

2013-12-04

Parameter Estimation Methods for Comprehensive Pyrolysis Modeling

Mihyun Esther Kim

Worcester Polytechnic Institute

Follow this and additional works at: <https://digitalcommons.wpi.edu/etd-dissertations>

Repository Citation

Kim, M. E. (2013). *Parameter Estimation Methods for Comprehensive Pyrolysis Modeling*. Retrieved from <https://digitalcommons.wpi.edu/etd-dissertations/408>

This dissertation is brought to you for free and open access by [Digital WPI](#). It has been accepted for inclusion in Doctoral Dissertations (All Dissertations, All Years) by an authorized administrator of Digital WPI. For more information, please contact wpi-etd@wpi.edu.

Parameter Estimation Methods for Comprehensive Pyrolysis Modeling

by

Mihyun Esther Kim

A Dissertation Submitted to the Faculty of
Worcester Polytechnic Institute
in partial fulfillment for the requirements for the
Degree of Doctor of Philosophy
in Fire Protection Engineering
February 2014

APPROVED:

Professor Nicholas A. Dembsey, Major Advisor

Professor Satya Shivkumar, Co-Advisor

Professor Albert Simeoni, Co-Advisor

Professor Kathy A. Notarianni, Head of Department

ABSTRACT

This dissertation documents a study on parameter estimation methods for comprehensive pyrolysis modeling. There are four parts to this work, which are (1) evaluating effects of applying different kinetic models to pyrolysis modeling of fiberglass reinforced polymer composites; (2); evaluation of pyrolysis parameters for fiberglass reinforced polymer composites based on multi-objective optimization; (3) parameter estimation for comprehensive pyrolysis modeling: guidance and critical observations; and (4) engineering guide for estimating material pyrolysis properties for fire modeling.

In the first part (Section 2), evaluation work is conducted to determine the effects of applying different kinetic models (KMs), developed based on thermal analysis using TGA data, when used in typical 1D pyrolysis models of fiberglass reinforced polymer (FRP) composites. The study shows that that increasing complexity of KMs to be used in pyrolysis modeling is unnecessary for the FRP samples investigated. Additionally, the findings from this research indicates that the basic assumption of considering thermal decomposition of each computational cell in comprehensive pyrolysis modeling as equivalent to that in a TGA experiment becomes inapplicable at depth and higher heating rates.

The second part of this dissertation (Section 3) reports the results from a study conducted to investigate the ability of global, multi-objective and multi-variable optimization methods to estimate material parameters for comprehensive pyrolysis models. The research materials are two fiberglass reinforced polymer (FRP) composites that share the same fiberglass mats but with two different resin systems. One resin system is composed of a single component and the other system is composed of two components (resin and fire retardant additive). The results show that for a well-configured parameter estimation exercise using the optimization method described above, (1) estimated results are within $\pm 100\%$ of the measurements in general; (2) increasing complexity of the kinetic modeling for a single component system has insignificant effect on estimated values; (3) increasing complexity of the kinetic modeling for a multiple component system with each element having different thermal characteristics has positive effect on estimated values; and (4) parameter estimation using an optimization method with appropriate level of complexity in kinetic model and optimization targets can find estimations that can be considered as effective material property values.

The third part of this dissertation (Section 4) proposes a process for conducting parameter estimation for comprehensive pyrolysis models. The work describes the underlying concepts considered in the proposed process and gives discussions of its limitations. Additionally, example cases of parameter estimation exercise are shown to illustrate the application of the parameter estimation process. There are four materials considered in the example cases – thermoplastics (PMMA), corrugated cardboard, fiberglass reinforced polymer composites and plywood.

In the last part (Section 5), the actual Guide, a standardized procedure for obtaining material parameters for input into a wide range of pyrolysis models is presented. This is a step-by-step process that provides a brief

description of modeling approaches and assumptions; a typical mathematical formulation to identify model parameters in the equations; and methods of estimating the model parameters either by independent measurements or optimization in pair with the model. In the Guide, example cases are given to show how the process can be applied to different types of real-world materials.

ACKNOWLEDGEMENTS

I thank my family for being supportive of my work. My husband found new ways to help me release the stress from the research work and gave his best effort to help me meet my paper deadlines. Without his support, I would have not been able to finish the 14 publications in journals, conference proceedings and reports, which were completed throughout the course of my ph.D. studies. My two beautiful children gave me the strength to come back to work as having them in my life and spending time with them reminded me that I was fully blessed. I thank my father, another WPI FPE graduate, for introducing me to this world of fire protection engineering and convincing me to follow his footsteps. He has taught me to have confidence in myself, although we are from a culture that doubts the need for highly educated female engineers. I greatly thank my mother who has always been there for me with prayer, long discussions over the phone, helping me with the kids, and so much more. Without her help mentally, physically and spiritually, I would not have been able to finish my studies. I thank Grandmother Kim for helping me with my family in time of great need.

I thank my advisor, Professor Nicholas A. Dembsey for his teachings, guidance and most of all his patience. I sincerely respect him for his willingness to understand and support my professional and personal decisions. I thank Professor Satya Shivkumar for introducing me to thermal analysis of polymers and the many discussions that we had about thermal decomposition. I also thank Professor Albert Simeoni and Kathy A. Notarianni for their assistance.

I thank Dr. Patricia A. Beaulieu for her guidance and friendship throughout my graduate school years. I thank Dr. Christopher W. Lautenberger for his assistance in using his comprehensive pyrolysis model, GPYRO and the property estimation algorithms in my work. I thank Mr. Ranall Harris for his help with most of the experimental works including the Cone Calorimeter, Fire Propagation Apparatus, muffle furnace, Thermogravimetric Analysis and Differential Scanning Calorimetry tests. I also thank all the FPE graduate students who worked with me in the Fire Laboratory over the years. I greatly appreciate the support for this work from DOC NIST Award Number 60NANB8D8106 (Federal Program Officer Dr. Kevin McGrattan). Special thanks go to Charles Dore for fabricating and donating the FRP composite materials used in this study.

TABLE OF CONTENTS

ABSTRACT.....	i
ACKNOWLEDGEMENTS.....	iii
TABLE OF CONTENTS.....	iv
LIST OF FIGURES.....	xv
LIST OF TABLES.....	xxviii

- Section 1 -

INTRODUCTION.....	Section 1 - 1
-------------------	---------------

- Section 2 -

EVALUATING EFFECTS OF APPLYING DIFFERENT KINETIC MODELS TO PYROLYSIS MODELING OF FIBERGLASS REINFORCED POLYMER COMPOSITES	Section 2 - 1
Abstract.....	Section 2 - 1
Nomenclature	Section 2 - 1
1. Introduction	Section 2 - 2
1. Background	Section 2 - 3
1.1. Kinetic Modeling Using Thermal Analysis	Section 2 - 3
1.2. Kinetic Modeling for Comprehensive Pyrolysis Models	Section 2 - 5
2. Materials	Section 2 - 6
3. Test Matrix	Section 2 - 7
4. Methodology: Experiments and Modeling	Section 2 - 9
4.1. Small-scale Experiments for Kinetic Modeling Using Thermal Analysis	Section 2 - 9

4.2.	Bench-scale Experiments for Pyrolysis Modeling	Section 2 - 9
4.3.	Screening Process: 1D Pyrolysis Modeling with Measured Temperature Gradient.....	Section 2 - 10
5.	Results and Discussion	Section 2 - 12
5.1.	Thermal Decomposition of Resins	Section 2 - 12
5.1.1.	Brominated Unsaturated Polyester Resin: BrUPE	Section 2 - 12
5.1.2.	Modified Acrylic with Inorganic Additive: MA+A.....	Section 2 - 14
5.2.	Kinetic Modeling Results: Comparison to TGA Data and Extrapolation	Section 2 - 15
5.3.	Pyrolysis Modeling	Section 2 - 21
6.	Conclusion.....	Section 2 - 26
7.	Acknowledgements.....	Section 2 - 26
8.	Reference	Section 2 - 27

- Section 3 -

	EVALUATION OF PYROLYSIS PARAMETERS FOR FIBERGLASS REINFORCED POLYMER COMPOSITES BASED ON MULTI-OBJECTIVE OPTIMIZATION	Section 3 - 1
	ABSTRACT.....	Section 3 - 1
1.	INTRODUCTION	Section 3 - 1
2.	SAMPLE MATERIAL.....	Section 3 - 2
3.	EXPERIMENTS.....	Section 3 - 3
4.	PARAMETER ESTIMATION VIA OPTIMIZATION METHOD	Section 3 - 4
5.	THERMAL DECOMPOSITION KINETIC MODELING	Section 3 - 5
6.	OPTIMIZATION TARGET	Section 3 - 8
7.	RESULTS AND DISCUSSION.....	Section 3 - 10
8.	CONCLUSIONS.....	Section 3 - 17
9.	ACKNOWLEDGEMENTS	Section 3 - 18

10. REFERENCES	Section 3 - 18
----------------------	----------------

- Section 4 -

PARAMETER ESTIMATION FOR COMPREHENSIVE PYROLYSIS MODELING: GUIDANCE AND CRITICAL OBSERVATIONS	Section 4 - 1
1. Abstract	Section 4 - 1
2. Keywords.....	Section 4 - 1
3. Introduction	Section 4 - 1
4. Background	Section 4 - 2
5. Applied Principals and Approaches in Developing the Parameter Estimation Process.....	Section 4 - 3
Consistency, Common-sense and Correctness	Section 4 - 3
Breaking Down the Problem into Groups	Section 4 - 3
Determining Appropriate Complexity of the Problem	Section 4 - 4
Measurements and/or Numerical Optimization	Section 4 - 5
6. Parameter Estimation Process	Section 4 - 7
7. Different Optimization Methods.....	Section 4 - 10
8. Limitations in Parameter Estimation	Section 4 - 11
Microstructure Effect.....	Section 4 - 12
Kinetic Modeling Effect	Section 4 - 13
Numerical Optimization Effect.....	Section 4 - 17
9. Application to Real-world Material Problems.....	Section 4 - 18
Results and Discussion	Section 4 - 19
10. Conclusion.....	Section 4 - 30
11. Acknowledgments.....	Section 4 - 31
12. References	Section 4 - 31

ENGINEERING GUIDE FOR ESTIMATING MATERIAL PYROLYSIS PROPERTIES FOR

FIRE MODELING Section 5 - 1

Chapter 1–Introduction Section 5 - 1

 Background Section 5 - 1

 Purpose Section 5 - 3

 Organization of the Guide..... Section 5 - 4

 References Section 5 - 4

Chapter 2–Determine Model Type Section 5 - 6

 Pyrolysis of materials Section 5 - 6

 Pyrolysis Models Section 5 - 8

 Process of Choosing Pyrolysis Model..... Section 5 - 10

Chapter 3–Empirical Models..... Section 5 - 14

 Understanding Model Section 5 - 14

 General Description of Models Section 5 - 14

 Governing Equations..... Section 5 - 15

 Model Parameters and Measurement Methods Section 5 - 16

 Virtual Material Section 5 - 16

 Model Parameter Table Section 5 - 16

 Model Parameter Measurement Methods..... Section 5 - 17

 Uncertainty Analysis Section 5 - 21

 Parameter Estimation Process..... Section 5 - 22

 Example Cases Overview Section 5 - 24

 Case 1: Burning Object..... Section 5 - 25

 General Model Parameter Table Section 5 - 25

 Example 3.1 Modeling Sofa Section 5 - 26

Case 2: Burning Flat Surfaces	Section 5 - 31
General Model Parameter Table	Section 5 - 31
Example 3.2 Modeling PMMA	Section 5 - 32
Example 3.3 Modeling Corrugated Cardboard	Section 5 - 35
Example 3.4 Modeling Fire Retarded FRP Composite	Section 5 - 38
Example 3.5 Modeling Plywood.....	Section 5 - 41
References	Section 5 - 44
Chapter 4–Simple Analytical Models	Section 5 - 45
Understanding Model	Section 5 - 45
General Description of Models	Section 5 - 45
Governing Equations.....	Section 5 - 46
Model Parameters and Measurement Methods	Section 5 - 49
Virtual Material	Section 5 - 49
Model-Parameter Table	Section 5 - 50
Model-Parameter-Measurement Methods	Section 5 - 50
Uncertainty Analysis	Section 5 - 63
Ignition Data Analysis.....	Section 5 - 63
Burning-Rate Data Analysis.....	Section 5 - 66
Parameter-Estimation Process.....	Section 5 - 67
Example Cases Overview	Section 5 - 69
Case 1: Thermally-Thick, Inert at Pre-Ignition with Steady Burning at Post-ignition.....	Section 5 - 70
Virtual Microstructure of Virgin Material	Section 5 - 70
General Model-Parameter Table	Section 5 - 70
Example 4.1 Modeling Poly(methylmethacrylate), PMMA	Section 5 - 71
Example 4.2 Modeling Corrugated Cardboard	Section 5 - 77

Example 4.3 Modeling Fire Retarded FRP Composite	Section 5 - 82
Example 4.4 Modeling Plywood.....	Section 5 - 87
Case 2: Thermally-Thin, Inert at Pre-Ignition with Steady Burning	
at Post-ignition.....	Section 5 - 92
Virtual Microstructure of Virgin Material	Section 5 - 92
General Model-Parameter Table	Section 5 - 92
Example 4.5 Modeling Sandwich Composite – GRP Skin	
with Balsawood Core	Section 5 - 93
Example 4.6 Modeling Thin FRP Composite	Section 5 - 98
References	Section 5 - 103
Chapter 5—Comprehensive Models	Section 5 - 105
Understanding Model	Section 5 - 105
General Description of Models	Section 5 - 105
Brief Description of Typical Pyrolysis Models Available in the	
Fire Community.....	Section 5 - 106
Governing Equations.....	Section 5 - 108
Model Parameters and Measurement Methods	Section 5 - 113
Virtual Microstructure of Virgin Material and Decomposition Kinetics Type....	Section 5 - 113
Model-Parameter Table	Section 5 - 116
Model-Parameter Measurement Methods	Section 5 - 118
Parameter-Estimation Process.....	Section 5 - 137
Sensitivity Analysis	Section 5 - 144
Example Case 1 and 2	Section 5 - 144
Example Case 3 (Global Sensitivity Analysis: Morris Method).....	Section 5 - 144
Uncertainty Analysis	Section 5 - 147
Optimization	Section 5 - 149

Example Cases Overview	Section 5 - 152
Case 1: Single-Step Decomposition Reaction without Residue Production	Section 5 - 153
Virtual Microstructure of Virgin Material	Section 5 - 153
Decomposition Kinetics Type	Section 5 - 153
General Model-Parameter Table	Section 5 - 153
Example 5.1 Modeling Poly(methylmethacrylate), PMMA	Section 5 - 154
Case 2: Single-Step Decomposition Reaction With Residue Production	Section 5 - 165
Virtual Microstructure of Virgin Material	Section 5 - 165
Decomposition Kinetics Type	Section 5 - 165
General Model Parameter Table	Section 5 - 165
Example 5.2 Modeling Triple-layered Corrugated Cardboard	Section 5 - 166
Case 3: Two-Step Decomposition Reaction With Residue Production	Section 5 - 178
Virtual Microstructure of Virgin Material	Section 5 - 178
Decomposition Kinetics Type	Section 5 - 178
General Model Parameter Table	Section 5 - 178
Example 5.3 Modeling FRP Composite with Modified Acrylic Resin with High-charring Inorganic Additive	Section 5 - 179
Example 5.4 Modeling Plywood	Section 5 - 197
References	Section 5 - 212
Chapter 6—Conclusions	Section 5 - 215
Appendix A - Uncertainty Analysis	Section 5 - 216
Type A Uncertainty	Section 5 - 217
Type B Uncertainty	Section 5 - 218
References	Section 5 - 219
Appendix B - Example Solutions for Chapter 3	Section 5 - 220
Example 3.1 Modeling Sofa	Section 5 - 220

Obtain Parameters via Experiment.....	Section 5 - 220
Validation and Commentary	Section 5 - 223
Example 3.2 Modeling PMMA	Section 5 - 226
Obtain Parameters via Experiment.....	Section 5 - 226
Validation and Commentary	Section 5 - 229
Example 3.3 Modeling Corrugated Cardboard	Section 5 - 231
Obtain Parameters via Experiment.....	Section 5 - 231
Validation and Commentary	Section 5 - 234
Example 3.4 Modeling Fire Retarded FRP Composite	Section 5 - 235
Obtain Parameters via Experiment.....	Section 5 - 235
Validation and Commentary	Section 5 - 238
Example 3.5 Modeling Plywood.....	Section 5 - 239
Obtain Parameters via Experiment.....	Section 5 - 239
Validation and Commentary	Section 5 - 242
References	Section 5 - 243
Appendix C - Example Solutions for Chapter 4	Section 5 - 244
Example 4.1 Modeling PMMA	Section 5 - 244
Measure Parameters.....	Section 5 - 244
Obtain Parameters via Data Analysis	Section 5 - 246
Validation	Section 5 - 258
Commentary	Section 5 - 265
Example 4.2 Modeling Corrugated Cardboard	Section 5 - 266
Measure Parameters.....	Section 5 - 266
Obtain Parameters via Data Analysis	Section 5 - 268
Validation	Section 5 - 279
Commentary	Section 5 - 283

Example 4.3 Modeling Fire-Retarded FRP Composite	Section 5 - 285
Measure Parameters.....	Section 5 - 285
Obtain Parameters via Data Analysis	Section 5 - 287
Validation	Section 5 - 299
Commentary	Section 5 - 303
Example 4.4 Modeling Plywood.....	Section 5 - 304
Measure Parameters.....	Section 5 - 304
Obtain Parameters via Data Analysis	Section 5 - 306
Validation	Section 5 - 317
Commentary	Section 5 - 321
Example 4.5 Modeling GRP with Balsa Wood Core Sandwich Composite	Section 5 - 322
Measure Parameters.....	Section 5 - 322
Obtain Parameters via Data Analysis	Section 5 - 324
Validation	Section 5 - 337
Commentary	Section 5 - 341
Example 4.6 Modeling Thin FRP Composite Sheet	Section 5 - 342
Measure Parameters.....	Section 5 - 342
Obtain Parameters via Data Analysis	Section 5 - 344
Validation	Section 5 - 355
Commentary	Section 5 - 359
References	Section 5 - 361
Appendix D - Example Solutions for Chapter 5.....	Section 5 - 362
Example 5.1 Modeling PMMA	Section 5 - 362
Measure Parameters.....	Section 5 - 362
Obtain Parameters via Numerical Optimization.....	Section 5 - 367
Validation	Section 5 - 372

Commentary	Section 5 - 378
Example 5.2 Modeling Corrugated Cardboard	Section 5 - 382
Measure Parameters.....	Section 5 - 382
Obtain Parameters via Numerical Optimization.....	Section 5 - 385
Validation	Section 5 - 391
Commentary	Section 5 - 398
Example 5.3 Modeling Modified Acrylic FRP Composite.....	Section 5 - 401
Measure Parameters.....	Section 5 - 403
Obtain Parameters via Numerical Optimization.....	Section 5 - 409
Validation	Section 5 - 416
Commentary	Section 5 - 428
Example 5.4 Modeling Plywood.....	Section 5 - 432
Measure Parameters.....	Section 5 - 432
Obtain Parameters via Numerical Optimization.....	Section 5 - 435
Validation	Section 5 - 441
Commentary	Section 5 - 448
References	Section 5 - 451
Appendix E - Chapter 5 Supplement: Morris' OAT Method	Section 5 - 453
References	Section 5 - 455

- Section 6 -

CONCLUSIONS.....	Section 6 - 1
FUTURE WORKS	Section 6 - 3

- Appendix -

Appendix A – Kinetic Effects on Pyrolysis Modeling of Fiberglass Reinforced Polymer Composites, *7th International Seminar of Fire & Explosion Hazards (ISFEH 2013)*

Appendix B – Thermo-Physical and Optical Parameter Estimation for Pyrolysis Modeling of Fiberglass Reinforced Polymer Composites, *ANTEC 2013*

Appendix C – Evaluation of Different Approaches for Property Estimation for Pyrolysis Modeling Applied to FRP Composites, *Fire and Materials 2011, 12th International Conference*

Appendix D – Evaluation of Different Approaches for Property Estimation for Pyrolysis Modeling Applied to FRP Composites, *Composites 2011*

Appendix E – Thermal Degradation Kinetics Modeling for Pyrolysis Modeling Using Fire Retarded Thermoset Polymer Resins, *Interflam 2010, 12th International Conference on Fire Science and Engineering*

Appendix F – Property Estimation for Pyrolysis Modeling Applied to Flame Retarded Modified Acrylic FRP Composites, *Composites & Polycon 2010*

Appendix G – Parameter Estimation for Pyrolysis Modeling Applied to Polyester FRP Composites with Different Glass Contents, *Fire and Materials 2009, 11th International Conference*

Appendix H – Property Estimation for Pyrolysis Modeling Applied to Polyester FRP Composites with Different Glass Contents, *Composites & Polycon 2009*

Appendix I – The Role of Decomposition Kinetics in Pyrolysis Modeling: Application to a Fire Retardant Polyester Composite, *Fire Safety Science - Proceedings of the 9th International Symposium*

LIST OF FIGURES

- Section 2 -

Figure 1. Schematic of the screening process: mass loss of FRP is simulated with conservation of mass and energy represented by the decomposition kinetics and temperature profile measurements from bench-scale experiment of FRP, respectively.

Figure 2. Results from iso-conversional method conducted on BrUPE (left) and MA+A (right) resins: both figures show the estimated activation energy of thermal decomposition with respect to conversion (α)

Figure 3. Heat flow measurements from DSC experiments for BrUPE and MA+A polymer resin samples with 20 °C/min heating rate using nitrogen purge. MA+A resin shows a significant endothermic heat at lower temperatures, which is speculated as the heat associated with thermal decomposition of the fire retardant additive (A) in the resin system. There is an overlap in another endothermic heat at relatively higher temperatures for both materials, which is considered to be the heat necessary for the thermal decomposition of the resins itself (BrUPE and MA).

Figure 4. Mass loss rates from TGA experiments (exp) and kinetic modeling A; B; C; D; E; and F are shown for BrUPE with 60 °C/min heating rate case. Applying various approaches in kinetic modeling results in minor changes in modeled mass loss rate.

Figure 5. Mass loss rates from TGA experiments (exp) and kinetic modeling A; B; C; D; E; and F are shown for MA+A with 60 °C/min heating rate case. Applying various approaches in kinetic modeling results in minor changes in modeled mass loss rate.

Figure 6. An extrapolation case at 200 °C/min heating rate for thermal decomposition of BrUPE (left) and MA+A (right) resins. Differences between different kinetic models (A through F) are similar to those observed in the lower heating rates.

Figure 7. Temperature data at front surface (T_s), 1/3 depth ($T_{1/3}$), 2/3 depth ($T_{2/3}$) and back surface (T_b) from Cone Calorimeter experiments with BrUPE and MA+A FRP samples tested at various heat flux levels ranging from 25 to 100 kW/m². These have been used in the simplified pyrolysis modeling with different kinetic models.

Figure 8. Example calculation using the simplified comprehensive pyrolysis model is shown for the surface location. Temperature data at front surface (T_s) from Cone Calorimeter experiments with applied heat flux of 50 kW/m² and simplified comprehensive pyrolysis modeling results using various kinetic models (A-F) at this location are shown for BrUPE (left) and MA+A (right) FRP composites.

Figure 9. Mass loss rates from Cone Calorimeter experiments (exp) and simplified comprehensive pyrolysis modeling (mod) are shown for BrUPE and MA+A FRP composites. Applied heat flux levels are 50, 70 and 100 kW/m² for BrUPE FRP composite and 25, 50 and 75 kW/m² for MA+A FRP composite. Good agreement between experiment data and modeling results is found from the cases that are less than 50kW/m².

- Section 3 -

Figure 1. Mass loss rates from TGA experiments (exp) and kinetic modeling (A-F) and are shown for BrUPE (a) and MA+A (b) with 60 °C/min heating rate case. Applying various approaches in kinetic modeling results in minor changes in modeled mass loss rate.

Figure 2. Mass loss rates from Cone Calorimeter experiments (exp) and simplified comprehensive pyrolysis modeling (mod) and are shown for BrUPE and MA+A FRP composites. Applied heat flux levels are 50, 70 and 100 kW/m² for BrUPE FRP composite ((a), (b) and (c), respectively) and 25, 50 and 75 kW/m² for MA+A FRP composite ((d), (e) and (f), respectively). Good agreement between experiment data and modeling results are found from (a) for BrUPE composite and (d) and (e) for MA+A composite.

Figure 3. Mass loss rate, front and back surface temperature histories from Cone Calorimeter experiments (exp) and comprehensive pyrolysis modeling results with parameters estimated from numerical optimization using three different kinetic models (B, C and F) are shown for BrUPE FRP composite. Applied heat flux level is 50 kW/m². Modeling outputs are mostly within the uncertainty bands of the experiment data.

Figure 4. Mass loss rate, front and back surface temperature histories from Cone Calorimeter experiments (exp) and comprehensive pyrolysis modeling results with parameters estimated from numerical optimization using two different kinetic models (B and C) are shown for MA+A FRP composite. Applied heat flux level is 50 kW/m². Modeling outputs are mostly within the uncertainty bands of the experiment data.

Figure 5. Comparison between measured specific heat values and estimated values from numerical optimization with different kinetic models – B, C and F – for two polymer resin systems of (a) BrUPE and (b) MA+A: Results show that compared to measured values there is some improvement in the estimated specific heat capacity of the resins for a single component system BrUPE and a significant improvement for two-component system MA+A when a more complex kinetic model is used in the estimation process.

Figure 6. Comparison of estimated (a) thermal conductivity and (b) specific heat capacity values for glass from numerical optimization process with different kinetic models – B, C and F – for two FRP composites of BrUPE and MA+A FRPs: Results show that compared to measured values there is insignificant effect in the estimated thermal conductivity and some improvement in the estimated specific heat capacity of the fiberglass for a single component system BrUPE. However, for two-component system MA+A, there is a significant improvement in the estimation for thermal conductivity and specific heat capacity for fiberglass when a more complex kinetic model is used.

- Section 4 -

Figure 1. Flow chart of parameter estimation for comprehensive pyrolysis models

Figure 2. Understanding manual optimization: (a) For a one-step thermal decomposition kinetics that takes place within temperature range of $T_a < T < T_b$, changing parameters related to reactants should affect fire behaviors at temperatures below T_a and changing parameters related to products should affect fire behaviors at temperatures above T_b ; (b) Reducing HoR increases mass loss rate peak; (c) Reducing thermal conductivity results in wider spread between T_{surf} and T_{back} ; (d) Reducing specific heat capacity results in faster increase in temperature throughout. Note that results from greater parameter value are shown in solid lines, while those from smaller value are shown in dashed lines.

Figure 3. Thermal conductivity of fiberglass estimated from measured thermal conductivities of polymer resin and fiberglass reinforced polymer (FRP) composite and volume (X) fraction of resin and fiberglass. The solid fill of the markers indicate the mean and the uncertainties are considered with unfilled markers. When $k < 0$, estimation is considered to be non-physical.

Figure 4. Actual pyrolysis phenomenon of a porous solid phase material under one-dimensional heating

Figure 5. Mass loss rates from Cone Calorimeter experiments (exp) and simplified comprehensive pyrolysis modeling (mod) and are shown for MA+A FRP composite. Applied heat flux levels are 25 (left), 50 (middle) and 75 (right) kW/m². Good agreement between experiment data and modeling results is found from the cases with applied heat flux level of 25 and 50kW/m². Deviation in simulation occurs from experiment data at 75 kW/m² case near the initial peak in the mass loss rate ($t < 300s$).

Figure 6. Mass loss rates from Cone Calorimeter experiments (exp) and simplified comprehensive pyrolysis modeling with different kinetic models (A through F) and are shown for BrUPE FRP composite at applied heat flux level of 50 kW/m². Generally, good agreement between experiment data and modeling results are found for all cases (A through F) except for case A where a large scatter is found near the mass loss rate peak and at the end of the simulation.

Figure 7. Mass loss rate (MLR, top row) and surface temperature (T_{surf} , bottom row) comparisons for PMMA between actual from experiment (exp) and modeled (mod) at applied heat flux of 23 (left), 46 (middle) and 64 (right) kW/m². Best simulation results were found from estimation with mostly non-optimization (i.e. independent measurements or literature search) approach for parameter estimation of PMMA.

Figure 8. Mass loss rate (MLR, top row) and surface temperatures (T_{surf} , bottom row) comparisons for corrugated cardboard between actual from experiment (exp) and modeled (mod) at applied heat flux of 20 (left), 60 (middle) and 110 (right) kW/m². The moderate heat flux case is used in optimization and the lower and higher heat flux cases are used in extrapolation exercise to examine modeling quality. Best simulation results were found from estimation with mostly optimization approach using shuffled complex evolution method for parameter estimation of triple layered corrugated cardboard.

Figure 9. Mass loss rate (MLR) and surface temperatures (T_{surf} , T_{back}) comparisons for fiberglass reinforced polymer (FRP) composite with modified acrylic resin with high-charring fire retardant additive between actual from experiment (exp) and modeled (mod) at applied heat flux of 25, 50 and 75 kW/m². The moderate heat flux case is used in optimization and the lower and higher heat flux cases are used in extrapolation exercise to examine modeling quality. Best simulation results were found from estimation with mostly optimization approach using either genetic algorithm or shuffled complex evolution method for parameter estimation of this fiberglass reinforced polymer composite.

Figure 10. Mass loss rate (MLR) and surface temperatures (T_{surf} , T_{back}) comparisons for plywood between actual from experiment (exp) and modeled (mod) at applied heat flux of 25, 50 and 75 kW/m². The moderate heat flux case is used in optimization and the lower and higher heat flux cases are used in extrapolation exercise to examine modeling quality. Simulation results are from estimation with manual optimization approach for parameter estimation of plywood.

- Section 5 -

Figure 2-1. Material category: Depending on material's characteristics, material can be grouped into 4 categories and examples for each category is given.

Figure 2-2. Model selection flowchart: By examining the cross-section of material and analyzing experiment data that presents its fire behavior, modeler may determine material's virtual microstructure and appropriate pyrolysis models available for its specific use.

Figure 3-1. Flow chart of parameter estimation for empirical pyrolysis models

Figure 3-2. Effect of ignition source strength: single seat sofas tested in furniture calorimeter test with different ignition source – ignition with 59 mL gasoline poured (a) or with 45 W butane gas flame (b)

Figure 3-3. Effect of ignition location: steel framed seat sofa mockups tested in furniture calorimeter test with different ignition location – ignition on center seat cushion (a) or seat cushion on right side (b)

Figure 4-1. Schematic of a piloted ignition experiment

Figure 4-2. Pyrolysis modeling set-up used for thermally-thick materials

Figure 4-3. Pyrolysis modeling set-up used for thermally-thin materials

Figure 4-4. Measuring surface temperature with a thermocouple

Figure 4-5. Heat balance at the surface of a burning cone calorimeter specimen

Figure 4-6. Flow chart of parameter estimation for simple analytical pyrolysis models

Figure 4-7 Mass-loss rate (MLR) comparisons for PMMA between actual MLR from experiment (exp) and Modeled MLR (sim) at different applied heat-flux levels – (a) MLR at 25 kW/m²; (b) MLR at 50 kW/m²; and (c) MLR at 75 kW/m². Note that data shown were used to estimate model parameter values.

Figure 4-8 Mass-loss rate (MLR) comparisons for PMMA between actual MLR from experiment (exp) and modeled MLR (sim) at different applied heat-flux levels – (a) MLR at 28.4 kW/m²; and (b) MLR at 60 kW/m². Note that data shown were not included in the model parameter estimation process; hence, these two cases are considered as extrapolation cases.

Figure 4-9 Mass-Loss Rate (MLR) comparisons for corrugated cardboard between actual MLR from experiment (exp) and modeled MLR (sim) at different applied heat-flux levels – (a) MLR at 25 kW/m²; (b) MLR at 50 kW/m²; and (c) MLR at 75 kW/m². Note that data shown were used to estimate model parameter values.

Figure 4-10 Mass-loss rate (MLR) comparisons for fire-retarded FRP composite between actual MLR from experiment (exp) and modeled MLR (sim) at different applied heat-flux levels – (a) MLR at 50 kW/m²; and (b) MLR at 75 kW/m². Note that data shown were used to estimate model parameter values.

Figure 4-10 Mass-loss rate (MLR) comparisons for plywood between actual MLR from experiment (exp) and modeled MLR (sim) at different applied heat-flux levels – (a) MLR at 25 kW/m²; (b) MLR at 50 kW/m²; and (c) MLR at 75 kW/m². Note that data shown were used to estimate model parameter values.

Figure 4-12 Mass-loss rate (MLR) comparisons for sandwich composite – GRP skin with balsawood core – between actual MLR from experiment (exp) of the composite and modeled MLR (sim) of GRP skin at different applied heat-flux levels – (a) MLR at 35 kW/m²; (b) MLR at 50 kW/m²; and (c) MLR at 75 kW/m². Note that data shown were used to estimate model parameter values.

Figure 4-13 Mass-loss rate (MLR) comparisons for thin FRP composite between actual MLR from experiment (exp) and modeled MLR (sim) at different applied heat-flux levels – (a) MLR at 25 kW/m²; (b) MLR at 50 kW/m²; and (c) MLR at 75 kW/m². Note that data shown were used to estimate model parameter values.

Figure 5-1. Typical DTG thermogram showing single peak

Figure 5-2. Schematic of conducting Ozawa, Flynn and Wall Iso-conversional Method

Figure 5-3. Schematic of conducting Friedman's Iso-conversional Method

Figure 5-4. Change in DTG curve with respect to changes made in n values using nth order reaction model

Figure 5-5. TG (weight loss) thermogram from TGA experiment (left) and heat flow diagram from DSC experiment (right) for decomposition of a rigid foam plastic

Figure 5-6. Melting points for a thermoplastic polymer as a function of DSC heating rates

Figure 5-7. Flow chart of parameter estimation for comprehensive pyrolysis models

Figure 5-8. Understanding manual optimization: (a) For a one-step thermal decomposition kinetics that takes place within temperature range of $T_a < T < T_b$, parameter estimation conductor may understand changing parameters related to reactant should affect fire behaviors at temperatures below T_a and changing parameters related to product should affect fire behaviors at temperatures above T_b ; (b) Reducing HoR increases mass loss rate peak; (c) Reducing thermal conductivity results in wider spread between T_{surf} and T_{back} ; (d) Reducing specific heat capacity results in faster increase in temperature throughout. Note that results from greater parameter value are shown in solid lines, while those from smaller value are shown in dashed lines.

Figure 5-9. Cone calorimeter test data of thick PMMA (thickness, δ ranging from 24 ~ 29 mm) impinged with effective heat fluxes (EHF) of 23, 46, and 69 kW/m²

Figure 5-10. TG/DTG curves at 10°C/min heating rate with different estimation results for kinetic parameters for thermal decomposition of PMMA

Figure 5-11. Mass-loss rate (MLR) comparisons for PMMA between actual MLR from experiment (data) and modeled MLR (A, B-GA, B-SCE, B-SHC, C-GA, C-SCE, C-SHC) at applied heat-flux of 46 kW/m². Note that data shown were used to estimate model parameter values via numerical optimization using GA, SCE or SHC routines.

Figure 5-12. Mass-loss rate (MLR) comparisons for PMMA between actual MLR from experiment (data) and modeled MLR (A, B-GA, B-SCE, B-SHC, C-GA, C-SCE, C-SHC) at applied heat flux of (a) 23 and (b) 64 kW/m². Note that data shown were not included in the model parameter estimation process; hence, these two cases are considered as extrapolation cases.

Figure 5-13. surface temperature (T_{surf}) comparisons for PMMA modeling using parameters estimated from different approaches – direct measurement, literature search, or approximation (A); measurement and numerical optimization (B-GA, B-SCE, B-SHC); mostly numerical optimization (C-GA, C-SCE, C-SHC) at applied heat flux of 46 kW/m². Note that data shown were used to estimate model parameter values via numerical optimization using GA, SCE or SHC routines.

Figure 5-14. Surface temperature (T_{surf}) comparisons for PMMA modeling using parameters estimated from different approaches – direct measurement, literature search, or approximation (A); measurement and numerical optimization (B-GA, B-SCE, B-SHC); mostly numerical optimization (C-GA, C-SCE, C-SHC) at applied heat flux of (a) 23 and (b) 64 kW/m². Note that data shown were not included in the model parameter estimation process; hence, these two cases are considered as extrapolation cases.

Figure 5-15. TGA thermograms of PMMA decomposition conducted under constant heating rates – 2, 5, 10 and 20K/min – and two different environments – (a) nitrogen and (b) air

Figure 5-16. Fire propagation apparatus (FPA) test data – (a) mass-loss rate; and (b) surface-temperature profile – of triple-wall corrugated cardboard, i.e., two layers of corrugated cardboard (thickness, δ is 30 mm) impinged with effective heat fluxes (EHF) of 20 to 110 kW/m²

Figure 5-17. TG/DTG curves at 10°C/min heating rate with different estimation results for kinetic parameters for thermal decomposition of corrugated cardboard: For better comparison, TG and DTG thermograms have been scaled to result in 100% conversion.

Figure 5-18. Mass-Loss Rate (MLR) comparisons for corrugated cardboard between actual MLR from experiment (Data) and modeled MLR (B-GA, B-SCE, B-SHC, C-GA, C-SCE, C-SHC) at applied heat flux of 60 kW/m². Note that data shown were used to estimate model parameter values via numerical optimization using GA, SCE or SHC routines.

Figure 5-19. Mass-Loss Rate (MLR) comparisons for corrugated cardboard between actual MLR from experiment (data) and modeled MLR (B-GA, B-SCE, B-SHC, C-GA, C-SCE, C-SHC) at applied heat flux of (a) 20 and (b) 110 kW/m². Note that data shown were not included in the model-parameter estimation process; hence, these two cases are considered as extrapolation cases.

Figure 5-20. Surface-temperature (T_{surf}) comparisons for corrugated cardboard between actual T_{surf} from experiment (data) and modeled T_{surf} (B-GA, B-SCE, B-SHC, C-GA, C-SCE, C-SHC) at applied heat flux of 60 kW/m². Note that data shown were used to estimate model parameter values via numerical optimization using GA, SCE or SHC routines.

Figure 5-21. Surface Temperature (T_{surf}) comparisons for corrugated cardboard between actual T_{surf} from experiment (data) and modeled T_{surf} (B-GA, B-SCE, B-SHC, C-GA, C-SCE, C-SHC) at applied heat flux of (a) 20 and (b) 110 kW/m². Note that data shown were not included in the model parameter estimation process; hence, these two cases are considered as extrapolation cases.

Figure 5-22. TGA thermograms of corrugated cardboard decomposition conducted under constant heating rate of 20 °C/min and two different environments – nitrogen and air

Figure 5-23. Cross-section of FRP composite with modified acrylic resin with high-charring inorganic additive

Figure 5-24. Total heat flux measured from sample surface during cone calorimeter test

Figure 5-25. Cone calorimeter (cone) test data of modified acrylic resin with high-charring additive FRP composite (thickness, δ is 8.9 ± 0.2 mm, density, ρ is 1900 kg/m³) impinged with effective heat fluxes (EHF) of 25 to 75 kW/m²

Figure 5-26. TG/DTG curves at 10°C/min heating rate with different estimation results for kinetic parameters for thermal decomposition of fire-retarded FRP composite: Testing of resin with additive sample (~10mg) with nitrogen purge

Figure 5-27. Mass-loss rate (MLR) comparisons for FRP composite with modified-acrylic resin with high-charring inorganic additive between actual MLR from experiment (data) and modeled MLR (GA, SCE, SHC) at applied heat flux of 50 kW/m². Note that data shown were used to estimate model parameter values via numerical optimization using GA, SCE or SHC routines.

Figure 5-28. Mass-loss rate (MLR) comparisons for FRP composite with modified-acrylic resin with high-charring inorganic additive between actual MLR from experiment (data) and modeled MLR (GA, SCE, SHC) at applied heat flux of (a) 25 and (b) 75 kW/m². Note that data shown were not included in the model parameter estimation process; hence, these two cases are considered as extrapolation cases.

Figure 5-29. Surface-temperature (T_{surf}) Comparisons for FRP composite with modified-acrylic resin with high-charring inorganic additive between actual T_{surf} from experiment (data) and modeled T_{surf} (GA, SCE, SHC) at applied heat flux of 50 kW/m². Note that data shown were used to estimate model parameter values via numerical optimization using GA, SCE or SHC routines.

Figure 5-30. Surface-temperature (T_{surf}) comparisons for FRP composite with modified-acrylic resin with high-charring inorganic additive between actual T_{surf} from experiment (data) and modeled T_{surf} (GA, SCE, SHC) at applied heat flux of (a) 25 and (b) 75 kW/m². Note that data shown were not included in the model parameter estimation process; hence, these two cases are considered as extrapolation cases.

Figure 5-31. Back-surface temperature (T_{back}) comparisons for FRP composite with modified-acrylic resin with high-charring inorganic additive between actual T_{back} from Experiment (Data) and Modeled T_{back} (GA, SCE, SHC) at applied heat flux of 50 kW/m². Note that data shown were used to estimate model parameter values via numerical optimization using GA, SCE or SHC routines.

Figure 5-32. Back-surface temperature (T_{back}) comparisons for FRP composite with modified-acrylic resin with high-charring inorganic additive between actual T_{back} from experiment (data) and modeled T_{back} (GA, SCE, SHC) at applied heat flux of (a) 25 and (b) 75 kW/m². Note that data shown were not included in the model parameter estimation process; hence, these two cases are considered as extrapolation cases.

Figure 5-33. Total heat flux measured from sample surface during cone calorimeter test

Figure 5-34. Cone calorimeter (cone) test data of plywood (thickness, δ is 11.1 ± 0.1 mm, density, ρ is 540 ± 10 kg/m³) impinged with effective heat fluxes (EHF) of 25 to 75 kW/m²

Figure 5-35. TG/DTG curves at 20°C/min heating rate with different estimation results for kinetic parameters for thermal decomposition of plywood: Testing of plywood sample (~10mg) with air purge

Figure 5-36. Mass-loss rate (MLR) comparisons for FRP composite with plywood between actual MLR from experiment (data) and modeled MLR (M&M) at applied heat flux of 50 kW/m². Note that data shown were used to estimate model parameter values via manual optimization.

Figure 5-37. Mass-loss rate (MLR) comparisons for FRP composite with plywood between actual MLR from experiment (data) and modeled MLR (M&M) at applied heat flux of (a) 25 and (b) 75 kW/m². Note that data shown were not included in the model parameter estimation process; hence, these two cases are considered as extrapolation cases.

Figure 5-38. Surface-temperature (T_{surf}) comparisons for plywood between actual T_{surf} from experiment (data) and modeled T_{surf} (M&M) at applied heat flux of 50 kW/m². Note that data shown were used to estimate model parameter values via manual optimization.

Figure 5-39. Surface-temperature (T_{surf}) comparisons for FRP composite with plywood between actual T_{surf} from experiment (data) and modeled T_{surf} (M&M) at applied heat flux of (a) 25 and (b) 75 kW/m². Note that data shown were not included in the model parameter estimation process; hence, these two cases are considered as extrapolation cases.

Figure 5-40. Back-surface temperature (T_{back}) comparisons for plywood between actual T_{back} from experiment (data) and modeled T_{back} (M&M) at applied heat flux of 50 kW/m². Note that data shown were used to estimate model parameter values via manual optimization.

Figure 5-41. Back-surface temperature (T_{back}) comparisons for plywood between actual T_{back} from experiment (data) and modeled t_{back} (M&M) at applied heat flux of (a) 25 and (b) 75 kW/m². Note that data shown were not included in the model parameter estimation process; hence, these two cases are considered as extrapolation cases.

Figure A(B)-1. Schematic of a furniture calorimeter

Figure A(B)-2. HRR curve from furniture calorimeter experiment of 4 identical tests of the same sofa mockup

Figure A(B)-3. Effect of ignition source strength: single seat sofas tested in furniture calorimeter test with different ignition source – ignition with 59 mL gasoline poured (a) or with 45 W butane gas flame (b)

Figure A(B)-4. Effect of ignition location: steel framed seat sofa mockups tested in furniture calorimeter test with different ignition location – ignition on center seat cushion (a) or seat cushion on right side (b)

Figure A(B)-5. Simplified representation of a cone calorimeter test of PMMA

Figure A(B)-6. MLR curve from cone calorimeter experiment of PMMA

Figure A(B)-7. Simplified representation of a cone calorimeter test of corrugated cardboard

Figure A(B)-8. MLR curve from cone calorimeter test of corrugated cardboard

Figure A(B)-9. Simplified representation of a cone calorimeter test of fire-retarded fiberglass-reinforced polymer (FRP) composite

Figure A(B)-10. MLR curve from cone calorimeter test of fire-retarded FRP composite

Figure A(B)-11. Simplified representation of a cone calorimeter test of plywood

Figure A(B)-12. MLR curve from cone calorimeter test of plywood

Figure A(C)-1. Simplified representation of a cone calorimeter test of PMMA

Figure A(C)-2. Plot of \dot{m}'' versus \dot{Q}''

Figure A(C)-3. Plot of steady MLR versus different applied heat-flux levels – 25, 50 and 75 kW/m²

Figure A(C)-4. Mass-loss rate (MLR) comparisons for PMMA between actual MLR from experiment (exp) and modeled MLR (sim) at 25 kW/m². Note that data shown were used to estimate model parameter values.

Figure A(C)-5. Mass-loss rate (MLR) comparisons for PMMA between actual MLR from experiment (exp) and modeled MLR (sim) at 50 kW/m². Note that data shown were used to estimate model parameter values.

Figure A(C)-6. Mass-loss rate (MLR) comparisons for PMMA between actual MLR from experiment (exp) and modeled MLR (sim) at 75 kW/m². Note that data shown were used to estimate model parameter values.

Figure A(C)-7. Mass-loss rate (MLR) comparisons for PMMA between actual MLR from experiment (exp) and modeled MLR (sim) at 28.4 kW/m². Note that data shown were not included in the model parameter estimation process; hence, this case is considered as extrapolation case.

Figure A(C)-9. Mass-loss rate (MLR) comparisons for PMMA between actual MLR from experiment (exp) and modeled MLR (sim) at 60 kW/m². Note that data shown were not included in the model parameter estimation process; hence, this case is considered as extrapolation case.

Figure A(C)-10. Simplified representation of a cone calorimeter test of corrugated cardboard

Figure A(C)-11. Plot of \dot{m}'' versus \dot{Q}''

Figure A(C)-12. Plot of steady MLR versus different applied heat-flux levels – 25 to 75 kW/m²

Figure A(C)-13. Mass-loss rate (MLR) comparisons for corrugated cardboard between actual MLR from experiment (exp) and modeled MLR (sim) at 25 kW/m². Note that data shown were used to estimate model parameter values.

Figure A(C)-14. Mass-loss rate (MLR) comparisons for corrugated cardboard between actual MLR from experiment (exp) and modeled MLR (sim) at 50 kW/m². Note that data shown were used to estimate model parameter values.

Figure A(C)-15. Mass-loss rate (MLR) comparisons for corrugated cardboard between actual MLR from experiment (exp) and modeled MLR (sim) at 75 kW/m². Note that data shown were used to estimate model parameter values.

Figure A(C)-16. Simplified representation of a cone calorimeter test of fire-retarded fiberglass-reinforced polymer (FRP) composite

Figure A(C)-17. Plot of \dot{m}'' versus \dot{q}''

Figure A(C)-18. Plot of steady MLR versus different applied heat flux levels – 25 to 75 kW/m²

Figure A(C)-19. Mass-loss rate (MLR) comparisons for fire-retarded FRP composite between actual MLR from experiment (exp) and modeled MLR (sim) at 50 kW/m². Note that data shown were used to estimate model parameter values.

Figure A(C)-20. Mass-loss rate (MLR) comparisons for fire-retarded FRP composite between actual MLR from experiment (exp) and modeled MLR (sim) at 75 kW/m². Note that data shown were used to estimate model parameter values.

Figure A(C)-21. Simplified representation of a cone calorimeter test of plywood

Figure A(C)-22. Plot of \dot{m}'' versus \dot{q}''

Figure A(C)-23. Plot of steady MLR versus different applied heat flux levels – 25 to 75 kW/m²

Figure A(C)-24. Mass-loss rate (MLR) comparisons for plywood between actual MLR from experiment (exp) and modeled MLR (sim) at 25 kW/m². Note that data shown were used to estimate model parameter values.

Figure A(C)-25. Mass-loss rate (MLR) comparisons for plywood between actual MLR from experiment (exp) and modeled MLR (sim) at 50 kW/m². Note that data shown were used to estimate model parameter values.

Figure A(C)-26. Mass-loss rate (MLR) comparisons for plywood between actual MLR from experiment (exp) and modeled MLR (sim) at 75 kW/m². Note that data shown were used to estimate model parameter values.

Figure A(C)-27. Simplified representation of a cone calorimeter test of sandwich composite

Figure A(C)-28. Plot of \dot{m}'' versus \dot{q}''

Figure A(C)-29. Plot of steady MLR versus different applied heat-flux levels – 25 to 75 kW/m²

Figure A(C)-30. Mass-loss rate (MLR) comparisons for GRP with balsa wood core sandwich composite between actual MLR from experiment (exp) and modeled MLR (sim) at 25 kW/m². Note that data shown were used to estimate model parameter values.

Figure A(C)-31. Mass-loss rate (MLR) comparisons for GRP with balsa wood core sandwich composite between actual MLR from experiment (exp) and modeled MLR (sim) at 50 kW/m². Note that data shown were used to estimate model parameter values.

Figure A(C)-32. Mass-loss rate (MLR) comparisons for GRP with balsa wood core sandwich composite between actual MLR from experiment (exp) and modeled MLR (sim) at 75 kW/m². Note that data shown were used to estimate model parameter values.

Figure A(C)-33. Simplified representation of a cone calorimeter test of FRP composite sheet

Figure A(C)-34. Plot of \dot{m}'' versus \dot{q}''

Figure A(C)-35. Plot of steady MLR versus different applied heat-flux levels – 25 to 75 kW/m²

Figure A(C)-36. Mass-loss rate (MLR) comparisons for thin FRP composite sheet between actual MLR from experiment (exp) and modeled MLR (sim) at 25 kW/m². Note that data shown were used to estimate model parameter values.

Figure A(C)-37. Mass-loss rate (MLR) comparisons for thin FRP composite sheet between actual MLR from experiment (exp) and modeled MLR (sim) at 50 kW/m². Note that data shown were used to estimate model parameter values.

Figure A(C)-38. Mass-loss rate (MLR) comparisons for thin FRP composite sheet between actual MLR from experiment (exp) and modeled MLR (sim) at 75 kW/m². Note that data shown were used to estimate model parameter values.

Figure A(D)-1. Thermal conductivity of PMMA

Figure A(D)-2. Heat capacity of PMMA

Figure A(D)-3. Kinetic modeling for decomposition of PMMA under nitrogen atmosphere: Arrhenius equation with n = 1 reaction model is used.

Figure A(D)-4. Simplified representation of a cone calorimeter test of PMMA

Figure A(D)-5. Cone experiment results of PMMA with effective heat flux and thickness ranging from 23 to 69 kW/m² and 24 to 29 mm, respectively

Figure A(D)-6. TG/DTG curves at 10°C/min heating rate with different estimation results for kinetic parameters for thermal decomposition of PMMA

Figure A(D)-7. Mass-loss rate (MLR) comparisons for PMMA between actual MLR from experiment (data) and modeled MLR (A, B-GA, B-SCE, B-SHC, C-GA, C-SCE, C-SHC) at applied heat flux of 46 kW/m². Note that data shown were used to estimate model parameter values via numerical optimization using GA, SCE or SHC routines.

Figure A(D)-8. Surface-temperature (T_{surf}) comparisons for PMMA modeling using parameters estimated from different approaches – direct measurement, literature search, or approximation (A); measurement and numerical optimization (B-GA, B-SCE, B-SHC); mostly numerical optimization (C-GA, C-SCE, C-SHC) at applied heat flux of 46 kW/m². Note that data shown were used to estimate model parameter values via numerical optimization using GA, SCE or SHC routines.

Figure A(D)-9. Mass-loss rate (MLR) comparisons for PMMA between actual MLR from experiment (data) and modeled MLR (A, B-GA, B-SCE, B-SHC, C-GA, C-SCE, C-SHC) at applied heat flux of (a) 23 and (b) 64 kW/m². Note that data shown were not included in the model parameter estimation process; hence, these two cases are considered as extrapolation cases.

Figure A(D)-10. Surface-temperature (T_{surf}) comparisons for PMMA modeling using parameters estimated from different approaches – direct measurement, literature search, or approximation (A); measurement and numerical optimization (B-GA, B-SCE, B-SHC); mostly numerical optimization (C-GA, C-

SCE, C-SHC) at applied heat flux of (a) 23 and (b) 64 kW/m². Note that data shown were not included in the model parameter estimation process; hence, these two cases are considered as extrapolation cases.

Figure A(D)-11. TGA thermograms of PMMA decomposition conducted under constant heating rates – 2, 5, 10 and 20K/min – and two different environments – (a) nitrogen and (b) air

Figure A(D)-12. TGA thermogram (TG and DTG) of corrugated cardboard decomposition conducted under 20K/min heating rate and nitrogen environment

Figure A(D)-13. Schematic of the FPA

Figure A(D)-14. FPA experiment results of corrugated cardboard with applied heat flux ranging from 20 to 110 kW/m²: (a) mass-loss rate and (b) surface-temperature measurements using pyrometer

Figure A(D)-15. TG/DTG curves at 10°C/min heating rate with different estimation results for kinetic parameters for thermal decomposition of corrugated cardboard: For better comparison, TG and DTG thermograms have been scaled to result in 100% conversion.

Figure A(D)-16. Mass-loss rate (MLR) comparisons for corrugated cardboard between actual MLR from experiment (data) and modeled MLR (B-GA, B-SCE, B-SHC, C-GA, C-SCE, C-SHC) at applied heat flux of 60 kW/m². Note that data shown were used to estimate model parameter values via numerical optimization using GA, SCE or SHC routines.

Figure A(D)-17. Surface-temperature (T_{surf}) comparisons for corrugated cardboard between actual T_{surf} from experiment (data) and modeled T_{surf} (B-GA, B-SCE, B-SHC, C-GA, C-SCE, C-SHC) at applied heat flux of 60 kW/m². Note that data shown were used to estimate model parameter values via numerical optimization using GA, SCE or SHC routines.

Figure A(D)-18. Mass-loss rate (MLR) comparisons for corrugated cardboard between actual MLR from experiment (data) and modeled MLR (B-GA, B-SCE, B-SHC, C-GA, C-SCE, C-SHC) at applied heat flux of (a) 20 and (b) 110 kW/m². Note that data shown were not included in the model parameter estimation process; hence, these two cases are considered as extrapolation cases.

Figure A(D)-19. Surface-temperature (T_{surf}) comparisons for corrugated cardboard between actual T_{surf} from experiment (data) and modeled T_{surf} (B-GA, B-SCE, B-SHC, C-GA, C-SCE, C-SHC) at applied heat flux of (a) 20 and (b) 110 kW/m². Note that data shown were not included in the model parameter estimation process; hence, these two cases are considered as extrapolation cases.

Figure A(D)-20. TGA thermograms of corrugated cardboard decomposition conducted under constant heating rate of 20 °C/min and two different environments – nitrogen and air

Figure A(D)-21. Cross-section of FRP composite with modified-acrylic resin with high-charring inorganic additive

Figure A(D)-22. TGA (a) and DSC (b) thermograms of decomposition of modified-acrylic resin with high-charring additive conducted under 20K/min heating rate and nitrogen environment

Figure A(D)-23. Estimated activation energy, E_a, with respect to conversion (1-α) based on Iso-conversional Method for decomposition of modified-acrylic resin with (a) and without (b) inorganic high-charring additive

Figure A(D)-24. Comparison of TGA experiment data (TG and DTG) at 20°C/min under nitrogen atmosphere with kinetic modeling results based on Model-fitting Method for modified-acrylic resin with inorganic high-charring additive

Figure A(D)-25. Simplified representation of a cone calorimeter test of FRP composite

Figure A(D)-26. Heat flux measured during cone calorimeter test of modified-acrylic resin with high-charring additive (MA+A) FRP composite at external heat flux level of 50kW/m²: Ignition occurs near $\tau = 3$ s/mm² and from this point additional heat flux impinges on the surface due to the flame

Figure A(D)-27. Cone calorimeter experiment results of modified-acrylic resin with high-charring additive (MA+A) FRP composite with applied heat flux ranging from 25 to 75 kW/m²: (a) Mass-loss rate and (b) surface-temperature and (c) back-surface-temperature measurements

Figure A(D)-28. Increase in model output fitness to targets – mass-loss rate, cumulative mass loss, surface and back-surface temperatures – from genetic algorithm (GA) optimization for estimating unknown parameters from simulating pyrolysis of modified-acrylic resin with high-charring additive (MA+A) FRP composite

Figure A(D)-29. Sensitivity coefficient (SC) for 21 parameters included in sensitivity analysis

Figure A(D)-30. TG/DTG curves at 10°C/min Heating rate with different estimation results for kinetic parameters for thermal decomposition of fire-retarded FRP composite: testing of resin with additive sample (~10mg) with nitrogen purge

Figure A(D)-31. Mass-loss rate (MLR) comparisons for FRP composite with modified-acrylic resin with high-charring inorganic additive between actual MLR from experiment (data) and modeled MLR (GA, SCE, SHC) at applied heat flux of 50 kW/m². Note that data shown were used to estimate model parameter values via numerical optimization using GA, SCE or SHC routines.

Figure A(D)-32. Surface-temperature (T_{surf}) comparisons for FRP composite with modified-acrylic resin with high-charring inorganic additive between actual T_{surf} from experiment (data) and modeled T_{surf} (GA, SCE, SHC) at applied heat flux of 50 kW/m². Note that data shown were used to estimate model parameter values via numerical optimization using GA, SCE or SHC routines.

Figure A(D)-33. Mass-loss rate (MLR) comparisons for FRP composite with modified-acrylic resin with high-charring inorganic additive between actual MLR from experiment (data) and modeled MLR (GA, SCE, SHC) at applied heat flux of (a) 25 and (b) 75 kW/m². Note that data shown were not included in the model parameter estimation process; hence, these two cases are considered as extrapolation cases.

Figure A(D)-34. Surface-temperature (T_{surf}) comparisons for FRP composite with modified-acrylic resin with high-charring inorganic additive between actual T_{surf} from experiment (data) and modeled T_{surf} (GA, SCE, SHC) at applied heat flux of (a) 25 and (b) 75 kW/m². Note that data shown were not included in the model parameter estimation process; hence, these two cases are considered as extrapolation cases.

Figure A(D)-35. Simplified representation of a cone calorimeter test of plywood

Figure A(D)-36. Total heat flux measured from plywood surface during cone calorimeter test at external heat flux level of 50kW/m²: Ignition occurs before $\tau = 1$ s/mm² and from this point additional heat flux impinges on the surface due to the flame

Figure A(D)-37. Cone calorimeter (cone) test data of plywood (thickness, δ is 11.1 ± 0.1 mm, density, ρ is 540 ± 10 kg/m³) impinged with effective heat fluxes (EHF) of 25 to 75 kW/m²

Figure A(D)-38. TG/DTG curves at 20°C/min heating rate with different estimation results for kinetic parameters for thermal decomposition of plywood: testing of plywood sample (~10mg) with air purge.

Figure A(D)-39. Mass-loss rate (MLR) comparisons for FRP composite with plywood between actual MLR from experiment (data) and modeled MLR (M&M) at applied heat flux of 50 kW/m². Note that data shown were used to estimate model parameter values via manual optimization.

Figure A(D)-40. Surface-temperature (T_{surf}) comparisons for plywood between actual T_{surf} from experiment (data) and modeled T_{surf} (M&M) at applied heat flux of 50 kW/m². Note that data shown were used to estimate model parameter values via manual optimization.

Figure A(D)- 41. Back-surface-temperature (T_{back}) comparisons for plywood between actual T_{back} from experiment (data) and modeled T_{back} (M&M) at Applied heat flux of 50 kW/m². Note that data shown were used to estimate model parameter values via manual optimization.

Figure A(D)-42. Mass-loss rate (MLR) comparisons for FRP composite with plywood between actual MLR from experiment (data) and modeled MLR (M&M) at applied heat flux of (a) 25 and (b) 75 kW/m². Note that data shown were not included in the model parameter estimation process; hence, these two cases are considered as extrapolation cases.

Figure A(D)-43. Surface-temperature (T_{surf}) comparisons for FRP composite with plywood between actual T_{surf} from experiment (data) and modeled T_{surf} (M&M) at applied heat flux of (a) 25 and (b) 75 kW/m². Note that data shown were not included in the model parameter estimation process; hence, these two cases are considered as extrapolation cases.

Figure A(D)-44. Back-surface-temperature (T_{back}) comparisons for plywood between actual T_{back} from experiment (data) and modeled T_{back} (M&M) at applied heat flux of (a) 25 and (b) 75 kW/m². Note that data shown were not included in the model parameter estimation process; hence, these two cases are considered as extrapolation cases.

LIST OF TABLES

- Section 2 -

Table 1. Different kinetic models considered in this study

Table 2. Estimation of kinetic parameters with 6 different kinetic modeling approaches for modeling BrUPE decomposition. Parameters with * are assumed values, with ** estimated values from the iso-conversional method and with *** calculated values from analytical solution. R1, R2 and R3 are the reactions for resin decomposition. β is the heating rate in °C/min. Note that kinetic model A and B have used single heating rate TGA data (60 °C/min) and model C, D and F have used multiple heating rate TGA data (5, 20, 40 and 60 °C/min).

Table 3. Estimation of kinetic parameters with 6 different kinetic modeling approaches for modeling MA+A decomposition. Parameters with * are assumed values, with ** estimated values from the iso-conversional method and with *** calculated values from analytical solution. R1, R2 and R3 are the reactions for resin decomposition and A is the reaction for additive decomposition. β is the heating rate in °C/min. Note that kinetic model A and B have used single heating rate TGA data (60 °C/min) and model C, D and F have used multiple heating rate TGA data (5, 20, 40 and 60 °C/min).

Table 4. Summary of maximum and average heating rates (°C/min) observed at front surface in bench-scale experiments of BrUPE and MA+A FRPs when tested at various applied heating rates. Data presented are average values where three or four identical tests are used and 95% confidence intervals are calculated using the student t distribution.

- Section 3 -

Table 1. Different kinetic models considered in this study

Table 2. Comparison between measured parameter values for thermal conductivity and emissivity of the polymer systems (BrUPE and MA+A) and FRP composites (BrUPE FRP and MA+A FRP) and estimated values from numerical optimization: Last column shows the percentage difference between measured (at room temperature) and estimated values where generally a reduction of difference occurs when more complicated kinetic model is used in the estimation process.

Table 3. Comparison of estimated emissivity of glass from parameter estimation exercise conducted for the two composites (BrUPE FRP and MA+A FRP) with different kinetic models: For both materials, as the complexity of applied kinetic model increases from B to F, the estimated emissivity values become closer to 0.9.

- Section 4 -

Table 1. Summary of thermal decomposition process utilized in three comprehensive pyrolysis models – pyrolysis model in FDS, Thermakin and GPYRO: process in red is accounted for in each model

Table 2. Different kinetic models considered in this study

Table 3. Overview of material examples used in parameter estimation process for comprehensive pyrolysis models

Table 4. Parameter estimation results with approach A for parameter values estimated from measurement, literature or approximation; approach B for estimation based on combination of non-optimization and optimization methods using GA, SCE and SHC numerical optimization routines; and approach C for estimation based on mostly optimization method using GA, SCE and SHC. Best simulation results were found from estimation with approach A (i.e. independent measurements or literature search) approach for parameter estimation of PMMA.

Table 5. Parameter estimation results with approach B for estimation based on combination of non-optimization and optimization methods using GA, SCE and SHC numerical optimization routines; and approach C for estimation based on mostly optimization method using GA, SCE and SHC. Best simulation results were found from estimation with approach C using shuffled complex evolution method for parameter estimation of triple layered corrugated cardboard.

Table 6. Parameter estimation results with estimation based on combination of non-optimization and optimization methods using GA, SCE and SHC numerical optimization routines. Best simulation results were found from estimation with GA or SCE method for parameter estimation of this fiberglass reinforced polymer composite.

Table 7. Parameter estimation results with estimation based on combination of non-optimization and manual optimization method. A single simulation results are found for parameter estimation of this plywood.

- Section 5 -

Table 2-1. Example materials in Chapter 3 – empirical models: materials are either considered as a burning object or flat surface in modeling

Table 2-2. Example materials in Chapter 4 – simple analytical models: materials are either considered as thermally-thick and inert at pre-ignition with steady burning at post-ignition or thermally-thin and inert at pre-ignition with steady burning at post-ignition in modeling

Table 2-3. Example materials in Chapter 5 – Comprehensive analytical models: materials are considered to decompose with single or multiple reaction(s) with or without residue production in modeling

Table 3-1. Model parameter table: summary of model parameters required to conduct pyrolysis modeling

Table 3-2. Ignition sources specified in standard fire tests

Table 3-3. ASTM standards for measurement of time to ignition of materials exposed to specified level of incident radiant heat source in intermediate/bench-scale Calorimeter Tests

Table 3-4. Overview of example cases using empirical pyrolysis models

Table 3-5. Model parameter table for Case 1 examples

Table 3-6. Model parameter table for Case 2 examples

Table 4-1. Model Parameter table: summary of model parameters required to conduct pyrolysis modeling

table 4-2. ASTM standards of calorimeter tests measuring ignition and burning properties of material

Table 4-3. Recommended hc values for different test apparatuses

Table 4-4. ASTM standards for measuring emissivity

Table 4-5. Overview of example cases using simple analytical pyrolysis models

Table 4-6. Model parameter table for Case 1 examples

Table 4-7. Model parameter table for Case 2 examples

Table 5-1. General governing equations for comprehensive pyrolysis models

Table 5-2. Various types of decomposition kinetics

Table 5-3. Model parameter table: summary of model parameters required to conduct pyrolysis modeling

Table 5-4. ASTM standards for measuring thermal conductivity using steady state methods

Table 5-5. ASTM standards for measuring thermal conductivity using transient methods

Table 5-6. ASTM standards for measuring specific heat capacity

Table 5-7. ASTM standards for measuring emissivity

Table 5-8. ASTM standards for thermogravimetry analysis (TGA)

Table 5-9. ASTM standard for measuring reaction enthalpies

Table 5-10. Three types of numerical optimization routines applied to comprehensive pyrolysis modeling in literature: Genetic Algorithm³³, Shuffled Complex Evolution, and Stochastic Hill-climber³⁵

Table 5-11. Overview of example cases using comprehensive pyrolysis models

Table 5-12. Model parameter table for Case 1 examples

Table 5-13. Comparison between experiment data from cone calorimeter test and modeling outputs using estimated parameter values via either direct measurement, literature search, or approximation (A); measurements and numerical optimization (B-GA, B-SCE, B-SHC); or mostly numerical optimization (C-GA, C-SCE, C-SHC)

Table 5-14. model parameter table for Case 2 examples

Table 5-15. Comparison between experiment data from fire propagation apparatus test and modeling outputs using estimated parameter values via either measurements and numerical optimization (B-GA, B-SCE, B-SHC) or mostly numerical optimization (C-GA, C-SCE, C-SHC)

Table 5-16. Model parameter table for Case 3 examples

Table 5-17. Comparison between experiment data from cone calorimeter test and modeling outputs using estimated parameter values using numerical optimization (GA, SCE, SHC)

Table 5-18. Comparison between experiment data from cone calorimeter test and modeling outputs using estimated parameter values via measurements and manual optimization

Table A(C)-1. Ignition data from cone calorimeter tests for PMMA

Table A(C)-2. Summary of model parameter table with estimated values via direct measurements, literature search or approximation

Table A(C)-3. versus

Table A(C)-4. Estimation of effective heat of combustion using cone calorimeter test results at applied heat flux of 25, 50 and 75 kW/m²

Table A(C)-5. Estimation of effective heat of gasification using cone calorimeter test results at applied heat flux of 25, 50 and 75 kW/m²

Table A(C)-6. Summary of model parameter table with estimated values with uncertainty

Table A(C)-7. Comparison of time to ignition at different heat flux levels from actual experiment and pyrolysis modeling

Table A(C)-8. Comparison of time to ignition at different heat flux levels from actual experiment and pyrolysis modeling

Table A(C)-9. Summary of model parameter table with estimated values via direct measurements, literature search or approximation

Table A(C)-10. versus

Table A(C)-11. Estimation of effective heat of gasification using cone calorimeter test results at applied heat flux ranging between 25 and 75 kW/m²

Table A(C)-12. Summary of model parameter table with estimated values with uncertainty

Table A(C)-13. Comparison of time to ignition at different heat flux levels from actual experiment and pyrolysis modeling

Table A(C)-14. Summary of model parameter table with estimated values via direct measurements, literature search or approximation

Table A(C)-15. versus

Table A(C)-16. Estimation of effective heat of gasification using cone calorimeter test results at applied heat flux ranging between 25 and 75 kW/m²

Table A(C)-17. Summary of model parameter table with estimated values with uncertainty

Table A(C)-18. Comparison of time to ignition at different heat flux levels from actual experiment and pyrolysis modeling

Table A(C)-19. Ignition data from cone calorimeter tests for plywood

Table A(C)-20. Summary of model parameter table with estimated values via direct measurements, literature search or approximation

Table A(C)-21. versus

Table A(C)-22. Estimation of effective heat of gasification using cone calorimeter test results at applied heat flux ranging between 25 and 75 kW/m²

Table A(C)-23. Summary of model parameter table with estimated values with uncertainty

Table A(C)-24. Comparison of time to ignition at different heat flux levels from actual experiment and pyrolysis modeling

Table A(C)-25. Ignition data from cone calorimeter tests for GRP with balsa wood core sandwich composite

Table A(C)-26. Summary of model parameter table with estimated values via direct measurements, literature search or approximation

Table A(C)-27. versus

Table A(C)-28. Estimation of effective heat of gasification using cone calorimeter test results at applied heat flux ranging between 30 and 90 kW/m²

Table A(C)-29. Summary of model parameter table with estimated values with uncertainty

Table A(C)-30. Comparison of time to ignition at different heat flux levels from actual experiment and pyrolysis modeling

Table A(C)-31. Ignition data from cone calorimeter tests for thin FRP composite sheet

Table A(C)-32. Summary of model parameter table with estimated values via direct measurements, literature search or approximation

Table A(C)-33. versus

Table A(C)-34. Estimation of effective heat of gasification using cone calorimeter test results at applied heat flux ranging between 17 and 75 kW/m²

Table A(C)-35. Summary of model parameter table with estimated values with uncertainty

Table A(C)-36. Comparison of time to ignition at different heat flux levels from actual experiment and pyrolysis modeling

Table A(D)-1. Summary of estimated uncertainty for each model parameter

Table A(D)-2. Summary of estimated uncertainty in PMMA Cone Calorimeter experiments based on 5 repeating tests under 49 kW/m² heat flux level with medium thickness sample (7.7 ~ 9.4 mm)

Table A(D)-3. Comparison between experiment data from cone calorimeter test and modeling outputs using estimated parameter values via either direct measurement, literature search, or approximation (A); measurements and numerical optimization (B-GA, B-SCE, B-SHC); or mostly numerical optimization (C-GA, C-SCE, C-SHC)

Table A(D)-4. Summary of necessary model parameters for simulating pyrolysis of Corrugated Cardboard

Table A(D)-5. Summary of estimated optimum with confidence interval (C.I.) for each model parameter

Table A(D)-6. Summary of estimated uncertainty in triple wall (2 layers) corrugated cardboard FPA experiments based on 2 repeating tests at 60 kW/m² heat flux level

Table A(D)-7. Outline of 5 parameter groups – kinetic parameters, heat of decomposition reaction and combustion, and emissivity of fuel and residue – varied in uncertainty analysis using one at a time method

Table A(D)-8. Comparison between experiment data from fire propagation apparatus test and modeling outputs using estimated parameter values via either measurements and numerical optimization (B-GA, B-SCE, B-SHC) or mostly numerical optimization (C-GA, C-SCE, C-SHC)

Table A(D)-9. Kinetic parameters for 2 step model – decomposition of additive (+A-R) and resin (R) – for modeling modified-acrylic resin with inorganic high-charring additive

Table A(D)-10. Summary of necessary model parameters for simulating pyrolysis of modified-acrylic resin with high-charring additive (MA+A) FRP composite

Table A(D)-11. Summary of unknown model parameters included in sensitivity analysis with searchable space defined with SA min and max: 4 levels (P1 though P4) and an increment of Δ are shown.

Table A(D)-12. Summary of estimated uncertainty in modified-acrylic resin with high-charring additive (MA+A) FRP composite cone calorimeter experiments based on 3 repeating tests at 50 kW/m² heat-flux level

Table A(D)-13. Outline of 5 parameters – MA_residue emissivity, A_residue thermal conductivity and GAMMA, fiberglass thermal conductivity and specific heat capacity T dependent terms – varied in uncertainty analysis using one-at-a-time method

Table A(D)-14. Comparison between experiment data from cone calorimeter test and modeling outputs using estimated parameter values using numerical optimization (GA, SCE, SHC)

Table A(D)-15. Summary of necessary model parameters for simulating pyrolysis of plywood

Table A(D)-16. Comparison between experiment data from cone calorimeter test and modeling outputs using estimated parameter values via measurements and manual optimization

Section 1

INTRODUCTION

INTRODUCTION

This dissertation consists four sections, which covers various aspects of parameter estimation problem for pyrolysis modeling. Section 2 is devoted to conducting thermal decomposition kinetic modeling using independent thermal analysis. This information is needed as an input to describe the thermal decomposition mechanism in the comprehensive pyrolysis models. Additional work is conducted to evaluate the effects of applying different kinetic models to pyrolysis modeling. Sample materials used were fiberglass (E-glass mats) reinforced polymer composites with two types of resin systems – brominated unsaturated polyester and modified acrylic with inorganic high-charring fire retardant additive. Section 3 is dedicated to investigate the ability of global, multi-objective/variable optimization methods to estimate material parameters for comprehensive pyrolysis models. The estimation exercise is prepared with carefulness in terms of selecting the appropriate kinetic model and the optimization targets. The estimated results are compared with independently measured or reference values. Same sample materials are used in Section 3 as in Section 2. In Section 4, a process for conducting parameter estimation for comprehensive pyrolysis model is proposed and the relevant concepts used in the process and the limitations are explained. In addition, example cases of conducting parameter estimation following the process proposed are shown for real-world materials – thermoplastics (PMMA), corrugated cardboard, fiberglass reinforced polymer composites and plywood. Section 5 is the actual step-by-step guide for conducting parameter estimation for a wide range of pyrolysis models including comprehensive pyrolysis models.

Section 2

EVALUATING EFFECTS OF APPLYING DIFFERENT KINETIC MODELS TO PYROLYSIS MODELING OF FIBERGLASS REINFORCED POLYMER COMPOSITES

[Type the abstract of the document here. The abstract is typically a short summary of the contents of the document. Type the abstract of the document here. The abstract is typically a short summary of the contents of the document.]

EVALUATING EFFECTS OF APPLYING DIFFERENT KINETIC MODELS TO PYROLYSIS MODELING OF FIBERGLASS REINFORCED POLYMER COMPOSITES

Kim, E.¹, Dembsey, N.^{1*}, and Shivkumar, S.²

¹WPI, Fire Protection Engineering Dept., Worcester, MA, USA

²WPI, Mechanical Engineering Dept., Worcester, MA, USA

*Corresponding author email: ndembsey@wpi.edu

ABSTRACT

This research evaluates the effects of applying different kinetic models (KMs), developed based on thermal analysis using TGA data, when used in typical 1D pyrolysis models of fiberglass reinforced polymer (FRP) composites. The effect of different KMs is isolated from the FRP heating by conducting pyrolysis modeling based on measured temperature gradients. Mass loss rate (MLR) simulations from this pyrolysis modeling with various KMs show changes in the simulations due to applying different KM approaches are minimal in general. Pyrolysis simulations with the most complex KM are conducted at several heat flux levels. MLR comparison shows there is good overlap between simulations and the experimental data at low incident heat fluxes. Comparison shows there is poor overlap at high incident heat fluxes. These results indicate that increasing complexity of KMs to be used in pyrolysis modeling is unnecessary for these FRP samples; and that the basic assumption of considering thermal decomposition of each computational cell in comprehensive pyrolysis modeling as equivalent to that in a TGA experiment becomes inapplicable at depth and higher heating rates.

KEYWORDS

thermal decomposition; kinetic modeling; thermal analysis; thermoset resin; pyrolysis modeling; fiberglass reinforced polymer

NOMENCLATURE

<i>a</i>	zero order rxn model slope (/K)
<i>b</i>	zero order rxn model intercept (-)
<i>e</i>	Euler's number (-)
<i>E</i>	activation energy (kJ/mol)
<i>f</i>	function
<i>k</i>	rate constant (/s)

r	rate (%/min)
R	gas constant (J/mol-K)
T	temperature (K)
t	time (s)

Greek

α	conversion (-)
β	heating rate (°C/min)

Subscripts

p	DTG peak
0	initial condition

1. INTRODUCTION

In the recent years, comprehensive pyrolysis models [1,2,3] have been released to the fire community. In contrast to previous pyrolysis models [4,5,6] where empirical or simple analytical approaches were used with many restrictions in terms of describing the material and modelling conditions, these comprehensive pyrolysis models allow greater flexibility mathematically as they explicitly solve for conservation of mass, energy and/or momentum of materials upon heating and/or thermal decomposition. Additionally, these models can simulate multi-step thermal decomposition reactions and materials with multiple homogeneous layers that have different decomposition behaviours. However, the downside of utilizing comprehensive pyrolysis models is related to the effort needed to estimate the models' input- parameters related to thermal decomposition kinetics, material properties and model fitting parameters. With empirical or simple analytical pyrolysis models, the number of input parameters is only a few and they are all obtained through direct measurements or simple data analysis from calorimeter experiments. For comprehensive pyrolysis models, the number of input parameters varies from a few to several orders of magnitude greater. Usually the estimation process involves a state-of-the-art practice where independent measurements are conducted and/or robust numerical optimization methods are used to solve an inverse problem to estimate the parameters [7,8,9,10,11]. These optimization methods are computationally intensive with the time needed for estimation increasing rapidly as the number of parameters increases.

When conducting comprehensive pyrolysis modelling, thermal decomposition kinetic modelling plays a critical role for determining the complexity of the entire problem. The complexity of kinetic modelling used determines the total number of input parameters involved in pyrolysis modelling. For example, applying single-step thermal decomposition kinetics, e.g. virgin \rightarrow char + vapour, results in two solid phase species: virgin and char. For this case, model parameters related to material properties – thermo-physical, optical and porosity characteristics – need to be estimated for the virgin and char. However, when two-step thermal decomposition kinetics is applied, e.g. virgin \rightarrow intermediate + vapour, intermediate \rightarrow char + vapour, three solid phase species virgin, intermediate and

char are introduced into the pyrolysis modelling, which results in one additional set of parameters related to material properties of the intermediate species to be estimated.

Accepted practice for conducting kinetic modelling for comprehensive pyrolysis models is to perform independent thermal analysis using small-scale experiments such as thermogravimetric analysis (TGA), differential scanning calorimetry (DSC), etc. The underlying assumption is that the computational cell in the comprehensive pyrolysis model is equivalent to a sample decomposing in a TGA, DSC, etc. In other words, depending on the temperature and residual mass in the computational cell, mass loss is predicted based on heat gain or loss from the decomposition reaction. Conventionally, single-step reactions are favoured to model thermal decomposition to limit the complexity of a given problem [12]. However, for the past few years, efforts have been undertaken to investigate more complex kinetic models which have the ability to allow multiple reactions for describing thermal decomposition kinetics [9,13,14,15]. To date, although it has been demonstrated that more complex kinetic models can be used in comprehensive pyrolysis modelling, strong justification for utilizing them as opposed to simpler kinetic models has been absent. This is especially true with inverse problems where any effect of applying different kinetic models can be compensated for during the optimization of other unknown parameter.

In this study, the following objectives are investigated using commercial thermoset polymer resins and their fiberglass reinforced polymer (FRP) composites as sample materials: First, conducting kinetic modelling, i.e. proposing thermal decomposition kinetic reactions and estimating relevant kinetic parameters, via independent thermal analysis with data obtained from thermogravimetric analysis (TGA) and differential scanning calorimetry (DSC) experiments. Kinetic models in this work are developed with minimal information about the polymer resins as for most real world materials that are commercially available details regarding the chemical structure of the base polymer, fire retardant additives, etc. are rarely accessible to the modelers due to the information being proprietary to the manufacturer. The models are intended to be simplified but sophisticated enough to capture the characteristics of the materials such as the fire retardancy via additives within a polymer matrix, environmental effects, etc. Second, understanding the effects of applying different kinetic models with various levels of complexity on comprehensive pyrolysis modelling. This is accomplished by performing a 1D pyrolysis modelling screening process, which utilizes kinetic modelling and temperature gradient measurements from bench-scale experiments as a proxy for conservation of energy with heat gain/loss from thermal decomposition reactions. This screening process allows the evaluation of applying different kinetic models to pyrolysis modelling without the need of estimating the corresponding model input parameters.

1. BACKGROUND

1.1. Kinetic Modeling Using Thermal Analysis

Kinetic modeling in thermal analysis is generally defined as a description of the sequence of chemical steps through which reactants are transformed into products. Although when a material is thermally decomposing with numerous reactions, most times there are rate determining steps. Kinetic modeling is conducted to simulate these rate determining steps. To find the rate determining steps for a thermally decomposing material, one should consider the

reaction rate controlling factor(s). There are three factors [16] to consider in reactions of solids where one or a combination of the factors controls the reaction rate. One is the chemical reaction factor that considers a bond redistribution step. This step usually occurs at a reaction interface and is the chemical control of reactivity. Another factor is the reaction geometry. A systematic variation in the reaction interface area with respect to the changes in the geometry of the reaction interface as the reaction proceeds exerts an important influence on the kinetic behavior. Last is the rate of diffusion of reaction participants. This factor can influence the rate of product formation. Based on the understanding of the reaction rate controlling factors, kinetic models can be developed to describe the thermal decomposition of a material.

In the small-scale experiments used in thermal analysis, milligram samples are decomposed under certain testing conditions so that their main reaction rate controlling factor may be the intrinsic chemical reaction with reaction geometry and/or diffusion being the sub-factors. Data obtained from these experiments, thermograms, are used in data analysis to estimate kinetic parameters either by linear regression or comparison between measured and calculated reaction profiles. Note that any changes made to the testing conditions, i.e. changes to the sample particle size, abrasion or damage to crystal surfaces, surface impurities and irradiation, local environment, a precursor step, etc. can affect the test results [16].

Typically in thermal analysis, the isothermal rate of degradation or conversion, $d\alpha/dt$, is assumed to be a linear function of the temperature dependent rate constant, $k(T)$, and a temperature independent function of the conversion, reaction model, $f(\alpha)$, where α indicates the conversion. This equation can be further expanded by using the Arrhenius expression for the rate constant. Within the Arrhenius expression, two more reaction dependent constants are introduced: the pre-exponential constant, A , and the activation energy, E_a (see Eq. 1). The temperature independent function of the conversion, $f(\alpha)$ is dependent upon the mechanism of the chemical reactions and there are three major types: accelerating, decelerating and sigmoidal (also called autocatalytic). It is noteworthy that the pressure dependence of kinetics is commonly ignored in thermal analysis because the testing conditions can be controlled to maintain a favorable environment for certain reactions to occur. The pressure effects on the decomposition processes can be profound for some cases, e.g. reversible decomposition reactions such as oxidation and/or reduction with gaseous reaction participants, but in general these are considered to be beyond the research scope of thermal analysis [17].

$$\frac{d\alpha}{dt} = k(T)f(\alpha) = \left[A \exp\left(-\frac{E_a}{RT}\right) \right] f(\alpha) \quad (1)$$

The iso-conversional method [18,19,20,21], also known as the “model-free method”, is the method applied to identify the minimum number of reactions necessary for a kinetic model. This method requires data from multiple non-isothermal (or dynamic) experiments, i.e. data tested with at least 4 different heating rates. The basis for this method is that at a constant conversion, α , $d\alpha/dt$ and $f(\alpha)$ become constants and therefore, E_a at each conversion is found without the pre-knowledge of the reaction mechanisms. When the E_a is found for the entire degradation process, the results provide insight for the minimum number of steps of elementary reactions needed to

address the global reaction. A global reaction composed of a single stage process will show no dependence of E_a on conversion, α . When the global reaction is a complex process, the E_a changes with respect to conversion, α . An increase in E_a with α typically indicates parallel reactions. A decrease in E_a with α suggests that either the process is reversible (concave shape) or there is a change in the rate determining step (convex shape). Therefore, by analyzing the shape of the curve of E_a with respect to conversion, α , a minimum number of elementary reactions are suggested [22].

When conducting kinetic modeling – proposing thermal decomposition kinetic reactions and estimating relevant kinetic parameters – using thermal analysis, there are two methods to increase the complexity of a kinetic model and increase the fitness of its calculated reaction profile to thermograms: The first approach is to apply a more complex reaction model, $f(\alpha)$ to a single step reaction model. In this case, the iso-conversional method should be used in advance to ensure that the estimated E_a 's dependency on conversion, α is minimal and therefore a single-step reaction model is sufficient to describe the kinetics. Kinetic parameters other than the activation energy can be estimated via model-free method as an extent to the iso-conversional method [23,24]. The second approach is to increase the number of elementary reactions in a kinetic model to develop a multiple-step reaction model using a model-fitting method [25,26]. This is applicable when estimated E_a 's from an iso-conversional method significantly vary with respect to conversion, α , i.e. complex kinetics. In this case, kinetic parameters are estimated via an optimization process that involves either linear or non-linear methods with the pre-selected reaction model, $f(\alpha)$ and typically the estimated E_a 's from an iso-conversional method are used as initial estimates.

One major concern when performing kinetic parameter estimation with thermal analysis is the “compensation effect” which exists between the kinetic parameters. This compensation effect allows estimation of multiple sets of kinetic parameters that give good fitness to the data. Theoretically, each component of kinetic parameters is associated with some fundamental behavior. E_a , A and $f(\alpha)$ can be considered as a certain energy barrier, frequency of vibrations of the activated complex [27], and reaction mechanism [28], respectively. However, due to the non-species specific nature of the thermal analysis measurements and complexity of the processes involved, estimating for the intrinsic kinetic parameters of a decomposition reaction is extremely difficult. Generally, the estimated parameters are considered to be “effective” and estimating for invariant kinetic parameters means finding a set of values that simulates reaction profiles – either rates or extents of conversions – that are in good correspondence with actual data, given the temperature range and/or heating rates. Therefore, when using thermal analysis, estimation of E_a based on the iso-conversional method where multiple heating rate thermograms are used in the estimation process is considered to be more reliable and preferred than that of a model-fitting method using single heating rate data.

1.2. Kinetic Modeling for Comprehensive Pyrolysis Models

When conducting kinetic modelling for comprehensive pyrolysis models, a basic assumption is that the computational cell is ideally a sample decomposing in a thermogravimetric analysis (TGA) experiment as mass transport effects are typically considered to be negligible. Mass loss rate of the cell is a function of temperature and residual mass as in Eq. (1) and/or occasionally the availability of gas phase reactant, oxygen. The kinetic parameters

used in comprehensive pyrolysis modelling are estimated from independent kinetic modelling based on thermal analysis. A sample decomposing in a TGA experiment is conducted under a well-defined condition to maximize the effect of the intrinsic chemical reaction on the thermal decomposition rate while limiting other factors and any changes made to the testing conditions can have significant effect on the decomposition kinetics. Therefore, extrapolating the thermal decomposition kinetic information gained from zero-dimensional thermal analysis to one- or higher-dimensional pyrolysis modelling should be conducted with caution as many of the conditions during pyrolysis of a slab sample is different from that of the milligram sample during decomposition in a TGA experiment.

When considering kinetic modelling as a part of comprehensive pyrolysis modelling, estimating for the invariant kinetic parameters becomes less important. Applying kinetic parameters that provide similar simulated reaction profiles mathematically to thermograms by making use of the compensation effect existing between the parameters can be sufficient for pyrolysis modelling purposes as those kinetic parameter sets should result in the same modelling outputs. However, it is recommended to estimate invariant kinetic parameters, for estimation of E_a at least when considering a possibility of compiling the estimated values in a database as those values may give insights to thermal behaviors of the materials. For example, materials with lower E_a indicate that they are thermally less stable than the ones with higher E_a as less energy is needed to initiate the decomposition process and having this understanding about the material can be beneficial for modelers.

2. MATERIALS

FRP composite panels were fabricated by vacuum bagging for relatively high glass content, using two different types of fiberglass (E-glass) mats – chopped strand mat and a woven roving mat – that were wetted with resin. The chopped strand mat is thinner and more porous than the woven mat. The laminate schedule is chopped strand mat and roving alternating 8 and 6 times with another chopped strand mat layer at the end for the brominated unsaturated polyester (BrUPE) and modified acrylic with inorganic additive (MA+A) FRP composites, respectively. Average overall glass contents in the FRP composites are 75% for BrUPE composite and 30% for MA+A composite by weight. Average thicknesses of these FRPs are 6 – 7 mm for BrUPE composites and 9 mm for MA+A composites. Visual inspection is made of a polished cross-section of the composite slab to confirm consistency with the provided laminate schedule. BrUPE is an unsaturated polyester resin with bromination for flame retardancy. The bromination is built in to the carbon back bone with 20% by weight, which is typically substituted by replacing the hydrogens. Along with the bromination, antimony trioxide is added as a synergist that assists the flame retardancy of the polymer resin. MA is a modified acrylic resin. This resin is essentially unsaturated polyester (UPE) with Methacrylic Acid (MMA) replacing most of the styrene monomers. MA+A is a modified acrylic resin (MA) with an inorganic additive (A) for fire retardancy. Typical inorganic additives are hydrates such as alumina trihydroxide (ATH) or magnesium hydroxide, antimony trioxide, borax, chalk, silica, etc. [29] Because this additive was known to give a high-charring effect with a strong endotherm, A is categorized with typical hydroxides used as flame retardant fillers. These hydroxides work as a flame retardant by an endothermic dehydration reaction that produces oxides and water [29,30]. The water produced by this reaction vaporizes and the vapor dilutes the gaseous phase. This flame retardant is added in a relatively large amount (50 to 65%) comparing to other types of additives.

3. TEST MATRIX

In this study, 6 different kinetic models developed from independent thermal analysis are investigated. See Table 1 for kinetic model summary. To investigate a range of kinetic models with different complexity, either different reaction models are utilized or the total number of elementary reactions is varied. The reaction model applied in this study is the reaction order models ($f(\alpha) = (1 - \alpha)^n$ with $n = 0, 1$ or n), which are commonly used in modeling pyrolysis of various polymers. The zero order reaction assumes that decomposition is a linear function of temperature (see Eq. (2)) and estimation of kinetic parameters are undertaken by data fitting (model fitting method [31,32]) to a single heating rate TGA data (60 °C/min). Note that the slope, a , is estimated as approximately 80% of the DTG peak, which is the differential thermogravimetric data equivalent to the mass loss rate divided by the initial sample weight. Although kinetic parameter estimation based on a single heating rate TGA data is considered to be unreliable in thermal analysis, this approach has been included in the test matrix as for comprehensive pyrolysis modeling purposes any parameter set that gives similar simulated reaction profile is sufficient for performing the calculations. When a first or n th order reaction model is applied, kinetic parameters other than activation energy are (1) calculated analytically by assuming at each DTG peak, the second derivative of conversion, α with respect to time is zero and activation energy of each reaction is significantly greater than $2RT_p$ (i.e. $E_a \gg 2RT_p$) where T_p is the temperature at DTG peak [33] (see Eq. (3) and (4)); or (2) estimated using a model fitting method with kinetic models – $f(\alpha) = 1 - \alpha$ or $(1 - \alpha)^n$.

$$\alpha = -aT + b \quad (2)$$

$$E_a \approx \frac{RT_p^2}{\beta} \frac{er_p}{(1 - \alpha_0)} \quad (3)$$

$$A \approx \frac{er_p}{(1 - \alpha_0)} \exp\left(\frac{E_a}{RT}\right) \quad (4)$$

Table 1. Different kinetic models considered in this study

BrUPE		MA+A	
Model	Model Assumptions / Data	Model	Model Assumptions / Data
A	R2: virgin \rightarrow char + vap \uparrow zero order reaction model using constant DTG with respect to temperature	A	R2: virgin \rightarrow char + vap \uparrow zero order reaction model using constant DTG with respect to temperature
B	R2: virgin \rightarrow char + vap \uparrow first order reaction model using DTG peak to estimate kinetic parameters	B	R2: virgin \rightarrow char + vap \uparrow first order reaction model using DTG peak to estimate kinetic parameters
C	R2: virgin \rightarrow char + vap \uparrow first order reaction model using multiple iso-heating rates TGA data to estimate kinetic parameters	C	R2: virgin \rightarrow char + vap \uparrow A: additive \rightarrow additive_residue + vap \uparrow first order reaction models using multiple iso-heating rates TGA data to estimate kinetic parameters
D	R2: virgin \rightarrow char + vap \uparrow nth order reaction model using multiple iso-heating rates TGA data to estimate kinetic parameters	D	R2: virgin \rightarrow char + vap \uparrow A: additive \rightarrow additive_residue + vap \uparrow nth order reaction models using multiple iso-heating rates TGA data to estimate kinetic parameters
E	R1: virgin \rightarrow intermediate + vap \uparrow R2: intermediate \rightarrow char + vap \uparrow R3: char \rightarrow residue + vap \uparrow first order reaction models using multiple iso-heating rates TGA data to estimate kinetic parameters	E	R1: virgin \rightarrow intermediate + vap \uparrow R2: intermediate \rightarrow char + vap \uparrow R3: char \rightarrow residue + vap \uparrow A: additive \rightarrow additive_residue + vap \uparrow first order reaction models using multiple iso-heating rates TGA data to estimate kinetic parameters
F	R1: virgin \rightarrow intermediate + vap \uparrow R2: intermediate \rightarrow char + vap \uparrow R3: char \rightarrow residue + vap \uparrow nth order reaction models using multiple iso-heating rates TGA data to estimate kinetic parameters	F	R1: virgin \rightarrow intermediate + vap \uparrow R2: intermediate \rightarrow char + vap \uparrow R3: char \rightarrow residue + vap \uparrow A: additive \rightarrow additive_residue + vap \uparrow nth order reaction models using multiple iso-heating rates TGA data to estimate kinetic parameters

The total number of elementary reactions has been varied from a single-step reaction to maximum of three- or four-step reactions for BrUPE or MA+A resins, respectively, based on analyzing iso-conversional method results (see section 5.1). Model A and B apply a single step reaction for BrUPE or MA+A polymer decomposition. Model C and D applies single step for BrUPE and two step for MA+A case where resin and additive decomposition reactions are considered separately. Model E and F are the most complex cases proposed from thermal analyses where three steps are applied for the additive-free resin case (BrUPE and MA) – decomposition reactions of resin to resin' (R1) and resin' to char (R2) and oxidation reaction of char to residue (R3) – and one step is applied for

modeling the additive decomposition (A). Justification for suggesting simple one or two step mechanisms rather than the three or four step mechanisms is the following: the uncertainty in TG, the thermogravimetric data equivalent to mass loss history divided by the initial sample weight, is compared with the total weight loss of a sample from each reaction and has shown typically that R1 and R3 are less than the uncertainty estimated for the two resin systems decomposing in TGA experiments. Therefore, decomposition due to R1 and R3 can be considered to be negligible.

4. METHODOLOGY: EXPERIMENTS AND MODELING

4.1. Small-scale Experiments for Kinetic Modeling Using Thermal Analysis

The instruments used in this study were manufactured from TA Instruments: Thermogravimetric Analysis Q50 (TGA) and the Differential Scanning Calorimetry Q20 (DSC). Throughout this study, TGA and DSC were used for non-isothermal test purposes and the tests were conducted in nitrogen and air environments to study pyrolysis and oxidation, respectively. Sample pan used in the TGA was made in platinum and no lid was used. For the DSC experiments, sample pan was a standard aluminium pan with a lid, which was prepared with a manufacturer's crimper. To allow better escape of the volatiles produced from decomposition, typically holes were placed on the lid manually with tweezers. Using the TGA, 4 different heating rates of 5, 20, 40 and 60°C/min. were applied to measure the mass loss history of each resin sample up to 800°C. Note that based on TGA experiments with various sample particle sizes, overall effects of variations in sample particle sizes in TGA data (TG and DTG) were considered to be minimal for the sample sizes used in this work (< 10mg for a single particle) for these two materials. Therefore, non-thermally lumped behavior affecting results reported in this work can be considered as insignificant. For the DSC, a constant heating rate of 20°C/min. was used to measure the heat flow through the sample during the thermal decomposition of resins up to 500°C using a sample amount of ~ 10 mg in a standard aluminium pan with a punctured lid so that gases may evolve freely away from the pan. The uncertainty in the mass loss (TG) measurements was quantified by plotting 3 or 4 weight loss curves from different tests with respect to temperature and finding the maximum standard deviation at each temperature ranging from ambient to 750 °C. The maximum standard deviation is then used to calculate 95% confidence intervals for each material by applying the student t distribution with a sample size of 3 or 4. Uncertainties in TG for BrUPE and MA+A resins are estimated to be ± 7 and ± 6 %, respectively.

4.2. Bench-scale Experiments for Pyrolysis Modeling

The Cone Calorimeter (Cone, ASTM E 1354 [34]) is a bench-scale fire test apparatus in which the sample is heated by an electrically powered rod in the shape of a cone. The sample is tested by applying a constant radiative heat flux set via temperature control of the rod. The Cone exposes the sample in an ambient environment which results in a natural flow field as the sample temperature increases allowing convective cooling above the sample surface. The ignition source is an intermittent sparker. Several modifications were made to the standard testing procedure. First,

when testing these FRPs, two different types of sample holders were used to produce nominal one-dimensional data: the standard non-insulated square holder with a metal edge frame and a round insulated holder [35]. Second, typically 4 thermocouples were installed to measure temperature change of the sample at various depths: exposed surface, 1/3, 2/3 and back surface. The uncertainties in experimental mass loss rate (MLR) and thermocouple measurements at surfaces (exposed, T_s and back, T_b) were quantified by comparing data from 3 or 4 identical FRP composite tests at 50 and 75kW/m² applied heat flux levels for BrUPE and MA+A composites, respectively. Note that normalized time, time divided by sample thickness square, i.e., $\tau = \text{time}/\delta^2$ is used to remove the effect of different sample thicknesses. Because the data is transient, values at different times ($\tau = 1, 3, 5 \text{ s/mm}^2$ for BrUPE and 1, 3, 5, 7 s/mm² for MA+A composites) from each test have been used to calculate the standard deviation at each time. Then these are averaged and used to estimate uncertainty by applying student t distribution with a sample size of 3 or 4 and calculating the 95% confidence interval. Uncertainties in MLR are $\pm 2.2 \text{ g/s-m}^2$ for BrUPE or 2.3 g/s-m² for MA+A composite. In the experimental mass loss rate curves reported in this paper show oscillations that have magnitudes which correspond well with the MLR uncertainty. Uncertainties in T_s and T_b are ± 67 or 30 °C, and ± 14 or 22 °C for BrUPE or MA+A composite. The uncertainty in TC bead location at depth is typically $\pm 1 \text{ mm}$. These uncertainty values were used to evaluate significant differences between the modeling results and experimental data.

4.3. Screening Process: 1D Pyrolysis Modeling with Measured Temperature Gradient

Assuming mass transport effects during pyrolysis are negligible, a typical assumption in comprehensive pyrolysis models; simulating pyrolysis requires an understanding of the heating of a material and the mass loss due to thermal decomposition. These two aspects of pyrolysis can be captured by considering conservation of energy and mass. To evaluate the effect of kinetic modeling on the thermal decomposition of FRPs, the effect of applying different kinetic modeling approaches must be isolated from the heating of the FRPs. By exposing FRPs to various thermal insults and measuring the resultant temperature profiles from the exposed surface to the back surface of the solid, a representation of conservation of energy on the FRPs can be acquired. The changes in temperature measured in the tests account for the heat transport phenomena within the material as well as the heat addition or loss from decomposition reactions. Therefore, to determine mass loss of an FRP, only conservation of mass needs to be considered which is represented by the decomposition kinetics. Decomposition simulations based on the temperature profiles then can be conducted by solving the rate of decomposition (da/dt) computed from a given assumed kinetic model.

To conduct this 1D simplified pyrolysis modeling, the solid material is discretized into $n+1$ number of cells in the z-direction (depth) with equal length of Δz except for the two cells at the surfaces (front and back) where a half-length ($1/2\Delta z$) is used (see Figure 1). In this work, temperature profiles at 4 different locations were obtained via experiments – front and back surfaces, 1/3 and 2/3 depths. With these temperatures known, temperatures at intermediate locations which are unknown are found using a 3rd order polynomial curve fit at each time step. Knowing the temperature of cells at each time step, weight loss of each cell is calculated by solving the rate of decomposition (da/dt) using an ODE solver (Runge-Kutta 4th order).

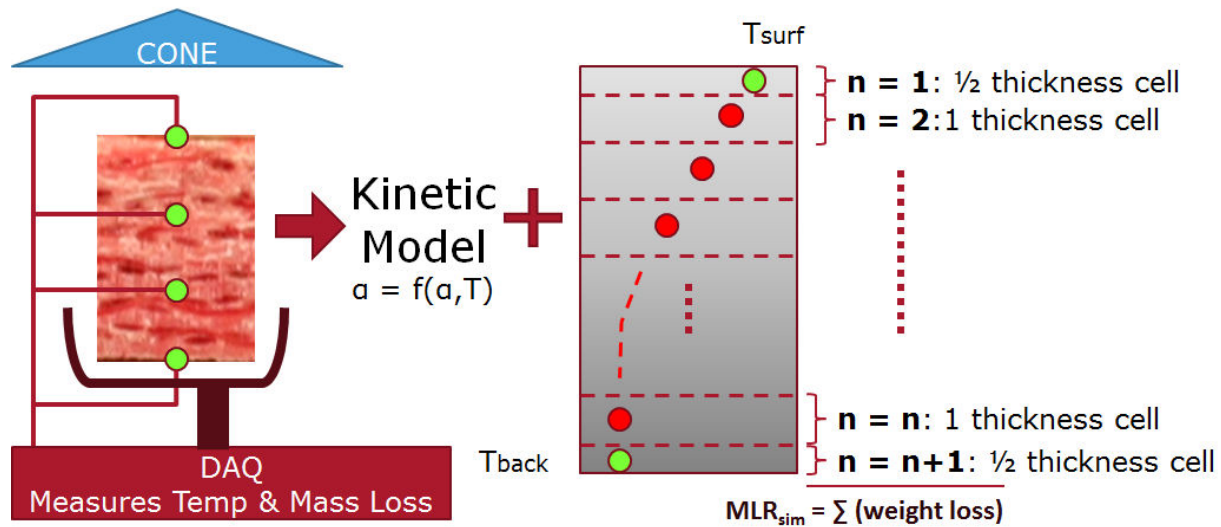


Figure 1. Schematic of the screening process: mass loss of FRP is simulated with conservation of mass and energy represented by the decomposition kinetics and temperature profile measurements from bench-scale experiment of FRP, respectively.

When instrumenting the thermocouples in the composites, 1.25 mm thickness drill bits were used to make the holes from the side. Hence, when a thermocouple is inserted, the bead where the temperature is actually being read may be located anywhere within this hole. When conducting the uncertainty analysis, the in-depth locations (1/3 and 2/3 of thickness) of the temperature measurements were varied by ± 1 mm to check the simulation outputs. Although the uncertainty is ± 0.625 mm considering the thickness of the drill bit, ± 1 mm was used in the uncertainty analysis to be more conservative. All the outputs show similar trends meaning considering the positional uncertainty of the TC beads do not change the results reported in this work. Note that in this exercise, only the cases that made physical sense (smooth decay of temperature from front surface to back) were selected to be included in the uncertainty analysis. The material's cross-section is considered as an effective homogeneous mixture of resin and fiberglass mats. This approach was utilized because although FRP composites are composed of layers of resin-wetted fiberglass mats stacked one after another, a clear distinction between resin and fiberglass layers was difficult to resolve based on visual inspection of the cross-section for these relatively high glass content FRPs considered in this study. Additionally, the effect of layering on the experiment data was not observed. When testing the same composite with lower glass content that was fabricated via hand lay-up method, which had apparent layers in the cross-section (visual inspection), oscillation in the mass loss rate or heat release rate curve was observed. This was due to the burning of the resin layers. As the pyrolysis front propagated towards the back surface of the composite, resin rich layer gave a higher mass loss or heat release but the fiberglass layers gave a lower mass loss or heat release. Because the resin rich and fiberglass layers alternated, the oscillating mass loss rate or heat release rate curves were reported. However, for this high glass content composite, the data showed no evidence of the layering cross-section. These suggested that adding more complexity to the modeling to account for the layering was superfluous.

5. RESULTS AND DISCUSSION

5.1. Thermal Decomposition of Resins

To understand thermal decomposition behavior, the iso-conversional method [18,19,20,21] was applied to iso-heating rate (5, 20, 40 and 60°C/min) TGA data. Using this method, activation energy with respect to conversion, α is calculated and plotted for both resin systems – BrUPE (see (a) in Figure 2) and MA+A (see (b) in Figure 2) – to understand their thermal decomposition characteristics in nitrogen (inert) and air (oxidative) environments.

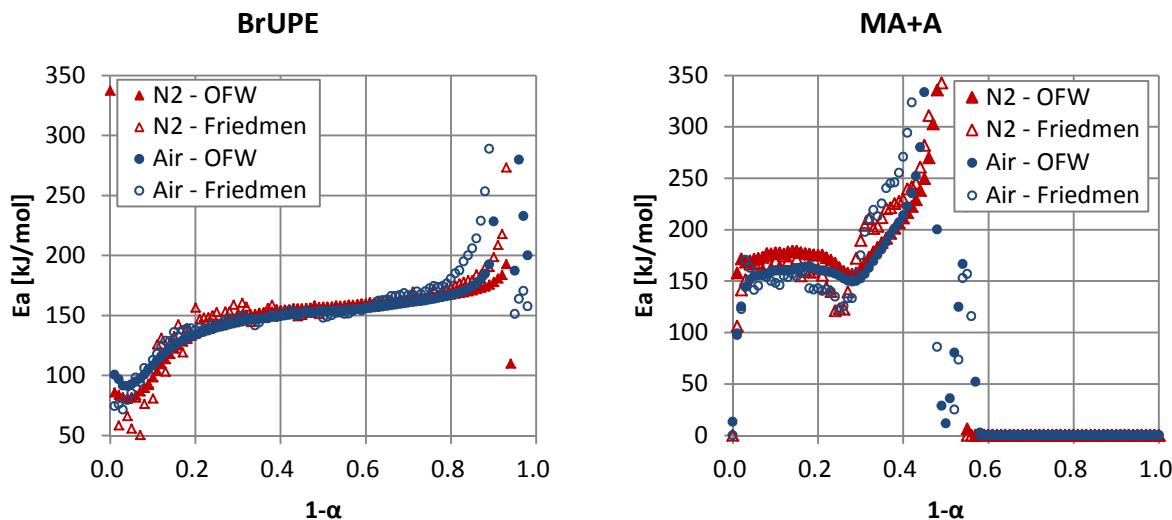


Figure 2. Results from iso-conversional method conducted on BrUPE (left) and MA+A (right) resins: both figures show the estimated activation energy of thermal decomposition with respect to conversion (α)

5.1.1. Brominated Unsaturated Polyester Resin: BrUPE

Based on the iso-conversional method, thermal decomposition of BrUPE can be grouped into three stages. The first stage is the initial mass loss where the activation energy increases with respect to α . The changes in the activation energies calculated for each conversion indicate that there is more than one reaction resulting in weight loss. At this stage, mass loss of approximately 10 to 20% of its initial weight is observed and the temperatures ranges from ambient to 300 – 400°C.

The second stage is the region where most of the mass loss is occurring and is identified with a profound, maximum peak in the DTG thermogram obtained from TGA experiments. As shown in (a) in Figure 2, the activation energies calculated for conversion of BrUPE are relatively constant for both nitrogen and air. This result indicates that a single step reaction can describe the degradation process within this stage. For BrUPE resin decomposing both in nitrogen and air, a significant mass loss occurs leaving residue less than 10% of its initial mass at this stage where temperatures range up to 400 – 500°C. The DSC heat flow measurements for BrUPE resin decomposition in nitrogen and air indicate that there is an endothermic reaction in this stage, which is stronger than that of the first stage (see Figure 3).

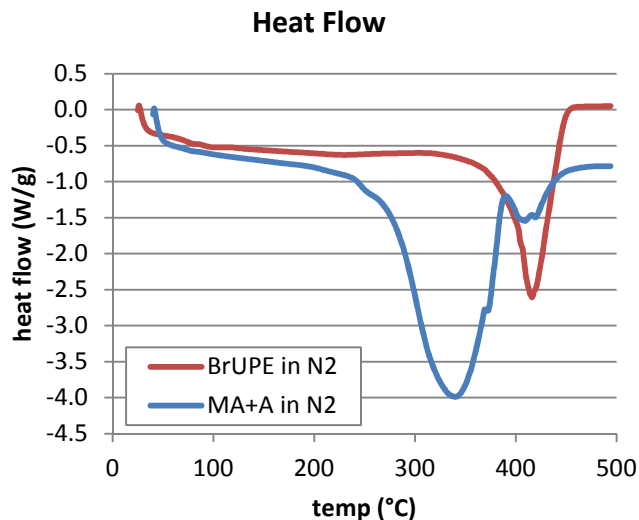


Figure 3. Heat flow measurements from DSC experiments for BrUPE and MA+A polymer resin samples with 20 °C/min heating rate using nitrogen purge. MA+A resin shows a significant endothermic heat at lower temperatures, which is speculated as the heat associated with thermal decomposition of the fire retardant additive (A) in the resin system. There is an overlap in another endothermic heat at relatively higher temperatures for both materials, which is considered to be the heat necessary for the thermal decomposition of the resins itself (BrUPE and MA).

The third stage is the region where final mass loss is observed at temperatures above 400-500°C leaving almost no mass behind. In this stage, increase in the activation energy with respect to α occurs for decomposition of BrUPE resin and it occurs earlier for decomposition in air than in nitrogen. This increase in estimated activation energy can be explained by two possible reasons: One is simply because having a minimal weight on the TGA scale and less change taking place in the mass at the end of the experiment. The other is due to a parallel reaction occurring in this stage. Based on the weight loss (TG) and mass loss rate (DTG) thermogram shapes from TGA experiments and the residue yield – 4-5% in nitrogen and less than 2% in air at 800°C, one can speculate that BrUPE decomposition in nitrogen results in a constant increase in activation energy because the weight loss is minimal in this stage, but for BrUPE decomposing in air, it occurs because a parallel, oxidative reaction exists. The oxygen diffusion through the sample seems to delay the decomposition process only slightly, probably because the sample sizes used in this experiment are small.

The results found from conducting the iso-conversional method are consistent with previous research [36,37,38,39] conducted for unsaturated polyester thermoset resins. A typical thermal degradation process of unsaturated polyester cross-linked with styrene monomers is described in the following. When unsaturated polyesters thermally degrade, a minor weight loss of less than 10% of its total weight is observed below 340°C to 350°C. This mass loss is mainly due to the escape of impurities, unreacted monomers and non-fully cross-linked oligomers within the polymer resin. BrUPE follows this general observation made for degradation of unsaturated polyesters. One thing to note is that BrUPE is identified as thermally less stable than the typical UPE knowing that the initial weight loss occurs up to 10-20% rather than a minor weight loss of less than 10%. This discrepancy is probably due to the antimony trioxide added in BrUPE as a flame retardant additive or other things that may have

been added inadvertently acting as an impurity. Even a small amount of impurities are known to affect the integrity or the stability of the polymer performance [40]. Additionally, adding antimony trioxide to a halogenated compound such as UPE is known to have an effect on lowering the charring temperature. This is due to the initial release of antimony trioxide and some hydrogen halide (HX) enhancing the dissociation of carbon halide chains (-C-X-) within the condensed phase. After the initial weight loss, the major decomposition step occurs. Studies have discovered that the decomposition occurs on the ester chain (-CO-C-) and the unsaturated chain (-C=C-) where the weakest chemical bonding exists. This region exists up to 400°C to 500°C depending on the heating rate and is observed in thermal degradations of BrUPE. In addition to this major decomposition step, weight loss up to 10% of the UPE samples' initial weight is noticed from the tests conducted in air. Considering that this only occurs in oxidative environment, the weight loss is understood as an oxidative degradation reaction that starts around 500°C and above.

5.1.2. *Modified Acrylic with Inorganic Additive: MA+A*

Based on the iso-conversional method, thermal decomposition of MA+A can be grouped into four stages – three similar to those of BrUPE and one additional stage where decomposition of the additive (A) is observed (see (b) in Figure 2). Although the detailed composition of the additive is unknown, additive (A) decomposition for the conversion region of $0.0 < \alpha < 0.3$ can be considered as follows: (1) a strong endothermic peak is observed from DSC heat flow measurements in the temperature range (~ 390°C) relevant to this conversion region (see Figure 3); (2) the estimated activation energies, E_a from the iso-conversional method in this region are relatively constant (160 ± 3 kJ/mol with normal distribution, 95% confidence interval) indicating that a single step reaction is sufficient to describe the reaction occurring in this conversion region; and (3) weight loss of ~20% is comparable to expected from additive decomposition.

The results found from the iso-conversional method and heat flow measurements show that the decomposition of the inorganic additive used in MA+A that gives high-charring effect is similar to the decomposition of polymers with typical hydroxides used as flame retardant fillers. Among various hydroxides, possibly alumina trihydroxide (ATH, $Al_2(OH)_3$) is used as the unknown additive in the resin and additive mixture considering that (1) the decomposition temperature of the additive is below 250°C; and (2) the weight loss of the additive after its decomposition reaction is approximately 30% of its initial mass. The decomposition temperature of ATH is 240°C and complete weight loss when decomposing to aluminium oxide (Al_2O_3) is 35% of its initial mass [41,42].

5.2. Kinetic Modeling Results: Comparison to TGA Data and Extrapolation

Activation energies for each reaction are estimated from the iso-conversional method when multiple heating rate TGA data are used in the estimation of kinetic parameters. Fitness of each kinetic model to TGA data is calculated by a least squares method. Estimated kinetic parameter values from 6 different approaches (A through F in Table 1) are summarized in Table 2 and Table 3 for decomposition of BrUPE and MA+A resins, respectively. Estimations based on a single heating rate TGA data at 60 °C/min are kinetic model A and B. Estimations based on multiple heating rates TGA data are kinetic model C, D and F where heating rates of 5, 20, 40 and 60 °C/min have been used. The activation energy values estimated from iso-conversional method has been kept as a constant while conducting model fitting method to estimate for other kinetic parameters. This approach is adopted to utilize the estimated values from iso-conversional method, which are known to be more reliable in terms of reproducing the actual reaction profiles independent of the heating rates (see section 1.2 for more discussion). Note that all cases provide good fitness (minimum r-square value of 0.98 with most values greater than 0.99) to TGA data (see Figure 4 and Figure 5).

Table 2. Estimation of kinetic parameters with 6 different kinetic modeling approaches for modeling BrUPE decomposition. Parameters with * are assumed values, with ** estimated values from the iso-conversional method and with *** calculated values from analytical solution. R1, R2 and R3 are the reactions for resin decomposition. β is the heating rate in °C/min. Note that kinetic model A and B have used single heating rate TGA data (60 °C/min) and model C, D and F have used multiple heating rate TGA data (5, 20, 40 and 60 °C/min).

Kinetic Model	Parameters	Reactions			Fitness		
		R1	R2	R3	β	r-sqaure (N ₂)	r-sqaure (Air)
A	weight frac.		0.93		5		
	a		0.014		20		
	b		10.1		40		
					60	0.9891	0.9938
				avg			
B	weight frac.		0.93		5		
	T _p (degC)		430		20		
	r _p (%/min)		98.24		40		
	β (degC/min)		60		60	0.9968	0.9913
	log A (log(/s))		13.3***		avg		
	E (kJ/mol)		197***				
	n (/)		1*				
C	weight frac.		0.93		5	0.9958	0.9925
	log A (log(/s))		10.2		20	0.9978	0.9963
	E (kJ/mol)		155**		40	0.9974	0.9974
	n (/)		1*		60	0.9956	0.9971
					avg	0.9966	0.9958
D	weight frac.		0.93		5	0.9931	0.9917
	log A (log(/s))		10.2		20	0.9956	0.9962
	E (kJ/mol)		155		40	0.9958	0.9958
	n (/)		0.7		60	0.9909	0.9961
					avg	0.9939	0.9950
E	weight frac.	0.10	0.83	0.05	5	0.9982	0.9989
	log A (log(/s))	13.4	10.2	7.7	20	0.9976	0.9989
	E (kJ/mol)	155**	155**	155**	40	0.9981	0.9982
	n (/)	1*	1*	1*	60	0.9937	0.9990
					avg	0.9969	0.9987
F	weight frac.	0.10	0.83	0.05	5	0.9986	0.9980
	log A (log(/s))	13.9	10.1	7.5	20	0.9992	0.9992
	E (kJ/mol)	155**	155**	155**	40	0.9993	0.9998
	n (/)	5	0.7	1*	60	0.9966	0.9997
					avg	0.9984	0.9992

Table 3. Estimation of kinetic parameters with 6 different kinetic modeling approaches for modeling MA+A decomposition. Parameters with * are assumed values, with ** estimated values from the iso-conversional method and with *** calculated values from analytical solution. R1, R2 and R3 are the reactions for resin decomposition and A is the reaction for additive decomposition. β is the heating rate in °C/min. Note that kinetic model A and B have used single heating rate TGA data (60 °C/min) and model C, D and F have used multiple heating rate TGA data (5, 20, 40 and 60 °C/min).

Kinetic Model	Parameters	Reactions				Fitness		
		R1	R2	R3	A	B	r-sqaure (N ₂)	r-sqaure (Air)
A	weight frac.		0.55			5		
	a		0.009			20		
	b		6.6			40		
						60	0.9872	0.9898
						Avg		
B	weight frac.		0.55			5		
	Tp(degC)		434			20		
	rp(%/min)		36.84			40		
	β (degC/min)		60			60	0.9765	0.9852
	logA(log(/s))		7.8***			Avg		
	E(kJ/mol)		126***					
n (/)		1*						
C	weight frac.		0.35		0.20	5	0.9918	0.9870
	logA(log(/s))		12		11.9	20	0.9927	0.9926
	E(kJ/mol)		183		160	40	0.9940	0.9963
	n (/)		1*		1*	60	0.9941	0.9960
						Avg	0.9932	0.9929
D	weight frac.		0.35		0.20	5	0.9927	0.9874
	logA(log(/s))		12.3		12.6	20	0.9942	0.9942
	E(kJ/mol)		183**		160**	40	0.9958	0.9985
	n (/)		0.9		5	60	0.9960	0.9973
						Avg	0.9947	0.9944
E	weight frac.	0.05	0.30	0.02	0.20	5	0.9956	0.9893
	logA(log(/s))	16.3	12.2	10.2	11.4	20	0.9949	0.9955
	E(kJ/mol)	183**	183**	183**	160**	40	0.9967	0.9975
	n (/)	1*	1*	1*	1*	60	0.9965	0.9961
						Avg	0.9959	0.9946
F	weight frac.	0.05	0.30	0.02	0.20	5	0.9981	0.9935
	logA(log(/s))	16.5	12.5	10.5	12.2	20	0.9978	0.9982
	E(kJ/mol)	183**	183**	183**	160**	40	0.9991	0.9985
	n (/)	5.0	1.3	1*	5.0	60	0.9992	0.9977
						Avg	0.9985	0.9970

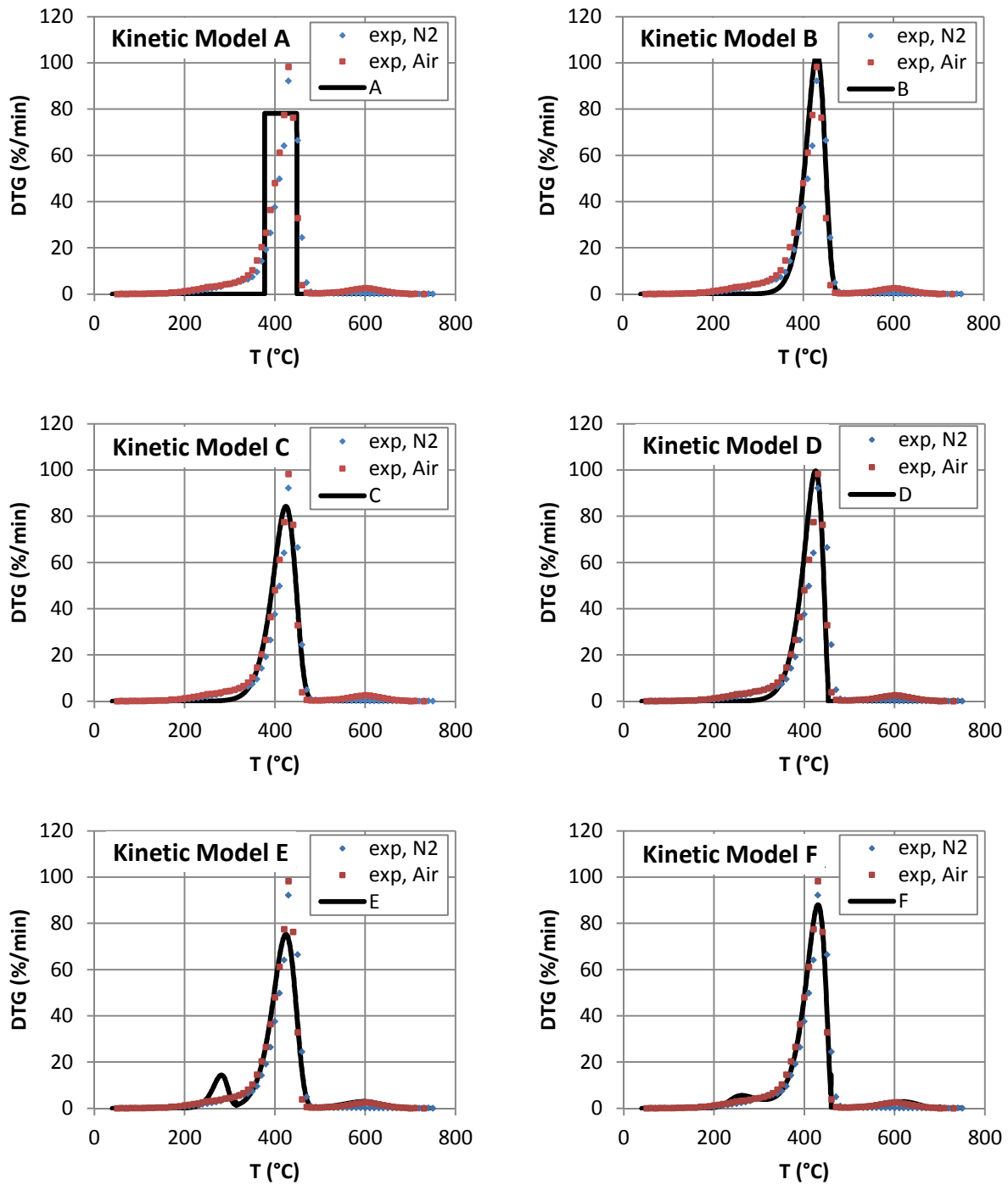


Figure 4. Mass loss rates from TGA experiments (exp) and kinetic modeling A; B; C; D; E; and F are shown for BrUPE with 60 °C/min heating rate case. Applying various approaches in kinetic modeling results in minor changes in modeled mass loss rate.

All kinetic models (A through F) are used to simulate an extrapolation case at 200 °C/min heating rate knowing that these models will be used in pyrolysis modeling of FRPs. The extrapolation case was found by considering the actual Cone test data. Among the various heating rates observed during bench-scale experiments of FRPs at applied heat fluxes ranging from 25 to 100 kW/m² those at the front surfaces are the highest. The maximum and the average heating rates from the Cone experiments are summarized in Table 4. The maximum heating rates reported in the table are observed within the first 10 seconds of exposure to the heating source. Therefore, the average heating rates over time which range from 30 to 140 °C/min were considered when determining the extrapolation case of the upper bound for the heating rate. The results (see Figure 6) show that the differences between different kinetic models are similar to those observed in the lower heating rates used in the kinetic parameter estimation (see Figure 4 and Figure 5).

Table 4. Summary of maximum and average heating rates (°C/min) observed at front surface in bench-scale experiments of BrUPE and MA+A FRPs when tested at various applied heating rates. Data presented are average values where three or four identical tests are used and 95% confidence intervals are calculated using the student t distribution.

Material		Applied Heat Flux Level (kW/m ²)				
		25	50	70	75	100
BrUPE FRP	max HR (°C/min)		1400 ± 500	1900 ± 400		1800 ± 600
	avg HR (°C/min)		120 ± 20	130 ± 10		140 ± 10
MA+A FRP	max HR (°C/min)	700 ± 300	1300 ± 500		1200 ± 500	
	avg HR (°C/min)	30 ± 1	60 ± 10		80 ± 2	

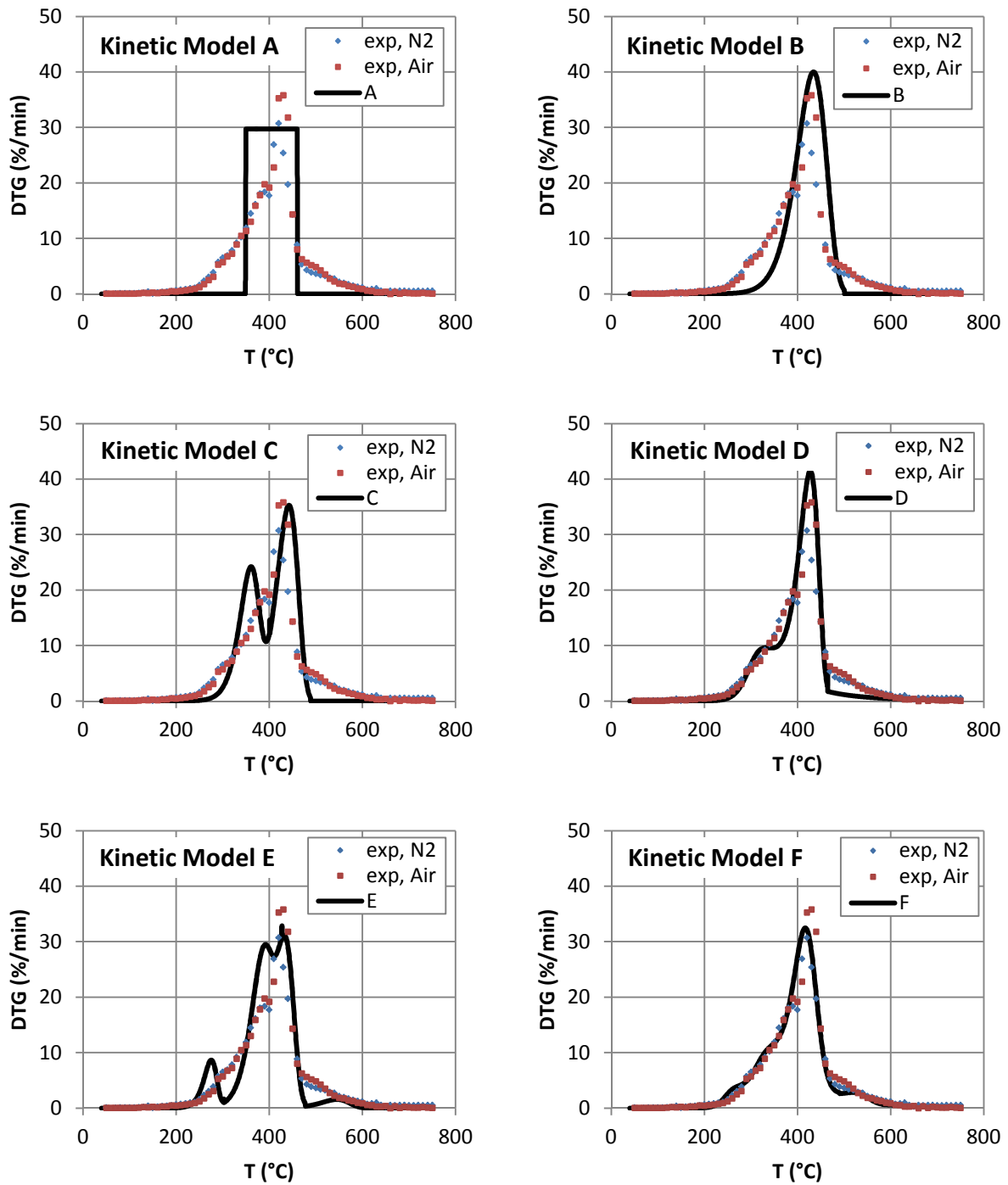


Figure 5. Mass loss rates from TGA experiments (exp) and kinetic modeling A; B; C; D; E; and F are shown for MA+A with 60 °C/min heating rate case. Applying various approaches in kinetic modeling results in minor changes in modeled mass loss rate.

For the extrapolation case, comparison with actual TGA data is not available. TGA experiments at this heating rate are undesirable as the samples experience significant thermal lag, mass transport effects, etc. resulting in a non-zero-order analysis condition. Hence, verifying the performances of the estimated kinetic parameters in modeling thermal decomposition at higher heating rates by directly comparing to TGA data is not possible. However, conducting the screening process introduced in this work allows modelers to determine whether the kinetic models developed from TGA experiments with relatively low heating rates will produce satisfying results or not for other conditions as extrapolation cases.

5.3. Pyrolysis Modeling

Simplified pyrolysis modeling of both composites irradiated at 50 kW/m^2 applied heat flux is conducted with different kinetic modeling approaches (A through F) to examine appropriateness of each case. Figure 7 shows the temperature data from the bench-scale experiment used in the screening process. Figure 8 shows an example calculation using the simplified comprehensive pyrolysis model at the surface location for the two sample materials. As shown in BrUPE FRP @ 50 kW/m^2 and MA+A FRP @ 50 kW/m^2 in Figure 9, changes in simulated mass loss rate due to applying different kinetic modeling approaches are minimal except for case A. There is a larger scatter of simulation points occurring near the peak and the beginning stage of the final decay for case A where significant changes are observed in the MLR curve. This can be explained by the unsmooth transition between the non-decomposing and decomposing stage in the modeled DTG curve shown in (a) in Figure 4 and Figure 5. There is some benefit in applying more complex three- and four-step decomposition models for modeling BrUPE and MA+A composites (case E and F), respectively, for they allow the pyrolysis model to capture the small amount of mass loss prior to ignition (shoulder before initial mass loss rate peak) and near mass loss end time. Other than these two advantages, applying more complex kinetic model either by utilizing a different reaction model or increasing the number of reaction steps becomes unnecessary in terms of conducting pyrolysis modeling to calculate mass loss rate as the effects are minimal.

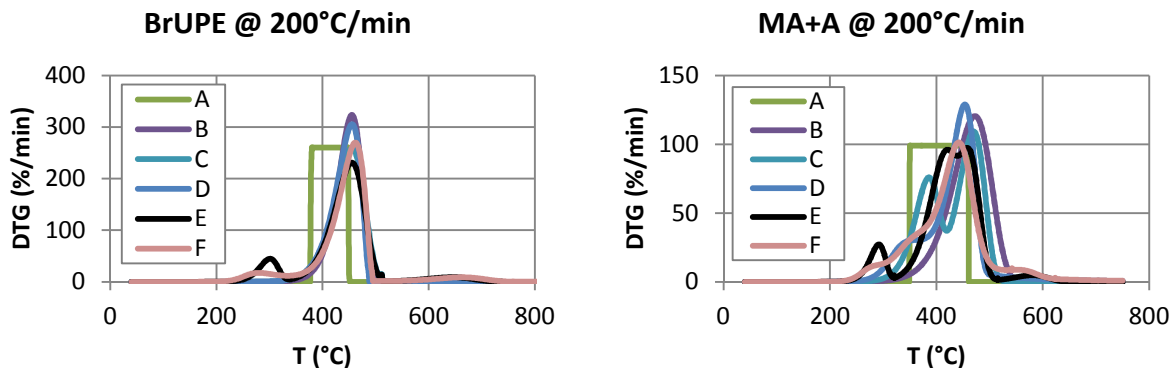


Figure 6. An extrapolation case at $200 \text{ }^\circ\text{C/min}$ heating rate for thermal decomposition of BrUPE (left) and MA+A (right) resins. Differences between different kinetic models (A through F) are similar to those observed in the lower heating rates.

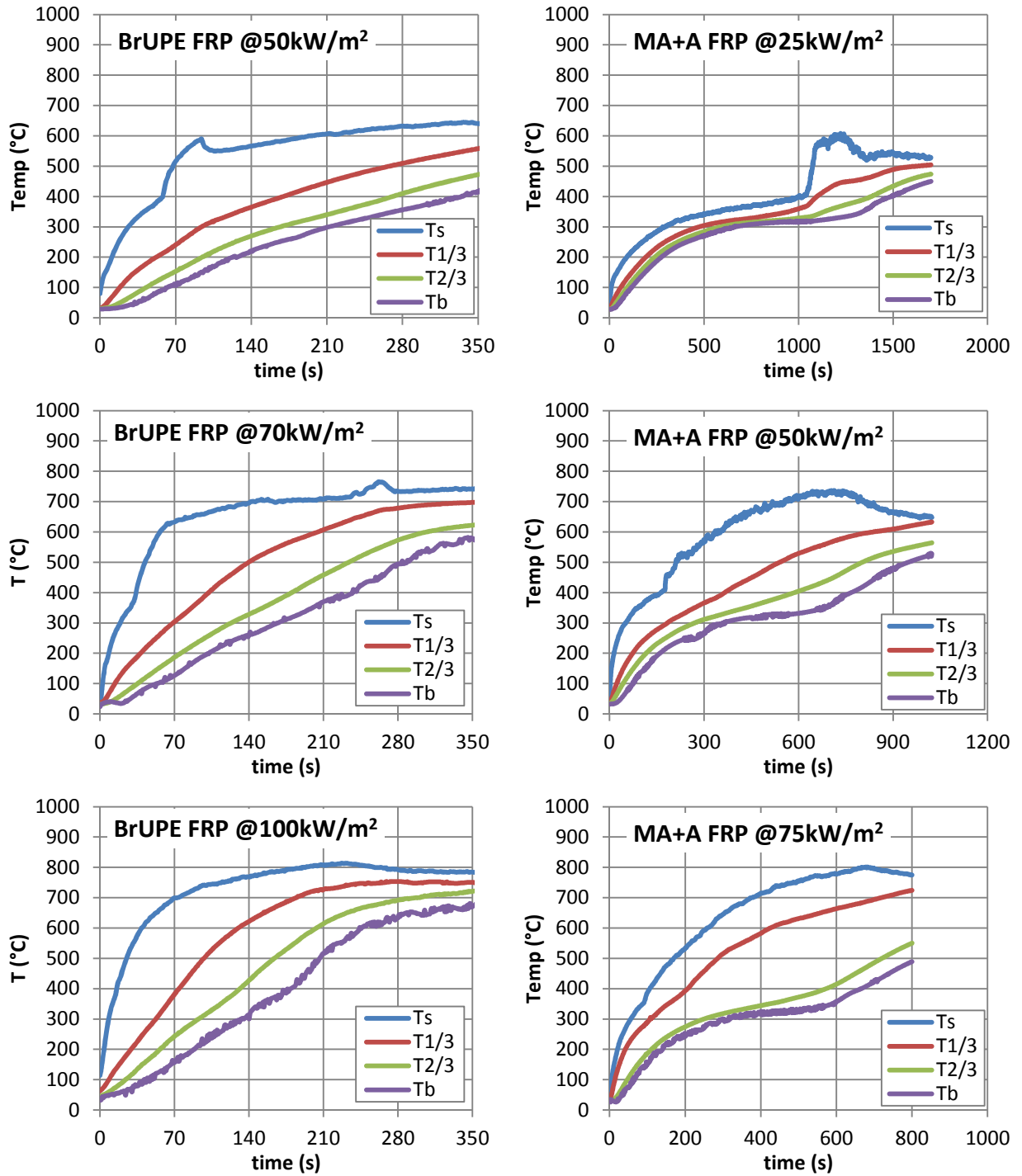


Figure 7. Temperature data at front surface (Ts), 1/3 depth (T1/3), 2/3 depth (T2/3) and back surface (Tb) from Cone Calorimeter experiments with BrUPE and MA+A FRP samples tested at various heat flux levels ranging from 25 to 100 kW/m². These have been used in the simplified pyrolysis modeling with different kinetic models.

Following this work, mass loss rate simulations of BrUPE and MA+A composites with all kinetic models (A through F) were conducted at applied heat flux levels of 50, 70 and 100 kW/m² and 25, 50 and 75 kW/m², respectively (see Figure 9). Similar trend is found in simulations of BrUPE and MA+A FRPs at different heat flux levels as in those found at 50 kW/m². Other than kinetic model case A having large scatter in the simulated mass loss rate near the peak and the beginning stage of the final decay, other models produce similar MLR curves. For modeling of both composites, good agreement with experiment data is shown for cases with relatively low applied heat flux of less than 50 kW/m². At higher heat flux levels, modeling deviates from experimental data for both FRP composites. For modeling of BrUPE composite at or above 70kW/m², a secondary peak in mass loss rate, which is comparable to the initial peak immediately occurring after ignition is observed and results in a shorter end time of the simulated mass loss than that of the experiment which has an extended tail. Modeling results of MA+A composite decomposing at 75 kW/m² show a significantly higher mass loss rate peak following ignition than that of experiment resulting in a shorter end time of mass loss than that of experiment. This finding indicates that although the temperatures are high enough to result in greater mass loss of the resin system based on TGA data, mass loss is reduced and/or delayed when the FRP is decomposing. This deviation is suggestive that as the pyrolysis front propagates from material front surface to back surface and the heating rate increases from low to high applied heat flux impinging at the front surface in bench-scale experiments, the assumption that a pyrolysis computational cell being equivalent to a sample decomposing in a TGA experiment becomes invalid whichever kinetic model is used. In other words, thermal decomposition kinetics of the resins at depth that results in mass loss after the initial peak in the mass loss rate curve are affected by conditions that are different from those experienced in the TGA experiments. This difference between the resin decomposition in an FRP composite and that in a TGA experiment can be attributed to the change in residence time of gaseous reaction participants, e.g. fuel volatiles, during decomposition. The inert fiberglass mats within the pyrolyzing FRP composite create a physical barrier to transport of gas phase products. The residence time of these gas phase volatiles in bench-scale experiments increases with respect to increasing depth. This is in contrast to the insignificant barriers to transport in a TGA experiment. The change in residence time can be expected to affect the decomposition kinetics and result in deviation from the proposed kinetic model based on thermal analysis.

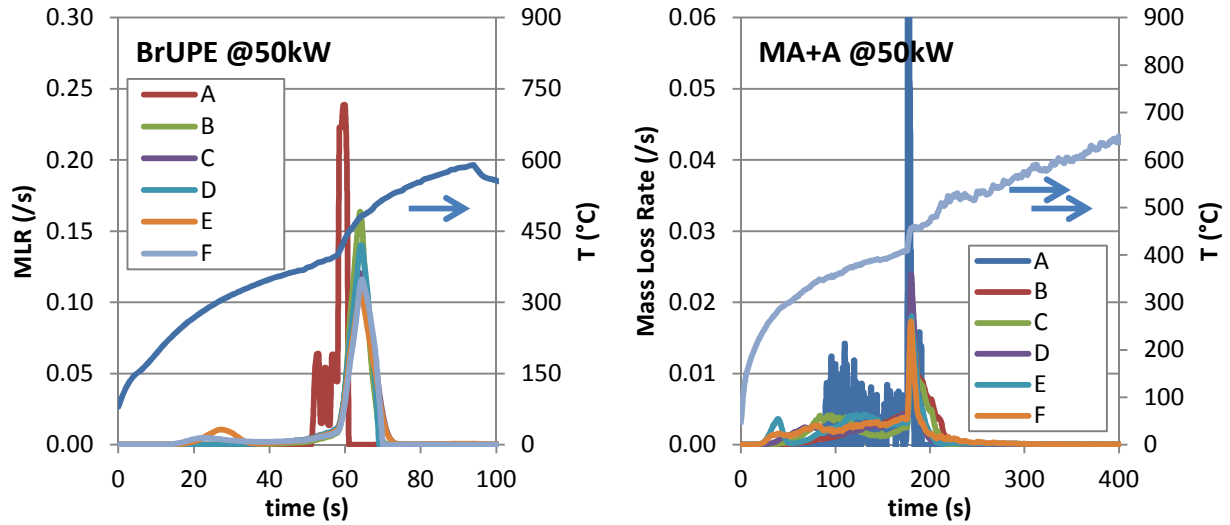


Figure 8. Example calculation using the simplified comprehensive pyrolysis model is shown for the surface location. Temperature data at front surface (T_s) from Cone Calorimeter experiments with applied heat flux of 50 kW/m^2 and simplified comprehensive pyrolysis modeling results using various kinetic models (A-F) at this location are shown for BrUPE (left) and MA+A (right) FRP composites.

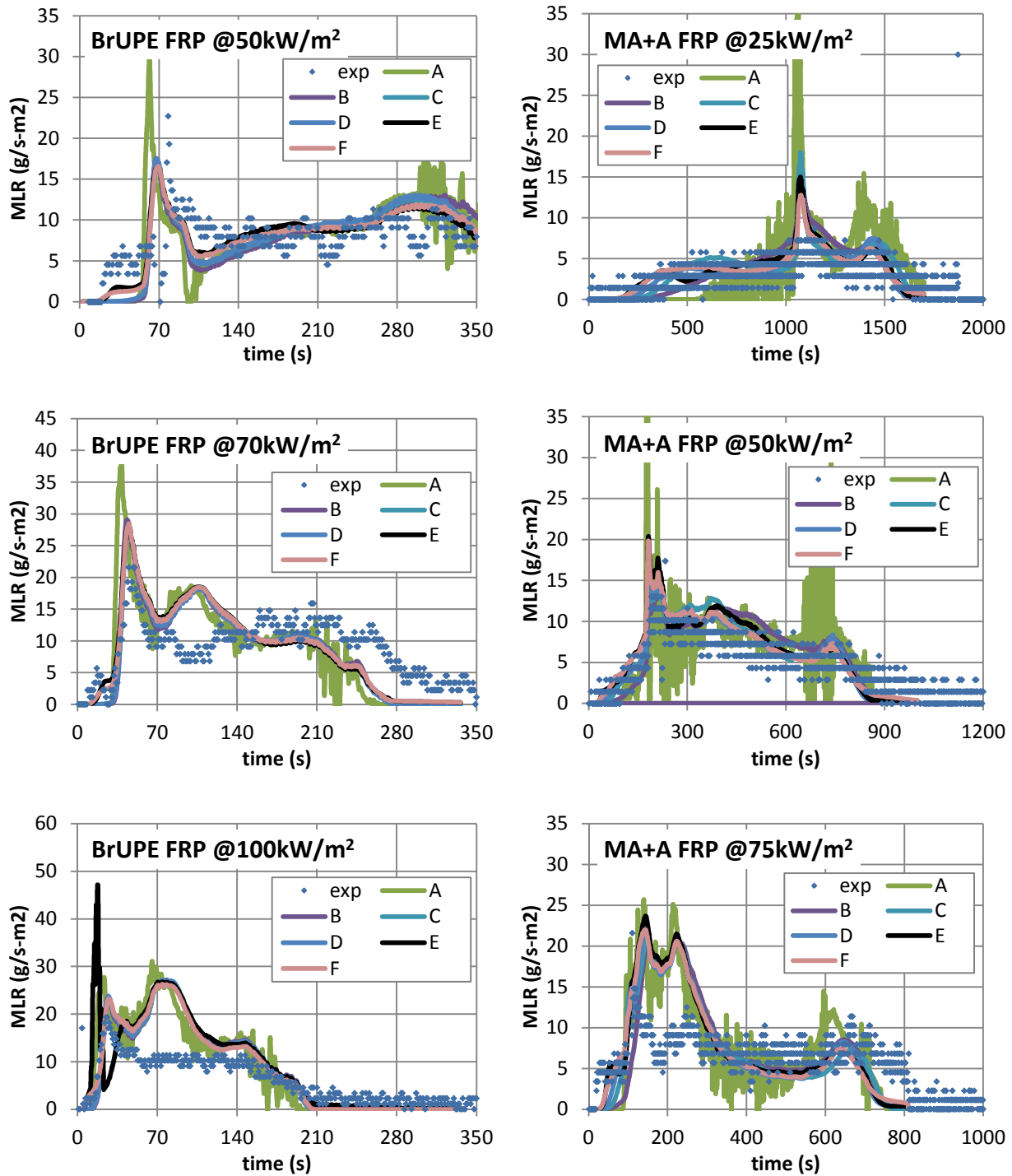


Figure 9. Mass loss rates from Cone Calorimeter experiments (exp) and simplified comprehensive pyrolysis modeling (mod) are shown for BrUPE and MA+A FRP composites. Applied heat flux levels are 50, 70 and 100 kW/m² for BrUPE FRP composite and 25, 50 and 75 kW/m² for MA+A FRP composite. Good agreement between experiment data and modeling results is found from the cases that are less than 50kW/m².

6. CONCLUSION

In this research, the effects of applying different kinetic models is evaluated when used in typical 1D comprehensive pyrolysis modeling where mass transport effects during pyrolysis are assumed to be negligible and each computational cell is assumed to be decomposing as in TGA experiments. The kinetic models are developed based on thermal analysis using TGA data. Two FRP composites are used as sample materials – BrUPE and MA+A composites. To examine the effect of kinetic modeling on the thermal decomposition of FRPs, the kinetic modeling approaches are isolated from the heating of the FRPs by conducting pyrolysis modeling which utilizes temperature measurement data from bench-scale experiments of FRP composites as a proxy for conservation of energy. Conservation of mass of the materials is represented by decomposition simulation with different kinetic models. Mass loss rate simulations with kinetic models A through F for both materials at moderate applied heat flux (50kW/m^2) show that changes in the simulation due to applying different kinetic modeling approaches are minimal except for case A where large scatter is observed due to the inherent limitations of this zero order kinetic model. In addition, simulations at various heat flux levels with kinetic models A through F are conducted and the mass loss rate results are compared to those of experiments. Results show that although at relatively low incident heat fluxes there is good overlap between simulations and the experimental data, at higher heat flux levels ($> 70\text{kW/m}^2$), simulated mass loss rates significantly deviate from the experimental data. These findings indicate that (1) increasing complexity of kinetic models by applying different reaction models or increasing the number of reaction steps to be used in comprehensive pyrolysis modeling is unnecessary for modeling of the FRP samples used in this research as the effects are minimal; and (2) the typical assumption of considering thermal decomposition of each computational cell in comprehensive pyrolysis modeling as equivalent to that in TGA experiments becomes inapplicable at depth and at higher heating rates, whichever kinetic model is used, indicating that for these conditions decomposition kinetics are apparently different from what has been captured by thermal analysis.

7. ACKNOWLEDGEMENTS

The authors greatly appreciate the support for this work from DOC NIST Award Number 60NANB8D8106 (Federal Program Officer Dr. Kevin McGrattan). Special thanks go to Charles Dore for fabricating and donating the FRP composite materials used in this study. Many thanks also to Randall Harris at WPI for conducting the Cone Calorimeter tests.

8. REFERENCE

1. Kevin McGrattan, Simo Hostikka, Jason Floyd, Howard Baum, Ronald Rehm, William Mell and Randall McDermott, Fire Dynamics Simulator (Version 5) Technical Reference Guide, NIST Special Publication 1018-5, October 29, 2010
2. S.I. Stoliarov, R.E. Lyon, Federal Aviation Administration Technical Note, DOT/FAA/AR-TN08/17, 2008; available for download at <http://www.fire.tc.faa.gov/reports/reports.asp>.
3. Lautenberger, C. & Fernandez-Pello, C., 2009. Generalized Pyrolysis Model for Combustible Solids, *Fire Safety Journal* 44(6), pp. 819-839.
4. Tewarson A., "Generation of Heat and Chemical Compounds in Fires", In *SFPE Handbook of Fire Protection Engineering*, 3rd ed., NFPA, Quincy, MA, USA (2002) Chapter 3-4.
5. Quintiere, J.G., and Harkleroad, M., "New Concepts for Measuring Flame Spread Properties", in *Fire Safety Science and Engineering*, ASTM STP 882, ASTM International, West Conshohocken, PA, USA (1985) 239-267.
6. Chen, Y., Delichatsios, M.A., and Motevalli, V., "Material Pyrolysis Properties, Part I: An Integral Model for One-Dimensional Transient Pyrolysis of Charring and Non-Charring Materials", *Combustion Science and Technology*, **88** (1993) 309-328.
7. Lautenberger, C, Rein, G., & Fernandez-Pello, C., 2006. The Application of a Genetic Algorithm to Estimate Material Properties for Fire Modeling from Bench-Scale Fire Test Data, *Fire Safety Journal* 41(3), pp. 204-214.
8. Stoliarov, S.I., Crowley, S., Lyon, R.E., & Linteris, G.T., 2009. Prediction of the Burning Rates of Non-Charring Polymers, *Combustion and Flame* 156(5), pp. 1068-1083.
9. Chaos M, Khan MM, Krishnamoorthy N, et al. Evaluation of optimization schemes and determination of solid fuel properties for CFD fire models using bench-scale pyrolysis tests. *P Combust Inst* 2011; 33(2): 2599–2606.
10. Webster, R., "Pyrolysis Model Parameter Optimization using a Customized Stochastic Hill-Climber Algorithm and Bench Scale Fire Test Data," MS Thesis, University of Maryland, 2009.
11. Marler, R. T., and Arora, J. S. (2004), "Survey of Multi-Objective Optimization Methods for Engineering," *Structural and Multidisciplinary Optimization*, 26 (6), 369-395.
12. Staggs, J.E.J., 1999. Modeling Thermal Degradation of Polymers Using Single-Step First-Order Kinetics, *Fire Safety Journal* 32(1), pp. 17-34.
13. G. Rein, C. Lautenberger, A.C. Fernandez-Pello, J.L. Torero, D.L. Urban, Application of Genetic Algorithms and Thermogravimetry to Determine the Kinetics of Polyurethane Foam in Smoldering Combustion, *Combustion and Flame* 146 (1-2), pp 95-108, 2006.
14. Lautenberger, C. & Fernandez-Pello, A.C., "A Model for the Oxidative Pyrolysis of Wood," *Combustion and Flame* **156** 1503-1513 (2009).
15. Lautenberger, C. & Fernandez-Pello, C., "Optimization Algorithms for Material Pyrolysis Property Estimation," *Fire Safety Science* **10** 751-764 (2011).
16. Handbook of Thermal analysis and Calorimetry. Vol.1: Principles and Practice. M.E. Brown, editor c 1998 Elsevier Science B.V.
17. A.K. Burnham, R.K. Weese, A.P. Wemhoff, J.L. Maienschein, A historical and current perspective on predicting thermal cookoff behavior, *J. Therm. Anal. Calorim.* 89 (2007) 407–415.
18. T. Ozawa, "A new method of analyzing thermogravimetric data," *Bull. Chem. Soc. Jpn.*, vol. 38, pp. 1881–1886, 1965.
19. J. H. Flynn and L. A. Wall, "A quick, direct method for the determination of activation energy from thermogravimetric data," *J. Polym. Sci. Polym. Lett.*, vol. 4, pp. 323–328, 1966.
20. H. L. Friedman, "Kinetics of thermal degradation of char-forming plastics from Thermogravimetry. Application to a phenolic plastic," *J. Polym. Sci., Pt. C* 6, 183-195 (1964).
21. J. H. Flynn, L. A. Wall, "A quick, direct method for the determination of activation energy from thermogravimetric data," *J. Polym. Sci. Polym. Lett.* 4, 323-328 (1966).
22. S.V. Vyazovkin and A.I. Lesnikovich, *Thermochim. Acta*, 165 (1990) 273
23. S. Vyazovkin, *The Handbook of Thermal Analysis & Calorimetry*, in: M.E. Brown, P.K. Gallagher (Eds.), *Recent Advances, Techniques and Applications*, vol. 5, Elsevier, 2008, p. 503.
24. S. Vyazovkin, A unified approach to kinetic processing of nonisothermal data, *Int. J. Chem. Kinet.* 28 (1996) 95–101.

-
25. L.A. Perez-Maqueda, J.M. Criado, P.E. Sanchez-Jimenez, Combined kinetic analysis of solid-state reactions: a powerful tool for the simultaneous determination of kinetic parameters and the kinetic model without previous assumptions on the reaction mechanism, *J. Phys. Chem. A* 110 (2006) 12456–12462.
 26. J. Opfermann, Kinetic analysis using multivariate non-linear regression I. Basic concepts, *J. Therm. Anal. Calorim.* 60 (2000) 641–658.
 27. P. Atkins, J. de Paula, *Physical Chemistry*, 9th ed., W.H. Freeman, New York, 2010 (discussion of negative activation energies is also found in earlier editions, see subject index under “activation energy, negative”).
 28. M.E. Brown, *Introduction to Thermal Analysis*, 2nd ed., Kluwer, Dordrecht, 2001.
 29. Anand K. Kulshreshtha, Cornelia Vasile (Editors), *Handbook of polymer blends and composites*, RAPRA Technology LTD, 2002
 30. LeVan, S.L., *The Chemistry of Solid Wood*; Chapter 14. *Chemistry of Fire Retardancy*, American Chemical Society, 1984
 31. Bras, M.L., Rose, N. and Bourbigot, S., The Degradation Front Model – A tool for the Chemical Study of the Degradation of Epoxy Resins in Fire, *Journal of Fire Sciences*, Vol. 14 – May/June (1996)
 32. Liu, J., He, D., Xu, L., Yang, H. and Wang, Q., Study of the Kinetics of the Combustion Reaction on Shuangya Mountain Coal Dust by TG, *Journal of Thermal Analysis and Calorimetry*, Vol. 58 (1999) 447-453
 33. Lyon RE, Safronava N and Oztekin E. A simple method for determining kinetic parameters for materials in fire models. *Fire Saf Sci* 2011; 10: 765–777.
 34. Standard Test Method for Heat and Visible Smoke Release Rates for Materials and Products Using an Oxygen Consumption Calorimeter, ASTM E 1354-02, ASTM, 100 Barr Harbor Drive, West Conshohocken, PA, U.S.
 35. de Ris, J.L. and Khan, M.M., “A sample holder for determining material properties,” *Fire and Materials*, 24, 219-226 (2000).
 36. Chrissafis, K., Paraskevopoulos, K.M., Bikiaris, D.N., Thermal degradation kinetics of the biodegradable aliphatic polyester, poly(propylene succinate), *Polymer Degradation and Stability* 91 (2006) 60-68
 37. Y. S. Yang and L. James Lee, Microstructure formation in the cure of unsaturated polyester resins *Polymer, Volume 29, Issue 10, October 1988, Pages 1793-1800*
 38. Chiu, H.T., Chiu, S.H., Jeng, R.E., Chung, J.S., A study of the combustion and fire-retardance behaviour of unsaturated polyester/phenolic resin blends, *Polymer Degradation and Stability* 70 (2000) 505-514
 39. Liliana B. Manfredi, Exequiel S. Rodri'guez, Maria Wladyka-Przybylak, Anali'a Va' zquez, Thermal degradation and fire resistance of unsaturated polyester, modified acrylic resins and their composites with natural fibres, *Polymer Degradation and Stability* 91 (2006) 255-261
 40. Reich, L., Stivala, S.S., Chapter 6. Factors Affecting Polymer Stability, *Elements of Polymer Degradation*, McGraw-Hill, Inc., c 1971
 41. Chen, I., Hwang, S., Chen, S., Chemical Kinetics and Reaction Mechanism of Thermal Decomposition of Aluminum Hydroxide and Magnesium Hydroxide at High Temperatures (973-1123K), *Ind. Eng. Chem. Res.*, **1989**, 28 (6), pp 738–742
 42. Hornsby, P. R. (1994), The application of magnesium hydroxide as a fire retardant and smoke-suppressing additive for polymers. *Fire and Materials*, 18: 269–276. doi: 10.1002/fam.810180502

Section 3

EVALUATION OF PYROLYSIS PARAMETERS FOR FIBERGLASS REINFORCED POLYMER
COMPOSITES BASED ON MULTI-OBJECTIVE OPTIMIZATION

EVALUATION OF PYROLYSIS PARAMETERS FOR FIBERGLASS REINFORCED POLYMER COMPOSITES BASED ON MULTI-OBJECTIVE OPTIMIZATION

Kim, E. and Dembsey, N.*

WPI, Fire Protection Engineering Dept., Worcester, MA, USA

*Corresponding author email: ndembsey@wpi.edu

ABSTRACT

This study was conducted to investigate the ability of global, multi-objective/variable optimization methods to estimate material parameters for comprehensive pyrolysis models – thermo-physical and optical properties of two Fiberglass Reinforced Polymer (FRP) composites that share the same fiberglass. With these optimization methods used in pair with a comprehensive pyrolysis model, parameter estimation was carefully conducted with considerations given to applying appropriate thermal decomposition kinetic models (three different models from simple to complex) and optimization targets (Cone Calorimeter data irradiated at 50kW/m²).

Estimation results are compared with independently measured effective properties – thermal conductivity, specific heat capacity and emissivity of polymer resins and FRPs. Additionally, fiberglass properties estimated from the two FRPs are compared to analyze for consistency in optimized values. The results show that for a well-configured parameter estimation exercise using the optimization method described above, (1) estimated results are within $\pm 100\%$ of the measurements in general and sometimes comparable to effective property values; (2) increasing complexity of the kinetic modeling for a single component system has insignificant effect on estimated values; and (3) increasing complexity of the kinetic modeling for a multiple component system with each element having different thermal characteristics has positive effect on estimated values.

1. INTRODUCTION

In the recent years, several comprehensive pyrolysis models [1,2,3] have been publically released to the fire community as a step forward in modeling materials' pyrolysis. Unlike previous versions of pyrolysis models where material pyrolysis has been modeled empirically or with simple analytical solutions, comprehensive pyrolysis models simulate a materials physical and chemical reaction to fire responses based on fundamental conservation equations. Typically, models are constructed to conserve mass and energy when the material is being heated and/or thermally decomposed. Numerical calculations are conducted using various methods – finite difference, finite element, etc. – to determine mass loss and temperature profiles from the heat exposed front surface to unexposed back surface with respect to increasing time. However, when applying these models to real world problems, generally model users experience significant challenges as these models require estimation of many model parameters by the users and there is no material database available to search for the unknown parameter values.

Typically, comprehensive pyrolysis model parameters can be grouped into three categories: parameters related to thermal decomposition kinetics and material properties, and model dependent parameters. Among these

parameters, only a few of them may be estimated via independent measurement based on standard tests: those for a material's initial non-decomposing stage. Measurement techniques do not exist for parameters during a material's decomposing stage or to measure parameters of residual species. To overcome this difficulty in estimating model parameters, parameter estimation using global, multi-objective and multi-variable numerical optimization methods have been introduced [4,5,6,7,8]. This approach integrates robust, global, numerical optimization methods (e.g. genetic algorithm, shuffled complex evolution, etc.) to pyrolysis modeling to optimize for the unknowns by iteratively comparing model outputs with optimization targets set as bench-scale experimental data such as mass loss rate and temperature profiles from Cone Calorimeter (ASTM E 1354 [9]) experiments. This has become more appealing recently due to the inexpensive and accessible nature of "high speed" computer resources.

Although these multi-objective optimization routines are global methods, applying them to parameter estimation naturally results in estimation of multiple near optimal parameter sets as typically there is no unique solution to solving this type of inverse problem [10]. The reason for resulting in many near optimals is due to the existing compensating effects between different model parameters, which have been already discussed by other researchers. For example, low activation energy used in kinetic model can be compensated by applying a lower pre-exponential factor [11], the effect of poorly estimated kinetic parameters on pyrolysis modeling can be compensated by adjusting other thermo-physical property related model parameters [12], etc.

The ability of multi-objective optimization methods to estimate comprehensive pyrolysis model parameters related to material properties is evaluated in this study. This exercise is performed to understand how sensible the estimated values via multi-objective optimization method can be in terms of being consistent with their effective material properties, independently measured by standard tests. To do so, parameter estimation is conducted with great caution in estimating model parameters of two Fiberglass Reinforced Polymer (FRP) composites that share the same fiberglass but have different polymer resins. Parameter estimation is conducted by considering the following: applying appropriate (1) thermal decomposition kinetic model and (2) optimization targets. First, suitable kinetic models that have different levels of complexity are proposed from thermal analysis of the polymer resins and their effect on 1D pyrolysis modeling of *integrated* overall mass loss rate is examined through a screening process which involves mass loss rate simulation of 1D FRP pyrolysis using kinetic models and temperature profiles from Cone Calorimeter tests. Following this work, optimization targets are selected from the same screening process with consideration of data over a range of heat flux levels applied during testing. Finally, parameter estimation exercises are conducted and the results are compared with several independently measured effective material properties – thermal conductivity, specific heat capacity and emissivity of polymer resins and FRPs. Additionally, fiberglass properties estimated from different parameter estimation exercises conducted for the two FRPs are compared to analyze consistency in optimized values.

2. SAMPLE MATERIAL

FRP composite panels were fabricated by vacuum bagging to ensure relatively high glass content, using two different types of fiberglass (E-glass) mats – chopped strand mat and a woven roving mat – that were wetted with

resin. The chopped strand mat is thinner and more porous than the woven mat. The laminate schedule is chopped strand mat and roving alternating 8 and 6 times with another chopped strand mat layer at the end for the brominated unsaturated polyester (BrUPE) and modified acrylic with inorganic high charring additive (MA+A) FRP composites resulting in average glass contents of 75% and 67% by weight, respectively. Typically, these composites had thickness ranging from 7 to 9 mm. Note that these two materials were chosen to represent FRPs with a thermally decomposable resin that has a single component (BrUPE) or a thermally decomposable resin (MA) and additive (A) mixture that has two distinct components with different thermal characteristics (MA+A). More detailed description of sample materials can be found in previous work [13].

3. EXPERIMENTS

The milli-scale instruments used in this study were manufactured from TA Instruments: Thermogravimetric Analysis Q50 (TGA) and the Differential Scanning Calorimetry Q20 (DSC). Throughout this study, TGA and DSC were used for non-isothermal test purposes under nitrogen or air environments to study pyrolysis and oxidation, respectively. Further descriptions are found in ref [13].

The Cone Calorimeter (Cone, ASTM E 1354 [14]) is a bench-scale fire test apparatus in which the sample is heated by an electrically powered rod in the shape of a cone. The sample is tested by applying a constant radiative heat flux set via temperature control of the rod. The Cone exposes the sample in an ambient environment which results in a natural flow field as the sample temperature increases allowing convective cooling above the sample surface. The ignition source is an intermittent sparker. Several modifications were made to the standard testing procedure. First, when testing these FRPs, two different types of sample holders were used to produce nominal one-dimensional data: the standard non-insulated square holder with a metal edge frame and a round insulated holder [15]. Second, typically 4 thermocouples were installed to measure temperature change of the sample at various depths: exposed surface, 1/3, 2/3 and back surface. The uncertainties in experimental mass loss rate (MLR) and thermocouple measurements at surfaces (exposed, T_s and back, T_b) were quantified by comparing data from 3 or 4 identical FRP composite tests at 50 and 75kW/m² applied heat flux levels for BrUPE and MA+A composites, respectively. Note that normalized time, time divided by sample thickness square, i.e., $\tau = \text{time}/\delta^2$ is used to remove the effect of different sample thicknesses. Because the data is transient, values at different times ($\tau = 1, 3, 5 \text{ s/mm}^2$ for BrUPE and 1, 3, 5, 7 s/mm² for MA+A composites) from each test have been used to calculate the standard deviation at each time. Then these are averaged and used to estimate uncertainty by applying student t distribution with a sample size of 3 or 4 and calculating the 95% confidence interval. Uncertainties in MLR, T_s and T_b are ± 2.2 or 2.3 g/s-m², ± 67 or 30 °C, and ± 14 or 22 °C for BrUPE or MA+A composite. The uncertainty in TC bead location at depth is typically ± 1 mm. These uncertainty values were used to evaluate significant differences between the modeling results and experiment data.

4. PARAMETER ESTIMATION VIA OPTIMIZATION METHOD

The comprehensive pyrolysis modeling and parameter estimation via numerical optimization reported here are conducted with a generalized pyrolysis model [3,8] that can be applied to a wide variety of condensed phase fuels. The model simultaneously calculates the condensed phase mass conservation, gas phase mass conservation, condensed phase species conservation, and condensed phase energy conservation equations. This model can be applied to 1D systems and is therefore capable of simulating “slab” (Cone Calorimeter) experiments. Extensive details are given in Ref. [3]. In this study, among various optimization routines available in this model, genetic algorithm (GA) or shuffled complex evolution (SCE) are used. These optimization routines are evolution optimization schemes with high efficiency and robustness that allow multi-objective and multi-variable optimization under limited knowledge of the problem. Note that when GA is used, although a parameter set with best fitness to targets may be found by the algorithm, multiple near optimal sets that have similar fitness can be identified and therefore any analysis in this work using GA optimization results is conducted with an average value for each estimated parameter from different optimal sets. For SCE, a single optimal set is found and that is used in the analysis. Note that when conducting the optimizations, a fairly wide searchable range – typically 2-3 orders of magnitude between minimum and maximum value – was applied for each unknown parameter.

Details of the modeling approach used in this comprehensive pyrolysis modeling are as follows. The FRP composite is construed as a homogeneous mixture of the polymer system and the fiberglass. Pyrolyzate volatiles produced from thermal decomposition of the condense phase polymer system is assumed to be released instantaneously to the gas phase without any interruption. Local thermal equilibrium is assumed between the condense phase and the volatiles. Any condensation of the gaseous products is negligible. Porosity effects are only accounted for in defining the bulk thermal conductivity of the composite. When simulating the bench-scale experiment, the surface is impinged with a constant radiative heat flux and the backing is insulated with a layer of insulation with known properties. The contact resistances (hcrz) between the FRP composite and the insulation and the insulation and ambient are estimated roughly as 10 W/m²K and 1 W/m²K, respectively, based on preliminary numerical work on model parameter sensitivity. For both materials, ignition phenomenon is interpreted as an additional constant heat flux of 20 kW/m² applied to the surface from a user-specified ignition time to simulation end time. This approach is utilized to simulate the effect of the flame after ignition and the value of 20 kW/m² is estimated from Cone experiments with a total heat flux gauge embedded in the sample. Thermal conductivity and specific heat capacity parameters of each condense-phase species are assumed to be temperature dependent: $k(T) = k_0 (T/T_r)^{n_k}$ and $c(T) = c_0 (T/T_r)^{n_c}$, respectively, where T_r is a reference temperature of 300 K. The average effective parameters are weighted based on condense-phase volume fractions for thermal conductivity (see Eq.1) and emissivity (see Eq.3), and mass fractions for specific heat capacity (see Eq.2). Note that G, R and A are abbreviation for fiberglass, resin and additive, respectively in the equations below.

$$\bar{k}_0 = X_{0,G}k_{0,G} + X_{0,R}k_{0,R} + X_{0,A}k_{0,A} \quad \text{Eq.1}$$

$$\bar{c}_0 = Y_{0,G}c_{0,G} + Y_{0,R}c_{0,R} + Y_{0,A}c_{0,A} \quad \text{Eq.2}$$

$$\bar{\varepsilon}_0 = X_{0,G}\varepsilon_{0,G} + X_{0,R}\varepsilon_{0,R} + X_{0,A}\varepsilon_{0,A} \quad \text{Eq.3}$$

Before evaluating whether parameter estimation via numerical optimization is capable of estimating physically sensible parameter values, the following must be considered as a basis for conducting reliable parameter estimation: applying an appropriate kinetic model for describing thermal decomposition process and selecting appropriate optimization targets.

5. THERMAL DECOMPOSITION KINETIC MODELING

The first step to configure the pyrolysis modeling problem mathematically for a material of interest is to determine the level of complexity needed for the thermal decomposition kinetics of the resin and any additives. Candidate kinetics models are developed based on thermal analysis [16,17,18,19] using TGA and DSC data. In a reduced form, thermal decomposition of BrUPE and MA+A can be grouped into a maximum of three and four stages, respectively – three for initial (ambient temperature to ~200°C), major (200°C to ~ 500°C), and final (500°C to ~ 700°C) resin (BrUPE or MA) decomposition and one additional stage where decomposition of the additive (A) is observed at relatively lower temperatures (200°C to ~ 400°C).

The final kinetic model for the FRP is chosen based on a screening procedure that simulates mass loss during 1D FRP pyrolysis by using bench scale temperature data from the Cone Calorimeter as a proxy for conservation of energy on the FRP. This approach assumes that thermal decomposition is a function of temperature only and products are instantaneously released to the gas phase without interruption, which is typically used in general comprehensive pyrolysis modeling in the fire community [1]. Additionally, the FRP composite is construed as a homogeneous mixture of a thermally decomposable component of polymer system and an inert fiberglass. This homogeneous cross-section is discretized into some number of cells and their mass loss is calculated based on the kinetic model proposed with the temperature information obtained from bench-scale experiments. The simulation results are a mass loss rate *integrated* over the cross-section of FRPs at different time steps. This screening process is capable of decoupling the kinetic simulation from the overall pyrolysis simulation and evaluating the appropriateness of each kinetic model proposed.

Six different kinetic models were tested which utilize the Arrhenius form (see Eq.4) with $n = 0$ (see Eq.5); 1 or nth order reaction models, $f(\alpha) = (1 - \alpha)^n$; simplified single step reaction to describe the entire decomposition process or multiple step reactions to explicitly describe for each process of different components in the resin mixture; and applying single or multiple iso-heating rate TGA data to estimate kinetic parameter values (see Table 1). Although the changes are minor, fitness of the kinetic models to TGA data increases from the simplest approach, A, to the most complex approach, F, as shown in Figure 1. The results of the screening procedure for 1D pyrolysis simulation at a moderate applied heat flux level of 50 kW/m² showed the following. The effects of applying models B through F on the *overall* simulation of mass loss rate is considered insignificant. This is because the difference in mass loss rate between kinetic models is less than the uncertainty of the experimental mass loss rate data. Applying

model A resulted in a larger scatter near the peak and the tail of the mass loss rate simulation; however, the trend follows well with the other case results. Further discussion can be found in ref [13].

Table 1. Different kinetic models considered in this study

BrUPE		MA+A	
Model	Model Assumptions / Data	Model	Model Assumptions / Data
A	virgin \rightarrow char + vap \uparrow zero order reaction model using constant DTG with respect to temperature	A	virgin \rightarrow char + vap \uparrow zero order reaction model using constant DTG with respect to temperature
B	virgin \rightarrow char + vap \uparrow first order reaction model using DTG peak to estimate kinetic parameters	B	virgin \rightarrow char + vap \uparrow first order reaction model using DTG peak to estimate kinetic parameters
C	virgin \rightarrow char + vap \uparrow first order reaction model using multiple iso-heating rates TGA data to estimate kinetic parameters	C	virgin \rightarrow char + vap \uparrow additive \rightarrow additive_residue + vap \uparrow first order reaction models using multiple iso-heating rates TGA data to estimate kinetic parameters
D	virgin \rightarrow char + vap \uparrow nth order reaction model using multiple iso-heating rates TGA data to estimate kinetic parameters	D	virgin \rightarrow char + vap \uparrow additive \rightarrow additive_residue + vap \uparrow nth order reaction models using multiple iso-heating rates TGA data to estimate kinetic parameters
E	virgin \rightarrow intermediate + vap \uparrow intermediate \rightarrow char + vap \uparrow char \rightarrow residue + vap \uparrow first order reaction models using multiple iso-heating rates TGA data to estimate kinetic parameters	E	virgin \rightarrow intermediate + vap \uparrow intermediate \rightarrow char + vap \uparrow char \rightarrow residue + vap \uparrow additive \rightarrow additive_residue + vap \uparrow first order reaction models using multiple iso-heating rates TGA data to estimate kinetic parameters
F	virgin \rightarrow intermediate + vap \uparrow intermediate \rightarrow char + vap \uparrow char \rightarrow residue + vap \uparrow nth order reaction models using multiple iso-heating rates TGA data to estimate kinetic parameters	F	virgin \rightarrow intermediate + vap \uparrow intermediate \rightarrow char + vap \uparrow char \rightarrow residue + vap \uparrow additive \rightarrow additive_residue + vap \uparrow nth order reaction models using multiple iso-heating rates TGA data to estimate kinetic parameters

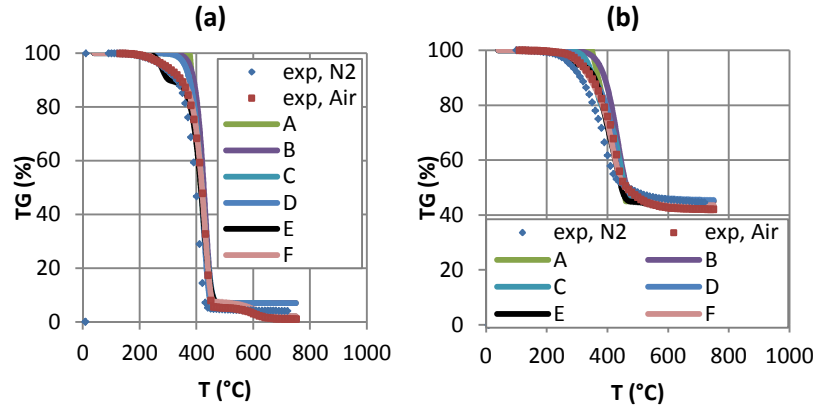


Figure 1. Mass loss rates from TGA experiments (exp) and kinetic modeling (A-F) and are shown for BrUPE (a) and MA+A (b) with 60 °C/min heating rate case. Applying various approaches in kinetic modeling results in minor changes in modeled mass loss rate.

$$\frac{d\alpha}{dt} = A \exp\left(-\frac{E_a}{RT}\right) f(\alpha) \quad \text{Eq.4}$$

$$\alpha = aT + b. \quad \text{Eq.5}$$

It is important to choose the appropriate level of complexity in kinetic modeling. As the kinetic modeling approach used in pyrolysis modeling becomes more complex, the number of species involved during pyrolysis increases meaning that the number of model parameters associated with those species will increase. Therefore, in terms of conducting parameter estimation for pyrolysis modeling, simpler kinetic modeling approaches are more desirable. Based on the screening procedure conducted previously, insignificant changes were observed in the simulations of mass loss rates *integrated* over the cross-section at each time step with different kinetic models (A through F). Although the effect of increasing complexity in kinetic model was trivial in the simulation of mass loss rate *integrated* over the cross-section, its effect on parameter estimation for pyrolysis modeling based on multi-objective optimization is unknown. Therefore, to understand this effect of kinetic modeling complexity on the parameter estimation process, kinetic models with different complexity – model B, C and F – are selected to be applied in the pyrolysis modeling problem for both FRP materials. The major differences between these models are how the different components in the resin mixture are described. For the BrUPE resin mixture, kinetic model B and C have a single step mechanism which simplifies the process into a single reaction; and model F has a three step mechanism to address decomposition of different species – resin, intermediate resin and char. For the MA+A resin mixture, kinetic model B has a single step mechanism lumping decomposition into a single reaction; model C has a two-step mechanism with one reaction for describing decomposition of the polymer (MA) and one reaction for describing decomposition of the additive (A); and model F has a four step mechanism to include decomposition of different species – resin, intermediate resin and char – from the polymer (MA) as well as the additive (A). When these kinetic models are applied, the total number of unknowns in model parameters ranged from less than 20 up to 40 using the comprehensive pyrolysis model, GPYRO [3,8].

6. OPTIMIZATION TARGET

Finding the appropriate targets is important as the numerical optimization routines are capable of optimizing the parameter values to compensate for any undesirable deviation from the given targets. When this happens, numerical optimization routines will be more likely to optimize to non-physical values for the model unknowns. The purpose of this study is in examining the ability of multi-objective optimization methods to estimate comprehensive pyrolysis model parameters related to material properties by evaluating how close are the estimated values to their effective material properties, independently measured by various standard tests. Therefore, caution is necessary in terms of selecting the appropriate optimization targets in the parameter estimation exercises – bench-scale experiment data of mass loss rate, front and back surface temperature histories – as this can affect the estimation results.

To find an appropriate optimization target for parameter estimation, screening simulations with kinetic model F (best fitness to TGA data) of mass loss rates are conducted (see Figure 2) for cases with different applied heat flux levels – 50, 70 and 100 kW/m² for BrUPE composite and 25, 50 and 75 kW/m² for MA+A composite to ensure consistency between simulation and data. The results show that at lower heat flux levels good agreement between experimental data and simulations are found where the averaged difference between data and simulations is less than the average uncertainty of mass loss rate data. However, at higher heat flux levels, there is a significant deviation in simulation results from measured MLR for both materials. This is suggestive that at higher heat flux levels, applying assumptions of thermal decomposition being only a function of temperature and residual mass and having no interruption during release of pyrolysis products becomes inappropriate.

Based on the screening procedure conducted above, the target data are from a single test with applied heat flux level of 50 kW/m² is used instead of utilizing multiple data sets with different applied heat flux levels. This ensures that these parameter estimations are performed within the bounds of the pyrolysis modeling assumptions, i.e. assuming thermal decomposition is a function of temperature only and products are instantaneously released to the gas phase without interruption. Otherwise, the effect of modeling results deviating from experimental data at earlier times with higher heat flux levels (see (b), (c) and (f) of Figure 2) will be accounted for in the estimated parameter values to compensate for this undesirable deviation.

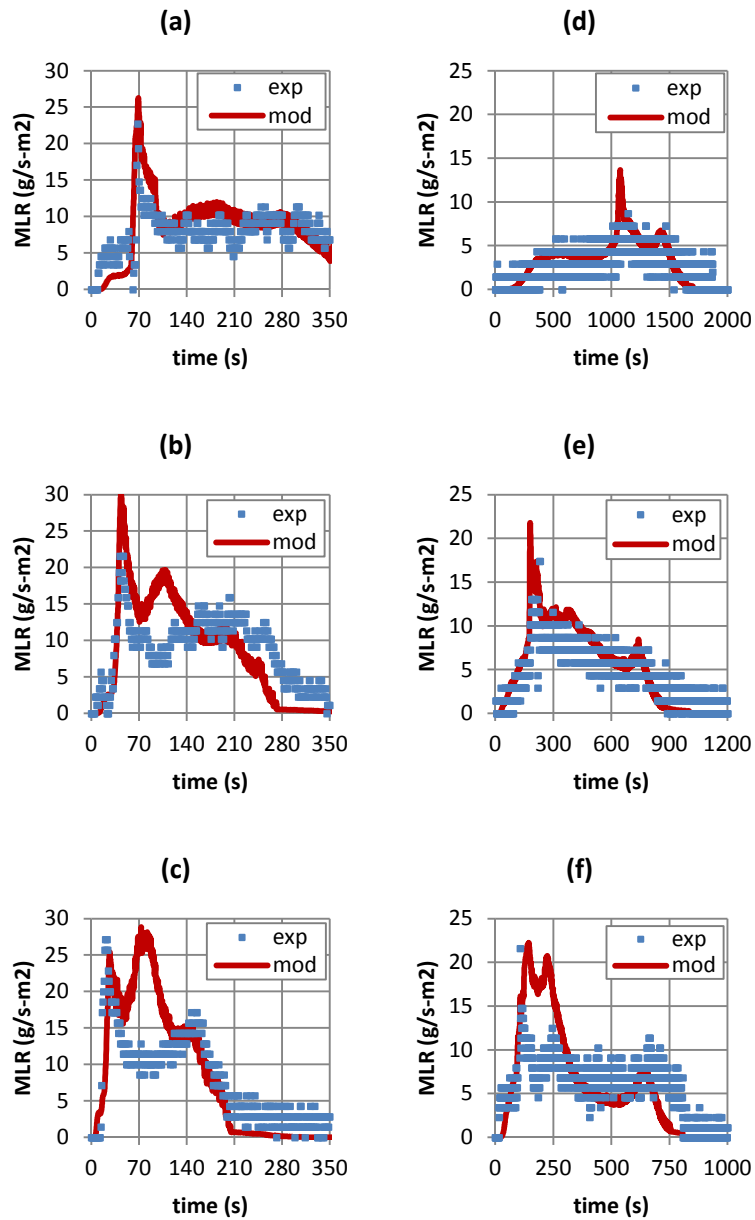


Figure 2. Mass loss rates from Cone Calorimeter experiments (exp) and simplified comprehensive pyrolysis modeling (mod) and are shown for BrUPE and MA+A FRP composites. Applied heat flux levels are 50, 70 and 100 kW/m² for BrUPE FRP composite ((a), (b) and (c), respectively) and 25, 50 and 75 kW/m² for MA+A FRP composite ((d), (e) and (f), respectively). Good agreement between experiment data and modeling results are found from (a) for BrUPE composite and (d) and (e) for MA+A composite.

7. RESULTS AND DISCUSSION

For the BrUPE FRP composite, the parameter estimation process was successful for all cases with the three kinetic models – B, C and F. For parameter estimation cases with kinetic models B and C, SCE routine was used and for that with kinetic model F, GA routine was used. When SCE is used, a single optimized parameter set is used to conduct further analysis. For GA optimized case, 100 near optimal parameter sets are used to calculate the average and the 95% confidence interval by applying a student t-distribution. The best-fit cases from parameter estimation with kinetic models B, C and F are shown with experiment data in Figure 3. Mass loss rate simulations from all cases are in good agreement with the data considering the experiment uncertainty. For simulations of front and back surface temperature histories, that of case F is in agreement with data for the entire time range – pre-ignition, ignition and post-ignition. Temperature simulations with kinetic model B and C have poor agreement during pre-ignition and near ignition time range ($t < 150$ s) where front and back surface temperatures are greater and lower than those of experiment data and the differences are greater than the data uncertainty.

The parameter estimation process for the MA+A FRP composite was successful for kinetic models B and C; however, parameter estimation with the most complex kinetic model among the three cases, kinetic model F was unsuccessful. For B and C cases, GA near optimal parameter sets of 50 and 20 are used, respectively, to estimate the average and 95% confidence intervals by applying a student t-distribution. The best-fit cases from parameter estimation with kinetic models B and C are shown with experiment data in Figure 4. Mass loss rate and front and back surface temperature history simulations with kinetic models B and C are in a good agreement with the data where modeling outputs are mostly within the uncertainty bands of the experiment data.

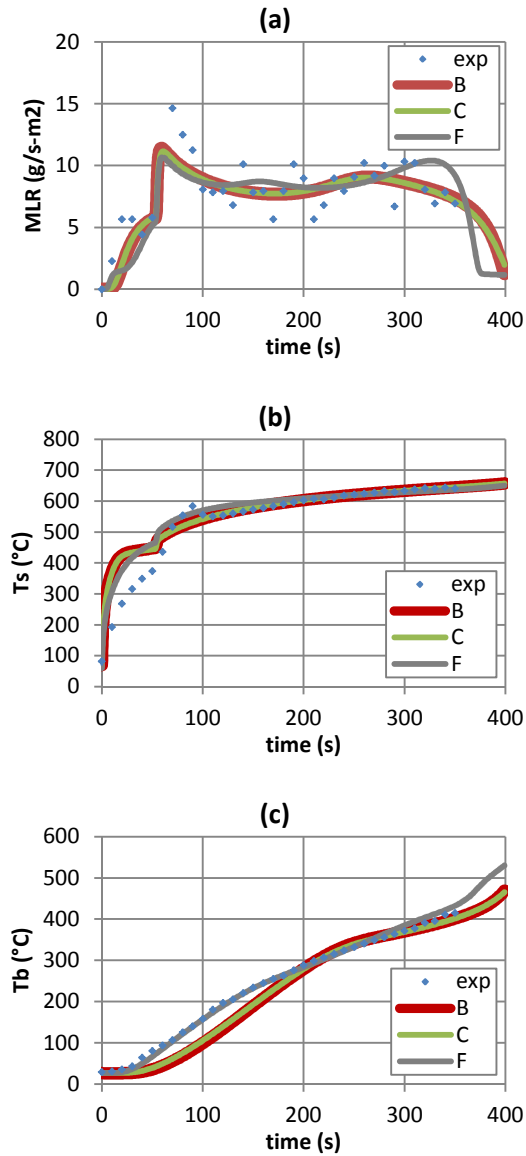


Figure 3. Mass loss rate, front and back surface temperature histories from Cone Calorimeter experiments (exp) and comprehensive pyrolysis modeling results with parameters estimated from numerical optimization using three different kinetic models (B, C and F) are shown for BrUPE FRP composite. Applied heat flux level is 50 kW/m². Modeling outputs are mostly within the uncertainty bands of the experiment data.

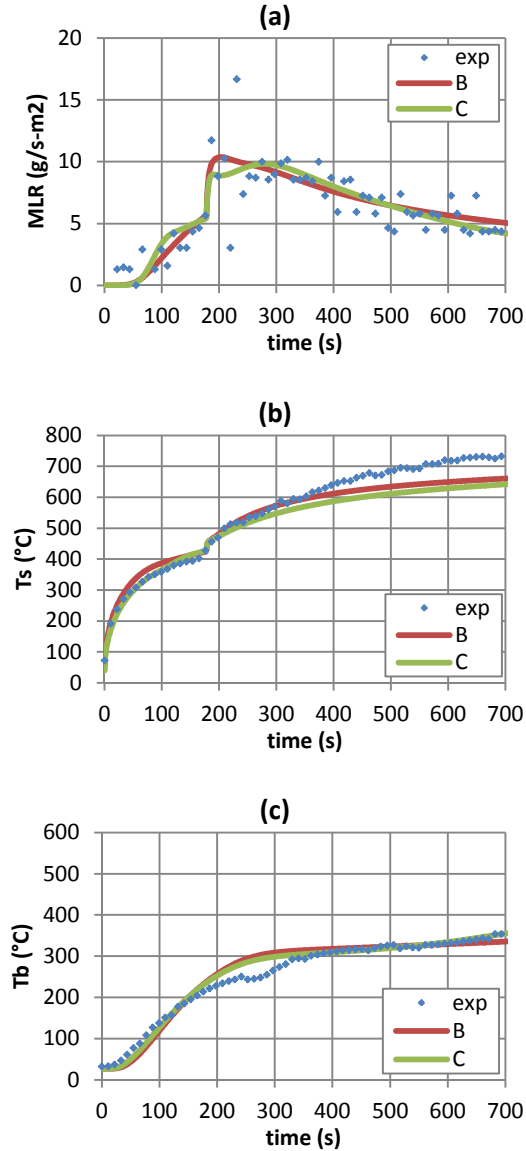


Figure 4. Mass loss rate, front and back surface temperature histories from Cone Calorimeter experiments (exp) and comprehensive pyrolysis modeling results with parameters estimated from numerical optimization using two different kinetic models (B and C) are shown for MA+A FRP composite. Applied heat flux level is 50 kW/m². Modeling outputs are mostly within the uncertainty bands of the experiment data.

The results of the successful optimization strategies with different kinetic models for the two composites – BrUPE and MA+A FRP composites – are evaluated by comparison to independent measurements made with standard tests [20,21,22,23] at temperatures below the FRPs’ decomposition temperature – thermal conductivity (k) of the polymer systems (BrUPE and MA+A) and the FRPs, specific heat capacity (c_p) of the polymer resin systems (BrUPE and MA+A), and emissivity (ϵ) of the FRP composites (see Table 2 and Figure 5). Note that the independent measurements have reported uncertainties of $\pm 20\%$, $\pm 5\%$ and ± 0.03 for thermal conductivity, specific heat capacity and emissivity, respectively. For thermal conductivity, the differences between the estimated and measured values reduce from 66 to 59% for the BrUPE resin and 80 to 40% for the BrUPE FRP composite with

respect to increasing complexity in kinetic model (B to F). A similar trend is found for the thermal conductivity estimations for MA+A resin and MA+A FRP composite, but with greater decrease in % difference between the estimated and measured values than those in BrUPE cases – 67 to 4% for the MA+A resin and 43 to 13% for the MA+A FRP composite. For specific heat capacity, although there is some improvement when kinetic model F is used where the average difference between estimation and measurement over the temperature range of interest decreases from 59% (kinetic model C) to 32% (kinetic model F), the estimated values with all kinetic models have poor correlation with the measured values for the BrUPE polymer resin. Good correlation is found between the estimations and measurement of specific heat capacity for the MA+A resin case when the more complex kinetic model C is used where the average difference between estimation and measurement over the temperature range of interest decreases from 31% (kinetic model B) to 8% (kinetic model C). For emissivity, estimations show that the differences between the estimated values and measured values range from 2 to 9% and 6 to 12% for BrUPE and MA+A FRP composites, respectively. With increasing complexity in applied kinetic model there is increasing difference between the estimation and measurement for emissivity of BrUPE FRP composite. The difference between the estimated emissivity values and the measured value for MA+A FRP composite becomes smaller as more complex kinetic model is applied.

Table 2. Comparison between measured parameter values for thermal conductivity and emissivity of the polymer systems (BrUPE and MA+A) and FRP composites (BrUPE FRP and MA+A FRP) and estimated values from numerical optimization: Last column shows the percentage difference between measured (at room temperature) and estimated values where generally a reduction of difference occurs when more complicated kinetic model is used in the estimation process.

Parameter	Material	Meas. Value	KM Type	Estimated Value	% Diff
k [W/m-K]	BrUPE	0.231 ± 0.046	B	0.078	66
			C	0.058	75
			F	0.368 ± 0.013	59
	MA+A	1.060 ± 0.212	B	0.349 ± 0.017	67
			C	1.018 ± 0.158	4
	BrUPE FRP	0.327 ± 0.065	B	0.067	80
			C	0.085	74
			F	0.197 ± 0.007	40
	MA+A FRP	0.573 ± 0.115	B	0.328 ± 0.012	43
			C	0.643 ± 0.090	13
ε [-]	BrUPE FRP	0.913 ± 0.03	B	0.909	2
			C	0.960	6
			F	0.831 ± 0.013	9
	MA+A FRP	0.912 ± 0.03	B	0.804 ± 0.020	12
			C	0.856 ± 0.028	6

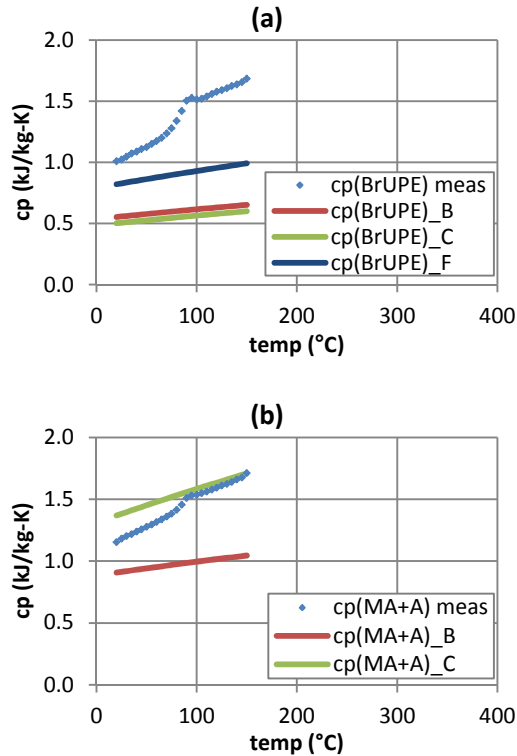


Figure 5. Comparison between measured specific heat values and estimated values from numerical optimization with different kinetic models – B, C and F – for two polymer resin systems of (a) BrUPE and (b) MA+A: Results show that compared to measured values there is some improvement in the estimated specific heat capacity of the resins for a single component system BrUPE and a significant improvement for two-component system MA+A when a more complex kinetic model is used in the estimation process.

From the above analysis, it is shown that when the complexity of the kinetic model increases (model B \rightarrow F) no apparent trend of improvement in the parameter estimations is observed for BrUPE resin/FRP cases. However, there is a significant improvement in the estimations for MA+A resin/FRP cases with respect to increasing kinetic modeling complexity (model B \rightarrow C). This is illustrated by comparing to independent measurements for thermal conductivity, specific heat capacity and emissivity. It is noteworthy that the difference between the estimated values from case C for MA+A resin/FRP material and those of independent measurements are less than the measurement uncertainty and therefore they can be considered as effective property values.

Considering that the fiberglass used in both FRP composites is the same, additional analysis is performed for the following fiberglass properties – thermal conductivity, specific heat capacity and emissivity (see Table 3 and Figure 6). For thermal conductivity of the fiberglass, a reference value for comparison with the estimated values has been calculated based on Eq.1 using measured values for the resin mixture and FRP composite at ambient temperature. The thermal conductivity values estimated for the BrUPE case is 0.0 ± 0.2 W/mK and for the MA+A case is 0.4 ± 0.2 W/mK as volume fraction of the fiberglass in the composite is 0.24 for BrUPE and 0.56 for MA+A FRP case. Because these are the same fiberglass mats used in the two composites, the true thermal conductivity of

the glass is considered to be near 0.2 W/mK where the two reference values overlap. The estimated thermal conductivities from different parameter estimation cases have shown that those from applying kinetic model C for BrUPE FRP case and kinetic model C for MA+A FRP case are the closest to 0.2 W/mK. For specific heat capacity of the fiberglass used in the FRP composites, a reference value of 0.8 kJ/kg-K at ambient temperature is used for comparison, which is found from [24]. Among various estimations of specific heat capacity, those from applying kinetic model F for BrUPE FRP case and kinetic model C for MA+A FRP case are the closest to the reference value. For emissivity of the fiberglass, reference values for comparison have been calculated based on Eq.3 similar to the thermal conductivity case using measured values for the resin mixture and FRP composite. The emissivity value calculated for the BrUPE case is 1.1 ± 0.2 and for the MA+A case is 0.9 ± 0.1 . Knowing that emissivity should range from 0.0 to 1.0 and the reference value from each FRP case should be consistent as they are the same fiberglass mats in two FRPs, the true emissivity of the glass is considered to be within the range 0.9 to 1.0. The estimated emissivities from different parameter estimation cases have shown that those from applying any kinetic model B through F for BrUPE FRP case and applying kinetic model C for MA+A FRP case are within 0.9 to 1.0 range. From the above analysis, when the complexity in a kinetic model increases (model B \rightarrow F) there is no apparent trend in improvement in the parameter estimations for BrUPE FRP cases. However, improvement in the estimations for MA+A FRP cases are observed as illustrated by making comparison to reference values for thermal conductivity, specific heat capacity and emissivity of the fiberglass used in the FRP composites.

Table 3. Comparison of estimated emissivity of glass from parameter estimation exercise conducted for the two composites (BrUPE FRP and MA+A FRP) with different kinetic models: For both materials, as the complexity of applied kinetic model increases from B to F, the estimated emissivity values become closer to 0.9.

Parameter	Material	KM Type	Estimated Value
ε [-]	BrUPE FRP	B	0.959
		C	0.985
		F	0.919 ± 0.014
	MA+A FRP	B	0.846 ± 0.032
		C	0.873 ± 0.041

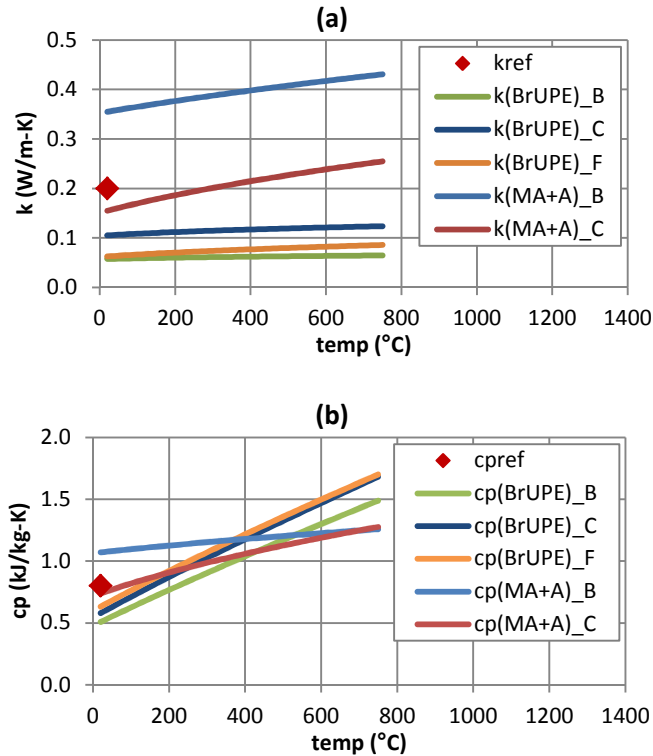


Figure 6. Comparison of estimated (a) thermal conductivity and (b) specific heat capacity values for glass from numerical optimization process with different kinetic models – B, C and F – for two FRP composites of BrUPE and MA+A FRPs: Results show that compared to measured values there is insignificant effect in the estimated thermal conductivity and some improvement in the estimated specific heat capacity of the fiberglass for a single component system BrUPE. However, for two-component system MA+A, there is a significant improvement in the estimation for thermal conductivity and specific heat capacity for fiberglass when a more complex kinetic model is used.

These findings are summarized as follows: (1) Excessively complex kinetic models that can reproduce TGA data with higher precision may result in too many unknowns resulting in unsuccessful parameter estimation using an optimization method which finds no solution for the given problem (e.g. kinetic model F for MA+A composite). (2) For the BrUPE resin/FRP cases, all cases – applying kinetic model B (single step reaction with single heating rate TGA data used for kinetic parameter estimation), model C (single step reaction with multiple heating rate TGA data used for kinetic parameter estimation) and model F (three step reaction to account for decomposition of intermediate species) – were successful in terms of finding an optimum parameter set via numerical optimization method. Comparing the estimated results to reference values for thermal conductivity, specific heat capacity and emissivity of the resin, FRP composite and fiberglass showed that there is no apparent trend in improvement in the estimations with respect to increasing kinetic model complexity. (3) For the MA+A resin/FRP cases, applying kinetic model B (single step with single heating rate TGA data used for kinetic parameter estimation) and model C (two step reaction to account for decomposition of different components (MA and A) in the resin mixture, separately) were successful with parameter estimation using optimization method. Comparing the estimated results to reference values for thermal conductivity, specific heat capacity and emissivity of the resin, FRP

composite and fiberglass showed that there is a significant improvement in the estimations when kinetic model complexity is increased. The increased complexity was to explicitly account for decomposition of the different components in the resin mixture, i.e. the base resin MA and the additive A, with separate reactions. Some of the estimated values of MA+A resin/FRP from case C can be considered as effective property values as the difference between the estimated values and those of independent measurements are less than the reported measurement uncertainty.

The above findings suggest following: (1) With a highly tuned parameter estimation exercise using global, multi-objective and multi-variable optimization method, estimated results will roughly be within $\pm 100\%$ of the measurements. (2) Increasing kinetic model complexity for a single component system as BrUPE to utilize multiple heating rate TGA data when estimating kinetic parameters with a single step global reaction (kinetic model C) or to account for decomposition of intermediate species with additional reactions (kinetic model F) have less influence in parameter estimation. (3) Increasing kinetic model complexity for a two-component system as MA+A to account for decomposition of different components in the resin mixture with separate reactions (kinetic model C) instead of applying a single step global reaction (kinetic model B) results in significant improvement in parameter estimation. (4) Parameter estimation using numerical optimization method with an appropriate level of complexity in the kinetic model used and optimization targets can find estimations that can be considered as effective material property values. (5) Good practice for kinetic modeling for pyrolysis modeling when using parameter estimation via optimization is to utilize the simpler approach of assuming a global single step reaction since increasing complexity results in more model parameters to estimate. However, when a decomposing material is known to be a multi-component system such as the MA+A resin investigated in this study, applying separate reactions for decomposition of each component is desirable since it improves the parameter estimation results to be more consistent with independent measurements.

8. CONCLUSIONS

In this study, parameter estimations for comprehensive pyrolysis modeling [3,8] of brominated unsaturated polyester (BrUPE, single component system) and modified acrylic with fire retardant additive (MA+A, two component system, MA and A) FRP composites are conducted to investigate the ability of global, multi-objective and multi-variable optimization methods to estimate model parameters related to material properties – thermo-physical and optical properties. To conduct meaningful parameter estimation, first, an appropriate kinetic model for describing the thermal decomposition process of the polymer resins needs to be identified. Kinetic modeling is conducted with independent thermal analyses using TGA and DSC experimental data and several kinetic models with different level of complexity have been proposed. Their effect on modeling is evaluated using a screening process that involves simulations of mass loss rate *integrated* over the cross-section at each time step of 1D FRP pyrolysis. The screening process utilizes bench-scale temperature data as a proxy for conservation of energy. Through this procedure, it has been shown that insignificant changes occur in the *integrated* mass loss rate simulation of 1D pyrolysis with respect to changes made in the kinetic model for both FRPs. Knowing this, different

kinetic models – B, C and F – are applied to the parameter estimation process to examine their effect on the estimation with numerical optimization. Second, optimization targets are carefully selected based on the same screening process used to evaluate kinetic models. This procedure showed that data from experiments with low to moderate applied heat flux levels are appropriate. Therefore, parameter estimation is conducted with three different kinetic models, from simple to complex, using optimization targets from Cone Calorimeter experimental data irradiated at 50kW/m². Estimation results are compared with independently measured effective material properties – thermal conductivity, specific heat capacity and emissivity of polymer resins and FRPs. Additionally, fiberglass properties estimated from different parameter estimation exercises conducted for the two FRPs are compared to analyze consistency in optimized values. These parameter estimation exercises have shown the following: (1) With a well-configured parameter estimation exercise using global, multi-objective and multi-variable optimization method, estimated results will be within $\pm 100\%$ of the measurements. (2) Increasing kinetic model complexity for a single component system as BrUPE have less influence in parameter estimation. (3) Increasing kinetic model complexity for a two-component system as MA+A to address decomposition of each component separately results in a significant improvement in parameter estimation. (4) Parameter estimation using numerical optimization method with appropriate level of complexity in kinetic model and optimization targets can find estimations that can be considered as effective material property values. (5) Good practice for kinetic modeling for pyrolysis modeling when used with parameter estimation via optimization method is to apply a simple single step reaction at first as increasing complexity results in more model parameters to estimate. However, when a decomposing material is known to be a multi-component system with different thermal characteristics (e.g. MA+A resin), applying separate reactions for decomposition of each component is desirable as it should improve the parameter estimation results to be more consistent with independent measurements.

9. ACKNOWLEDGEMENTS

The authors greatly appreciate the support for this work from DOC NIST Award Number 60NANB8D8106 (Federal Program Officer Dr. Kevin McGrattan). Special thanks goes to Charles Dore for fabricating and donating FRP composite materials used in this study. Many thanks also to Randall Harris at WPI for conducting the Cone Calorimeter tests.

10. REFERENCES

-
1. Kevin McGrattan, Simo Hostikka, Jason Floyd, Howard Baum, Ronald Rehm, William Mell and Randall McDermott, Fire Dynamics Simulator (Version 5) Technical Reference Guide, NIST Special Publication 1018-5, October 29, 2010
 2. S.I. Stoliarov, R.E. Lyon, Federal Aviation Administration Technical Note, DOT/FAA/AR-TN08/17, 2008; available for download at <http://www.fire.tc.faa.gov/reports/reports.asp>.
 3. Lautenberger, C., Gpyro – A Generalized Pyrolysis Model for Combustible Solids, Technical Reference, Version 0.700, February 19, 2009

-
4. Lautenberger, C, Rein, G., & Fernandez-Pello, C., 2006. The Application of a Genetic Algorithm to Estimate Material Properties for Fire Modeling from Bench-Scale Fire Test Data, *Fire Safety Journal* 41(3), pp. 204-214.
 5. Stoliarov, S.I., Crowley, S., Lyon, R.E., & Linteris, G.T., 2009. Prediction of the Burning Rates of Non-Charring Polymers, *Combustion and Flame* 156(5), pp. 1068-1083.
 6. Chaos M, Khan MM, Krishnamoorthy N, et al. Evaluation of optimization schemes and determination of solid fuel properties for CFD fire models using bench-scale pyrolysis tests. *P Combust Inst* 2011; 33(2): 2599–2606.
 7. Marler, R. T., and Arora, J. S. (2004), "Survey of Multi-Objective Optimization Methods for Engineering," *Structural and Multidisciplinary Optimization*, 26 (6), 369-395.
 8. Lautenberger C and Fernandez-Pello C. Optimization algorithms for material pyrolysis property estimation. *Fire Saf Sci* 2011; 10: 751–764.
 9. Standard Test Method for Heat and Visible Smoke Release Rates for Materials and Products Using an Oxygen Consumption Calorimeter, ASTM E 1354-02, ASTM, 100 Barr Harbor Drive, West Conshohocken, PA, USA
 10. Rick Aster, Brian Borchers, Cliff Thurber, Preface, In: Richard C. Aster, Brian Borchers and Clifford H. Thurber, Editor(s), *International Geophysics*, Academic Press, 2005, Volume 90, Parameter Estimation and Inverse Problems, Pages xi-xii, ISSN 0074-6142, ISBN 9780120656042, DOI: 10.1016/S0074-6142(05)80014-2.
 11. Matala, A., Lautenberger, C., & Hostikka, S., "Generalized direct method for pyrolysis kinetics parameter estimation and comparison to existing methods," *Journal of Fire Sciences* 30 339-356 (2012).
 12. Bal, Nicolas, Uncertainty and complexity in pyrolysis modeling, PhD Dissertation, The University of Edinburgh, 2012, <http://hdl.handle.net/1842/6511>
 13. Kim, E., Dembsey, N., and Shivkumar, S., Evaluating Effects of Applying Different Kinetic Models to Pyrolysis Modeling of Fiberglass Reinforced Polymer Composites, *submitted for review in Fire and Materials Journal*
 14. Standard Test Method for Heat and Visible Smoke Release Rates for Materials and Products Using an Oxygen Consumption Calorimeter, ASTM E 1354-02, ASTM, 100 Barr Harbor Drive, West Conshohocken, PA, U.S.
 15. de Ris, J.L. and Khan, M.M., "A sample holder for determining material properties," *Fire and Materials*, 24, 219-226 (2000).
 16. T. Ozawa, "A new method of analyzing thermogravimetric data," *Bull.Chem. Soc. Jpn.*, vol. 38, pp. 1881–1886, 1965.
 17. J. H. Flynn and L. A. Wall, "A quick, direct method for the determination of activation energy from thermogravimetric data," *J. Polym. Sci. Polym. Lett.*, vol. 4, pp. 323–328, 1966.
 18. H. L. Friedman, "Kinetics of thermal degradation of char-forming plastics from Thermogravimetry. Application to a phenolic plastic," *J. Polym. Sci., Pt. C* 6, 183-195 (1964)
 19. J. H. Flynn, L. A. Wall, "A quick, direct method for the determination of activation energy from thermogravimetric data," *J. Polym. Sci. Polym. Lett.* 4, 323-328 (1966).
 20. Standard Test Method for Steady State Thermal Transmission Properties by Means of the Heat Flow Meter Apparatus, ASTM C518, ASTM, 100 Barr Harbor Drive, West Conshohocken, PA, USA
 21. Standard Test Method for Thermal Conductivity of Solids by Means of the Guarded Comparative Longitudinal Heat Flow Technique, ASTM E1225, 100 Barr Harbor Drive, West Conshohocken, PA, USA
 22. Standard Test Method for Determining Specific Heat Capacity by Differential Scanning Calorimetry, ASTM E1269, 100 Barr Harbor Drive, West Conshohocken, PA, USA
 23. Standard Test Methods for Total Normal Emittance of Surfaces Using Inspection Meter Techniques, ASTM E408, 100 Barr Harbor Drive, West Conshohocken, PA, USA
 24. Hust, J.G., Callanan, J.E. and Sullivan, S.A. (1988). Specific Heat of Insulations. In: Yarbrough, D.W. (ed.), *Thermal Conductivity* 19, pp. 533-550, Plenum, N.Y.

Section 4

PARAMETER ESTIMATION FOR COMPREHENSIVE PYROLYSIS MODELING: GUIDANCE AND
CRITICAL OBSERVATIONS

PARAMETER ESTIMATION FOR COMPREHENSIVE PYROLYSIS MODELING: GUIDANCE AND CRITICAL OBSERVATIONS

E. Kim¹ and, N. Dembsey¹

¹Fire Protection Engineering, WPI

1. ABSTRACT

A process for conducting parameter estimation for comprehensive pyrolysis models is proposed in this study. This estimation process was developed based on the following: (1) parameter estimation is about being consistent, applying engineering common-sense and correctly following the steps in this guide; (2) parameter estimation is conducted by breaking down the problem into groups of unknowns of similar character and considering them separately; (3) parameter estimation is conducted in consideration of an appropriate complexity in model set-up using certain approximations for simplifications; and (4) parameter estimation is conducted with direct measurements of parameters from independent experiments, literature search and/or numerical optimization paired with certain pyrolysis models. Additionally, limitations in parameter estimation are discussed by considering example cases. They are shown to demonstrate how simplifying the microstructure, modeling thermal decomposition kinetics and applying numerical optimization methods affect the estimation results. The process developed is applied to modeling of real-world materials: thermoplastics (PMMA), corrugated cardboard, fiberglass reinforced polymer composites and plywood. Understanding the limitations in parameter estimation, it was noted that (1) the estimated parameter values are compensated by other parameter values in a parameter set allowing optimization method to optimize for multiple optimal, *linked* parameter sets; however, (2) when modeling is well-configured with optimum complexity, the optimized parameter values may become closer to those of independent measurements, highlighting the possibility of utilizing the optimization method to estimate for effective material properties.

2. KEYWORDS

comprehensive pyrolysis modeling; parameter estimation; numerical optimization

3. INTRODUCTION

In recent years with the availability of increased computational power, there has been growing demand for conducting Computational Fluid Dynamics (CFD) simulations in the fire community. Along with this, there has been an increased interest in development of pyrolysis models as sub-models to CFD models that can provide information about solid phase decomposition. Early pyrolysis models used in the fire field were empirical and simple analytical models [1,2] that only considered solids in an aggregate manner. The next pyrolysis models developed were integral models [3,4,5,6,7] where solids were divided into two parts: pre-decomposed and decomposed. Recently, comprehensive pyrolysis models have gained notice [8,9,10]. In comparison to simpler pyrolysis models, comprehensive pyrolysis models have greater flexibility in describing the pyrolysis of a solid

mathematically. The comprehensive models explicitly solve for conservation of mass and energy on the solid. However, they require significant effort in estimating model parameters, because the total numbers of unknown parameters may vary from less than 10 to over 100 for each and every type of solid material of interest. This makes it difficult for users to utilize these models.

Understanding this difficulty in conducting comprehensive pyrolysis modeling, a process of parameter estimation is proposed in this study. This process is applied to four real-world materials – thermoplastic (PMMA), corrugated cardboard, fiberglass reinforced polymer composite, and plywood. Then, limitations in parameter estimation were evaluated by following the proposed process. The effects of simplifying the microstructure, modeling thermal decomposition kinetics independently using thermal analysis, and applying numerical and optimization methods to parameter estimation are examined in detail by showing example cases to illustrate how these modeling assumptions, simplifications and approaches affect parameter estimation results. The work presented in this paper – the proposed parameter estimation process and the example cases – has been formatted to a guide as well [11].

4. BACKGROUND

Comprehensive pyrolysis models are models those account for physical and chemical responses of materials exposed to fire conditions [8,9,10]. These models utilize fundamental conservation equations to describe the changes in a material during its pyrolysis process. Typically, models are constructed to conserve mass and energy when the material is being heated and/or thermally decomposed. Numerical calculations are conducted using various methods – finite difference, finite element, or integral formats where governing equations are transformed to systems of ODEs instead of PDEs using simplifications – to determine mass loss and temperature profiles from the heat exposed front surface to unexposed back surface with respect to increasing time.

Thermal decomposition processes in comprehensive pyrolysis modeling can be modeled by two different approaches – reactions that are infinitely fast or finite. When thermal decomposition is infinitely fast, the pyrolysis front becomes an infinitely thin reaction zone where reactants are consumed instantaneously into products releasing or consuming reaction heat. In this case, heat transfer is considered as a limiting factor for modeling the pyrolysis problem. Typically, a pre-determined pyrolysis temperature is used to locate the pyrolysis front. When thermal decomposition reaction rate is modeled as finite, the pyrolysis front has a finite thickness. Whether a virgin material is pyrolyzed completely (single solid state case) or partially (multiple solid state case) to fuel vapor, the assumption used in this approach allows the model to approximate the pyrolysis kinetics as well as the heat transfer throughout the solid fuel. When pyrolysis kinetics are explicitly considered in modeling, pyrolyzates can be produced at various locations within the pyrolysis front. By performing numerical calculations in these comprehensive pyrolysis models, temperature profiles are obtained for a solid fuel and depending on the local temperature pyrolysis reaction(s) rates are calculated allowing the reactants to be consumed to produce pyrolyzates or other types of solid phase materials with associated energy consumption. Typically, an Arrhenius type expression is used for describing

the pyrolysis kinetics. Some models of this kind consider mass and heat transfer of gases through a decomposed solid phase product layer, which requires additional governing equations to be solved.

Although accounting for physical and chemical mechanisms observed explicitly during pyrolysis is a merit of comprehensive models, difficulties arise when using these models due to the numerous unknown model parameters that need to be estimated by the user. The ability of modeling various aspects of the pyrolysis problem results in greater complexity of the model. Therefore, the numbers of parameters involved in the simulation can dramatically increase, which results in significant effort to estimate the additional unknown parameters.

5. APPLIED PRINCIPALS AND APPROACHES IN DEVELOPING THE PARAMETER ESTIMATION PROCESS

Given all the parameters that are required for modeling, it is very likely that unknown parameters will need to be estimated to perform pyrolysis simulations. This process is called parameter estimation. A guide is proposed in this study to find an appropriate approach to estimating parameters for comprehensive pyrolysis modeling. There are 4 major principals and approaches taken in developing this guide: (1) parameter estimation is about being consistent, applying engineering common-sense and correctly following the steps in this guide; (2) parameter estimation is conducted by breaking down the problems into groups of unknowns of similar character and considering them separately; (3) parameter estimation is conducted with consideration to an appropriate complexity chosen for pyrolysis modeling; and (4) parameter estimation is conducted with measurements of parameters from experiments and/or numerical optimization paired with certain pyrolysis models.

Consistency, Common-sense and Correctness

Due to the complexity of the parameter estimation problem, there is no simple right or wrong answers to estimating unknown model parameters. Therefore, a guide for estimating model parameters is prepared in this study based on the following principals. First, the guide is to allow users to estimate unknowns in a consistent manner. Second, the guide is developed based on common-sense. Third, the guide provides enough detail to allow the users to correctly follow along.

Breaking Down the Problem into Groups

When estimating parameters, a complete list of model parameters should be created first. It is good practice for users to build their model parameter list by certain groups or categories considering their characteristics. Model parameters are related to heat transfer, mass transfer and thermal decomposition kinetics. Parameters can be grouped into (1) parameters related to modeling **thermal decomposition** process; (2) **material properties** that are *intrinsic*, i.e. they depend on chemical and physical structure of the material or *effective* due to neglecting actual microstructure of the material and considering the material as homogeneous; and (3) **model-dependent fitting parameters**, which are not material properties but parameter constants that provide the best fitness of model output to experiment results.

Parameters used in **thermal decomposition** modeling are the pyrolysis onset temperature for applying the infinitely thin reaction zone assumption or kinetic parameters for applying the finite thickness reaction zone assumption, and reaction heat. In general, good practice is to determine these by independent kinetic modeling. Parameters in this group are crucial as they structure the problem by setting the number of decomposition reactions. For example, consider decomposition as “virgin \rightarrow char + gas”. In this case, as a result of this one-step kinetic modeling with two solid phase species, estimation of model parameters of material properties are needed for virgin and char. **Material properties** can be considered in three groups: (1) thermo-physical properties – density, thermal conductivity and specific heat capacity; (2) porous media characteristics – porosity and permeability; and (3) optical properties – absorption coefficient and emissivity. Material property parameters are “ideal” when they are measured by independent experiment. However, there are limitations and disadvantages in direct or indirect measurements, which will be discussed below. An example of a **model-dependent fitting parameter** is “ γ ” used in GPYRO [10], where this parameter governs the effective conductivity attributed to radiative heat transfer across pores. Parameters in this group are only obtainable through optimization rather than measurements, as they are directly linked to the pyrolysis model of use. With an understanding of these model parameters for each group, an estimation strategy can be planned for each parameter.

Determining Appropriate Complexity of the Problem

Depending on the complexity of the modeling approach, the total number of model parameters that need to be estimated may vary. There is a tradeoff between increasing modeling complexity to define the material of interest more precisely and increasing effort necessary to estimate the model parameters. For example, consider having more than one reaction in kinetic modeling. If one global decomposition reaction is broken into two elementary reactions to be more precise in reproducing the DTG (mass loss rate) curve from TGA experiments, the list of model parameters that need to be estimated will be doubled to 4 species. Therefore, determining the appropriate level of complexity for modeling is important for parameter estimation. Some of the questions that need to be answered are – Should a material’s cross-section be modeled as a homogeneous single layer or heterogeneous multiple layers? How many reactions are necessary for modeling thermal decomposition kinetics of the material of interest? Should some of the material properties be considered as constants or temperature dependent parameters? Are there any possible approximations that can be made to simplify the material’s fire behavior (e.g. emissivity of charred surface approximated as 1)? A rule of thumb for determining the appropriate complexity level in modeling is as follows: start modeling with the simplest approach and apply additional complexity to the problem when simulation results deviate from experimental bench marks in a significant manner. the needed level of complexity should reduce the differences between simulations and experiments to a non-significant level. This requires some trial and error exercises; however, once the user has enough experience in how things change in the modeling outputs with respect to certain variations in model parameters, finding a good balance between modeling complexities with its gains becomes less challenging.

Measurements and/or Numerical Optimization

Parameter estimation can be conducted using three different approaches: (1) measuring each parameter via independent experiment; (2) searching the literature for measurement values of similar materials or use approximations; (3) conducting numerical optimization by pairing a pyrolysis model with an optimization routine. The above approaches can be used by itself or in pair to estimate the entire unknown model parameter set.

When the unknown parameters are estimated by measurement using independent experiments, typically small-scale experiments are used based on standard tests such as ASTM or ISO. This approach only allows measurement of model parameters related to material properties and modeling thermal decomposition kinetics. In general, estimating parameters by measurements is challenging due to the following reasons: First, it is noteworthy that material parameters obtained through this approach are not always *intrinsic*, but in many cases are *effective*. Due to the limited sample size used in small-scale tests, material parameters measured via independent experiments are generally accepted as *intrinsic*. However, in many cases for real world heterogeneous materials, the material parameter measured becomes *effective*. Because, the small amount of sample used in these tests are treated as homogeneous by neglecting the heterogeneity of the material. Second, there may be a disconnection between the model parameter obtained in a small-scale experiment and the model parameter required by the pyrolysis model. For example, a naturally high-charring phenolic resin decomposing during a Thermogravimetric Analysis (TGA) experiment in a powder form – a typical approach when conducting TGA experiment to reduce thermal lag– cannot represent decomposition of this same material in a bench-scale calorimeter test as a flat surface. The resin prepared in a powder form results in significantly larger surface area (interface) exposed to the gas phase per unit mass or volume. On the other hand, resin prepared as a flat surface has relatively smaller surface area exposed to the gas phase per unit mass or volume. This difference results in great deviation when comparing thermal decomposition of this material, because the smaller surface area per unit mass or volume is proportional to formation of more thermally stable carbonated char during decomposition. For example, a neat phenolic resin tested in the TGA under air environment at 20°C/min iso-heating rate with sample particle size of 0.5 mg results in 57% loss by weight at 600°C, while the same material tested with sample particle size of 2.2 mg results in 36% loss at 600°C. Obtaining kinetic parameters from a TGA experiment using a powder type sample and applying them to pyrolysis modeling to describe thermal decomposition occurring on a flat surface results in the parameters being *effective*. Third, material parameters required in pyrolysis modeling during material decomposition cannot be measured via independent experiments. Typically when measuring material parameters in small-scale experiments, decomposition of the sample is considered to be undesirable. Because the gases from decomposition may affect the measurements, which makes it impossible to make measurements for parameters of intermediate species involved in kinetic modeling. Fourth, measuring material parameters and conducting thermal analysis for modeling thermal decomposition kinetics through a commercial laboratory require significant time and financial investment.

Another approach to estimating model parameters is searching through the literature for measurement values of similar materials or using certain approximations. Although using this approach is most practical (because it is less time-consuming and inexpensive), caution should be given to the following: First, understanding the

material and its condition is essential. Certain polymers may have the same nomenclature, but depending on their polymer chain size, length and shapes, its character, e.g. thermal conductivity [12], may vary. The same material with higher moisture containment may show different thermal decomposition kinetics, because water molecules physically and/or chemically interfere in the process [13]. The same material with significant aging – e.g. scratches, cracks, etc. – may start to decompose at a lower temperature than that without aging [14]. These are some examples of how a material and its condition during experiments can affect the measurement results. Second, consideration of model parameter sensitivity and uncertainty is needed. In addition to the uncertainty reported for the measurement value in the literature, a greater uncertainty should be taken into account when using that value in pyrolysis modeling, as two “similar” materials may have subtle differences physically or chemically as noted above. Also, when approximation is used to estimate certain model parameters for simplification of the problem, the user should be aware of the sensitivity of that parameter on modeling outputs of interest and check whether small changes to the approximated parameter value significantly alter the modeling results or not.

The third approach of estimating model parameters is conducting numerical optimization by pairing a pyrolysis model with manual optimization or an optimization routine [15,16,17,18,19,20]. To overcome the limitation in estimating parameters through measurements (first approach) or by literature search or approximations (second approach), the unknowns in pyrolysis modeling can be obtained by comparing modeling outputs with optimizing targets – experimental data such as mass loss rate and temperature profiles from bench-scale test results. Then find the optimum parameter set that provides the best fitness to the target. When unknown parameters in a pyrolysis model are estimated by comparing certain modeling outputs with a target, using numerical optimization, this is considered as an inverse problem. These inverse problems in pyrolysis modeling are difficult to solve due to the following reasons [21]: First, when the data contains noise or the mathematical model does not account for important physics and/or chemistry of the real problem, there may be no optimum that fits the data exactly, i.e. the solution to the problem may not exist (existence of solution). In other words, when data uncertainty is high and/or the model is too simplified, the model solution may not be determined through this process [22]. For example, when model parameters are estimated by utilizing this approach for certain laminated fiberglass reinforced polymer (FRP) composites with relatively high glass content, successful optimization for the parameters separately for the two components of the composite, resin and fiberglass mats, may be unsatisfying because the variation in mass loss rate data used as targets generally do not show the effect of the alternating layers of resin and fiberglass mats in the composite. Second, even when a solution is found, it may not be unique (uniqueness of solution) [22,24]. This occurs usually when the data used in solving the problem is significantly smoothed or biased. Also, it may occur due to the compensating effects that exist among model parameters. Therefore, multi-objective/variable numerical optimization routines are typically able to converge to many near optimal solutions for these characteristics of the problem (see example cases). In resolving this problem, a typical approach is to reduce the total number of unknowns by fixing the unknown parameters to some values utilizing other approaches discussed previously, then conducting numerical optimization for all the parameters. Third, inverse problems are, in most cases, ill-posed, where a small change in a solution can lead to an enormous change in the modeling output. It is known as the instability problem of a solution (instability of solution) [21]. Therefore, an effort should be given to check the

applicability of the solution upon extrapolation to other modeling conditions not considered during numerical optimization knowing that this may result in significant deviation from actual phenomena [23]. Fourth, the optimized parameters should be considered as a *linked* parameter set, in general. Once numerical optimization is used, the optimized parameter value takes into account any assumptions used in pyrolysis modeling, all the intrinsic or effective parameter values with their uncertainty which were obtained through other means, etc. Hence, an optimized value for one parameter may not be used for other pyrolysis modeling cases. However, sometimes when the estimation is conducted carefully with appropriate kinetic model and optimization targets, the estimated values may be considered to be effective properties [24]. This is possible when the estimated values are significantly close to the measured ones, i.e. the difference between the estimated and measured values are within the limit of measurement uncertainty. Last, when applying this method, the estimation process can become confusing. Without a consistent approach it can lead to unsatisfying results.

6. PARAMETER ESTIMATION PROCESS

This work is focused on presenting a process for estimating model parameters that allows users to conduct parameter estimation based on commonsense, consistency and correctness. The process of parameter estimation can also be considered as an exercise of creating a virtual material in comprehensive pyrolysis models. This process is composed of the three approaches discussed above: (1) measuring each parameter via independent experiment; (2) searching literature for measurement values on similar materials or use of approximation; (3) conducting numerical optimization by pairing a pyrolysis model with an optimization routine. In addition to these, consideration of the uncertainty of estimation of each model parameter and its propagation into the pyrolysis modeling uncertainty is given in the context of defining the criteria for satisfying or unsatisfying parameter estimation. Typically, estimation based on measurement of the maximum possible number of parameters will be considered first. Then estimate parameters by literature review, as they can become practical constraints when conducting numerical optimization for solving unknowns. Therefore, estimation based on use of a numerical optimization routine in pair with pyrolysis modeling will be considered as the last option.

To create a virtual material in comprehensive pyrolysis models, the following tasks must be considered:

Step 1: Create the microstructure of the virtual material

Step 2: Identify the decomposition kinetics type

Step 3: Create a list of model inputs

Step 4: Obtain the model unknown inputs via measurement or literature search

When the above tasks are done and every unknown has been estimated, validation work is needed to understand the performance of the estimated parameter set:

Step 5: Run model

Step 6: Analyze simulation quality with consideration of uncertainties in modeling outputs and data

Step 7: Add commentary

When there are additional unknowns that need to be estimated, the users may conduct optimization in pair with the pyrolysis model. This process of obtaining unknowns via optimization should be followed by validation work as well. Obtaining parameters using an optimization and validation process should include the following:

Step 8: Run model in pair with optimization

Step 9: Analyze simulation quality with consideration of uncertainties in modeling outputs and data

Step 10: Validate simulation quality upon extrapolation

Step 11: Add commentary

When presenting the parameter estimation results, three summary tables will be introduced: Model Parameters, Validation and Commentary sections. The Model Parameters section includes the model parameters necessary to conduct pyrolysis modeling, their estimated values, and methods of estimating the unknowns. The Validation section consists of the following information: description of modeling goal, pyrolysis model type and modeling approach used in the exercise, experiment type and its data used to compare data to modeling outputs or optimize for unknowns, and uncertainty information of experimental data and modeling outputs. The Commentary section discusses any limitations of pyrolysis modeling conducted above, which has been summarized in the Model Parameters and Validation sections. For better visualization of the problem, a flowchart can be used (see Figure 1).

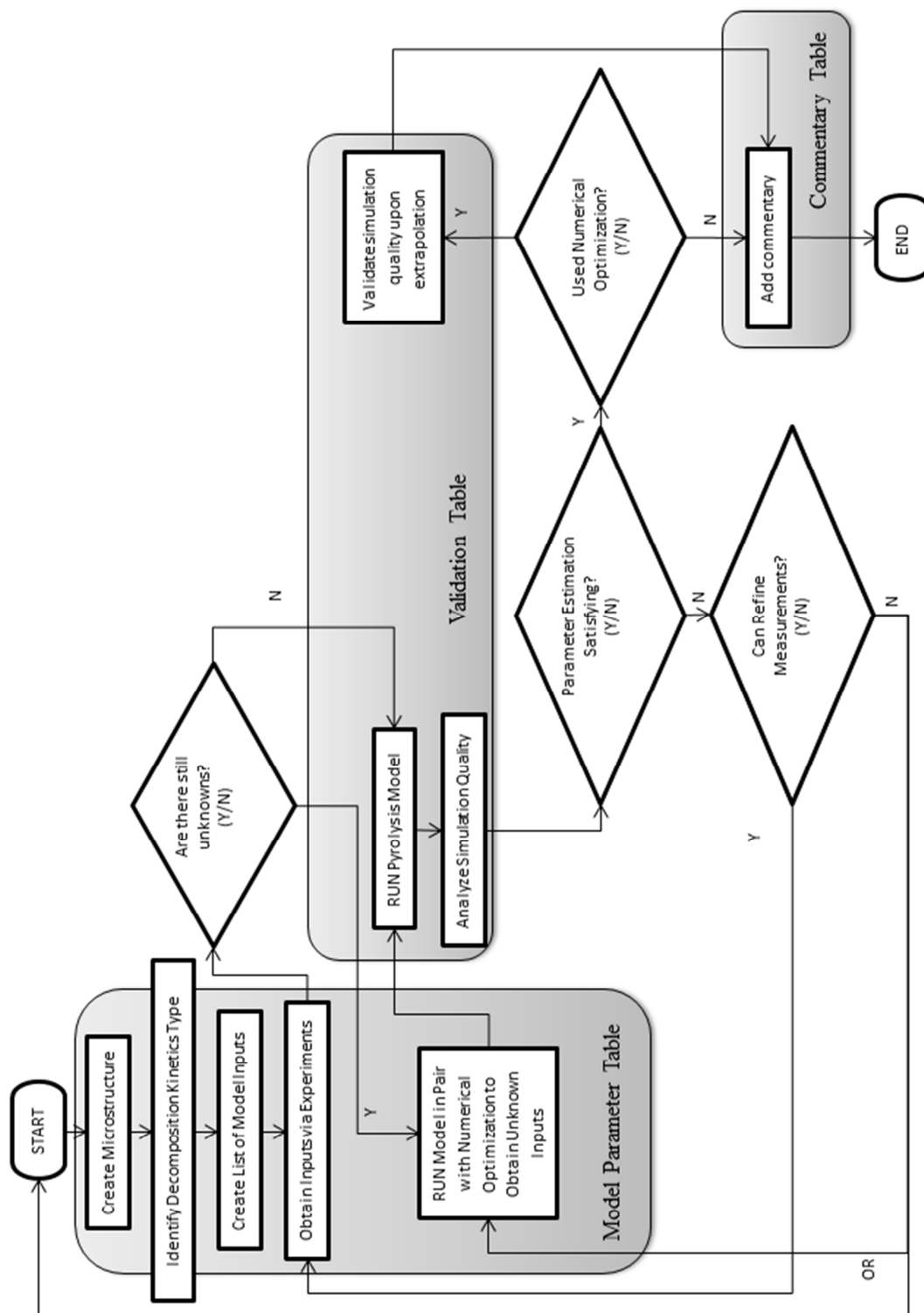


Figure 1. Flow chart of parameter estimation for comprehensive pyrolysis models

7. DIFFERENT OPTIMIZATION METHODS

There are two types of optimization methods applied in the examples: manual optimization or numerical optimization routines. The manual optimization can be done for simple cases, e.g. estimating unknown parameters for two solid phase species involved in one-step thermal decomposition kinetics; however, it requires many iterations of trial and error. Rules of thumb for conducting manual optimization are as follows. Consider having optimization targets as experiment data from bench-scale tests such as the mass loss rate and temperature at various depths, which is a typical case. First, conduct kinetic modeling independently to understand at what temperatures each species will exist. Assume that the decomposition reaction occurs at temperatures between T_a and T_b where $T_a < T_b$. Any changes made in parameters related to reactants should affect fire behaviors at temperature smaller than T_a and any changes made in parameters related to products should affect behaviors at temperatures greater than T_b (see (a) in Figure 2). Second, understand that any changes made in heat of reaction (HoR) affects the mass loss rate peak. When HoR is reduced, the peak becomes taller (see (b) in Figure 2). Third, understand that thermal conductivity (k) affects the temperature gradient throughout the specimen thickness. Reducing k results in a wider spread between the surface and the back surface temperature profiles (see (c) in Figure 2). Fourth, understand that specific heat capacity (c_p) determines how soon a material heats up, i.e. increases its body temperature. Applying smaller c_p results in faster increase in temperature profiles throughout, from surface to back surface (see (d) in Figure 2). Last, for estimating optical properties, apply simple approximations, e.g. having emissivity equal to 1 for surfaces that are close to black or quickly becomes black after exposure to radiative heating. Knowing these tips helps conducting manual optimization for estimation of unknown model parameters.

For numerical optimization routines, there are three types that had been applied to fire pyrolysis modeling so far and they were applied for the parameter estimation exercise conducted in this study also – genetic algorithm (GA) [15,16], shuffled complex evolution (SCE) [17,18,19] and stochastic hill-climber (SHC) [20]. These are evolution optimization schemes with high efficiency and robustness that allow multi-objective and multi-variable optimization under limited knowledge of the problem. All three optimization routines can be considered in terms of four processes: (1) Initialization of individuals, which refers to the set of initial guesses of unknown parameters; (2) Evolutionary process of selection and reproduction – selection from population for reproduction conducted for individuals with good fitness, i.e. better adaptation to their environment and reproduction resulting in new generation derived from a previous one while ensuring convergence, i.e. increase in fitness; (3) Termination of evolution at a user-defined termination condition.

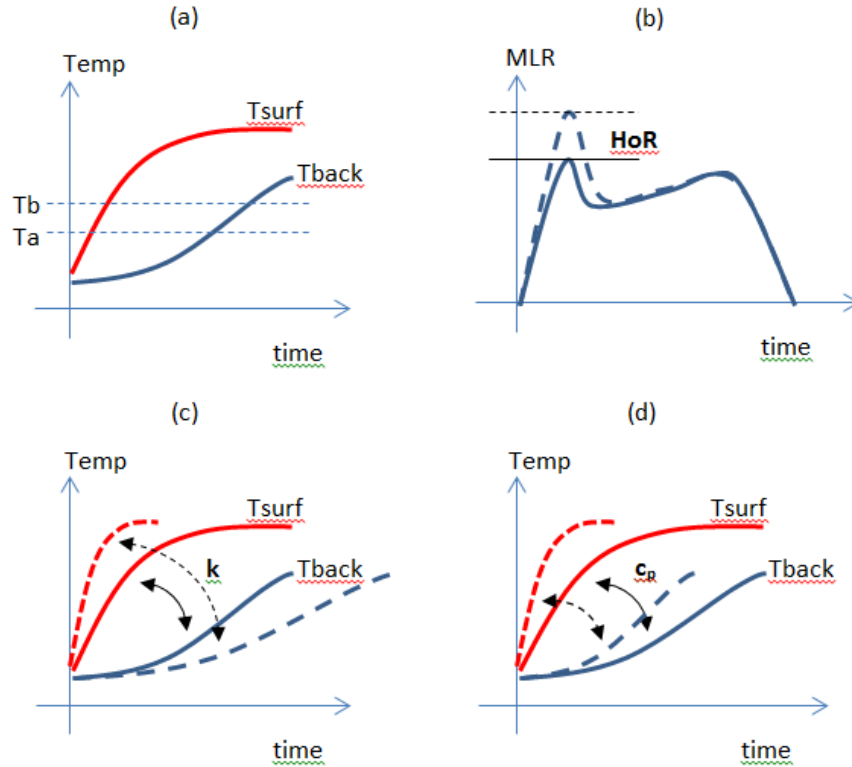


Figure 2. Understanding manual optimization: (a) For a one-step thermal decomposition kinetics that takes place within temperature range of $T_a < T < T_b$, changing parameters related to reactants should affect fire behaviors at temperatures below T_a and changing parameters related to products should affect fire behaviors at temperatures above T_b ; (b) Reducing HoR increases mass loss rate peak; (c) Reducing thermal conductivity results in wider spread between T_{surf} and T_{back} ; (d) Reducing specific heat capacity results in faster increase in temperature throughout. Note that results from greater parameter value are shown in solid lines, while those from smaller value are shown in dashed lines.

8. LIMITATIONS IN PARAMETER ESTIMATION

Although parameter estimation is carefully conducted following the process discussed above, consideration should be given to what each estimated parameter value means. The parameter estimation process gives guidance to apply desirable model assumptions and simplifications, before users begin to estimate the parameter values of the problem. This means the estimated parameter values incorporate the effect of how the problem was set up to conduct parameter estimation. Therefore, depending on how the modeling was set up, the same parameter for the same material may result in different estimations. In the following, discussions of the microstructure, kinetic modeling and numerical optimization effects on parameter estimation results are given to illustrate the limitations in estimated results.

Microstructure Effect

Generally, in FPE practice, heterogeneous materials are assumed to be a homogeneous mixture of components, when pyrolysis modeling is conducted for simplification of the problem. However, when the microstructure effect of the material on parameter estimation for pyrolysis modeling is neglected, inconsistency may be observed in parameter estimation for the same material component existing in different materials. For example, consider estimating the fiberglass thermal conductivity simply from thermal conductivities of polymer resin and fiberglass reinforced polymer (FRP) composite at the pre-decomposition stage at ambient temperature. Knowing the thermal conductivity values of the polymer resin and FRP composite measured from independent tests, thermal conductivity of the fiberglass may be estimated by considering the volume (X) fractions of resin and fiberglass in the FRP composite: $k_G = (k_{FRP} - X_R k_R) / X_G$ [8,9,10]. Although the composite has alternating resin and fiberglass layers laminated, this approach of estimating thermal conductivity assumes a homogeneous mixture of resin and fiberglass in the composite. This exercise is performed for the following two FRP composites – brominated unsaturated polyester (BrUPE) and modified acrylic with fire retardant additive (MA+A) FRP composites – with the same fiberglass used in the lamination. As shown in Figure 3, the estimated thermal conductivities of the same fiberglass are 0.4 ± 0.2 W/mK for the BrUPE FRP case and -1.0 ± 1.2 W/mK for the MA+A FRP case. The uncertainty band of estimated thermal conductivity of fiberglass can be found by considering the uncertainty limits of standard measurements, which were reported as ± 15 to 16%. Uncertainty calculations are performed with $\pm 20\%$ to be more conservative. Considering that the negative values are non-physical and both estimations are for the same fiberglass mats used in different FRPs, the actual thermal conductivity of the fiberglass should be near 0.2 W/mK where the two estimations overlap. This value is the lower limit of the estimation for the BrUPE FRP case and the upper limit of the estimation for the MA+A FRP case. Therefore, it shows that when microstructure effects are neglected by assuming the material is a homogeneous mixture of different components, parameter estimations for each component, e.g. thermal conductivity of fiberglass, may be non-physical (negative mean) or have a narrow overlap between two estimations. The above example shows this is true even for estimations solely with measured values from standard tests.

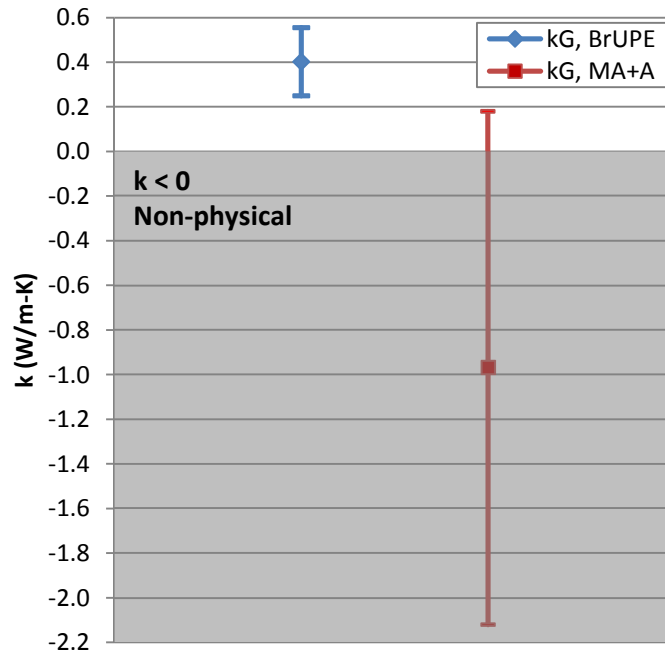


Figure 3. Thermal conductivity of fiberglass estimated from measured thermal conductivities of polymer resin and fiberglass reinforced polymer (FRP) composite and volume (X) fraction of resin and fiberglass. The solid fill of the markers indicate the mean and the uncertainties are considered with unfilled markers. When $k < 0$, estimation is considered to be non-physical.

Kinetic Modeling Effect

To understand the kinetic modeling effects on parameter estimation, thermal decomposition during pyrolysis should be considered first. Typical materials under decomposition with respect to one-dimensional heating of the solid phase material from the surface with a known heat flux of \dot{q}'' is shown in Figure 4 and can be considered similar to that of a bench-scale calorimeter experiment. Assumptions are that the solid material is porous and a gas phase reactant is required for decomposition. When a material is exposed to heating from one side (surface), the decomposition process can be expressed in 7 stages (A \rightarrow G) [25]. First, diffusion of the gas phase reactant needs to occur through a boundary layer from the gas phase to the solid phase (A). The gas phase reactant needs to continue to diffuse through the voids in the porous solid phase (condense phase) to locate the solid particle where reaction will be occurring, which is located within the reaction zone with a finite thickness (B). This is known as the intra-particle diffusion. After locating the solid particle, adsorption of the reactant occurs at the reaction site, i.e. the reactant is diffusing through the solid particle to find other active reactant(s) (C). With all the reaction participants at the reaction site, chemical reaction occurs, which can be considered as “intrinsic” (D). The gas phase product(s) resulting from this reaction need to diffuse through the solid particle (condense phase) to be set off to the gas phase (E). This process is desorption of the gas phase products. Additionally, intra-particle diffusion of the products occurs following the desorption (F). At the end, products need to diffuse through the boundary layer to enter into the bulk gas phase (G).

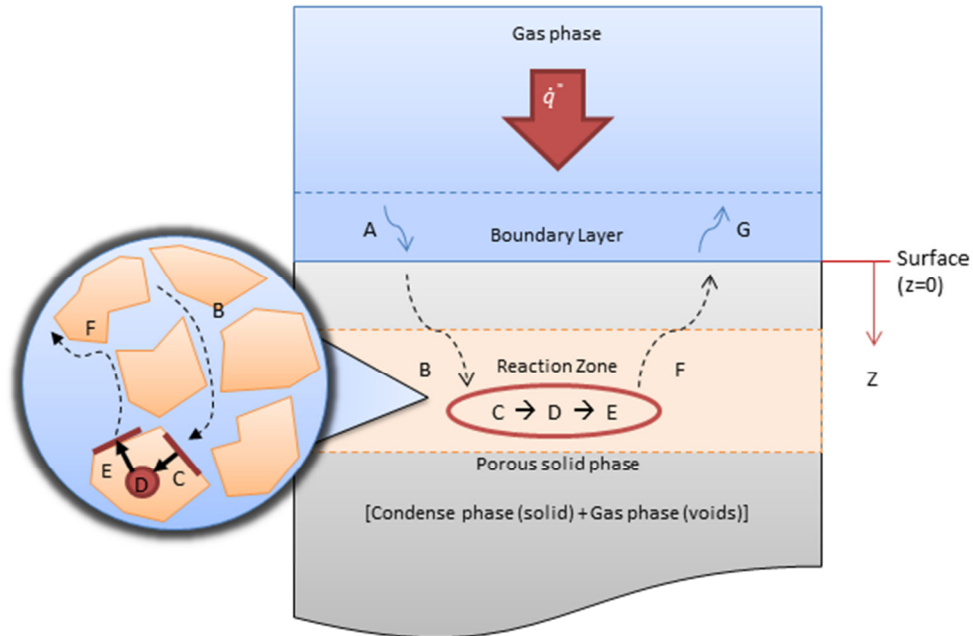


Figure 4. Actual pyrolysis phenomenon of a porous solid phase material under one-dimensional heating

Understanding these 7 stages of thermal decomposition in a slab, one may consider how they are simplified in the well-known comprehensive pyrolysis models: the pyrolysis model in FDS [8], Thermakin [9] and GPYRO [10] (see Table 1). First, in the case of FDS's pyrolysis model, the 7 stages of decomposition process are lumped into one where everything is represented by a process of decomposition chemical reaction. This model allows transformation of a single solid phase component into another type of solid phase component and/or volatiles that are freely released to the bulk gas phase above the solid phase surface. Second, for Thermakin, the 7 stages of decomposition process are reduced to modeling the decomposition chemical reaction with gaseous products transfer due to concentration gradient ($D \rightarrow F$). In this model, decomposition kinetics are assumed to be a single solid phase component or two solid phase components together becoming another type of single or two solid phase component(s) and/or volatiles. Third, GPYRO includes three out of 7 stages – intra-particle diffusion of the gaseous reactant, chemical reaction and intra-particle diffusion of the gaseous products ($B \rightarrow D \rightarrow F$). Additionally, GPYRO has the most flexibility in defining chemical reactions – reactions can be heterogeneous (gas phase – condense phase) or homogeneous (gas phase – gas phase).

Table 1. Summary of thermal decomposition process utilized in three comprehensive pyrolysis models – pyrolysis model in FDS, Thermakin and GPYRO: process in red is accounted for in each model

Model Type	Decomposition Process
FDS	$A \rightarrow B \rightarrow C \rightarrow D \rightarrow E \rightarrow F \rightarrow G$
Thermakin	$A \rightarrow B \rightarrow C \rightarrow D \rightarrow E \rightarrow F \rightarrow G$
GPYRO	$A \rightarrow B \rightarrow C \rightarrow D \rightarrow E \rightarrow F \rightarrow G$

Although different models have their own ways of describing the decomposition processes of a solid phase material, every model assumes that the parameters in their kinetic model can be determined through independent kinetic modeling using thermal analysis. All models assume that the model's discretized unit is equivalent to a TGA (or equivalent) sample. Throughout the sample, for the first two models – FDS and Thermakin – the decomposition chemical reaction rate is determined based on the temperature and the mass fraction of this unit only. For GPYRO, this rate is determined based on unit's temperature, mass fraction and availability of gaseous reactant(s), when reactions involving gaseous reactant(s) are utilized. These assumptions and simplifications in describing the thermal decomposition kinetics for pyrolysis modeling should have certain effects on parameter estimation process, and they are illustrated with examples below.

First, in some cases, the effect of thermal decomposition processes neglected in pyrolysis modeling is considerable. For example, consider taking kinetic modeling results from independent thermal analysis of modified acrylic with high-charring inorganic fire retardant additive polymer resin and applying to pyrolysis modeling of fiberglass reinforced polymer (FRP) composite [26]. Based on thermal analysis using TGA and DSC experiments, thermal decomposition of the additive in this polymer resin sample was found to be diffusion controlled, i.e. process E in Figure 4 is the rate determining factor. General guidance in conducting experiments with this type of material is to significantly reduce the sample particle size used in TGA or DSC to eliminate or limit mass transfer effects on thermal decomposition. Following the above, the kinetic model estimated from thermal analysis should be free of process E affecting decomposition. However, when this kinetic model is applied to model pyrolysis of the FRP composite using a pyrolysis model that assumes negligible mass transport effect on decomposition (C and E in Figure 4) as discussed previously and the results are compared with bench-scale pyrolysis data, the effect of neglecting process E in both kinetic and pyrolysis models is identified in [26]. As shown in Figure 5, good agreement between modeling and data can be found when modeling pyrolysis at lower heating rates (applied heat flux of 25 and 50 kW/m²), where enough travel time is given for mass transfer with respect to temperature increase. Poor agreement between modeling and data is found, when modeling pyrolysis is done at higher heating rates (applied heat flux of 75 kW/m²). In this case shorter travel time is given for mass transfer with respect to temperature increase. Therefore, when parameter estimation is conducted for this case, the estimated model parameter values implicitly account for the effect of process E in actual pyrolysis, because it was considered to be negligible in both kinetic and pyrolysis modeling.

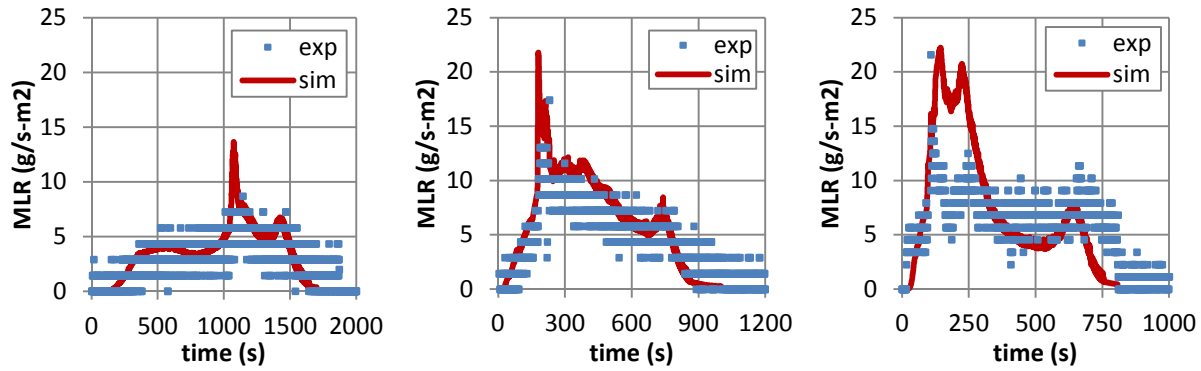


Figure 5. Mass loss rates from Cone Calorimeter experiments (exp) and simplified comprehensive pyrolysis modeling (mod) and are shown for MA+A FRP composite. Applied heat flux levels are 25 (left), 50 (middle) and 75 (right) kW/m². Good agreement between experiment data and modeling results is found from the cases with applied heat flux level of 25 and 50kW/m². Deviation in simulation occurs from experiment data at 75 kW/m² case near the initial peak in the mass loss rate ($t < 300$ s).

Second, in many cases, increasing complexity in kinetic modeling for describing thermal decomposition reaction (D) results in insignificant effect on overall pyrolysis modeling [26,27]. For example, consider taking kinetic modeling results from independent thermal analysis of a thermosetting polymer resin – brominated unsaturated polyester –, and applying to pyrolysis modeling of the fiberglass reinforced polymer (FRP) composites [26]. In general practice for thermal analysis, increasing fitness to thermograms from TGA or DSC by increasing complexity in kinetic model is favored to study the decomposition mechanism in detail. To understand the effect of kinetic model complexity in pyrolysis modeling, various kinetic models are considered – single- or multi-step mechanism and zero-, first- or nth-order reaction model in Arrhenius expression: model A through F, from the simplest to the most complex (see Table 2). Based on this work, it was shown that increasing complexity in kinetic model to account for various aspects of decomposition behavior had an insignificant impact on the simulated *overall* mass loss rate at low to moderate applied heat flux levels (see Figure 6). Although kinetic model case A shows a large scatter in the simulated mass loss rate near the peak and the beginning stage of the final decay, other models produce similar MLR curves independent of the kinetic modeling approach. Therefore, when parameter estimation is conducted for these materials, increasing kinetic model complexity (increasing unknown parameters) to increase fitness to TGA data only results in incremental improvements to modeling outputs.

Table 2. Different kinetic models considered in this study

Model	Model Assumptions / Data	Model	Model Assumptions / Data
A	1 zero order rxn/constant DTG	D	1 or 2 nth order rxn/multi-heating rate
B	1 first order rxn/ peak DTG	E	3 or 4 first order rxn/multi-heating rate
C	1 or 2 first order rxn/multi-heating rate	F	3 or 4 nth order rxn/multi-heating rate

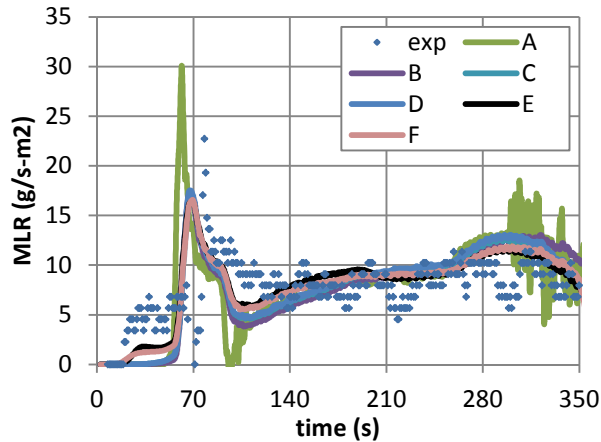


Figure 6. Mass loss rates from Cone Calorimeter experiments (exp) and simplified comprehensive pyrolysis modeling with different kinetic models (A through F) and are shown for BrUPE FRP composite at applied heat flux level of 50 kW/m^2 . Generally, good agreement between experiment data and modeling results are found for all cases (A through F) except for case A where a large scatter is found near the mass loss rate peak and at the end of the simulation.

Numerical Optimization Effect

As mentioned in the previous section, conducting parameter estimation is solving an inverse problem, i.e. applying multi-objective, multi-variable numerical optimization routines to a pyrolysis model of choice to estimate unknowns iteratively, is challenging due to the following reasons: existence, uniqueness and instability of solutions. Hence, whenever parameter estimation is conducted with these numerical optimization methods, the problem should be carefully constructed in terms of applying an appropriate kinetic model representing the actual decomposition process in slab pyrolysis, use of experimental data for optimization targets which have behavior consistent with the model formulation, etc. With a well bounded parameter estimation exercise with appropriate kinetic model and optimization targets, the estimated results using numerical optimization method have been shown to produce good correlation with the measured values [24]. In this reference, parameter estimation exercise is conducted for two material systems: single component brominated unsaturated polyester (BrUPE) fiberglass reinforced polymer (FRP) composite and two components modified acrylic with high charring additive (MA+A) fiberglass reinforced polymer (FRP) composite. The study shows that the estimated results are within $\pm 100\%$ of the measurements, considering thermal conductivity, specific heat capacity and emissivity of the resin or FRP. Additionally, increasing kinetic model complexity for the single component system BrUPE gives less influence in parameter estimation. However, increasing kinetic model complexity for the two-component system MA+A to address decomposition of each component separately results in a significant improvement in parameter estimation. For this case of MA+A, some of the difference between the estimations and measurements are within the limit of the measurement uncertainty, and therefore the estimated values via numerical optimization can be considered as effective material property values.

9. APPLICATION TO REAL-WORLD MATERIAL PROBLEMS

The parameter estimation process introduced above has been applied to create virtual materials for the following real-world materials – PMMA, cardboard, fiberglass reinforced polymer composite and plywood. These materials are selected to cover a wide range of material groups. PMMA is a thermoplastic and has been used in pyrolysis studies frequently for its homogeneous characteristics and relatively simple pyrolysis behavior. Corrugated cardboard is a cellulose material that is widely used as a packaging material. Fiberglass reinforced polymer composite is considered to study parameter estimation for pyrolysis of a mixture of different components, in this case thermally decomposing polymer and inert fiberglass. Plywood is a wood composite product with wood and thin resin alternating layers laminated with pressure.

Applying the first two steps in the parameter estimation process, these materials are assumed to have homogeneous cross-section (step 1). Their thermal decomposition has been assumed to be a single- or two-step reaction without or with residue production (step 2). The lists of model inputs are shown in Table 4 through Table 7 with the estimated values (step 3). The estimation approaches applied for the example materials were mostly non-optimization (i.e. independent measurements or literature search, step 4), comparable non-optimization and numerical optimization, mostly numerical optimization, or manual optimization (see Table 3). When all of the unknowns are estimated through independent measurements or literature search (step 4), step 5 through 7 are conducted. When there are additional unknowns estimated based on optimization, step 8 through 11 are conducted. Details of the analyses are found in Ref [11]

Table 3. Overview of material examples used in parameter estimation process for comprehensive pyrolysis models

Material Example	PMMA	Corrugated Cardboard	Fire Retarded FRP Composite	Plywood
Case Description	Single-step Decomposition RxN w/o Residue	Single-step Decomposition RxN w/ Residue	Two-step Decomposition RxN w/ Residue	Drying and Single-step Decomposition RxN w/ Residue
Estimation Approach	Mostly Non-optimization	PMMA – A		
	Comparable Non-optimization and Optimization	PMMA – B	Cardboard – B	Composite – B
	Mostly Optimization	PMMA – C	Cardboard – C	
	Manual Optimization			Plywood – D

Results and Discussion

Parameter estimation results with good agreement with data are shown in Figure 7, Figure 8, Figure 9 and Figure 10 and the estimated values are summarized in Table 4, Table 5, Table 6 and Table 7. They are parameter estimation for pyrolysis modeling of PMMA, triple layered corrugated cardboard, fiberglass reinforced polymer (FRP) composite with modified acrylic resin with high-charring fire retardant additive and plywood, respectively. For each material, experimental data and simulation results are shown for mass loss rate and temperature profiles at surfaces at three different heat flux levels ranging from low to high. The moderate heat flux case is used in optimization and the lower and higher heat flux cases are used in the extrapolation exercise to examine modeling quality.

Parameter estimation of PMMA shows that the best agreement with data can be found when the parameter values are all estimated by independent measurement, literature referencing and approximated using engineering judgment (approach A, see Figure 7 and Table 4). The results show that this approach gave better results in terms of following the data trend than other approaches examined in this example (approach B and C). Additionally, the estimated values for the same parameters show variation depending on the specific routine (GA, SCE or SHC) used in the exercise when a numerical optimization method is applied. The findings are suggestive of the following: (1) This exercise shows that the approach of starting with independent measurements, literature reference or approximation rather than applying only numerical optimization method discussed in the parameter estimation process (see Figure 1) is justified. (2) Having variation in the estimated values when applying different optimization routines indicates that there are compensating effects between each parameter allowing the algorithm to optimize for different optimal parameter sets.

Table 4. Parameter estimation results with approach A for parameter values estimated from measurement, literature or approximation; approach B for estimation based on combination of non-optimization and optimization methods using GA, SCE and SHC numerical optimization routines; and approach C for estimation based on mostly optimization method using GA, SCE and SHC. Best simulation results were found from estimation with approach A (i.e. independent measurements or literature search) approach for parameter estimation of PMMA.

ID		A	B-GA	B-SCE	B-SHC	C-GA	C-SCE	C-SHC
Parameter	Unit	Measurement, Literature, or Approximation	Comparable Non-optimization and Optimization			Mostly Optimization		
Thermo-physical Property	ρ_i	1200 ± 60	1200 ± 60			1200 ± 60		
		Measurement	Measurement			Measurement		
	k_i	0.18 ± 0.01	0.30 ± 0.01	0.21	0.33	0.29 ± 0.01	0.29	0.19
		Literature*	GA	SCE	SHC	GA	SCE	SHC
c_i	J/kg-K	2.2 ± 0.1	1.8 ± 0.1	0.7	1.7	2.0 ± 0.1	1.1	1.7
		Literature**,***	GA	SCE	SHC	GA	SCE	SHC
Optical Property	κ_i	2700 ± 1400	150000 ± 86000	1000000	3600000	2200 ± 500	790000	350000
		Literature****	GA	SCE	SHC	GA	SCE	SHC
	ε_i	0.85 ± 0.16	0.91 ± 0.01	0.66	0.89	0.66 ± 0.01	0.99	0.54
		Literature****	GA	SCE	SHC	GA	SCE	SHC
Thermal Decomposition Kinetics and Heats	n_k	1	1			0.5 ± 0.1	0.5	1.5
		Approximated	Approximated			GA	SCE	SHC
	Z_k	(8.5 ± 4.3) × 10 ¹²	(8.5 ± 4.3) × 10 ¹²			(1.3 ± 0.6) × 10 ¹⁶	3.3 × 10 ¹⁵	5.3 × 10 ¹⁹
		Model Fitting w/ multiple heating rate TGA data	Model Fitting with multiple heating rate TGA data			GA	SCE	SHC
	E_k	(1.88 ± 0.06) × 10 ⁵	(1.88 ± 0.06) × 10 ⁵			(1.77 ± 0.01) × 10 ⁵	2.27 × 10 ⁵	2.43 × 10 ⁵
		Model Fitting w/ multiple heating rate TGA data	Model Fitting with multiple heating rate TGA data			GA	SCE	SHC
ΔH_k	kJ/kg	870 ± 130	870 ± 130			1100 ± 21	1300	520
		Literature**	Literature ^{Error! Bookmark not defined.}			GA	SCE	SHC
Dependent Parameter	h_{crz}	0	12 ± 3	2	14	38 ± 4	3	-32
		Approximated adiabatic condition at back surface	GA	SCE	SHC	GA	SCE	SHC

* J. Brandrup, E.H. Immergut, E.A. Grulke, A. Abe, D.R. Bloch (Eds.), Polymer Handbook, fourth ed., John Wiley & Sons, New York, 1999.

** S.I. Stoliarov and R.N. Walters, Polym. Degrad. Stab. **93** (2008), pp. 422–427.

*** Brandrup J, Immergut EH, Grulke EA, Abe A, Bloch DR, editors. Polymer handbook. 4th ed. New York: John Wiley and Sons; 1999.

**** Stanislav I. Stoliarov, Sean Crowley, Richard E. Lyon, Gregory T. Linteris, Prediction of the burning rates of non-charring polymers, Combustion and Flame, Volume 156, Issue 5, May 2009, Pages 1068-1083, ISSN 0010-2180, DOI: 10.1016/j.combustflame.2008.11.010.

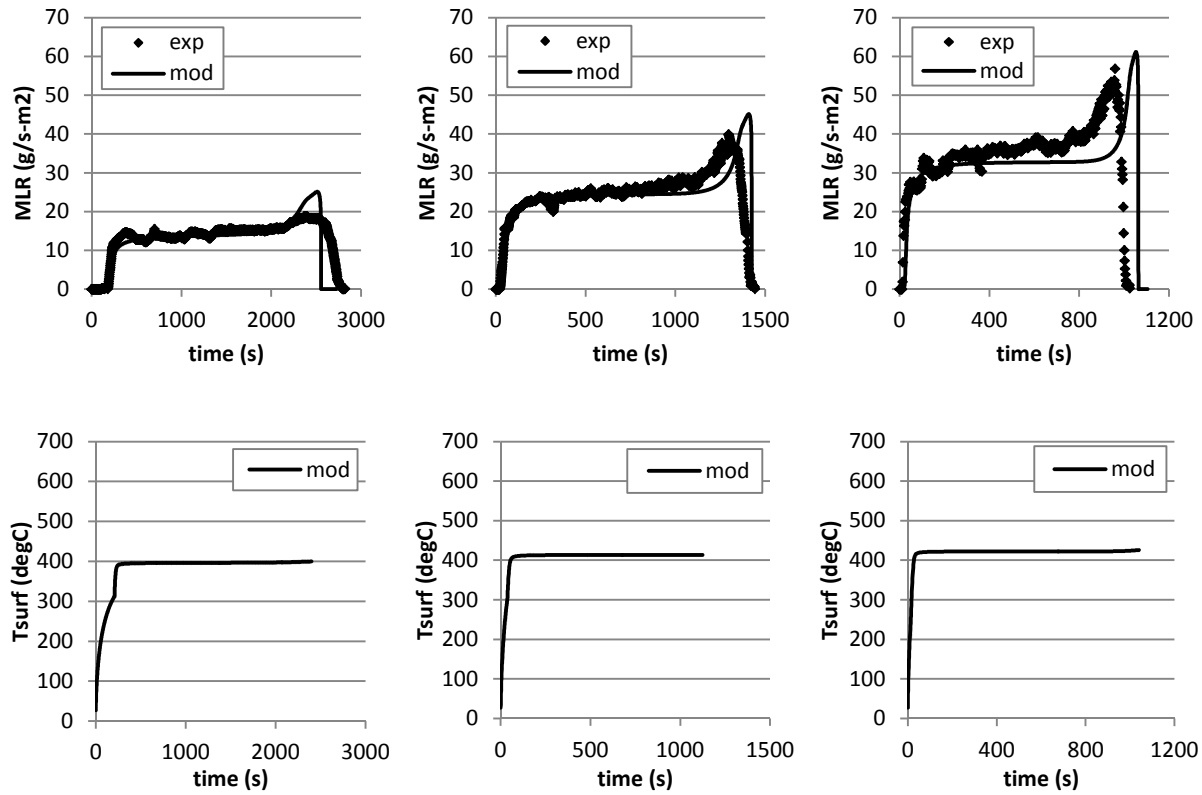


Figure 7. Mass loss rate (MLR, top row) and surface temperature (T_{surf} , bottom row) comparisons for PMMA between actual from experiment (exp) and modeled (mod) at applied heat flux of 23 (left), 46 (middle) and 64 (right) kW/m^2 . Best simulation results were found from estimation with mostly non-optimization (i.e. independent measurements or literature search) approach for parameter estimation of PMMA.

Parameter estimation of triple layered corrugated cardboard shows that the best agreement with data can be found when the parameter values are estimated by mostly optimization using SCE (approach C-SCE, see Figure 8 and Table 5). The results show that the optimization and the upper limit extrapolation cases have good agreement to the experimental data in terms of having similar data trends for all approaches (approach B and C) except for the C-SHC approach. However, the lower limit extrapolation case from all approaches shows significantly poor agreement to the experimental data near the initial mass loss rate peak. Among various results, the lower limit extrapolation case from mostly optimization using SCE approach was closest to the experimental data. Additionally, the estimated values for the same parameters show variation depending on the specific routine (GA, SCE or SHC) used in the exercise when numerical optimization method is applied. The findings are suggestive of the following. (1) Comparing the three optimization techniques, GA and SCE gave better estimations of optimal parameter sets than SHC, though the computing time needed for SHC to conduct the optimization was an order of magnitude less than the other two. (2) When the material is significantly simplified mathematically, e.g assuming a homogeneous cross-section for a complicated structured heterogeneous material such as this example, estimated parameter values must take into account of the effect of simplification. Therefore, pyrolysis modeling has a higher chance of producing diverging results when simulating extrapolation cases as shown in this lower limit extrapolation case. (3) Although the approach of starting with independent measurements, literature reference or approximation rather than applying only numerical optimization method should be favored, in this case the mostly optimization case show a better agreement with data. This can also be explained by the simplifications made in the modeling set-up and the estimated parameter values taking into account of the simplifications. In such cases, allowing the optimization routine to have greater flexibility in searching for the near optimums by leaving the parameters as variables instead of fixing them as a constant with measured values. (4) The variation shown in the estimated values when using different optimization routines (GA, SCE or SHC) indicates that there are compensating effects between each parameter allowing the algorithm to optimize for different optimal parameter sets.

Table 5. Parameter estimation results with approach B for estimation based on combination of non-optimization and optimization methods using GA, SCE and SHC numerical optimization routines; and approach C for estimation based on mostly optimization method using GA, SCE and SHC. Best simulation results were found from estimation with approach C using shuffled complex evolution method for parameter estimation of triple layered corrugated cardboard.

ID		B-GA	B-SCE	B-SHC	C-GA	C-SCE	C-SHC			
Parameter		Comparable Non-optimization and Optimization			Mostly Optimization					
Thermo-physical Property	i = 1 (fuel)	ρ_i	kg/m ³	110			110			
		k_i	W/m-K	0.08 ± 0.01			0.13	0.21	0.21	
				Measurement			GA	SCE	SHC	
		c_i	J/kg-K	2.8	2.3	0.6	2.0	2.4	1.7	
				GA	SCE	SHC	GA	SCE	SHC	
				25	20	11	26	10	43	
	i = 2 (residue)	ρ_i	kg/m ³	GA	SCE	SHC	GA	SCE	SHC	
				0.29	0.32	0.32	0.20	0.35	0.20	
		k_i	W/m-K	GA	SCE	SHC	GA	SCE	SHC	
				1.5	1.1	0.2	1.0	0.8	2.2	
		c_i	J/kg-K	GA	SCE	SHC	GA	SCE	SHC	
				10 ⁶			10 ⁶			
Optical Property	i = 1 (fuel)	κ_i	/m	10 ⁶			10 ⁶			
				Approximated as opaque			Approximated as opaque			
		ε_i	-	0.88 ± 0.01			0.72	0.50	0.65	
				Measurement			GA	SCE	SHC	
	i = 2 (residue)	κ_i	/m	10 ⁶			10 ⁶			
				Approximated as opaque			Approximated as opaque			
		ε_i	-	1			0.82	0.93	0.96	
				Approximated			GA	SCE	SHC	
Thermal Decomposition Kinetics and Heats	n_k	-	1			3.7	3.0	2.2		
			Approximated			GA	SCE	SHC		
			Z_k	/s	1.1 x 10 ²¹			3.9 x 10 ⁶	9.8 x 10 ¹⁹	6.0 x 10 ¹⁴
					Model Fitting with single heating rate TGA data			GA	SCE	SHC
	E_k	J/mol	2.49 x 10 ⁵			7.0 x 10 ⁴	2.47 x 10 ⁵	3.02 x 10 ⁵		
			Model Fitting with single heating rate TGA data			GA	SCE	SHC		
	ΔH_k	kJ/kg	123	512	809	88	54	0.7		
			GA	SCE	SHC	GA	SCE	SHC		
Model Dependent Parameter	h_{crz}	W/m ² -K	19	8	14	10	8	10		
			GA	SCE	SHC	GA	SCE	SHC		
	$n_{kz}(i=1)$	-	5.6	4.6	7.6	0				
			GA	SCE	SHC	Approximated				

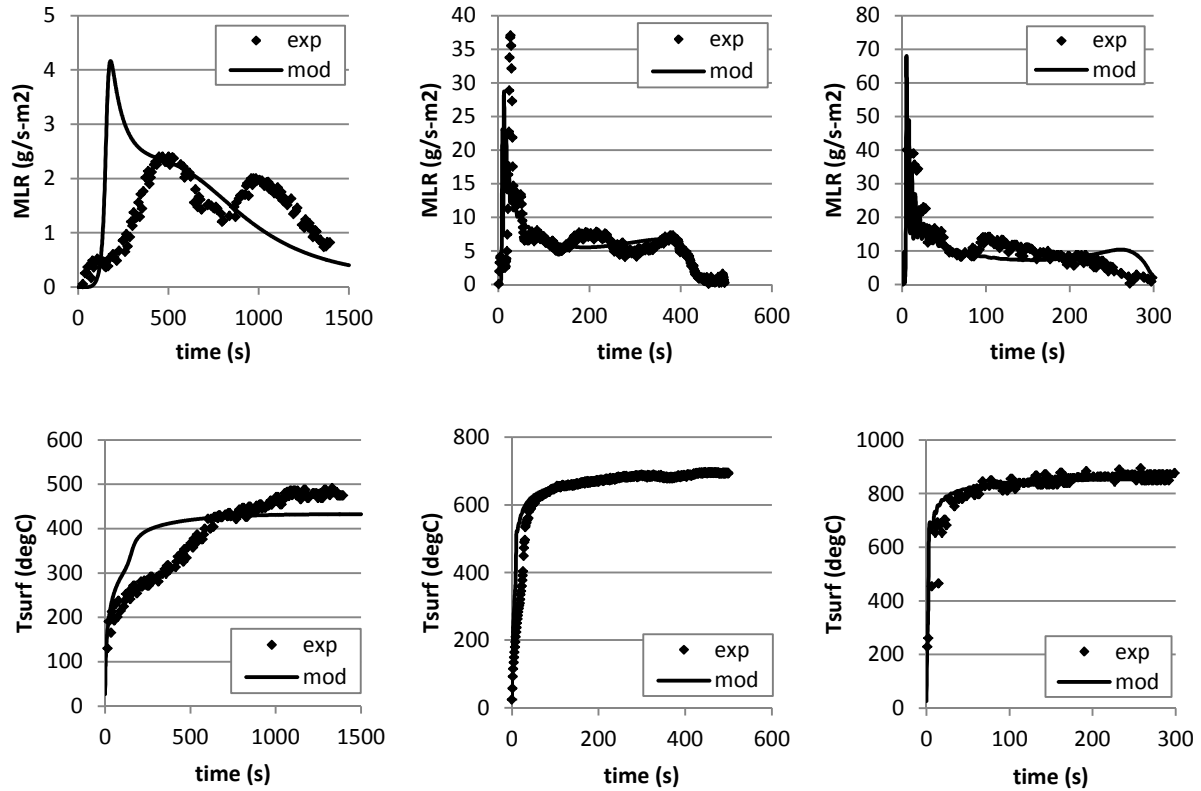


Figure 8. Mass loss rate (MLR, top row) and surface temperatures (T_{surf} , bottom row) comparisons for corrugated cardboard between actual from experiment (exp) and modeled (mod) at applied heat flux of 20 (left), 60 (middle) and 110 (right) kW/m^2 . The moderate heat flux case is used in optimization and the lower and higher heat flux cases are used in extrapolation exercise to examine modeling quality. Best simulation results were found from estimation with mostly optimization approach using shuffled complex evolution method for parameter estimation of triple layered corrugated cardboard.

Parameter estimation of fiberglass reinforced polymer (FRP) composite shows that the best agreement with data can be found when the parameter values are estimated by mostly optimization using optimization routines other than SHC (see Figure 9 and Table 6). The results show that both optimization and extrapolation cases produce simulations that follows the experimental data trends well for GA and SCE cases. The estimated values for the same parameters show variation depending on the specific optimization routine used in the exercise. Some values are compared with measured or referenced from literatures values – thermal conductivity, specific heat capacity and emissivity of the resin, FRP composite and fiberglass. This exercise is similar to the work conducted in Ref [24]. Based on this comparison, it has shown that more than half of the estimated values discussed above are close to measured or reference values and their differences are less than the measurement uncertainty. The findings are suggestive of the following. (1) GA and SCE were able to optimize better than SHC. (2) The variation shown in the estimated values when using different optimization routines (GA, SCE or SHC) indicates that there are compensating effects between each parameter allowing the algorithm to optimize for different optimal parameter sets. (3) However, when modeling is well-configured with an optimum level of complexity, estimated values with optimization method can be close to the independent measurements, which are considered to be effective properties of a material.

Table 6. Parameter estimation results with estimation based on combination of non-optimization and optimization methods using GA, SCE and SHC numerical optimization routines. Best simulation results were found from estimation with GA or SCE method for parameter estimation of this fiberglass reinforced polymer composite.

		ID		GA(avg)	GA(best)	SCE	SHC	
Parameter		Unit	Comparable Non-optimization and Optimization					
Thermo-physical Property	i = 1 (Resin)	ρ_i	kg/m ³	1200 Measurement				
		k_i	W/m-K	0.23 ± 0.02 GA	0.21 GA	0.54 SCE	0.04 SHC	
		c_i	J/kg-K	1400 ± 100 GA	2200 GA	300 SCE	1300 SHC	
		i = 2 (R_residue)	ρ_i	kg/m ³	253 Measurement, Kinetic Modeling			
			k_i	W/m-K	0.19 ± 0.02 GA	0.12 GA	0.08 SCE	0.31 SHC
			c_i	J/kg-K	1900 ± 200 GA	1600 GA	1800 SCE	1800 SHC
	i = 3 (Additive)		ρ_i	kg/m ³	2300 Measurement			
		k_i	W/m-K	1.22 ± 0.10 GA	1.44 GA	0.82 SCE	2.74 SHC	
		c_i	J/kg-K	1200 ± 100 GA	930 GA	2500 SCE	2400 SHC	
		i = 4 (A_residue)	ρ_i	kg/m ³	1558 Measurement, Kinetic Modeling			
	k_i		W/m-K	0.24 ± 0.04 GA	0.22 GA	0.59 SCE	0.36 SHC	
	c_i		J/kg-K	1200 ± 100 GA	2200 GA	300 SCE	780 SHC	
	i = 5 (Glass)		ρ_i	kg/m ³	2600 Reference (MSDS)			
		k_i	W/m-K	0.18 ± 0.02 GA	0.15 GA	0.30 SCE	0.09 SHC	
		c_i	J/kg-K	400 ± 100 GA	170 GA	300 SCE	110 SHC	
		Optical Property	i = 1 (R)	κ_i	/m	10 ⁰ Approximated as opaque		
	ϵ_i			-	0.84 ± 0.03 GA	0.81 GA	0.82 SCE	1.24 SHC
	i = 2 (R_res)		κ_i	/m	10 ⁰ Approximated as opaque			
ϵ_i			-	0.90 ± 0.03 GA	0.87 GA	1.00 SCE	0.97 SHC	
i = 3 (A)	κ_i		/m	10 ⁰ Approximated as opaque				
	ϵ_i		-	0.81 ± 0.04 GA	0.77 GA	1.00 SCE	0.84 SHC	
i = 4 (A_res)	κ_i		/m	10 ⁰ Approximated as opaque				
	ϵ_i		-	0.89 ± 0.03 GA	0.96 GA	1.00 SCE	0.42 SHC	
i = 5 (Glass)	κ_i		/m	10 ⁰ Approximated as opaque				
	ϵ_i		-	0.88 ± 0.02 GA	0.90 GA	1.00 SCE	1.41 SHC	
Kinetics and Heats	k = 1	n_k	-	1.3		Model Fitting with Multiple Heating Rate TGA Data		
	R → R _{residue} + vap↑	Z_k	/s	3.2 x 10 ¹²				

		E_k	J/mol	1.83×10^5				
		ΔH_k	kJ/kg	$(2.5 \pm 0.2) \times 10^3$	2.0×10^3	2.6×10^3	2.6×10^3	
				GA	GA	SCE	SHC	
	k = 2 A → A _{residue + vap} ↑	n_k	-	5.0		Model Fitting with Multiple Heating Rate TGA Data		
		Z_k	/s	1.6×10^{12}				
		E_k	J/mol	1.60×10^5				
		ΔH_k	kJ/kg	3760 ± 1130 (30%) Measurement, DSC				
	Model Dependent Parameter	n_{kz} (i=5)	-	0.59 ± 0.06	0.58	0.01	0.18	
				GA	GA	SCE	SHC	
		n_c (i=5)	-	0.53 ± 0.06	0.37	0.88	-0.26	
GA				GA	SCE	SHC		
γ (i=2)		m	0.00348 ± 0.00134	0.00051	0.00002	0.02482		
			GA	GA	SCE	SHC		
γ (i=4)		m	0.00475 ± 0.00184	0.00625	0.00001	0.05832		
			GA	GA	SCE	SHC		
γ (i=5)		m	0.00769 ± 0.00225	0.00001	0.00003	-0.02453		
			GA	GA	SCE	SHC		

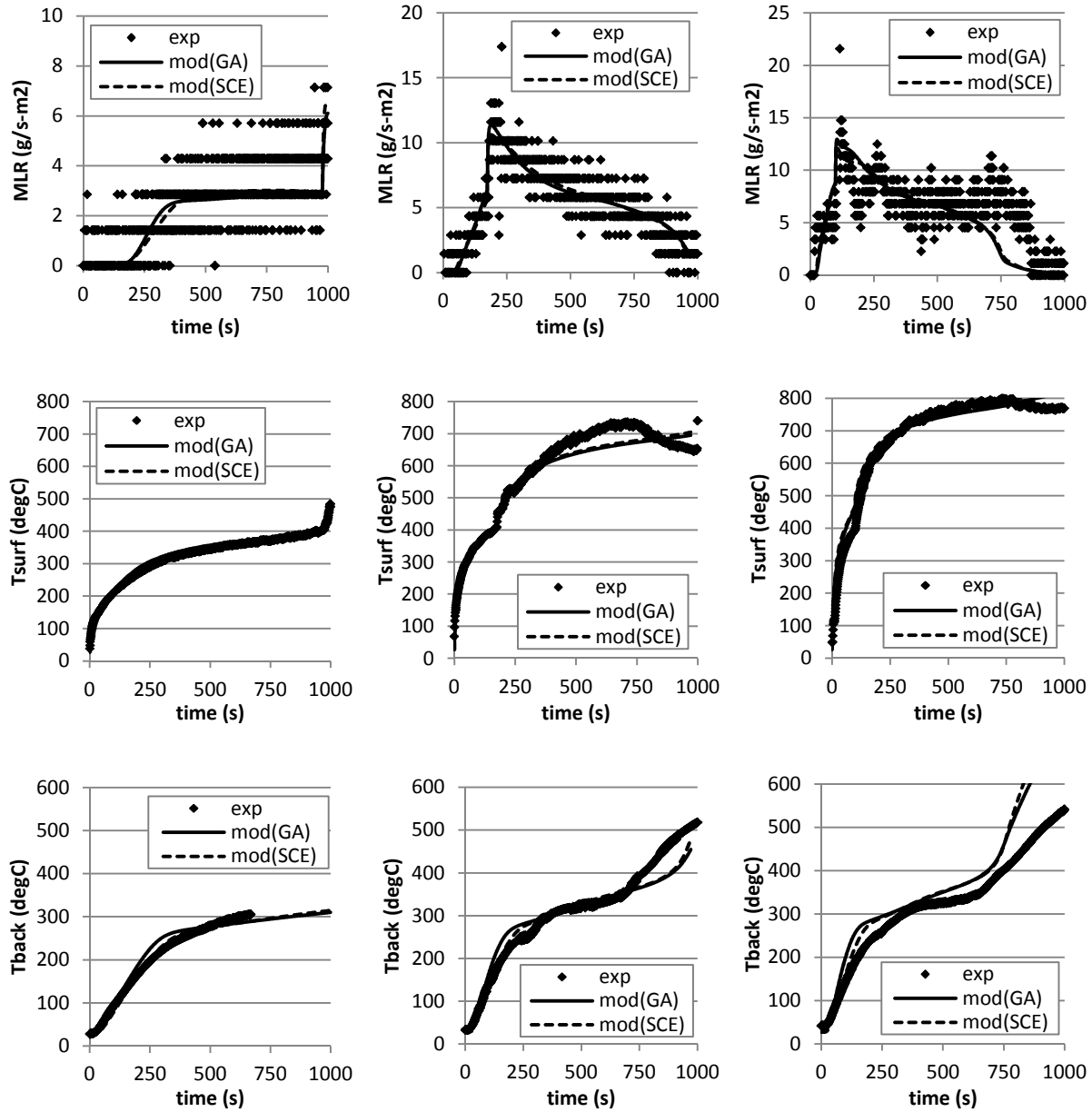


Figure 9. Mass loss rate (MLR) and surface temperatures (T_{surf} , T_{back}) comparisons for fiberglass reinforced polymer (FRP) composite with modified acrylic resin with high-charring fire retardant additive between actual from experiment (exp) and modeled (mod) at applied heat flux of 25, 50 and 75 kW/m^2 . The moderate heat flux case is used in optimization and the lower and higher heat flux cases are used in extrapolation exercise to examine modeling quality. Best simulation results were found from estimation with mostly optimization approach using either genetic algorithm or shuffled complex evolution method for parameter estimation of this fiberglass reinforced polymer composite.

Parameter estimation of plywood shows that there is good agreement with data when manual optimization is used (see Figure 10 and Table 7). The results show that both optimization and extrapolation cases have good agreement to the experimental data in terms of following the data trend to a certain degree. In this example, parameter values from independent measurements, literature reference or approximation are mostly used as initial values in the manual optimization process. Other unknown parameters were optimized via trial-and-error method as discussed in the previous section. This example illustrates the successful use of manual optimization.

Table 7. Parameter estimation results with estimation based on combination of non-optimization and manual optimization method. A single simulation results are found for parameter estimation of this plywood.

Parameter		Unit	Comparable Non-optimization and Manual Optimization			
Thermo-physical Property	i = 1 (water)	ρ_i	kg/m ³	1000	Reference*	
		k_i	W/m-K	0.6		
		c_i	J/kg-K	4200		
	i = 2 (dry_wood)	ρ_i	kg/m ³	504 ± 10		Measurement
		k_i	W/m-K	0.26		Manual Optimization with Initial Guess of 0.122 measured at 20 °C (dry_wood, ASTM C518/E1225)
		c_i	J/kg-K	2400		Manual Optimization with Initial Guess of 1200 measured at 20 °C (dry_wood, ASTM E1269)
	i = 3 (char)	ρ_i	kg/m ³	173	Measurement	
		k_i	W/m-K	0.12	Manual Optimization with Initial Guess of 0.122 measured at 20 °C (dry_wood, ASTM C518/E1225)	
		c_i	J/kg-K	3700	Manual Optimization with Initial Guess of 1200 measured at 20 °C (dry_wood, ASTM E1269)	
	Optical Property	i = 1 (water)	ε_i	-	1.00	Approximated
		i = 2 (dry_wood)	κ_i	/m	10 ⁶	Approximated as opaque
			ε_i	-	0.891 ± 0.018	Measurement, ASTM E903
i = 3 (char)		κ_i	/m	10 ⁶	Approximated as opaque	
		ε_i	-	1.00	Approximated	
Kinetics and Heats		k = 1 water → vap↑	n_k	-	5.0	Model Fitting with Multiple Heating Rate TGA Data
	Z_k		/s	2.5 × 10 ¹²		
	E_k		J/mol	83 × 10 ⁴		
	ΔH_k		kJ/kg	2500 ± 800 (30%)	Measurement, DSC	
	k = 2 dry_wood → char + vap↑	n_k	-	1.7	Model Fitting with Multiple Heating Rate TGA Data	
		Z_k	/s	5.0 × 10 ¹⁶		
		E_k	J/mol	2.10 × 10 ⁵		
		ΔH_k	kJ/kg	631		Manual Optimization
	Model Dependent Parameter	γ (i=3)	m		0.0036	Manual Optimization

* NIST Chemistry WebBook, <http://webbook.nist.gov/>

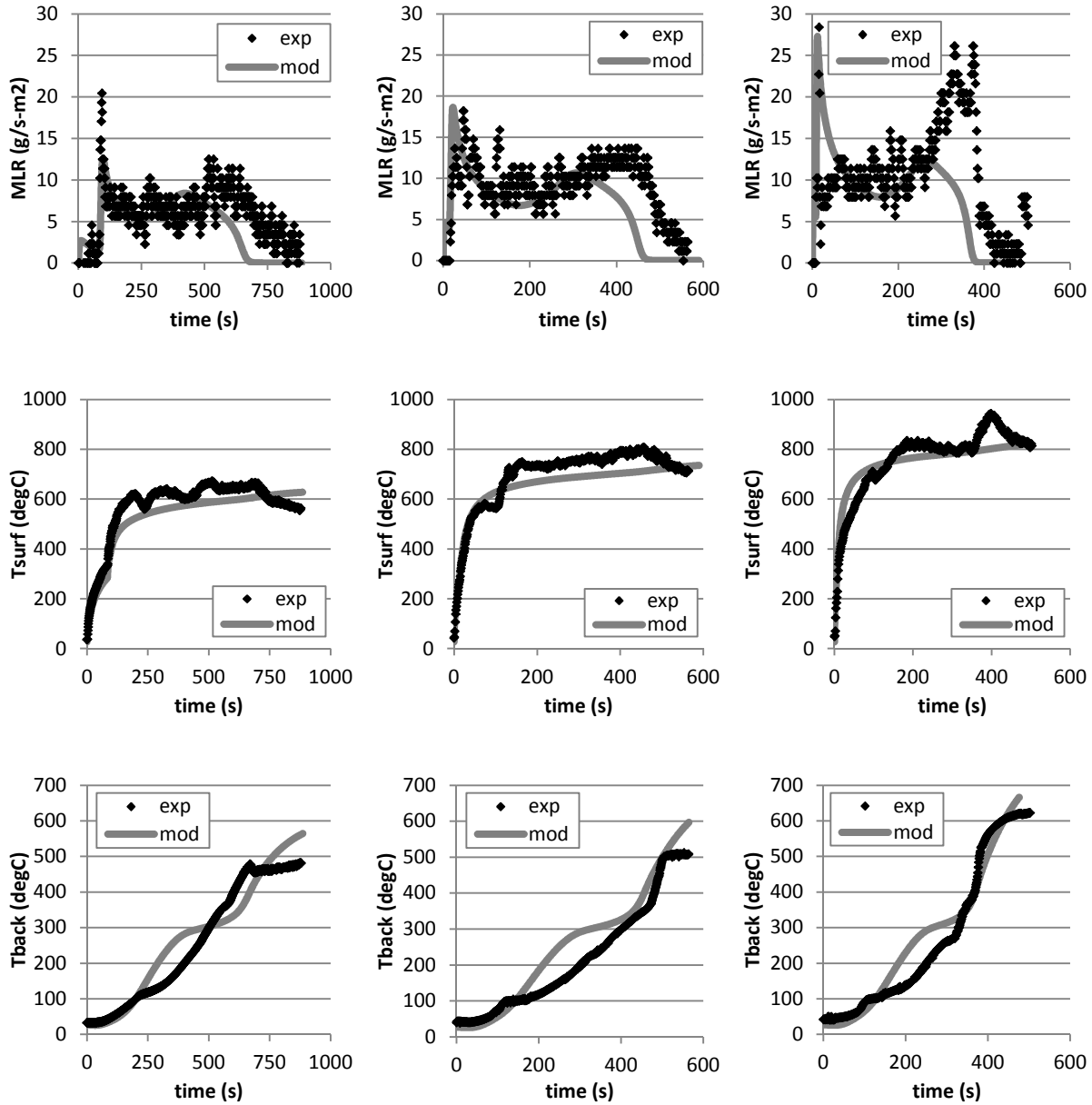


Figure 10. Mass loss rate (MLR) and surface temperatures (T_{surf} , T_{back}) comparisons for plywood between actual from experiment (exp) and modeled (mod) at applied heat flux of 25, 50 and 75 kW/m^2 . The moderate heat flux case is used in optimization and the lower and higher heat flux cases are used in extrapolation exercise to examine modeling quality. Simulation results are from estimation with manual optimization approach for parameter estimation of plywood.

The parameter estimation process proposed in this study has been applied to these four real-world materials – PMMA, corrugated cardboard, fiberglass reinforced polymer (FRP) composite and plywood. The results have shown that the estimations were successful in terms of producing modeling outputs that have good agreement with experimental data. The approach of starting the parameter estimation with independent measurements, literature reference or approximation rather than applying only numerical optimization method has shown to produce better

results for PMMA where much of the material's characteristics are mathematically described in modeling. This is consistent with the parameter estimation process proposed in this work. For the corrugated cardboard example where greater simplifications were made in modeling set-up, e.g. homogeneous cross-section, estimation via mostly numerical optimization gave better results. This is due to the estimated parameter values taking into account of the simplifications. For this case, allowing the optimization routine to have greater flexibility in searching for the near optimum by leaving the parameters as variables is better than fixing them with measured values. In all example cases, variations in estimated values were identified when using different approaches. This indicates that there is a compensating effect between each parameter in a parameter set and the optimization routines are able to find multiple optimums. In other words, each estimated parameter set should be considered as a *linked* parameter set. The FRP composite example has shown that, although in general each estimated parameter set is a *linked* parameter set, when modeling is well-configured with an optimum level of complexity, sometimes the difference between the estimated values from an optimization method and measured values can be less than the measurement uncertainty. In this case, one can consider the estimated values as effective material properties. From the plywood example, it was demonstrated that manual optimization can be successful in estimating model parameters.

10. CONCLUSION

In this study, a process for conducting parameter estimation for comprehensive pyrolysis models was proposed. The estimation process was developed based on the following four principals and approaches: (1) parameter estimation is about being consistent, applying engineering common-sense and correctly following the steps in this guide; (2) parameter estimation is conducted by breaking down the problem into groups of unknowns of similar characters and considering them separately; (3) parameter estimation is conducted with consideration to an appropriate complexity in model set-up using certain approximations for simplifications; and (4) parameter estimation is conducted with direct measurements of parameters with independent experiments, literature search and/or numerical optimization paired with certain pyrolysis models. Following this, limitations in parameter estimation was discussed by considering how simplifying the microstructure of a heterogeneous material to homogeneous mixture, modeling thermal decomposition kinetics independently using thermal analysis and applying multi-objective and multi-variable numerical optimization method affect the estimation results. Examples were given to show any assumptions and conditions used during parameter estimation process are accounted for in the estimated value itself and/or other parameter values in the parameter set. The process developed was applied to modeling of real-world materials of thermoplastic (PMMA), corrugated cardboard, fiberglass reinforced polymer composite and plywood and the estimation results – mass loss rate and temperature profiles at front and back surfaces – were shown. Understanding the limitations in parameter estimation, it was noted that when parameter estimation is conducted via numerical optimization, the estimated parameter values are compensated by other parameter values in a parameter set. This allows optimization method to optimize for multiple optimal parameter sets. In other words, each estimated parameter set should be considered as a *linked* parameter set. However, when modeling is well-configured with optimum complexity, the optimized parameter values become closer to those of independent measurements. This highlights the possibility of utilizing the optimization method to estimate for effective material properties.

11. ACKNOWLEDGMENTS

The authors greatly appreciate the support for this work from DOC NIST Award Number 60NANB8D8106 (Federal Program Officer Dr. Kevin McGrattan). Special thanks goes to Charles Dore for fabricating and donating the FRP composite materials used in this study. Many thanks also to Randall Harris at WPI for conducting the Cone Calorimeter tests.

12. REFERENCES

-
- ¹ Tewarson A., "Generation of Heat and Chemical Compounds in Fires", In SFPE Handbook of Fire Protection Engineering, 3rd ed., NFPA, Quincy, MA, USA (2002) Chapter 3-4.
 - ² Quintiere, J.G., and Harkleroad, M., "New Concepts for Measuring Flame Spread Properties", in Fire Safety Science and Engineering, ASTM STP 882, ASTM International, West Conshohocken, PA, USA (1985) 239-267.
 - ³ Hopkins, D. and Quintiere, J.G., "Material Fire Properties and Predictions for Thermoplastics", Fire Safety Journal, 26 (1996) 241-268.
 - ⁴ Chen, Y., Delichatsios, M.A., and Motevalli, V., "Material Pyrolysis Properties, Part I: An Integral Model for One-Dimensional Transient Pyrolysis of Charring and Non-Charring Materials", Combustion Science and Technology, 88 (1993) 309-328.
 - ⁵ Theuns, E., Merci, B., Vierendeels, J. and Vandavelde, P., "Extension and Evaluation of the Integral Model for Transient Pyrolysis of Charring Materials", Fire and Materials, 29 (2005) 195-212.
 - ⁶ Theuns E., Merci B., Vierendeels, J. and Vandavelde, P., "Critical Evaluation of an Integral Model for the Pyrolysis of Charring Materials", Fire Safety Journal, 40 (2005) 121-140.
 - ⁷ Delichatsios, M., Paroz, B., and Bhargava, A., "Flammability Properties for Charring Materials", Fire Safety Journal, 38:3 (2003) 219-228.
 - ⁸ Kevin McGrattan, Simo Hostikka, Jason Floyd, Howard Baum, Ronald Rehm, William Mell and Randall McDermott, Fire Dynamics Simulator (Version 5) Technical Reference Guide, NIST Special Publication 1018-5, October 29, 2010
 - ⁹ S.I. Stoliarov, R.E. Lyon, Federal Aviation Administration Technical Note, DOT/FAA/AR-TN08/17, 2008; available for download at <http://www.fire.tc.faa.gov/reports/reports.asp>.
 - ¹⁰ Lautenberger, C., Gpyro – A Generalized Pyrolysis Model for Combustible Solids, Technical Reference, Version 0.700, February 19, 2009
 - ¹¹ Kim, Mihyun Esther, Parameter Estimation Methods for Comprehensive Pyrolysis Models, Ph.D. Dissertation, Worcester Polytechnic Institute, Department of Fire Protection Engineering, 2013
 - ¹² S. Rudtsch, H.-P Ebert, F. Hemberger, G. Barth, R. Brandt, U. Groß, W. Hohenauer, K. Jaenicke-Roessler, E. Kaschnitz, E. Pfaff, W. Pöbnecker, G. Pottlacher, M. Rhode and B. Wilthan, Intercomparison between thermophysical property measurements on an austenitic stainless steel, International Journal of Thermophysics, Vol. 26, p. 855 - 867, (2005)
 - ¹³ Oztekin, E.S., Crowley, S.B., Lyon, R.E., Stoliarov, S.I., Patel, P., and Hull, T.R., "Sources of variability in fire test data: A case study on poly(aryl ether ether ketone) (PEEK)", Combustion and Flame, Vol. 159, Issue 4, pp. 1720-1731, Apr 2012.
 - ¹⁴ Mikiya Ito, Kazukiyo Nagai, Degradation issues of polymer materials used in railway field, Polymer Degradation and Stability, Volume 93, Issue 10, October 2008, Pages 1723-1735, ISSN 0141-3910, 10.1016/j.polymdegradstab.2008.07.011. (<http://www.sciencedirect.com/science/article/pii/S0141391008002218>)
 - ¹⁵ C. Lautenberger, G. Rein and C. Fernandez-Pello, "The Application of a Genetic Algorithm to Estimate Material Properties", Fire Safety Journal 41 (2006), pp. 204–214.
 - ¹⁶ Matala, A., "Estimation of Solid Phase Reaction Parameters for Fire Simulation," MS Thesis, University of Technology, Helsinki, 2008.
 - ¹⁷ Duan, Q., Gupta, V.K., & Sorooshian, S., 1993. Shuffled Complex Evolution Approach for Effective and Efficient Global Minimization, Journal of Optimization Theory and Applications 76, pp. 501-521.

-
- ¹⁸ Chaos, M., Khan, M.M., Krishnamoorthy, N., de Ris, J.L., & Dorofeev, S.B., Bench-Scale Flammability Experiments: Determination of Material Properties Using Pyrolysis Models for Use in CFD Fire Simulations. In: *Interflam 2010*, July 5-7, 2010, Nottingham, UK..
- ¹⁹ Chaos, M., Khan, M.M., Krishnamoorthy, N., de Ris, J.L., & Dorofeev, S.B., 2010. Evaluation of Optimization Schemes and Determination of Solid Fuel Properties for CFD Fire Models using Bench-scale Pyrolysis Tests, *Proceedings of the Combustion Institute 33*, in press, doi:10.1016/j.proci.2010.07.018
- ²⁰ Webster, R., "Pyrolysis Model Parameter Optimization using a Customized Stochastic Hill-Climber Algorithm and Bench Scale Fire Test Data," MS Thesis, University of Maryland, 2009.
- ²¹ Rick Aster, Brian Borchers, Cliff Thurber, Preface, In: Richard C. Aster, Brian Borchers and Clifford H. Thurber, Editor(s), *International Geophysics*, Academic Press, 2005, Volume 90, Parameter Estimation and Inverse Problems, Pages xi-xii, ISSN 0074-6142, ISBN 9780120656042, DOI: 10.1016/S0074-6142(05)80014-2.
- ²² Kim, E., Dembsey, N.A., and Dore, C.H., "Property Estimation for Pyrolysis Modeling Applied to Flame Retarded Modified Acrylic FRP Composites", in *Proceedings of Composites & Polycon 2010*, American Composites Manufacturers Association, Mandalay Bay, Las Vegas, NV, USA, 9-11 February (2010). *Best Fire Technical Paper Award at Composites and Polycon 2010*
- ²³ E. Kim, N. Dembsey, and C Lautenberger, Parameter Estimation for Pyrolysis Modeling Applied to Polyester FRP Composites with Different Glass Contents, in *Fire and Materials 2009, 11th International Conference*, 26-28 January 2009, Hyatt Hotel at Fishermans Wharf, San Francisco, CA, USA
- ²⁴ Kim, E. and Dembsey, N., Assessing Parameter Estimation Method Using Multi-objective Optimization for Pyrolysis Modeling of Fiberglass Reinforced Polymer Composites, *submitted for review in Fire and Materials Journal*
- ²⁵ A. Gómez-Barea, P. Ollero, and, and C. Fernández-Baco, Diffusional Effects in CO₂ Gasification Experiments with Single Biomass Char Particles. 1. Experimental Investigation, *Energy & Fuels* 2006 20 (5), 2202-2210
- ²⁶ Kim, E., Dembsey, N., and Shivkumar, S., Evaluating Effects of Applying Different Kinetic Models to Pyrolysis Modeling of Fiberglass Reinforced Polymer Composites, *submitted for review in Fire and Materials Journal*
- ²⁷ Matala, A., Lautenberger, C., & Hostikka, S., "Generalized direct method for pyrolysis kinetics parameter estimation and comparison to existing methods," *Journal of Fire Sciences* **30** 339-356 (2012).

Section 5

ENGINEERING GUIDE FOR ESTIMATING MATERIAL PYROLYSIS PROPERTIES FOR FIRE MODELING

ENGINEERING GUIDE FOR ESTIMATING MATERIAL PYROLYSIS PROPERTIES FOR FIRE MODELING

Kim, E.¹, Dembsey, N.^{1*}, and Shivkumar, S.²

¹WPI, Fire Protection Engineering Dept., Worcester, MA, USA

NIST Award Number 60NANB8D8106

Federal Program Officer Dr. Kevin McGrattan

Chapter 1–Introduction

BACKGROUND

The use of fire models in Fire Protection Engineering (FPE) is widespread, and as a tool these models are vital to the practicing engineer especially in performance-based design. Typical classes of fire models are algebraic,¹ zone,² and field/CFD.³ The input data required for these models can be generally characterized as gas phase (combustion and radiation sub-models) and solid phase (heating and pyrolysis sub-models). A significant challenge for the practicing engineer is compiling and developing input data consistent with model assumptions, as FPE is yet to develop standard input databases.

Recognizing this absence of input databases, a standard guide on creating model input data has been developed as ASTM E 1591,⁴ which was developed for zone models. The standard describes the input data required by a model mathematically and presents guidelines to obtain the data. The existence of this guide has enabled users to develop input data in a consistent manner for zone models. Similarly, this new guide will enable the users to develop input data in a consistent manner for different pyrolysis models and various materials.

Among fire-model inputs, in general, gas-phase input is readily available to the practicing engineer, as a range of standard information for certain materials can be found in the combustion literature. In contrast, solid-phase input for heating and thermal decomposition of materials is rarely available. Some standard information on heating may be found in the heat transfer literature for certain materials. However, this information is significantly limited compared to the needs of practitioners. Hence, other practical methods are necessary to estimate model parameters to conduct fire modeling.

In search of a method for estimating parameters, over the past few decades numerous approaches have been developed to extract solid-phase pyrolysis parameters from bench-scale fire test data for computer model input. Examples of early research involving ignition temperature and steady burning are the work performed by Tewarson,⁵ and Quintiere and Harkleroad.⁶ These approaches consider only the aggregate behavior of solids (time-to-ignition and MLR) but not details of the decomposition of the solids. Parameter estimation is accomplished via slope-based plotting techniques of the bench scale data. Field/CFD models^{3,7} use essentially the same thermal model as described in these references, but field/CFD models do not have any built-in parameter estimation method, like the slope based techniques. These pyrolysis models have shown good success at providing meaningful parameters for thermoplastic solids. Charring solids and other complex systems (composites: thin linings over substrates, fiber-reinforced polymers, plywood, etc.) have not shown as good success. Flame-spread models^{8,9} based on this approach have been created that have demonstrated some degree of success.

Building on this work, development of pyrolysis (ignition) temperature based solid integral pyrolysis models^{10,11,12,13,14} that address certain details of the decomposition of solids have been undertaken. The key detail of decomposition included in these models is propagation of a regression or charring front through the solid. Each of these models has an associated bench-scale testing procedure to develop data needed for the associated parameter-estimation procedure using the model. The model of Theuns et al.^{12,13} has been coupled to a field/CFD model. These models have shown good success with thermoplastic-type solids and classic charring solids (wood). Complex systems have not been shown to be successful.

Recently, pyrolysis modeling focusing on details of solid decomposition, including “microstructure” and (multi-step) kinetics, have been developed with accompanying procedures to estimate parameters.^{15,16,17,18,19} Parameter estimation is accomplished via optimization routines. These models have the potential to handle complex solids that need to have “micro structure” explicitly detailed as well as multi-step kinetics.

These pyrolysis models are relatively new and have not yet been extensively evaluated against a range of solids, including complex ones. Initial assessment of the

models shows promise. An interesting observation of the above high quality work is that the focus has been on the important tasks of developing pyrolysis models and parameter-estimation routines as well as showing their potential with “limited” data comparison. As the work has been incorporated into the body of FPE knowledge, the assumptions and limitations of the models have not in general been clearly identified, accepted, and followed by practitioners. Accepted methods for comparing the models and estimated parameters, as well as guidance on how to use the parameters correctly in flame spread and other models, are also lacking. This points to the equally important tasks of interfacing these “theoretical” tools with proper empirical techniques to develop data strictly consistent with the assumptions and limitations of the models. Additionally the “robustness” and utility of the parameters needs to be assessed so as to allow comparison and proper use of the parameters.

In recent years, there has been a high demand for conducting Computational Fluid Dynamics (CFD) simulations in the fire community. The importance of accurate pyrolysis data for the continued use and development of CFD fire models becomes quite clear, especially given that none of the models has a pyrolysis-parameter database, and users are required to develop their own parameters. The current state of the art in procedures for development of model input data, ASTM E 15914, is out-of-date, as it focuses only on zone models and does not address solid-phase pyrolysis. This situation had set the stage for development of a standard guide for estimation of pyrolysis parameters for various types of fire pyrolysis models based on the current knowledge about solid pyrolysis models and parameters, and proper empirical techniques to develop “robust” pyrolysis parameters for fire models.

PURPOSE

With this *Guide*, standardized procedures for obtaining material parameters for input into fire-pyrolysis models are presented, such as empirical, simple analytical and comprehensive pyrolysis models.

ORGANIZATION OF THE GUIDE

The following section (Chapter 2) offers guidance to show what pyrolysis models are available for modelers and what may be appropriate for their modeling needs. To provide standardized procedures for obtaining material-pyrolysis parameters for input into fire models, pyrolysis models are grouped into three categories based on their modeling characteristics, understanding that most of the model-input unknowns are related to the solid phase during thermal decomposition. The three categories are Empirical Models (Chapter 3), Simple Analytical Models (Chapter 4), and Comprehensive Models (Chapter 5). For each model category the following information is provided:

- A brief description of its modeling approach and assumptions applied to simplify the problem.
- A typical mathematical formulation with identification of model parameters in the equations.
- Methods of estimating the unknown parameters either by independent measurements or numerical optimization in pair with the model.

Using this information, example cases are introduced for better understanding of the parameter-estimation procedure described for each model category. Additionally, the Appendix provides thorough explanation of example solutions from different chapters.

REFERENCES

¹ Walton, W.D.; and Thomas, P.H., "Estimating Temperatures in Compartment Fires," In *SFPE Handbook of Fire Protection Engineering*, 3rd ed., NFPA, Quincy, MA, USA (2002) Chapter 3-6.

² Walton, W.D., "Zone Computer Fire Models for Enclosures," In *SFPE Handbook of Fire Protection Engineering*, 3rd ed., NFPA, Quincy, MA, USA (2002) Chapter 3-7.

³ Cox, G.; and Kumar, S., "Modeling Enclosure Fires Using CFD," In *SFPE Handbook of Fire Protection Engineering*, 3rd ed., NFPA, Quincy, MA, USA (2002) Chapter 3-8.

⁴ Standard Guide for Obtaining Data for Deterministic Fire Models, ASTM E 1591, ASTM International, West Conshohocken, PA, USA (2000).

⁵ Tewarson A., "Generation of Heat and Chemical Compounds in Fires," In *SFPE Handbook of Fire Protection Engineering*, 3rd ed., NFPA, Quincy, MA, USA (2002) Chapter 3-4.

-
- ⁶ Quintiere, J.G.; and Harkleroad, M., "New Concepts for Measuring Flame Spread Properties." in *Fire Safety Science and Engineering*, ASTM STP 882, ASTM International, West Conshohocken, PA, USA (1985) 239-267.
- ⁷ McGrattan, Kevin; Hostikka, Simo; Floyd, Jason; Baum, Howard; Rehm, Ronald; Mell, William and McDermott, Randall, *Fire Dynamics Simulator (Version 5) Technical Reference Guide*, NIST Special Publication 1018-5, October 29, 2010.
- ⁸ Quintiere, J.G., "A Simulation Model for Fire Growth on Materials Subject to a Room-Corner Test," *Fire Safety Journal*, 20 (1993) 313-339.
- ⁹ Lattimer B.Y.; Hunt, S.P.; Wright, M.; and Sorathia, U., "Modeling Fire Growth in a Combustible Corner," *Fire Safety Journal*, 38 (2003) 771-796.
- ¹⁰ Hopkins, D.; and Quintiere, J.G., "Material Fire Properties and Predictions for Thermoplastics," *Fire Safety Journal*, 26 (1996) 241-268.
- ¹¹ Chen, Y.; Delichatsios, M.A.; and Motevalli, V., "Material Pyrolysis Properties, Part I: An Integral Model for One-Dimensional Transient Pyrolysis of Charring and Non-Charring Materials," *Combustion Science and Technology*, 88 (1993) 309-328.
- ¹² Theuns, E.; Merci, B.; Vierendeels, J.; and Vandeveld, P., "Extension and Evaluation of the Integral Model for Transient Pyrolysis of Charring Materials," *Fire and Materials*, 29 (2005) 195-212.
- ¹³ Theuns, E.; Merci, B.; Vierendeels, J.; and Vandeveld, P., "Critical Evaluation of an Integral Model for the Pyrolysis of Charring Materials," *Fire Safety Journal*, 40 (2005) 121-140.
- ¹⁴ Delichatsios, M.; Paroz, B.; and Bhargava, A., "Flammability Properties for Charring Materials," *Fire Safety Journal*, 38:3 (2003) 219-228.
- ¹⁵ Lautenberger, C.W.; Rein, G.; and Fernandez-Pello, A.C., "The Application of a Genetic Algorithm to Estimate Material Properties for Fire Modeling from Bench-Scale Fire Test Data," *Fire Safety Journal*, 41 (2006) 204-214.
- ¹⁶ Rein, G.; Lautenberger, C.; Fernandez-Pello, A.C.; Torero, J.L.; and Urban, D.L., "Application of Genetic Algorithms and Thermogravimetry to Determine the Kinetics of Polyurethane Foam in Smoldering Combustion," *Combustion and Flame*, 146 (2006) 95-108.
- ¹⁷ Ferriol, M.; Gentilhomme, A.; Cochez, M.; Oget, N.; and Mieloszynski, "Thermal Degradation of Poly(methylmethacrylate) (PMMA): Modelling of DTG and TG curves," *Polymer Degradation and Stability*, 79 (2003) 271-181.
- ¹⁸ Lautenberger, C.W.; and Fernandez-Pello, A.C., "A Generalized Pyrolysis Model for Simulating Charring, Intumescent, Smoldering, and Noncharring Gasification," *Combustion Processes Laboratories, Fire Science, UC Berkeley, eScholarship Repository* (2006), <http://repositories.cdlib.org/cpl/fs/LautenbergerGenPyro>.
- ¹⁹ Lefebvre, J., et al., "Thermal Stability and Fire Properties of Conventional Flexible Polyurethane Foam Formulations," *Polymer Degradation and Stability*, 88:1 (2005) 28-34.

Chapter 2–Determine Model Type

In this chapter, guidance is given to the modeler to help her/him to select certain types of pyrolysis models by considering processes involved in pyrolysis, characteristics of typical materials, and the models available today that incorporate various assumptions. For more information about each model type in terms of mathematical expressions and application, see the following chapters: Chapter 3 – Empirical Models, Chapter 4 – Simple Analytical Models, and Chapter 5 – Comprehensive Models.

PYROLYSIS OF MATERIALS

Pyrolysis refers to the thermal decomposition of porous or non-porous solid-phase materials caused by heating during exposure to fire conditions. Pyrolysis is a complicated phenomenon, which is a combination of the following interactive processes: heat transfer through materials from fire exposure; thermal decomposition that produces combustible or non-combustible pyrolyzates in gas, liquid or solid form; and mass transfer of oxygen from ambient and those pyrolyzates.

Materials subject to pyrolysis can be first categorized into one of two groups depending on the geometry of interest: an object or a flat surface (see Figure 2-1). The object covers situations where the material's geometry is non-flat or complex in its fire behavior. Whether materials are considered an object or a flat surface, their physical structure may or may not remain stable during pyrolysis. When changes in structural stability do occur, those are typically due to melting, flowing and/or dripping, expanding, popping due to steam expansion, collapsing, etc. When materials maintain their structural stability throughout pyrolysis, further categorization can be applied depending on the location of thermal decomposition sites – Is thermal decomposition occurring near the surface or surface and at in-depth?

Examples of each material group are as follow: (1) Objects: furniture, boxed products, products in pressurized containers, electronics, and more; (2) Flat surfaces that experience structural instability during pyrolysis: flowing and/or dripping thermoplastics due to low melting and glass transition points, intumescent materials, plastic foams that liquefy, phenolic resin that pops, etc; (3) Flat surfaces that maintain their structural stability during pyrolysis and have decomposition occurring mostly on surface: non-flowing thermoplastics, etc; and (4) Flat

surfaces that maintain their structural stability during pyrolysis and have decomposition occurring near surface and at in-depth: wood, highly cross-linked thermosets, plastics with charring additives, etc.

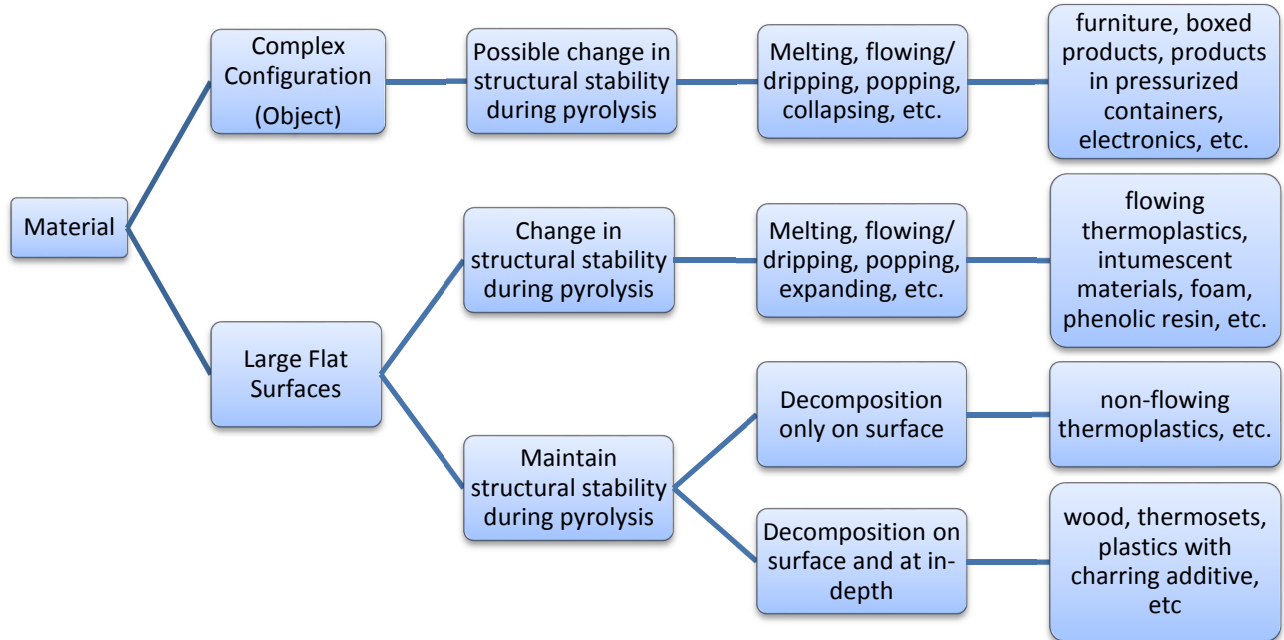


Figure 2-1. Material category: Depending on material's characteristics, material can be grouped into 4 categories and examples for each category is given.

PYROLYSIS MODELS

As aforementioned, pyrolysis is a complicated phenomenon and is a combination of heat transfer, thermal decomposition, and mass transfer. When pyrolysis is modeled, various approaches can be taken by approximating the three processes of pyrolysis. Note that the goal of conducting pyrolysis modeling in fire engineering is to simulate the mass-loss rate per unit area as a result of decomposition of a solid-phase material under fire conditions. This information can be then used as input parameters for pyrolysis sub-models in a zone or CFD model.

The simplest approach of modeling pyrolysis is utilizing empirical data from calorimetry experiments: Empirical Models. Heat transfer, thermal decomposition, and mass-transfer effects are confounded assuming that the difference between testing and modeling conditions are negligible at all times. Another simple approach but more sophisticated than Empirical Models is using analytical solutions to describe pyrolysis: Simple Analytical Models. This approach analytically solves for heat transfer of pyrolyzing materials at the pre-ignition stage by assuming materials as inert and semi-infinite or lumped. Thermal decomposition is modeled by having an ignition criterion, ignition temperature (T_{ig}) at surface. At the post-ignition stage, steady-state burning is assumed. Any mass-transfer effects on pyrolysis are neglected.

The most complex approach available for fire problems is directly solving for the three processes using conservation equations: Comprehensive Models. In this approach, heat transfer is modeled using conservation of energy, which allows the most flexibility in specifying boundary conditions for front and back surfaces, i.e., in specifying heating and cooling at material boundaries. Thermal decomposition is modeled by using conservation of mass and either a pyrolysis criterion, pyrolysis temperature (T_p), or defining a finite reaction rate through kinetic modeling. This approach may also account for mass-transfer effects; however, in this *Guide*, Comprehensive Models will be considered without modeling mass-transfer effects on pyrolysis due to the lack of current understanding of these effects.

Empirical Models can be used for any kind of materials from any of the four material groups discussed previously. Simple Analytical Models can be used only for flat surfaces that maintain their structural stability during pyrolysis. Additionally, strictly, due to model assumptions these models should be applied to thermally-thick or thermally-thin behaving flat surface materials that have decomposition occurring mostly at the surface and resulting in steady-state burning after ignition. Despite this limitation, some modeling work has been

conducted on charring materials such as wood by conducting analysis with data that has a short pre-ignition period followed by a quasi-steady burning. These behaviors allow the assumptions of thermally-thick or thermally-thin behavior and inert at the pre-ignition stage followed by steady-state burning at post-ignition stage to be applied. Comprehensive Models can be used to model all materials that are flat surfaces that maintain their structural stability during pyrolysis. However, caution should be used for modeling materials that have mass transfer of pyrolyzates and gas-phase reactants that significantly affect pyrolysis given the lack of knowledge in this area.

PROCESS OF CHOOSING PYROLYSIS MODEL

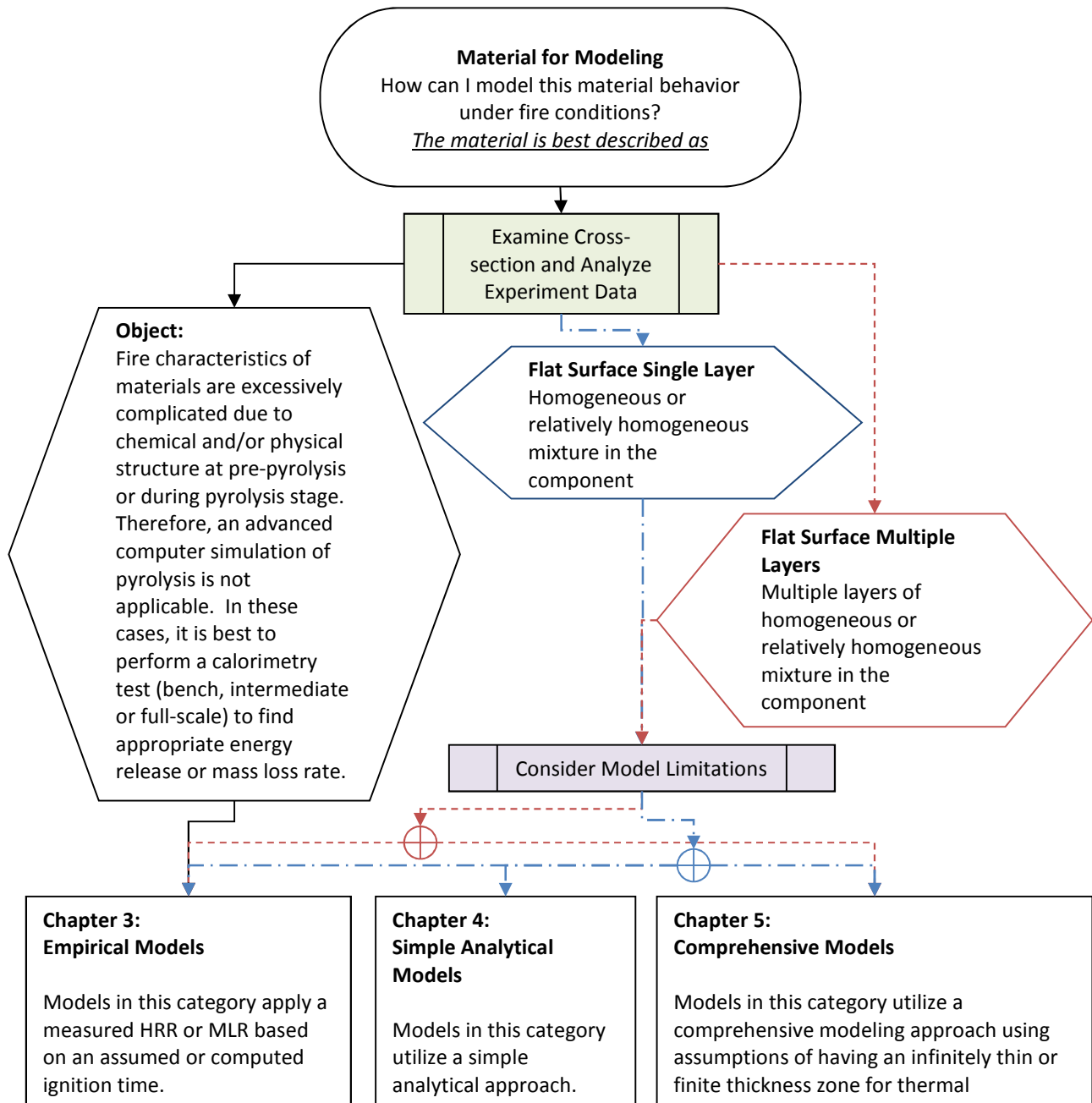


Figure 2-2. Model selection flowchart: By examining the cross-section of material and analyzing experiment data that presents its fire behavior, modeler may determine the material's virtual microstructure and appropriate pyrolysis models available for its specific use.

A flow chart is shown above (see Figure 2-2) to describe the process of model selection. As shown in this chart, a material's virtual microstructure is decided through "Examine Cross-section and Analyze Experiment Data." The virtual microstructure can be **Object**, **Flat Surface Single Layer**, or **Flat Surface Multiple Layers**.

Object is for materials without homogeneous or relatively homogeneous mixture *layers* based on this guide at the pre-pyrolysis stage or during pyrolysis stage, i.e., material geometry that cannot be considered one-dimensional knowing that typically pyrolysis models assume a one-dimensional geometry.

Flat Surface Multiple Layers is for materials that satisfy the following three conditions:

- (1) Distinctive homogeneous or relatively homogeneous mixture layers based on visual inspection
- (2) Experiment data, such as Heat Release Rate or Mass Loss Rate, from a bench-scale test that identify any effects of having multiple layers on material's thermally decomposing or burning characteristics
- (3) That those effects found from analyzing data with consideration of the assumed microstructure are important for modeling purposes, and therefore multiple layers microstructure is necessary, although it adds more complexity to modeling

Flat Surface Single Layer is for materials either with one homogeneous or relatively homogeneous mixture layer, or with multiple homogeneous or relatively homogeneous mixture layers but does not satisfy all three conditions listed above for Flat Surface Multiple Layers.

The modeler now can select the model of his/her interest from the three model categories – **Empirical Models**, **Simple Analytical Models**, and **Comprehensive Models** – depending on its assumed microstructure (Object, Flat Surface Single Layer, or Flat Surface Multiple Layers) and each model's limitations ("Consider Model Limitations"). Note that the complexity of the model increases as model category changes from Empirical Models to Comprehensive Models. This means that the number of parameters that need to be estimated increases as well.

Empirical Models can be used for modeling materials with any microstructure discussed previously – Object, Flat Surface Single Layer, or Multiple Layers. The advantage of utilizing this approach is that it is simple, i.e., unknown model parameters are minimal and easy to obtain through various scale calorimetry experiments. Typically, these models are for materials that have excessively complicated fire behaviors due to either material geometry/structural stability at

pre-pyrolysis stage (e.g., sofa, chair, bookshelf, etc.) or burning behavior during pyrolysis stage (e.g., melting, dripping, non-uniform expanding, etc.). The disadvantage of using models in this category is that, because empirical data such as the heat-release rate or mass-loss rate from a certain test is directly applied to modeling, effects of variation in fire conditions (e.g., ignition scenario, environment, etc.) of the fire scenario from a standard test condition is not considered. See Chapter 3 – Empirical Models for more description. There are five different materials considered as example cases in this chapter (see Table 2-1).

Table 2-1. Example materials in Chapter 3 – Empirical Models: materials are either considered as a burning object or flat surface in modeling

	Burning Object	Burning Flat Surfaces			
Example Materials	Sofa	PMMA	Corrugated Cardboard	Fire-Retarded FRP Composite	Plywood

Simple Analytical Models are for materials that have Flat Surface Single Layer geometry only. The advantage of considering models in this category is that, due to the simplicity of model, only a few unknown model parameters exist, and they are easily estimated typically using bench-scale test results. The disadvantage of using models in this category is that pyrolysis conditions under fire environment need to be applicable to many assumptions used in developing the model – material is considered to be homogeneous, thermally-thick or thermally-thin behavior, and results in steady burning after ignition. See more details on model assumptions and description in Chapter 4 – Simple Analytical Models. There are six different materials considered as example cases in this chapter (see Table 2-2).

Table 2-2. Example materials in Chapter 4 – Simple Analytical Models: materials are considered either thermally-thick and inert at pre-ignition with steady burning at post-ignition, or thermally-thin and inert at pre-ignition with steady burning at post-ignition in modeling

	Thermally-thick and Inert at Pre-ignition, Steady Burning at Post-ignition				Thermally-thin and Inert at Pre-ignition, Steady Burning at Post-ignition	
Example Materials	PMMA	Corrugated Cardboard	Fire Retarded FRP Composite	Plywood	Vinyl Ester GRP and Balsa Wood Core Sandwich Panel	Class C FRP Composite Sheet

Comprehensive Models are for materials that have either Flat Surface Single Layer or Multiple Layers geometry. The advantage of utilizing these models is that the modeler has much flexibility in setting up the pyrolysis problem mathematically. Generally, these models explicitly solve for heating of material during pyrolysis and account for weight loss due to thermal decomposition by conserving mass and energy. Some models even track mass transfer effects such as interactions between pyrolysis products, diffusion of oxygen from surface, etc. The disadvantage of using these models is that significant effort may be needed to estimate unknown model parameters, knowing that the number of unknowns can dramatically increase with respect to increasing modeling complexity. It can range from less than 10 unknowns up to 100 or even more. See Chapter 5 – Comprehensive Models for more description. There are four different materials considered as example cases in this chapter (see Table 2-3).

Table 2-3. Example materials in Chapter 5 – Comprehensive Analytical Models: materials are considered to decompose with single or multiple reaction(s) with or without residue production in modeling

	single-step decomposition RxN w/o residue	single-step decomposition RxN w/ residue	two-step decomposition RxN w/ residue	drying and single-step decomposition RxN w/ residue
Example Materials	PMMA	Corrugated Cardboard	Fire Retarded FRP Composite	Plywood

Chapter 3—Empirical Models

UNDERSTANDING MODEL

General Description of Models

This chapter focuses on empirical methods to estimate the pyrolysis rate of **Objects** (complex geometry) and **Flat Surfaces** materials in a fire scenario, typically in a compartment-fire situation. These methods are referred to as “Empirical Models.” This is the easiest approach to estimate the burning rate of an object or flat surfaces, where heat release and mass loss rate data measured in a test is directly applied to describe a material’s pyrolysis behavior. Data for burning of an object can be obtained through full-scale test with various ignition sources and locations, e.g., furniture calorimeter test. For flat surfaces, data can be obtained through intermediate/bench-scale calorimeter test at a specified heat flux.

Principle assumption is that the ignition scenario and exposure conditions in the fire are comparable to those used in the laboratory. In addition, Empirical Models for flat surfaces assume that (1) heat and mass transfer is one-dimensional, i.e., perpendicular to the exposed surface; (2) edge effects in material testing are not included; and (3) applied heat-flux level during testing is representative average (over space and time) for the fire scenario that is being modeled.¹

Governing Equations

Mathematically the model for estimating the onset (ignition) and subsequent rate of pyrolysis can be described as follows:

$$(t_{ig})_{mod} = (t_{ig})_{exp} \quad \text{Eq.3-1}$$

and

$$(\dot{Q}'')_{mod} = (\dot{Q}'')_{exp} = \Delta h_{c,eff} (\dot{m}'')_{exp} \quad \text{Eq.3-2}$$

where

$(t_{ig})_{mod}$ = ignition time used in the pyrolysis model (s)

$(t_{ig})_{exp}$ = ignition time measured in the calorimeter (s)

$(\dot{Q}'')_{mod}$ = heat release rate used in the compartment fire model (kW/m²)

$(\dot{Q}'')_{exp}$ = heat release rate measured in the calorimeter (kW/m²)

$(\dot{m}'')_{exp}$ = mass loss rate measured in the calorimeter (g/ m²·s)

$\Delta h_{c,eff}$ = effective heat of combustion of the fuel (kJ/g)

Note that heat-release and mass-loss rates measured in a small- and intermediate-scale calorimeter are usually expressed as rate per unit exposed area (hence the double prime). However, for data obtained in a full-scale calorimeter experiment are typically expressed as rate.

MODEL PARAMETERS AND MEASUREMENT METHODS

Virtual Material

Virtual material is an energy source releasing heat to gas phase expressed in terms of heat-release rate or mass-loss rate and effective heat of combustion without certain geometry, whether material is an object or a flat surface.

Model Parameter Table

The following table (see Table 3-1) summarizes model parameters that need to be estimated:

Table 3-1. Model parameter table: summary of model parameters required to conduct pyrolysis modeling

Ignition Parameters	t_{ig}		Time-to-Ignition	
Burning-Rate Parameters	Using HRR		Using MLR and HoC	
	$\dot{Q}''(t)$	Heat-Release Rate	$\dot{m}''(t)$	Mass-Loss Rate
			$\Delta h_{c,eff}$	Effective Heat-of-Combustion

Model Parameter Measurement Methods

1. Time to Ignition

For burning of an object with a complex geometry, full-scale tests such as Furniture (maximum capacity of 1 MW) or Larger (maximum capacity of 40 MW) Calorimeters are conducted. Various ignition sources are used in these tests and they are placed at certain locations for some specified time at the start of each test. Typically, due to this testing procedure, ignition time is at the start of the test. A number of ASTM standards have been tabulated below for full-scale calorimeter tests (see Table 3-2):

Table 3-2. Ignition sources specified in standard fire tests

Test Method	Specimen	Gas Burner Ignition Source			Location of Application
		No.	Type	Heat Output	
ASTM E 603	Various	1	Square	Various	Various
ASTM E 1537 CAL TB 133	Single chair	1	Square	19 kW for 80 s	Horizontal seating surface
ASTM E 1822	Stacked chairs	1	Line	18 kW for 80 s	Bottom chair front edge
ASTM E 1590	Mattress (set)	1	Line	18 kW for 180 s	Front bottom edge
CAL TB 603 16 CFR 1633	Mattress (set)	2	Line Line	19 kW for 70 s 10 kW for 50 s	Top surface Vertical along side
NFPA 286	Wall / Ceiling Lining	1	Square	40 kW for 300 s 160 kw for 600 s	Room corner

For burning of a flat surface material, an intermediate/bench-scale calorimeter test(s) is conducted at a specified heat flux. In these tests, an apparatus that consists of a radiant panel that exposes the specimen to a preset irradiance is used to measure the ignition time. The heat source can be a gas panel or consist of one or several electrical heating elements. A small flame, electric spark or hot wire is usually present in the gas phase above the specimen surface (horizontal specimen orientation) or at the top edge of the specimen (vertical or inclined surface). Time of ignition is typically determined on the basis of visual observations. This can be tricky when the material exhibits extensive flashing before sustained flaming. An alternative method based on the second time derivative of the mass of the specimen has been suggested to alleviate this problem.² Ignition criteria based on a critical mass loss rate of $1 \text{ g/m}^2\cdot\text{s}$ or a critical heat-release rate

of 24 kW/m² have also been proposed.³ A number of ASTM standards have been tabulated below (see Table 3-3) for measuring the time to ignition of a material exposed to a specified level of incident radiant heat and intermediate/bench-scale calorimeter tests:

Table 3-3. ASTM standards for measurement of time-to-ignition of materials exposed to specified level of incident radiant heat source in intermediate/bench-scale calorimeter tests

Standard Test	Description
ASTM E 1321 – 09	<i>Standard Test Method for Determining Material Ignition and Flame Spread Properties</i>
ASTM E 1354 – 11b	<i>Standard Test Method for Heat and Visible Smoke Release Rates for Materials and Products Using an Oxygen Consumption Calorimeter</i>
ASTM E 2058 – 09	<i>Standard Test Methods for Measurement of Synthetic Polymer Material Flammability Using a Fire Propagation Apparatus (FPA)</i>

2. Heat-Release Rate or Mass-Loss Rate and Effective Heat of Combustion

HEAT RELEASE RATE

Heat-release rate is measured via calorimetry test in various scales. Two major methods used since the early 1980s are oxygen-consumption and carbon-oxides generation techniques. Oxygen-consumption method is based on test results of organic fuels showing a nearly constant net amount of heat, E, is released per unit mass of oxygen consumed for complete combustion.^{4,5} Carbon-oxides generation method is based on the fact that amount of heat released per mass unit of carbon dioxide and carbon monoxide generated is also relatively constant within a category of fuels or polymers. This method is particularly useful for oxidizers.⁶ See section for measurement of Time to Ignition for a list of ASTM standards for calorimetry tests.

MASS-LOSS RATE

The energy release by material pyrolysis can also be expressed in terms of mass-loss rate and effective heat of combustion. Mass-loss rate is found from direct measurement of mass loss, as calorimeters are often equipped with a scale. The mass-loss rate of the specimen in a test is then determined by continuously weighing the

specimen during the test and by subsequently calculating the time derivative of the mass vs. time curve.

EFFECTIVE HEAT OF COMBUSTION

The effective heat of combustion, $\Delta h_{c,eff}$, is equal to the net heat-release rate divided by the mass-loss rate measured in a calorimeter (see Eq.3-3):

$$\Delta h_{c,eff} \equiv \frac{\dot{Q}}{\dot{m}} = \frac{\dot{Q}''}{\dot{m}''} \quad \text{Eq.3-3}$$

The effective heat of combustion at a particular time t can be calculated by substituting the values for \dot{Q} (or \dot{Q}'') and \dot{m} (or \dot{m}'') at that time as in above equation. The average effective heat of combustion over a specified time period is equal to the cumulative heat released over the specified period divided by the mass loss over the specified period. Theoretically it is possible to calculate $\Delta h_{c,eff}$ at every data scan. In practice, however, there are several challenges.

1. The heat-release rate and mass-loss rate measurements are not completely synchronized. This may result in significant errors, in particular at times when there is a rapid change in the burning rate.
2. Measurement errors are amplified during periods of slow burning, as both numerator and denominator in Eq.3-3 are small.
3. Even if a general math filter is used, calculated mass-loss rates can still be very noisy, resulting in fluctuations in the calculated effective heat of combustion values.

For this reason it usually better to report the average effective heat of combustion over a specified period of time, i.e., the cumulative heat released over the specified period divided by the mass loss over the specified period. It is very common to report the average effective heat of combustion over the entire test (see Eq.3-4):

$$(\Delta h_{c,eff})_{avg} = \frac{Q_{tot}}{m_0 - m_f} \quad \text{Eq.3-4}$$

where

$(\Delta h_{c,eff})_{avg}$ = average effective heat of combustion over the entire test (kJ/g);

Q_{tot} = total heat released over the entire test duration (kJ);

m_0 = specimen mass at the start of the test (g); and
 m_f = specimen mass at the end of the test (g).

Dillon et al. found the average effective heat of combustion over the peak burning period to be useful for predicting fire growth of wall linings (flat surfaces) in a room/corner test on the basis of Cone Calorimeter data.⁷ The peak burning period was defined in this study as the time during which the heat release rate in the Cone Calorimeter is equal to or higher than 80% of the (first) peak heat release rate.

UNCERTAINTY ANALYSIS

An engineering fire safety analysis involving compartment fire modeling must take into account the uncertainty of the input data in order to determine the uncertainty of the results of the analysis. This process is referred to a “propagation of uncertainty.” Some input data, such as the dimensions of the compartment, are relatively well known and their uncertainty can be neglected. Other input parameters, such as the heat release rate of an object, are significantly more variable and the uncertainty of these parameters must be accounted for. A distinction is made between two types of uncertainty: Type A and Type B. The former is uncertainty due to uncertainty due to random variation, while the latter is due to lack of (complete) knowledge. A brief and general discussion of the two types of uncertainty can be found in Appendix A.

Considering that the model input parameters are time-to-ignition and heat-release rate directly found from certain tests, uncertainty in measurements from calorimetry tests in the literature are searched for. For a large-scale apparatus, a 3 MW quantitative HRR facility at NIST has been assessed to calculate the HRR uncertainty.⁸ This work has taken into account the basic measurement inputs, which are the instrument voltages, thermocouple temperatures, and constant parameters used in calculations, and has showed that the relative uncertainties were ± 7.5 , ± 5.3 , and $\pm 5.3\%$ for HRR at 0.05, 0.65, and 2.7MW, respectively. There are studies that have addressed the uncertainty associated with the HRR calculation for bench-scale apparatuses – Cone Calorimeter and Fire Propagation Apparatus (FPA).^{9,10} Enright and Fleischmann⁹ have reported that the relative HRR uncertainty is about $\pm 5.5\%$ for the HRR in the range of 200–500kW/m². Zhao and Dembsey¹⁰ have estimated the relative HRR uncertainties are 20 to 30%, 10% and 10% for 1 kW, 3 kW and 5 kW methane fires, respectively.

PARAMETER ESTIMATION PROCESS

To create a virtual material, these tasks must be considered:

- Create a list of model inputs, which needs to be determined
- Obtain model unknown inputs via measurement or literature search

When the above is done and every unknown has been estimated, validation work and commentary is needed to understand the performance of the estimated parameter set:

- Run model
- Analyze simulation quality with consideration of uncertainties in modeling outputs and data
- Add commentary

When presenting the parameter estimation results, three summary tables will be introduced: Model Parameter Table, Validation, and Commentary sections. Model Parameter Table includes the model parameters necessary to conduct pyrolysis modeling, their estimated values, and methods of estimating the unknowns. Validation work consists of the following information: description of modeling goal, pyrolysis model type and modeling approach used in the exercise, experiment type and its data used to empirically simulate material's heat release rate and uncertainty information of experimental data, and modeling outputs. Commentary section discusses any limitations of pyrolysis modeling conducted above, which has been summarized in Model Parameter and Validation Tables.

For better visualization of the problem, a flowchart is shown below (see Figure 3-1):

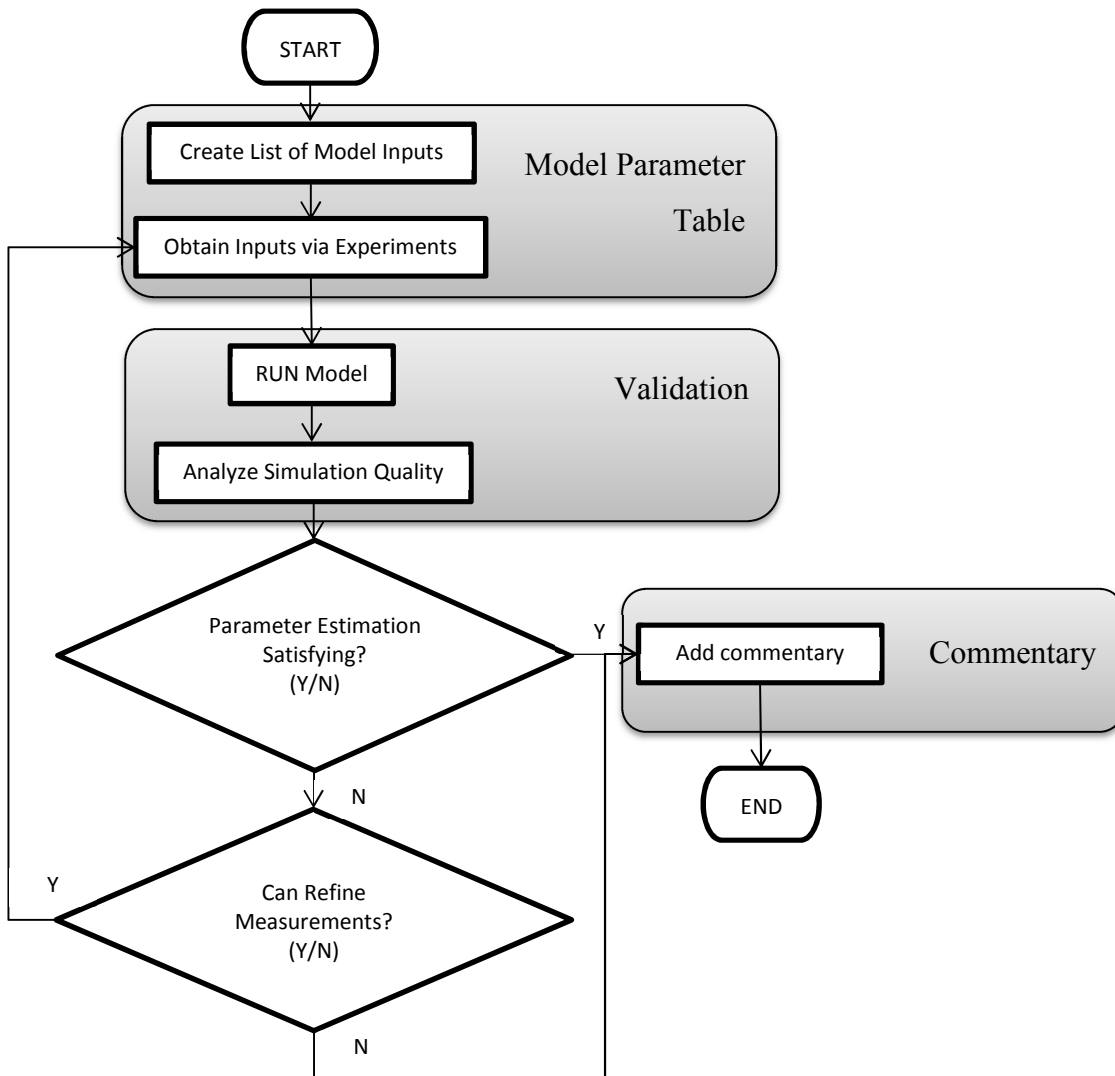


Figure 3-1. Flow chart of parameter estimation for empirical pyrolysis models

EXAMPLE CASES OVERVIEW

Table 3-4. Overview of example cases using empirical pyrolysis models

Case	Description	Examples
1	Burning Objects	Sofa
2	Burning Flat Surfaces	PMMA
		Corrugated Cardboard
		Fire-Retarded FRP Composite
		Plywood

In the following, summarized results are shown for each example case. Detailed solutions of these example cases are given in Appendix B.

CASE 1: BURNING OBJECT

General Model Parameter Table

Table 3-5. Model-parameter table for Case 1 examples

Ignition Parameters	t_{ig}		Time-to-Ignition	
Burning-Rate Parameters	Using HRR		Using MLR and HoC	
	$\dot{Q}''(t)$	Heat-Release Rate	$\dot{m}''(t)$	Mass-Loss Rate
			$\Delta h_{c,eff}$	Effective Heat-of-Combustion

Example 3.1 Modeling Sofa

3.1.1 Model Parameter Table

Model Parameters		Unit	Estimated Values and Estimation Methods
Ignition Parameters	t_{ig}	s	80
			Measurement, Furniture Calorimeter
Burning-Rate Parameters	HRR	kW	
			Measurement, Furniture Calorimeter

3.1.2 Validation

3.1.2.1 MODELING GOAL

Estimate model parameters for conducting modeling of pyrolysis of an object under well-ventilated condition.

3.1.2.2 MODEL TYPE

Empirical Pyrolysis Model

3.1.2.3 MODELING APPROACH

- Pre-ignition stage is:
 - Inert: decomposition before ignition is neglected
 - Always the same as in Furniture Calorimeter test
- Ignition scenario is the same as in Furniture Calorimeter experiment: time to ignition is the same in modeling as determined in experiment
- Post-ignition stage is:

- Considered to have instantaneous release of volatiles from solid to gas phase: typically, an area is specified that can be correlated to the actual burning object where energy is released to the gas phase
- Considered to be the same as in Furniture Calorimeter test in terms of heat-release rate or mass-loss rate

3.1.2.4 EXPERIMENT DESCRIPTION

Furniture Calorimeter test

3.1.2.5 DATA SET

Experiment data of a single-seat sofa mockup is found for pyrolysis modeling using Empirical Model. This sofa mockup was burned under a hood of a furniture calorimeter. The mockup consisted of a steel frame with untreated polyurethane foam cushions (80% of the combustible mass) and a cotton fabric (20% of the combustible mass). Total combustible mass was 3.93 kg. The test was performed according to *ASTM E 1537* and CAL TB 133. The ignition source consisted of a 0.25 m square tubular propane burner producing a 19 kW flame for 80 seconds applied to the top of the seat cushion.

3.1.2.6 UNCERTAINTY

Uncertainty in Experiment Data

- Data reproducibility is checked by repeating four identical sofa mockup tests
- Uncertainty of HRR is estimated by first calculating the confidence interval for 95% confidence level ($\alpha = 0.05$) assuming student t distribution with a sample size of 3 (four data sets) at each time step. Then an average confidence interval is calculated for the time interval of interest ($0 < t < 800$ min), which results in ± 20.4 kW.
- Assume:
 - Uncertainties are comparable to those of similar objects pyrolyzing in a compartment fire

Uncertainty in Modeling Outputs

- Same as in experiment data

3.1.3 Commentary

When using the Empirical Model to simulate pyrolysis of a sofa, furniture calorimeter test data has been utilized to estimate the time to ignition from exposure to a propane burner and the energy released from burning. As noted in the Understanding Model part of the chapter, this approach is limited as follows in terms of the conditions being comparable to those found in the fire scenario of interest:

- Ignition scenario and exposure conditions

The basic assumption used in Empirical Models is that the ignition scenario and exposure conditions in the fire are comparable to those used in the laboratory. Therefore, any changes made in the ignition scenario and exposure conditions have to be accounted for by the model user when applying the data to Empirical Models. The furniture calorimeter experiment in this example is conducted under certain conditions: ignition is achieved by applying propane flame on the horizontal surface (seating cushion) for 80 s and sufficient supply of air is provided throughout its burning phase. To illustrate the effect of altering the conditions in HRR curves, two other HRR curves are shown below:

Effect of ignition source strength (see Figure 3-2): Two identical single-seat sofas were obtained for testing. In the first test the sofa was ignited with a 45 W butane gas flame applied to the center of the seat cushion for 20 s. In the second test 59 ml (2 oz) of gasoline was poured on the seat cushion to simulate an incendiary fire. The resulting heat-release rate measurements are shown below. In this case the use of the weaker ignition source delays the propagation to full involvement by approximately 170 s. For this case the effect of ignition source strength can relatively easily be accounted for, although in practice it may not be trivial to determine the exact time period over which to shift the HRR curve. The effect can be much more pronounced when the source strength is close to the level needed to obtain sustained burning.

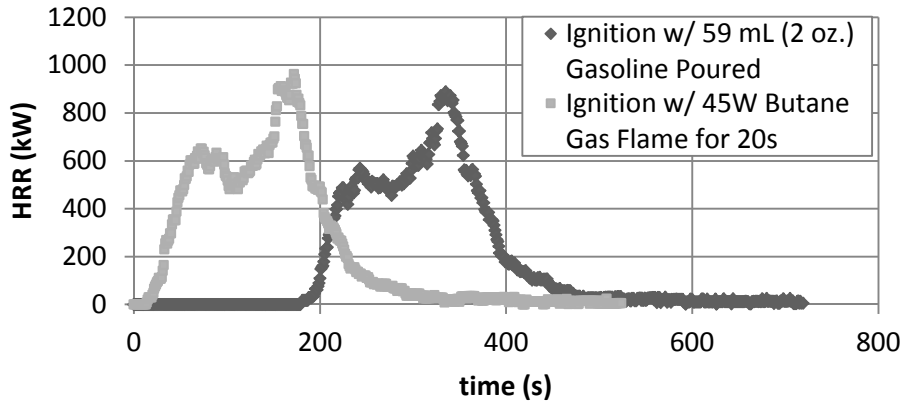


Figure 3-2. Effect of ignition source strength: single-seat sofas tested in furniture calorimeter test with different ignition sources – ignition with 59 mL gasoline poured (♦) or with 45 W butane gas flame (■)

Effect of ignition location (see Figure 3-3): Two tests were conducted on a steel-framed-seat sofa mockup according to the same procedure and using the same padding and fabric as in the tests described in the Example case. In the first test the burner flame was applied to the seat cushion on the right side. In the second test the burner was applied to the center seat cushion. The resulting HRR measurements are compared in Figure 3-3 below. In the first test the flames spread from the right side to the left side. When the flames reached the armrest on the left side, part of the material on the right side had already been consumed. This resulted in a relatively steady HRR that peaked slightly above 400 kW. In the second test the flames spread in two directions. As a result the heat rate continuously increased until the two armrests ignited and a peak heat-release rate of close to 1 MW was reached. This case illustrates that a seemingly small difference in the ignition scenario can have a surprisingly dramatic effect on fire growth.

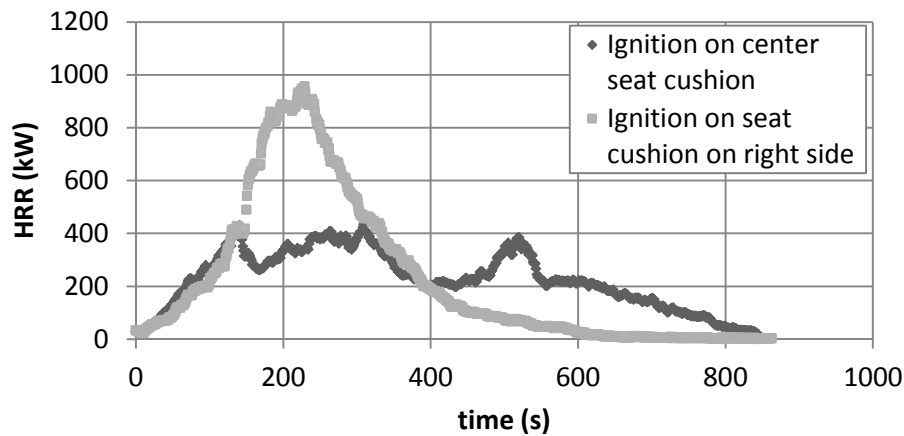


Figure 3-3. Effect of ignition location: steel-framed seat sofa mockups tested in furniture calorimeter test with different ignition locations – ignition on center seat cushion (♦) or seat cushion on right side (■)

- Heat and mass transfer

This is a multi-dimensional problem, and the dimensional effect is implicitly addressed in modeling by a single parameter – HRR or MLR and effective heat of combustion.

CASE 2: BURNING FLAT SURFACES

General Model Parameter Table

Table 3-6. Model Parameter Table for Case 2 Examples

Ignition Parameters	t_{ig}		Time-to-Ignition	
Burning-Rate Parameters	Using HRR		Using MLR and HoC	
	$\dot{Q}''(t)$	Heat-Release Rate	$\dot{m}''(t)$	Mass-Loss Rate
			$\Delta h_{c,eff}$	Effective Heat-of-Combustion

Example 3.2 Modeling PMMA

3.2.1 Model Parameter Table

Model Parameters		Unit	Estimated Values and Estimation Methods
Ignition Parameters	t_{ig}	s	22
			Measurement, Cone Calorimeter
Burning-Rate Parameters	MLR	g/s- m ²	
			<p>* Measurement is made at applied heat flux of 50 kW/m² in Cone Calorimeter.</p>
	HoC	kJ/g	24.8 ± 0.1 Measurement, Cone Calorimeter

3.2.2 Validation

3.2.2.1 MODELING GOAL

Estimate model parameters for conducting modeling of pyrolysis of a flat surface under well-ventilated condition.

3.2.2.2 MODEL TYPE

Empirical Pyrolysis Model

3.2.2.3 MODELING APPROACH

- Pre-ignition stage is
 - Inert: decomposition with bubbling before ignition is neglected
 - Always the same as in Cone Calorimeter test with a specified heat flux impinging on material's surface (typically $\sim 50 \text{ kW/m}^2$ is used)
- Ignition phenomenon is the same as in Cone Calorimeter experiment: time to ignition is the same in modeling as determined in experiment
- Post-ignition stage is
 - Considered to have instantaneous release of volatiles from solid to gas phase: bubbling layer is neglected and is considered as a surface phenomena
 - Considered to be the same as in Cone Calorimeter test in terms of heat-release rate or mass-loss rate per unit area

3.2.2.4 EXPERIMENT DESCRIPTION

Cone Calorimeter test

3.2.2.5 DATA SET

Cone Calorimeter test data of black PMMA with thickness of 18 mm, density of 1170 kg/m^3 and applied heat flux of 50 kW/m^2 is found.

3.2.2.6 UNCERTAINTY

Uncertainty in Experiment Data

- Uncertainty in time-to-ignition and mass-loss rate: From the experiment work done by Beaulieu and Dembsey¹¹ on thermally-thick behaving black PMMA using AFM apparatus, the experiment uncertainty in time-to-ignition and mass-loss rate at steady burning were determined as $\pm 2 \text{ s}$ and $\pm 3 \text{ g/m}^2\text{s}$, respectively. The test results were compared with other literature values using different apparatuses such as Cone Calorimeter as well, which were considered as consistent.
- Assume:
 - Uncertainties are comparable to those of similar flat surfaces pyrolyzing under heating

Uncertainty in Modeling Outputs

- Same as in experiment data

3.2.3 Commentary

When using Empirical Model to simulate pyrolysis of PMMA, PMMA test data from a bench-scale Cone Calorimeter experiment at a set heat-flux level has been utilized to estimate the time-to-ignition from exposure to heating and the energy released from burning of PMMA. As noted in the Understanding Model part of the chapter, this approach is limited as follows in terms of the conditions being comparable to those found in the fire scenario on interest:

- Ignition scenario: piloted ignition with an electric sparker
- Exposure conditions: electrically heated coil uniformly heating PMMA with a set heat flux impinging on the front surface, where this applied heat-flux level during testing is assumed to be representative average (over space and time) for the fire scenario that is being modeled
- Heat and mass transfer: one-dimensional, i.e., perpendicular to the exposed surface
- Surface-burning data: edge effects in material testing are not included; therefore, data per unit area can be applied to simulate larger areas by simply multiplying by the material surface area involved in fire

Example 3.3 Modeling Corrugated Cardboard

3.3.1 Model Parameter Table

Model Parameters		Unit	Estimated Values and Estimation Methods
Ignition Parameters	t_{ig}	s	32 ± 4
			Measurement, Cone Calorimeter (4 tests at 25 kW/m ² average and 95% C.I. using student t distribution)
Burning-Rate Parameters	MLR	g/s-m ²	
			* Measurement is made at applied heat flux of 25 kW/m ² in Cone Calorimeter.
	HoC	kJ/g	13.5 ± 0.5 Measurement, Cone Calorimeter (2 tests at 25 kW/m ² average and 2 times standard deviation)

3.3.2 Validation

3.3.2.1 MODELING GOAL

Estimate model parameters for conducting modeling of pyrolysis of a flat surface under well-ventilated condition.

3.3.2.2 MODEL TYPE

Empirical Pyrolysis Model

3.3.2.3 MODELING APPROACH

- Pre-ignition stage is
 - Inert: non-uniform charring is considered to be evenly distributed
 - Always the same as in Cone Calorimeter test with a specified heat flux impinging on material's surface
- Ignition phenomenon is the same as in Cone Calorimeter experiment: time-to-ignition is the same in modeling as determined in experiment
- Post-ignition stage is
 - Considered to have instantaneous release of volatiles from solid to gas phase
 - Considered to be the same as in Cone Calorimeter test in terms of heat-release rate or mass-loss rate per unit area

3.3.2.4 EXPERIMENT DESCRIPTION

Cone Calorimeter test

3.3.2.5 DATA SET

Cone Calorimeter test data of triple-layer cardboard with thickness of 15 mm, density of 116 kg/m^3 , and applied heat flux of 25 kW/m^2 is found.

3.3.2.6 UNCERTAINTY

Uncertainty in Experiment Data

- The uncertainty in the mass-loss rate data is estimated via statistical approach, taking the standard deviation (0.58 g/sm^2) from the mean of a steady burning of five identical PMMA tests conducted in a Cone Calorimeter¹². The estimated uncertainty is 1.4 g/sm^2 , which is found by calculating the 95% confidence interval applying student t distribution with a sample size of 5.
- The uncertainty in time to ignition data is estimated via statistical approach, taking four identical Cone Calorimeter test data at heat flux 25 kW/m^2 of this cardboard. 95% confidence interval is calculated for each heat-flux level assuming student t distribution.
- The uncertainty in effective heat-of-combustion is estimated by average heat-release rate divided by average mass-loss rate of two identical tests. Two times the standard deviation is used as its uncertainty band.
- Assume:
 - Uncertainties are comparable to those of similar flat surfaces pyrolyzing under heating

Uncertainty in Modeling Outputs

- Same as in experiment data

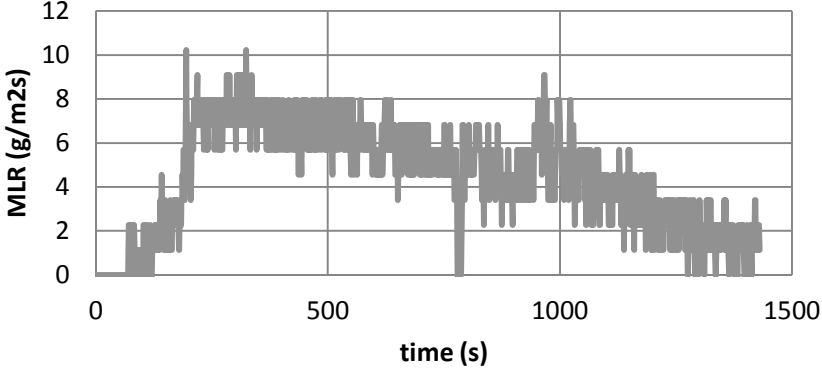
3.3.3 Commentary

When using Empirical Model to simulate pyrolysis of this triple-layer cardboard, test data from a bench-scale Cone Calorimeter experiment at a set heat-flux level has been utilized to estimate the time to ignition from exposure to heating and the energy released from burning of this cardboard. As noted in the Understanding Model part of the chapter, this approach is limited as follows in terms of the conditions being comparable to those found in the fire scenario of interest:

- Ignition scenario: piloted ignition with an electric sparker
- Exposure conditions: electrically heated coil uniformly heating sample with a set heat flux impinging on the front surface, where this applied heat-flux level during testing is assumed to be representative average (over space and time) for the fire scenario that is being modeled
- Heat and mass transfer: one-dimensional, i.e., perpendicular to the exposed surface
- Surface-burning data: edge effects in material testing are not included ; therefore, data per unit area can be applied to simulate larger areas by simply multiplying by the material surface area involved in fire

Example 3.4 Modeling Fire Retarded FRP Composite

3.4.1 Model Parameter Table

Model Parameters		Unit	Estimated Values and Estimation Methods
Ignition Parameters	t_{ig}	s	175 ± 36
			Measurement, Cone Calorimeter (4 tests at 50 kW/m ² average and 95% C.I. using student t distribution)
Burning-Rate Parameters	MLR	g/s-m ²	 <p>* Measurement is made at applied heat flux of 50 kW/m² in Cone Calorimeter.</p>
			Measurement, Cone Calorimeter
	HoC	kJ/g	14.7 ± 3.8 Measurement, Cone Calorimeter (4 tests at 50 kW/m ² average and 95% C.I. using student t distribution)

3.4.2 Validation

3.4.2.1 MODELING GOAL

Estimate model parameters for conducting modeling of pyrolysis of a flat surface under well-ventilated condition.

3.4.2.2 MODEL TYPE

Empirical Pyrolysis Model

3.4.2.3 MODELING APPROACH

- Pre-ignition stage is
 - Inert: non-uniform charring is considered to be evenly distributed
 - Always the same as in Cone Calorimeter test with a specified heat flux impinging on material's surface
- Ignition phenomenon is the same as in Cone Calorimeter experiment: time-to-ignition is the same in modeling as determined in experiment
- Post-ignition stage is:

- Considered to have instantaneous release of volatiles from solid to gas phase
- Considered to be the same as in Cone Calorimeter test in terms of heat-release rate or mass-loss rate per unit area

3.4.2.4 EXPERIMENT DESCRIPTION

Cone Calorimeter test

3.4.2.5 DATA SET

Cone Calorimeter test data of FRP composite with thickness of 9.2 mm, density of 1900 kg/m³, and applied heat flux of 50 kW/m² is found.

3.4.2.6 UNCERTAINTY

Uncertainty in Experiment Data

- The uncertainty in the mass loss rate data is estimated via statistical approach, taking the standard deviation (0.58 g/sm²) from the mean of a steady burning of five identical PMMA tests conducted in a Cone Calorimeter.¹² The estimated uncertainty is 1.4 g/sm², which is found by calculating the 95% confidence interval applying student t distribution with a sample size of five.
- The uncertainty in time to ignition data is estimated via statistical approach, taking four identical Cone Calorimeter test data at heat flux 50 kW/m² of this cardboard. 95% confidence interval is calculated for each heat-flux level assuming student t distribution.
- The uncertainty in effective heat of combustion is estimated by average heat release rate divided by average mass loss rate of four identical tests. 95% confidence interval is calculated for each heat-flux level assuming student t distribution.
- Assume:
 - Uncertainties are comparable to those of similar flat surfaces pyrolyzing under heating

Uncertainty in Modeling Outputs

- Same as in experiment data

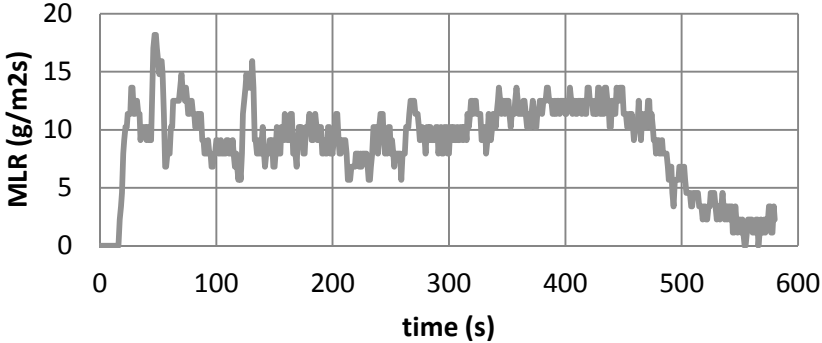
3.4.3 Commentary

When using Empirical Model to simulate pyrolysis of this fire retarded FRP composite, test data from a bench-scale Cone Calorimeter experiment at a set heat-flux level has been utilized to estimate the time to ignition from exposure to heating and the energy released from burning of this material. As noted in the Understanding Model part of the chapter, this approach is limited as follows in terms of the conditions being comparable to those found in the fire scenario of interest:

- Ignition scenario: piloted ignition with an electric sparker
- Exposure conditions: electrically heated coil uniformly heating sample with a set heat flux impinging on the front surface, where this applied heat flux level during testing is assumed to be representative average (over space and time) for the fire scenario that is being modeled
- Heat and mass transfer: one-dimensional, i.e., perpendicular to the exposed surface
- Surface-burning data: edge effects in material testing are not included; therefore, data per unit area can be applied to simulate larger areas by simply multiplying by the material surface area involved in fire

Example 3.5 Modeling Plywood

3.5.1 Model Parameter Table

Model Parameters		Unit	Estimated Values and Estimation Methods
Ignition Parameters	t_{ig}	s	27 ± 9
			Measurement, Cone Calorimeter (3 tests at 50 kW/m ² average and 95% C.I. using student t distribution)
Burning-Rate Parameters	MLR	g/s-m ²	 <p>* Measurement is made at applied heat flux of 50 kW/m² in Cone Calorimeter.</p>
			Measurement, Cone Calorimeter
	HoC	kJ/g	11.0 ± 0.3
			Measurement, Cone Calorimeter (2 tests at 50 kW/m ² average and 2 times standard deviation)

3.5.2 Validation

3.5.2.1 Modeling Goal

Estimate model parameters for conducting modeling of pyrolysis of a flat surface under well-ventilated condition.

3.5.2.2 Model Type

Empirical Pyrolysis Model

3.5.2.3 Modeling Approach

- Pre-ignition stage is:
 - Inert: non-uniform charring is considered to be evenly distributed
 - Always the same as in Cone Calorimeter test with a specified heat flux impinging on material's surface
- Ignition phenomenon is the same as in Cone Calorimeter experiment: time to ignition is the same in modeling as determined in experiment
- Post-ignition stage is:
 - Considered to have instantaneous release of volatiles from solid to gas phase
 - Considered to be the same as in Cone Calorimeter test in terms of heat-release rate or mass loss rate per unit area

3.5.2.4 Experiment Description

Cone Calorimeter test

3.5.2.5 Data Set

Cone Calorimeter test data of triple-layer cardboard with thickness of 11.1 mm, density of 542 kg/m³ and applied heat flux of 50 kW/m² is found.

3.5.2.6 Uncertainty

Uncertainty in Experiment Data

- The uncertainty in the mass loss rate data is estimated via statistical approach, taking the standard deviation (0.58 g/sm²) from the mean of a steady burning of five identical PMMA tests conducted in a Cone Calorimeter.¹² The estimated uncertainty is 1.4 g/sm², which is found by calculating the 95% confidence interval applying student t distribution with a sample size of five.
- The uncertainty in time-to-ignition data is estimated via statistical approach, taking three identical Cone Calorimeter test data at heat flux 50 kW/m² of this cardboard. 95% confidence interval is calculated for each heat flux level assuming student t distribution.
- The uncertainty in effective heat of combustion is estimated by average heat release rate divided by average mass loss rate of two identical tests. Two times the standard deviation is used as its uncertainty band.
- Assume:
 - Uncertainties are comparable to those of similar flat surfaces pyrolyzing under heating

Uncertainty in Modeling Outputs

- Same as in experiment data

3.5.3 Commentary

When using Empirical Model to simulate pyrolysis of this plywood, test data from a bench-scale Cone Calorimeter experiment at a set heat-flux level has been utilized to estimate the time-to-ignition from exposure to heating and the energy released from burning of this material. As noted in the Understanding Model part of the chapter, this approach is limited as follows in terms of the conditions being comparable to those found in the fire scenario of interest:

- Ignition scenario: piloted ignition with an electric sparker
- Exposure conditions: electrically heated coil uniformly heating sample with a set heat flux impinging on the front surface where this applied heat-flux level during testing is assumed to be representative average (over space and time) for the fire scenario that is being modeled
- Heat and mass transfer: one-dimensional, i.e., perpendicular to the exposed surface
- Surface-burning data: edge effects in material testing are not included; therefore, data per unit area can be applied to simulate larger areas by simply multiplying the by material surface area involved in fire

REFERENCES

- ¹ Babrauskas, V., "Specimen Heat Fluxes for Bench-Scale Heat Release Rate Testing," *Fire and Materials*, 19, 243-252, 1995.
- ² Khan, M.; and deRis, J., "Determination of Operator Independent Ignition for Polymeric Solids," in *9th Fire and Materials Conference*, Interscience Co.mmunications, London, England., 2005, 11-22.
- ³ Lyon, R.; and Quintiere, J., "Criteria for Piloted Ignition of Combustible Solids," *Combustion and Flame*, 151, 551-559, 2007.
- ⁴ Thornton, W., "The Relation of Oxygen to the Heat of Combustion of Organic Compounds," *Philosophical Magazine and Journal of Science*, 33, 1917.
- ⁵ Huggett, C., "Estimation of the Rate of Heat Release by Means of Oxygen Consumption Measurements," *Fire and Materials*, 12, 61-65, 1980.
- ⁶ Buc, E., *Oxidizer Classification Research Project: Tests and Criteria*, Final Report, Fire Protection Research Foundation, Quincy, MA, 2009.
- ⁷ Dillon, S., *et al.*, "Determination of Properties and the Prediction of the Energy Release Rate of Materials in the ISO 9705 Room-Corner Test," National Institute of Standards and Technology, Gaithersburg, MD NIST-GCR-98-753, 1998
- ⁸ Bryant, R.A.; Ohlemiller, T.J.; Johnsson, E.L.; Hammins, A.; Grove, B.S.; Guthrie, W.F.; Maranghides, A.; and Mulholland, G.W., The NIST 3 Megawatt quantitative heat release rate facility. NIST Special Publication 1007. NIST, Gaithersburg, MD, December 2003.
- ⁹ Enright, P.; and Fleischmann, C.; Uncertainty of heat release rate calculation of the ISO5660-1 Cone Calorimeter Standard Test Method. *Fire Technology* 1999; 35(2):153–169.
- ¹⁰ Zhao, Lei; and Dembsey, Nicholas A. 2008. Measurement uncertainty analysis for calorimetry apparatuses. *Fire and Materials*. 32(1), 1-26.
- ¹¹ Beaulieu, P.A.; and Dembsey, N.A., "Effect of Oxygen on Flame Heat Flux in Horizontal and Vertical Orientations," *Fire Safety Journal*, 43:6 (2008) 410-428.
- ¹² Zhao, Lei, Bench Scale Apparatus Measurement Uncertainty and Uncertainty Effects on Measurement of Fire Characteristics of Material Systems, MS Thesis, Fire Protection Engineering, WPI, 2005-04-27, ETD-050105-182456.

Chapter 4—Simple Analytical Models

UNDERSTANDING MODEL

General Description of Models

In this model category, surface temperature of a material is solved based on transient heat conduction equation using either thermally-thick or thermally-thin assumption. When the thermally-thick assumption is used, material is considered as a semi-infinite inert solid up until ignition from time-of-exposure to heating. The rate of surface-temperature increase is dependent upon the thermal inertia ($k\rho c$) of the material. The thermally-thin approach can be used for materials that are subject to heating under condition of greater convective resistance between solid and gas phase than conductive resistance within solid phase. This condition allows the material to be modeled with thermally-lumped analysis to calculate its temperature increase during pre-ignition stage where any temperature gradient within the solid phase and mass loss is neglected. The rate of temperature increase is dependent upon the density multiplied by heat capacity (ρc) of the material. For both approaches, the material is assumed to ignite when its surface temperature reaches a material-dependent value (T_{ig}). Following ignition the mass-loss rate of the material is determined based on the net heat flux at the exposed surface and the heat of gasification (Δh_g). Finally the heat release rate is determined by multiplying the mass-loss rate by the effective heat of combustion ($\Delta h_{c,eff}$).

Principal assumptions are the same as those for Empirical Models for flat surfaces. In addition, the methods to obtain the two combustion properties ($\Delta h_{c,eff}$ and Δh_g) are based on the assumptions of steady burning on the material surface.

Governing Equations

Assuming that the material is a thermally-thick solid being heated on one side by applying a constant heat flux with the other side insulated (see Figure 4-1), conservation of energy with initial and boundary conditions can be written as below (see Eq. 4-1 through Eq. 4-4):

$$\rho c \frac{\partial T}{\partial t} = k \frac{\partial^2 T}{\partial x^2} \quad \text{Eq. 4-1}$$

$$T_{t=0} = T_{\infty} \quad \text{Eq. 4-2}$$

$$-k \left. \frac{\partial T}{\partial x} \right|_{x=0} = \dot{q}_{net} \quad \text{Eq. 4-3}$$

$$-k \left. \frac{\partial T}{\partial x} \right|_{x=\delta} = 0 \quad \text{Eq. 4-4}$$

where

- T = temperature (K);
- x = distance from the exposed surface of the specimen (m);
- δ = specimen thickness (m);
- T_{∞} = ambient and initial temperature (K);
- ε = surface emissivity/absorptivity;
- h_c = convection coefficient ($\text{kW}/\text{m}^2 \cdot \text{K}$);
- T_s = surface temperature (K); and
- σ = Boltzmann constant ($5.67 \cdot 10^{-11} \text{ kW}/\text{K}^4 \cdot \text{m}^2$).

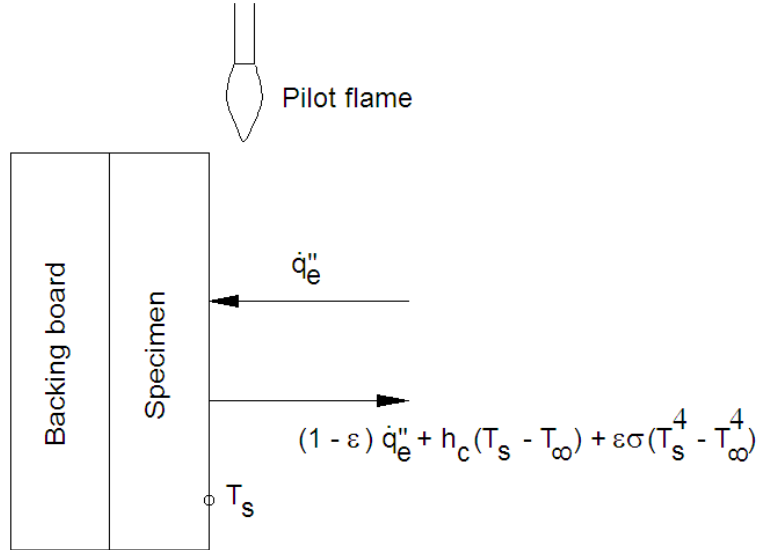


Figure 4-1. Schematic of a piloted ignition experiment

For the thermally-thin approach, the following governing equation is used (see Eq. 4-5 and Eq. 4-6):

$$\rho c \delta \frac{dT}{dt} = \dot{q}_{net}'' \quad \text{Eq. 4-5}$$

$$T_{t=0} = T_\infty \quad \text{Eq. 4-6}$$

By assuming that the applied heat flux is constant, time-to-ignition can be solved as below (see Eq. 4-7 and Eq. 4-8):

$$t_{ig} = \frac{\pi}{4} k \rho c \frac{(T_{ig} - T_\infty)^2}{(\dot{q}_{net}'')^2} \quad (\text{thermally-thick}) \quad \text{Eq. 4-7}$$

$$t_{ig} = \rho c \delta \frac{(T_{ig} - T_\infty)}{\dot{q}_{net}''} \quad (\text{thermally-thin}) \quad \text{Eq. 4-8}$$

where typically, \dot{q}_{net}'' impinging on material surface for times prior to ignition in an intermediate or bench-scale calorimetry tests can be expressed as below assuming material is inert and opaque:

$$\dot{q}_{net}'' = \varepsilon \dot{q}_e'' - h_c (T_s - T_\infty) - \varepsilon \sigma (T_s^4 - T_\infty^4) \quad \text{Eq. 4-9}$$

To determine whether the material of interest is acting thermally-thick or thermally-thin, one may examine the time-to-ignition data and plot them as $1/t_{ig}^n$ vs. applied heat flux and vary the exponent of t_{ig} , n value from 0.5 to 1.0. When data gives its best fitness at $n \rightarrow 0.5$, the material may be considered as thermally-thick behaving material. When data gives its best fitness at $n \rightarrow 1$, the material can be considered as thermally-thin. Hence, careful examination of the ignition data should be done prior to parameter estimation for simple analytical pyrolysis modeling, because the model takes into account the material's thermal characteristics to simplify the model equations.

For both thermally-thick and -thin behaving materials, heat release at steady burning following ignition is calculated from Eq. 4-10:

$$\dot{Q}(t) = \begin{cases} 0 & \text{for } t < t_{ig} \\ \frac{\Delta h_{c,eff}}{\Delta h_g} \dot{q}_{net}''(t) & \text{for } t \geq t_{ig} \end{cases} \quad \text{Eq. 4-10}$$

MODEL PARAMETERS AND MEASUREMENT METHODS

Virtual Material

For modeling transient heating of an inert, semi-infinite homogeneous material and pyrolysis after ignition, the following set-up is used (see Figure 4-2):

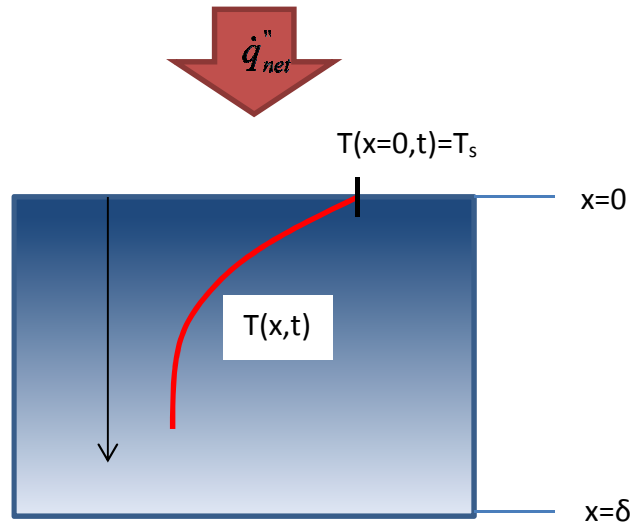


Figure 4-2. Pyrolysis modeling set-up used for thermally-thick materials

For modeling transient heating of an inert, thermally-thin homogeneous material and pyrolysis after ignition, the following set-up is used (see Figure 4-3):

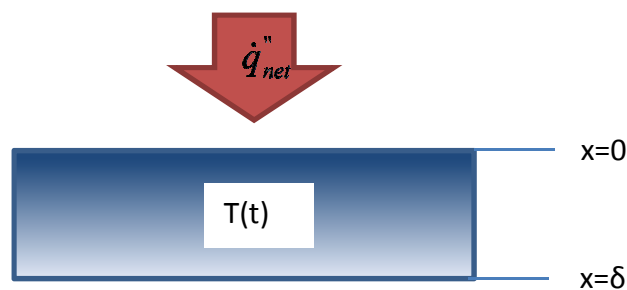


Figure 4-3. Pyrolysis modeling set-up used for thermally-thin materials

Model-Parameter Table

Table 4-1. Model-parameter table: summary of model parameters required to conduct pyrolysis modeling

Ignition Parameters	T_{ig}	Surface Temperature at Ignition
	\dot{q}_{cr}''	Critical Heat Flux for Ignition
	$k\rho c$	Thermal Inertia (Thermally-thick)
	$\rho c\delta$	Thermal Capacity (Thermally-thin)
Burning-Rate Parameters	$\Delta h_{c,eff}$	Effective Heat of Combustion
	Δh_g	Heat of Gasification
Parameters for Specifying Conditions	h_c	Convection Coefficient
	T_∞	Ambient Temperature
	ε	Surface Emissivity/Absorptivity
	Δt_{burn}	Burn Duration

Model-Parameter-Measurement Methods

1. Surface Temperature at Ignition

DIRECT MEASUREMENT

The most common approach for directly measuring surface temperature at ignition involves the use of fine thermocouples. The wire diameter has to be as small as possible to avoid having the thermocouple alter the material's response in the test. Although pre-welded type K unsheathed thermocouples are available with wire diameters down to 0.013 mm, it is extremely tedious to handle wires that are less than 0.25 mm in diameter. Butt-welded thermocouples are preferred because they have no bead. Since the smallest diameter of commercially available butt-welded thermocouples is 0.25 mm, it is recommended that these be used instead of 0.13-mm standard beaded wire thermocouples.

Thermocouples are installed on the surface by drilling two small holes through the specimen at 5–10 mm from opposite sides of its center. The wires are pulled through the holes and taped to the back side of the specimen, so that the thermocouple junction is in

the middle between the holes and in contact with the specimen surface. It is beneficial to make a small incision between the holes so that the exposed part of the thermocouple wire is partially below the surface (see Figure 4-4(a)). It is critical to apply the right tension so that the wire is neither pulled into the material (see Figure 4-4(b)) nor loses contact with the surface (see Figure 4-4(c)).

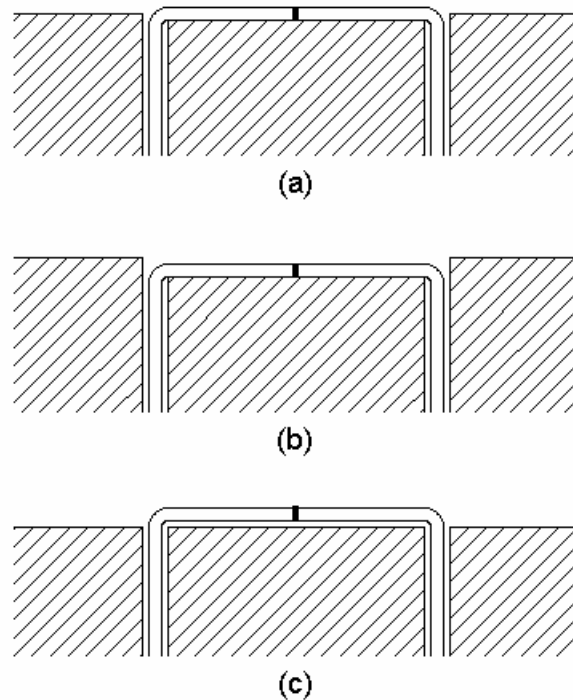


Figure 4-4. Measuring surface temperature with a thermocouple

It is very difficult and time-consuming to accurately measure the surface temperature of a specimen in a fire test with a thermocouple. The problems of this technique can be avoided by using a non-contact method that relies on an optical pyrometer or infrared camera. However, this approach is not without challenges either. First of all, it may not be possible to position the pyrometer or camera so that the instrument has a clear unobstructed view of the target surface. Often the radiant panel of the test apparatus is in the way and the pyrometer has to be positioned at an angle. Second, if the absorptivity of the target surface is less than unity, part of the incident heat flux from the radiant panel is reflected. The pyrometer or camera signal has to be corrected to account for this reflection. Finally, to accurately measure surface temperature with an optical pyrometer or infrared camera, the absorption of radiation,

e.g., by CO₂ and water vapor,¹ in the space between the target and the sensor has to be accounted for. This presents a major challenge when measuring the surface temperature of a burning specimen due to the radiation from the flame and interference of the flame with the radiation from the surface. This challenge has been successfully addressed by using a narrow-band pyrometer that operates in the 8–10 μm range of the IR spectrum, i.e., outside the absorption/emission bands of carbon dioxide and water vapor.^{2,3}

Investigators in Sweden have recently experimented with the use of thermographic phosphors to measure the surface temperature in fire tests.^{4,5,6} This technique relies on the fact that the phosphorescence lifetime and spectral properties of UV laser-induced emissions from a thermographic phosphor applied to the surface of a test specimen are a function of the temperature of the phosphor. This method is still in its infancy, and more work is needed to demonstrate that it can be used for a wide range of materials and fire-test conditions.

The surface temperature at ignition of a thermoplastic is reasonably constant and independent of heat flux.^{7,8} A number of investigators measured T_{ig} for a range of wood products.^{9,10,11,12,13,14} Reasonably constant values were found for each material at heat fluxes ≥ 25 kW/m². All studies reported a significant increase of T_{ig} at lower heat fluxes (50 °C–150 °C at 15 kW/m²). This is due to the fact that pyrolysis and char formation at the surface are no longer negligible for ignition times exceeding 3 min. Under those conditions one of the basic assumptions of thermal-ignition theory, i.e., that the specimen behaves as an inert solid, is no longer valid.

A number of ASTM standards have been tabulated below for calorimeter tests that allow measurements of ignition and burning properties of materials (see Table 4-2):

Table 4-2. ASTM standards of calorimeter tests measuring ignition and burning properties of material

Standard Test	Description
ASTM D 1929 – 11	<i>Standard Test Method for Determining Ignition Temperature of Plastics</i>
ASTM E 1321 – 09	<i>Standard Test Method for Determining Material Ignition and Flame Spread Properties</i>
ASTM E 1354 – 11b	<i>Standard Test Method for Heat and Visible Smoke Release Rates for Materials and Products Using an Oxygen Consumption Calorimeter</i>
ASTM E 2058 – 09	<i>Standard Test Methods for Measurement of Synthetic Polymer Material Flammability Using a Fire Propagation Apparatus (FPA)</i>

IGNITION DATA ANALYSIS

Because it is very tedious to measure T_{ig} directly, it is much more common to determine ignition properties on the basis of an analysis of time-to-ignition data obtained over a range of heat fluxes. The analysis is usually based on a simple heat conduction model, which assumes that the solid is inert (negligible pyrolysis prior to ignition) and thermally-thick (heat wave does not reach the back surface prior to ignition) or thermally-thin (heat wave does reach the back surface prior to ignition; therefore, temperature gradient can be neglected within solid phase). It is important to understand that material properties obtained from such analyses are model parameters, which are not necessarily a good estimate of the real values.

THERMALLY-THICK MATERIALS

Quintiere and Harkleroad developed a practical method for analyzing ignition data obtained with the LIFT apparatus.¹⁵ The method is described in ASTM E 1321. The first step of the method consists of conducting ignition tests starting at a radiant heat-flux level near the maximum for the apparatus (60–65 kW/m²). Time-to-ignition is obtained at heat-flux levels in descending order at intervals of 5 kW/m² to 10 kW/m², preferably with some replicates. When ignition time becomes sufficiently long (of the order of 10 min), data is obtained at heat-flux levels more closely together (1.5 kW/m² to 2 kW/m² intervals). At a certain level, ignition will no longer occur within the (arbitrary) maximum test duration of 20 min. The critical heat flux is taken to be slightly above this

level. Usually, a few more tests are conducted around this level to confirm its value. Once the critical heat flux is known, T_{ig} can be calculated from a heat balance at the surface (see Figure 4-1) after very long exposure, since heat conduction into the specimen then becomes negligible (see Eq. 4-11):

$$\varepsilon \dot{q}_{cr}'' = h_c (T_{ig} - T_\infty) + \varepsilon \sigma (T_{ig}^4 - T_\infty^4) \quad \text{Eq. 4-11}$$

THERMALLY-THIN MATERIALS

The same approach can be applied to estimate T_{ig} for thermally-thin materials.

2. Critical Heat Flux for Ignition

A quantity related to T_{ig} is the minimum heat flux for ignition, \dot{q}_{min}'' . The minimum heat flux is just sufficient to heat the material surface to T_{ig} for very long exposure times (theoretically ∞). It is not a true material property, because it depends on the rate of convective cooling from the surface. This, in turn, depends primarily on the orientation, size, and flow field around the exposed surface. Since these are different in a small-scale test vs. a real fire, the minimum heat flux determined based on test data is an approximate value. To make the distinction, it is referred as the critical heat flux for ignition, \dot{q}_{cr}'' when measured directly. The critical heat flux may also vary between different small-scale test apparatuses due to differences in convective cooling. For example, DiTenberger obtained critical heat flux values of 14.3 kW/m² and 18.8 kW/m² for conditioned redwood in the Cone Calorimeter (*ASTM E 1354*) and Lateral Ignition and Flame spread Test (LIFT) apparatus (*ASTM E 1321*) respectively.¹⁶

The critical heat flux, \dot{q}_{cr}'' , can be determined by bracketing, i.e., by conducting experiments at incrementally decreasing heat flux levels until ignition does not occur within a specified period (usually 10 or 20 min).

3. *Thermal Inertia or Thermal Capacity per Unit Area*

The thermal inertia, $k\rho c$, is a measure of how fast the surface temperature of a thermally-thick material rises when exposed to heat. A material with lower $k\rho c$ will ignite faster than a material with higher $k\rho c$ and the same T_{ig} exposed to the same heat flux. Similar to thermal inertia, for materials that are thermally-thin, thermal capacity per unit area, $\rho c\delta$, is a measure of how fast the material's lumped body temperature rises when exposed to heat.

DIRECT MEASUREMENT

This parameter can be determined by measuring thermal conductivity, density, and specific heat separately. Methods for measuring k , ρ , and c are described in the section on thermophysical parameters (see Chapter 5). Since k and c are temperature-dependent, the question is, at which temperature should these parameters be determined? A possible approach involves using average parameter values for the temperature range between ambient and T_{ig} .

IGNITION DATA ANALYSIS

Similar to measuring T_{ig} directly, direct measurement of $k\rho c$ or $\rho c\delta$ requires investment of time and financial commitment. Therefore, it is more common to determine this parameter on the basis of an analysis of time-to-ignition data obtained over a range of heat fluxes. The analysis is usually based on a simple heat-conduction model, which assumes that the solid is inert (negligible pyrolysis prior to ignition) and thermally-thick (heat wave does not reach the back surface prior to ignition) or thermally-thin (heat wave does reach the back surface prior to ignition; therefore, temperature gradient can be neglected within solid phase). It is important to understand that material properties obtained from such analyses are model parameters, which are not necessarily a good estimate of the real values.

THERMALLY-THICK MATERIALS

Once the \dot{q}_{cr}'' and T_{ig} are known, total heat-transfer coefficient at ignition, h_{ig} , can be calculated from a heat balance at the surface after very long exposure, since heat conduction into the specimen then becomes negligible (see Eq. 4-12):

$$\varepsilon \dot{q}_{cr}'' = h_c (T_{ig} - T_\infty) + \varepsilon \sigma (T_{ig}^4 - T_\infty^4) \equiv h_{ig} (T_{ig} - T_\infty) \quad \text{Eq. 4-12}$$

where

$$h_{ig} = \text{total heat transfer coefficient at ignition (kW/m}^2\cdot\text{K)}.$$

Surface temperature measurements under steady-state conditions for a number of inert materials and some combustible materials resulted in the following fit¹⁵:

$$\dot{q}_{cr}'' = 0.015(T_{ig} - T_\infty) + \sigma(T_{ig}^4 - T_\infty^4) \equiv h_{ig} (T_{ig} - T_\infty) \quad \text{Eq. 4-13}$$

Thus, if specimens are heated for a sufficiently long time in the LIFT apparatus, it may be assumed that $\varepsilon = 1$ and that $h_c = 15 \text{ W/m}^2\cdot\text{K}$. Once T_{ig} is calculated from the empirical value for \dot{q}_{cr}'' via Eq. 4-11, a total heat-transfer coefficient from the surface at ignition can be obtained by rearranging this equation as follows (see Eq. 4-14):

$$h_{ig} \equiv \frac{\dot{q}_{cr}''}{T_{ig} - T_\infty} = 0.015 + \sigma \frac{T_{ig}^4 - T_\infty^4}{T_{ig} - T_\infty} \quad \text{Eq. 4-14}$$

Based on approximate solutions of Eq. 4-1 through Eq. 4-4 with linearized heat losses from the exposed surface, the surface temperature at ignition for exposure to a constant radiant heat flux is approximated by (see Eq. 4-15):

$$T_{ig} = T_\infty + \frac{\dot{q}_e''}{h_{ig}} F(t_{ig}) \quad \text{with} \quad F(t) = \begin{cases} \frac{2 h_{ig} \sqrt{t}}{\sqrt{\pi k \rho c}} & \text{small } t \\ 1 & \text{large } t \end{cases} \quad \text{Eq. 4-15}$$

where

$$t_{ig} = \text{time to ignition at incident heat flux } \dot{q}_e'' \text{ (s); and}$$

$$F = \text{function of time.}$$

This leads to the following expression for correlation of piloted-ignition data (see Eq. 4-16):

$$\frac{\dot{q}_{cr}''}{\dot{q}_e''} = F(t_{ig}) = \begin{cases} \frac{2 h_{ig} \sqrt{t_{ig}}}{\sqrt{\pi k \rho c}} & t_{ig} \leq t^* \\ 1 & t_{ig} > t^* \end{cases} \quad \text{Eq. 4-16}$$

where

t^* = time to reach steady conditions (s).

Thus, all data are plotted in a graph of $\dot{q}_{cr}'' / \dot{q}_e''$ versus $\sqrt{t_{ig}}$. An “apparent” value for $k\rho c$ can be calculated from the slope of the line through zero that best fits the data. This line crosses $\dot{q}_{cr}'' / \dot{q}_e'' = 1$ at t^* , the time needed to reach “steady-state” conditions. The functional form of Eq. 4-16 for small times is identical to that of the solution of the one-dimensional heat conduction equation for a semi-infinite solid exposed to a constant heat flux without heat losses from the surface. Consequently, $k\rho c$ values obtained with this procedure are higher than actual average values. The same procedure can be used to analyze piloted-ignition data obtained with the Cone Calorimeter, provided an adjustment is made to h_c to account for the differences in convective cooling conditions.

THERMALLY-THIN MATERIALS

Similar to what has been done for thermally-thick materials, ignition theory can be applied to thermally-thin materials. The only difference from the method introduced above is the $F(t)$ function (see Eq. 4-17):

$$\frac{\dot{q}_{cr}''}{\dot{q}_e''} = F(t_{ig}) = \begin{cases} \frac{h_{ig} t_{ig}}{\rho c \delta} & t_{ig} \leq t^* \\ 1 & t_{ig} > t^* \end{cases} \quad \text{Eq. 4-17}$$

where $\rho c \delta$ is the thermal capacity per unit area. This parameter is comparable to thermal inertia in equations derived for thermally-thick behaving material, which may be estimated from the slope of the line from linear regression method.

4. Effective Heat of Combustion

See Chapter 3.

5. Heat-of-Gasification

The heat-of-gasification, $\Delta h_{c,g}$, is defined as the net heat flow into a specimen required to convert one mass unit of solid material to volatiles. The net heat flux can be obtained from an energy balance at the surface of the specimen. Typically, a specimen exposed in a small-scale calorimeter is heated by external heaters and by its own flame. Heat is lost from the surface in the form of radiation. A schematic of the heat balance at the surface of a burning specimen in the Cone Calorimeter (*ASTM E 1354*) is shown in Figure 4-1. Hence, $\Delta h_{c,g}$ is defined as (see Eq. 4-18):

$$\Delta h_g \equiv \frac{\dot{q}_{net}''}{\dot{m}''} = \frac{\dot{q}_e'' + \dot{q}_f'' - \dot{q}_l''}{\dot{m}''} \quad \text{Eq. 4-18}$$

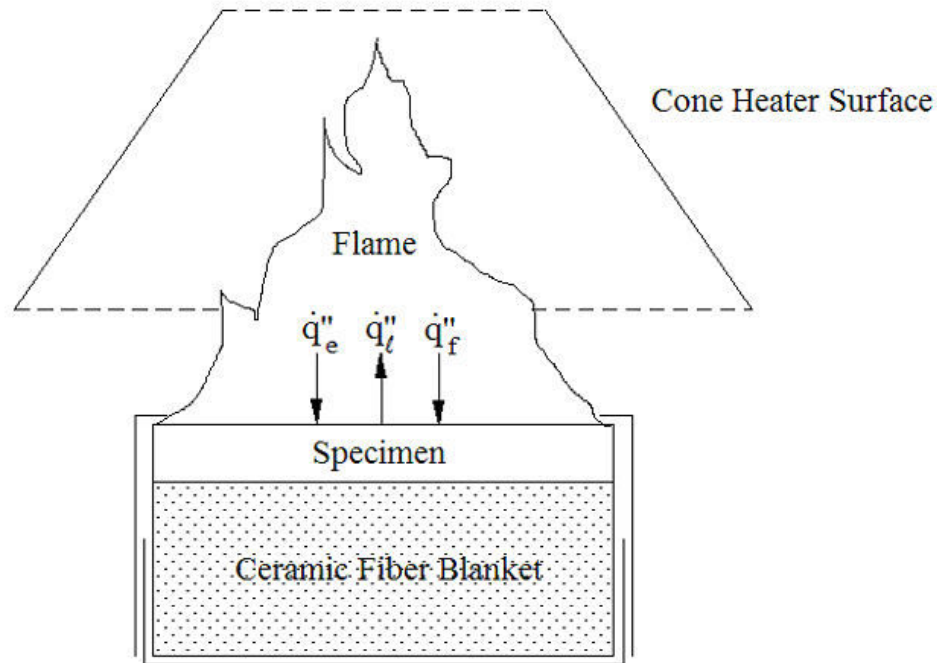


Figure 4-5. Heat balance at the surface of a burning cone calorimeter specimen

where

\dot{q}_{net}'' = net heat flux into the specimen (kW/m^2);

\dot{q}_e'' = heat flux to the specimen surface from external sources (kW/m^2);

- \dot{q}_f'' = heat flux to the specimen surface from the flame (kW/m²); and
 \dot{q}_l'' = heat losses from the exposed surface (kW/m²).

The heat of gasification is defined by Eq. 4-18. If the flame is approximated as a homogeneous grey gas volume, the heat flux from the flame can be expressed as follows (see Eq. 4-19):

$$\dot{q}_f'' = \dot{q}_{f,c}'' + \dot{q}_{f,r}'' = h(T_f - T_s) + \sigma \epsilon_f T_f^4 \quad \text{Eq. 4-19}$$

where

- $\dot{q}_{f,c}''$ = convective fraction of the flame flux (kW/m²);
 $\dot{q}_{f,r}''$ = radiative fraction of the flame flux (kW/m²);
 h^* = convection coefficient corrected for blowing (kW/m²·K);
 T_f = flame temperature (K);
 T_s = surface temperature (K);
 σ = Boltzmann constant (5.67·10⁻¹¹ kW/m²·K⁴); and
 ϵ_f = emissivity of the flame.

The flow of combustible volatiles emerging through the exposed surface of the specimen adversely affects the convective heat transfer between the flame and the surface. This effect is referred to as “blowing.” The flame flux in a small-scale calorimeter is primarily convective, in particular in the vertical orientation, and flame absorption of external heater and specimen surface radiation can be neglected.

The heat losses from the surface can be expressed as Eq. 4-20:

$$\dot{q}_l'' = \sigma \epsilon_s (T_s^4 - T_\infty^4) \quad \text{Eq. 4-20}$$

where

- ϵ_s = surface emissivity of the specimen; and
 T_∞ = ambient temperature (K).

Some materials exhibit nearly steady mass-loss rates when exposed to a fixed radiant-heat flux. T_s for these materials reaches a steady value after a short initial transient period, and all terms in Eq. 4-20 are approximately constant. Δh_g can then be

obtained by measuring steady mass-loss rates at different radiant-heat flux levels, and by plotting \dot{m}'' as a function of \dot{q}_e'' . The reciprocal of the slope of a straight line fitted through the data points is equal to Δh_g . The intercept of the line with the abscissa is equal to $\dot{q}_i'' - \dot{q}_f''$. Tewarson et al.¹⁷ and Petrella¹⁸ have used this technique to obtain average Δh_g values for a large number of materials. Tewarson et al. also conducted tests in vitiated O₂/N₂ mixtures and found \dot{q}_f'' to decrease linearly with decreasing oxygen concentration. Analysis of these additional experiments made it possible to separate \dot{q}_f'' and \dot{q}_i'' .

Many materials, in particular those that form an insulating char layer as they burn, take a long time to reach steady burning conditions or may never reach steady conditions. Eq. 4-18 is still valid for such materials, but the heat and mass fluxes and resulting Δh_g values vary with time. Tewarson and Petrella have used the method described in the previous paragraph to determine average Δh_g values for non-steady burning materials using average mass-loss rates. They found that average \dot{m}'' is still an approximately linear function of \dot{q}_e'' . However, the average heat-of-gasification values obtained in this manner may not have any physical meaning. For example, Janssens demonstrated that the values based on average mass loss rates are too high for wood, and suggested a method to determine Δh_g as a function of char depth.

6. Convection Coefficient

The convection coefficient depends on the apparatus that was used to obtain the piloted ignition data. Table 4-3 summarizes recommended h_c values for different apparatuses.

Table 4-3. Recommended h_c values for different test apparatuses

Apparatus	Orientation	h_c (kW/m ² ·K)
ISO Ignitability Test	Horizontal	0.011
Cone Calorimeter	Horizontal	0.012
Cone Calorimeter	Vertical	0.016
LIFT	Vertical	0.015
Fire Propagation Apparatus	Horizontal	0.010

7. Ambient Temperature

Typically, ambient temperature is directly measured using a thermometer measuring room temperature located in the lab where testing is conducted.

8. Surface Emissivity / Absorptivity

The emissivity can be (1) obtained from the literature; (2) assumed to be equal to 1, or close to 1 (which is reasonable for many materials); or (3) measured according to a standard test method (see Table 4-4).

Table 4-4. ASTM standards for Measuring Emissivity

Standard Test	Description
ASTM C 835	<i>Standard Test Method for Total Hemispherical Emittance of Surfaces up to 1400°C</i>
ASTM C 1371	<i>Standard Test Method for Determination of Emittance of Materials Near Room Temperature Using Portable Emissometers</i>

9. Burn Duration

Burn duration is the time of burning, i.e., time of complete burnout minus time of ignition. This parameter can be calculated by considering steady burning rate after ignition and available amount of fuel mass to burn. At a certain level of applied heat flux, the modeler can estimate the burning rate from linear-regression plotting external applied heat flux, \dot{q}_e'' versus burning rate, \dot{m}'' (see Eq. 4-17). Burn duration can be estimated by Eq. 4-21:

$$\Delta t_{burn} = \frac{\rho \delta}{\dot{m}''} \quad \text{Eq. 4-21}$$

UNCERTAINTY ANALYSIS

When a parameter is obtained via direct measurement, a statistical approach may be used to quantify the uncertainty. Use at least three identical measurements to analyze confidence interval, assuming data is not biased due to inherent problem during data collection. When parameters are obtained via data analysis, uncertainty can be calculated using the Law of Propagation of Uncertainty. These are shown below:

Ignition Data Analysis

Thermally-thick Materials

ΔT_{ig}

This parameter is a function of \dot{q}_{cr}'' , h_c , and T_∞ . Knowing the uncertainty of \dot{q}_{cr}'' , h_c and T_∞ uncertainty of T_{ig} can be estimated as below using the Law of Propagation of Uncertainty.

Recall the heat-balance equation at the front surface during steady burning (see Eq. 4-11). Using the Law of Propagation of Uncertainty, the following mathematical expression is found (see Eq. 4-22):

$$\delta \dot{q}_{cr}'' = \sqrt{\left(\frac{\partial \dot{q}_{cr}''}{\partial \varepsilon} \delta \varepsilon \right)^2 + \left(\frac{\partial \dot{q}_{cr}''}{\partial h_c} \delta h_c \right)^2 + \left(\frac{\partial \dot{q}_{cr}''}{\partial T_\infty} \delta T_\infty \right)^2 + \left(\frac{\partial \dot{q}_{cr}''}{\partial T_{ig}} \delta T_{ig} \right)^2} \quad \text{Eq. 4-22}$$

Therefore, the uncertainty of T_{ig} becomes (see Eq. 4-23):

$$\delta T_{ig} = \left(\frac{\partial \dot{q}_{cr}''}{\partial T_{ig}} \right)^{-1} \sqrt{(\delta \dot{q}_{cr}'')^2 - \left(\left(\frac{\partial \dot{q}_{cr}''}{\partial \varepsilon} \delta \varepsilon \right)^2 + \left(\frac{\partial \dot{q}_{cr}''}{\partial h_c} \delta h_c \right)^2 + \left(\frac{\partial \dot{q}_{cr}''}{\partial T_\infty} \delta T_\infty \right)^2 \right)} \quad \text{Eq. 4-23}$$

where

$$\frac{\partial \dot{q}_{cr}''}{\partial T_{ig}} = \frac{h_c + 4\varepsilon\sigma T_{ig}^3}{\varepsilon}$$

$$\frac{\partial \dot{q}_{cr}''}{\partial \varepsilon} = \frac{-\dot{q}_{cr}'' + \sigma(T_{ig}^4 - T_\infty^4)}{\varepsilon}$$

$$\frac{\partial \dot{q}_{cr}''}{\partial h_c} = \frac{T_{ig} - T_\infty}{\varepsilon}$$

$$\frac{\partial \dot{q}_{cr}''}{\partial T_{\infty}} = \frac{-h_c - 4\varepsilon\sigma T_{\infty}^3}{\varepsilon}$$

$\Delta(K\rho C)$

This parameter is a function of estimated slope of the best-fit line that represents the relationship between $\dot{q}_{cr}'' / \dot{q}_e''$ and $\sqrt{t_{ig}}$ and h_{ig} where h_{ig} is a function of $\varepsilon, \dot{q}_{cr}'', T_{ig}$ and T_{∞} .

$$\text{Recall } k\rho C = \frac{4 h_{ig}^2}{\pi \cdot (\text{slope})^2} \text{ and } \varepsilon \dot{q}_{cr}'' \equiv h_{ig} (T_{ig} - T_{\infty}) .$$

By substituting h_{ig} , thermal inertia can be rearranged to Eq. 4-24:

$$k\rho C = \frac{4}{\pi \cdot (\text{slope})^2} \left(\frac{\varepsilon \dot{q}_{cr}''}{T_{ig} - T_{\infty}} \right)^2 \quad \text{Eq. 4-24}$$

Therefore, using the Law of Propagation of Uncertainty, the following mathematical expression is found (see Eq. 4-25):

$$\delta(k\rho C) = \sqrt{\left(\frac{\partial(k\rho C)}{\partial(\text{slope})} \delta(\text{slope}) \right)^2 + \left(\frac{\partial(k\rho C)}{\partial\varepsilon} \delta\varepsilon \right)^2 + \left(\frac{\partial(k\rho C)}{\partial\dot{q}_{cr}''} \delta\dot{q}_{cr}'' \right)^2 + \left(\frac{\partial(k\rho C)}{\partial T_{ig}} \delta T_{ig} \right)^2 + \left(\frac{\partial(k\rho C)}{\partial T_{\infty}} \delta T_{\infty} \right)^2} \quad \text{Eq. 4-25}$$

where

$$\frac{\partial(k\rho C)}{\partial(\text{slope})} = \frac{-8}{\pi \cdot (\text{slope})^3} \left(\frac{\varepsilon \dot{q}_{cr}''}{T_{ig} - T_{\infty}} \right)^2$$

$$\frac{\partial(k\rho C)}{\partial\varepsilon} = \frac{8}{\pi \cdot (\text{slope})^2} \left(\frac{\dot{q}_{cr}''}{T_{ig} - T_{\infty}} \right)^2 \varepsilon$$

$$\frac{\partial(k\rho C)}{\partial\dot{q}_{cr}''} = \frac{8}{\pi \cdot (\text{slope})^2} \left(\frac{\varepsilon}{T_{ig} - T_{\infty}} \right)^2 \dot{q}_{cr}''$$

$$\frac{\partial(k\rho C)}{\partial T_{ig}} = \frac{-8}{\pi \cdot (\text{slope})^2} \left(\frac{\varepsilon \dot{q}_{cr}''}{T_{ig} - T_{\infty}} \right)^2 \frac{1}{T_{ig} - T_{\infty}}$$

$$\frac{\partial(k\rho C)}{\partial T_{\infty}} = \frac{8}{\pi \cdot (\text{slope})^2} \left(\frac{\varepsilon \dot{q}_{cr}''}{T_{ig} - T_{\infty}} \right)^2 \frac{1}{T_{ig} - T_{\infty}}$$

Thermally-thin Materials

ΔT_{ig}

Uncertainty of this parameter is the same as in thermally-thick case.

$\Delta(\rho c \Delta)$

This parameter is a function of the estimated slope of the best-fit line that represents the relationship between $\dot{q}_{cr}'' / \dot{q}_e''$ and t_{ig} and h_{ig} where h_{ig} is a function of ε , \dot{q}_{cr}'' , T_{ig} and T_∞ .

$$\text{Recall } \rho c \delta = \frac{h_{ig}}{\text{slope}} \text{ and } \varepsilon \dot{q}_{cr}'' \equiv h_{ig} (T_{ig} - T_\infty)$$

By substituting h_{ig} , thermal capacity per unit area can be rearranged to Eq. 4-26:

$$\rho c \delta = \frac{1}{\text{slope}} \left(\frac{\varepsilon \dot{q}_{cr}''}{T_{ig} - T_\infty} \right) \quad \text{Eq. 4-26}$$

Therefore, using the Law of Propagation of Uncertainty, the following mathematical expression is found as Eq. 4-27:

$$\delta(\rho c \delta) = \sqrt{\left(\frac{\partial(\rho c \delta)}{\partial(\text{slope})} \delta(\text{slope}) \right)^2 + \left(\frac{\partial(\rho c \delta)}{\partial \varepsilon} \delta \varepsilon \right)^2 + \left(\frac{\partial(\rho c \delta)}{\partial \dot{q}_{cr}''} \delta \dot{q}_{cr}'' \right)^2 + \left(\frac{\partial(\rho c \delta)}{\partial T_{ig}} \delta T_{ig} \right)^2 + \left(\frac{\partial(\rho c \delta)}{\partial T_\infty} \delta T_\infty \right)^2} \quad \text{Eq. 4-27}$$

where

$$\frac{\partial(\rho c \delta)}{\partial(\text{slope})} = \frac{-1}{(\text{slope})^2} \left(\frac{\varepsilon \dot{q}_{cr}''}{T_{ig} - T_\infty} \right)$$

$$\frac{\partial(\rho c \delta)}{\partial \varepsilon} = \frac{1}{(\text{slope})} \left(\frac{\dot{q}_{cr}''}{T_{ig} - T_\infty} \right)$$

$$\frac{\partial(\rho c \delta)}{\partial \dot{q}_{cr}''} = \frac{1}{(\text{slope})} \left(\frac{\varepsilon}{T_{ig} - T_\infty} \right)$$

$$\frac{\partial(\rho c \delta)}{\partial T_{ig}} = \frac{-1}{(\text{slope})} \left(\frac{\varepsilon \dot{q}_{cr}''}{T_{ig} - T_\infty} \right) \frac{1}{T_{ig} - T_\infty}$$

$$\frac{\partial(\rho c \delta)}{\partial T_\infty} = \frac{1}{(\text{slope})} \left(\frac{\varepsilon \dot{q}_{cr}''}{T_{ig} - T_\infty} \right) \frac{1}{T_{ig} - T_\infty}$$

Burning-Rate Data Analysis

$\Delta\Delta H_G$

This parameter is estimated by calculating the reciprocal of the slope of the best-fit line of \dot{m}'' versus \dot{q}_e'' using mass-loss rate data obtained from Cone tests at different

heat-flux levels. Recall $\Delta h_g \equiv \frac{\dot{q}_{net}''}{\dot{m}''} = \frac{\dot{q}_e'' + \dot{q}_f'' - \dot{q}_l''}{\dot{m}''}$ during steady burning and therefore

$\dot{m}'' = \frac{1}{\Delta h_g} \dot{q}_e'' + \frac{(\dot{q}_f'' - \dot{q}_l'')}{\Delta h_g}$. The uncertainty of the slope ($=1/\Delta h_g$) can be estimated

through calculating the standard error of the slope of the best-fit line. Knowing the uncertainty of the slope, calculation of uncertainty of Δh_g becomes possible by considering the boundary values.

PARAMETER-ESTIMATION PROCESS

To create a virtual material, these tasks must be considered:

- Create a list of model inputs, which needs to be determined
- Obtain model unknown inputs via measurement or literature search

When the above is done and every unknown has been estimated, validation work and commentary is needed to understand the performance of the estimated parameter set:

- Run model
- Analyze simulation quality with consideration of uncertainties in modeling outputs and data
- Add commentary

When presenting the parameter-estimation results, three summary tables will be introduced: Model-Parameter Table, Validation, and Commentary sections. The Model-Parameter Table includes the model parameters necessary to conduct pyrolysis modeling, their estimated values, and methods of estimating the unknowns. The Validation section consists of the following information: description of modeling goal, pyrolysis model type, and the modeling approach used in the exercise, experiment type and its data used to empirically simulate the material's heat-release rate and uncertainty information of experimental data and modeling outputs. The Commentary section discusses any limitations of pyrolysis modeling conducted above, which has been summarized in the Model Parameter Table and Validation sections.

For better visualization of the problem, a flowchart is shown below (see Figure 4-6):

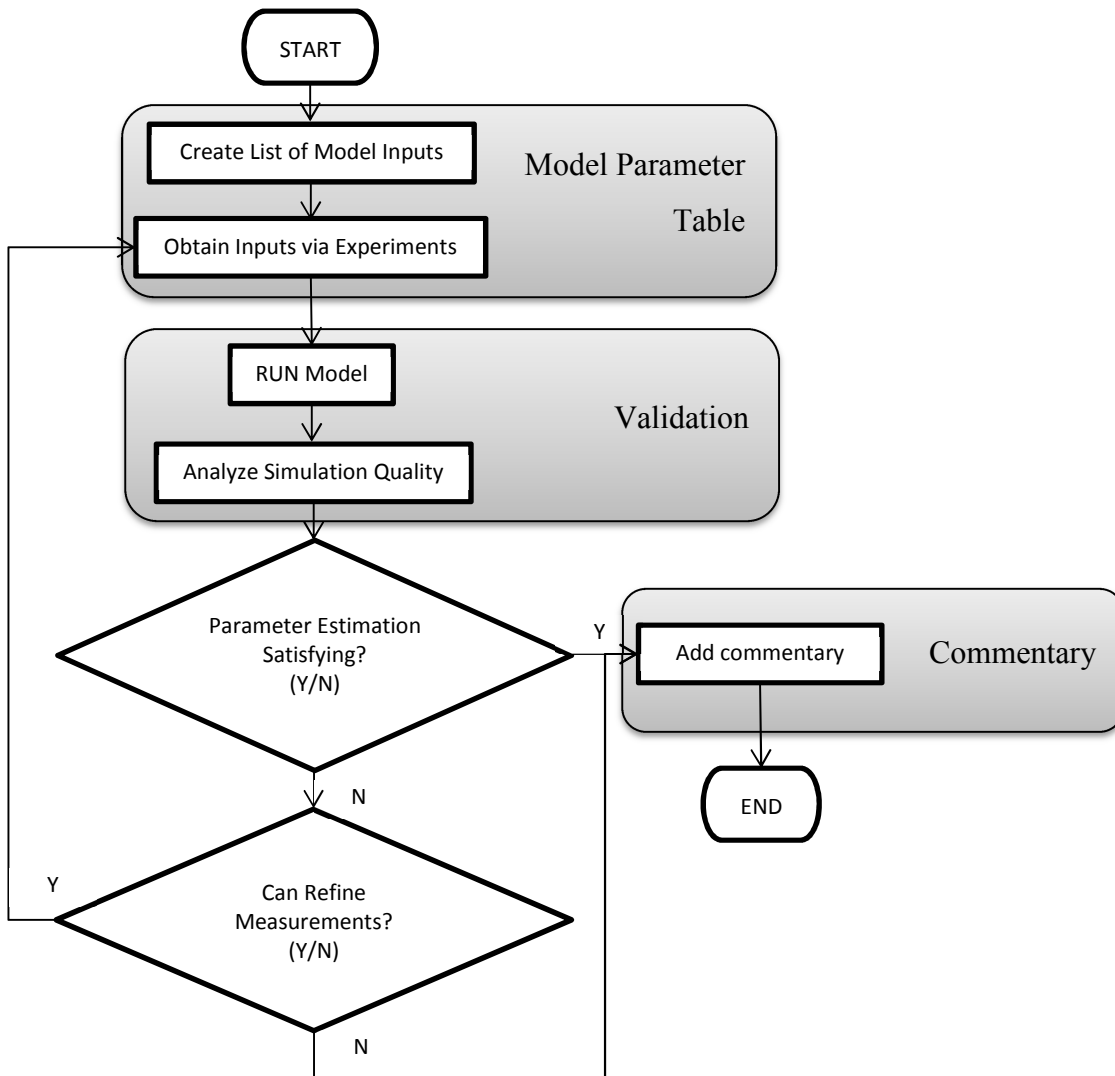


Figure 4-6. Flow chart of parameter estimation for simple analytical pyrolysis models

EXAMPLE CASES OVERVIEW

Table 4-5. Overview of example cases using simple analytical pyrolysis models

Case	Description	Examples
1	Thermally-thick, inert at pre-ignition with steady burning at post-ignition	PMMA
		Corrugated Cardboard
		Fire-Retarded FRP Composite
		Plywood
2	Thermally-thin, inert at pre-ignition with steady burning at post-ignition	Sandwich Composite
		Thin FRP Composite

In the following, summarized results are shown for each example case. Detailed solutions of these example cases are given in Appendix C.

CASE 1: THERMALLY-THICK, INERT AT PRE-IGNITION WITH STEADY BURNING AT POST-IGNITION

Virtual Microstructure of Virgin Material

- Homogeneous flat surface single layer in horizontal position
- Pre-ignition stage: inert, semi-infinite thickness (i.e., thermally-thick)
- Post-ignition stage: steady burning

General Model-Parameter Table

- Ignition and burning-rate parameters are considered in this example
- Reduced Model Parameter Table (see Table 4-6):

Table 4-6. Model Parameter Table for Case 1 Examples

Ignition Parameters	T_{ig}	Surface Temperature at Ignition
	\dot{q}_{cr}''	Critical Heat Flux for Ignition
	$k\rho c$	Thermal Inertia (Thermally-thick)
Burning-Rate Parameters	$\Delta h_{c,eff}$	Effective Heat-of-Combustion
	Δh_g	Heat-of-Gasification
Parameters for Specifying Conditions	h_c	Convection Coefficient
	T_∞	Ambient Temperature
	ε	Surface Emissivity/Absorptivity
	Δt_{burn}	Burn Duration

Example 4.1 Modeling Poly(methylmethacrylate), PMMA

4.1.1 Model Parameter Table

Model Parameters		Unit	Estimated Values and Estimation Methods
Ignition Parameters	T_{ig}	°C	318 ± 4
			Ignition Data Analysis
	\dot{q}_{cr}''	kW/m ²	10.5 ± 0.5
			Measurement, Cone Calorimeter by bracketing
	k _{pc}	kJ ² /m ⁴ K ² s	0.649 ± 0.151
Ignition Data Analysis			
Burning-Rate Parameters	$\Delta h_{c,eff}$	g/s-m ²	24.6 ± 0.9
			Burning-Rate Data Analysis
	Δh_g	kJ/g	2.9 ± 1.0
			Burning-Rate Data Analysis
Parameters for Specifying Conditions	h_c	W/m ² K	12 ± 0.5
			Reference value for horizontal position in cone calorimeter
	T_∞	°C	20 ± 2
			Measurement
	ε	-	0.9 ± 0.09
			Approximated
	Δt_{burn}	s	$\frac{(1170)(18)}{0.351\dot{q}_e'' + 8.896}$
Burning-Rate Data Analysis			

4.1.2 Validation

4.1.2.1 MODELING GOAL

Estimate model parameters for conducting modeling of pyrolysis of PMMA under various heating rates – heat-flux levels ranging up to $\sim 100\text{kW/m}^2$.

4.1.2.2 MODEL TYPE

Thermally-thick model for ignition analysis (Quintiere and Harkleroad, ASTM E 1321) and steady burning model

4.1.2.3 MODELING APPROACH

- Pre-ignition stage is
 - Inert: decomposition with bubbling before ignition is neglected
 - Thermally-thick: heat transfer does not reach back surface
- Post-ignition stage is
 - Considered to have instantaneous release of volatiles from solid to gas phase: bubbling layer is neglected and is considered as a surface phenomenon
 - Considered to have a constant thickness: regression of PMMA is neglected
 - Steady burning: heat loss equals heat gain at front surface

4.1.2.4 EXPERIMENT DESCRIPTION

Cone Calorimeter test

4.1.2.5 DATA SET

- Cone Calorimeter test data of black PMMA with thickness of 18 mm, density of 1170 kg/m^3 and applied heat-flux levels ranging from 10 to 75 kW/m^2 is found.
- For ignition data analysis, only time-to-ignition with respect to applied heat-flux data will be used.
- For burning-rate data analysis, data for the entire testing time duration at HF = 25, 50, and 75 kW/m^2 , mass loss and heat release during testing period with respect to applied heat flux will be used.
- PMMA AFM tests¹⁹ conducted under 28.4 and 60 kW/m^2 are used to compare data with extrapolated modeling cases – time of ignition and MLR at steady burning stage.

4.1.2.6 UNCERTAINTY

Uncertainty in Experiment Data

- Uncertainty in time to ignition and mass loss rate: From the experimental work done by Beaulieu and Dembsey¹⁹ on thermally-thick behaving black PMMA using AFM apparatus, the experiment uncertainty in time-to-ignition and mass-loss rate at steady burning were determined as ± 2 s and ± 3 g/m²s, respectively. The test results were compared with other literature values using different apparatuses, such as Cone Calorimeter as well, which were considered as consistent.
- Assume:
 - Uncertainties are comparable to those of similar flat surfaces pyrolyzing under heating

Uncertainty in Modeling Outputs

- Uncertainty in t_{ig} and \dot{m}'' can be estimated from linear regression process and using the Law of Propagation of Uncertainty

4.1.2.7 MODELING OUTPUT: MASS LOSS RATE (MLR)

- Ignition and Burning-Rate Data Analysis

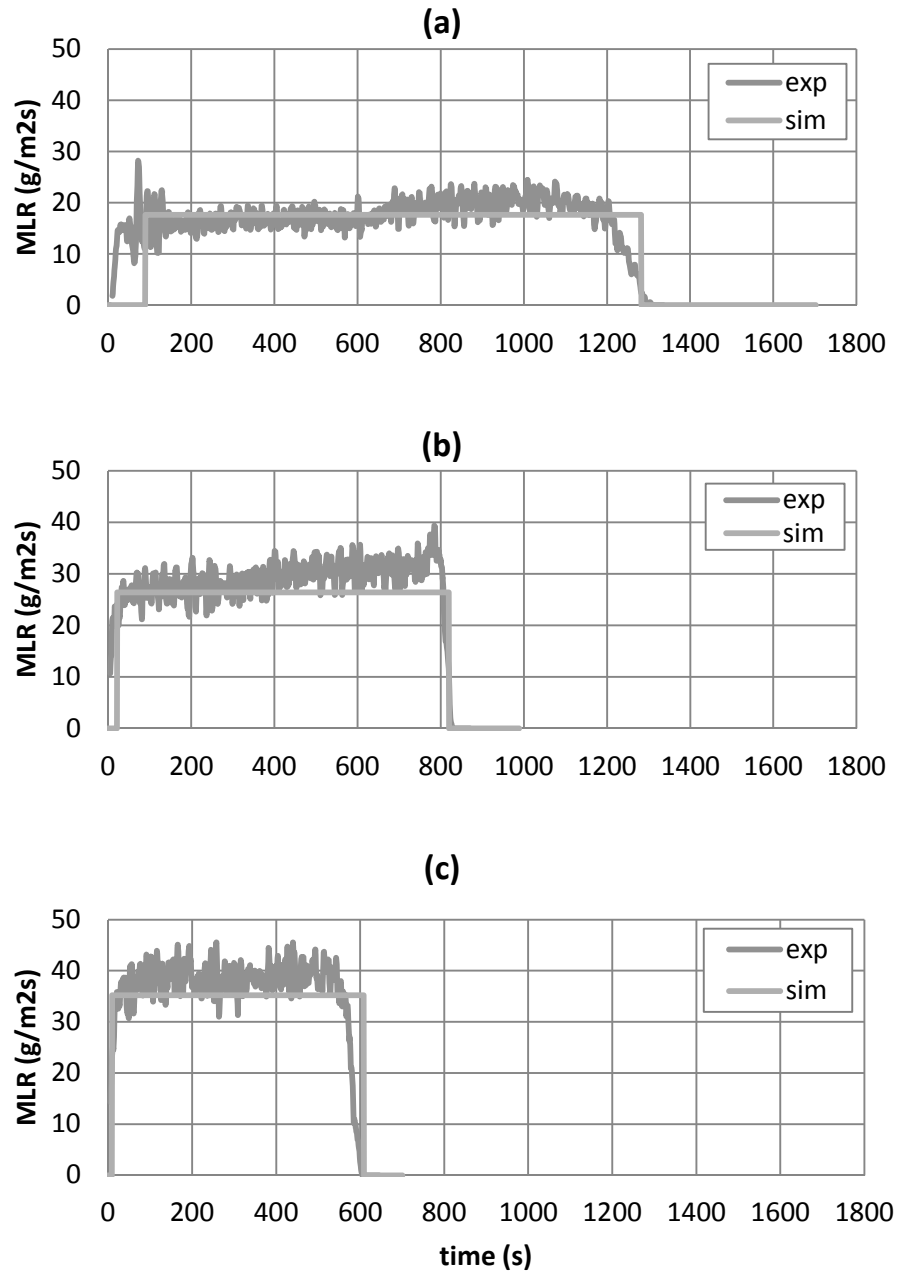


Figure 4-7 Mass-loss rate (MLR) comparisons for PMMA between actual MLR from experiment (exp) and modeled MLR (sim) at different applied heat-flux levels – (a) MLR at 25 kW/m²; (b) MLR at 50 kW/m²; and (c) MLR at 75 kW/m². Note that data shown were used to estimate model-parameter values.

- Extrapolation

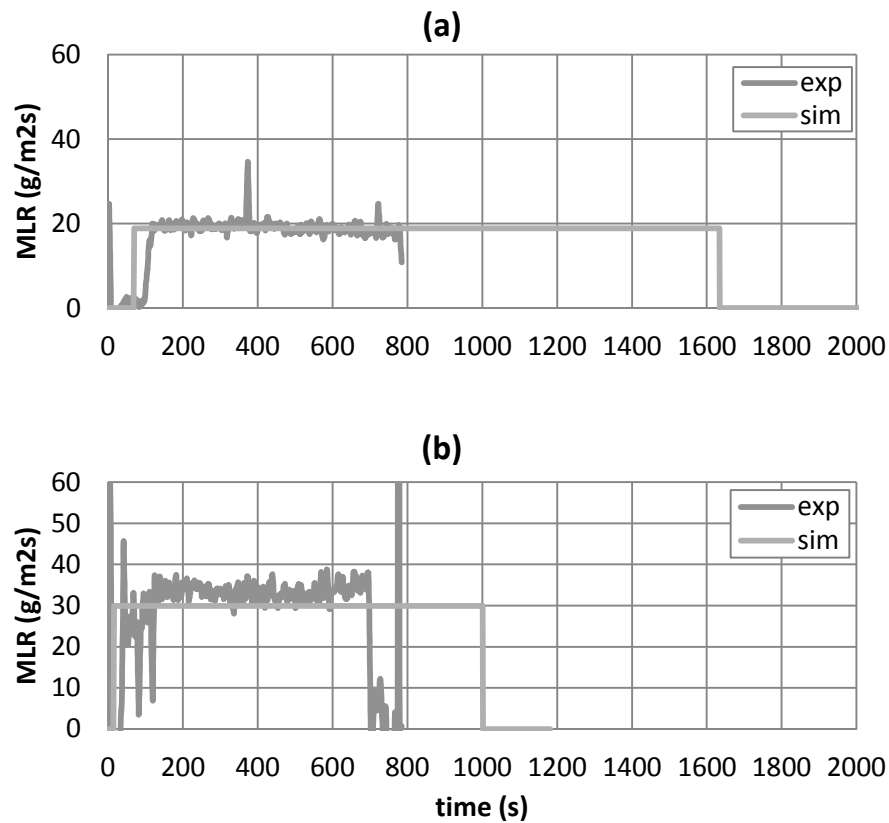


Figure 4-8 Mass-loss rate (MLR) comparisons for PMMA between actual MLR from experiment (exp) and modeled MLR (sim) at different applied heat-flux levels – (a) MLR at 28.4 kW/m²; and (b) MLR at 60 kW/m². Note that data shown were not included in the model-parameter-estimation process; hence, these two cases are considered as extrapolation cases.

4.1.3 Commentary

GENERAL COMMENTS ABOUT MLR

- Ignition and Burning-Rate Data Analysis at HF = 25, 50 and 75 kW/m²: Good agreement exists between experiment data and all modeling results
- Extrapolation at HF = 28.4 and 60 kW/m²: Generally, good agreement exists between MLR data and modeling results, except near ignition stage. In modeling time-to-ignition, the model's outputs are shorter than those from AFM tests for both heat-flux levels. This discrepancy can be explained by considering the in-depth absorption of radiation during heating of PMMA. The data from AFM tests, where IR lamps are used to heat the samples, possibly were subject to in-depth radiative absorption delaying ignition, knowing that the PMMA samples are somewhat transparent. However, this phenomenon is not accounted for in modeling assumptions and in parameter estimation process where Cone Calorimeter test data is used – in the Cone, radiation is absorbed mostly on the surface.

LIMITATION IN MODELING

- When using the Simple Analytical Model to simulate pyrolysis of black PMMA (density 1170 kg/m³, thickness 18 mm), test data from a bench-scale Cone Calorimeter experiment at several heat flux levels have been utilized to estimate the time-to-ignition from exposure to heating and the mass-loss rate at steady-burning stage after ignition. The comparison between the model outputs (time-to-ignition and steady-burning rate) and the data from bench-scale experiment showed good agreement for both checking purposes, where the same heat flux levels (25, 50 and 75 kW/m²) used in parameter estimation have been considered and extrapolation purposes where heat-flux levels (28.4 and 60 kW/m²) not included in parameter estimation process have been considered.
- Although the modeling predictions of time-to-ignition and steady-burning rate in this example seem to be reasonable, limitations of Simple Analytical Modeling has been acknowledged in literature for modeling black PMMA at relatively high applied heat-flux levels. At high-heat flux levels, the assumption of having an inert condition during pre-ignition stage and neglecting thermal decomposition behavior- such as bubbling- cannot be made where these effects become more profound on temperature profile and ignition process of PMMA. Therefore, caution should be given when conducting modeling for cases with higher heat-flux levels.

Example 4.2 Modeling Corrugated Cardboard

4.2.1 Model Parameter Table

Model Parameters		Unit	Estimated Values and Estimation Methods
Ignition Parameters	T_{ig}	°C	293 ± 17
			Ignition Data Analysis
	\dot{q}_{cr}''	kW/m ²	9 ± 1
			Measurement, Cone Calorimeter by bracketing
	kpc	kJ ² /m ⁴ K ² s	0.297 ± 0.101
		Ignition Data Analysis	
Burning-Rate Parameters	$\Delta h_{c,eff}$	g/s-m ²	13.9 ± 1.3
			Burning-Rate Data Analysis
	Δh_g	kJ/g	21.6 ± 10.9
			Burning-Rate Data Analysis
Parameters for Specifying Conditions	h_c	W/m ² K	12 ± 0.5
			Reference value for horizontal position in Cone Calorimeter
	T_∞	°C	293 ± 17
			Ignition Data Analysis
	ε	-	0.9 ± 0.09
			Approximated
Δt_{burn}	s	$\frac{(116)(15.1)}{0.046\dot{q}_e'' + 5.530}$	
		Burning-Rate Data Analysis	

4.2.2 Validation

4.2.2.1 MODELING GOAL

Estimate model parameters for conducting modeling of pyrolysis of triple-layer corrugated cardboard under various heating rates – heat flux levels ranging up to ~ 75 kW/m².

4.2.2.2 MODEL TYPE

Thermally-thick model for ignition analysis (Quintiere and Harkleroad, ASTM E 1321) and steady-burning model

4.2.2.3 MODELING APPROACH

- Pre-ignition stage is
 - Inert: non-uniform charring is considered to be evenly distributed
 - Thermally-thick: heat transfer does not reach back surface
- Post-ignition stage is
 - Considered to have instantaneous release of volatiles from solid to gas phase
 - Considered to have a constant thickness: exfoliation of surface layers is neglected
 - Steady burning: heat loss equals heat gain at front surface

4.2.2.4 EXPERIMENT DESCRIPTION

Cone Calorimeter test

4.2.2.5 DATA SET

- Cone Calorimeter test data of triple-layered corrugated cardboard with thickness of 15 mm, density of 116 kg/m³ and applied heat-flux levels ranging from 8 to 75 kW/m² is found.
- For ignition-data analysis, only time-to-ignition with respect to applied heat-flux data will be used.
- For burning-rate data analysis, data for the entire testing time duration mass loss and heat release during testing period with respect to applied heat flux will be used.

4.2.2.6 UNCERTAINTY

Uncertainty in Experiment Data

- The uncertainty in the mass loss rate data used for comparison between data and model outputs is estimated via statistical approach, taking the standard deviation (0.58 g/sm^2) from the mean of a steady burning of five identical PMMA tests conducted in a Cone Calorimeter.²⁰ The estimated uncertainty is 1.4 g/sm^2 , which is found by calculating the 95% confidence interval applying student t distribution with a sample size of 5.
- The uncertainty in time-to-ignition data used for comparison is estimated via statistical approach, taking two to four identical Cone Calorimeter test data at heat fluxes ranging from 25 to 75 kW/m^2 of this cardboard. A 95% confidence interval is calculated for each heat-flux level assuming student t distribution.
- Assume:
 - Uncertainties are comparable to those of similar flat surfaces pyrolyzing under heating

Uncertainty in Modeling Outputs

- Uncertainty in t_{ig} and \dot{m}'' can be estimated from a linear regression process and using the Law of Propagation of Uncertainty

MODELING OUTPUT: MASS LOSS RATE (MLR)

- Ignition and Burning-Rate Data Analysis

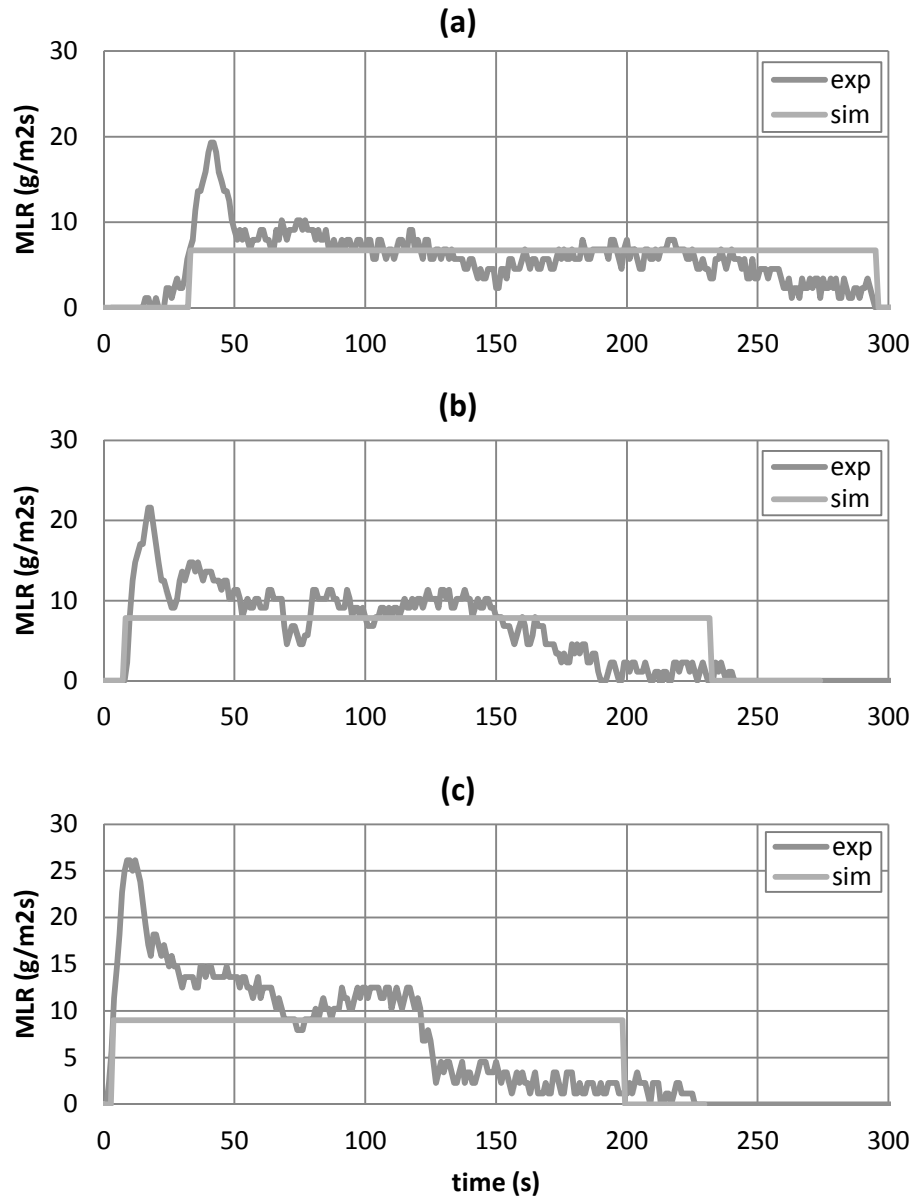


Figure 4-9 Mass-loss rate (MLR) comparisons for corrugated cardboard between actual MLR from experiment (exp) and modeled MLR (sim) at different applied heat-flux levels – (a) MLR at 25 kW/m²; (b) MLR at 50 kW/m²; and (c) MLR at 75 kW/m².

Note that data shown were used to estimate model-parameter values.

4.2.3 Commentary

GENERAL COMMENTS ABOUT MLR

- Ignition and Burning-Rate Data Analysis at HF = 25, 50 and 75 kW/m²: Good agreement exists between experiment data and all modeling results
- The peaks are not captured in all cases, for averaged mass-loss rates have been used to estimate burning rate in the model.

LIMITATION IN MODELING

- When using the Simple Analytical Model to simulate pyrolysis of triple-layered corrugated cardboard (density 116 kg/m³, thickness 15 mm), test data from a bench-scale Cone Calorimeter experiment at several heat-flux levels have been utilized to estimate the time-to-ignition from exposure to heating and the mass-loss rate at steady-burning stage after ignition. The comparison between the model outputs (time-to-ignition and steady-burning rate) and the data from bench-scale experiment showed good agreement for both checking purposes, where the same heat flux levels (25, 50, and 75 kW/m²) used in parameter estimation have been considered.
- Although the modeling predictions of time-to-ignition and steady-burning rate in this example seems to be reasonable, limitation of this Simple Analytical Modeling should be noted, which is that the model is for thermally-thick-behaving materials and steady burning after ignition.

Example 4.3 Modeling Fire Retarded FRP Composite

4.3.1 Model Parameter Table

Model Parameters	Unit	Estimated Values and Estimation Methods
Ignition Parameters	T_{ig}	523 ± 5
		Ignition Data Analysis
	\dot{q}_{cr}''	29 ± 1
		Measurement, Cone Calorimeter by bracketing
	kpc	1.834 ± 0.408
	Ignition Data Analysis	
Burning-Rate Parameters	$\Delta h_{c,eff}$	18.3 ± 6.7
		Burning-Rate Data Analysis
	Δh_g	13.7 ± 3.5
	Burning-Rate Data Analysis	
Parameters for Specifying Conditions	h_c	12 ± 0.5
		Reference value for horizontal position in Cone Calorimeter
	T_∞	23 ± 3.45
		Measurement
	ε	0.9 ± 0.09
		Approximated
Δt_{burn}	s	$\frac{(609)(8.9)}{0.073\dot{q}_e'' + 0.830}$
		Burning-Rate Data Analysis

4.3.2 Validation

4.3.2.1 MODELING GOAL

Estimate model parameters for conducting modeling of pyrolysis of fire retarded FRP composite under various heating rates – heat-flux levels ranging up to $\sim 75 \text{ kW/m}^2$.

4.3.2.2 MODEL TYPE

Thermally-thick model for ignition analysis (Quintiere and Harkleroad, ASTM E 1321) and steady burning model

4.3.2.3 MODELING APPROACH

- Pre-ignition stage is
 - Inert: non-uniform charring is considered to be evenly distributed
 - Thermally-thick: heat transfer does not reach back surface
- Post-ignition stage is
 - Considered to have instantaneous release of volatiles from solid to gas phase
 - Considered to have a constant thickness
 - Steady burning: heat loss equals heat gain at front surface

4.3.2.4 EXPERIMENT DESCRIPTION

Cone Calorimeter test

4.3.2.5 DATA SET

- Cone Calorimeter test data of FRP composite with thickness of 9.2 mm, density of 1900 kg/m^3 , and applied heat-flux levels ranging from 20 to 75 kW/m^2 is found.
- For ignition-data analysis, only time-to-ignition with respect to applied heat-flux data will be used.
- For burning-rate data analysis, data for the entire testing time duration mass loss and heat release during testing period with respect to applied heat flux will be used.

4.3.2.6 UNCERTAINTY

Uncertainty in Experiment Data

- The uncertainty in the mass-loss rate data used for comparison between data and model outputs is estimated via statistical approach, taking the standard deviation (0.58 g/sm^2) from the mean of a steady burning of five identical PMMA tests conducted in a Cone Calorimeter²⁰. The estimated uncertainty is 1.4 g/sm^2 , which is found by calculating the 95% confidence interval applying student t distribution with a sample size of five.
- The uncertainty in time-to-ignition data used for comparison is estimated via statistical approach, taking four to five identical Cone Calorimeter test data at heat fluxes ranging from 50 and 75 kW/m^2 of this cardboard. A 95% confidence interval is calculated for each heat-flux level assuming student t distribution.
- Assume:
 - Uncertainties are comparable to those of similar flat surfaces pyrolyzing under heating

Uncertainty in Modeling Outputs

- Uncertainty in t_{ig} and \dot{m}'' can be estimated from the linear-regression process and using the Law of Propagation of Uncertainty

4.3.2.7 MODELING OUTPUT: MASS LOSS RATE (MLR)

- Ignition and Burning-Rate Data Analysis

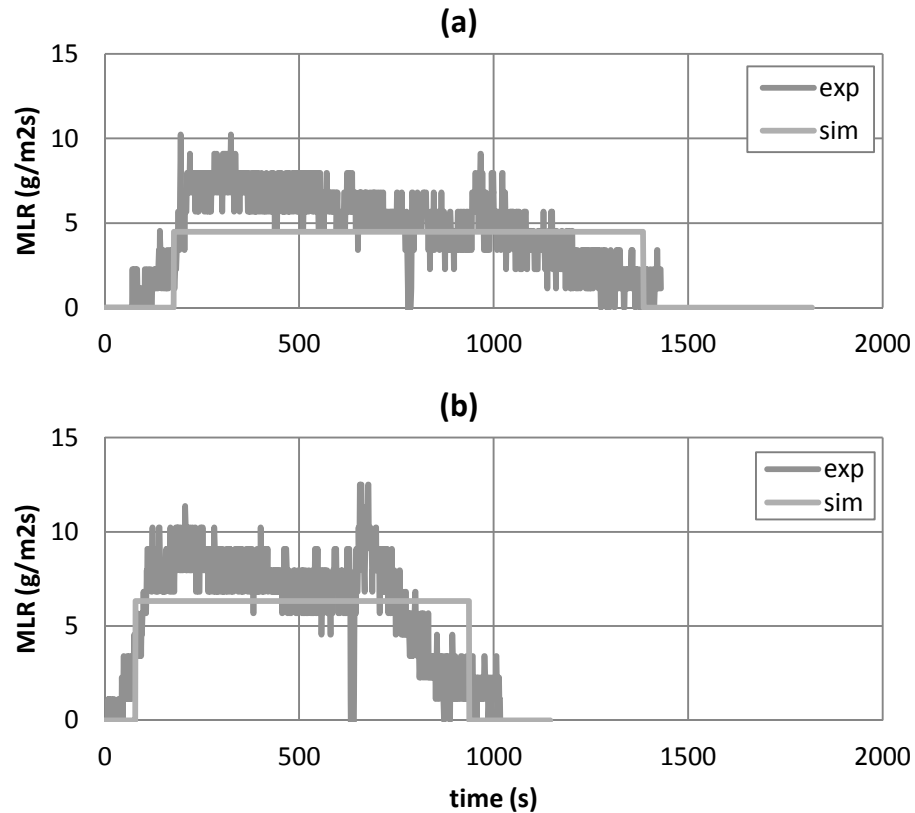


Figure 4-10 Mass-loss rate (MLR) comparisons for fire-retarded FRP composite between actual MLR from experiment (exp) and modeled MLR (sim) at different applied heat-flux levels – (a) MLR at 50 kW/m²; and (b) MLR at 75 kW/m². Note that data shown were used to estimate model-parameter values.

4.3.3 Commentary

GENERAL COMMENTS ABOUT MLR

- Ignition and Burning-Rate Data Analysis at HF = 25, 50, and 75 kW/m²: Good agreement exists between experiment data and all modeling results
- The peaks are not captured in all cases, for averaged mass-loss rates have been used to estimate burning rate in the model

LIMITATION IN MODELING

- When using the Simple Analytical Model to simulate pyrolysis of a fire-retarded fiberglass-reinforced polymer (FRP) composite (density 2100 kg/m³, thickness 8.9 mm, 71 wt% of composite remains as residue), test data from a bench-scale Cone Calorimeter experiment at several heat-flux levels have been utilized to estimate the time to ignition from exposure to heating and the mass-loss rate at steady-burning stage after ignition. The comparison between the model outputs (time-to-ignition and steady-burning rate) and the data from bench-scale experiment showed good agreement for both checking purposes- where the same heat-flux levels (50 and 75 kW/m²) used in parameter estimation have been considered.
- Although the modeling predictions of time-to-ignition and steady-burning rate in this example seems to be reasonable, limitation of this Simple Analytical Modeling should be noted, which is that the model is for thermally-thick-behaving materials and steady burning after ignition.

Example 4.4 Modeling Plywood

4.4.1 Model Parameter Table

Model Parameters		Unit	Estimated Values and Estimation Methods
Ignition Parameters	T_{ig}	°C	377 ± 11
			Ignition Data Analysis
	\dot{q}_{cr}''	kW/m ²	14.5 ± 1
			Measurement, Cone Calorimeter by bracketing
	kpc	kJ ² /m ⁴ K ² s	0.501 ± 0.138
Ignition Data Analysis			
Burning-Rate Parameters	$\Delta h_{c,eff}$	g/s-m ²	14.4 ± 1.2
			Burning-Rate Data Analysis
	Δh_g	kJ/g	8.0 ± 1.1
			Burning-Rate Data Analysis
Parameters for Specifying Conditions	h_c	W/m ² K	12 ± 0.5
			Reference value for horizontal position in Cone Calorimeter
	T_∞	°C	20 ± 2
			Measurement
	ε	-	0.9 ± 0.09
			Approximated
	Δt_{burn}	s	$\frac{(542)(11.1)}{0.125\dot{q}_e'' + 4.110}$
Burning-Rate Data Analysis			

4.4.2 Validation

4.4.2.1 MODELING GOAL

Estimate model parameters for conducting modeling of pyrolysis of plywood under various heating rates – heat-flux levels ranging up to $\sim 100 \text{ kW/m}^2$.

4.4.2.2 MODEL TYPE

Thermally-thick model for ignition analysis (Quintiere and Harkleroad, ASTM E 1321) and steady-burning model

4.4.2.3 MODELING APPROACH

- Pre-ignition stage is
 - Inert
 - Thermally thick: heat transfer does not reach back surface
- Post-ignition stage is
 - Considered to have instantaneous release of volatiles from solid to gas phase: any mass transportation effect on pyrolysis is neglected and pyrolysis is considered as surface phenomenon only
 - Considered to have a constant thickness: shrinkage, regression and bending near the end is neglected
 - Steady burning: heat loss equals heat gain at front surface

4.4.2.4 EXPERIMENT DESCRIPTION

Cone Calorimeter test

4.4.2.5 DATA SET

- Cone Calorimeter test data of Douglas Fir plywood with thickness of $11.1 \pm 0.1 \text{ mm}$, density of $542 \pm 11 \text{ kg/m}^3$ and applied heat flux levels ranging from 14 to 100 kW/m^2 is found (student t distribution, $\alpha = 0.05$, sample size of 10).
- For ignition data analysis, only time-to-ignition with respect to applied heat-flux data will be used.
- For burning-rate data analysis, data for the entire testing time duration mass loss and heat release during testing period with respect to applied heat flux will be used.

4.4.2.6 UNCERTAINTY

Uncertainty in Experiment Data

- The uncertainty in the mass-loss rate data used for comparison between data and model outputs is estimated via statistical approach, taking the standard deviation (0.58 g/sm^2) from the mean of a steady burning of five identical PMMA tests conducted in a Cone Calorimeter²⁰. The estimated uncertainty is 1.4 g/sm^2 , which is found by calculating the 95% confidence interval applying student t distribution with a sample size of five.
- The uncertainty in time-to-ignition data used for comparison is estimated via statistical approach, taking three to four identical Cone Calorimeter test data at heat fluxes ranging from 25 to 75 kW/m^2 of this cardboard. A 95% confidence interval is calculated for each heat-flux level assuming student t distribution.
- Assume:
 - Uncertainties are comparable to those of similar flat surfaces pyrolyzing under heating

Uncertainty in Modeling Outputs

- Uncertainty in t_{ig} and \dot{m}'' can be estimated from linear regression process and using the Law of Propagation of Uncertainty

4.4.2.7 MODELING OUTPUT: MASS LOSS RATE (MLR)

- Ignition and Burning-Rate Data Analysis

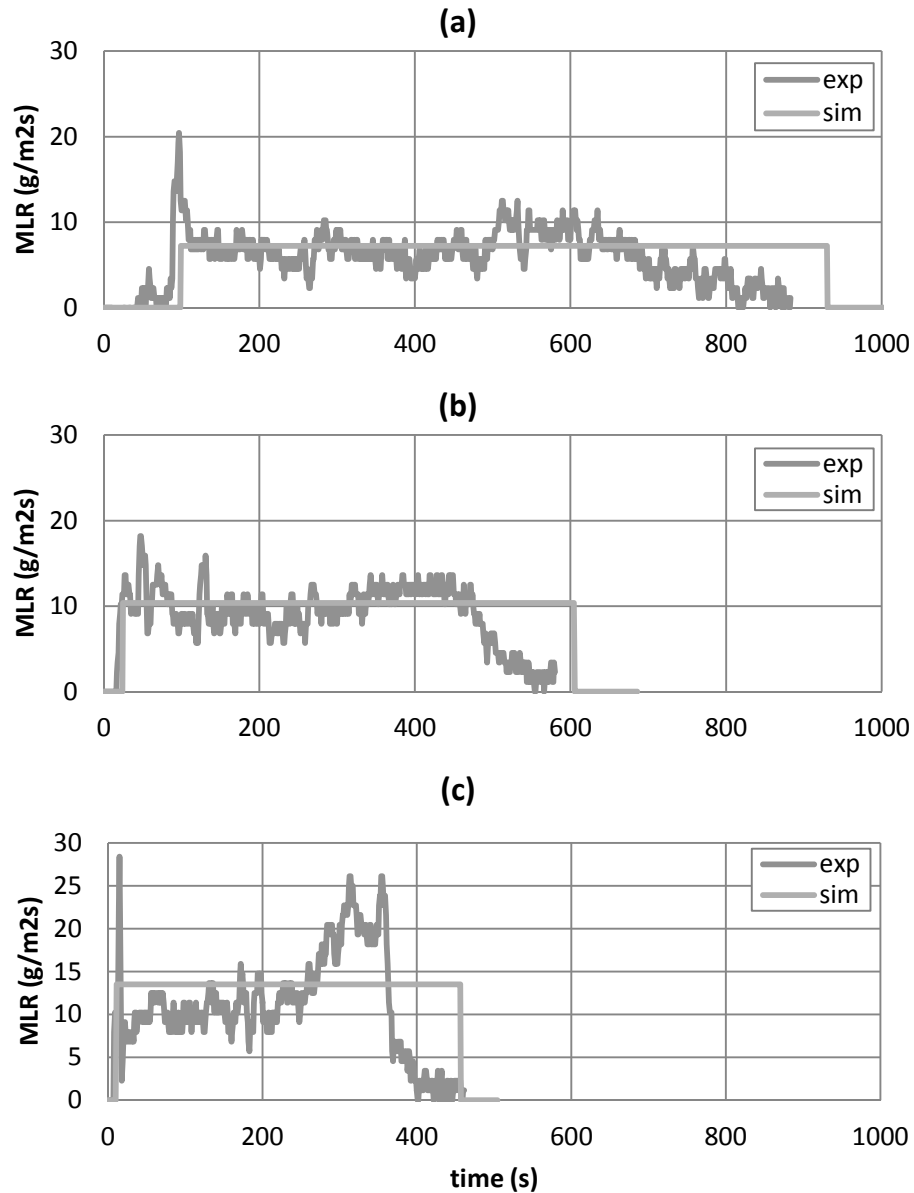


Figure 4-11 Mass-loss rate (MLR) comparisons for plywood between actual MLR from experiment (exp) and modeled MLR (sim) at different applied heat-flux levels – (a) MLR at 25 kW/m²; (b) MLR at 50 kW/m²; and (c) MLR at 75 kW/m². Note that data shown were used to estimate model-parameter values.

4.4.3 Commentary

GENERAL COMMENTS ABOUT MLR

- Ignition and Burning-Rate Data Analysis at HF = 25, 50 and 75 kW/m²: Good agreement exists between experiment data and all modeling results

LIMITATION IN MODELING

- When using the Simple Analytical Model to simulate pyrolysis of Douglas Fir Plywood, test data from a bench-scale Cone Calorimeter experiment at several heat flux levels have been utilized to estimate the time-to-ignition from exposure to heating and the mass-loss rate at steady-burning stage after ignition. The comparison between the model outputs (time-to-ignition and steady-burning rate) and the data from bench-scale experiment showed good agreement for both checking purposes where the same heat-flux levels (25, 50 and 75 kW/m²) used in parameter estimation have been considered.
- Although the modeling predictions of time-to-ignition and steady-burning rate in this example seems to be reasonable, limitation of this Simple Analytical Modeling should be noted, which is that the model is for thermally-thick-behaving materials and steady burning after ignition.

CASE 2: THERMALLY-THIN, INERT AT PRE-IGNITION WITH STEADY BURNING AT POST-IGNITION

Virtual Microstructure of Virgin Material

- Homogeneous flat surface single layer in horizontal position
- Pre-ignition stage: inert, thermally thin
- Post-ignition stage: steady burning

General Model-Parameter Table

- Ignition and burning-rate parameters are considered in this example
- Reduced Model Parameter Table (see Table 4-7):

Table 4-7. Model Parameter Table for Case 2 Examples

Ignition Parameters	T_{ig}	Surface Temperature at Ignition
	\dot{q}_{cr}''	Critical Heat Flux for Ignition
	$\rho c \delta$	Thermal Capacity (Thermally-thin)
Burning-Rate Parameters	$\Delta h_{c,eff}$	Effective Heat-of-Combustion
	Δh_g	Heat-of-Gasification
Parameters for Specifying Conditions	h_c	Convection Coefficient
	T_∞	Ambient Temperature
	ε	Surface Emissivity/Absorptivity
	Δt_{burn}	Burn Duration

Example 4.5 Modeling Sandwich Composite – GRP Skin with Balsawood Core

This material is composed of approximately 1 mm thickness of laminated glass-reinforced polymer (GRP) over approximately 25 mm thickness of resin-soaked balsa wood core as a skin layer (sandwich construction). The resin used in the GRP and with balsa wood is vinyl ester (VEX). The light weight core, balsa wood acts as an insulating layer for the thin GRP skin and allows the ignition data to behave thermally thin. This thermal behavior is examined by plotting $1/t_{ig}^n$ vs. applied heat flux where its best fitness of a linear regression occurs near $n = 0.9$.

4.5.1 Model Parameter Table

Model Parameters		Unit	Estimated Values and Estimation Methods
Ignition Parameters	T_{ig}	°C	350 ± 36
			Ignition Data Analysis
	\dot{q}_{cr}''	kW/m ²	12.5 ± 2.5
			Measurement, Cone Calorimeter by bracketing
k _{pc}	kJ ² /m ⁴ K ² s	7.625 ± 19.1	
		Ignition Data Analysis	
Burning-Rate Parameters	$\Delta h_{c,eff}$	g/s-m ²	23.5 ± 2.1
			Burning-Rate Data Analysis
	Δh_g	kJ/g	8.7 ± 1.4
Parameters for Specifying Conditions	h_c	W/m ² K	12 ± 0.5
			Reference value for horizontal position in Cone Calorimeter
	T_∞	°C	20 ± 5
			Measurement
	ε	-	0.9 ± 0.09
			Approximated
Δt_{burn}	s	$\frac{(600)(1.3)}{0.129\dot{q}_e'' + 7.415}$	
		Burning-Rate Data Analysis	

4.5.2 Validation

4.5.2.1 MODELING GOAL

Estimate model parameters for conducting modeling of pyrolysis of vinyl ester glass-reinforced polymer (GRP) skin with 1" thick resin soaked balsa wood core sandwich composite under various heating rates – heat-flux levels ranging up to $\sim 90 \text{ kW/m}^2$.

4.5.2.2 MODEL TYPE

Thermally-thin model for ignition analysis and steady-burning model

4.5.2.3 MODELING APPROACH

- Pre-ignition stage is
 - Inert: decomposition with bubbling and changing color on surface before ignition is neglected
 - Thermally-thin GRP skin: heat transfer does not reach back surface quickly and the surface layer (vinyl ester resin GRP) is considered to have uniform temperature throughout
 - Control volume for ignition analysis is the thermally-thin GRP skin layer on the front surface facing the heating source
- Post-ignition stage is
 - Considered to have instantaneous release of volatiles from solid to gas phase: any mass-transportation effect on pyrolysis is neglected and pyrolysis is considered as surface phenomenon only
 - Considered to have a constant thickness
 - Steady burning: heat loss equals heat gain at front surface
 - 30% of the GRP skin layer (density of 2000 kg/m^3) is consumed via burning, and this information is used to calculate the model's burnout time prediction

4.5.2.4 EXPERIMENT DESCRIPTION

Cone Calorimeter test

4.5.2.5 DATA SET

- Cone Calorimeter test data of this sandwich composite panel with thickness of 28 mm, density of 500 kg/m^3 and applied heat flux levels ranging from 15 to 90 kW/m^2 is found.
- For ignition data analysis, only time-to-ignition with respect to applied heat-flux data will be used.
- For burning-rate data analysis, data for the entire testing time duration mass loss and heat release during testing period with respect to applied heat flux will be used.

4.5.2.6 UNCERTAINTY

Uncertainty in Experiment Data

- The uncertainty in the mass-loss rate data used for comparison between data and model outputs is estimated via a statistical approach, taking the standard deviation (0.58 g/sm^2) from the mean of a steady burning of five identical PMMA tests conducted in a Cone Calorimeter.²⁰ The estimated uncertainty is 1.4 g/sm^2 , which is found by calculating the 95% confidence interval applying student t distribution with a sample size of five.
- The uncertainty in time-to-ignition data used for comparison is estimated via a statistical approach, taking three to four identical Cone Calorimeter test data at heat fluxes ranging from 35 to 75 kW/m^2 of this cardboard. A 95% confidence interval is calculated for each heat-flux level assuming student t distribution.
- Assume:
 - Uncertainties are comparable to those of similar flat surfaces pyrolyzing under heating

Uncertainty in Modeling Outputs

- Uncertainty in t_{ig} and \dot{m}'' can be estimated from a linear regression process and using the Law of Propagation of Uncertainty

4.5.2.7 MODELING OUTPUT: MASS LOSS RATE (MLR)

- Ignition and Burning-Rate Data Analysis

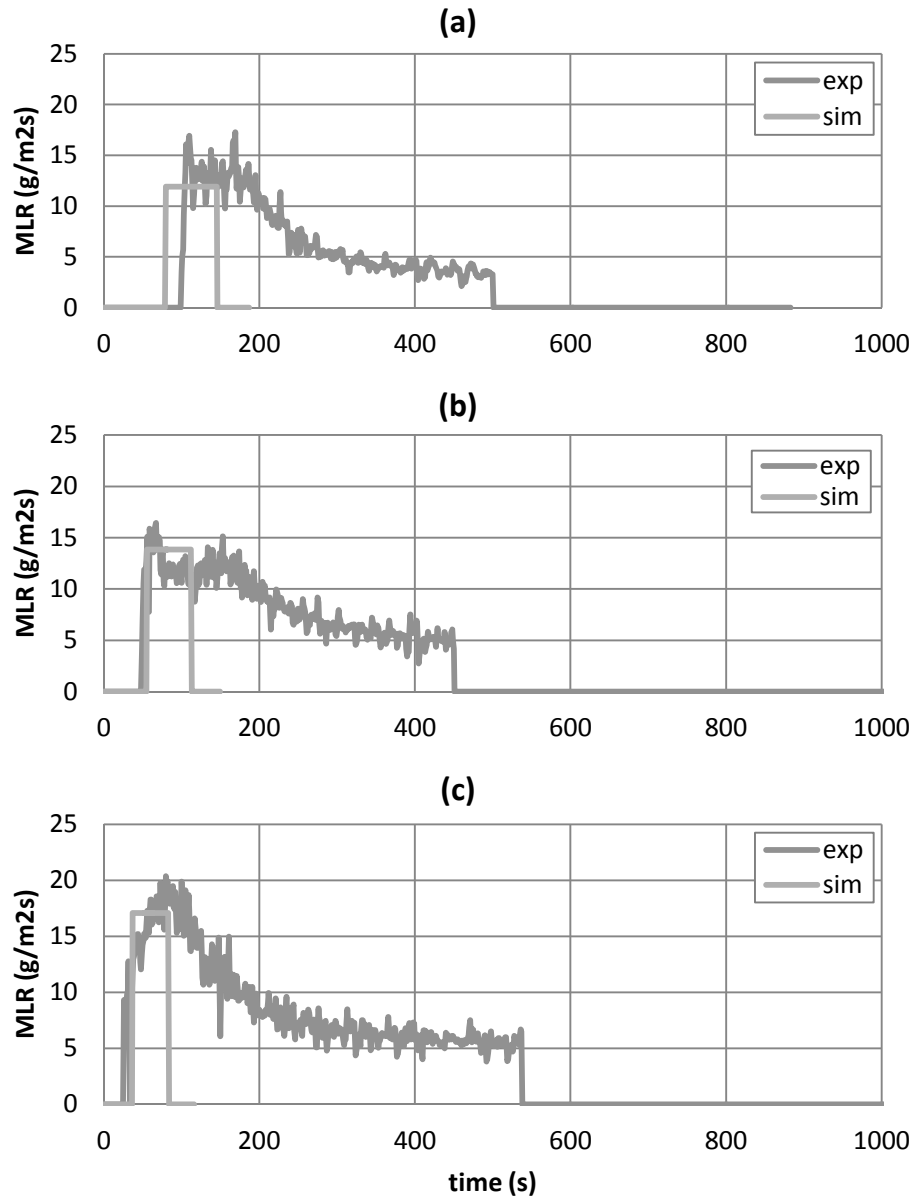


Figure 4-12 Mass-loss rate (MLR) comparisons for sandwich composite – GRP skin with balsawood core – between actual MLR from experiment (exp) of the composite and modeled MLR (sim) of GRP skin at different applied heat-flux levels – (a) MLR at 35 kW/m²; (b) MLR at 50 kW/m²; and (c) MLR at 75 kW/m². Note that data shown were used to estimate model-parameter values.

4.5.3 Commentary

GENERAL COMMENTS ABOUT MLR

- Ignition and Burning-Rate Data Analysis at HF = 35, 50 and 75 kW/m²: Good agreement exists between experiment data and all modeling results

LIMITATION IN MODELING

- When using the Simple Analytical Model to simulate pyrolysis of Douglas Fir Plywood, test data from a bench-scale Cone Calorimeter experiment at several heat flux levels have been utilized to estimate the time-to-ignition from exposure to heating and the mass-loss rate at steady-burning stage after ignition. The comparison between the model outputs (time-to-ignition and steady-burning rate) and the data from bench-scale experiment showed good agreement for both checking purposes where the same heat-flux levels (35, 50 and 75 kW/m²) used in parameter estimation have been considered.
- Although the modeling predictions of time-to-ignition and steady-burning rate in this example seem to be reasonable, limitation of this Simple Analytical Modeling should be noted, which is that the model is for thermally-thick-behaving materials and steady burning after ignition.

Example 4.6 Modeling Thin FRP Composite

The rigid FRP panel chosen for use in full-scale testing is commercially available and advertised for use as ceiling and wall linings (flat surfaces) in environments designed to be moisture- and mold-free. The panel has a Class C (ASTM E84) flame-spread rating. It is consisted of modified polyester copolymer and inorganic fillers as the resin base and reinforced with a weave of random chopped fiberglass. The panel's thickness is 0.09" (2.3 mm) nominal, with a smooth backface and a pebbled, embossed white front surface. When this material is tested for ignition in Cone Calorimeter test, thermally-thin behavior is observed. This thermal characteristic is examined by plotting $1/t_{ig}^n$ vs. applied heat flux where its best fitness of a linear regression occurs near $n = 1.0$.

4.6.1 Model Parameter Table

Model Parameters		Unit	Estimated Values and Estimation Methods
Ignition Parameters	T_{ig}	°C	397 ± 10
			Ignition Data Analysis
	\dot{q}_{cr}''	kW/m ²	16 ± 1
Measurement, Cone Calorimeter by bracketing			
k _{pc}	kJ ² /m ⁴ K ² s	4.333 ± 4.369	
		Ignition Data Analysis	
Burning-Rate Parameters	$\Delta h_{c,eff}$	g/s-m ²	25.5 ± 1.8
			Burning-Rate Data Analysis
	Δh_g	kJ/g	16.3 ± 4.7
			Burning-Rate Data Analysis
Parameters for Specifying Conditions	h_c	W/m ² K	12 ± 0.5
			Reference value for horizontal position in Cone Calorimeter
	T_∞	°C	23 ± 3.45
			Measurement
ε	-	0.9 ± 0.09	
		Approximated	
Δt_{burn}	s	$\frac{(600)(2.0)}{0.061\dot{q}_e'' + 1.194}$	
		Burning-Rate Data Analysis	

4.6.2 Validation

4.6.2.1 MODELING GOAL

Estimate model parameters for conducting modeling of pyrolysis of this Class C FRP composite under various heating rates – heat-flux levels ranging up to $\sim 75 \text{ kW/m}^2$.

4.6.2.2 MODEL TYPE

Thermally-thin model for ignition analysis and steady burning model

4.6.2.3 MODELING APPROACH

- Pre-ignition stage is
 - Inert: decomposition with crackling sound and changing color on surface before ignition is neglected
 - Thermally thin: heat transfer does not reach back surface quickly, and the entire layer is considered to have uniform temperature throughout
 - Control volume for ignition analysis is the thermally-thin GRP skin layer on the front surface facing the heating source
- Post-ignition stage is
 - Considered to have instantaneous release of volatiles from solid to gas phase: any mass-transportation effect on pyrolysis is neglected and pyrolysis is considered as a surface phenomenon only
 - Considered to have a constant thickness
 - Steady burning: heat loss equals heat gain at front surface
 - 40% of the FRP composite sheet (density of 1500 kg/m^3) is consumed via burning, and this information is used to calculate the model's burnout time prediction

4.6.2.4 EXPERIMENT DESCRIPTION

Cone Calorimeter test

4.6.2.5 DATA SET

- Cone Calorimeter test data of this sandwich composite panel with thickness of 2 mm, density of 1500 kg/m^3 and applied heat-flux levels ranging from 15 to 75 kW/m^2 is found.
- For ignition data analysis, only time-to-ignition with respect to applied heat-flux data will be used.
- For burning-rate data analysis, data for the entire testing time duration mass loss and heat release during testing period with respect to applied heat flux will be used.

4.6.2.6 UNCERTAINTY

Uncertainty in Experiment Data

- The uncertainty in the mass-loss rate data used for comparison between data and model outputs is estimated via a statistical approach, taking the standard deviation (0.58 g/sm^2) from the mean of a steady burning of five identical PMMA tests conducted in a Cone Calorimeter²⁰. The estimated uncertainty is 1.4 g/sm^2 , which is found by calculating the 95% confidence interval applying student t distribution with a sample size of five.
- The uncertainty in time-to-ignition data used for comparison is estimated via a statistical approach, taking two to three identical Cone Calorimeter test data at heat fluxes ranging from 25 to 75 kW/m^2 of this cardboard. A 95% confidence interval is calculated for each heat-flux level assuming student t distribution.
- Assume:
 - Uncertainties are comparable to those of similar flat surfaces pyrolyzing under heating

Uncertainty in Modeling Outputs

- Uncertainty in t_{ig} and \dot{m}'' can be estimated from a linear regression process and using the Law of Propagation of Uncertainty

4.6.2.7 MODELING OUTPUT: MASS LOSS RATE (MLR)

- Ignition and Burning-Rate Data Analysis

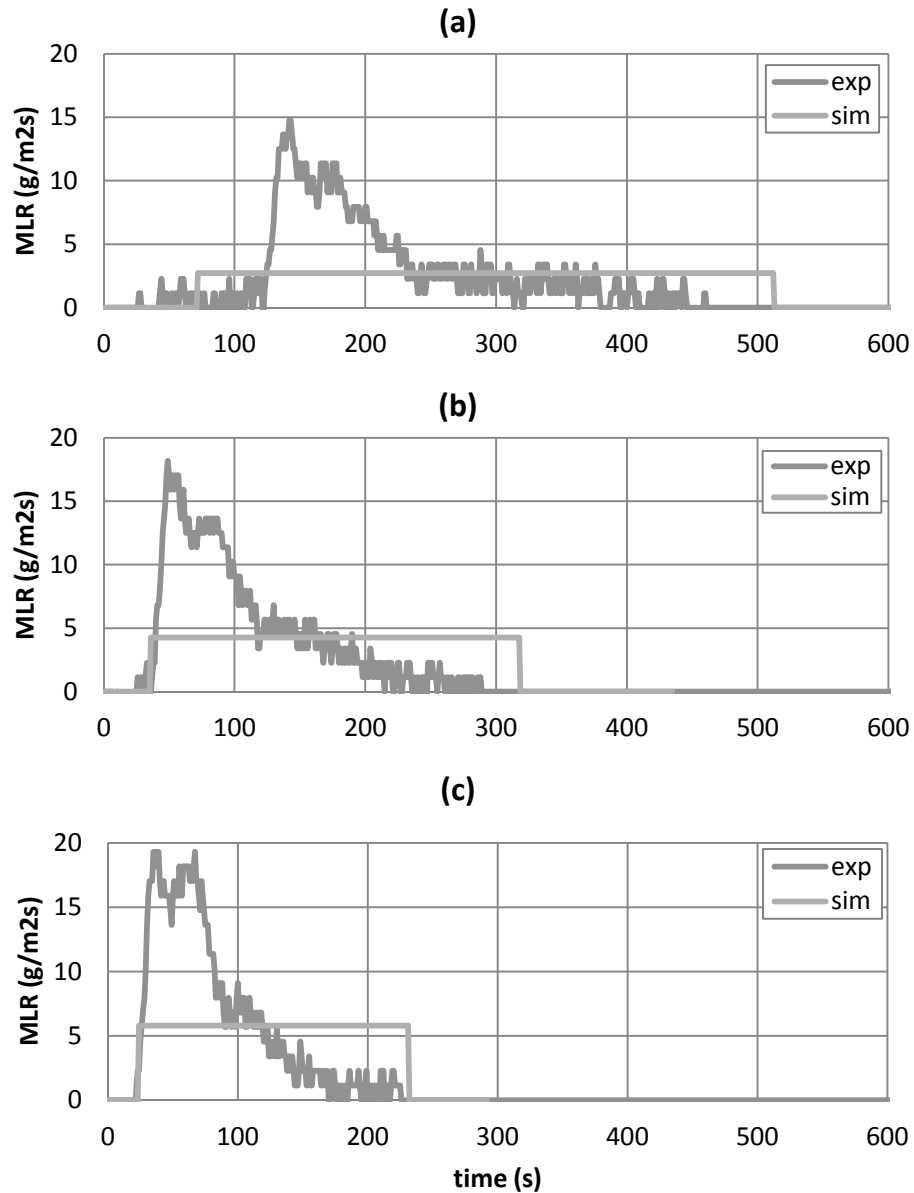


Figure 4-13 Mass-loss rate (MLR) comparisons for thin FRP composite between actual MLR from experiment (exp) and modeled MLR (sim) at different applied heat-flux levels – (a) MLR at 25 kW/m²; (b) MLR at 50 kW/m²; and (c) MLR at 75 kW/m². Note that data shown were used to estimate model-parameter values.

4.6.3 Commentary

GENERAL COMMENTS ABOUT MLR

- Ignition and Burning-Rate Data Analysis at HF = 25, 50 and 75 kW/m²: Good agreement exists between experiment data and all modeling results
- The peaks are not captured in all cases, for averaged mass-loss rates have been used to estimate burning rate in the model

LIMITATION IN MODELING

- In this example, the Simple Analytical Model is used to simulate pyrolysis of thermally -thin-behaving FRP composite sheet. Test data from a bench-scale Cone Calorimeter experiment at several heat-flux levels have been utilized to estimate the time-to-ignition from exposure to heating and the mass-loss rate at steady-burning stage after ignition. The comparison between the model outputs (time-to-ignition and steady-burning rate) and the data from bench-scale experiment showed good agreement for both checking purposes where the same heat-flux levels (25, 50 and 75 kW/m²) used in parameter estimation have been considered. To improve modeling results, one may consider taking the peak average of the mass-loss rate and the heat-release rates to estimate heat-of-gasification, for most of the burning occurs near the peak. The tail following the peak (MLR or HRR curve) extends for a longer period of time until flame-out, where smaller percentage of the combustible resin between fiber glass layers is burning off at in-depth.
- Although the modeling predictions of time-to-ignition and steady-burning rate in this example seems to be reasonable, limitation of this Simple Analytical Modeling should be noted, which is that the model is for thermally-thick-behaving materials and steady burning after ignition.

REFERENCES

-
- ¹ Fuss, S.; and Hamins, A., "An Estimate of the Correction Applied to Radiant Flame Measurements due to Attenuation by Atmospheric CO₂ and H₂O," *Fire Safety Journal*, vol. 37, 181-190, 2002.
- ² Urbas, J.; and Parker, W., "Surface Temperature Measurement in a Fire Environment Using an Infrared Pyrometer," in *Eighth International Symposium on Fire Safety Science*, Beijing, China, 2005, 1401-1412.
- ³ Urbas, J., *et al.*, "Surface Temperature Measurements on Burning Materials Using an Infrared Pyrometer: Accounting for Emissivity and Reflection Of External Radiation," *Fire and Materials*, vol. 28, 33-53, 2004.
- ⁴ Omrane, A., *et al.*, "Surface Temperature Measurement of Flame Spread Using Thermographic Phosphors," in *Seventh International Symposium on Fire Safety Science*, Worcester, MA, 2003, 141-152
- ⁵ Göransson, U.; and Omrane, A., "Surface Temperature Measurements in the Cone Calorimeter Using Phosphorescence," in *10th Interflam Conference*, Edinburgh, Scotland, 2004, 1431-1442.
- ⁶ Omrane, A., *et al.*, "Surface Temperature of Decomposing Construction Materials Studied by Laser-Induced Phosphorescence," *Fire and Materials*, vol. 29, 39-51, 2005.
- ⁷ Thomson, H.; and Drysdale, D., "Flammability of Plastics, I: Ignition Temperatures," *Fire and Materials*, vol. 11, 163-172, 1987.
- ⁸ Thomson, H., *et al.*, "An Experimental Evaluation of Critical Surface Temperature as a Criterion for Piloted Ignition of Solid Fuels," *Fire Safety Journal*, vol. 13, 185-196, 1988.
- ⁹ Abu-Zaid, M., "Effect of Water on Ignition of Cellulosic Materials," Ph.D. Thesis, Michigan State University, East Lansing, MI, 1988.
- ¹⁰ Atreya, A., "Pyrolysis, Ignition and Fire Spread on Horizontal Surfaces of Wood," Ph.D. Thesis, Harvard University, Cambridge, MA, 1983.
- ¹¹ Atreya, A., *et al.*, "Effect of Sample Orientation on Piloted Ignition and Flame Spread," in *First International Symposium on Fire Safety Science*, Gaithersburg, MD, 1985, 97-109.
- ¹² Fangrat, J., *et al.*, "Surface Temperature at Ignition of Wooden Based Slabs," *Fire Safety Journal*, vol. 27, 249-259, 1996.
- ¹³ Janssens, M., "Thermophysical Properties of Wood and their Role in Enclosure Fire Growth," Ph.D. Thesis, University of Ghent, Ghent, Belgium, 1991.
- ¹⁴ Yudong, L.; and Drysdale, D., "Measurement of the Ignition Temperature of Wood," *Fire Safety Science*, vol. 1, 25-30, 1992.
- ¹⁵ Quintiere, J.; and Harkleroad, M., "New Concepts for Measuring Flame Spread Properties," in *Fire Safety: Science and Engineering, ASTM STP 882*, June 16-17, 1984, Denver, CO, 1985, 239-267.
- ¹⁶ Dietenberger, M., "Ignitability Analysis Using the Cone Calorimeter and LIFT Apparatus," in *Twenty-Second International Conference on Fire Safety*, Columbus, OH, 1996.
- ¹⁷ Tewarson, A.; and Pion, R., "Flammability of Plastics. I. Burning Intensity," *Combustion & Flame*, vol. 26, 85-103, 1976.
- ¹⁸ Petrella, V., "The Mass Burning Rate of Polymers, Wood and Liquids," *Journal of Fire and Flammability*, vol. 11, 3-21, 1980.
- ¹⁹ Beaulieu, P.A.; and Dembsey, N.A., *Fire Safe*. J. 43 (2008) 410-428

²⁰ Zhao, Lei, Bench Scale Apparatus Measurement Uncertainty and Uncertainty Effects on Measurement of Fire Characteristics of Material Systems, MS Thesis, Fire Protection Engineering, WPI, 2005-04-27, ETD-050105-182456.

Chapter 5—Comprehensive Models

UNDERSTANDING MODEL

General Description of Models

Comprehensive pyrolysis models are models that account for physical and chemical responses of fire characteristics of a solid material.^{1,2,3} These models utilize fundamental conservation equations to describe the changes in a material during pyrolysis. Typically, models are constructed to conserve mass and energy when material is being heated and/or thermally decomposed. Numerical calculations are conducted using various methods – finite difference, finite element, or integral formats, where governing equations are transformed to system of ODEs instead of PDEs using simplifications – to determine mass loss and temperature profile from the heat-exposed front surface to unexposed back surface with respect to increasing time.

The thermal-decomposition process in comprehensive pyrolysis modeling can be modeled by two different approaches: reactions that are infinitely fast or finite. When thermal decomposition is infinitely fast, pyrolysis front becomes an infinitely thin reaction zone where reactants are consumed instantaneously into products with releasing or consuming reaction heat. In this case, heat transfer is considered as a limiting factor for modeling the pyrolysis problem. Typically, a pre-determined pyrolysis temperature is used to locate the pyrolysis front. When thermal-decomposition reaction rate is modeled as finite, pyrolysis front has a finite thickness. Whether the virgin material pyrolyzes completely (single solid-state case) or partially (multiple solid-state case) to fuel vapor, the assumption used in this approach allows the model to approximate the pyrolysis kinetics as well as the heat transfer throughout the solid fuel. When pyrolysis kinetics is explicitly considered in modeling, pyrolyzates can be produced at various locations within the pyrolysis front, which has a finite thickness. By performing numerical calculations in these comprehensive pyrolysis models, the temperature profile is obtained for a solid fuel, and, depending on the local temperature, the pyrolysis reaction(s) rate is calculated, allowing the reactants to be consumed to produce pyrolyzates or other types of solid phase materials with associated energy consumption. Typically, an Arrhenius-type expression is used for describing the pyrolysis kinetics. Some models of this kind

consider mass and heat transfer of gases through a decomposed solid-phase product layer, which requires additional governing equations to be solved.

Although accounting for physical and chemical phenomena observed during pyrolysis explicitly is a merit for comprehensive models, difficulties arise when using these models due to the numerous unknowns of model parameters that the model user needs to estimate. The ability of modeling various aspects of the pyrolysis problem results in greater complexity of the model. Therefore, the number of parameters involved in the simulation can dramatically increase, which results in the need of extra effort in estimating the additional unknown parameters.

Brief Description of Typical Pyrolysis Models Available in the Fire Community

In this section, a brief discussion of well-known comprehensive pyrolysis models available to fire community is given. These include a pyrolysis model in Fire Dynamics Simulator (FDS) version 5¹, Thermakin², and GPYRO.³ Typically, pyrolysis modeling is composed of modeling of mass, energy and momentum transfers, and decomposition kinetics within the decomposing material.

Pyrolysis Model in FDS version 5¹

In FDS, mass transfer within a porous solid phase material is not modeled. The assumption is that, when decomposition reaction occurs, the volatile from solid decomposition is released instantaneously to the gas phase. Additionally, condensation of gaseous products within the solid phase is assumed to be negligible. Energy transfer within a solid is described via a one-dimensional heat conduction equation for the solid phase, including the voids from the pores, which allows the model to track temperature changes of the solid phase with respect to time and space. This approach is allowed due to the local thermal equilibrium assumed between the solid and the volatiles at all times. In this equation, the heat-source term is included and it accounts for heat release or absorption due to chemical reactions, radiative absorption, and emission-in-depth. In-depth radiative absorption and emission is modeled as a “two-flux” model based on the Schuster-Schwarzschild approximation,⁴ where the radiative intensity is assumed to be constant at the “forward” and “backward” hemispheres. At the front surface boundary,

convective heat transfer is modeled via combination of natural and forced convection correlation for horizontal or vertical surfaces. Momentum transfer is not solved for the solid phase in this model. Decomposition kinetics is modeled using an Arrhenius type expression with an n^{th} order reaction model. This kinetic model allows decomposition of a single solid-phase component into another type of solid-phase component and/or volatiles to be modeled. The model can configure multiple layers with multiple reactions for decomposition.

Thermakin²

Thermakin models gas-phase mass transfer within a porous solid-phase material; however, the condense phase is immobile. The traveling of gases within the solid is governed by concentration gradient. Gases can be produced by chemical reactions and released to the gas phase. The model tracks the changes of gases in the volume. Transportation of energy is modeled by taking into account the conductive heat transfer through solids (condense phase in porous solid phase) via the Fourier law, convective heat transfer from one element to another due to the travel of gases and heat generation or consumption due to chemical reactions. Radiation transport within the condensed phase is modeled by considering a single element absorbing the external radiation via a maximum-absorption or random-absorption algorithm. For both cases, the external radiation modeled to penetrate material and behave in accordance with Beer-Lambert's law.⁵ These approaches assume that the absorbing element also acts as a gray-body reflector and emitter. Convective heat transfer is modeled at the front surface boundary using a simple Newtonian heat-transfer equation, where the convection coefficient is a user-specified input parameter. Momentum transfer is not solved for the solid phase in this model. Decomposition kinetics is modeled using an Arrhenius-type expression with a first-order reaction model. This kinetic model allows decomposition of a single solid/liquid/gas phase component or two together into another type of a single or two solid/liquid/gas phase component(s) to be modeled. The model can configure multiple components with multiple reactions for decomposition.

GPYRO³

In GPYRO, the condense phase and the gas phase within a porous solid material can be modeled separately. Transfer of condense phase is prohibited by the model. Mass

transfer of gases within the porous solid material is modeled by considering the convective transfer, where conversion of condensed phase mass to gas phase via chemical reactions is accounted for in the source term. Any changes in species mass due to reactions in condense or gas phases are conserved. Transportation of energy in the condense phase is modeled by considering heat transfer via conduction using Fourier's law; source terms that account for volumetric rate of heat release (or absorption) due to condense phase and volumetric rate of heat transfer from the condense phase to the gas phase; and in-depth radiative heat transfer. In this model, in-depth radiative heat transfer accounts only for "one-way" radiation, meaning the penetration of radiation into the solid is calculated, but the emission from interior parts of the solid is not calculated. For energy transfer in the gas phase, conductive and diffusive heat transfers have been included in the model. For calculating the diffusive flux term, Fickian diffusion is applied, and all gases are assumed to have the same diffusion coefficient for simplification. Momentum transfer within the gas phase is conserved in this model by assuming a Darcian flow of the gases with buoyancy. For modeling of decomposition kinetics, an Arrhenius type expression with various reaction models is allowed to describe heterogeneous (gas phase – condense phase) or homogeneous (gas phase – gas phase) reactions. The model can configure multiple layers with multiple reactions for decomposition.

The advantage of using GPYRO is that only this pyrolysis model comes with various numerical optimization algorithms, including Genetic Algorithm (GA), Shuffled Complex Evolution (SCE), and Stochastic Hill Climber (SHC). These algorithms can be used to estimate unknown model parameters by comparing modeling outputs to certain optimization targets, e.g., experiment data.

Governing Equations

Although the effect of the porous nature of the material can be simulated directly by considering the gas phase and the pore-free condense phase separately^{3,6} in comprehensive pyrolysis modeling, a more simplified and general approach is to consider a single mixture of the two phases: gas and condense phase. By doing so, material porosity is accounted for indirectly.

In Table 5-1, the system of equations is given for a Comprehensive Model, where conservation equations are solved for a single, porous, condense phase. Note that the equations are presented in a one-dimensional form in the z-direction, considering that typical pyrolysis modeling is conducted in 1D. Additionally, basic assumptions are the volume change of a cell is negligible ($\Delta z = const$), and gases produced from thermal decomposition leave the porous-condense phase instantaneously without any restriction. These equations are a simplified version of GPYRO's; hence, similarities in mathematical expression exist. See the technical³ and user's guide⁶ of GPYRO (<http://code.google.com/p/gpyro>) for more information.

The major difference in the system of equations between models in Comprehensive Models with finite-thickness pyrolysis fronts and those with infinitely thin pyrolysis fronts is the approach in mathematically describing the decomposition reaction in terms of its speed (finite or infinitely fast). In general, the location of the infinitely thin reaction zone is identified by a material-dependent temperature known as the pyrolysis temperature, T_p , that remains on the pyrolyzing surface for non-charring materials or propagates toward in-depth, leaving a char layer behind near the surface for charring materials. At this location, pyrolysis heat, ΔH_p , is consumed, and reaction reactants and products are consumed and released, respectively.

Table 5-1. General governing equations for comprehensive pyrolysis models

Governing Equations	Material Property Parameters
<p>Condensed-phase mass conservation</p> $\frac{\partial \bar{\rho}}{\partial t} = -\dot{\omega}_{fg}^m$	$\bar{\rho}, \rho_i$
<p>Condensed-phase species conservation</p> $\frac{\partial (\bar{\rho} Y_i)}{\partial t} = \dot{\omega}_{fi}^m - \dot{\omega}_{di}^m$	\bar{k}, k_i ΔH_k \bar{c}, c_i $\Delta H_{m,i}$
<p>Condensed-phase energy conservation</p> $\frac{\partial (\bar{\rho} \bar{h})}{\partial t} = -\frac{\partial}{\partial z} \left(\underbrace{\dot{q}_{z,z}''}_{\text{Fourier's Law for cond.} : \dot{q}'' = -\bar{k} \frac{\partial T}{\partial z}} \right) + \underbrace{\sum_{k=1}^K \dot{\omega}_{s,k}^m}_{\text{sum of heat release/loss due to condense phase rxns, } \Delta H} - \frac{\partial}{\partial z} \left(\underbrace{\dot{q}_{z,z}''}_{\text{in-depth rad heat transfer}} + \underbrace{\sum_{i=1}^M (\dot{\omega}_{fi}^m - \dot{\omega}_{di}^m) h_i}_{\text{sum of gas phase prod. sensible enthalpy}} \right)$ <p>where $\bar{h} = \sum_{i=1}^M Y_i h_i = \sum_{i=1}^M Y_i \left(\int_{T_d}^T c_i(\theta) d\theta \right) + \sum_{i=1}^M X_i k_i, \bar{c} = \sum_{i=1}^M Y_i c_i$</p>	n_k, Z_k, E_k
<p>* Heterogeneous-reaction rate of the k^{th} gas-phase reaction for a general n^{th} order reaction when reaction zone is modeled with finite thickness (i.e., destruction rate of condensed-phase species A_k)</p> $r_k = \dot{\omega}_{dA_k}^m = \underbrace{f(\alpha_{A_k})}_{=(1-\alpha_{A_k})^{n_k}} \frac{(\bar{\rho} Y_{A_k} \Delta z)_{\Sigma}}{\Delta z} Z_k \exp\left(-\frac{E_k}{RT}\right)$	

Initial and Boundary Conditions	Parameters for Specifying Conditions Related to Porous Solid Phase
<p>Condensed-phase mass conservation</p> $\bar{\rho} \Big _{r=0} = \sum_{i=1}^M X_{i0} \rho_{i0}$ <p>Condensed-phase species conservation</p> $\bar{\rho} Y_i \Big _{r=0} = \sum_{i=1}^M (X_{i0} \rho_{i0}) Y_{i0}$ <p>Condensed-phase energy conservation</p> $T^o \Big _{r=0} = T_0 \Rightarrow \bar{h}^o \Big _{r=0} = \sum_{i=1}^M (Y_{i0} h_{i0}(T_0))$ $-\bar{k} \frac{\partial T}{\partial z} \Big _{z=0} = \underbrace{\dot{q}''_{front surf.}}_{\text{Specified flux at front surf.}}$ $-\bar{k} \frac{\partial T}{\partial z} \Big _{z=\delta} = \underbrace{\dot{q}''_{back surf.}}_{\text{Specified flux at back surf.}}$	X_{i0} Y_{i0} X_{j0} Y_{j0} $\bar{\epsilon}, \epsilon_i$

Nomenclature	
Letters	Greek symbols
<i>c</i> Specific-heat capacity (J/kg-K)	δ Thickness (m)
<i>E</i> Activation energy (kJ/mole)	ε Emissivity (-)
<i>h</i> Enthalpy (J/kg)	κ In-depth radiation absorption coefficient (m^{-1})
ΔH Change in enthalpy (J/kg)	ρ Density (kg/m^3)
<i>k</i> Thermal conductivity (W/m-K)	$\dot{\omega}'''$ Volumetric reaction rate (kg/m^3-s)
\dot{m}'' Mass flux (kg/m^2-s)	Subscripts
<i>n</i> Exponent (reaction order)	<i>A</i> Species <i>A</i>
\dot{q}'' Heat flux (W/m^2)	<i>d</i> Destruction or datum
\dot{Q}''' Volumetric rate of heat release or absorption (W/m^3)	<i>f</i> Formation
<i>r</i> Reaction rate (kg/m^3-s)	<i>g</i> Gaseous, gas phase, or gasification
<i>t</i> Time (s)	<i>i</i> Condensed phase species <i>i</i>
<i>T</i> Temperature (K)	<i>k</i> Heterogeneous reaction <i>k</i>
<i>X</i> Volume fraction (-)	<i>m</i> Melting
<i>Y</i> Mass fraction (-)	<i>p</i> Pyrolysis
<i>z</i> Distance (m)	<i>0</i> Initial (as in T_0)
<i>Z</i> Condensed-phase pre-exponential factor (s^{-1})	∞ Ambient
	Superscripts
	($\bar{\quad}$) Weighted or averaged
	\circ Value at present time

MODEL PARAMETERS AND MEASUREMENT METHODS

Virtual Microstructure of Virgin Material and Decomposition Kinetics Type

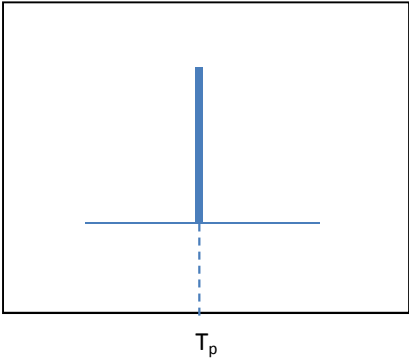
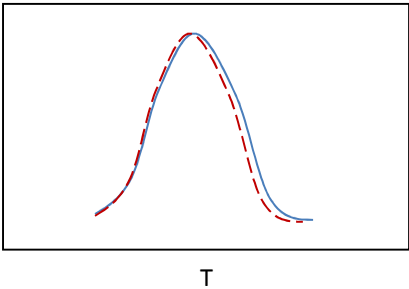
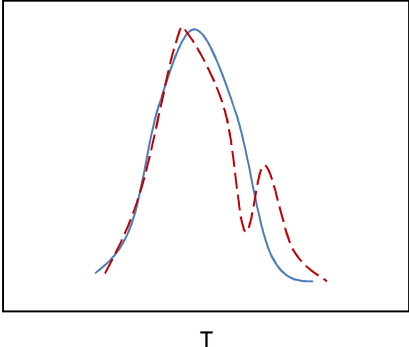
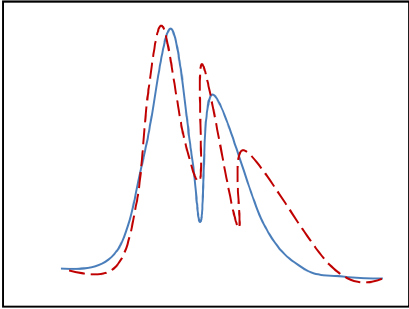
When conducting parameter estimation for a material of interest, visual inspection should be conducted first to model its microstructure. Considering that typical pyrolysis models are available in one-dimension in the direction of the depth from the sample surface, the material's cross-section should be examined to determine whether the virtual microstructure should be considered as a **single layer of homogeneous material** or **multiple layers of homogeneous materials**. Note that, when the virtual microstructure is determined as a single layer of homogeneous material, the modeler has an option of utilizing models of either type of Comprehensive Model. However, when multiple layers of homogeneous materials are necessary to describe the material's microstructure, using Comprehensive Models with pyrolysis fronts of finite thickness are required.

Despite the increase in modeling complexity, multiple layers of homogeneous materials can be necessary. Rule of thumb of when to utilize multiple layers structure is as follows: (1) the virgin material is composed of several distinctive layers that bear significantly different pyrolyzing characteristics; (2) different pyrolyzing characteristics can be identified in experiment data, where layers exist in test samples; and (3) this effect is desired to be captured in the simulations.

The next step should be determining the decomposition kinetics type for each layer of homogeneous material identified above. In the following (see Table 5-2), typical decomposition thermograms observed from a Thermogravimetric Analysis (TGA) experiments are shown for fire problems, which will be dealt with in the example cases in this *Guide*. Based on the characteristics of the TGA curve, the modeler may choose the type of example case to consider for their problem. Note that decomposition kinetics should be identified for each layer of the specified microstructure or decomposable component of the material composing a layer. In the following table, different types of decomposition kinetics and the corresponding minimum number of elementary reactions to describe materials' full decomposition are shown based on TGA data (DTG) obtained from nitrogen and air environments. Conduct a minimum of three TGA experiments with

heating rates lower than $10^{\circ}\text{C}/\text{min.}$, sample sizes smaller than 10 mg, and various sample shapes, assuming that, with these conditions, chemical reaction becomes the decomposition kinetic controlling factor rather than diffusion.

Table 5-2. Various Types of Decomposition Kinetics

Type	Inert (solid, typically nitrogen) and Oxidative (dash, typically air) Environments	
0		<p>Weight-loss rate (DTG) with respect to temperature can be described with a single line independent of the testing environment (inert or oxidative) at pyrolysis temperature, T_p.</p> <p><u>Minimum of 1 reaction</u></p>
1		<p>Weight-loss rate (DTG) with respect to temperature can be described with a single peak independent of the testing environment (inert or oxidative). In DSC experiments, endotherm is observed for tests conducted in both environments.</p> <p><u>Minimum of 1 reaction</u></p>
2		<p>Weight-loss rate (DTG) with respect to temperature in inert environment can be described with a single peak. However, when sample is tested in oxidative environment (air), additional, secondary peak is observed at higher temperature range, typically considered as “char oxidation reaction.” From DSC experiments, the first and second peak in TGA should correspond to an endothermic and exothermic peak, respectively.</p> <p><u>Minimum of 2 reactions</u></p>
3		<p>Weight-loss rate (DTG) with respect to temperature in inert environment should be described with multiple (k) peaks. When sample is tested in oxidative environment (air), additional peak is observed at higher temperature range, typically considered as “char oxidation reaction.” From DSC experiments, the first few and last peak in TGA should correspond to endothermic and exothermic peaks, respectively.</p> <p><u>Minimum of $k+1$ reactions</u></p>

Model-Parameter Table

With the virtual microstructure set and decomposition-kinetics type determined for each layer of the specified microstructure or decomposable component of the material composing a layer, the modeler is able to identify every species in the porous-condense phase (*i*) and decomposition reaction involved in pyrolysis modeling.

To mathematically describe a pyrolyzing solid-phase material in comprehensive pyrolysis modeling in fire, a set of parameters are needed. Model parameters are related to heat transfer, mass transfer, and thermal-decomposition kinetics. Parameters consist of (1) **material properties** that are *intrinsic*, i.e., they depend on chemical and physical structure of the material or *effective* due to neglecting actual microstructure of the material and considering the material as homogeneous; (2) parameters related to modeling the **thermal-decomposition** process; and (3) **model-dependent fitting parameters**, which are not material properties but parameter constants that provide the best fitness of model output to experiment results. Typically, **material properties** can be considered in three groups: (1) thermo-physical properties – density, thermal conductivity, specific-heat capacity; (2) porous media characteristics – porosity, permeability; and (3) optical properties – absorption coefficient and emissivity. Parameters used in **thermal decomposition** modeling are pyrolysis onset temperature or kinetic parameters for applying infinitely thin or finite-thick reaction zone assumption, respectively, and reaction heats. An example of **model-dependent fitting parameters** can be exponent or constants used to describe temperature dependence of thermal conductivity, k : $k(T) = k_0(T/T_r)^{n_k}$ or $k(T) = a + bT + cT^2 + dT^3$.

This allows the modeler to construct a model parameter table as below (see Table 5-3). Note that in this table only model-independent parameters are included. There can be other parameters related to material property in different models. For example, in GPYRO γT^3 term is used in the effective thermal conductivity to model radiative heat transfer through pores when material is porous, where γ is a fitting parameter. These model-dependent parameters should be identified and obtained after setting up the problem in a model of choice in the validation part.

Table 5-3. Model parameter table: Summary of model parameters required to conduct pyrolysis modeling

		Condense Phase (<i>i</i>)	
Material Property		ρ_i	Density
		k_i	Thermal conductivity
		c_i	Specific-heat capacity
		κ_i	Absorption coefficient
Parameters for Specifying Conditions		X_{i0}	Volume fraction
		Y_{i0}	Mass fraction
		ε_i	Emissivity
		Heterogeneous RxN (<i>k</i>)	
Thermal Decomposition	Infinitely Thin Reaction Zone	T_p	
		ΔH_p	
	Finite Thickness Reaction Zone	n_k	Reaction order
		Z_k	Pre-exponential factor
		E_k	Activation energy
		ΔH_k	heat

Model-Parameter Measurement Methods

This section provides descriptions of how the model parameters identified above can be obtained via direct measurement using experiments. Relevant standard tests are listed when found. However, the most efficient approach for obtaining parameter values through independent measurements involves making contact with a commercial laboratory and consulting with them about the nature of your sample (brittle, soft, isotropic, melting, porous, etc.). Density, thermal conductivity and specific-heat capacity are thermophysical properties. Absorption coefficient and emissivity are optical properties. Kinetic parameters and heats are properties of thermal-decomposition kinetics. A modeler may search for test methods or labs that measure these properties.

1. Density

The bulk density of a porous solid material can be determined by measuring the mass of a representative specimen of the material and then dividing it by the measured volume of the specimen. Mass is generally measured with an analytical balance or scale. Volume can be determined, for example, by measuring the dimensions of the specimen or by submerging the specimen in a liquid and measuring the resulting displacement of the liquid. The bulk density of a material can also be determined on the basis of its specific gravity, i.e., the ratio of the density of the material to the density of a reference material. Although there are number of ASTM standards for measuring density or specific gravity at ambient temperature of specific materials, the typical approach in pyrolysis modeling is measuring the bulk density as noted above.

2. Thermal Conductivity

Various methods have been developed to measure the thermal conductivity of solids. In these methods the thermal conductivity is determined either under steady state or under transient conditions. The general principles of the two types of methods are summarized below.

STEADY-STATE METHODS

The one-dimensional heat-conduction equation based on Fourier's Law for a slab with infinitely large surface area and finite thickness, L- is as follows (see Eq.5-1):

$$\dot{q}'' = k \frac{\Delta T}{L} \quad \text{Eq.5-1}$$

where \dot{q}'' = heat flux through the slab (W/m²)
k = thermal conductivity of the slab material (W/m·K)
 ΔT = temperature difference between two faces of the slab (K)
L = thickness of the slab (m)

Steady-state methods are based on the above equation and are classified into two categories: absolute and comparative. In absolute methods, ΔT and \dot{q}'' are measured, and k is determined from the equation. The test specimen (a slab of the material of which the thermal conductivity is to be determined) is sandwiched between a heater and a cooled plate. The temperature is measured on both faces of the specimen. To ensure one-dimensional heat transfer, guard heaters and insulation are used around the perimeter of the main heater and the specimen, respectively.

The main drawback of absolute methods is that it takes several hours to get to steady-state conditions with low thermal conductivity materials. Comparative methods were developed to reduce the test time (at the expense a slight reduction in accuracy). In comparative methods the heat flux is determined from the temperature gradient over a slab of a reference material with a known thermal conductivity. The specimen and reference material slabs are sandwiched between a heat source and a heat sink. The difference between the heat source and the heat sink is approximately 50-100K.

ASTM has standardized and published several steady-state methods (see Table 5-4). ASTM C 177 and ASTM E 1530 are absolute methods while the other two standards describe a comparative method.

Table 5-4. ASTM standards for measuring thermal conductivity using steady state methods

Standard Test	Description
ASTM C 177	<i>Standard Test Method for Steady-State Heat Flux Measurements and Thermal Transmission Properties by Means of the Guarded-Hot-Plate Apparatus</i>
ASTM C 518	<i>Standard Test Method for Steady-State Thermal Transmission Properties by Means of the Heat Flow Meter Apparatus</i>

TRANSIENT METHODS

The limitations of steady-state methods are: (1) it takes a long time to reach steady conditions (even when a comparative approach is used); (2) a relative large quantity of material is needed; and (3) it is not easy to perform measurements at elevated temperature. Transient methods are generally not as accurate, but they do not have the limitations of steady-state methods. Two well-known ASTM standards are shown in Table 5-5.

Table 5-5. ASTM standards for measuring thermal conductivity using transient methods

Standard Test	Description
ASTM C 1113	<i>Standard Test Method for Thermal Conductivity of Refractories by Hot Wire (Platinum Resistance Thermometer Technique)</i>
ASTM D 5930	<i>Standard Test Method for Thermal Conductivity of Plastics by Means of a Transient Line-Source Technique</i>

The hot-wire method is a typical example of a transient method. A fine metallic wire is placed at the center between two pieces of the material. The temperature of the wire is changed in step-wise fashion by incrementally increasing the current flowing through the wire. The generated heat flows in all radial directions and produces a temperature field in the material that increases with time. In most cases the wire itself serves as a temperature sensor as its resistance changes with temperature. The thermal conductivity of the material is a direct function of the heat dissipated in the wire and the rate at which its temperature rises. ASTM has developed standards that describe the use

of the hot-wire method specifically for measuring the thermal conductivity of refractory materials and plastics.

Variations of the hot-wire method have been developed with different heat-source geometries (strip, plane, disc, or spiral) and an energy pulse instead of step-wise increases of the heat generated in the source. Adl-Zarrabi et al. used the Transient Plane Source (TPS) method to measure the thermal conductivity of concrete and wood at elevated temperatures and obtained reasonable agreement with literature values.⁷ The TPS method was developed by Gustafsson and Long^{8,9} and uses a heat source in the shape of a disc.

Bentz recently developed a transient method to determine the thermal conductivity of fire resistive materials.^{10,11} The basic specimen configuration consists of a “sandwich,” with a square central stainless-steel plate (slug) surrounded on two sides by a slab of the test material. This sandwich configuration provides an adiabatic boundary condition at the central axis of the slug plate, which greatly simplifies the analysis. The edges of the steel plate and specimens are insulated using a low thermal-conductivity fumed silica board. Two metal plates manufactured from a high-temperature alloy provide a frame for placing the entire sandwich specimen slightly in compression. The entire configuration is centrally placed at the bottom of an electrically heated box furnace, and the temperatures of the metal slug and exterior specimen surfaces are monitored during multiple heating and cooling cycles. Knowing the heat capacities and densities of the steel slug and the specimen material, an effective thermal conductivity can be estimated. The effective thermal conductivity of the specimen is influenced by its true thermal conductivity and by any endothermic or exothermic reactions or phase changes occurring within the specimens. The method is now standardized as ASTM E 2584.

3. Specific Heat Capacity

The enthalpy of a solid material is related to the kinetic energy of the particles in the solid. In the absence of chemical reactions or phase changes, the enthalpy of a solid material increases when it is heated. The rate at which it increases with respect to

temperature is referred to as the specific-heat capacity. The specific-heat capacity for most solids varies with temperature.

Table 5-6. ASTM standard for measuring specific heat capacity

Standard Test	Description
ASTM E 1269	<i>Test Method for Determine Specific Heat Capacity by Differential Scanning Calorimetry</i>

Differential Scanning Calorimetry (DSC) is an accurate and convenient method to obtain specific heat capacities of solid materials at elevated temperatures. A standard procedure is described in ASTM E 1269 (see Table 5-6). In a DSC, a milligram-size sample and a reference are heated at a constant rate. The power required to increase the temperature of the sample and reference at the specified rate is proportional to their heat capacities. The sample heat capacity is determined on the basis of the power measured during the test, the baseline, and calibrations with a material with known heat capacity over the temperature range of interest (typically sapphire). The specific-heat capacity of the sample is then obtained by dividing the measured heat capacity by the sample mass. If the mass of the sample changes as a function of temperature, the heat capacity at a specified temperature should be divided by the sample mass at that same temperature. The latter can be obtained from TGA measurements performed under the same conditions, i.e., same heating rate, same purge gas, etc. DSC and TGA are often combined in a single instrument, which facilitates specific-heat capacity measurements.

As with TGA, DSC tests can be performed with different sample pans (aluminum, platinum or ceramic; open or sealed, with or without a pin hole), heating rates (typically between 1°C/min. and 60°C/min.), purge gases (typically air, nitrogen, or argon) and purge-gas rates. DSC tests are routinely performed at temperature ranging from ambient to 600°C. Many instruments can reach much higher temperatures.

4. Absorption Coefficient

With the absorption coefficient for radiation, a material's ability to allow penetration of thermal radiation in-depth can be quantified. Having a large radiative absorption coefficient means that the incident thermal radiation is attenuated quickly after

passing through the material, i.e., the material is opaque and most of thermal radiation is absorbed near the surface. Having a lower value means that the material is more transparent; therefore, more in-depth radiation is occurring. Note that the absorption coefficient is strongly wavelength-dependent; therefore, some averaged value should be used to remove wavelength dependency. Additionally, it is known that obtaining accurate property data that characterizes the in-depth absorption (normally, the “gray” absorption coefficient) can be difficult.

5. Emissivity

Emissivity is a measure of a material's ability to emit energy by radiation at the surface. Although emissivity changes with respect to temperature, emission angle, wavelength, and more, a typical simplification made when determining this value is applying a grey body assumption, resulting in a wavelength- and temperature-independent constant. See Table 5-7 for relevant standard tests for measuring emissivity.

Table 5-7. ASTM standards for measuring emissivity

Standard Test	Description
ASTM C835 - 06	<i>Standard Test Method for Total Hemispherical Emittance of Surfaces up to 1400°C</i>
ASTM E 408-71	<i>Standard Test Methods for Total Normal Emittance of Surfaces Using Inspection-Meter Techniques</i>

6. Parameters Related to Thermal Decomposition

INFINITELY-THIN REACTION-ZONE CASE

Assuming that the ignition temperature of a material is comparable to its pyrolysis temperature, this parameter can be directly measured using experiments or estimated using Ignition Data Analysis. See Chapters 3 and 4 for details.

REACTION ZONE WITH A FINITE-THICKNESS CASE

Mass as a function of temperature is most conveniently measured through thermogravimetric analysis (TGA). A TGA apparatus consists of a high-precision balance with a pan (usually aluminum, platinum, or ceramic) loaded with the sample. The sample mass is typically of the order of one milligram. It is kept as small as possible (to ensure uniform temperature) and depends on the material that is tested. The sample pan is placed in a small computer-controlled furnace with a thermocouple to accurately measure the temperature. The atmosphere may be purged with an inert gas (e.g., nitrogen or argon) to prevent oxidation or other undesired reactions. During a test, the furnace temperature is either kept constant or increased at a fixed rate (typically between 1 and 60 °C/min.) to a predefined maximum temperature (routinely 1000°C or higher). The result consists of a plot of mass (percentage) as a function of time and/or temperature.

For TGA testing and comparison of data, one needs to consider heating rates and atmosphere when studying mass-loss data relevant for fire models. Heating rates will affect the rate of thermal decomposition of a polymer, but in TGA faster heating rates tend to push the mass-loss curves to higher temperatures. Therefore, one should not compare different polymers unless they were tested at the same heating rate.

Atmosphere has a very important effect on TGA data in that a polymer will decompose in different chemical pathways under inert and oxidizing atmospheres. These changes in polymer decomposition chemistry can result in very different mass-loss rate curves, and so data for the same polymer collected under inert vs. oxidizing atmospheres can be compared qualitatively but not quantitatively. Likewise data for two different polymers collected under different atmospheres should not be compared. Of final note, it is always good practice to conduct TGA experiment in inert and oxidizing atmosphere to make comparison and understand the effect of the change in the environment. Generally, oxygen is known to affect only thermal decomposition prior to ignition. After the material ignites all oxygen is known to be consumed at the flame front. In this sense, TGA data collected under inert atmospheres tends to be far more useful for understanding polymer decomposition and pyrolysis behavior under fire conditions.¹² This is why NIST created its gasification apparatus to study mass loss pyrolysis behavior in the absence of flaming combustion.^{13,14,15} However, there are cases when the availability of oxygen affects the burning rate of the material as well, e.g., PMMA, wood, etc. Therefore, a careful consideration of the effect of atmosphere on TGA data should be given prior to modeling. See Table 5-8 for ASTM standards related to using TGA for studying thermal decomposition kinetics.

Table 5-8. ASTM standards for thermogravimetry analysis (TGA)

Standard Test	Description
ASTM E 2550	<i>Standard Test Method for Thermal Stability by Thermogravimetry</i>
ASTM E 1641	<i>Standard Test Method for Decomposition Kinetics by Thermogravimetry</i>

In the following section, brief descriptions of estimating methods for kinetic parameters using TGA data (single- or multiple-rate data) are provided. In both cases, decomposition kinetics is represented by an Arrhenius expression as below (see Eq.5-2):

$$\frac{d\alpha}{dt} = k(T)f(\alpha) = \left[A \exp\left(-\frac{E_a}{RT}\right) \right] f(\alpha) \quad \text{Eq.5-2}$$

where

$k(T)$ = temperature dependent rate constant

$f(\alpha)$ = temperature independent kinetic function of conversion, α (typically, $\alpha = 1 - m/m_0$) and this function is dependent upon the mechanism of decomposition

A = pre-exponential factor

E_a = activation energy

ESTIMATION BASED ON SINGLE HEATING RATE TGA DATA USING DTG
PEAK VALUES ($T_{\text{PEAK}}, R_{\text{PEAK}}$)¹⁶

Assuming that every peak in the DTG thermogram from the iso-heating rate (dynamic) TGA experiment can be considered as a single reaction with first-order reaction model (i.e., $f(\alpha) = (1-\alpha)^1$), this approach models the kinetics as follows: a condense-phase reactant thermally degrades to fuel vapor directly or to a secondary condense phase, which may or may not degrade further, producing fuel vapor and releasing it to the gas phase.

Consider an arbitrary DTG curve shown as below (see Figure 5-1). There is a single peak in this thermogram. Based on this approach, the modeler can assume a reaction for modeling thermal decomposition of this material. Apply a constant heating rate of $\beta = dT/dt$ and first-order kinetic model to above Arrhenius expression for describing decomposition. Rearranging it results in Eq.5-3:

$$\frac{d\alpha}{dT} = \frac{A}{\beta} \exp\left(-\frac{E_a}{RT}\right) (1-\alpha) \quad \text{Eq.5-3}$$

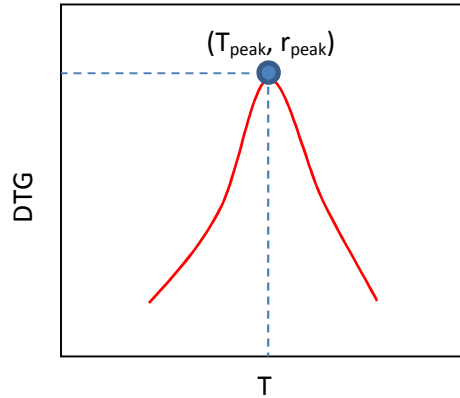


Figure 5-1. Typical DTG thermogram showing single peak

Assuming that, at each peak the second derivative of conversion, α , with respect to time is zero, and activation energy of each reaction is significantly greater than $2RT_p$ (i.e. $E_a \gg 2RT_p$), estimation of A and E_a for each reaction can be done using the following equations (see Eq.5-4 and Eq.5-5):

$$E_a \approx \frac{RT_p^2}{\beta} \frac{er_p}{(1-\alpha_0)} \quad \text{Eq.5-4}$$

$$A \approx \frac{er_p}{(1-\alpha_0)} \exp\left(\frac{E_a}{RT}\right) \quad \text{Eq.5-5}$$

ESTIMATION BASED ON MULTIPLE HEATING RATE TGA DATA USING ISO-CONVERSIONAL AND MODEL FITTING METHODS

Estimation of kinetic parameters based on multiple heating-rate data obtained from TGA experiments tries to take into account of any changes that may occur in thermally degrading behavior as the heating rate is changed. This approach requires a minimum of four iso-heating rate (dynamic) TGA data. The four heating rates should spread out in the range of less than 10 K/min. to above 40 K/min.

The Iso-conversional Method allows one to determine activation energy in terms of conversion with a minimum of four TGA tests with different heating rates without assuming the kinetic function. Two methods are introduced below:

Method of Ozawa, Flynn and Wall^{17,18} (OFW)

Apply a constant heating rate $\beta = dT/dt$ to the above Arrhenius expression for describing decomposition. Rearranging it results in Eq.5-6:

$$\ln(\beta) = \ln\left(\frac{dT}{dt}\right) = \ln\left(\frac{A \exp\left(-\frac{E_a}{RT}\right) f(\alpha)}{\frac{d\alpha}{dt} / \beta}\right) = \ln\left(\frac{A f(\alpha)}{\frac{d\alpha}{dt} / \beta}\right) - \frac{E_a}{RT} \quad \text{Eq.5-6}$$

A plot of $\ln(\beta)$ versus $1/T$ should give a slope of $-E_a/R$ for a wide range of conversion, α . For example, at $\alpha = \alpha^*$, four $\ln(\beta)$ values are found – $\ln(\beta_1)$, $\ln(\beta_2)$, $\ln(\beta_3)$ and $\ln(\beta_4)$ – at four different temperatures – T_1 , T_2 , T_3 and T_4 – when data from four iso-heating rate TGA tests are used as in the first figure below. These data points can be plotted in a $\ln(\beta)$ versus $1/T$ graph and the slope of the four points gives $-E_a/R$ at $\alpha = \alpha^*$ as shown in the second figure. This can be repeated for α ranging from 1 to 0, and the estimated E_a can be plotted with respect to alpha as in the last figure below (see Figure 5-2.)

Figure 5-2. Schematic of conducting Ozawa, Flynn, and Wall Iso-conversional Method

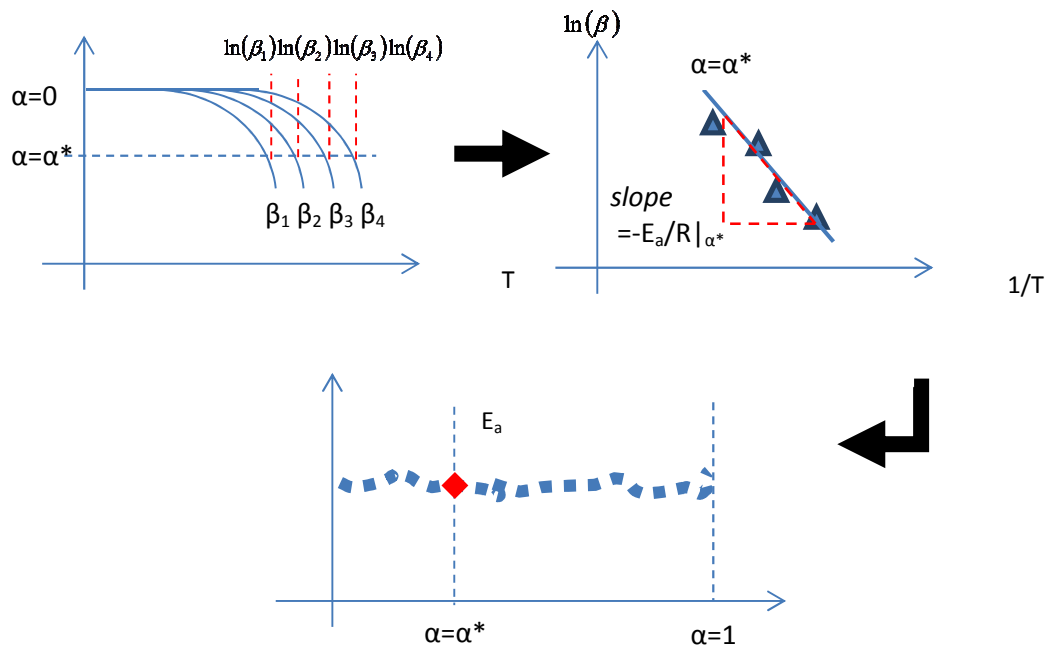


Figure 5-2. Schematic of conducting Ozawa, Flynn, and Wall Iso-conversional Method

Method of Friedman^{19,20} (Friedmen)

$$\ln\left(\frac{d\alpha}{dt}\right) = \ln\left(A \exp\left(-\frac{E_a}{RT}\right) f(\alpha)\right) = \ln(Af(\alpha)) - \frac{E_a}{RT} \quad \text{Eq.5-7}$$

A plot of $\ln(d\alpha/dt)$ versus $1/T$ is used to find the slope of $-E_a/R$ (see Eq.5-7). For example, at $\alpha = \alpha^*$, four $d\alpha/dt$ values are found – $(d\alpha/dt)_{\beta_1}$, $(d\alpha/dt)_{\beta_2}$, $(d\alpha/dt)_{\beta_3}$ and $(d\alpha/dt)_{\beta_4}$ – at four different temperatures – T_1 , T_2 , T_3 and T_4 – when data from four iso-heating rate TGA tests are used as in the first figure below. These data points can then be plotted in a $\ln(d\alpha/dt)$ versus $1/T$ graph and the slope of the four points gives $-E_a/R$ at $\alpha = \alpha^*$ as shown in the second figure. This can be repeated for α ranging from 1 to 0 and the estimated E_a can be plotted with respect to alpha as in the last figure below (see Figure 5-3).

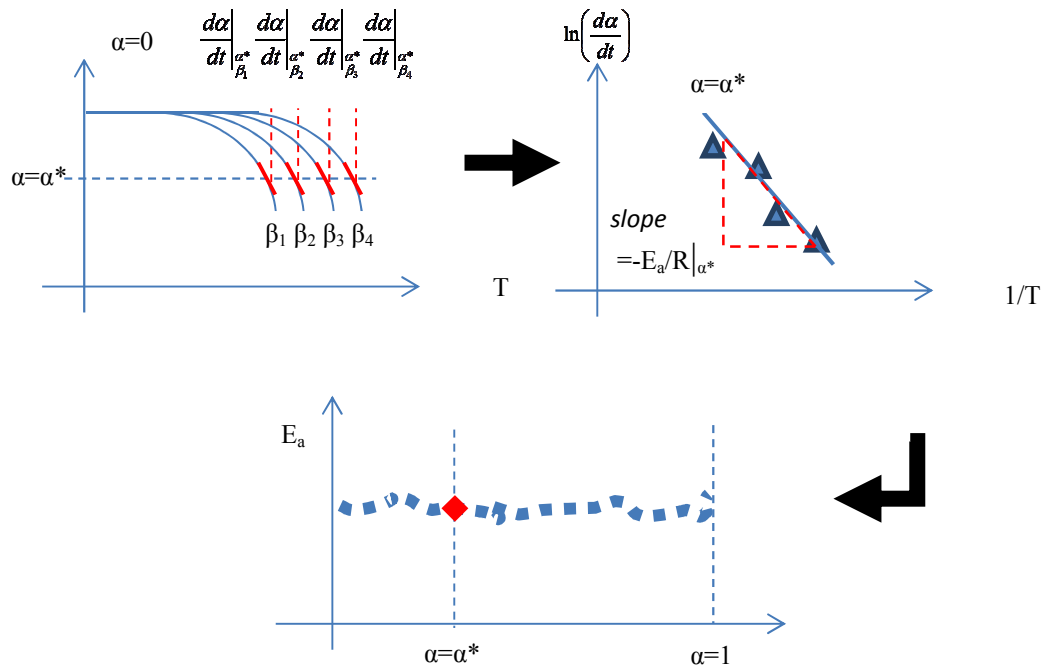


Figure 5-3. Schematic of conducting Friedman's Iso-conversional Method

Interpreting Results from the Iso-conversional Method

When the E_a is found for the entire degradation process, the results provide insight for the minimum number of steps of elementary reactions needed to characterize the global reaction.²¹ A global reaction composed of a single stage process will show no dependence of E_a on conversion, α . When the global reaction is a complex process, the

E_a changes with respect to conversion, α . An increase in E_a with α typically indicates parallel reactions. A decrease in E_a with α suggests that either the process is reversible (concave shape) or there is a change in the rate determining step (convex shape). Therefore, by analyzing the shape of the curve plotted with E_a with respect to conversion, α , a minimum number of elementary reactions are suggested.

Model Fitting Method

Once the minimum number of reactions and their activation energies are estimated by conducting the Iso-conversional Method, other kinetic parameters to fully mathematically describe the decomposition of MA+A need to be estimated as well. This is done by conducting the model-fitting method with a kinetic model assumed. Typically, an nth order reaction model is used due to its flexibility in providing good fitness between the data and the model. Therefore, an nth order will be utilized in this example.

Based on the model-fitting method, estimation for weight-loss fraction (f), pre-exponential constant (A), and exponent in the nth order kinetic model (n) is conducted for each reaction. Note that the estimation has been done with a least-square method by comparing TGA data (TG and DTG from iso-heating rate tests) with the kinetic modeling's output. The kinetic modeling's output is a sum of properly scaled elementary reactions with the weight-loss fraction found for each reaction. Without scaling, every reaction results in 100% conversion. Each reaction is calculated by applying the Runge-Kutta 4th order method (ODE solving method) to decomposition and constant heating rate ODE equations: two dependent variables (α , T) with time (t) as the independent variable (see Eq.5-8 and Eq.5-9).

$$\frac{d\alpha(t)}{dt} = \left[A \exp\left(-\frac{E_a}{RT(t)}\right) \right] (1 - \alpha(t))^n \quad \text{Eq.5-8}$$

$$\frac{dT(t)}{dt} = \beta \quad \text{Eq.5-9}$$

Weight-loss fraction (f): This parameter is for determining how much of the total weight of the entire sample (100%) is consumed by each reaction. Note that kinetic modeling is conducted in terms of conversion, $1-\alpha$, and each reaction results in 100% conversion. Therefore, mathematically, weight loss ($d\alpha/dt$) should be properly scaled with the weight-loss fraction parameter (f) to have the summation of weight loss due to all elementary reactions and any solid-phase leftover (typically labeled as residue) at temperatures exceeding maximum temperature considered in TGA experiment to equal 100%. For this example, where two elementary reactions have been proposed, total weight loss (conversion) and weight-loss rate (derivative of conversion) can be expressed as follows (see Eq.5-10 and Eq.5-11).

$$\alpha_{Total} = f_R\alpha_R + f_{+A-R}\alpha_{+A-R} + f_{residue} \quad \text{Eq.5-10}$$

$$\frac{d\alpha_{Total}}{dt} = f_R \frac{d\alpha_R}{dt} + f_{+A-R} \frac{d\alpha_{+A-R}}{dt} \quad \text{Eq.5-11}$$

To optimize for this parameter (f), consider results from the Iso-conversional Method to find an initial guess.

Pre-exponential constant (A): This parameter, also known as the collision frequency, is originally from the Collision Theory²² defined as the average number of collisions experienced by a reacting molecule with other molecules. However, in solid-state reactions, classical frequency factor becomes inappropriate, as reactions do not occur with molecules colliding but due to molecules being mostly stationary during solid-state decomposition. Although this parameter is different from that of Collision Theory, the A value can provide a measure of reactivity of the decomposition reaction.

When optimizing for this parameter, the modeler should be aware of the compensation effect²³ between the activation energy and pre-exponential constant, i.e., there are several sets of E_a and A that result in similar reaction rates. An increase in E_a can be compensated by a decrease in A and vice versa. Currently, no theory is accepted as explaining this effect, but it is well acknowledged that this exists. Therefore, it is important to estimate the activation energy value based on the Iso-conversional Method and optimize for A value using a model-fitting method.

Exponent in nth order kinetic model (n): Typically, n values considered for this reaction-order-type kinetic model (nth order) are between 0 and 3. Changing n value results in changes in the shape of DTG, i.e., an increase in n results in a lower peak in the DTG curve with wider temperature range as shown below (see Figure 5-4).

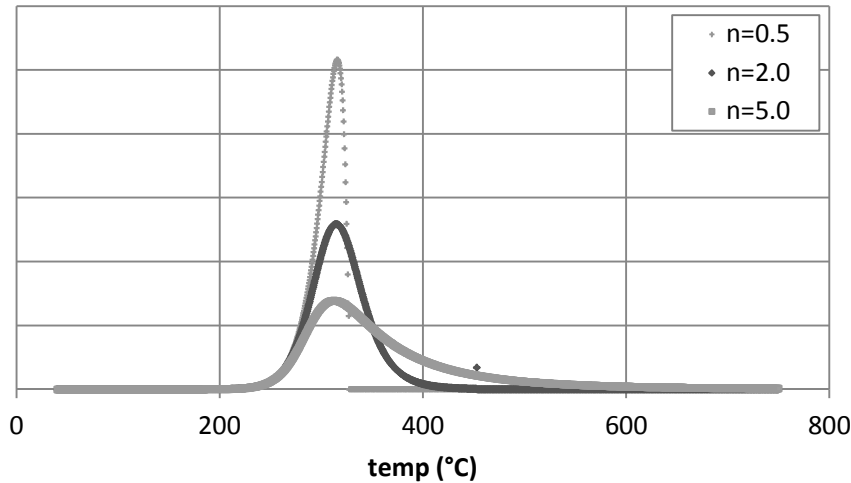


Figure 5-4. Change in DTG curve with respect to changes made in n values using nth order reaction model

Optimization: When optimizing for the parameters, an initial guess should be given for the weight fractions (f) for each reaction as the mid-values within the optimization range found via examining TGA and DSC data and results from the Iso-conversional Method. Additionally, an initial guess of the n value can be given as 1, where a first-order reaction model is the most simple and common model used to fit the data. The next step is to estimate the pre-exponential constants. Typically, the initial guess of this parameter can start from 10^{10} . The pre-exponential constant, A, for each reaction can be adjusted with other parameters set as their initial values to match the temperature range of the model's mass-loss rate peak (DTG) with the known temperature range found from analyzing the TGA and DSC data and results from the Iso-conversional Method. After this step, the n values can be optimized to match the peak of the mass-loss rate (DTG) from modeling to that of the data. As mentioned in the previous section, changing n value results in changes in the shape of DTG, i.e., increase in n results in lower peak in the DTG curve with wider temperature range. After going through these steps, manually each parameter can be optimized by comparing the kinetic modeling

results (mass loss or mass loss rate, i.e., TG or DTG) to data from the TGA experiment. In general, a correlation coefficient can be calculated to evaluate the fitness of the estimation to actual data, e.g., as the square of the correlation coefficient (R^2) becomes close to 1 by optimizing each parameter, it reflects that a stronger linear relationship exists between the modeling results (x) and data (y). See Eq.5-12.

$$R = \frac{\sum(x - \bar{x})(y - \bar{y})}{\sqrt{\sum(x - \bar{x})^2 \sum(y - \bar{y})^2}} \quad \text{Eq.5-12}$$

where \bar{x} and \bar{y} are sample means.

7. Heats

If the DSC sample goes through a transition, such as a phase change (e.g., evaporation of bound water) or a chemical reaction (e.g., pyrolysis), the associated enthalpy changes (e.g., the latent heat-of-vaporization or the heat-of-pyrolysis) will be recorded by the instrument. An example of decomposing polyurethane foam is shown in Figure 5-5.

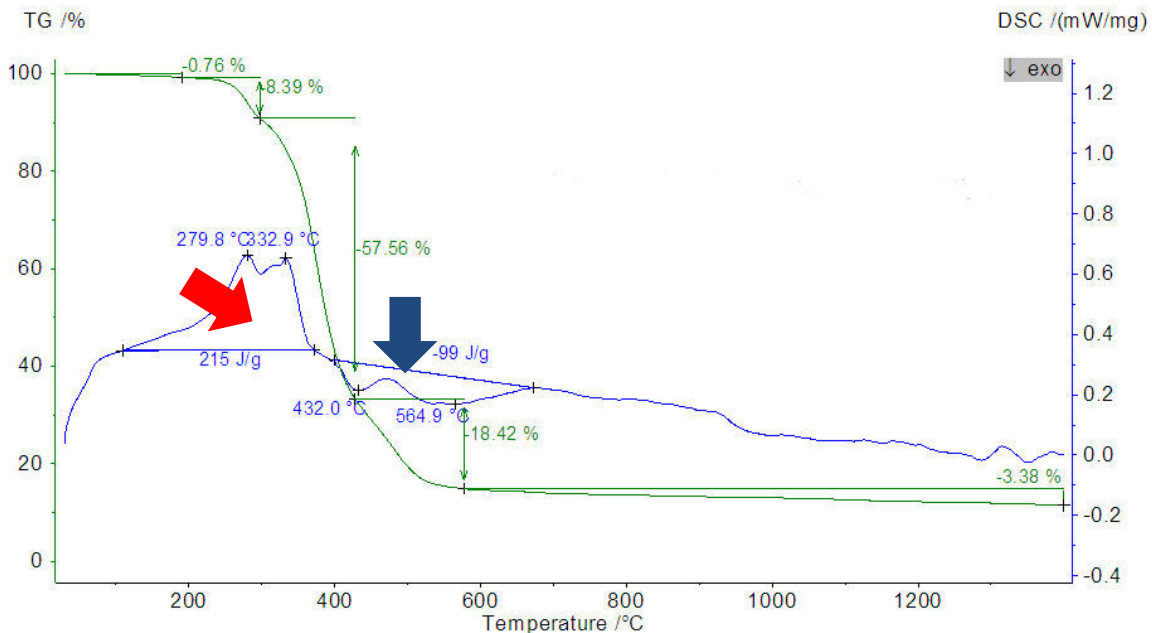


Figure 5-5. TG (weight loss) thermogram from TGA experiment (left) and heat-flow diagram from DSC experiment (right) for decomposition of a rigid-foam plastic

The polyurethane foam loses 85% of its mass between 100°C and 600°C. The thermal degradation is initially endothermic as the enthalpy rises above the baseline (see red

arrow). Between 400°C and 600°C the enthalpy drops below the baseline, which is characteristic of exothermic reactions (see blue arrow). The heat-of-pyrolysis associated with the endothermic reactions is determined from the area under the peaks and is approximately 215 J/g. The heat-of-pyrolysis associated with the exothermic reactions is determined in a similar way and is equal to approximately -99 J/g (since heat is released in exothermic reactions, the enthalpy change is negative). The fact that there are two separate peaks indicates that there are two distinct endothermic reactions. Likewise, the two valleys imply that there are two distinct exothermic reactions. To model the thermal degradation of this material, the data suggest a four-step reaction scheme, which is not obvious from inspection of the TGA curve. The uncertainty of the baseline can result in significant errors of heat-of-transition values obtained with this method. ASTM D 3418 (see Table 5-9) provides some guidance on how to address this problem.

Table 5-9. ASTM standard for measuring reaction enthalpies

Standard Test	Description
ASTM D 3418	<i>Standard Test Method for Transition Temperatures and Enthalpies of Fusion and Crystallization of Polymers by Differential Scanning Calorimetry</i>

The main experimental parameter that can affect DSC results is the heating rate. Faster heating rates can cause some thermal events to disappear or blur together (such as glass transition temperatures and low-energy melting events) as well as shift the temperatures of events. An example of this is shown below for an engineering crystalline thermoplastic. As the heating rate is increased, the melting point shifts to lower temperature (see Figure 5-6, Figure 5-5). While the range of peak melt temperatures is not so large for this sample (332-335 °C), one should not assume that this is true for all materials. Therefore, some consideration needs to be given to the heating rate when selecting DSC data for different polymers in a model. Of particular importance is the effect of the heating rate on the onsets of thermal decomposition (an endothermic event) or potential exothermic events (such as cross-linking). So, DSC data on different polymers should only be compared to each other if the data was collected at the same heating rate. Note that the above-mentioned trend will not be seen in combined

TGA/DSC experiments, as the loss of sample mass (evaporative cooling) will dominate the heat-transfer effects in the DSC measurements once the polymer begins to decompose. So one can argue that stand-alone DSC instruments are more accurate for measuring thermal events below thermal decomposition temperature, whereas TGA/DSC instruments are more accurate (or appropriate) for measuring thermal events where the polymer has begun to lose mass and is pyrolyzing/burning. However, in general TGA/DSC instruments are sufficient for fire pyrolysis modeling purposes, because more interest is given in the post-decomposition stage, where weight loss is considered in terms of heat being released.

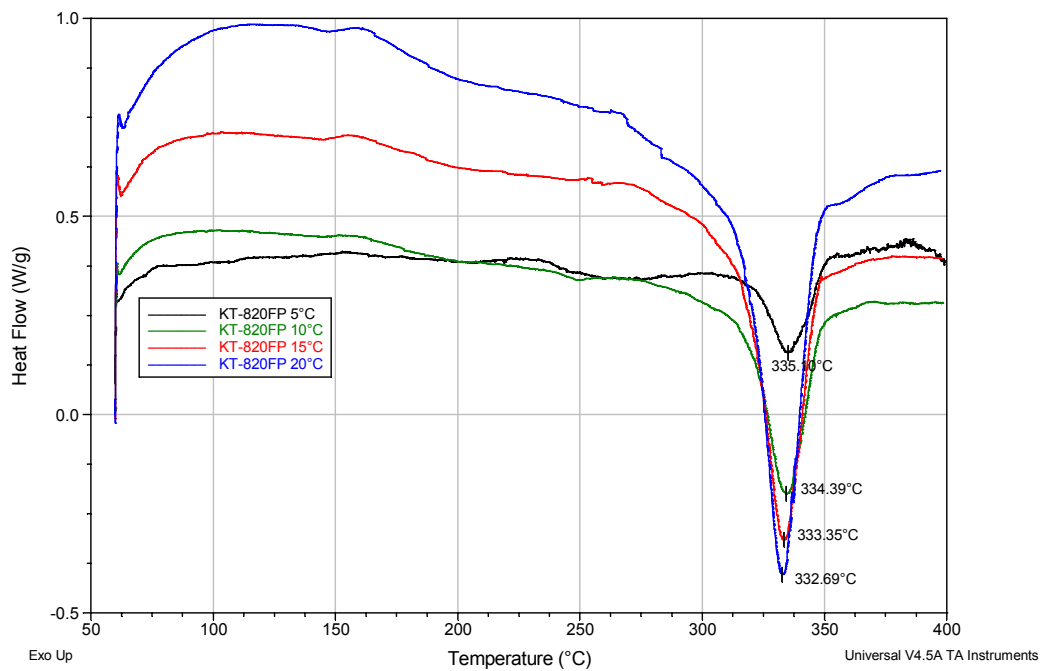


Figure 5-6. Melting points for a thermoplastic polymer as a function of DSC heating rates

Atmosphere choice in the DSC is typically not a parameter that gets changed, but some dual TGA/DSC units now commercially available can allow a material to have DSC data collected under oxidizing atmospheres while stand-alone DSC instruments are almost always tested under nitrogen. The atmosphere to which a polymer is exposed will affect its decomposition chemistry and therefore its kinetics of mass-loss rate. Likewise, a sample in a dual TGA/DSC unit will have very different behavior in nitrogen vs. air atmospheres (aerobic vs. anaerobic thermal decomposition). Therefore, any data from

these types of units should only be compared to other polymer data on the same instrument if they are collected under the same atmosphere. Certainly, however, the results from the same polymer in air vs. nitrogen could be studied and compared, and this can be very useful in the above-mentioned TGA/DSC experiments. For standalone DSC instruments, which are closed-cell systems, it is highly recommended that the polymer not be taken to decomposition temperatures – and definitely not in air – so that the sensitive DSC heating cell is not damaged or contaminated with polymer-decomposition products. The reason for this is that these decomposition products will condense out into the cell and change the heat sensitivity/thermal conductivity of the cell over time.

PARAMETER-ESTIMATION PROCESS

Knowing all the parameters required in modeling to create a virtual material, unknown parameters need to be estimated to perform actual calculations. This process is called parameter estimation. Parameter estimation for comprehensive pyrolysis modeling can be done using three different approaches: (1) measure each parameter via independent experiment; (2) search literature for measurement values on similar materials or use approximation; (3) conduct numerical optimization by pairing the pyrolysis model with an optimization routine. These approaches can be used alone or paired to estimate the entire unknown model-parameter set.

When the unknown parameters are estimated by measurement using independent experiment, typically small-scale experiments are used based on standard tests, such as ASTM or ISO. This approach only allows measurement of model parameters that are material properties and parameters related to modeling the thermal-decomposition process. It is noteworthy that material properties obtained through this approach are not always *intrinsic*, but in many cases are *effective*. Due to the limited sample size used in small-scale tests, material properties measured via independent experiment are generally accepted as *intrinsic*. However, in many cases for real-world heterogeneous materials, the material property measured becomes the *effective* property, as the small amount of sample used in these tests is also heterogeneous but treated as homogeneous by neglecting the heterogeneity nature of the material. Therefore, a caution should be given to a common misconception of understanding that measurements always result in obtaining *intrinsic* material properties whereas often *effective* properties are measured. In general, applying this approach of conducting experiments to directly measure model parameters is challenging due to the following reasons: First, there may be a discontinuity in model parameter obtained in a small-scale experiment and in model parameter required in the pyrolysis model. For example, a naturally high-charring phenolic resin decomposing during a Thermogravimetric Analysis (TGA) experiment in a powder form – a typical approach when conducting TGA experiment to reduce thermal lag effect – cannot represent decomposition of this same material in a bench-scale calorimeter test as a flat surface. This resin prepared in a powder form results in significantly large surface area (interface) exposed to the gas phase per unit mass or

volume. On the other hand, resin prepared as a flat surface has relatively smaller surface area exposed to the gas phase per unit mass or volume compared to resin in powder form. This difference results in great deviation when comparing thermal decomposition of this material, because the smaller surface area per unit mass or volume is proportional to the formation of more thermally stable carbonaceous char during decomposition. Therefore, for this case, obtaining kinetic parameters from a TGA experiment using powder-type sample and applying them to pyrolysis modeling to describe thermal decomposition occurring on a flat surface is not applicable. Second, material properties required in pyrolysis modeling that occurs while material is decomposing cannot be measured via independent experiments. Typically, when measuring material properties in small-scale experiments, decomposition of the sample is not allowed, which makes it impossible to make measurements for material properties of intermediate species involved in kinetic modeling. Third, measuring material properties and conducting thermal analysis for modeling thermal-decomposition kinetics through a commercial laboratory require significant financial investment.

Another approach to estimating model parameters is searching through literature for measurement values on similar materials or using certain approximations. Although using this approach is most practical because it is less time-consuming and inexpensive, caution should be given for the following: First, understanding of the material and its condition is essential. Certain polymers may have the same nomenclature, but depending on their polymer chain size, length and shapes, its character may vary.²⁴ Same material with moisture may show different thermal decomposition kinetics than that at dry state by water molecules chemically or physically interfering in the process.^{25,26,27,28} Same material with significant aging – e.g., scratches, cracks, etc. – may start to decompose at a lower temperature than that without aging.²⁹ These are some examples of how material and its conditions during experiments can affect the measurement results. Second, consideration to model parameter sensitivity and uncertainty is needed. In addition to the uncertainty reported for the measurement value in a literature, a greater uncertainty should be taken into account when using that value in pyrolysis modeling, for the two materials may have subtle differences physically or chemically as noted above. Also, when approximation is used to estimate certain model parameters for simplification of the

problem, modeler should be aware of the sensitivity of that parameter on modeling outputs of interest and check whether or not small changes to the approximated parameter value do not significantly alter the modeling results.

The third approach to estimating model parameters is by conducting numerical optimization by pairing the pyrolysis model with an optimization routine.^{30,31,32,33,34,35} To overcome the limitation in estimating parameters through measurements (first approach) or by literature search or approximations (second approach), the unknowns in pyrolysis modeling can be obtained by comparing modeling outputs with optimizing targets – experiment data such as mass-loss rate and temperature profiles from bench-scale test results – and finding the optimum parameter set that provides the best fitness to the target. When unknown parameters in a pyrolysis model are estimated using numerical optimization by comparing certain modeling outputs with a target, this is considered an inverse problem. These inverse problems in pyrolysis modeling are hard due to following reasons:³⁶ First, when the data contains noise or the mathematical model does not account for important physics and/or chemistry of the real problem, there may be no optimum that fits the data exactly, i.e., the solution to the problem may not exist (existence of solution). In other words, when data uncertainty is high enough to exert certain characteristics of a material through the acquired data and/or the model is too simplified, the model solution may not be determined through this process. For example, when model parameters are estimated by utilizing this approach for certain laminated fiberglass reinforced polymer (FRP) composite with relatively high glass content, successful optimization for the parameters separately for the two components of the composite, resin and fiberglass mats, may be unsatisfying, because the variation in mass-loss rate data used as targets generally do not show the effect of the alternating layers of resin and fiberglass mats in the composite.

Second, even when a solution is found, that may not be unique (uniqueness of solution). This occurs usually when the data used in solving the problem is significantly smoothed or biased. In resolving this problem, the typical approach is to reduce the total number of unknowns. This can be accomplished by fixing the unknown parameters to some values by utilizing approaches other than numerical optimization, as discussed previously.

Third, inverse problems are in most cases ill-posed, where a small change in a solution can lead to an enormous change in the modeling output, which is known as the instability problem of a solution (instability of solution). Therefore, effort should be given to always check the applicability of the solution upon extrapolation to other modeling conditions, which were not considered during numerical optimization, knowing that this may result in significant deviation from actual phenomena.

Fourth, the optimized parameters should be considered as a *linked* parameter set. Once numerical optimization is used, the optimized parameter value takes into account any assumptions used in pyrolysis modeling, all the intrinsic or effective parameter values with their uncertainty which were obtained through other means, etc. Hence, an optimized value for one parameter may not be used for other pyrolysis modeling cases, in general. Last, when applying this method, the estimation process can become confusing, and without a consistent approach it can lead to unsatisfying results.

This *Guide* is focused on presenting a process for estimating model parameters that allows modelers to conduct parameter estimation based on commonsense, consistency, and correctness. This process of creating a virtual material is composed of the three approaches discussed above: (1) measure each parameter via independent experiment; (2) search the literature for measurement values on similar materials or use approximation; (3) conduct numerical optimization by pairing the pyrolysis model with an optimization routine. In addition to these approaches, consideration is given to uncertainty of estimation of each model parameter and its propagation into pyrolysis modeling uncertainty, in the context of defining the criteria for satisfying or dissatisfying parameter estimation. Typically, estimation based on measurement of the maximum number of parameters possible will be considered first, then by literature review, as those can become practical constraints when conducting numerical optimization for solving unknowns. Therefore, estimation based on numerical optimization routine in pair with pyrolysis modeling will be considered as the last option.

To create a virtual material, these tasks must be considered:

- Create microstructure of the virtual material
- Identify decomposition kinetics type

- Create a list of model inputs, which needs to be determined
- Obtain model unknown inputs via measurement or literature search

When the above is done and every unknown has been estimated, validation work is needed to understand the performance of the estimated parameter set:

- Run model
- Analyze simulation quality with consideration of uncertainties in modeling outputs and data
- Add commentary

When there are additional unknowns that need to be estimated, the modeler may conduct numerical optimization in pair with modeling. This process of obtaining unknowns via numerical optimization should be followed by validation work as well. Obtaining parameters using numerical optimization and validation should consist the following:

- Run model in pair with numerical optimization
- Analyze simulation quality with consideration of uncertainties in modeling outputs and data
- Validate simulation quality upon extrapolation
- Add commentary

When presenting the parameter estimation results, three summary tables will be introduced: Model Parameter Table, Validation, and Commentary sections. The Model Parameter Table includes the model parameters necessary to conduct pyrolysis modeling, their estimated values, and methods of estimating the unknowns. Validation consists of the following information: description of modeling goal, pyrolysis model type and modeling approach used in the exercise, experiment type and its data used to compare data to modeling outputs or numerically optimize for unknowns, and uncertainty information of experimental data and modeling outputs. Commentary discusses any limitations of pyrolysis modeling conducted above, which has been summarized in the Model Parameter Table and Validation sections.

For better visualization of the problem, a flowchart is shown below (see Figure 5-7):

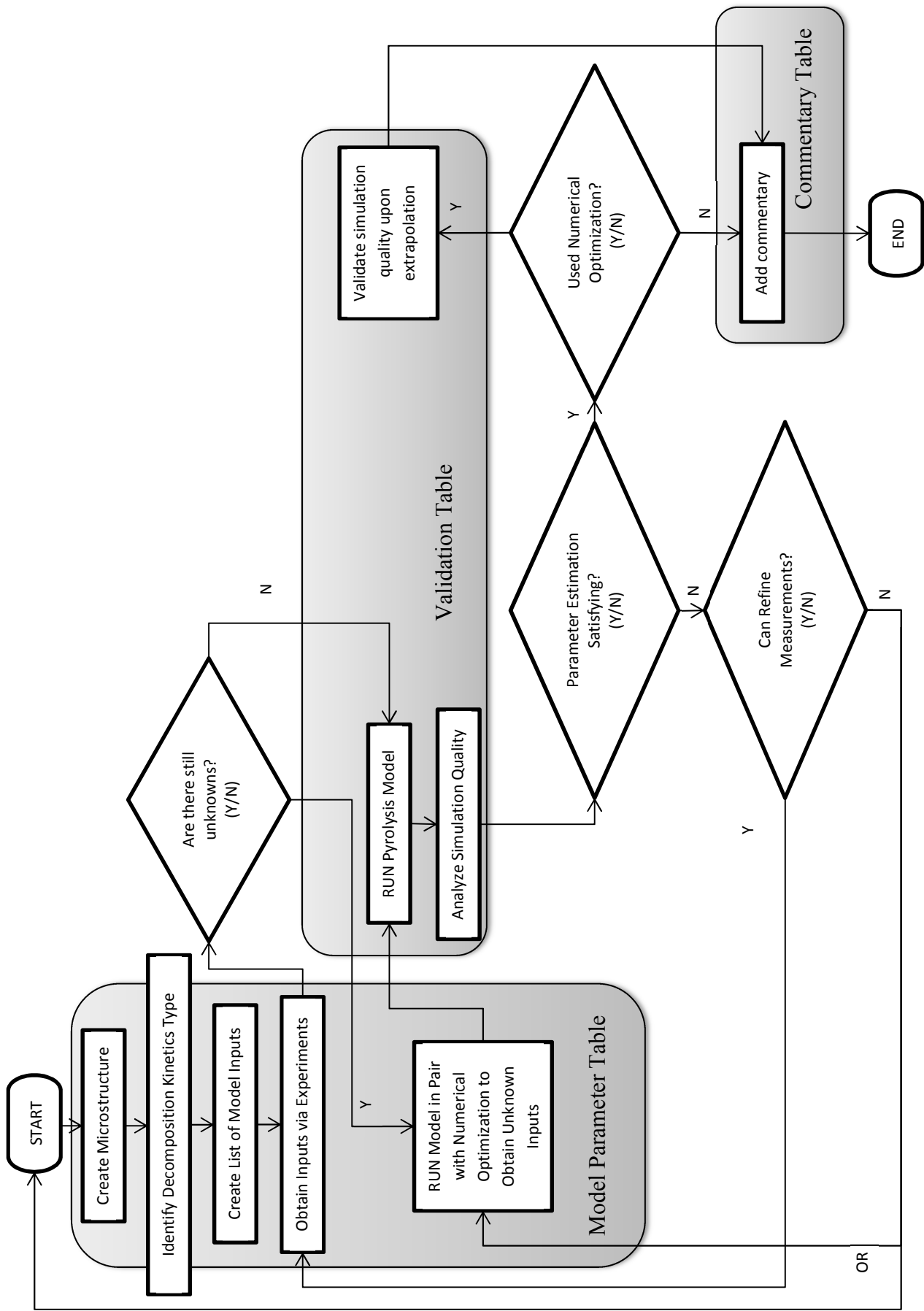


Figure 5-7. Flow chart of parameter estimation for comprehensive pyrolysis models
Section 5 - 143

SENSITIVITY ANALYSIS

Example Case 1 and 2

For these example cases, less than a total of 20 parameters are necessary due to the single step thermal decomposition kinetic modeling applied in these problems. Therefore, extensive sensitivity analysis is not necessary to determine sensitive parameters on model outputs of interest, because work conducted by Stoliarov³⁷ and Chaos³⁸ for similar cases considers the effect of variation in material properties on the rate of burning. According to those, it was recognized that the knowledge of parameters related to emissivity of virgin and char material and the decomposition reaction – Arrhenius pre-exponential factor, activation energy, heats, char yield – are significantly important for predicting the peak, average burning rates and surface temperatures. Based on this result, when determining the uncertainty of the model output, only these parameters will be considered where simulation quality is analyzed by comparing the model output with its uncertainty with experiment data with its uncertainty. Further details on sensitivity of each parameter can be found in this reference.^{37,38}

Example Case 3 (Global Sensitivity Analysis: Morris Method)

For these example cases, a greater number of parameters is involved in pyrolysis modeling. Therefore, a structured global sensitivity analysis technique is used to determine the sensitivity of model input parameters. Among various global analysis techniques, screening design is one of the simplest methods to identify important parameters.^{39,40,41} Typical screening designs are one-at-a-time (OAT) experiments, where a value is changed and its impact is evaluated in turn. It is known that classical OAT experiments are less meaningful if the model of interest is affected by nonlinearities, which causes drastically different “sensitivities” when parameter changes around the “control” scenario, depending on the chosen “control” scenarios. To address this limitation, Morris (1991) has proposed a global OAT design method, by covering the entire space in which the parameters may vary independently of the specific initial “control” scenario with which one may commence the experiment. A global OAT design assumes that the model is characterized by a large number of parameters and/or is

computationally expensive (regarding computational time and computational resources) to run.

Although originally the Morris method was used for unitless parameters, for these problems it was used for parameters with units. Because the Morris method allowed the user to interpret the effect of changes made in the inputs to the model outputs in terms of simulation variation observed in dimensional units (i.e., seconds for time, °C for temperature and g/m²-s for mass-loss rate), one was able to apply the significance level (see below) directly. This allows the user to rank the sensitivity of each parameter with a quantifiable variation.

To identify the sensitive parameters of a model via a sensitivity analysis, there needs to be a measure to determine the sensitivity. This measure, defined as the level of significance, should be able to distinguish which effects shown in the simulation results due to changes made in the inputs are significant and which are not. A typical sensitivity analysis allows the user to rank the input parameters in terms of its sensitivity to model outputs. Defining the level of significance allows the user also to determine how many of the parameters from the top ranking should be set with caution, because those significantly affect the simulation results. The level of significance that defines the sensitivity of an input parameter should be predetermined by the user based on one's goal of conducting the simulation. When the best simulation accuracy is desired, the level of significance should be determined by the experimental uncertainty obtained by tests identical to the simulation set-up, such as the cone calorimeter tests. For example, if the ignition time has an uncertainty of +/- 20 sec. in the cone calorimeter tests, any changes in the model input that allows more than +/- 20 sec. in the model output should be considered as a "significant change." However, there are situations where low simulation accuracy is acceptable for one's simulation purposes. In these cases, the level of significance can be set by the modeler to be greater than the experimental uncertainty, and this approach results in less parameter being considered as sensitive to model outputs.

After identifying the necessary parameters for pyrolysis modeling with a model of choice and selecting the significance level, a sensitivity analysis is performed to identify sensitive input parameters to model output. To determine the region of experimentation for the Morris method, a minimum and maximum range for each parameter is selected by

the user through common sense. Four levels, P1 through P4, are used in this *Guide* example cases ($p = \{0, 1/3, 2/3, 1\}$) with an increment of $\Delta = p/[2(p-1)] = 2/3$ following the guide presented by Morris. Four cases are simulated in each example case, which results in four elementary effects for each parameter.

To calculate an elementary effect, first a baseline case needs to be constructed. The baseline is a group of the entire parameters with their values randomly chosen from **P1 or P2**. This is because there are four levels in this analysis, and when conducting the analysis, adding Δ should not exceed the region of experiment. Next, a random order should be created for each case, where this order is used to change the parameter value from its baseline by Δ one at a time. The effect of changing a parameter by Δ is evaluated by running the model and evaluating the changes made in the model output of interest. Using these four effects found from four cases for each parameter, the modeler now can calculate the mean and its standard deviation or variance of changes that occurred due to an increase/decrease made to a single parameter value by Δ . Any parameter resulting in a significant change in model outputs when changed by Δ (i.e., a large mean and/or standard deviation/variance for changes made in the modeling outputs) are considered to be “sensitive.” Based on this analysis, when determining the uncertainty of the model output, only parameters that are “sensitive” will be considered, where simulation quality is analyzed by comparing the model output with its uncertainty versus experiment data with its uncertainty.

UNCERTAINTY ANALYSIS

To conduct uncertainty analysis for modeling outputs of interest, the uncertainty of each parameter value should be estimated first. When model parameters are estimated using experiment measurements or by literature search, the uncertainty of the measured value is typically estimated through the experiments. However, when numerical optimization is used to estimate unknown model parameters, estimating the uncertainties associated with those optimized values is nontrivial.

Assuming that the uncertainty of every parameter is known and each parameter can be considered as independent, the uncertainty propagated to pyrolysis modeling outputs of interest may be calculated via the Law of Propagation of Uncertainty. To conduct this calculation, first the sensitive parameters should be identified based on sensitivity analysis. Then those parameters are varied to their boundary values (minimum or maximum from representative values by considering parameter uncertainty) in modeling one at a time from its baseline case, which is the one modeled with all representative values for each parameter. The effect of variation is calculated by determining the modeling outputs of interest – e.g., peak heat-release rate, average heat-release rate, time-to-ignition, time to peak heat-release rate, etc. – and comparing the changes occurring from those in the baseline case. At the end, the overall summation of each maximum effect of changing one sensitive parameter at a time is calculated by the Law of Propagation of Uncertainty, which is used as a measure of the uncertainty in modeling results of interest.

When numerical optimization is utilized to estimate unknown parameters, one possible approach of addressing the uncertainty of those parameters is to use the near optimal parameter sets, or “best solutions,” to generate a relatively large population of parameter sets. A multi-objective optimization algorithm such as Genetic Algorithm (GA) applied to pyrolysis modeling typically produces many near-optimal sets or “best solutions,” which are a set of solutions that represent tradeoffs between many objective functions. Each parameter value from each set can be evaluated together to determine whether a near-optimal value of one parameter changes significantly from one set to another. Computing a histogram to understand the distribution of the optimized values and estimating uncertainty for each parameter would be a good practice.

Another possible approach for determining the uncertainty of optimized parameter values is using asymptotic methods.³² This approach is conceptually appealing and easy to implement. However, when problems are highly nonlinear, they may be a poor representation of the actual uncertainties of optimized parameters, for they are calculated locally at the optimum point found by the optimization routine. Nevertheless, the uncertainties estimated can become a useful indication of the reliability of the optimized parameters. At a certain optimum point, the standard error of the parameter estimates is approximated by a variance-covariance matrix based on the Jacobian of the model response. This matrix is then used along with the t-distribution at some desired confidence level to estimate the uncertainty. The set of equations shown below summarizes this approach:

$$\mathbf{COV} = \frac{\|\mathbf{f}(\hat{\mathbf{p}})\|_2^2}{n_d - n_p} (\mathbf{J}^T \mathbf{J})^{-1}; f(\hat{\mathbf{p}}) = y_{\text{exp}_i} - y_{\text{mod}_i}(\hat{\mathbf{p}}); i=1, \dots, n_d$$

$$\mathbf{J} = \begin{bmatrix} \left. \frac{\partial y_{\text{mod}1}(\mathbf{p})}{\partial p_1} \right|_{\hat{\mathbf{p}}} & \dots & \left. \frac{\partial y_{\text{mod}1}(\mathbf{p})}{\partial p_{n_p}} \right|_{\hat{\mathbf{p}}} \\ \vdots & \ddots & \vdots \\ \left. \frac{\partial y_{\text{mod}n_d}(\mathbf{p})}{\partial p_1} \right|_{\hat{\mathbf{p}}} & \dots & \left. \frac{\partial y_{\text{mod}n_d}(\mathbf{p})}{\partial p_{n_p}} \right|_{\hat{\mathbf{p}}} \end{bmatrix}$$

$$\hat{\mathbf{p}} = \hat{\mathbf{p}} \pm t^{-1}(CL; n_d - n_p) \sqrt{\text{diag}[\mathbf{COV}]}$$

Where $\hat{\mathbf{p}}$ is the optimum parameter vector (i.e., set of material properties), n_d is the number of data points used for optimization, n_p is the number of parameters (i.e., material properties), \mathbf{COV} and \mathbf{J} are the covariance and Jacobian matrices, respectively, \mathbf{f} is the vector of differences between model results (y_{mod}) and experimental data (y_{exp}), and t^{-1} is the value of the inverse t-distribution at a given confidence level (CL) and degrees of freedom ($n_d - n_p$). The availability of the the Jacobian matrix further allows for the computation of the sensitivity of model responses to changes in input parameters.

OPTIMIZATION

There are two types of optimization method applied in this *Guide*: manual optimization or numerical optimization routines. The manual optimization can be done for simple cases, e.g., estimating unknown parameters for two solid-phase species involved in one-step thermal decomposition kinetics; however, it requires many trials and errors. Rules-of-thumb for conducting manual optimization are as follows. Consider having optimization targets as experiment data from bench-scale tests, such as the mass loss rate and temperature at various depths, which is a typical case. First, conduct kinetic modeling independently to understand at what temperatures each species will exist. Assume that the decomposition reaction occurs at temperatures between T_a and T_b , where $T_a < T_b$. The parameter estimation conductor may understand any changes made in parameters related to reactant should affect fire behaviors at temperature smaller than T_a , and any changes made in parameters related to product should affect behaviors at temperatures greater than T_b (see (a) in Figure 5-8). With this in mind, manual optimization can be done. Second, understand that any changes made in heat-of-reaction (HoR) affects the mass-loss rate peak. When HoR is reduced, the peak becomes taller (see (b) in Figure 5-8). Third, understand that thermal conductivity (k) affects the temperature gradient throughout the specimen thickness. Reducing k results in a wider spread between the surface and the back surface temperature profiles (see (c) in Figure 5-8). Fourth, understand that specific-heat capacity (c_p) determines how soon material heats up, i.e., increases its body temperature. Applying smaller c_p results in faster increase in temperature profiles throughout, from surface to back surface (see (d) in Figure 5-8). Last, for estimating optical properties, apply simple approximations, e.g., having emissivity equal to 1, for surfaces that are close to black or quickly become black after exposure to radiative heating. Knowing these tips help manual optimization for estimation of unknown model parameters.

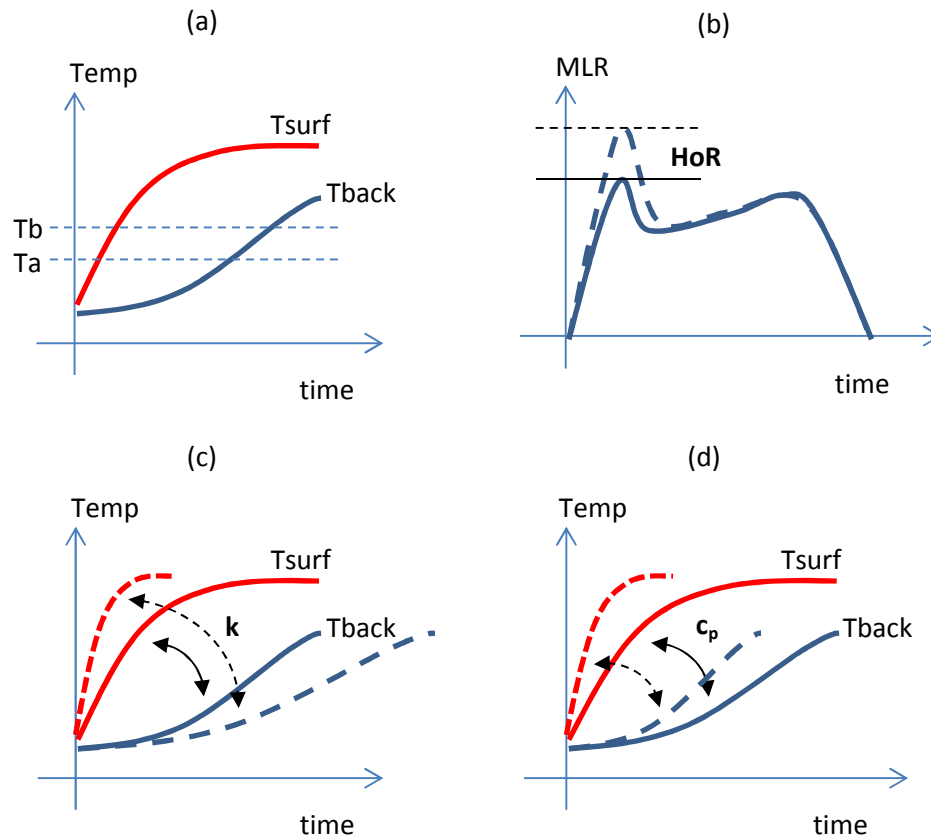


Figure 5-8. Understanding manual optimization: (a) For a one-step thermal-decomposition kinetics that takes place within temperature range of $T_a < T < T_b$, the parameter-estimation conductor may understand changing parameters related to reactant should affect fire behaviors at temperatures below T_a , and changing parameters related to product should affect fire behaviors at temperatures above T_b ; (b) Reducing HoR increases mass-loss rate peak; (c) Reducing thermal-conductivity results in wider spread between T_{surf} and T_{back} ; (d) Reducing specific-heat capacity results in faster increase in temperature throughout. Note that results from greater parameter value are shown in solid lines, while those from smaller value are shown in dashed lines.

There are three types of numerical optimization routines that have been applied to fire pyrolysis modeling so far. In Table 5-11, these numerical optimization routines are introduced and compared. These are evolution-optimization schemes with high efficiency and robustness that allow multi-objective and multi-variable optimization under limited knowledge of the problem. All three optimization routines can be considered in terms of four processes: (1) Initialization of individuals, which refers to the set of initial guesses of unknown parameters; (2) Evolutionary process of selection and reproduction – selection from population for reproduction conducted for individuals with

good fitness, i.e., better adaptation to their environment and reproduction resulting in new generation derived from a previous one while ensuring convergence, i.e., increase in fitness; (3) Termination of evolution at a user-defined termination condition.

Table 5-10. Three types of numerical optimization routines applied to comprehensive pyrolysis modeling in literature: Genetic Algorithm,^{33,34} Shuffled Complex Evolution,^{42,43,44} and Stochastic Hill-climber³⁵

		Genetic Algorithm (GA)	Shuffled Complex Evolution (SCE)	Stochastic Hill-climber (SHC)
Process	Initialization	Initial traits of individuals are customarily randomly generated within a user-defined parameter space as many as the user-defined population size.	Random set of material properties is initial selected within the feasible parameter space (i.e., a population) and partitions it into several subsets or “complexes.”	Initial traits of individuals are customarily randomly generated within a user-defined parameter space as many as the user-defined population size.
	Evolutionary Process of Selection and Reproduction	Probability of selection is customarily based on fitness. Reproduction occurs through the genetic processes of crossover (also called recombination) and/or mutation.	Each complex is allowed to evolve independently and, after a specified number of iterations, all points in each complex are combined back into a single population, ranked according to their objective function value, and then re-partitioned, i.e., shuffling the complexes. This procedure is iteratively repeated and allows for more extensive and freer exploration of the parameter space due to the partition of complexes. Shuffling enhances survivability by sharing information about the space gained independently by each complex.	Probability of selection is customarily based on fitness. Reproduction occurs through the genetic processes of random mutation only, i.e., same with genetic algorithm but without cross-mutation and a population of two - parent and child. The parents outlive the children if they are better adapted to the environment.
	Termination	The evolutionary process is continued until a user-defined termination condition is reached.	The evolutionary process is continued until a user-defined termination condition is reached.	The evolutionary process is continued until a user-defined termination condition is reached.
Computational Expense		High	High	Low

EXAMPLE CASES OVERVIEW

Table 5-11. Overview of example cases using comprehensive pyrolysis models

		Case 1	Case 2	Case 3	
Case Description		Single-step Decomposition RxN w/o Residue	Single-step Decomposition RxN w/ Residue	Two-step Decomposition RxN w/ Residue	Drying and single-step decomposition RxN w/ residue
Material Example		PMMA	Corrugated Cardboard	Fire Retarded FRP Composite	Plywood
Estimation Approach	Mostly Non-optimization	Case 1 – A			
	Comparable Non-optimization and Optimization	Case 1 – B	Case 2 – B	Case 3 – B	
	Mostly Optimization	Case 1 – C	Case 2 – C		
	Manual Optimization				Case 3 – D

In the following, summarized results are shown for each example case. Detailed solutions for these example cases are given in Appendix D.

CASE 1: SINGLE-STEP DECOMPOSITION REACTION WITHOUT RESIDUE PRODUCTION

Virtual Microstructure of Virgin Material

- Homogeneous single layer

Decomposition Kinetics Type

- Type 0 or 1: fuel (solid) → pyrolyzates (gas)
- No solid-phase residue formed
- Weight-loss rate (DTG) with respect to temperature described with a single peak independent of the testing environment (inert or oxidative)

General Model-Parameter Table

- Virgin material is nonporous (no gas phase, only condense phase considered in modeling)
- Reduced-Model Parameter Table (see Table 5-12)

Table 5-12. Model-parameter table for Case 1 examples

		No	Condense Phase ($i=1$)	
Material Property		1	ρ_i	Density
		2	k_i	Thermal conductivity
		3	c_i	Specific heat capacity
		4	κ_i	Absorption coefficient
Parameters for Specifying Conditions		5	ε_i	Emissivity
			Heterogeneous RxN ($k=1$)	
Thermal Decomposition	Finite Thickness Reaction Zone	6	n_k	Reaction order
			Z_k	Pre-exponential factor
			E_k	Activation energy
		7	ΔH_k	heat
	Infinitely Thin Reaction Zone	6	T_p	Pyrolysis temperature
		7	ΔH_p	heat

Example 5.1 Modeling Poly(methylmethacrylate), PMMA

5.1.1 Model-Parameter Table

ID		A	B-GA	B-SCE	B-SHC	C-GA	C-SCE	C-SHC	
Parameter	Unit	Measurement, Literature, or Approximation	Comparable Non-optimization and Optimization			Mostly Optimization			
Thermo-physical Property	ρ_i	kg/m ³	1200 ± 60	1200 ± 60			1200 ± 60		
			Measurement	Measurement			Measurement		
	k_i	W/m-K	0.18 ± 0.01	0.30 ± 0.01	0.21	0.33	0.29 ± 0.01	0.29	0.19
			Literature ⁴⁵	GA	SCE	SHC	GA	SCE	SHC
	c_i	J/kg-K	2.2 ± 0.1	1.8 ± 0.1	0.7	1.7	2.0 ± 0.1	1.1	1.7
Literature ^{46,47}			GA	SCE	SHC	GA	SCE	SHC	
Optical Property	κ_i	/m	2700 ± 1400	150000 ± 86000	1000000	3600000	2200 ± 500	790000	350000
			Literature ⁴⁸	GA	SCE	SHC	GA	SCE	SHC
	ε_i	-	0.85 ± 0.16	0.91 ± 0.01	0.66	0.89	0.66 ± 0.01	0.99	0.54
			Literature ⁴⁸	GA	SCE	SHC	GA	SCE	SHC
Thermal Decomposition Kinetics and Heats	n_k	-	1	1			0.5 ± 0.1	0.5	1.5
			Approximated	Approximated			GA	SCE	SHC
	Z_k	/s	(8.5 ± 4.3) x 10 ¹²	(8.5 ± 4.3) x 10 ¹²			(1.3 ± 0.6) x 10 ¹⁶	3.3 x 10 ¹⁵	5.3 x 10 ¹⁹
			Model Fitting w/ multiple heating rate TGA data	Model Fitting with multiple heating rate TGA data			GA	SCE	SHC
	E_k	J/mol	(1.88 ± 0.06) x 10 ⁵	(1.88 ± 0.06) x 10 ⁵			(1.77 ± 0.01) x 10 ⁵	2.27 x 10 ⁵	2.43 x 10 ⁵
			Model Fitting w/ multiple heating rate TGA data	Model Fitting with multiple heating rate TGA data			GA	SCE	SHC
	ΔH_k	kJ/kg	870 ± 130	870 ± 130			1100 ± 21	1300	520
Literature ⁴⁶			Literature ⁴⁶			GA	SCE	SHC	
Model Dependent Parameter	h_{crz}	W/m ² -K	0	12 ± 3	2	14	38 ± 4	3	-32
			Approximated adiabatic condition at back surface	GA	SCE	SHC	GA	SCE	SHC

*Note that GA, SCE and SHC refer to optimization routines – Genetic Algorithm, Shuffled Complex Evolution, and Stochastic Hill-climber. The GA's summarized parameter values are averaged values from near optimal parameter sets as sample population.

5.1.2 Validation

5.1.2.1 MODELING GOAL

Estimate model parameters for conducting modeling of pyrolysis of PMMA under various heating rates – heat-flux levels ranging up to $\sim 100\text{kW/m}^2$.

5.1.2.2 MODEL TYPE

GPYRO

5.1.2.3 MODELING APPROACH

- Instantaneous release of volatiles from solid to the gas phase
- Local thermal equilibrium between the solid and the volatiles
- No condensation of gaseous products
- No porosity effects

When conducting the GPYRO simulation for the cone calorimeter set-up, metal edge frame will be ignored, and backing is insulated. The ignition phenomenon is interpreted as the following in the simulations: at a known time-of-ignition (from experiment data), additional heat flux of 20 kW/m^2 is applied to the surface to simulate heat flux from the flame. This is the reference value found from the work of Beaulieu⁴⁹, where actual measurement of the flame heat flux of a black PMMA was conducted. The heat-of-combustion was determined using micro-scale combustion calorimeter⁵⁰ operating in following condition: pyrolysis in nitrogen atmosphere by heating samples (2 to 4 mg) at a fixed rate of 1 K/s from 373 to 1173 K. Value is normalized by initial sample weight: $\Delta H_c = 24100\text{ kJ/kg}$

5.1.2.4 EXPERIMENT DESCRIPTION

Cone calorimeter test

5.1.2.5 DATA SET

- Cone calorimeter test data of thick PMMA (thickness, δ ranging from 24 ~ 29 mm) impinged with effective heat fluxes (EHF) of 23, 46, and 69 kW/m^2 is found to show the burning behavior under various heat-flux levels that are less than 100 kW/m^2 . Data were reproduced from Stoliarov's paper⁴⁸, which are shown in Figure 5-9:

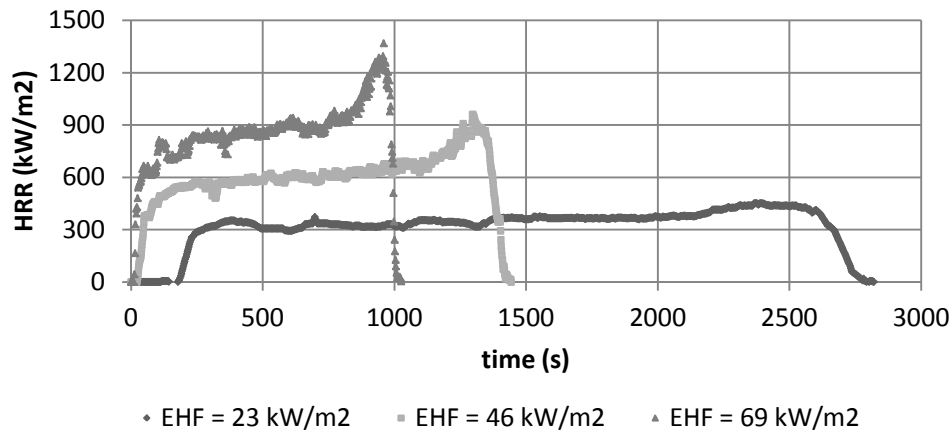


Figure 5-9. Cone calorimeter test data of thick PMMA (thickness, δ ranging from 24 ~ 29 mm) impinged with effective heat fluxes (EHF) of 23, 46, and 69 kW/m²

- Surface temperature measured at steady burning during cone tests of black PMMA decomposing under various heat flux levels is found from Beaulieu’s work⁴⁹ on black PMMA to be within 350 ± 50°C.

5.1.2.6 OPTIMIZATION TARGETS

MLR at EHF = 46 kW/m² with thick PMMA sample from cone calorimeter test

5.1.2.7 SENSITIVE PARAMETERS

$$\varepsilon_i, n_k, Z_k, E_k, \Delta H_k$$

5.1.2.8 UNCERTAINTY

Uncertainty in Experiment Data

- Data reproducibility is checked by repeating 5 identical PMMA tests under 49 kW/m² heat flux level with medium thickness samples (thickness, δ ranging from 7.7 ~ 9.4 mm)
- Uncertainty of peak HRR, average HRR and time to peak HRR are estimated via taking 2 standard deviation of the difference and normalizing them by the mean of this parameter – 17%, 7% and 17%, respectively
- Assume:
 - Uncertainty of HRR is comparable to that of MLR
 - Uncertainties are comparable to those of thicker PMMA tested at various heat-flux levels
 - Data set found above is close to the averaged curves from multiple identical tests under same conditions

- Uncertainty in surface temperature during steady burning is $\pm 50^{\circ}\text{C}$

Uncertainty in Modeling Outputs

- Baseline case: $\text{HF} = 46 \text{ kW/m}^2$, thickness = 29 mm
- Sensitive parameters varied one at a time from baseline to its max and min by considering uncertainty; however, due to compensation effect, pre-exponential factor and activation energy will be considered in pair to have max and min decomposition temperature
- Uncertainty is considered for GA optimization cases (B-GA, C-GA) only using 50 near-optimal parameter sets
- Integration of uncertainty is calculated by Law of Propagation of Uncertainty

5.1.2.9 TG / DTG PREDICTIONS AT $10^{\circ}\text{C}/\text{MIN}$ HEATING RATE USING ESTIMATED KINETIC PARAMETERS

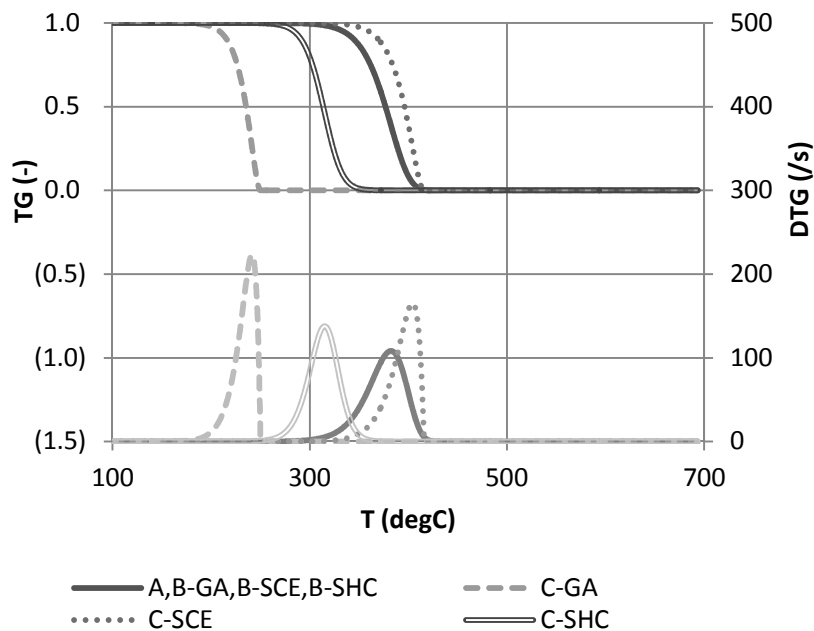


Figure 5-10. TG/DTG curves at $10^{\circ}\text{C}/\text{min}$ heating rate with different estimation results for kinetic parameters for thermal decomposition of PMMA

5.1.2.10 COMPARISON BETWEEN DATA AND COMPUTED-MODELING OUTPUTS

- Modeling is conducted for case with HF = 46 kW/m², thickness = 29 mm

Table 5-13. Comparison between experiment data from cone calorimeter test and modeling outputs using estimated parameter values via either direct measurement, literature search, or approximation (A); measurements and numerical optimization (B-GA, B-SCE, B-SHC); or mostly numerical optimization (C-GA, C-SCE, C-SHC)

	Data	A	B-GA	B-SCE	B-SHC	C-GA	C-SCE	C-SHC
Peak MLR (g/m ² s)	36.9 ±6.3	45.1 ±10.6	40.9 ±5.3	32.6	39.3	27.5 ±0.7	34.4	67.0
Avg MLR (g/m ² s)	24.9 ±1.7	24.2 ±5.2	26.7 ±2.7	25.9	26.6	24.0 ±0.5	26.4	28.0
t to pMLR (s)	1310 ±223	1408 ±252	1285 ±123	1317	1284	1391 ±32	1297	1233
Ts (°C)	350 ±50	413 ±21	433 ±20	407	409	244 ±3	419	343

5.1.2.11 MODELING OUTPUT: MASS LOSS RATE (MLR)

- Case used in optimization process

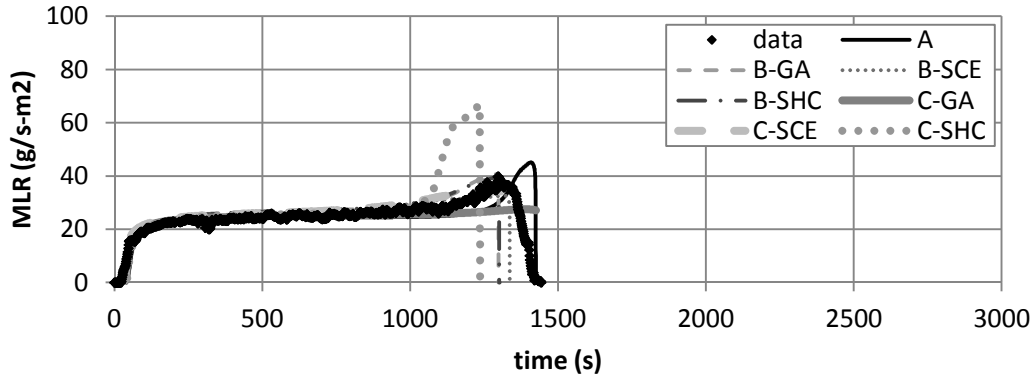


Figure 5- 11. Mass-loss rate (MLR) comparisons for PMMA between actual MLR from experiment (data) and modeled MLR (A, B-GA, B-SCE, B-SHC, C-GA, C-SCE, C-SHC) at applied heat flux of 46 kW/m². Note that data shown were used to estimate model-parameter values via numerical optimization using GA, SCE, or SHC routines.

- Extrapolation

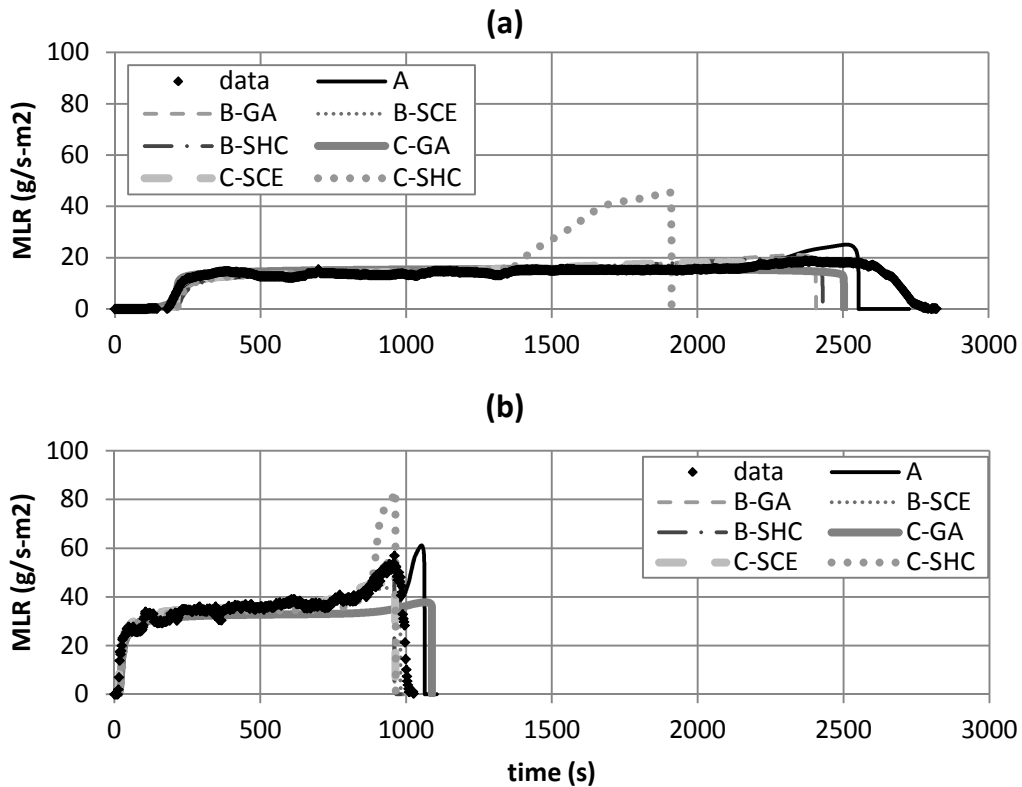


Figure 5-12. Mass-loss rate (MLR) comparisons for PMMA between actual MLR from experiment (data) and modeled MLR (A, B-GA, B-SCE, B-SHC, C-GA, C-SCE, C-SHC) at applied heat flux of (a) 23 and (b) 64 kW/m². Note that data shown were not included in the model-parameter-estimation process; hence, these two cases are considered as extrapolation cases.

5.1.2.12 MODELING OUTPUT: SURFACE TEMPERATURE (T_{SURF})

- Case used in optimization process

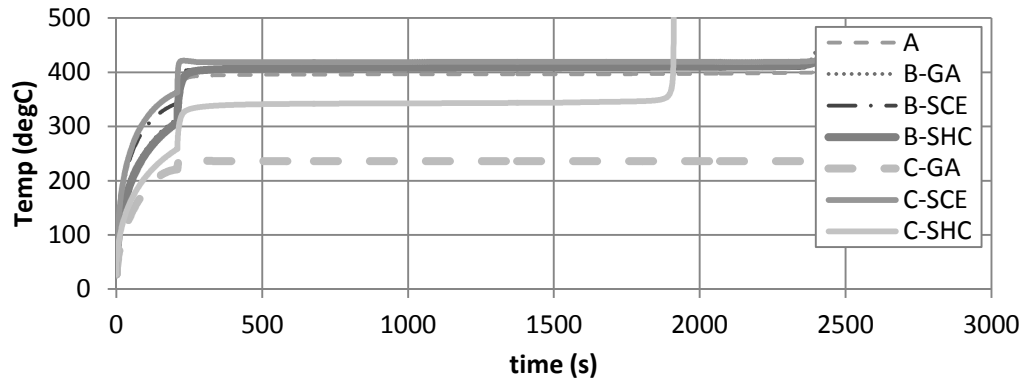


Figure 5-13. Surface-temperature (T_{surf}) comparisons for PMMA modeling using parameters estimated from different approaches – direct measurement, literature search, or approximation (A); measurement and numerical optimization (B-GA, B-SCE, B-SHC); mostly numerical optimization (C-GA, C-SCE, C-SHC) at applied heat flux of 46 kW/m^2 . Note that data shown were used to estimate model-parameter values via numerical optimization using GA, SCE, or SHC routines.

- Extrapolation

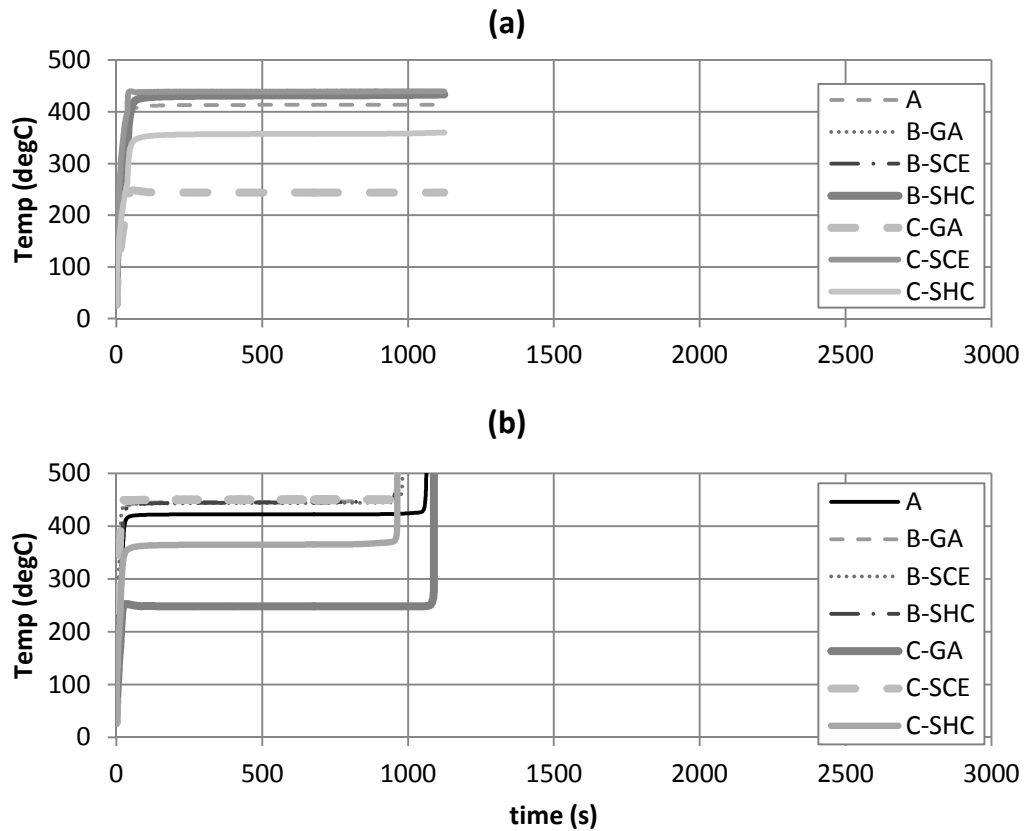


Figure 5-14. Surface-temperature (T_{surf}) comparisons for PMMA modeling using parameters estimated from different approaches – direct measurement, literature search, or approximation (A); measurement and numerical optimization (B-GA, B-SCE, B-SHC); mostly numerical optimization (C-GA, C-SCE, C-SHC) at applied heat flux of (a) 23 and (b) 64 kW/m². Note that data shown were not included in the model-parameter-estimation process; hence, these two cases are considered as extrapolation cases.

5.1.3 Commentary

GENERAL COMMENTS

- TG/DTG
 - Whether kinetic modeling is conducted independently using TGA data (A, B-GA, B-BSE, B-SHC) or as a part of numerical optimization (C-GA, C-SCE, C-SHC), decomposition of PMMA is considered to occur within the temperature range of 200°C to 400°C.
 - Among GA, SCE and SHC, estimation of SCE was closest, followed by SHC and GA to TGA data
 - Having surface temperature data as an additional optimization, target should have provided constraints to the optimization problem, because kinetic parameters directly determine the surface temperature. However, this approach was not utilized, for uncertainty in surface temperature measurement was too high – $350 \pm 50^\circ\text{C}$
- Comparison Between Data and Computed-Modeling Outputs
 - Better agreement between data and modeling outputs for the peak MLR is found when kinetic parameters are estimated through a separate process using TGA data (A, B-GA, B-BSE, B-SHC) compared with numerical optimization along with estimating other unknowns together (C-GA, C-SCE, C-SHC)
 - Average MLR and time-to-peak-MLR from all modeling cases show good agreement with data
 - Simulated surface temperature at steady burning of PMMA is greater (less than 10 s) than that of measurement for cases B-GA, B-SCE, B-SHC and C-SCE, while simulated surface temperature is lower (greater than 50 s) than that of measurement for case C-GA. Results from cases A and C-SHC are in good agreement.
- MLR
 - Direct Measurement or Optimization at $\text{HF} = 46 \text{ kW/m}^2$: Good agreement exists between experiment data and all modeling results, whether modeled with measured parameters or optimized in the time frame of exposure to heating source up to steady burning. However, in the later time, where the peak occurs, the result from C-SHC becomes unsatisfying, considering the data with its uncertainty, while others can be considered as satisfying.
 - Direct Measurement or Extrapolation at $\text{HF} = 23 \text{ kW/m}^2$: Good agreement exists between experiment data and all modeling results, except for C-SHC case.
 - Direct Measurement or Extrapolation at $\text{HF} = 64 \text{ kW/m}^2$: Good agreement exists between experiment data and all modeling results, except for C-GA and C-SHC case.

- Surface Temperature
 - See above

LIMITATION IN MODELING

- When considering limitation of the parameters in simulating PMMA, the modeler should take into account the applicability of the parameters and their associated uncertainties. For example, any assumptions used when determining a parameter value via experiment direct or indirect measurements can be utilized to understand when the parameter value becomes inappropriate. For this example of pyrolysis modeling of PMMA, most consideration can be given to the parameters related to decomposition kinetics.
- In this example, kinetic modeling was conducted with TGA data obtained from nitrogen environment. However, studies^{49,51,52} have suggested that PMMA decomposes differently with respect to heating rates and availability of oxygen. The decomposition rate of PMMA increases with respect to oxygen concentration, because oxygen aids unzipping of the polymer by being involved in the depolymerization process of the polymer. Also, the oxygen dependency increases at lower heating rates than at higher heating rates. Possible explanation for this can be given by considering the diffusion of oxygen from nearby gas phase to the condense phase. At lower heating rates, decomposition rate is relatively slow; therefore, the time allowed for oxygen to diffuse to the polymer layer and be involved in the decomposition process is relatively longer. However, at higher heating rates, decomposition rate is relatively higher even without the involvement of oxygen in the decomposition process. This results in a shorter time scale for transportation of oxygen via diffusion to the condense phase. In other words, the positive effect of enhancing decomposition by having oxygen involved in the process, compared to decomposition in non-oxidative condition, is compensated by the time necessary for oxygen diffusion to occur from the gas phase to the condense phase. Hence, the increase in decomposition rate of PMMA due to the presence of oxygen in the gas phase is more profound in conditions with lower heating rates than in higher heating rates. Visual observations of the surface phenomena during PMMA decomposition also provide evidence that above explanation is reasonable. Based on experimental work conducted by Beaulieu⁴⁹ during decomposition of PMMA, “bubbling” occurs on the surface. The bubbles are relatively large, forming a thick layer of bubbles when irradiated at lower heat-flux levels and they are smaller, forming a thin bubbling layer, when irradiated at higher heat-flux levels. Considering the bubbling is an effective way of the polymer to

enhance oxygen diffusion and larger bubbles entrains more oxygen, reduction in decomposition rate due to increasing time necessary for oxygen diffusion at higher heat-flux levels seems plausible, with bubbles becoming smaller as increasing from a lower heat flux to a higher heat flux.

- Figure 5-15 shows TGA thermograms of PMMA decomposition conducted under constant heating rates – 2, 5, 10 and 20 K/min – and two different environments – nitrogen and air (data obtained from work conducted by Matala³⁴). As shown below and discussed earlier, there is significant difference between the curves produced from nitrogen and air tests. This indicates that decomposition kinetics is different in two cases, and the difference is due to oxygen diffusion from the gas phase surrounding the solid sample surface with respect to the “bubbling” phenomenon.

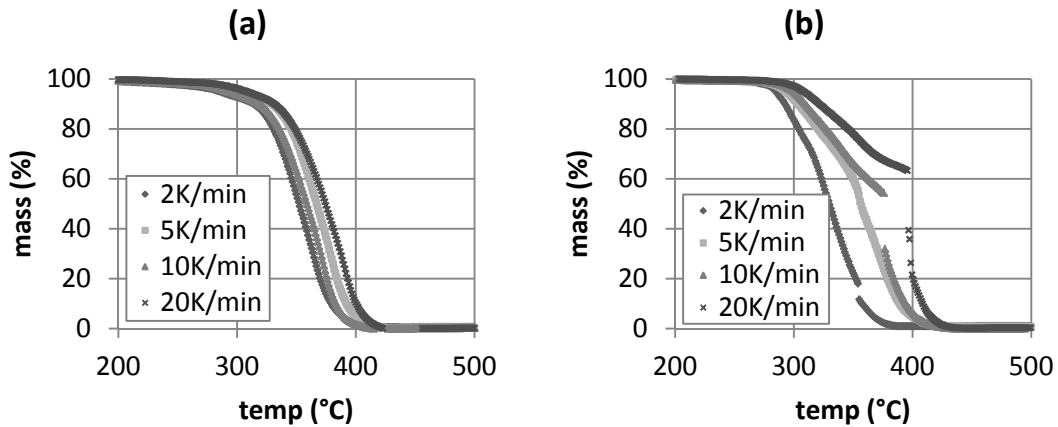


Figure 5-15. TGA thermograms of PMMA decomposition conducted under constant-heating rates – 2, 5, 10, and 20K/min – and two different environments – (a) nitrogen and (b) air

CASE 2: SINGLE-STEP DECOMPOSITION REACTION WITH RESIDUE PRODUCTION

Virtual Microstructure of Virgin Material

- Homogeneous single layer

Decomposition Kinetics Type

- Type 0 or 1: fuel (solid) → residue (solid) + pyrolyzates (gas)
- Weight-loss rate (DTG) with respect to temperature described with a single peak independent of the testing environment (inert or oxidative)

General Model Parameter Table

- Although actual virgin material is porous, porous nature of material is implicitly accounted for in density only (no gas phase, only condense phases – virgin state fuel and residue – considered in modeling)
- Reduced Model Parameter Table (see Table 5-14)

Table 5-14. Model-parameter table for Case 2 examples

		No	Condense Phase ($i=1,2$)	
Material Property		1	ρ_i	Density
		2	k_i	Thermal conductivity
		3	c_i	Specific-heat capacity
		4	κ_i	Absorption coefficient
Parameters for Specifying Conditions		5	ε_i	Emissivity
			Heterogeneous RxN ($k=1$)	
Thermal Decomposition	Finite-Thickness Reaction Zone	6	n_k	Reaction order
			Z_k	Pre-exponential factor
			E_k	Activation energy
		7	ΔH_k	Heat
	Infinitely-Thin Reaction Zone	6	T_p	Pyrolysis temperature
		7	ΔH_p	heat

Example 5.2 Modeling Triple-layered Corrugated Cardboard

5.2.1 Model Parameter Table

ID			B-GA	B-SCE	B-SHC	C-GA	C-SCE	C-SHC	
Parameter		Unit	Comparable Non-optimization and Optimization			Mostly Optimization			
Thermo-physical Property	i = 1 (fuel)	ρ_i	kg/m ³	110			110		
				Measurement			Measurement		
		k_i	W/m-K	0.08 ± 0.01			0.13	0.21	0.21
			Measurement			GA	SCE	SHC	
		c_i	J/kg-K	2.8	2.3	0.6	2.0	2.4	1.7
				GA	SCE	SHC	GA	SCE	SHC
	i = 2 (residue)	ρ_i	kg/m ³	25	20	11	26	10	43
				GA	SCE	SHC	GA	SCE	SHC
		k_i	W/m-K	0.29	0.32	0.32	0.20	0.35	0.20
				GA	SCE	SHC	GA	SCE	SHC
	c_i	J/kg-K	1.5	1.1	0.2	1.0	0.8	2.2	
			GA	SCE	SHC	GA	SCE	SHC	
Optical Property	i = 1 (fuel)	κ_i	/m	10 ⁶			10 ⁶		
				Approximated as opaque			Approximated as opaque		
		ε_i	-	0.88 ± 0.01			0.72	0.50	0.65
				Measurement			GA	SCE	SHC
	i = 2 (residue)	κ_i	/m	10 ⁶			10 ⁶		
				Approximated as opaque			Approximated as opaque		
Thermal Decomposition Kinetics and Heats		n_k	-	1			3.7	3.0	2.2
				Approximated			GA	SCE	SHC
		Z_k	/s	1.1 x 10 ²¹			3.9 x 10 ⁶	9.8 x 10 ¹⁹	6.0 x 10 ¹⁴
				Model Fitting with single heating rate TGA data			GA	SCE	SHC
		E_k	J/mol	2.49 x 10 ⁵			7.0 x 10 ⁴	2.47 x 10 ⁵	3.02 x 10 ⁵
				Model Fitting with single heating rate TGA data			GA	SCE	SHC
		ΔH_k	kJ/kg	123	512	809	88	54	0.7
				GA	SCE	SHC	GA	SCE	SHC
	Model Dependent Parameter	h_{crz}	W/m ² -K	19	8	14	10	8	10
				GA	SCE	SHC	GA	SCE	SHC
$n_{kz}(i=1)$		-	5.6	4.6	7.6	0			
			GA	SCE	SHC	Approximated			

*Note that GA, SCE and SHC refer to optimization routines – Genetic Algorithm, Shuffled Complex Evolution, and Stochastic Hill-climber.

5.2.2 Validation

5.2.2.1 MODELING GOAL

Estimate model parameters for conducting modeling of pyrolysis of triple-layered corrugated cardboard under various heating rates – heat-flux levels ranging up to ~ 100kW/m².

5.2.2.2 MODEL TYPE

GPYRO

5.2.2.3 MODELING APPROACH

- Instantaneous release of volatiles from solid to the gas phase
- Local thermal equilibrium between the solid and the volatiles
- No condensation of gaseous products
- No porosity effects

Further details can be found from Reference 43.

When conducting the 1D simulation for the FPA set-up, insulation at back surface is not modeled explicitly but included as some heat loss to the back surface. In this example case, only AN FPA experiment with nitrogen as purge gas will be considered; hence, there is no ignition phenomenon to be modeled.

5.2.2.4 EXPERIMENT DESCRIPTION

Fire Propagation Apparatus Test

5.2.2.5 DATA SET

- Fire Propagation Apparatus (FPA) test data of triple-wall corrugated cardboard, i.e., two layers of corrugated cardboard (thickness, δ is 30 mm) impinged with effective heat fluxes (EHF) of 20 to 110 kW/m² is found. Data were reproduced from Chaos' paper⁴³, which are shown below for 20, 60 and 110 kW/m² cases for mass loss rate (MLR) and surface temperature measurements using pyrometer (see Figure 5-16):

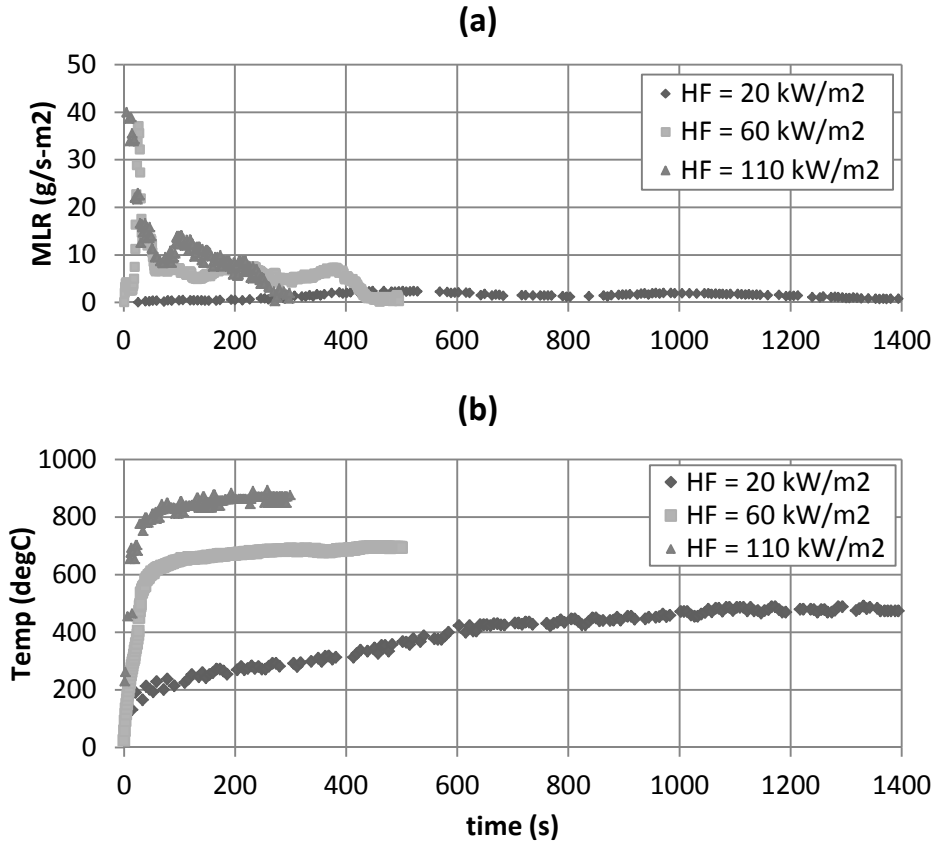


Figure 5-16. Fire propagation apparatus (FPA) Test Data – (a) mass-loss rate; and (b) surface-temperature profile – of triple-wall corrugated cardboard, i.e., two layers of corrugated cardboard (thickness, δ is 30 mm) impinged with effective heat fluxes (EHF) of 20 to 110 kW/m²

5.2.2.6 OPTIMIZATION TARGETS

MLR, cumulative mass loss (CML), and surface-temperature data with triple-layered corrugated cardboard sample from Fire Propagation Apparatus test at HF = 60 kW/m²

5.2.2.7 SENSITIVE PARAMETERS

$$\varepsilon_i, \rho_{i=2}, n_k, Z_k, E_k, \Delta H_k$$

5.2.2.8 UNCERTAINTY

Uncertainty in Experiment Data

- Data is acquired from two repeating FPA tests of triple-wall corrugated cardboard under 60 kW/m^2 heat-flux level with nitrogen atmosphere.
- Uncertainty analysis is conducted based on these two data sets. The uncertainties are quantified with confidence intervals with $\alpha = 0.05$ and assuming normal distribution of population (size 2).
- Assume:
 - Uncertainties are comparable to the same sample tested at various heat-flux levels

Uncertainty in Modeling Outputs

- Typically, uncertainty is considered for GA optimization cases (B-GA, C-GA) only by taking an average of a large population of near-optimals with their confidence intervals to quantify uncertainty when numerical optimization is used to estimate unknowns. However, in this case, GA found the best optimized parameter set that has relatively large fitness than other near-optimals. Therefore, estimation of uncertainty of GA's optimization was not possible; hence, was considered as certain.

5.2.2.9 TG / DTG PREDICTIONS AT 10 °C/MIN HEATING RATE USING ESTIMATED KINETIC PARAMETERS

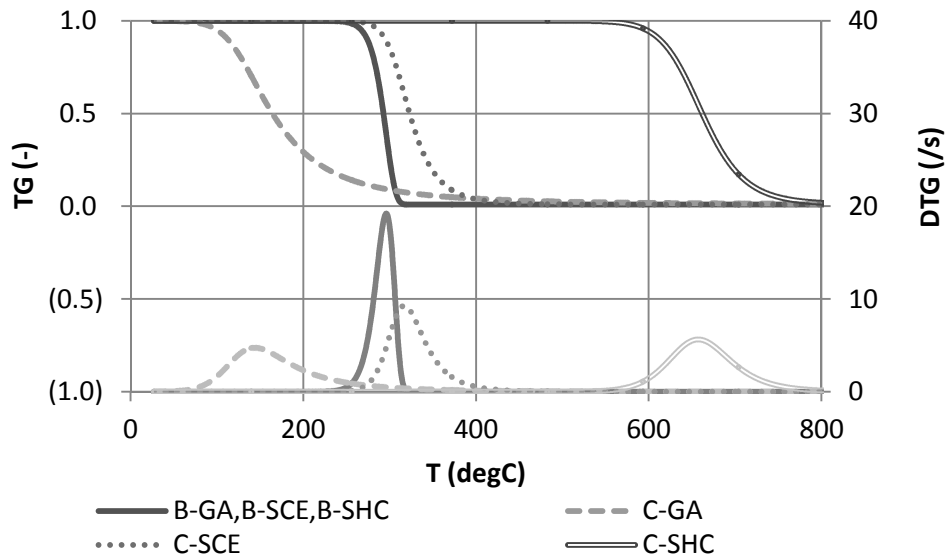


Figure 5-17. TG/DTG Curves at 10°C/min heating rate with different estimation results for kinetic parameters for thermal decomposition of corrugated cardboard: For better comparison, TG and DTG thermograms have been scaled to result in 100% conversion.

5.2.2.10 COMPARISON BETWEEN DATA AND COMPUTED-MODELING OUTPUTS

- Modeling is conducted for case with HF = 46 kW/m², thickness = 29 mm

Table 5-15. Comparison between experiment data from fire-propagation apparatus test and modeling outputs using estimated parameter values via either measurements and numerical optimization (B-GA, B-SCE, B-SHC) or mostly numerical optimization (C-GA, C-SCE, C-SHC)

	Data	B-GA	B-SCE	B-SHC	C-GA	C-SCE	C-SHC
Peak MLR (g/m ² s)	35 ± 4	28	24	53	23	29	N/A
Avg MLR (g/m ² s)	5.7 ± 0.6	4.6	5.4	5.9	4.8	6.0	N/A
t to pMLR (s)	27 ± 1	19	13	19	4	12	N/A
Ts at 300 s (°c)	696 ± 16	685	682	684	679	679	685

5.2.2.11 MODELING OUTPUT: MASS-LOSS RATE (MLR)

- Case used in optimization process

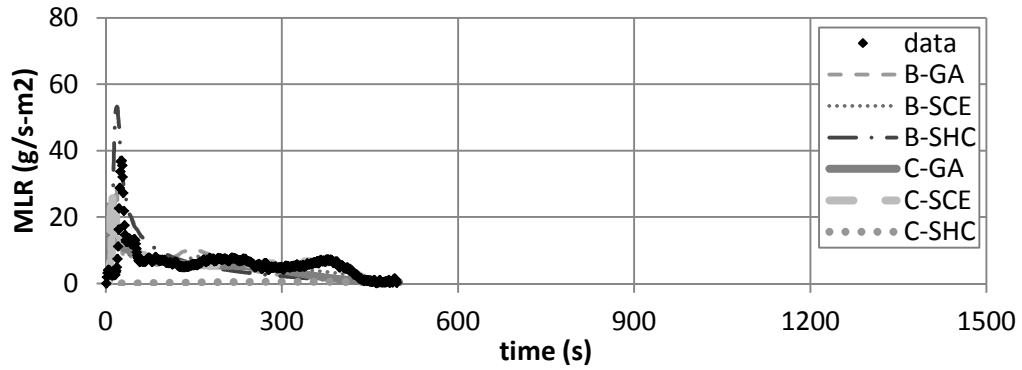


Figure 5-18. Mass-loss rate (MLR) comparisons for corrugated cardboard between actual MLR from experiment (data) and modeled MLR (B-GA, B-SCE, B-SHC, C-GA, C-SCE, C-SHC) at applied heat flux of 60 kW/m². Note that data shown were used to estimate model-parameter values via numerical optimization using GA, SCE, or SHC routines.

- Extrapolation

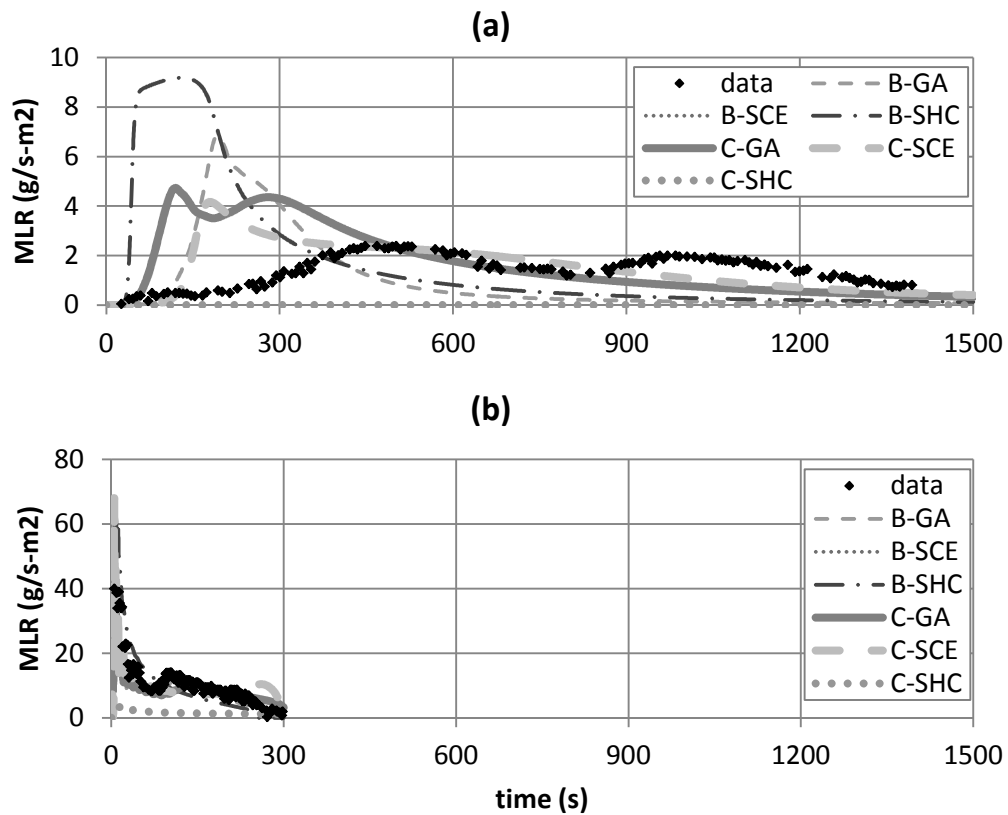


Figure 5-19. Mass-loss rate (MLR) comparisons for corrugated cardboard between actual MLR from experiment (data) and modeled MLR (B-GA, B-SCE, B-SHC, C-GA, C-SCE, C-SHC) at applied heat flux of (a) 20 and (b) 110 kW/m². Note that data shown were not included in the model parameter estimation process; hence, these two cases are considered as extrapolation cases.

5.2.2.12 MODELING OUTPUT: SURFACE TEMPERATURE (T_{SURF})

- Case used in optimization process

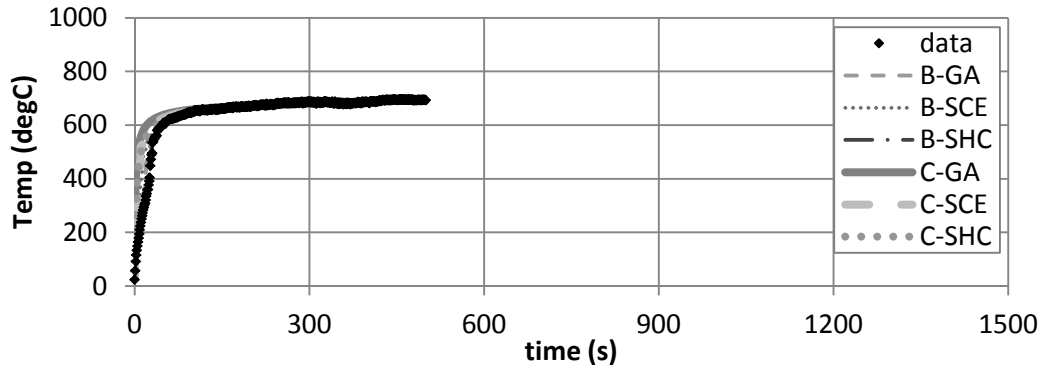


Figure 5-20. Surface-temperature (T_{surf}) comparisons for corrugated cardboard between actual T_{surf} from experiment (data) and modeled T_{surf} (B-GA, B-SCE, B-SHC, C-GA, C-SCE, C-SHC) at applied heat flux of 60 kW/m^2 . Note that data shown were used to estimate model-parameter values via numerical optimization using GA, SCE or SHC routines.

- Extrapolation

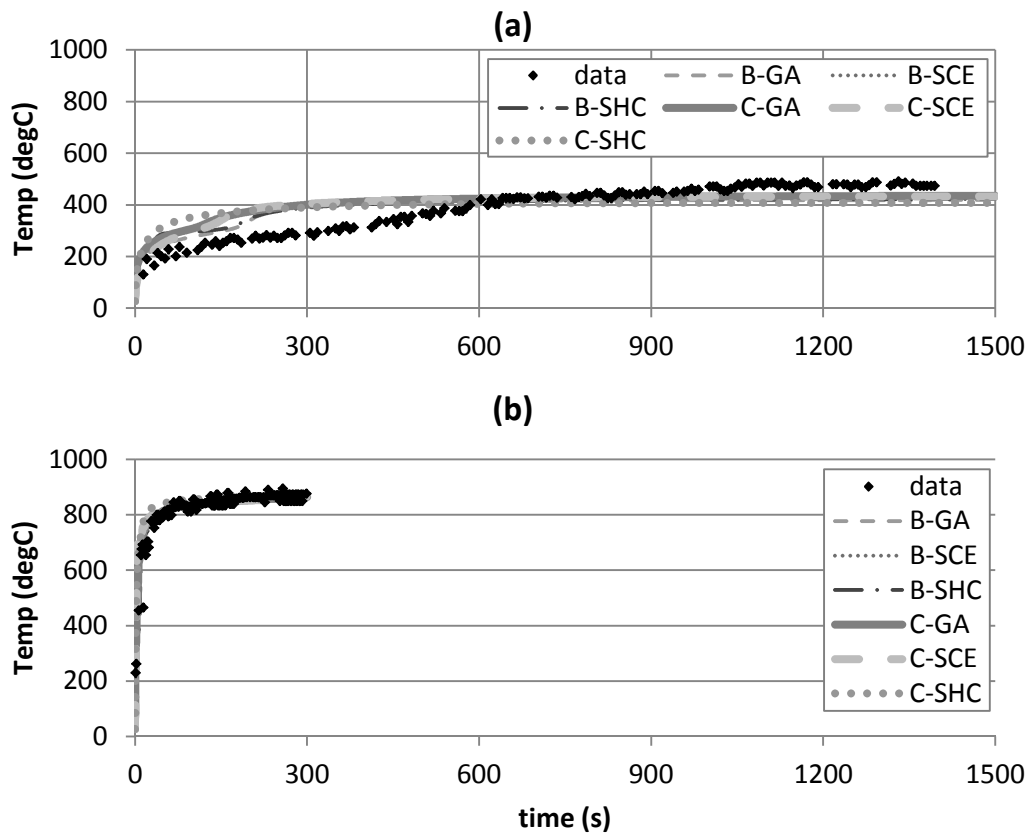


Figure 5-21. Surface-temperature (T_{surf}) comparisons for corrugated cardboard between actual T_{surf} from experiment (data) and modeled T_{surf} (B-GA, B-SCE, B-SHC, C-GA, C-SCE, C-SHC) at applied heat flux of (a) 20 and (b) 110 kW/m². Note that data shown were not included in the model-parameter-estimation process; hence, these two cases are considered as extrapolation cases.

5.2.3 Commentary

GENERAL COMMENTS

- TG/DTG
 - When kinetic modeling is conducted independently using TGA data (B-GA, B-BSE, B-SHC), the DTG peak exist near 300°C.
 - Among GA, SCE, and SHC, optimization of SCE of kinetic parameters as part of other unknown parameter estimation is closest to actual TGA data (B-GA, B-SCE, B-SHC), followed by GA and SHC.
 - Optimization of SHC of kinetic parameters along with other unknown parameter estimation is considered as unsuccessful, because decomposition temperature is excessively high (see mass-loss rate optimization and extrapolation results)
- Comparison between Data and Computed-Modeling Outputs
 - Generally, better agreement between data and modeling outputs is found when kinetic parameters are estimated through a separate process using TGA data (B-GA, B-BSE, B-SHC) than numerical optimization, along with estimating other unknowns together (C-GA, C-SCE, C-SHC)
 - None of the modeled peak MLRs is in quantitative agreement with data
 - Average MLR of B-SCE, B-SHC and C-SCE are in good agreement with data
 - None of the modeled time to peak MLRs is in quantitative agreement with data
 - Surface temperatures at 300 s of B-GA, B-SCE, B-SHC, and C-SHC are in good agreement with data
- MLR
 - Optimization at $HF = 60 \text{ kW/m}^2$: Although the peak may be off for some cases, generally good agreement exists between experiment data and all modeling results considering the trend, except for that of C-SHC, indicating that optimization of C-SHC – optimizing for all unknowns using SHC – was unsuccessful. Oscillation in the MLR curve is due to the inhomogeneity of the sample – corrugated cardboard – which is not captured in modeling due to the homogeneous assumption made when solving the problem.
 - Extrapolation at $HF = 20 \text{ kW/m}^2$: Poor agreement exists between experiment data and all modeling results. None of the modeling cases is able to capture the slow increase in mass-loss rate in the earlier times after exposure to heating source.
 - Extrapolation at $HF = 110 \text{ kW/m}^2$: Good agreement exists between experiment data and all modeling results, except for C-SHC case.
- Surface Temperature
 - Optimization at $HF = 60 \text{ kW/m}^2$: Generally good agreement exists between experiment data and all modeling results considering the trend, even for that of C-SHC. Also, when thermal conductivity of the sample at

its virgin state was independently measured and that value was used, modeling was able to capture the slow increase in surface temperature up until 400°C followed by a jump up to ~550°C.

- Extrapolation at HF = 20 kW/m²: Poor agreement exists between experiment data and all modeling results. None of the modeling cases is able to capture the slow increase in surface temperature in the earlier times after exposure to heating source.
- Extrapolation at HF = 110 kW/m²: Good agreement exists between experiment data and all modeling results, including C-SHC case.

LIMITATION IN MODELING

- When considering limitation of the parameters in modeling corrugated cardboard, the modeler should take into account the applicability of the parameters and their associated uncertainties. For example, any assumptions used when determining a parameter value via experiment direct or indirect measurements can be utilized to understand when the parameter value becomes inappropriate. For this example of pyrolysis modeling of corrugated cardboard, most consideration can be given to the parameters related to decomposition kinetics.
- As shown in the figure below of corrugated cardboard decomposed in TGA at 20 K/min under nitrogen and air atmosphere, the simplified kinetic modeling using a one-step decomposition mechanism is only true for a “dry” sample tested in nitrogen. Clearly, decomposition of a “dry” sample in air results in two distinct DTG peaks. Therefore, the effect of the simplification (one-step) made to kinetic modeling should be addressed when discussing large-scale simulation quality of the parallel panel experiment using the optimized parameter set from this exercise.

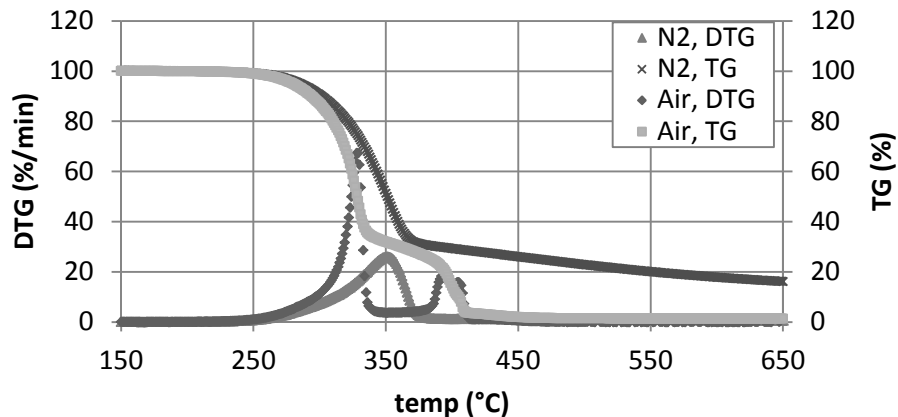


Figure 5-22. TGA thermograms of corrugated cardboard decomposition conducted under constant-heating rate of 20 °C/min and two different environments – nitrogen and air

CASE 3: TWO-STEP DECOMPOSITION REACTION WITH RESIDUE PRODUCTION

Virtual Microstructure of Virgin Material

- Effective homogeneous single layer

Decomposition Kinetics Type

- Type 3 with two-step reaction
 - Reactant₁ (solid) → Product₁ (solid) + pyrolyzates (gas)
 - Reactant₂ (solid) → Product₂ (solid) + pyrolyzates (gas)
- Weight-loss rate (DTG) with respect to temperature described with two overlapping peaks independent of the testing environment (inert or oxidative)

General Model Parameter Table

- Although actual virgin material is porous, the porous nature of the material is implicitly accounted for in density only (no gas phase, only condense phases – Reactant 1 and 2, Product 1 and 2 – considered in modeling)
- Reduced Model Parameter Table (see Table 5-16)

Table 5-16. Model-parameter table for Case 3 examples

	No	Condense Phase ($i=1,2,3,4$)	
Material Property	1	ρ_i	Density
	2	k_i	Thermal conductivity
	3	c_i	Specific-heat capacity
	4	κ_i	Absorption coefficient
Parameters for Specifying Conditions	5	ε_i	Emissivity
		Heterogeneous RxN ($k=1,2$)	
Kinetic Parameters and Heats Assuming n^{th} Order Model and Arrhenius-type Expression	6	n_k	Reaction order
		Z_k	Pre-exponential factor
		E_k	Activation energy
	7	ΔH_k	Heat

Example 5.3 Modeling FRP Composite with Modified Acrylic Resin with High-charring Inorganic Additive

An example case is shown for a fiberglass-reinforced polymer (FRP) composite with modified-acrylic resin with high-charring inorganic fire-retardant additive. Most of the approach and reference values of the input parameters for this simulation were obtained from Kim and Dembsey's work.³⁰

Modified-acrylic resin (MA) is essentially unsaturated polyester (UPE) with Methacrylic Acid (MMA) replacing most of the styrene monomers. Flame-retarded resin with MA is manufactured by adding a filler-type inorganic additive (A) as an additive where its loading versus resin is **MA:A = 0.38:0.62** by weight. Typical inorganic additives are hydrates such as alumina trihydroxide (ATH) or magnesium hydroxide, antimony trioxide, borax, chalk, silica, etc.⁵³ Because this additive was known to give a high-charring effect, A was categorized with typical hydroxides used as flame-retardant fillers. These hydroxides work as a flame retardant by resulting in an endothermic dehydration reaction that produces oxides and water.^{54,55} The water produced by this reaction vaporizes, which is an endothermic reaction, and the vapor dilutes the gaseous phase. The oxides remain in the char layer, which adds an insulative effect. This flame retardant is added with a relatively large amount (50 to 65%) compared with other types of additives. By adding a significant amount of an inorganic flame retardant, the polymer becomes more brittle. Because this is an inorganic additive, inserting this material into the polymer system by 50 to 65 wt% of its original polymer reduces the available fuel within the condensed phase. In addition to this effect, usually the additive has a higher heat capacity compared with the base polymer; hence, the flame retarded polymers with these types of hydroxides require more energy to increase the body temperature to its pyrolysis level. According to the product description, this resin with the flame-retardant additive is formulated to be Class I per ASTM E 84⁵⁶ (flame spread index < 20 and smoke developed < 225). **→Propose two parallel reactions for MA and A thermal decomposition**



Figure 5-23. Cross-section of FRP composite with modified-acrylic resin with high-charring inorganic additive

Composite panels were fabricated by vacuum bagging for a relatively high glass-content composite (31 ± 2 wt% of glass, thickness of 8.9 ± 0.2 mm) using two different types of fiberglass mats that were wetted with resin (see Figure 5-23 for cross-section of composite). The two types of fiberglass (E-glass) used in the composite are a chopped-strand mat and a glass-roving woven mat with an area density of 25 g/m^2 and 880 g/m^2 , respectively. The chopped-strand mat is thinner and more porous than the woven mat. The laminate schedule (provided by the manufacturer) is chopped-strand mat and roving alternating three times with another chopped-strand mat layer at the end. Visual inspection of a polished cross-section of the composite slab is consistent with this laminate schedule, but with polymer-resin layers between each fiberglass layer. The chopped-strand mat layer is difficult to identify in the cross section, perhaps because more resin is soaked into this layer than the roving layer. The roving layer is observed as a prominent glass layer possibly because the resin is absorbed only at the fiberglass layer surfaces leaving the interior with primarily glass. **→ Apply effective homogeneous single layer of resin, additive and fiberglass mixture**

5.3.1 Model Parameter Table

ID		GA(avg)	GA(best)	SCE	SHC			
Parameter		Unit						
		Comparable Non-optimization and Optimization						
Thermo-physical Property	i = 1 (Resin)	ρ_i	kg/m ³	1200 Measurement				
		k_i	W/m-K	0.23 ± 0.02 GA	0.21 GA	0.54 SCE	0.04 SHC	
		c_i	J/kg-K	1400 ± 100 GA	2200 GA	300 SCE	1300 SHC	
		i = 2 (R_residue)	ρ_i	kg/m ³	253 Measurement, Kinetic Modeling			
			k_i	W/m-K	0.19 ± 0.02 GA	0.12 GA	0.08 SCE	0.31 SHC
			c_i	J/kg-K	1900 ± 200 GA	1600 GA	1800 SCE	1800 SHC
	i = 3 (Additive)		ρ_i	kg/m ³	2300 Measurement			
		k_i	W/m-K	1.22 ± 0.10 GA	1.44 GA	0.82 SCE	2.74 SHC	
		c_i	J/kg-K	1200 ± 100 GA	930 GA	2500 SCE	2400 SHC	
		i = 4 (A_residue)	ρ_i	kg/m ³	1558 Measurement, Kinetic Modeling			
	k_i		W/m-K	0.24 ± 0.04 GA	0.22 GA	0.59 SCE	0.36 SHC	
	c_i		J/kg-K	1200 ± 100 GA	2200 GA	300 SCE	780 SHC	
	i = 5 (Glass)		ρ_i	kg/m ³	2600 Reference (MSDS)			
		k_i	W/m-K	0.18 ± 0.02 GA	0.15 GA	0.30 SCE	0.09 SHC	
		c_i	J/kg-K	400 ± 100 GA	170 GA	300 SCE	110 SHC	
		Optical Property	i = 1 (R)	κ_i	/m	10 ⁶ Approximated as opaque		
	ε_i			-	0.84 ± 0.03 GA	0.81 GA	0.82 SCE	1.24 SHC
	i = 2 (R_res)		κ_i	/m	10 ⁶ Approximated as opaque			
			ε_i	-	0.90 ± 0.03 GA	0.87 GA	1.00 SCE	0.97 SHC
	i = 3 (A)		κ_i	/m	10 ⁶ Approximated as opaque			
ε_i			-	0.81 ± 0.04 GA	0.77 GA	1.00 SCE	0.84 SHC	

	i = 4 (A_res)	κ_i	/m	10^6			
				Approximated as opaque			
		ε_i	-	0.89 ± 0.03 GA	0.96 GA	1.00 SCE	0.42 SHC
	i = 5 (Glass)	κ_i	/m	10^6			
				Approximated as opaque			
		ε_i	-	0.88 ± 0.02 GA	0.90 GA	1.00 SCE	1.41 SHC
Kinetics and Heats	k = 1 R → R _{residue} +vap↑	n_k	-	1.3		Model Fitting with Multiple-Heating-Rate TGA Data	
		Z_k	/s	3.2×10^{12}			
		E_k	J/mol	1.83×10^5			
		ΔH_k	kJ/kg	(2.5 ± 0.2) × 10 ³ GA	2.0 × 10 ³ GA	2.6 × 10 ³ SCE	2.6 × 10 ³ SHC
		k = 2 A → A _{residue} + vap↑	n_k	-	5.0		Model Fitting with Multiple-Heating-Rate TGA Data
	Z_k		/s	1.6×10^{12}			
	E_k		J/mol	1.60×10^5			
	ΔH_k		kJ/kg	3760 ± 1130 (30%) Measurement, DSC			
	Model-Dependent Parameter		n_{kz} (i=5)	-	0.59 ± 0.06 GA	0.58 GA	0.01 SCE
		-		0.53 ± 0.06 GA	0.37 GA	0.88 SCE	-0.26 SHC
Υ (i=2)		m	0.00348 ± 0.00134 GA	0.00051 GA	0.00002 SCE	0.02482 SHC	
		m	0.00475 ± 0.00184 GA	0.00625 GA	0.00001 SCE	0.05832 SHC	
Υ (i=5)		m	0.00769 ± 0.00225 GA	0.00001 GA	0.00003 SCE	-0.02453 SHC	
		m	0.00769 ± 0.00225 GA	0.00001 GA	0.00003 SCE	-0.02453 SHC	

*Note that GA, SCE and SHC refer to optimization routines – Genetic Algorithm, Shuffled Complex Evolution, and Stochastic Hill-climber. For GA, there are two cases. GA(avg) is the average estimated values from ~50 near-optimal-parameter-sets population. GA(best) is the parameter set with best fitness among those near-optimal population.

5.3.2 Validation

5.3.2.1 MODELING GOAL

Estimate model parameters for conducting modeling of pyrolysis of modified-acrylic resin with high-charring additive FRP composite under various heating rates – heat-flux levels ranging from 25 kW/m² to 75kW/m².

5.3.2.2 MODEL TYPE

GPYRO

5.3.2.3 MODELING APPROACH

- Instantaneous release of volatiles from solid to the gas phase
- Local thermal equilibrium between the solid and the volatiles
- No condensation of gaseous products
- No porosity effects
- When conducting the GPYRO simulation for the cone calorimeter set-up, metal edge frame will be ignored, and backing is insulated. The ignition phenomenon is interpreted as the following in the simulations: at a known time-of-ignition (from experiment data), additional heat flux of 20 kW/m² is applied to the surface to simulate heat flux from the flame. This value is estimated from a measurement from this material pyrolyzing in the cone with a total heat-flux gauge measuring heat flux impinging on the sample surface (see Figure 5-24– test conducted at 50 kW/m² applied heat flux; from time-of-ignition an increase in measured heat flux is observed due to flame).

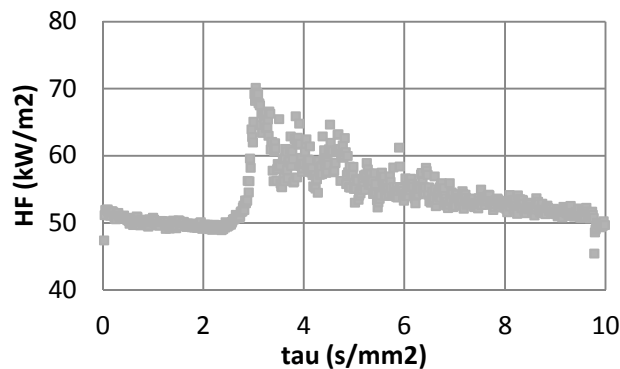


Figure 5-24. Total heat flux measured from sample surface during cone calorimeter test

- For the back surface, an additional layer of insulation with known properties is modeled to simulate some heat loss through the back. The contact resistance (hcrz) between the FRP composite and the insulation is estimated as roughly as 10 W/m²K and that of insulation layer and ambient as 1 W/m²K.
- In addition to the parameters introduced in the previous section (see parameter table), the model (GPYRO) has a coefficient (γ , GAMMA) that is used to model

radiative heat transfer through the pores. This parameter with T^3 is a model-dependent parameter that is added as another term in the effective thermal conductivity. γ is used for porous fiberglass and decomposed solid species, which results in more a porous state due to the weight loss; therefore, more radiative-heat transfer through the gas phase pores, i.e., for condense-phase species $i = 2$ (A_residue), 4 (MA_residue) and 5 (G).

- Another set of parameters included as unknowns is the temperature-dependent terms used to describe the variation of thermal conductivity and specific-heat capacity with respect to temperature increase: $k(T) = k_0(T/T_r)^{n_k}$ and $c(T) = c_0(T/T_r)^{n_c}$, respectively, where T_r is a reference temperature. Only properties of fiberglass is temperature dependent knowing that for high glass-content FRP composite, glass may be a controlling factor for its fire behavior. This approach is utilized to give much flexibility during parameter estimation for fiberglass.

5.3.2.4 EXPERIMENT DESCRIPTION

Cone calorimeter Test

5.3.2.5 DATA SET

- Cone calorimeter (cone) test data of modified-acrylic resin with high-charring additive FRP composite (thickness, δ is 8.9 ± 0.2 mm, density, ρ is 1900 kg/m^3) impinged with effective heat fluxes (EHF) of 25 to 75 kW/m^2 is obtained and are shown below (see Figure 5-25) for mass-loss rate (MLR), surface and back-face temperature measurements:

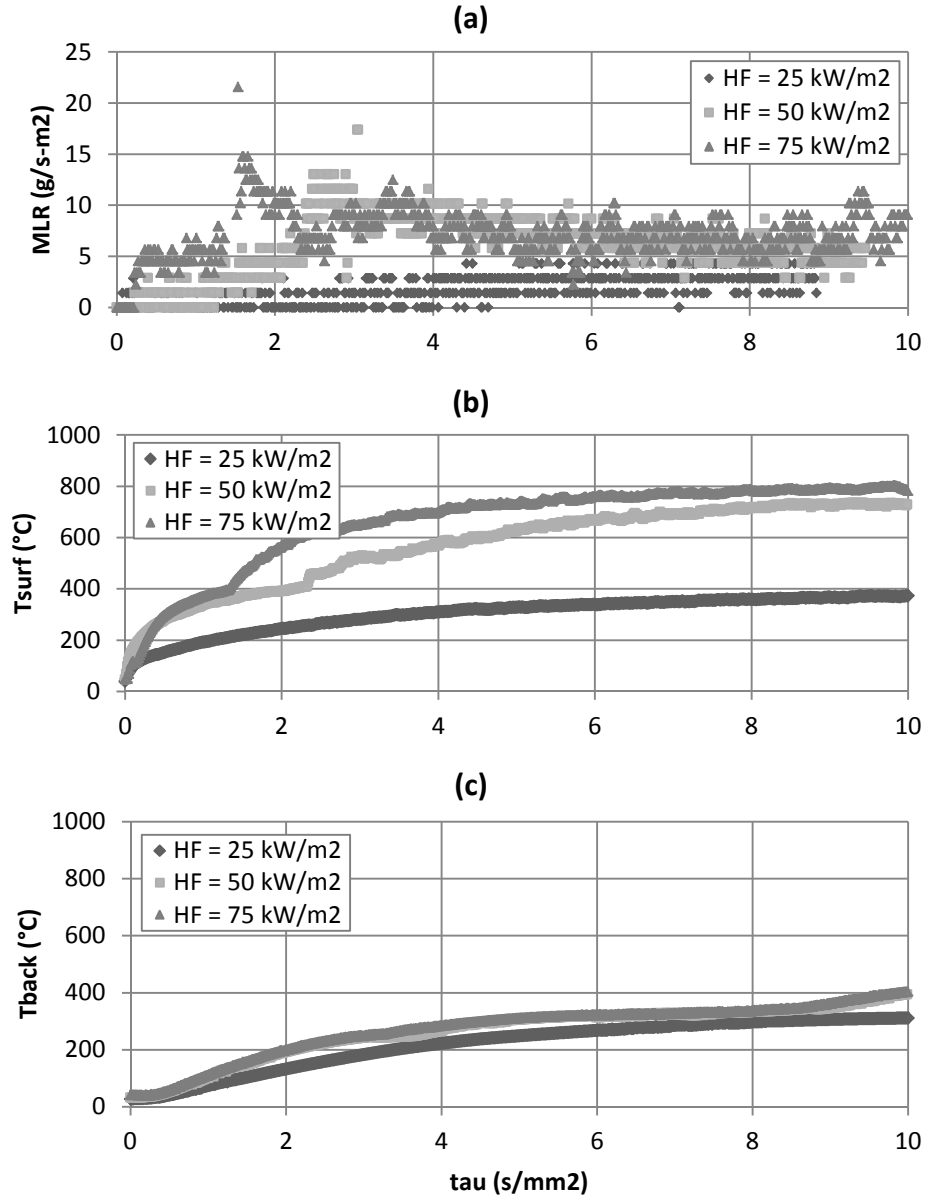


Figure 5-25. Cone calorimeter

Cone test data of modified-acrylic resin with high-charring additive FRP composite (thickness, δ is 8.9 ± 0.2 mm, density, ρ is 1900 kg/m^3) impinged with effective heat fluxes (EHF) of 25 to 75 kW/m^2

5.3.2.6 OPTIMIZATION TARGETS

Mass-loss rate (MLR), cumulative mass loss (CML), surface (T_s), and back (T_b) surface temperature data with FRP composite sample from cone calorimeter test at HF = 50 kW/m²

5.3.2.7 SENSITIVE PARAMETERS

- Identified by conducting OAT method (see Appendix for detail)
- R residue's ϵ , A_residue's k , A_residue's γ , G's n_k , G's n_c

5.3.2.8 UNCERTAINTY

Uncertainty in Experiment Data

- Data is acquired from three repeating cone tests of modified-acrylic resin with inorganic high-charring additive FRP composite with relatively high glass content under 50 kW/m² heat flux level.
- The uncertainties in the MLR and thermocouple measurements at front surface were quantified by comparing data from these three identical FRP composite tests. Note that normalized time, time divided by sample thickness square, i.e., $\tau = \text{time}/\delta^2$, is used to remove the effect of different sample thicknesses when comparing. Because the data is transient, values at different times ($\tau = 1, 3, 5$ and 7 s/mm^2) from each test have been used to calculate the standard deviation at each time. Then these are averaged and used to estimate uncertainty by applying student t distribution with a sample size of three and calculating the 95% confidence interval: uncertainty in MLR and T_s are $\pm 2.2\text{g/sm}^2$ and $\pm 67^\circ\text{C}$, respectively.
- Assume:
 - Uncertainties are comparable to the same sample tested at various heat flux levels
 - Data set found above is close to the averaged curves from multiple identical tests under same conditions

Uncertainty in Modeling Outputs

- Baseline case: HF = 50 kW/m², thickness = 8.7 mm
- Sensitive parameters varied one at a time from baseline to its max and min by considering uncertainty
- Uncertainty is considered for GA optimization case only using ~50 near-optimal parameter sets
- Integration of uncertainty is calculated by the Law of Propagation of Uncertainty: uncertainty in model's MLR, T_s , and T_b are $\pm 1.2\text{g/sm}^2$, $\pm 6^\circ\text{C}$ and $\pm 43^\circ\text{C}$, respectively.

5.3.2.9 TG / DTG PREDICTIONS AT 10 °C/MIN HEATING RATE USING ESTIMATED KINETIC PARAMETERS

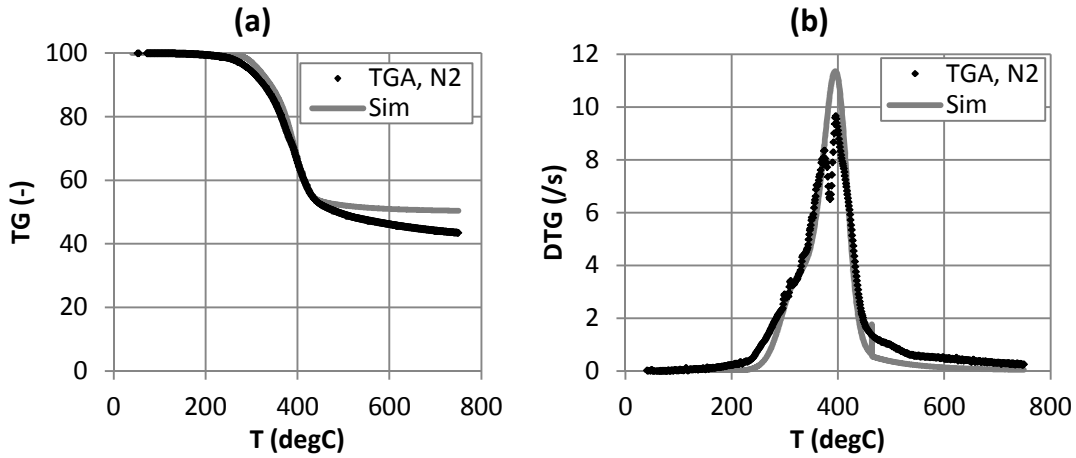


Figure 5-26. TG/DTG curves at 10°C/min heating rate with different estimation results for kinetic parameters for thermal decomposition of fire retarded-FRP composite: testing of resin with additive sample (~10mg) with nitrogen purge

5.3.2.10 COMPARISON BETWEEN DATA AND COMPUTED-MODELING OUTPUTS

- Modeling is conducted for case with HF = 46 kW/m², thickness = 29 mm

Table 5-17. Comparison between experiment data from cone calorimeter test and modeling outputs using estimated parameter values using numerical optimization (GA, SCE, SHC)

	Data	GA(avg)	GA(best)	SCE	SHC
Peak MLR (g/m ² s)	27 ± 31	10.7 ± 1.2	11.4	10.6	12.4
Avg MLR (g/m ² s)	5.8 ± 1.6	6.3 ± 1.2	6.1	6.2	8.1
t to pMLR (s)	200 ± 70	196	189	189	196
Ts at τ = 1 s/mm ² (°C)	341 ± 54	336 ± 6	327	339	326
Ts at τ = 3 s/mm ² (°C)	541 ± 100	496 ± 6	515	519	450
Ts at τ = 5 s/mm ² (°C)	632 ± 9	583 ± 6	607	611	517
Tb at τ = 1 s/mm ² (°C)	101 ± 14	111 ± 43	117	91	133
Tb at τ = 3 s/mm ² (°C)	240 ± 23	274 ± 43	276	265	289
Tb at τ = 5 s/mm ² (°C)	299 ± 25	302 ± 43	302	302	330

5.3.2.11 MODELING OUTPUT: MASS-LOSS RATE (MLR)

- Case used in optimization process

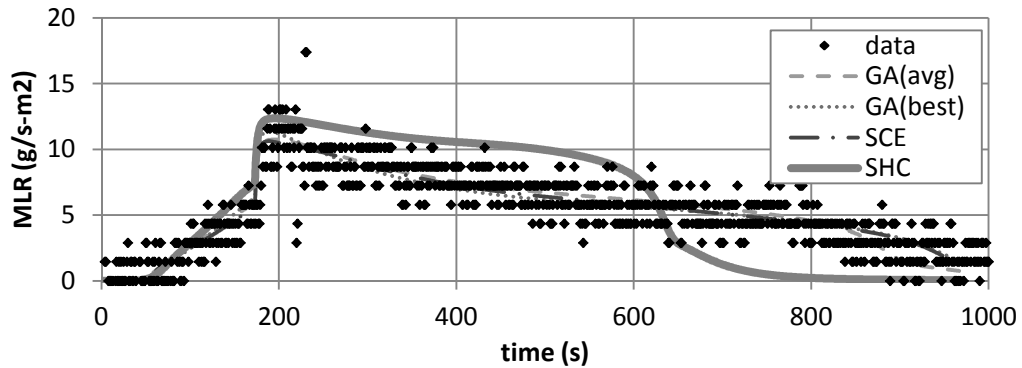


Figure 5-27. Mass-loss rate (MLR) comparisons for FRP composite with modified acrylic resin with high-charring inorganic additive between actual MLR from experiment (data) and modeled MLR (GA, SCE, SHC) at applied heat flux of 50 kW/m^2 . Note that data shown were used to estimate model-parameter values via numerical optimization using GA, SCE, or SHC routines.

- Extrapolation

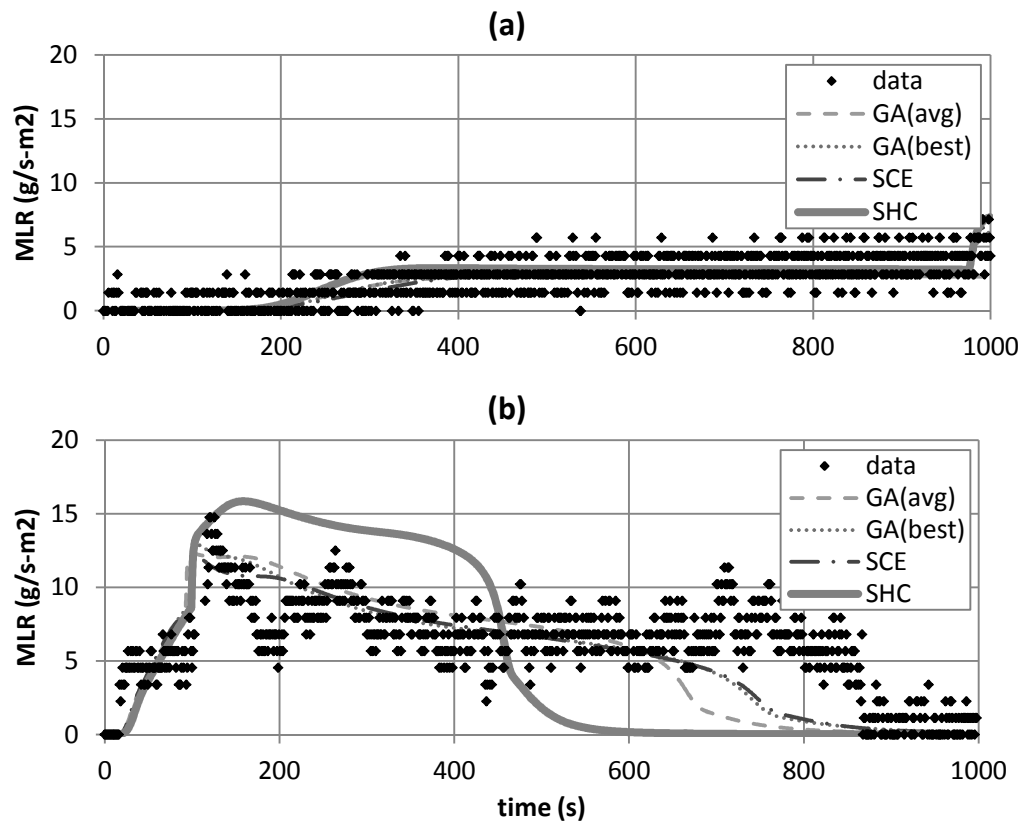


Figure 5-28. Mass-loss rate (MLR) comparisons for FRP composite with modified acrylic resin with high-charring inorganic additive between actual MLR from experiment (data) and modeled MLR (GA, SCE, SHC) at applied heat flux of (a) 25 and (b) 75 kW/m². Note that data shown were not included in the model-parameter-estimation process; hence, these two cases are considered as extrapolation cases.

5.3.2.12 MODELING OUTPUT: SURFACE TEMPERATURE (T_{SURF})

- Case used in optimization process

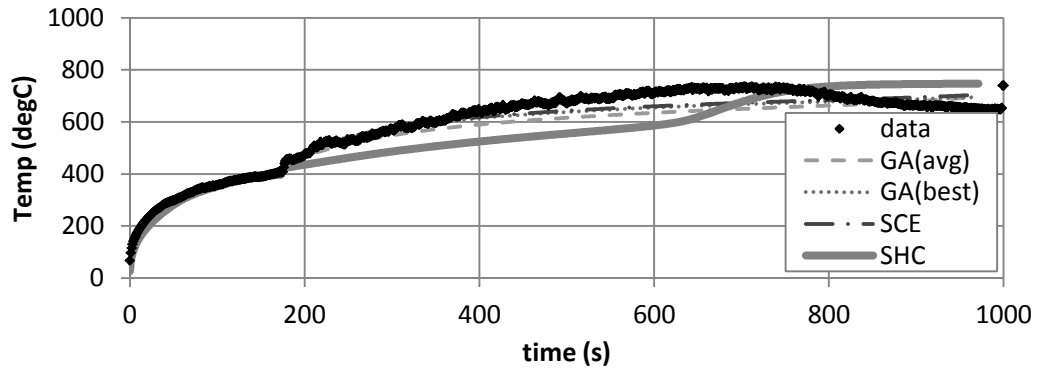


Figure 5-29. Surface-temperature (T_{surf}) comparisons for FRP composite with modified-acrylic resin with high-charring inorganic additive between actual T_{surf} from experiment (data) and modeled T_{surf} (GA, SCE, SHC) at applied heat flux of 50 kW/m^2 . Note that data shown were used to estimate model-parameter values via numerical optimization using GA, SCE, or SHC routines.

- Extrapolation

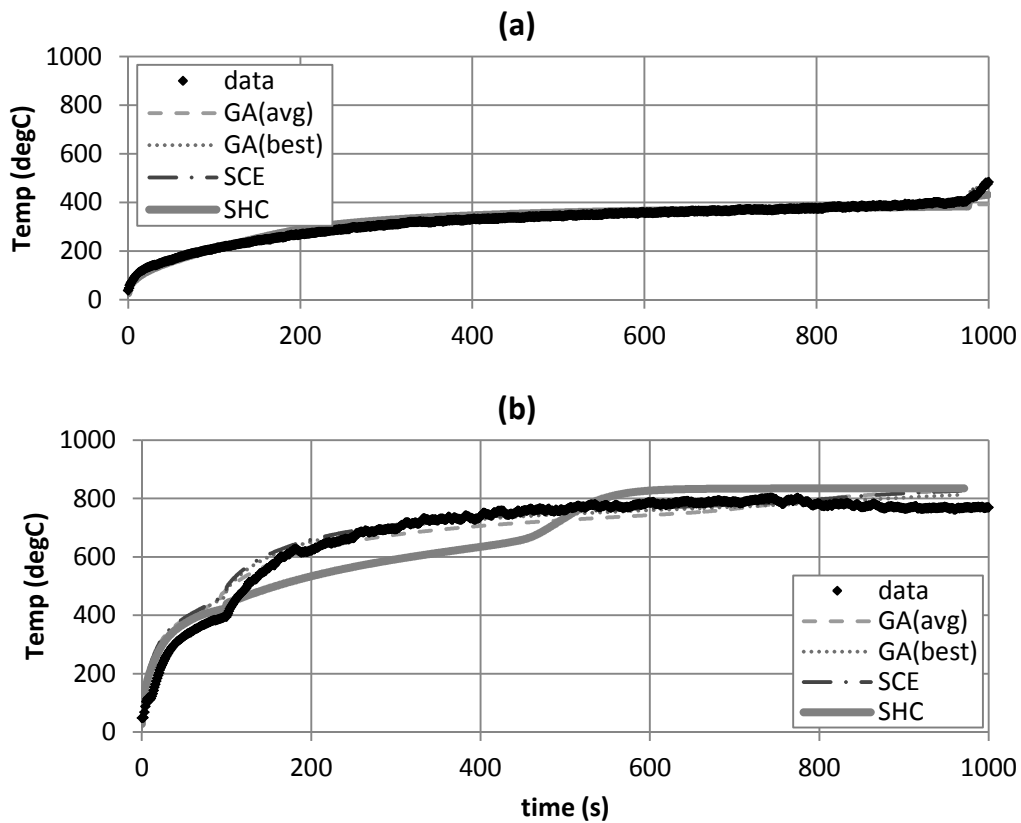


Figure 5-30. Surface-temperature (T_{surf}) comparisons for FRP Composite with modified acrylic resin with high-charring inorganic additive between actual T_{surf} from experiment (data) and modeled T_{surf} (GA, SCE, SHC) at applied heat flux of (a) 25 and (b) 75 kW/m^2 . Note that data shown were not included in the model-parameter-estimation process; hence, these two cases are considered as extrapolation cases.

5.3.2.13 MODELING OUTPUT: BACK SURFACE TEMPERATURE (T_{BACK})

- Case used in optimization process

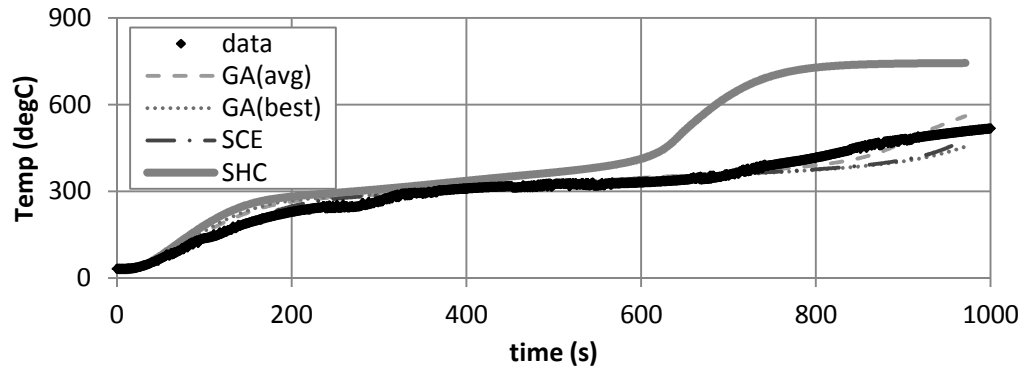


Figure 5-31. Back-surface-temperature (T_{back}) comparisons for FRP composite with modified-acrylic resin with high-charring inorganic additive between actual T_{back} from experiment (data) and modeled T_{back} (GA, SCE, SHC) at applied heat flux of 50 kW/m^2 . Note that data shown were used to estimate model-parameter values via numerical optimization using GA, SCE, or SHC routines.

- Extrapolation

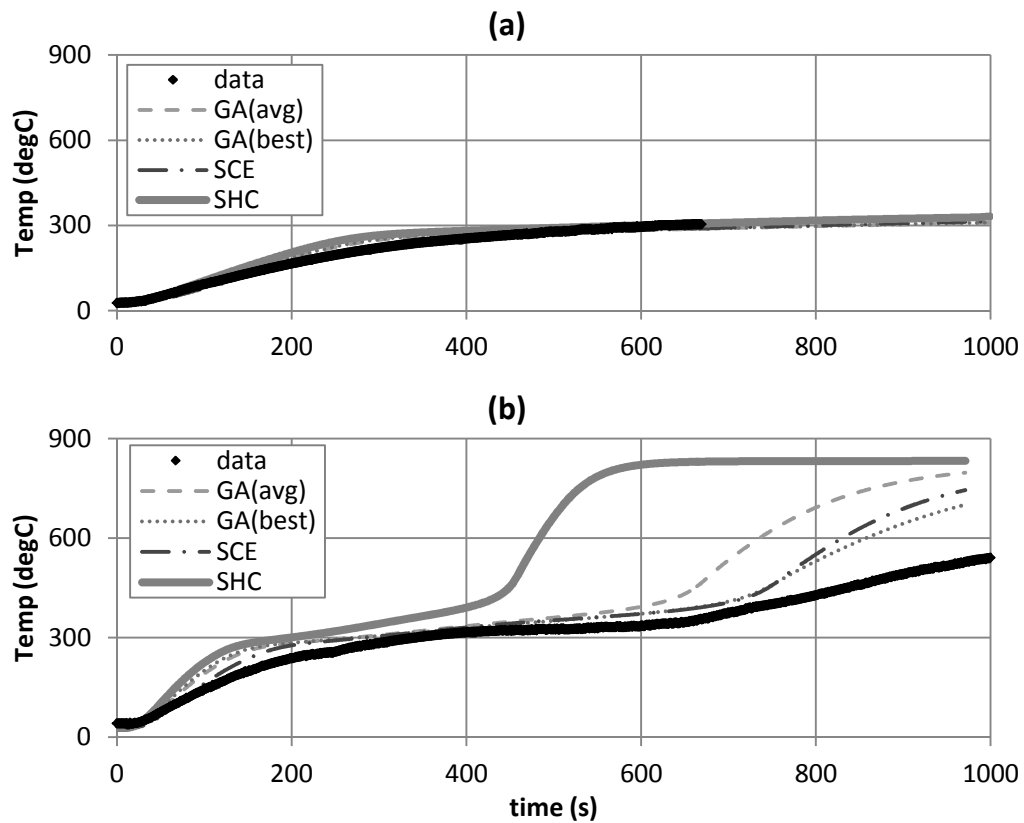


Figure 5-32. Back-surface-temperature (T_{back}) comparisons for FRP composite with modified acrylic resin with high-charring inorganic additive between actual T_{back} from experiment (data) and modeled T_{back} (GA, SCE, SHC) at applied heat flux of (a) 25 and (b) 75 kW/m². Note that data shown were not included in the model-parameter-estimation process; hence, these two cases are considered as extrapolation cases.

5.3.3 Commentary

GENERAL COMMENTS

- TG/DTG
 - Good agreement between simulated TG/DTG thermograms and those of actual from TGA experiment is shown when thermal decomposition kinetics is modeled using multiple heating rate data.
 - Proposed kinetic model does not account for minor mass loss at relatively lower and higher temperature range.
- Comparison between Data and Computed Modeling Outputs
 - Modeled peak MLRs are all in quantitative agreement with data considering its uncertainty.
 - Avg MLRs of modeling are in good agreement with data except for that of SHC
 - Modeled time to peak MLRs are all in quantitative agreement with data
 - Modeled surface temperatures at earlier time ($\tau = 1 \text{ s/mm}^2$) show good agreement with data while at later times ($\tau = 3$ and 5 s/mm^2) modeling results deviates from experiment results; however, considering that there is flame interfering with data collection from surface thermocouple, uncertainty in data should probably be larger.
 - Modeled back-surface temperatures at different times from GA(avg) show good agreement with data considering the modeling uncertainty. Those from GA(best), SCE and SHC are off by $\sim 10 \text{ }^\circ\text{C}$ from experiment results.
- MLR
 - Optimization at $\text{HF} = 50 \text{ kW/m}^2$: Generally good agreement exists between experiment data and all modeling results considering the trend, except for that of SHC indicating that optimization of SHC was close to being unsuccessful.
 - Extrapolation at $\text{HF} = 25 \text{ kW/m}^2$: Good agreement exists between experiment data and all modeling results. All of the modeling cases are able to capture the slow increase in mass-loss rate in the earlier times after exposure to heating source and a jump near 1000 s due to ignition.
 - Extrapolation at $\text{HF} = 75 \text{ kW/m}^2$: Good agreement exists between experiment data and all modeling results, except for SHC case. SHC's prediction is slightly higher than data and predictions from other cases; however, considering the uncertainty in the data, this falls within the acceptable bounds.
- Surface Temperature
 - Optimization at $\text{HF} = 50 \text{ kW/m}^2$: Generally good agreement exists between experiment data and all modeling results considering the trend, even for that of SHC. Note that after ignition (post-ignition stage) the flame interferes with data reading of thermocouple on surface.

- Extrapolation at $HF = 25 \text{ kW/m}^2$: Good agreement exists between experiment data and all modeling results.
- Extrapolation at $HF = 75 \text{ kW/m}^2$: Good agreement exists between experiment data and all modeling results, except for SHC case.

LIMITATION IN MODELING

- When considering limitation of the parameters in modeling this fire-retarded FRP composite, the modeler should take into account the applicability of the parameters and their associated uncertainties. For example, any assumptions used when determining a parameter value via experiment direct or indirect measurements can be utilized to understand when the parameter value becomes inappropriate. For this example, most consideration can be given to the parameters related to decomposition kinetics. One should be cautious that these findings can cause this FRP composite to behave differently under changing conditions, which were not included in the parameter-estimation process.
- First, the reaction-order-type kinetic model can be used to fit the DTG data with some degree of satisfaction for all reactions (see +A-R and R). However, the estimated reaction order is high as 5 for +A-R reaction. This indicates that the model is forced to fit the data, knowing that the reaction order in this magnitude is rare to find in the literatures. Also, the DSC data confirms that the reaction-order-type model was inappropriate for +A-R as well. Although the model is giving high correlation coefficients between the data and modeling for +A-R reaction, the DSC data show that +A-R should exist from 200°C and end before 400°C , where a strong endotherm is observed. When the data is fit with a reaction-order-type kinetic model, the additive decomposition temperature range extends beyond 400°C , ending near 600°C .
- Second, the decomposition of the additive reaction is best described by a kinetic model that describes a diffusion-controlled reaction (Jander's type model). The model type is reasonable considering that the model simulates the weight loss to be slow initially with respect to temperature increase and decays relatively fast after the weight-loss rate peak. This modeling becomes suitable for an additive decomposing within a resin-polymer system resulting in a time delay due to the time necessary to degrade the polymer near the additive. Consider the additive being mixed within the resin polymer. For the additive to undergo a decomposition reaction, the degradation of the resin polymer should occur simultaneously, because the additive is aggregated within the resin. Having the additive decomposition temperature lower than that of the resin, the decomposition of the additive is delayed until the temperature is higher to allow the resin to decompose. When this model is actually applied, it provides good estimate of the slow weight loss at the initial stage near 200°C and the temperature range for the entire reaction. Additionally, when this model is used,

the modeling results for weight-loss rate after 300°C matches well with the actual DTG data together with R reaction described with a reaction-order-type kinetic model.

- Third, although kinetic modeling has been conducted to give best fitness between the modeling and the DTG data obtained over various heating rates (5 to 60°C/min), assuming that the kinetics are identical irrespective of heating rates, changes in the kinetic over four heating rates have been noticed. At lower heating rates, the portion of the sample weight consumed via R_residue oxidation increases where at higher heating rates it decreases. This can be explained by understanding that the R_residue oxidation reaction is controlled by oxygen diffusion from the ambient to the condense phase. At a low heating rate, more time is available for oxygen diffusion with respect to temperature change, allowing an increase in the weight loss due to oxidation. However, when the heating rate is higher, the conditions become the opposite and pyrolysis reaction (R) dominates. The fitness of the model to DTG data increases when this effect is accounted for in the modeling.

Example 5.4 Modeling Plywood

5.4.1 Model Parameter Table

Parameter		Unit	Comparable Non-optimization and Manual Optimization		
Thermo-physical Property	i = 1 (water)	ρ_i	kg/m ³	1000 Reference ⁵⁷	
		k_i	W/m-K	0.6 Reference ⁵⁷	
		c_i	J/kg-K	4200 Reference ⁵⁷	
	i = 2 (dry_wood)	ρ_i	kg/m ³	504 ± 10 Measurement	
		k_i	W/m-K	0.26 Manual Optimization with Initial Guess of 0.122 Measured at 20 °C (dry_wood, ASTM C518/E1225)	
		c_i	J/kg-K	2400 Manual Optimization with Initial Guess of 1200 Measured at 20 °C (dry_wood, ASTM E1269)	
	i = 3 (char)	ρ_i	kg/m ³	173 Measurement	
		k_i	W/m-K	0.12 Manual Optimization with Initial Guess of 0.122 Measured at 20 °C (dry_wood, ASTM C518/E1225)	
		c_i	J/kg-K	3700 Manual Optimization with Initial Guess of 1200 Measured at 20 °C (dry_wood, ASTM E1269)	
	Optical Property	i = 1 (water)	ε_i	-	1.00 Approximated
					i = 2 (dry_wood)
		i = 3 (char)	κ_i	/m	
ε_i					-
		ε_i	-	1.00 Approximated	
Kinetics and Heats				k = 1 water → vap↑	n_k
	Z_k	/s	2.5 x 10 ¹²		
	E_k	J/mol	83 x 10 ⁴		
	ΔH_k	kJ/kg	2500 ± 800 (30%) Measurement, DSC		

	k = 2 dry_wood → char + vap ↑	n_k	-	1.7	Model Fitting with Multiple-Heating-Rate TGA Data
		Z_k	/s	5.0×10^{16}	
		E_k	J/mol	2.10×10^5	
		ΔH_k	kJ/kg	631	
	Manual Optimization				
Model-Dependent Parameter	Υ (i=3)	m	0.0036		
			Manual Optimization		

5.4.2 Validation

5.4.2.1 MODELING GOAL

Estimate model parameters for conducting modeling of pyrolysis of plywood under various heating rates – heat-flux levels ranging from 25 kW/m² to 75kW/m².

5.4.2.2 MODEL TYPE

GPYRO

5.4.2.3 MODELING APPROACH

- Instantaneous release of volatiles from solid to the gas phase
- Local thermal equilibrium between the solid and the volatiles
- No condensation of gaseous products
- No porosity effects
- When conducting the GPYRO simulation for the cone calorimeter set-up, metal edge frame will be ignored and backing is insulated. The ignition phenomenon is interpreted as the following in the simulations: at a known time-of-ignition (from experiment data), additional heat flux of 20 kW/m² is applied to the surface to simulate heat flux from the flame. This value is estimated from a measurement from this material pyrolyzing in the cone with a total-heat-flux gauge measuring heat flux impinging on the sample surface. Figure 5-33 shows the total-heat-flux measurement from sample surface (test conducted at 50 kW/m² applied heat flux). From the time-of-ignition ($\tau \sim 0.1$ s/mm²) an increase above the 50 kW/m² line in measured heat flux is observed due to flame. The oscillation in data in the time interval of ignition to $\tau = 1$ s/mm² is an artifact due to water evaporation, which had condensed near the water-cooled heat-flux gauge.

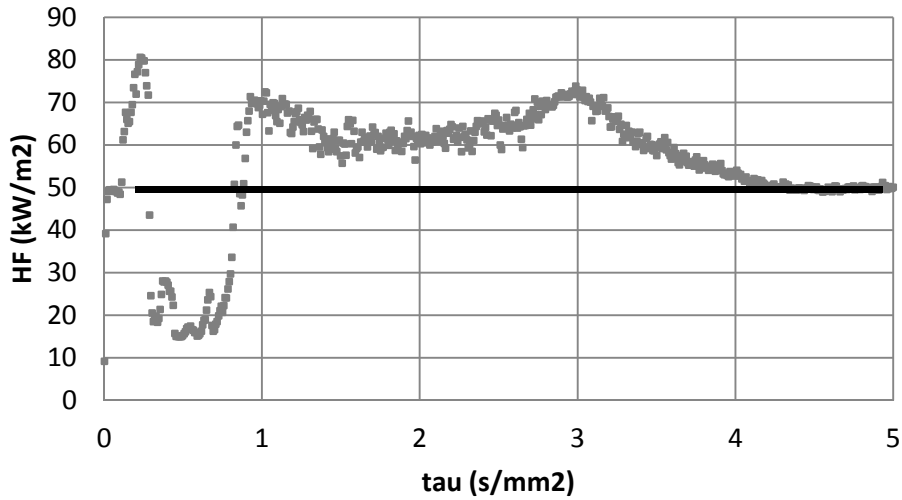


Figure 5-33. Total heat flux measured from sample surface during cone calorimeter test

- For the back surface, an additional layer of insulation with known properties is modeled to simulate some heat loss through the back. The contact resistance (h_{crz}) between the FRP composite and the insulation is estimated as roughly 10 W/m²K and that of insulation layer and ambient as 1 W/m²K.
- In addition to the parameters introduced in the previous section (see parameter table), the model (GPYRO) has a coefficient (γ , GAMMA) that is used to model radiative heat transfer through the pores. This parameter with T3 is a model dependent parameter that is added as another term in the effective thermal conductivity. γ is used for porous fiberglass and decomposed solid species, which results in a more porous state due to the weight loss; therefore, more radiative heat transfer through the gas phase pores, i.e., for condense phase specie $i = 2$ (char).

5.4.2.4 EXPERIMENT DESCRIPTION

Cone Calorimeter Test

5.4.2.5 DATA SET

- Cone calorimeter (cone) test data of plywood (thickness, δ is 11.1 ± 0.1 mm, density, ρ is 540 ± 10 kg/m³) impinged with effective heat fluxes (EHF) of 25 to 75 kW/m² is obtained and are shown below for mass-loss rate (MLR), surface and back face temperature measurements (see Figure 5-34):

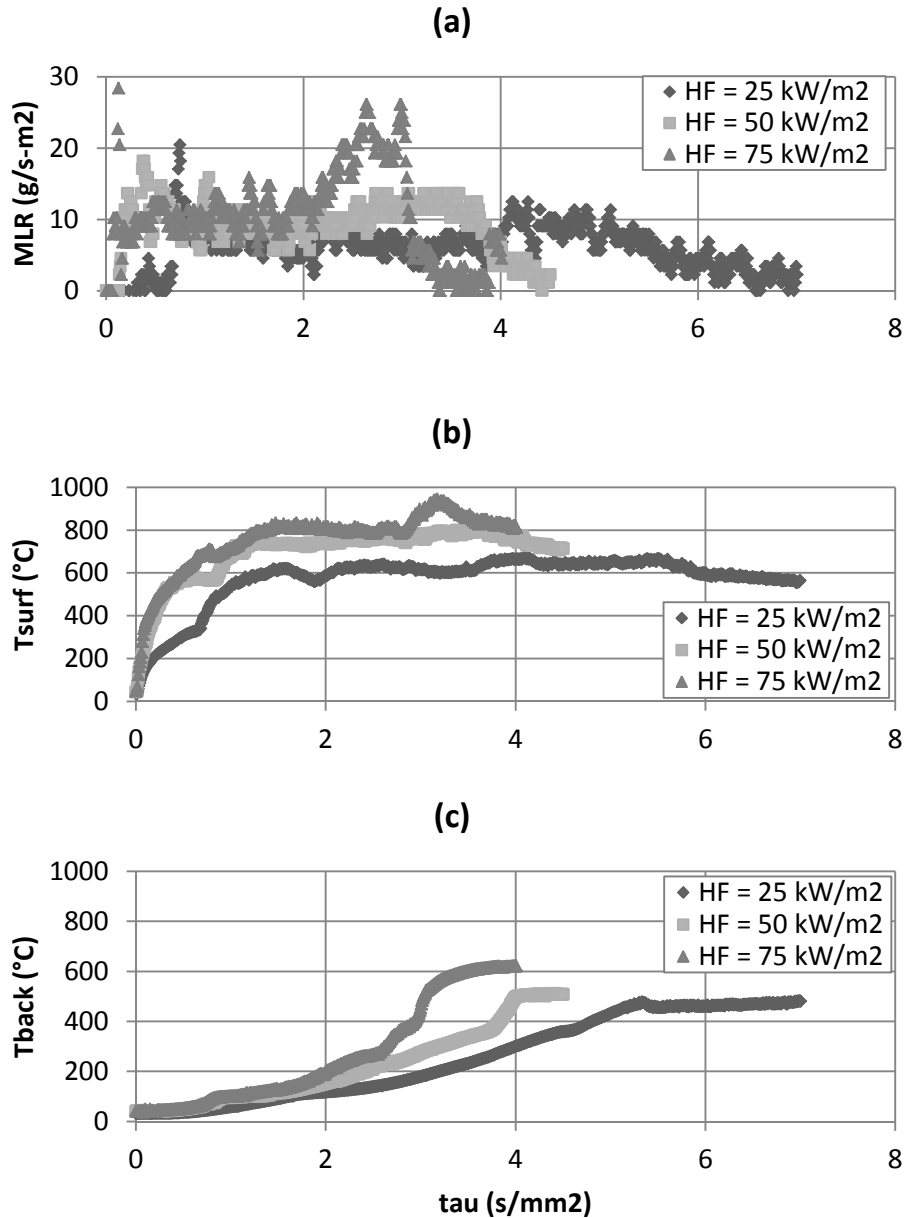


Figure 5-34. Cone calorimeter (cone) test data of plywood (thickness, δ is 11.1 ± 0.1 mm, density, ρ is 540 ± 10 kg/m³) impinged with effective heat fluxes (EHF) of 25 to 75 kW/m²

5.4.2.6 OPTIMIZATION TARGETS

Mass-loss rate (MLR), surface (T_s), and back (T_b) surface temperature data with plywood sample from cone calorimeter test at $HF = 50 \text{ kW/m}^2$

5.4.2.7 SENSITIVE PARAMETERS

- $\varepsilon_i, \rho_{i=2}, \Delta H_k$
- Kinetic parameters are considered to be certain in this example case.

5.4.2.8 UNCERTAINTY

Uncertainty in Experiment Data

- Data is acquired from two repeating cone tests of plywood under 50 kW/m^2 heat flux level.
- The uncertainties in the MLR and thermocouple measurements at front surface were quantified by comparing data from these two identical FRP composite tests. Note that the effect of different sample thicknesses was considered to be negligible for sample thicknesses in two tests were 11.1 and 11.2 mm. Because the data is transient, the standard deviation at each time step was calculated. Then these are averaged and multiplied by 2 to estimate uncertainty: uncertainty in MLR, T_s and T_b are $\pm 3.4\text{g/sm}^2$, $\pm 54 \text{ }^\circ\text{C}$ and $\pm 27 \text{ }^\circ\text{C}$, respectively.
- Assume:
 - Uncertainties are comparable to the same sample tested at various heat-flux levels
 - Data set found above is close to the averaged curves from multiple identical tests under same conditions

Uncertainty in Modeling Outputs

- Baseline case: $HF = 50 \text{ kW/m}^2$, thickness = 8.7 mm
- Sensitive parameters – density of dry_wood and char, emissivity of water, dry_wood and char, heat-of-reaction for drying process, and thermal decomposition of dry_wood to char – varied one at a time from baseline to its max and min: $\pm 10\%$ of estimated value or uncertainty limits found from measurement experiment.
- Kinetic parameters are considered to be certain in this example
- Integration of uncertainty is calculated by the Law of Propagation of Uncertainty: uncertainty in model's MLR, T_s and T_b are $\pm 7.2\text{g/sm}^2$, $\pm 57 \text{ }^\circ\text{C}$ and $\pm 157 \text{ }^\circ\text{C}$ respectively.

5.4.2.9 TG / DTG PREDICTIONS AT 20 °C/MIN HEATING RATE USING ESTIMATED KINETIC PARAMETERS

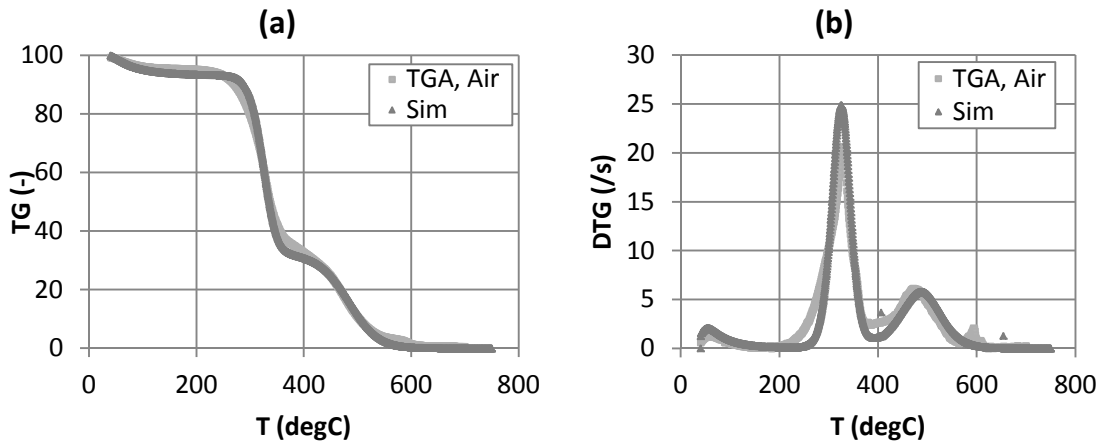


Figure 5-35. TG/DTG curves at 20°C/min heating rate with different estimation results for kinetic parameters for thermal decomposition of plywood: testing of plywood sample (~10mg) with air purge

* Note that only the first two peaks in the DTG curve in $T < 400^{\circ}\text{C}$ have been included in kinetic modeling for simplification of the parameter-estimation problem. This approach is considered to be reasonable, knowing that the third peak is due to char oxidation (confirmed by comparing thermograms from nitrogen and air-purge runs) and while flame exists on the surface, it is commonly accepted that char oxidation becomes minimal due to the oxygen-diffusion-limiting condition.

5.4.2.10 COMPARISON BETWEEN DATA AND COMPUTED MODELING OUTPUTS

- Modeling is conducted for case with HF = 50 kW/m², thickness = 11.2 mm

Table 5-18. Comparison between experiment data from cone calorimeter test and modeling outputs using estimated parameter values via measurements and manual optimization

	Data (Based on 2 tests, uncertainty as 2 times standard deviation)	Measurements and Manual Optimization
Peak MLR (g/m ² s)	19.9 ± 4.8	18.1 ± 7.2
Avg MLR (g/m ² s)	6.8 ± 0.5	6.6 ± 7.2
t to pMLR (s)	81 ± 113	23
Ts at 100 s (°C)	604 ± 112	628 ± 57
Ts at 200 s (°C)	734 ± 10	670 ± 57
Ts at 300 s (°C)	732 ± 45	689 ± 57
Tb at 100 s (°C)	68 ± 20	56 ± 157
Tb at 200 s (°C)	118 ± 1	185 ± 157
Tb at 300 s (°C)	196 ± 10	291 ± 157

5.4.2.11 MODELING OUTPUT: MASS-LOSS RATE (MLR)

- Case used in optimization process

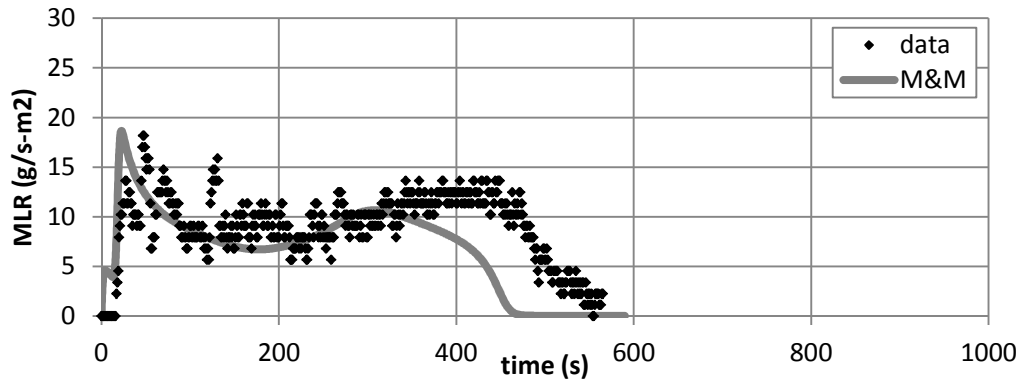


Figure 5-36. Mass-loss rate (MLR) comparisons for FRP composite with plywood between actual MLR from experiment (data) and modeled MLR (M&M) at applied heat flux of 50 kW/m². Note that data shown were used to estimate model-parameter values via manual optimization.

- Extrapolation

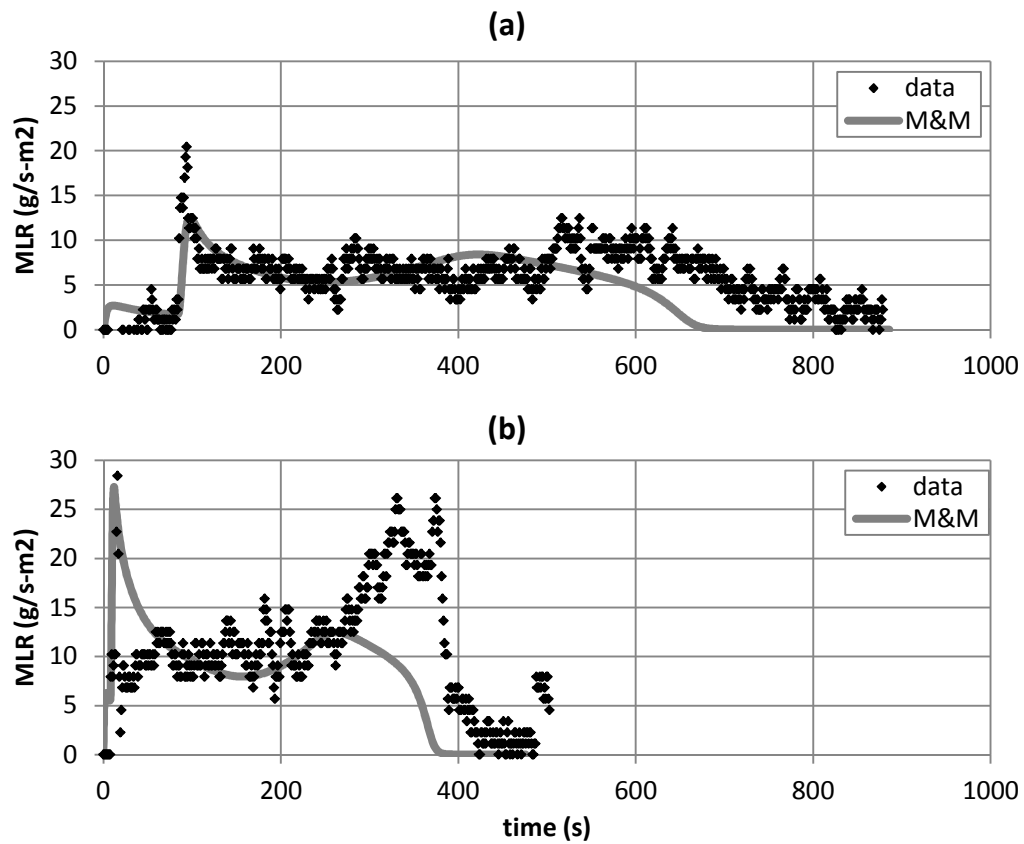


Figure 5-37. Mass-loss rate (MLR) comparisons for FRP composite with plywood between actual MLR from experiment (data) and modeled MLR (M&M) at applied heat flux of (a) 25 and (b) 75 kW/m². Note that data shown were not included in the model-parameter-estimation process; hence, these two cases are considered as extrapolation cases.

5.4.2.12 MODELING OUTPUT: SURFACE TEMPERATURE (T_{SURF})

- Case used in optimization process

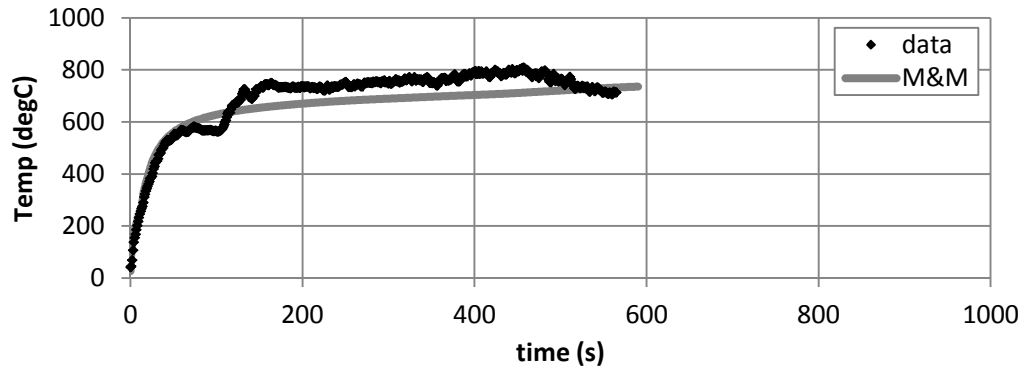


Figure 5-38. Surface-temperature (T_{surf}) comparisons for plywood between actual T_{surf} from experiment (data) and modeled T_{surf} (M&M) at applied heat flux of 50 kW/m^2 . Note that data shown were used to estimate model-parameter values via manual optimization.

- Extrapolation

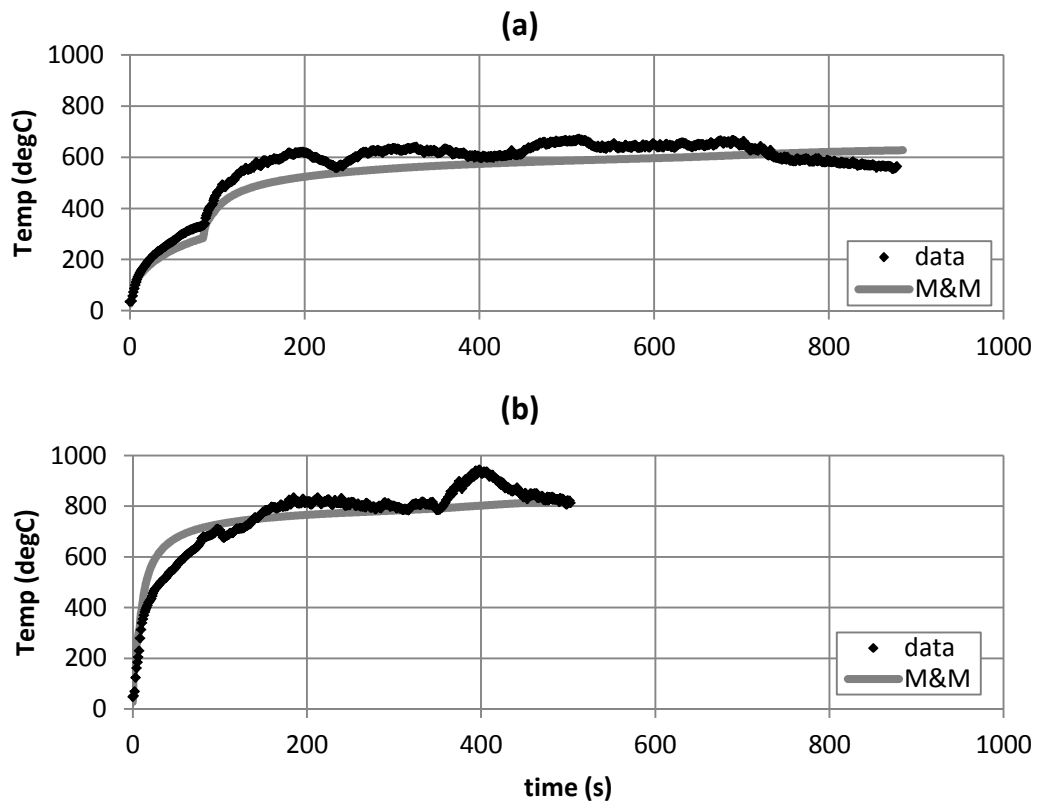


Figure 5-39. Surface-temperature (T_{surf}) comparisons for FRP composite with plywood between actual T_{surf} from experiment (data) and modeled T_{surf} (M&M) at applied heat flux of (a) 25 and (b) 75 kW/m². Note that data shown were not included in the model-parameter-estimation process; hence, these two cases are considered as extrapolation cases.

5.4.2.13 MODELING OUTPUT: BACK-SURFACE TEMPERATURE (T_{BACK})

- Case used in optimization process

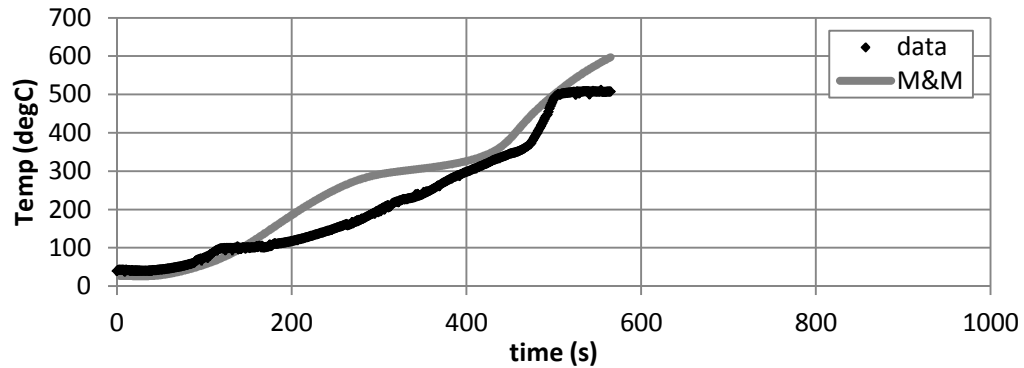


Figure 5-40. Back-surface-temperature (T_{back}) comparisons for plywood between actual T_{back} from experiment (data) and modeled T_{back} (M&M) at applied heat flux of 50 kW/m^2 . Note that data shown were used to estimate model-parameter values via manual optimization.

- Extrapolation

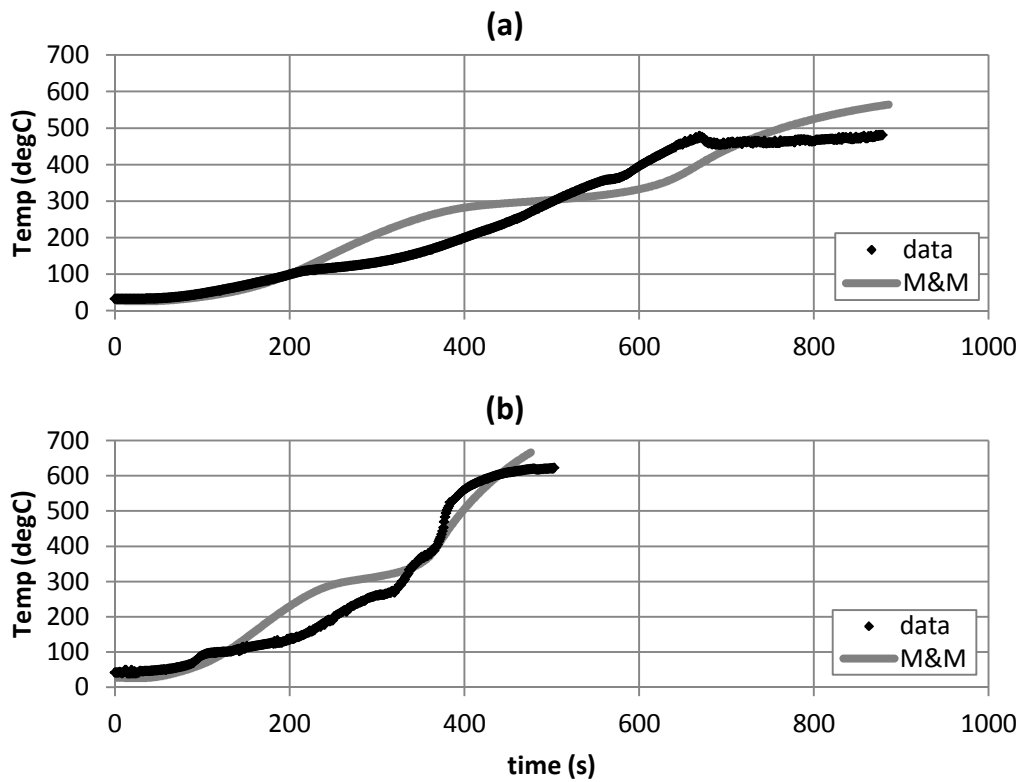


Figure 5-41. Back-surface-temperature (T_{back}) comparisons for plywood between actual T_{back} from experiment (data) and modeled T_{back} (M&M) at applied heat flux of (a) 25 and (b) 75 kW/m². Note that data shown were not included in the model-parameter-estimation process; hence, these two cases are considered as extrapolation cases.

5.4.3 Commentary

GENERAL COMMENTS

- TG/DTG
 - Good agreement between simulated TG/DTG thermograms and those of actual from TGA experiment is shown when thermal decomposition kinetics is modeled using multiple heating-rate data.
 - Proposed kinetic model does not account for mass loss due to char oxidation at relatively higher temperature range ($T > 400^{\circ}\text{C}$).
- Comparison between Data and Computed Modeling Outputs
 - Modeled peak MLR, Avg MLR, time to peak MLR, and T_s and T_b at various times are all in quantitative agreement with data, considering its uncertainty.
- MLR
 - Optimization at $\text{HF} = 50 \text{ kW/m}^2$: Generally good agreement exists between experiment data and all modeling results, considering the trend. Some deviation of modeling results from data is shown at later times, where the second peak is observed in the MLR curve. Near this region, bending of the sample toward the front surface occurs with respect to a rapid temperature increase throughout the back surface. This phenomenon is strictly a 3D behavior, which is not explicitly accounted for in current 1D model. Additionally, mass loss due to minor char oxidation at this region is speculated, for flame height becomes smaller and bending of sample may allow an ease to oxygen diffusion to solid phase.
 - Extrapolation at $\text{HF} = 25 \text{ kW/m}^2$: Good agreement exists between experiment data and modeling results. Modeling is able to capture the initial mass-loss rate peak followed by a decrease qualitatively and quantitatively. A qualitative agreement between data and modeling results exists for the second mass-loss rate peak; however, actual sample in cone testing extends for a longer period of time ($\sim 100 \text{ s}$), while in modeling burn out time occurs earlier. This is probably due to excluding char oxidation in kinetic modeling.
 - Extrapolation at $\text{HF} = 75 \text{ kW/m}^2$: Good agreement exists between experiment data and modeling results, except for the second peak in mass-loss rate curve. See above for discussion.
- Surface Temperature
 - Optimization at $\text{HF} = 50 \text{ kW/m}^2$: Generally good agreement exists between experiment data and modeling results, considering the trend. Note that after ignition (post-ignition stage) the flame interferes with data reading of thermocouple on surface.
 - Extrapolation at $\text{HF} = 25 \text{ kW/m}^2$: Good agreement exists between experiment data and modeling results.

- Extrapolation at $HF = 75 \text{ kW/m}^2$: Good agreement exists between experiment data and modeling results.

LIMITATION IN MODELING

- When considering limitation of the parameters in modeling this plywood, the modeler should take into account the applicability of the parameters and their associated uncertainties. For example, any assumptions used when determining a parameter value via experiment direct or indirect measurements can be utilized to understand when the parameter value becomes inappropriate. For this example, most consideration can be given to the parameters related to decomposition kinetics. One should be cautious that these findings can cause this FRP composite to behave differently under changing conditions, which were not included in the parameter-estimation process.
- In this example, drying is simplified as a heterogeneous reaction (i.e., an Arrhenius law temperature-dependent evaporation rate), which occurs near $100 \text{ }^\circ\text{C}$ based on TGA experiment results. However, water evaporation from a wet wood is governed by transport phenomena of liquid-phase water and vapor diffusion. Additionally, typically the water travels toward the back surface during heating and re-condensation may occur, allowing the back surface to be colder. This phenomenon will not be captured in this modeling.
- Any char oxidation has been considered to be minimal in this example, considering that with a flame sheet on material surface, oxygen diffusion becomes limited. However, when analyzing the cone calorimeter results, some oxidation is speculated, for the sample loses ~ 4 to 6% more of the initial sample weight comparing to TGA experiment.

REFERENCES

- ¹ McGrattan, Kevin; Hostikka, Simo; Floyd, Jason; Baum, Howard; Rehm, Ronald ; Mell, William; and McDermott, Randall, Fire Dynamics Simulator (Version 5) Technical Reference Guide, NIST Special Publication 1018-5, October 29, 2010.
- ² Stolarov, S.I.; and Lyon, R.E., Federal Aviation Administration Technical Note, DOT/FAA/AR-TN08/17, 2008; available for download at <http://www.fire.tc.faa.gov/reports/reports.asp>.
- ³ Lautenberger, C., Gpyro – A Generalized Pyrolysis Model for Combustible Solids, Technical Reference, Version 0.700, February 19, 2009.
- ⁴ Siegel, R.; and Howell, J.R., Thermal Radiation Heat Transfer. Taylor & Francis, New York, 4th edition, 2002.
- ⁵ Atkins, P.W., *Physical Chemistry*, W.H. Freeman and Company, San Francisco, CA, 1978, 582-611.
- ⁶ Lautenberger, C., Gpyro – A Generalized Pyrolysis Model for Combustible Solids, Users' Guide, Version 0.700, February 19, 2009.
- ⁷ Adl-Zarrabin, B., *et al.*, "Using the TPS Method for Determining the Thermal Properties of Concrete and Wood at Elevated Temperature," *Fire and Materials*, 30:359-369, 2006.
- ⁸ Gustafsson, S., "Transient Plane Source (TPS) Technique for Thermal Conductivity and Thermal Diffusivity Measurements of Solid Materials," *Review of Scientific Instruments*, 62:797–804, 1991.
- ⁹ Gustafsson, S.; and Long, T., "Transient Plane Source (TPS) Technique for Measuring Thermal Properties of Building Materials," *Fire and Materials*, 19:43–49, 1995.
- ¹⁰ Bentz, D., *et al.*, "A Slug Calorimeter for Evaluating the Thermal Performance of Fire Resistive Materials," *Fire and Materials*, 30:257-270, 2006.
- ¹¹ Bentz, D., *et al.*, "Towards a Methodology for the Characterization of Fire Resistive Materials with Respect to Thermal Performance Models," *Fire and Materials*, 30:311-321, 2006.
- ¹² Liu, W., *et al.*, "Understanding the Decomposition and Fire Performance Processes in Phosphorus and Nanomodified High Performance Epoxy Resins and Composites," *Polymer*, 48:2345-2354, 2007.
- ¹³ Kashiwagi, T., *et al.*, "Flame Retardant Mechanism of Polyamide-6 Nanocomposites," *Polymer*, 45:881-891, 2004.
- ¹⁴ Gilman, J., *et al.*, "A Study of the Flammability Reduction Mechanism of Polystyrene-Layered Silicate Nanocomposite: Layered Silicate Reinforced Carbonaceous Char," *Polym. Adv. Technol.*, 17:263-271, 2006.
- ¹⁵ Zanetti, M., *et al.*, "Cone Calorimeter Combustion and Gasification Studies of Polymer Layered Silicate Nanocomposites," *Chem. Mater.*, 14:881-887, 2002.
- ¹⁶ Lyon, R.E.; Safronava, N.; and Oztekin, E., A simple method for determining kinetic parameters for materials in fire models. *Fire Saf Sci* 2011; 10: 765–777.
- ¹⁷ Ozawa, T., "A new method of analyzing thermogravimetric data," *Bull. Chem. Soc. Jpn.*, 38:1881–1886, 1965.
- ¹⁸ Flynn, J.H.; and Wall, L.A., "A quick, direct method for the determination of activation energy from thermogravimetric data," *J. Polym. Sci. Polym. Lett.*, 4:323–328, 1966.
- ¹⁹ Friedman, H. L., "Kinetics of thermal degradation of char-forming plastics from Thermogravimetry. Application to a phenolic plastic," *J. Polym. Sci., Pt. C* 6, 183-195, 1964.
- ²⁰ Flynn, J.H.; and Wall, L.A., "A quick, direct method for the determination of activation energy from thermogravimetric data," *J. Polym. Sci. Polym. Lett.* 4, 323-328, 1966.
- ²¹ Vyazovkin, S.V.; and Lesnikovich, A.I., *Thermochim. Acta*, 165 (1990) 273.
- ²² IUPAC Compendium of Chemical Terminology, 2nd ed. 1997 (<http://old.iupac.org/goldbook>)

-
- ²³ Galwey, Andrew K.; and Brown, Michael E., Arrhenius parameters and compensation behaviour in solid-state decompositions, *Thermochimica Acta*, Vol. 300, Issues 1–2, 15 October 1997, 107-115, ISSN 0040-6031, 10.1016/S0040-6031(96)03120-6.
(<http://www.sciencedirect.com/science/article/pii/S0040603196031206>)
- ²⁴ Odian, G., *Principles of Polymerization*, John Wiley & Sons, 3rd ed., 1991.
- ²⁵ Simms, D.L.; and Law, Margaret, The ignition of wet and dry wood by radiation, combustion and flame, Volume 11, Issue 5, October 1967, 377-388, ISSN 0010-2180, 10.1016/0010-2180(67)90058-2.
- ²⁶ Galgano, Antonio; and Di Blasi, Colomba, Modeling the propagation of drying and decomposition fronts in wood, combustion and flame, Vol. 139, Issues 1–2, October 2004, 16-27, ISSN 0010-2180, 10.1016/j.combustflame.2004.07.004.
- ²⁷ Khan, M.; De Ris, J.L.; and Ogden, S.D., Effect of moisture on ignition time of cellulosic materials, in: *Proceedings of the Ninth International Symposium on Fire Safety Science*, 2008, 167–178.
- ²⁸ Oztekin, Ezgi S.; Crowley, Sean B.; Lyon, Richard E.; Stoliarov, Stanislav I.; Patel, Parina; and Hull, T. Richard, Sources of variability in fire test data: A case study on poly(aryl ether ether ketone) (PEEK), *Combustion and Flame*, Vol. 159, Issue 4, April 2012, 1720-1731, ISSN 0010-2180, 10.1016/j.combustflame.2011.11.009.
- ²⁹ Takemori, M.T., (1984) *Polymer Fatigue*, *Ann Rev. Mater Sci* 14:171–204.
- ³⁰ Kim, E.; Dembsey, N.A.; and Dore, C.H., "Property Estimation for Pyrolysis Modeling Applied to Flame Retarded Modified Acrylic FRP Composites", in *Proceedings of Composites & Polycon 2010*, American Composites Manufacturers Association, Mandalay Bay, Las Vegas, NV, USA, 9-11 February, 2010, *Best Fire Technical Paper Award at Composites and Polycon 2010*
- ³¹ Kim, E.; Dembsey, N.I and Lautenberger, C., Parameter Estimation for Pyrolysis Modeling Applied to Polyester FRP Composites with Different Glass Contents, *Fire and Materials 2009*, 11th International Conference, 26-28 January 2009, Hyatt Hotel at Fishermans Wharf, San Francisco, CA, USA.
- ³² Chaos, Marcos; Khan, M.; Krishnamoorthy, N.; Chatterjee, P.; Wang, Y.; Dorofeev, Experiments and Modeling of Single- and Triple-Wall Corrugated Cardboard: Effective Material Properties and Fire Behavior, in *Fire and Materials 2011*, 12th International Conference and Exhibition, 31 January–2 February 2011, Fisherman's Wharf, San Francisco, CA, USA.
- ³³ Lautenberger, C.; Rein, G.; and Fernandez-Pello, C., "The Application of a Genetic Algorithm to Estimate Material Properties", *Fire Safety Journal* 41 (2006), 204–214.
- ³⁴ Matala, A., "Estimation of Solid Phase Reaction Parameters for Fire Simulation," MS Thesis, University of Technology, Helsinki, 2008.
- ³⁵ Webster, R., "Pyrolysis Model Parameter Optimization using a Customized Stochastic Hill-Climber Algorithm and Bench Scale Fire Test Data," MS Thesis, University of Maryland, 2009.
- ³⁶ Aster, Richard C.; Borchers, Brian; and Thurber, Clifford H, Preface, in Aster, Borchers; Thurber, (Eds.) *International Geophysics*, Academic Press, 2005, Volume 90, Parameter Estimation and Inverse Problems, Pages xi-xii, ISSN 0074-6142, ISBN 9780120656042, DOI: 10.1016/S0074-6142(05)80014-2.
- ³⁷ Stoliarov, S. I.; Safronava, N.; and Lyon, R. E., (2009), The effect of variation in polymer properties on the rate of burning. *Fire and Materials*, 33: 257–271. doi: 10.1002/fam.1003.
- ³⁸ Chaos, M.; Khan, M.M.; Krishnamoorthy, N.; de Ris, J.L.; and Dorofeev, S.B., Material Properties for CFD Fire Models, FM Global Open Source CFD Fire Modeling Workshop 2010, <http://docs.google.com/viewer?a=v&pid=sites&srcid=ZGVmYXVsdGRvbWFpbnxmaXJlbW9kZWxpbmd3b3Jrc2hvcHxneDo0NGE0YTlkOWQ3OGUzYWQw>.

-
- ³⁹ Cacuci, Dan G.; Ionescu-Bujor, Mihaela; and Navon, Ionel Micheal, *Sensitivity and Uncertainty Analysis; Theory; Volume 1*, Chapman & Hall / CRC Taylor & Francis Group, c 2005.
- ⁴⁰ Cacuci, Dan G.; Ionescu-Bujor, Michael; and Navon, Ionel Micheal, *Sensitivity and Uncertainty Analysis; Applications to Large-Scale Systems; Volume 2*, Chapman & Hall / CRC Taylor & Francis Group, c 2005.
- ⁴¹ Saltelli, A.; Chan, K.; and Scott, E.M., *Sensitivity Analysis*, Wiley, c 2000.
- ⁴² Duan, Q.; Gupta, V.K.; and Sorooshian, S., 1993, Shuffled Complex Evolution Approach for Effective and Efficient Global Minimization, *Journal of Optimization Theory and Applications* 76, 501-521.
- ⁴³ Chaos, M.; Khan, M.M.; Krishnamoorthy, N.; de Ris, J.L.; and Dorofeev, S.B., Bench-Scale Flammability Experiments: Determination of Material Properties Using Pyrolysis Models for Use in CFD Fire Simulations in *Interflam 2010*, July 5-7, 2010, Nottingham, UK.
- ⁴⁴ Chaos, M.; Khan, M.M.; Krishnamoorthy, N.; de Ris, J.L.; and Dorofeev, S.B., 2010, Evaluation of Optimization Schemes and Determination of Solid Fuel Properties for CFD Fire Models using Bench-scale Pyrolysis Tests, *Proceedings of the Combustion Institute* 33, in press, doi:10.1016/j.proci.2010.07.018.
- ⁴⁵ Brandrup, J.; Immergut, E.H.; Grulke, E.A.; Abe, A.; and Bloch, D.R., (Eds.) *Polymer Handbook*, fourth ed., John Wiley & Sons, New York, 1999.
- ⁴⁶ Stoliarov, S.I.; and Walters, R.N., *Polym. Degrad. Stab.* 93 (2008), 422–427.
- ⁴⁷ Brandrup, J.; Immergut, E.H.; Grulke, E.A.; Abe, A.; and Bloch, D.R., (Eds.) *Polymer handbook*. 4th edition, New York: John Wiley and Sons; 1999.
- ⁴⁸ Stoliarov, Stanislav I.; Crowley, Sean; Lyon, Richard E.; and Linteris, Gregory T., Prediction of the burning rates of non-charring polymers, *Combustion and Flame*, Vol. 156, Issue 5, May 2009, 1068-1083, ISSN 0010-2180, DOI: 10.1016/j.combustflame.2008.11.010.
- ⁴⁹ Beaulieu, P.A.; and Dembsey, N.A., "Effect of Oxygen on Flame Heat Flux in Horizontal and Vertical Orientations", *Fire Safety Journal*, 43:6 (2008) 410-428.
- ⁵⁰ ASTM Standard D 7309-07, Test Method for Determining Flammability Characteristics of Plastics and Other Solid Materials Using Microscale Combustion Calorimetry, ASTM International, West Conshohocken, PA, 2007.
- ⁵¹ Kashiwagi, T.; and Ohlemiller, T.J., "A study of oxygen effects on nonflaming transient gasification of PMMA and PE during thermal irradiation," *Proceedings of the Combustion Institute*, 19: 815–823, 1982.
- ⁵² Kashiwagi T., Polymer combustion and flammability—role of the condensed phase. *Twenty-fifth Symposium (International) on Combustion*, Irvine, CA, 1994, 1423–1437.
- ⁵³ Kulshreshtha, Anand K.; and Vasile, Cornelia, *Handbook of polymer blends and composites*.
- ⁵⁴ Lewin, M., Synergism and Catalysis in Flame Retardancy of Polymers, *Polym. Adv. Technol.* 12, 215-222 (2001).
- ⁵⁵ LeVan, S.L., *The Chemistry of Solid Wood*; Chapter 14, *Chemistry of Fire Retardancy*, American Chemical Society, 1984.
- ⁵⁶ Standard Test Method for Surface Burning Characteristics of Building Materials, ASTM E 84-05, ASTM, 100 Barr Harbor Drive, West Conshohocken, PA, U.S.
- ⁵⁷ NIST Chemistry WebBook, <http://webbook.nist.gov/>.

Chapter 6–Conclusions

As an effort to create input data for fire models in a consistent manner and allow for compilation of accepted model input databases for various materials, a *Guide* for estimating material pyrolysis properties for fire modeling has been developed. The *Guide* provides standardized procedures for obtaining fire-model-input parameters related to the thermal decomposition of materials. Considering that these unknowns are dependent on the certain pyrolysis model of choice, this *Guide* describes a method to determine model type to be used for a material of interest (Chapter 2) followed by parameter-estimation procedures for three types of pyrolysis models: empirical (Chapter 3), simple analytical (Chapter 4), and comprehensive (Chapter 5) pyrolysis models.

Each chapter was designed to describe the pyrolysis-model type by presenting the modeling approach and assumptions used with its mathematical formulation identifying the model parameters to be obtained. This was followed by methods of estimating the unknown parameters via independent experiments for measurements or numerically using optimization routines. At the end, example cases are included for better understanding of the procedure discussed previously. For each example in the three chapters – Chapter 3, 4, and 5 – detailed problem solutions are given in the appendices.

Appendix A - Uncertainty Analysis

The objective of a measurement is to determine the value of the measurand, i.e., the physical quantity that needs to be measured. The value of the measurand is generally not obtained from a direct measurement, but is determined as a function (f) from N input quantities X_1, X_2, \dots, X_N (see Eq.A(A)-1):

$$Y = f(X_1, X_2, \dots, X_N) \quad \text{Eq.A(A)-1}$$

where

Y = true value of the measurand;

f = functional relationship between measurand and input quantities; and

X_i = true values of the input quantities ($i = 1 \dots N$).

The input quantities may be categorized as:

- quantities whose values and uncertainties are directly determined from single or repeated observation; or
- quantities whose values and uncertainties are brought into the measurement from external sources, such as reference data obtained from handbooks.

An estimate of the value of the measurand, y, is obtained from Eq.A(A)-1 using input estimates x_1, x_2, \dots, x_N for the values of the N input quantities (see Eq.A(A)-2):

$$y = f(x_1, x_2, \dots, x_N) \quad \text{Eq.A(A)-2}$$

The standard uncertainty of y is obtained by appropriately combining the standard uncertainties of the input estimates x_1, x_2, \dots, x_N . If all input quantities are independent, the combined standard uncertainty of y is given by Eq.A(A)-3:

$$u_c(y) = \sqrt{\sum_{i=1}^N \left[\left. \frac{\partial f}{\partial X_i} \right|_{x_i} \right]^2 u^2(x_i)} \equiv \sqrt{\sum_{i=1}^N [c_i u(x_i)]^2} \quad \text{Eq.A(A)-3}$$

where

u = standard uncertainty;

u_c = combined standard uncertainty; and

c_i = sensitivity coefficients.

Eq.A(A)-3 is referred to as the law of propagation of uncertainty^{1,2} and based on a first-order Taylor series approximation of $Y = f(X_1, X_2, \dots, X_N)$. When the nonlinearity of f is significant, higher-order terms must be included. When the input quantities are correlated, Eq.A(A)-3 must be revised to include the covariance terms. The combined standard uncertainty of y is then calculated from Eq.A(A)-4:

$$u_c(y) = \sqrt{\sum_{i=1}^N [c_i u(x_i)]^2 + 2 \sum_{i=1}^{N-1} \sum_{j=i+1}^N c_i c_j u(x_i) u(x_j) r(x_i, x_j)} \quad \text{Eq.A(A)-4}$$

Where

$r(x_i, x_j)$ = estimated correlation coefficient between X_i and X_{ij} .

Since the values of the input quantities are not known, the correlation coefficient is estimated on the basis of the measured values of the input quantities. The combined standard uncertainty in Eq.A(A)-3 and Eq.A(A)-4 is usually multiplied by a coverage factor to raise the confidence level, to obtain the “expanded” uncertainty. A multiplier of 2 is often used, which corresponds to a confidence level of approximately 95%.

The standard uncertainty of an input estimate x_i is obtained from the distribution of possible values of the input quantity X_i . There are two types of evaluations depending on how the distribution of possible values is obtained: Type A and Type B

TYPE A UNCERTAINTY

Type A uncertainty is also known as aleatory, stochastic, variability and irreducible uncertainty. This uncertainty is characterized by inherent randomness, which cannot be reduced further. Typically, Type A uncertainty is modeled with a probability distribution projected with repeated data acquisition, i.e., evaluation of this standard uncertainty of x_i is based on the frequency distribution, which is estimated from a series of n repeated observations $x_{i,k}$ ($k = 1 \dots n$). See Eq.A(A)-5:

$$u(x_i) \approx \sqrt{s^2(\bar{x}_i)} = \sqrt{\frac{s^2(\bar{x}_i)}{n}} = \sqrt{\frac{\sum_{k=1}^n (x_{i,k} - \bar{x}_i)^2}{n(n-1)}} \quad \text{Eq.A(A)-5}$$

TYPE B UNCERTAINTY

Type B uncertainty³ is also known as the state-of-knowledge uncertainty, subjective uncertainty, or reducible uncertainty. This uncertainty is characterized by the degree of understanding of the given problem, which is not directly based on repeated measurements. In this case the uncertainty is determined from previous measurements, experience or general knowledge, manufacturer specifications, data provided in calibration certificates, uncertainties assigned to reference data taken from handbooks, etc. Type B uncertainty can be reduced by increasing the understanding of the problem by collecting relevant data.

An example of taking into account for Type B uncertainty is considering the effect of different ignition scenarios in pyrolysis modeling using Empirical Models (see Chapter 3). To consider this effect, the modeler may conduct a series of experiments using different ignition scenarios that are plausible. Then modeler can decide to conduct modeling with the most sever scenario that may have a small but non-negligible probability of occurrence.

REFERENCES

¹ Taylor, B.N.; and Kuyatt, C.E., Guidelines for evaluating and expressing the uncertainty of NIST measurement results. *NIST Technical Note 1297*. NIST, Gaithersburg, MD, USA, 1994.

² 12. ISO. *Guide to the Expression of Uncertainty in Measurement*, ISBN 92-67-10188-9. International Organization for Standardization, Geneva, Switzerland, 1993.

³ Swiler, Laura P.; Paez, Thomas L.; and Mayes, Randall L., Epistemic Uncertainty Quantification Tutorial, http://dakota.sandia.gov/papers/294_swi.pdf

Appendix B - Example Solutions for Chapter 3

EXAMPLE 3.1 MODELING SOFA

Obtain Parameters via Experiment

Run model

SELECT MODEL: EMPIRICAL USING FULL-SCALE CALORIMETER DATA

UNDERSTAND EXPERIMENT

A furniture calorimeter typically consists of a weighing platform placed on the floor of the laboratory beneath a hood connected to an instrumented exhaust duct (see Figure A(B)-1). The specimen is placed on the platform and ignited with the specified ignition source. The products of combustion are collected in the hood and extracted through the exhaust duct. Measurements of the concentration of oxygen (and typically also carbon dioxide and carbon monoxide), flow rate (from bidirectional probe and thermocouple measurements) and light transmission in the exhaust duct are used to determine heat release and smoke-production rate as a function of time.

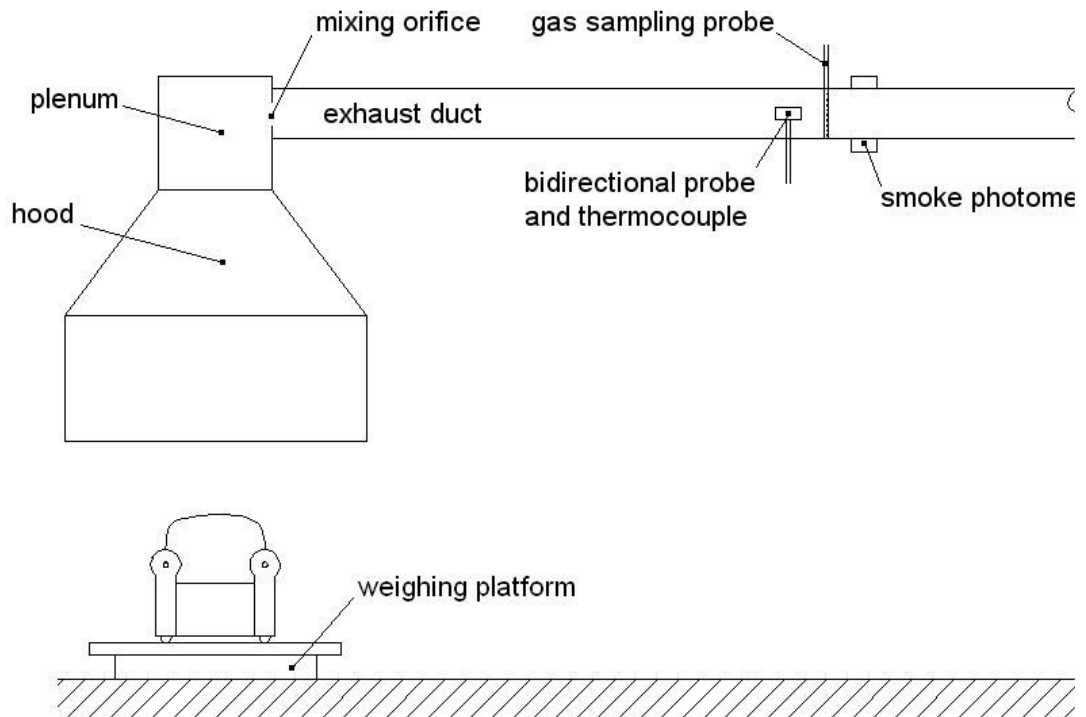


Figure A(B)-1. Schematic of a furniture calorimeter

Furniture calorimeters were initially developed in the 1980s. These calorimeters have since been used to obtain heat-release rate and related data for a wide range of other types of combustibles.³⁰

CONFIGURE MODEL CONDITIONS BASED ON UNDERSTANDING OF EXPERIMENT

In the model, the phenomena discussed above are simulated as below. Basic assumptions are as follows:

- Pre-ignition stage is
 - Inert: decomposition before ignition is neglected
 - Always the same as in furniture calorimeter test
- Ignition scenario is the same as in furniture calorimeter experiment: time-to-ignition is the same in modeling as determined in experiment
- Post-ignition stage is
 - Considered to have instantaneous release of volatiles from solid to gas phase: typically an area is specified that can be correlated to the actual burning object where energy is released to the gas phase
 - Considered to be the same as in furniture calorimeter test in terms of heat-release rate or mass-loss rate

ACQUIRE DATA SETS THAT CAN REPRESENT BURNING BEHAVIOR OF INTEREST

Experiment data of a single seat sofa mockup is found for pyrolysis modeling using Empirical Model. This sofa mockup was burnt under a hood of a furniture calorimeter. The mockup consisted of a steel frame with untreated polyurethane foam cushions (80% of the combustible mass) and a cotton fabric (20% of the combustible mass). Total combustible mass was 3.93 kg. The test was performed according to *ASTM E 1537* and *CAL TB 133*. The ignition source consisted of a 0.25 m square tubular propane burner producing a 19 kW flame for 80 seconds applied to the top of the seat cushion.

ESTIMATE UNKNOWNNS

1. Time-to-Ignition

Time-to-ignition of the furniture is found from the experiment procedure, where a propane burner producing a 19 kW flame is placed to the furniture for 80 sec. in the initial phase of the test.

2. HRR

To check repeatability of the data, four identical tests of the same sofa mockup have been conducted (see Figure A(B)-2). Using these data, an average heat-release rate is calculated at each time step and will be used as an input for pyrolysis modeling with Empirical Model for burning objects.

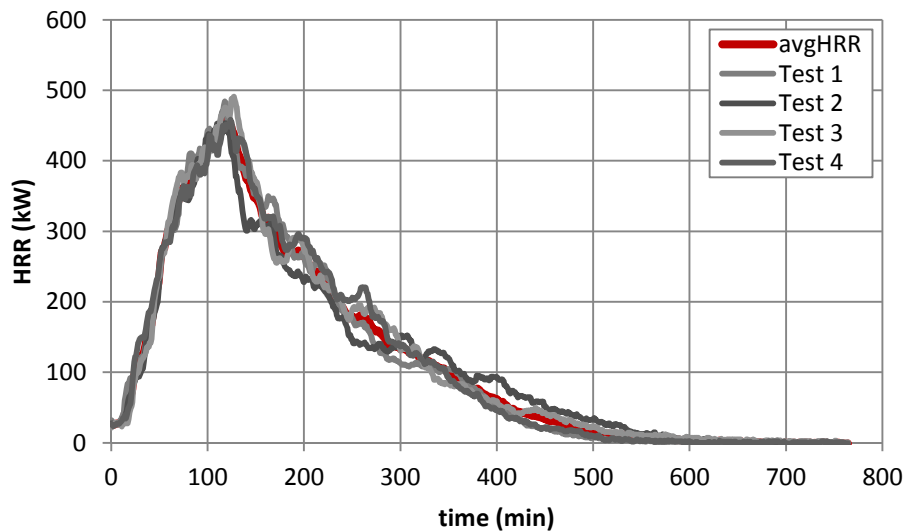


Figure A(B)-2. HRR curve from furniture calorimeter experiment of 4 identical tests of the same sofa mockup

Obtain Uncertainty for Estimated Parameters

Because time-to-ignition is directly given from the experiment procedure, this parameter can be considered as certain. For the uncertainty in HRR, uncertainty analysis is conducted based on above four data sets. The uncertainty of HRR is estimated by first calculating the confidence interval for 95% confidence level ($\alpha = 0.05$), assuming student t distribution with a sample size of three (four data sets) at each time step. Then an average confidence interval is calculated for the time interval of interest ($0 < t < 800$ min), which results in ± 20.4 kW.

Validation and Commentary

When using Empirical Model to simulate pyrolysis of a sofa, furniture-calorimeter test data has been utilized to estimate the time-to-ignition from exposure to a propane burner and the energy released from burning. As noted in the Understanding Model section of the chapter, this approach is limited as follows in terms of the conditions being comparable to those found in the fire scenario on interest:

- Ignition scenario and exposure conditions

A basic assumption used in empirical models is that the ignition scenario and exposure conditions in the fire are comparable to those used in the laboratory. Therefore, any changes made in the ignition scenario and exposure conditions have to be accounted for by the model user when applying the data to empirical models. The furniture-calorimeter experiment in this example is conducted under certain conditions: ignition is achieved by applying propane flame on the horizontal surface (seating cushion) for 80 s and sufficient supply of air is provided throughout its burning phase. To illustrate the effect of altering the conditions in HRR curves, two other HRR curves are shown below:

- Effect of ignition source strength:

Two identical single-seat sofas were obtained for testing (see Figure A(B)-3). In the first test the sofa was ignited with a 45 W butane gas flame applied to the center of the seat cushion for 20 s. In the second test 59 ml (2 oz) of gasoline was poured on the seat cushion to simulate an incendiary fire. The resulting heat-release-rate measurements are shown below. In this case the use of the weaker ignition source delays the propagation to full involvement

by approximately 170 s. For this case the effect of ignition-source strength can relatively easily be accounted for, although in practice it may not be trivial to determine the exact time period over which to shift the HRR curve. The effect can be much more pronounced when the source strength is close to the level needed to obtain sustained burning.

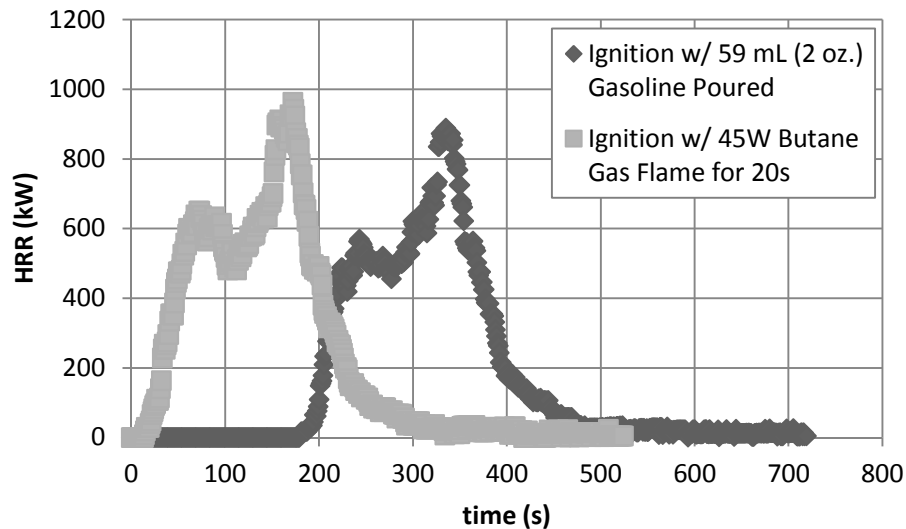


Figure A(B)-3. Effect of ignition source strength: single-seat sofas tested in furniture-calorimeter test with different ignition source – ignition with 59 mL gasoline poured (♦) or with 45 W butane gas flame (■)

○ Effect of ignition location:

Two tests were conducted on a steel-framed-seat sofa mockup according to the same procedure and using the same padding and fabric as in the tests described in this example case (see Figure A(B)-4). In the first test the burner flame was applied to the seat cushion on the right side. In the second test the burner was applied to the center seat cushion. The resulting HRR measurements are compared in Figure A(B)-4. In the first test the flames spread from the right side to the left side. When the flames reached the armrest on the left side, part of the material on the right side had already been consumed. This resulted in a relatively steady HRR that peaked slightly above 400 kW. In the second test the flames spread in two directions. As a result, the heat rate continuously increased until the two armrests ignited and a

peak heat-release rate of close to 1 MW was reached. This case illustrates that a seemingly small difference in the ignition scenario can have a surprisingly dramatic effect on fire growth.

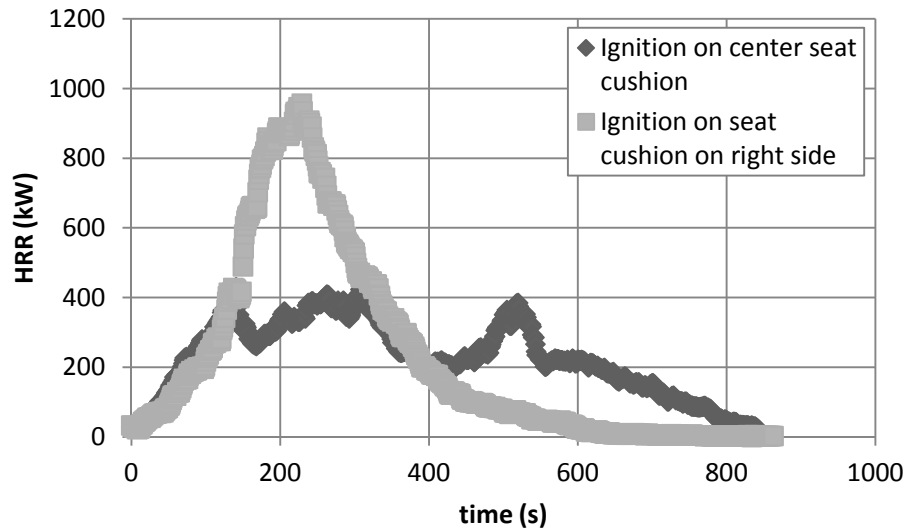


Figure A(B)-4. Effect of ignition location: steel-framed-seat sofa mockups tested in furniture-calorimeter test with different ignition location – ignition on center seat cushion (◆) or seat cushion on right side (■)

- Heat and mass transfer

This is a multi-dimensional problem, and the dimensional effect is implicitly addressed in modeling by a single parameter – HRR or MLR and effective heat of combustion.

EXAMPLE 3.2 MODELING PMMA

Obtain Parameters via Experiment

Run model

SELECT MODEL: EMPIRICAL USING BENCH-SCALE CALORIMETER DATA

UNDERSTAND EXPERIMENT

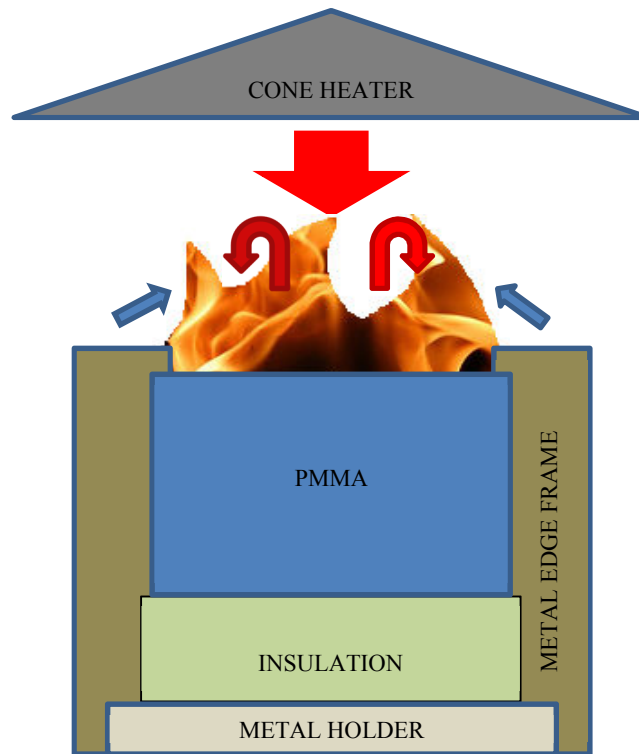


Figure A(B)-5. Simplified representation of a cone calorimeter test of PMMA

A simplified representation of a cone calorimeter test of PMMA is shown in Figure A(B)-5. The sample is placed on top of an insulation, which sits on a metal holder. Another metal frame is placed on top of the sample, insulation, and the holder. A metal edge frame is used as well.

Front Surface: As heating starts by opening the shutter to allow radiation from the cone heater to impinge on the sample surface (large red arrow), cooling also begins via natural convection (blue arrows) and re-radiation. The surface decomposes with bubbling with respect to temperature increase occurring through heat conduction and/or in-depth radiative transport. The pyrolyzates leave through the surface until complete burn-off because this material leaves no residue. When ignition occurs as the fuel vapor concentration above the surface exceeds its LFL (lower flammable limit), additional heat

flux from the flame is introduced on the surface (red arrows). Regression of the sample surface with respect to consumption of PMMA in pyrolysis occurs.

Back surface: The sample is placed on top of insulation. In the experiment, air gap of few millimeters thickness exist between the sample and the insulation due to thermal contact. Due to the insulation, nothing leaves through the back face when 1D assumption holds for the experiment.

CONFIGURE MODEL CONDITIONS BASED ON UNDERSTANDING OF EXPERIMENT

In the model, the phenomena discussed above are simulated as below. Basic assumptions are as follows:

- Pre-ignition stage is
 - Inert: decomposition with bubbling before ignition is neglected
 - Always the same as in cone calorimeter test with a specified heat flux impinging on material's surface (typically $\sim 50 \text{ kW/m}^2$ is used)
- Ignition phenomenon is the same as in cone calorimeter experiment: time-to-ignition is the same in modeling as determined in experiment
- Post-ignition stage is
 - Considered to have instantaneous release of volatiles from solid to gas phase: bubbling layer is neglected and is considered as a surface phenomena
 - Considered to be the same as in cone calorimeter test in terms of heat release rate or mass-loss rate per unit area

ACQUIRE DATA SETS THAT CAN REPRESENT BURNING BEHAVIOR OF INTEREST

Cone calorimeter test data of black PMMA with thickness of 18 mm, density of 1170 kg/m^3 , and applied heat flux of 50 kW/m^2 is found.

ESTIMATE UNKNOWNNS

1. Time-to-Ignition

$t_{ig} = 22$ s after exposure to heating

2. MLR and Effective HoC

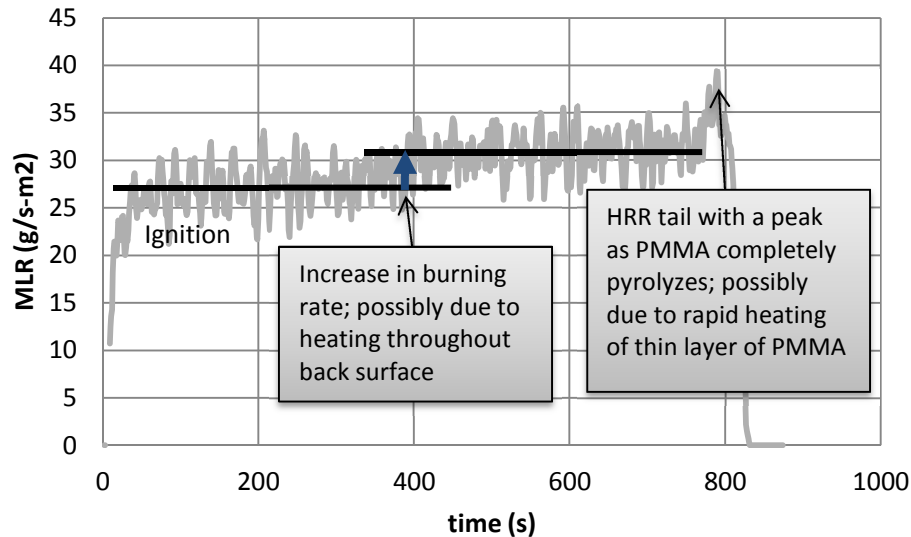


Figure A(B)-6. MLR curve from cone calorimeter experiment of PMMA

MLR curve with effective heat of combustion calculated from a cone experiment will be used directly (see Figure A(B)-6). This MLR data is from a PMMA test at 50kW/m^2 with sample thickness of 18 mm. The MLR profile changes with respect to the burning history of the sample. From time-of-ignition, initial steady-state-burning phase occurs. Then, near $t = 400$ s after exposure to heating, second steady-state-burning phase is reached, which has a slightly higher mass-loss rate than the initial phase, possibly due to the thermal wave penetrating to the back surface and increasing heating. At the end of the test, a mass-loss rate peak is observed. This is probably due to the rapid heating of thin layer of residual PMMA. Understanding the MLR profile enables modelers to adjust the curve when using it as an input to a pyrolysis model if needed. For example, the modeler may decide to only use data from time-to-ignition up to the initial steady-state burning phase if PMMA involved in a fire scenario of interest has a thickness greater than what has been used in the experiment (18 mm).

Effective heat-of-combustion is calculated from the heat-release rate and mass-loss rate data at every measurement, as discussed in Model Parameter Measurement

Methods. The average with its confidence interval with 95% confidence is: **24.8 ± 0.1 kJ/g**. Note that this average and confidence interval has been obtained for the steady-burning phases only due to significant changes in effective heat-of-combustion values near ignition and burn-off periods at the start and the end of testing, respectively.

Obtain Uncertainty for Estimated Parameters

For estimating the uncertainty in parameters, experimental uncertainty can be used, as the parameters are obtained from data directly. From the experiment work done by Beaulieu and Dembsey¹ on thermally-thick-behaving black PMMA using AFM apparatus, the experiment uncertainty in time-to-ignition and mass-loss rate at steady burning were determined as ± 2 s and ± 3 g/m²s, respectively. The test results were compared with other literature values using different apparatuses, such as cone calorimeter as well, which were considered as consistent. This uncertainty information will be used when comparing modeling output to experiment data.

Validation and Commentary

When using Empirical Model to simulate pyrolysis of PMMA, PMMA test data from a bench-scale cone calorimeter experiment at a set heat-flux level has been utilized to estimate the time-to-ignition from exposure to heating and the energy released from burning of PMMA. As noted in the Uncertainty part of the chapter, this approach is limited as follows in terms of the conditions being comparable to those found in the fire scenario of interest:

- Ignition scenario: piloted ignition with an electric sparker
- Exposure conditions: electrically heated coil uniformly heating PMMA with a set heat flux impinging on the front surface where this applied heat-flux level during testing is assumed to be representative average (over space and time) for the fire scenario that is being modeled
- Heat and mass transfer: one-dimensional, i.e., perpendicular to the exposed surface

- Surface burning data: edge effects in material testing are not included; therefore, data per unit area can be applied to simulate larger areas by simply multiplying the material surface area involved in fire

EXAMPLE 3.3 MODELING CORRUGATED CARDBOARD

Obtain Parameters via Experiment

Run model

SELECT MODEL: EMPIRICAL USING BENCH-SCALE CALORIMETER DATA

UNDERSTAND EXPERIMENT

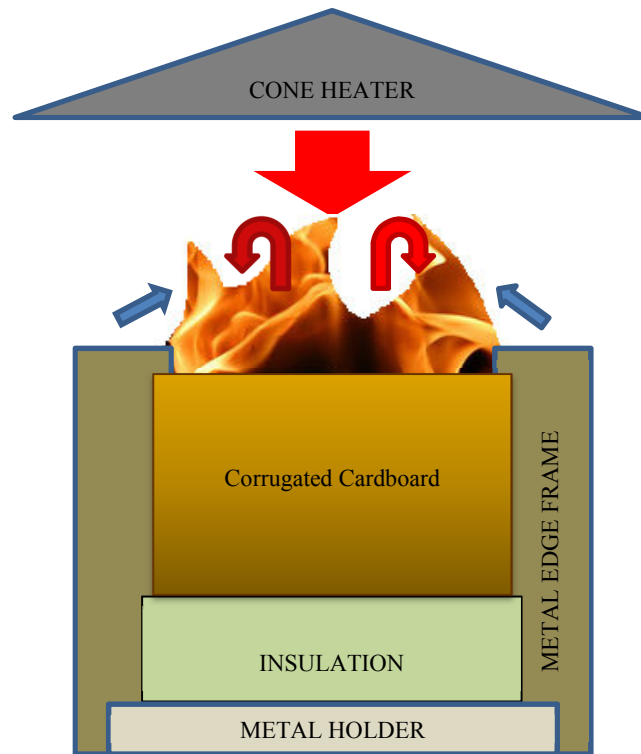


Figure A(B)-7. Simplified representation of a cone calorimeter test of corrugated cardboard

A simplified representation of a cone calorimeter test of triple-layered corrugated cardboard is shown above (see Figure A(B)-7). The sample is placed on top of an insulation, which sits on a metal holder. Another metal frame is placed on top of the sample, insulation, and the holder. A metal edge frame is used as well.

Front Surface: As heating starts by opening the shutter to allow radiation from the cone heater to impinge on sample surface (large red arrow), cooling also begins via natural convection (blue arrows) and re-radiation. The surface decomposes with charring, i.e., surface becoming black and white smoke, which typically indicates moisture loss with heating of the sample. Note that the surface becomes non-uniformly black due to corrugation showing linear shading. As the surface layer is burned away, it exfoliates toward the sides and opens up, allowing the first layer of the corrugation to

appear on the surface. Then the middle flat layer of the cardboard, which separates the two layers of corrugation, starts to burn, allowing the heat release to grow. As this layer is decomposed throughout, the second layer of the corrugation becomes involved in the burning process. Followed by the burning of the second corrugation layer, the last flat layer of the cardboard – back surface of the sample – burns. This results in another growing phase in the heat-release-rate curve. When ignition occurs as the fuel vapor concentration above the surface exceeds its LFL (lower flammable limit), additional heat flux from the flame is introduced on the surface (red arrows).

Back surface: The sample is placed on top of insulation. In the experiment, an air gap of few millimeters thickness exists between the sample and the insulation due to thermal contact. Nothing leaves through the back face with the insulation when 1D assumption holds for the experiment.

CONFIGURE MODEL CONDITIONS BASED ON UNDERSTANDING OF EXPERIMENT

In the model, the phenomena discussed above are simulated as below. Basic assumptions are as follows:

- Pre-ignition stage is
 - Inert: non-uniform charring is considered to be evenly distributed
 - Always the same as in cone calorimeter test with a specified heat flux impinging on material's surface
- Ignition phenomenon is the same as in cone calorimeter experiment: time-to-ignition is the same in modeling as determined in experiment
- Post-ignition stage is
 - Considered to have instantaneous release of volatiles from solid to gas phase
 - Considered to be the same as in cone calorimeter test in terms of heat-release rate or mass-loss rate per unit area

ACQUIRE DATA SETS THAT CAN REPRESENT BURNING BEHAVIOR OF INTEREST

Cone calorimeter test data of triple-layer cardboard with thickness of 15 mm, density of 116 kg/m³, and applied heat flux of 25 kW/m² is found.

ESTIMATE UNKNOWNNS

1. Time-to-Ignition

$$t_{ig} = 32 \pm 4 \text{ s after exposure to heating}$$

2. MLR and Effective HoC

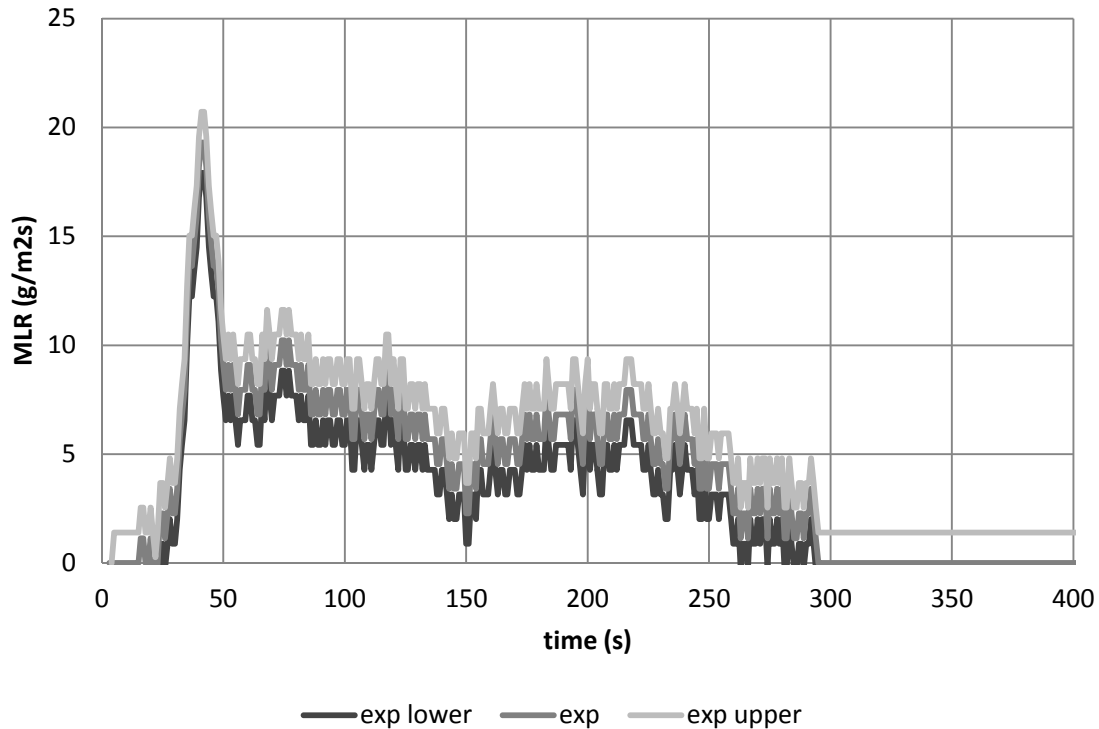


Figure A(B)-8. MLR curve from cone calorimeter test of corrugated cardboard

MLR curve with effective heat-of-combustion calculated from a cone experiment will be used directly (see Figure A(B)-8). This MLR data is from a triple-layer cardboard test at 25 kW/m^2 with sample thickness of 15 mm. The MLR profile changes with respect to the burning history of the sample.

Effective heat-of-combustion is calculated from the heat-release rate and mass-loss-rate data at every measurement, as discussed in Model Parameter Measurement Methods. The average of two tests with its confidence interval calculated by 2 times the standard deviation is: **$13.5 \pm 0.5 \text{ kJ/g}$** .

Obtain Uncertainty for Estimated Parameters

The uncertainty in the mass-loss-rate data is estimated via statistical approach, taking the standard deviation (0.58 g/sm^2) from the mean of a steady burning of five identical PMMA tests conducted in a cone calorimeter.² The estimated uncertainty is 1.4 g/sm^2 , which is found by calculating the 95% confidence interval applying student t distribution with a sample size of five.

The uncertainty in time-to-ignition data is estimated via statistical approach, taking four identical cone calorimeter test data at heat flux 25 kW/m^2 of this cardboard. 95% confidence interval is calculated for each heat-flux level assuming student t distribution.

The uncertainty in effective heat-of-combustion is estimated by average heat-release rate divided by average mass-loss rate of two identical tests. 2 times the standard deviation is used as its uncertainty band.

Validation and Commentary

When using Empirical Model to simulate pyrolysis of this triple-layer cardboard, test data from a bench-scale cone calorimeter experiment at a set heat-flux level has been utilized to estimate the time-to-ignition from exposure to heating and the energy released from burning of this cardboard. As noted in the Understanding Model part of the chapter, this approach is limited as follows in terms of the conditions being comparable to those found in the fire scenario on interest:

- Ignition scenario: piloted ignition with an electric sparker
- Exposure conditions: electrically heated coil uniformly heating sample with a set heat flux impinging on the front surface, where this applied heat-flux level during testing is assumed to be representative average (over space and time) for the fire scenario that is being modeled
- Heat and mass transfer: one-dimensional, i.e., perpendicular to the exposed surface
- Surface-burning data: edge effects in material testing are not included; therefore, data per unit area can be applied to simulate larger areas by simply multiplying the material surface area involved in fire

EXAMPLE 3.4 MODELING FIRE RETARDED FRP COMPOSITE

Obtain Parameters via Experiment

Run model

SELECT MODEL: EMPIRICAL USING BENCH-SCALE CALORIMETER DATA

UNDERSTAND EXPERIMENT

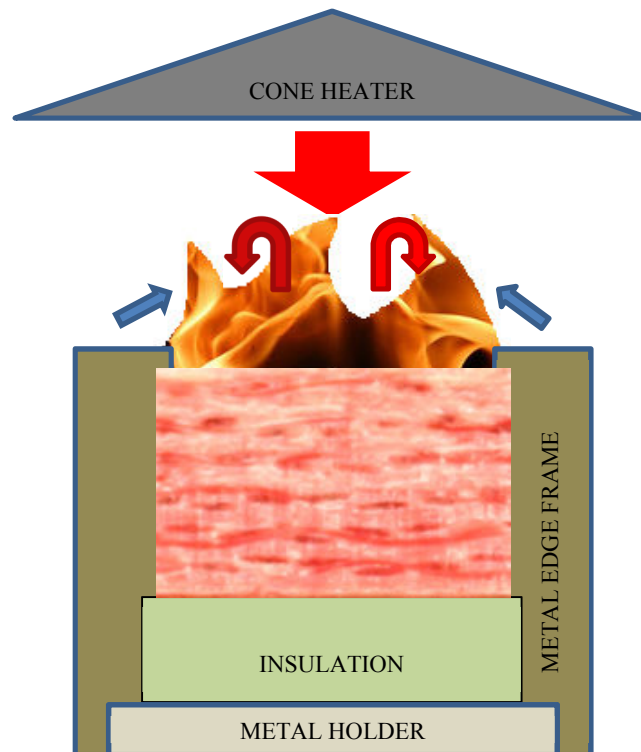


Figure A(B)-9. Simplified representation of a cone calorimeter test of fire-retarded fiberglass-reinforced polymer (FRP) Composite

A simplified representation of a cone calorimeter test of fire-retarded fiberglass-reinforced polymer (FRP) composite is shown in Figure A(B)-9. The sample is placed on top of an insulation, which sits on a metal holder. Another metal frame is placed on top of the sample, insulation, and the holder. A metal edge frame is used as well.

Front Surface: As heating starts by opening the shutter to allow radiation from the cone heater to impinge on sample surface (large red arrow), cooling also begins via natural convection (blue arrows) and re-radiation. The surface decomposes with charring, i.e., surface becoming black and white smoke, which typically indicates moisture loss with heating of the sample. Note that the surface becomes non-uniformly

black. As thermal decomposition of the resin with additive progresses, blackened surface becomes white, as the resin leaves a white powder-type residue (possible due to decomposition of fire-retardant additive). Shrinkage or regression during pyrolysis can be considered to be minimal for this material. When ignition occurs as the fuel vapor concentration above the surface exceeds its LFL (lower flammable limit), additional heat flux from the flame is introduced on the surface (red arrows).

Back surface: The sample is placed on top of insulation. In the experiment, an air gap of few millimeters thickness exist between the sample and the insulation due to thermal contact. Nothing leaves through the back face with the insulation when 1D assumption holds for the experiment.

CONFIGURE MODEL CONDITIONS BASED ON UNDERSTANDING OF EXPERIMENT

In the model, the phenomena discussed above are simulated as below. Basic assumptions are as follows:

- Pre-ignition stage is
 - Inert: non-uniform charring is considered to be evenly distributed
 - Always the same as in cone calorimeter test with a specified heat flux impinging on material's surface
- Ignition phenomenon is the same as in cone calorimeter experiment: time-to-ignition is the same in modeling as determined in experiment
- Post-ignition stage is
 - Considered to have instantaneous release of volatiles from solid to gas phase
 - Considered to be the same as in cone calorimeter test in terms of heat-release rate or mass-loss rate per unit area

ACQUIRE DATA SETS THAT CAN REPRESENT BURNING BEHAVIOR OF INTEREST

Cone calorimeter test data of this FRP composite with thickness of 9.2 mm, density of 1900 kg/m³, and applied heat flux of 50 kW/m² is found.

ESTIMATE UNKNOWNNS

1. Time-to-Ignition

$$t_{ig} = 175 \pm 36 \text{ s after exposure to heating}$$

2. MLR and Effective HoC

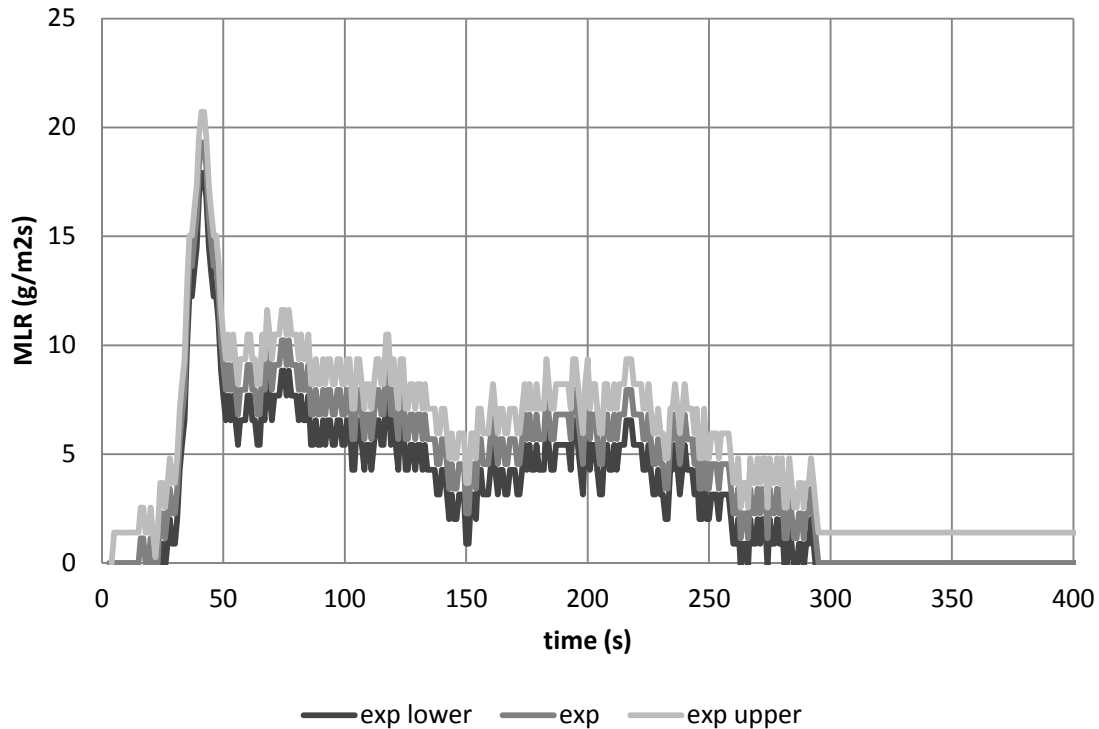


Figure A(B)-10. MLR curve from cone calorimeter test of fire-retarded FRP composite

MLR curve with effective heat-of-combustion calculated from a cone experiment will be used directly (see Figure A(B)-10). This MLR data is from FRP composite test at 50 kW/m^2 with sample average thickness of 9.2 mm. The MLR profile changes with respect to the burning history of the sample.

Effective heat-of-combustion is calculated from the heat-release rate and mass-loss-rate data at every measurement as discussed in Model Parameter Measurement Methods. The average of four tests with its confidence interval calculated by 95% confidence using student t distribution is: **$14.7 \pm 3.8 \text{ kJ/g}$** .

Obtain Uncertainty for Estimated Parameters

The uncertainty in the mass-loss-rate data is estimated via statistical approach, taking the standard deviation (0.58 g/sm^2) from the mean of a steady burning of five identical PMMA tests conducted in a cone calorimeter². The estimated uncertainty is 1.4 g/sm^2 , which is found by calculating the 95% confidence interval applying student t distribution with a sample size of five.

The uncertainty in time-to-ignition data is estimated via statistical approach, taking four identical cone calorimeter test data at heat flux 50 kW/m^2 of this cardboard. 95% confidence interval is calculated for each heat-flux level assuming student t distribution.

The uncertainty in effective heat-of-combustion is estimated by average heat-release rate divided by average mass-loss rate of four identical tests. 95% confidence interval is calculated for each heat-flux level assuming student t distribution.

Validation and Commentary

When using Empirical Model to simulate pyrolysis of this fire-retarded FRP composite, test data from a bench-scale cone calorimeter experiment at a set heat-flux level has been utilized to estimate the time-to-ignition from exposure to heating and the energy released from burning of this material. As noted in the Understanding Model part of the chapter, this approach is limited as follows in terms of the conditions being comparable to those found in the fire scenario of interest:

- Ignition scenario: piloted ignition with an electric sparker
- Exposure conditions: electrically heated coil uniformly heating sample with a set heat flux impinging on the front surface, where this applied heat-flux level during testing is assumed to be representative average (over space and time) for the fire scenario that is being modeled
- Heat and mass transfer: one-dimensional, i.e., perpendicular to the exposed surface
- Surface-burning data: edge effects in material testing are not included and therefore data per unit area can be applied to simulate larger areas by simply multiplying the material surface area involved in fire

EXAMPLE 3.5 MODELING PLYWOOD

Obtain Parameters via Experiment

Run model

SELECT MODEL: EMPIRICAL USING BENCH-SCALE CALORIMETER DATA

UNDERSTAND EXPERIMENT

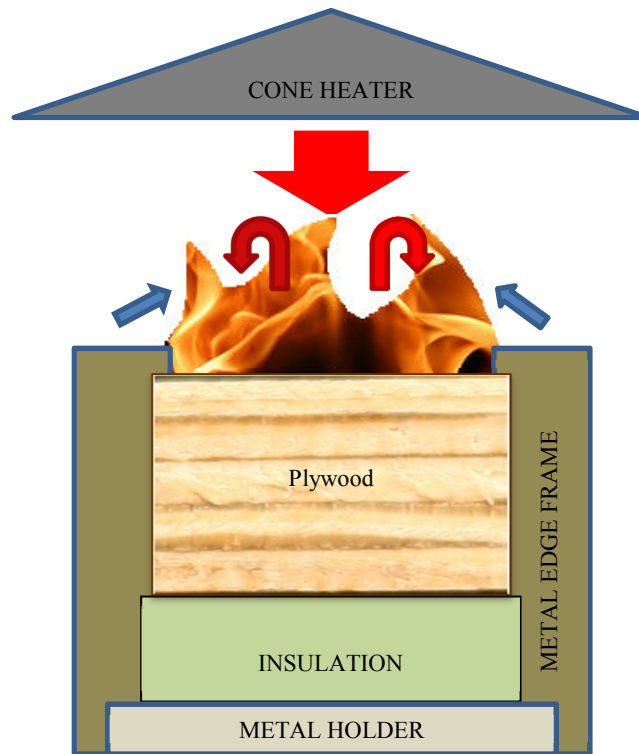


Figure A(B)-11. Simplified representation of a cone calorimeter test of plywood

A simplified representation of a cone calorimeter test of plywood is shown in Figure A(B)-11. The sample is placed on top of an insulation, which sits on a metal holder. Another metal frame is placed on top of the sample, insulation and the holder. A metal edge frame is used as well.

Front Surface: As heating starts by opening the shutter to allow radiation from the cone heater to impinge on sample surface (large red arrow), cooling also begins via natural convection (blue arrows) and re-radiation. The surface decomposes with moisture loss at first appearing as white smoke followed by thermal decomposition of the wood component. When ignition occurs as the fuel vapor concentration above the surface exceeds its LFL (lower flammable limit), additional heat flux from the flame is introduced on the surface (red arrows). As decomposition occurs under flaming

condition, relatively uniform cracks appear on the surface with some shrinkage, allowing easy evacuation of the pyrolyzates to the gas phase even as the pyrolysis front propagates toward in-depth. Near the burn-out leaving grey residue, the center of the sample bends upward then quickly falls apart resulting in flame out.

Back surface: The sample is placed on top of insulation. In the experiment, an air gap of few millimeters thickness exists between the sample and the insulation resulting in some thermal resistance. Due to the insulation, nothing leaves through the back face when 1D assumption holds for the experiment.

CONFIGURE MODEL CONDITIONS BASED ON UNDERSTANDING OF EXPERIMENT

In the model, the phenomena discussed above are simulated as below. Basic assumptions are as follows:

- Pre-ignition stage is
 - Inert: non-uniform charring is considered to be evenly distributed
 - Always the same as in cone calorimeter test with a specified heat flux impinging on material's surface
- Ignition phenomenon is the same as in cone calorimeter experiment: time to ignition is the same in modeling as determined in experiment
- Post-ignition stage is
 - Considered to have instantaneous release of volatiles from solid to gas phase
 - Considered to be the same as in cone calorimeter test in terms of heat release rate or mass loss rate per unit area

ACQUIRE DATA SETS THAT CAN REPRESENT BURNING BEHAVIOR OF INTEREST

Cone calorimeter test data of triple-layer cardboard with thickness of 11.1 mm, density of 542 kg/m³, and applied heat flux of 50 kW/m² is found.

ESTIMATE UNKNOWNNS

1. Time-to-Ignition

$$t_{ig} = 27 \pm 9 \text{ s after exposure to heating}$$

2. MLR and Effective HoC

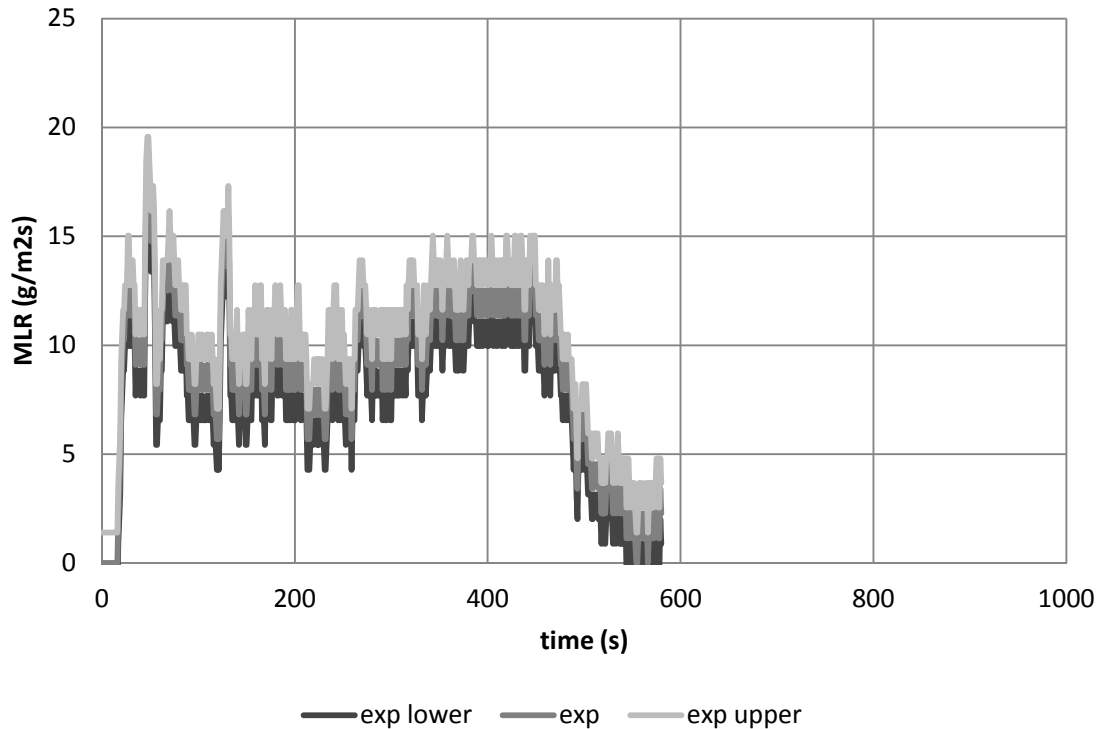


Figure A(B)-12. MLR curve from cone calorimeter test of plywood

MLR curve with effective heat-of-combustion calculated from a cone experiment will be used directly (see Figure A(B)-12). This MLR data is from a triple-layer cardboard test at 50 kW/m^2 with sample thickness of 11.1 mm. The MLR profile changes with respect to the burning history of the sample.

Effective heat-of-combustion is calculated from the heat-release rate and mass-loss-rate data at every measurement as discussed in Model Parameter Measurement Methods. The average of two tests with its confidence interval calculated by 2 times the standard deviation is: **$11.0 \pm 0.3 \text{ kJ/g}$** .

Obtain Uncertainty for Estimated Parameters

The uncertainty in the mass-loss-rate data is estimated via statistical approach, taking the standard deviation (0.58 g/sm^2) from the mean of a steady burning of five

identical PMMA tests conducted in a cone calorimeter.² The estimated uncertainty is 1.4 g/sm², which is found by calculating the 95% confidence interval applying student t distribution with a sample size of 5.

The uncertainty in time-to-ignition data is estimated via statistical approach, taking four identical cone calorimeter test data at heat flux 25 kW/m² of this cardboard. 95% confidence interval is calculated for each heat flux level assuming student t distribution.

The uncertainty in effective heat-of-combustion is estimated by average heat-release rate divided by average mass-loss rate of two identical tests. 2 times the standard deviation is used as its uncertainty band.

Validation and Commentary

When using Empirical Model to simulate pyrolysis of this plywood, test data from a bench-scale cone calorimeter experiment at a set heat-flux level has been utilized to estimate the time-to-ignition from exposure to heating and the energy released from burning of this material. As noted in the Understanding Model part of the chapter, this approach is limited as follows in terms of the conditions being comparable to those found in the fire scenario of interest:

- Ignition scenario: piloted ignition with an electric sparker
 - Exposure conditions: electrically heated coil uniformly heating sample with a set heat flux impinging on the front surface where this heat-flux level during testing is assumed to be representative average (over space and time) for the fire scenario that is being modeled
 - Heat and mass transfer: one-dimensional, i.e., perpendicular to the exposed surface
- Surface-burning data: edge effects in material testing are not included; therefore, data per unit area can be applied to simulate larger areas by simply multiplying the material surface area involved in fire

REFERENCES

¹ Beaulieu, P.A.; and Dembsey, N.A., "Effect of Oxygen on Flame Heat Flux in Horizontal and Vertical Orientations", *Fire Safety Journal*, 43:6 (2008) 410-428.

² Zhao, Lei, Bench Scale Apparatus Measurement Uncertainty and Uncertainty Effects on Measurement of Fire Characteristics of Material Systems, MS Thesis, Fire Protection Engineering, WPI, 2005-04-27, ETD-050105-182456

Appendix C - Example Solutions for Chapter 4

EXAMPLE 4.1 MODELING PMMA

Measure Parameters

1. Ambient Temperature

Direct measurement of ambient temperature is made as 20°C.

2. Surface Temperature at Ignition

This parameter will be obtained via Ignition Data Analysis, i.e., no direct measurements will be performed.

3. Critical Heat Flux for Ignition

By bracketing to within +/- 0.5 kW/m² in cone calorimeter tests, \dot{q}_{cr}'' has been determined to be 10.5 kW/m². Ignition data is provided below for PMMAs with thickness of 18.0 mm, density of 1170 kg/m³ (see Table A(C)-1):

Table A(C)-1. Ignition data from cone calorimeter tests for PMMA

Heat Flux (kW/m ²)	t _{ig} (s)
10	NI
11	1138
12	961
15	471
25	87
25	84
25	97
25	90
50	24
50	22
75	14
75	11

4. Thermal Inertia

This parameter will be obtained via Ignition Data Analysis, i.e., no direct measurements will be performed.

5. Effective Heat-of-Combustion

This parameter will be obtained via Burning-Rate Data Analysis, i.e., no direct measurements will be performed.

6. Heat-of-Gasification

This parameter will be obtained via Burning-Rate Data Analysis, i.e., no direct measurements will be performed.

7. Convection Coefficient

Because this is a material laid in horizontal position in a cone calorimeter, $h_c = 12$ W/m²K is used based on literature reference.

8. Surface Emissivity/Absorptivity

Emissivity is approximated as 0.9.

Summary

Table A(C)-2. Summary of model parameter table with estimated values via direct measurements, literature search, or approximation

Ignition Parameters	T_∞	20 °C
	T_{ig}	Ignition Data Analysis
	\dot{q}_{cr}''	10.5 kW/m ²
	$k\rho c$	Ignition Data Analysis
Burning-Rate Parameters	$\Delta h_{c,eff}$	Burning-Rate Data Analysis
	Δh_g	Burning-Rate Data Analysis
	h_c	12 W/m ² K
	ε	0.9

Obtain Parameters via Data Analysis

Run model

SELECT MODEL: THERMALLY THICK MODEL FOR IGNITION ANALYSIS (QUINTIERE AND HARKLEROAD, ASTM E 1321) AND STEADY-BURNING MODEL

UNDERSTAND EXPERIMENT AND FIRE CHARACTERISTICS OF MATERIAL

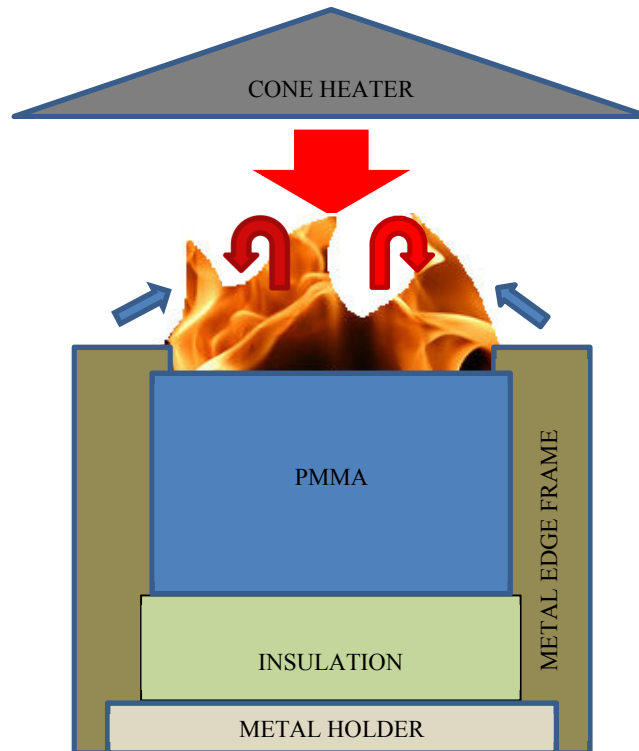


Figure A(C)-1. Simplified representation of a cone calorimeter test of PMMA

A simplified representation of a cone calorimeter test of PMMA is shown in Figure A(C)-1. The sample is placed on top of an insulation, which sits on a metal holder. Another metal frame is placed on top of the sample, insulation and the holder. A metal edge frame is used as well.

Front Surface: As heating starts by opening the shutter to allow radiation from the cone heater to impinge on sample surface (large red arrow), cooling also begins via natural convection (blue arrows) and re-radiation. The surface decomposes with bubbling with respect to temperature increase occurring through heat conduction and/or in-depth radiative transport. The pyrolyzates leave through the surface until complete burn-off, because this material leaves no residue. When ignition occurs as the fuel-vapor concentration above the surface exceeds its LFL (lower flammable limit), additional heat

flux from the flame is introduced on the surface (red arrows). Regression of the sample surface occurs with respect to consumption of PMMA in pyrolysis.

Back surface: The sample is placed on top of insulation. In the experiment, an air gap of a few millimeters thickness exists between the sample and the insulation due to thermal contact. Due to the insulation, nothing leaves through the back face when 1D assumption holds for the experiment.

Configure model conditions based on understanding of experiment and material characteristics

In the model, the phenomena discussed above are simulated as below. Basic assumptions are as follows:

- Pre-ignition stage is:
 - Inert: decomposition with bubbling before ignition is neglected
 - Thermally thick: heat transfer does not reach back surface
- Post-ignition stage is:
 - Considered to have instantaneous release of volatiles from solid to gas phase: bubbling layer is neglected and is considered as a surface phenomenon
 - Considered to have a constant thickness: regression of PMMA is neglected
 - Steady burning: heat loss equals heat gain at front surface

ACQUIRE DATA SETS

Cone calorimeter test data of black PMMA with thickness of 18 mm, density of 1170 kg/m³, and applied heat-flux levels ranging from 10 to 75 kW/m² is found. For Ignition Data analysis, only time-to-ignition with respect to applied heat-flux data will be used. For burning-rate-data analysis, data for the entire testing time duration, mass loss and heat release during testing period with respect to applied heat flux will be used.

CONDUCT IGNITION DATA ANALYSIS

1. Estimate T_{ig}

Heat balance at front surface during steady burning is as follow:

$$\varepsilon \dot{q}_{cr}'' = h_c (T_{ig} - T_{\infty}) + \varepsilon \sigma (T_{ig}^4 - T_{\infty}^4)$$

Knowing that emissivity is approximated as 0.9, critical heat flux is estimated as 10.5 kW/m², and heat-transfer coefficient in cone calorimeter experiment is estimated as 12.0 W/m²K, ignition temperature, T_{ig} is calculated as:

$$T_{ig} = 318\text{ }^{\circ}\text{C}$$

2. Estimate h_{ig}

h_{ig} is the total heat-transfer coefficient at ignition; therefore, at steady-state burning stage, the following can be defined:

$$\varepsilon \dot{q}_{cr}'' \equiv h_{ig} (T_{ig} - T_{\infty})$$

Knowing the ignition temperature, h_{ig} can be calculated:

$$h_{ig} = 31.7\text{ W/m}^2\text{K}$$

3. Calculate $\dot{q}_{cr}'' / \dot{q}_e''$ versus $\sqrt{t_{ig}}$ from ignition data (see Table A(C)-3)

Table A(C)-3. $\dot{q}_{cr}'' / \dot{q}_e''$ versus $\sqrt{t_{ig}}$

Heat Flux (kW/m ²)	t _{ig} (s)	CHF/HF	t _{ig} ^{0.5} (s ^{0.5})
10	NI		
11	1138	0.9546	33.73
12	961	0.8750	31.00
15	471	0.7000	21.70
25	87	0.4200	9.33
25	84	0.4200	9.17
25	97	0.4200	9.85
50	22	0.2100	4.69
75	11	0.1400	3.32

4. Plot $\dot{q}_{cr}'' / \dot{q}_e''$ versus $\sqrt{t_{ig}}$ to estimate the time needed to reach “steady-state”

burning, t* and thermal inertia, kpc

$$\text{Recall } \frac{\dot{q}_{cr}''}{\dot{q}_e''} = F(t_{ig}) = \begin{cases} \frac{2 h_{ig} \sqrt{t_{ig}}}{\sqrt{\pi k \rho c}} & t_{ig} \leq t^* \\ 1 & t_{ig} > t^* \end{cases} \quad \text{for piloted-ignition data where } t^* \text{ is}$$

the time when $\dot{q}_{cr}'' / \dot{q}_e'' = 1$. Thermal inertia can be estimated from the best-fit line through

$t = 0$. Its slope at $0 < t < t^*$ is $\frac{2 h_{ig}}{\sqrt{\pi k \rho c}}$; therefore, $k \rho c = \frac{4 h_{ig}^2}{\pi \cdot (slope)^2}$. Note that in the

analysis, few data points at lower heat-flux levels with large time-to-ignition data were excluded (see Figure A(C)-2, open circles) to increase fitness of the best-fit line. This approach is reasonable, considering that at this region analysis assumptions of having inert and thermally thick conditions are less likely to be satisfied.

$$k \rho c = 0.649 \text{ kJ}^2/\text{m}^4\text{K}^2\text{s}$$

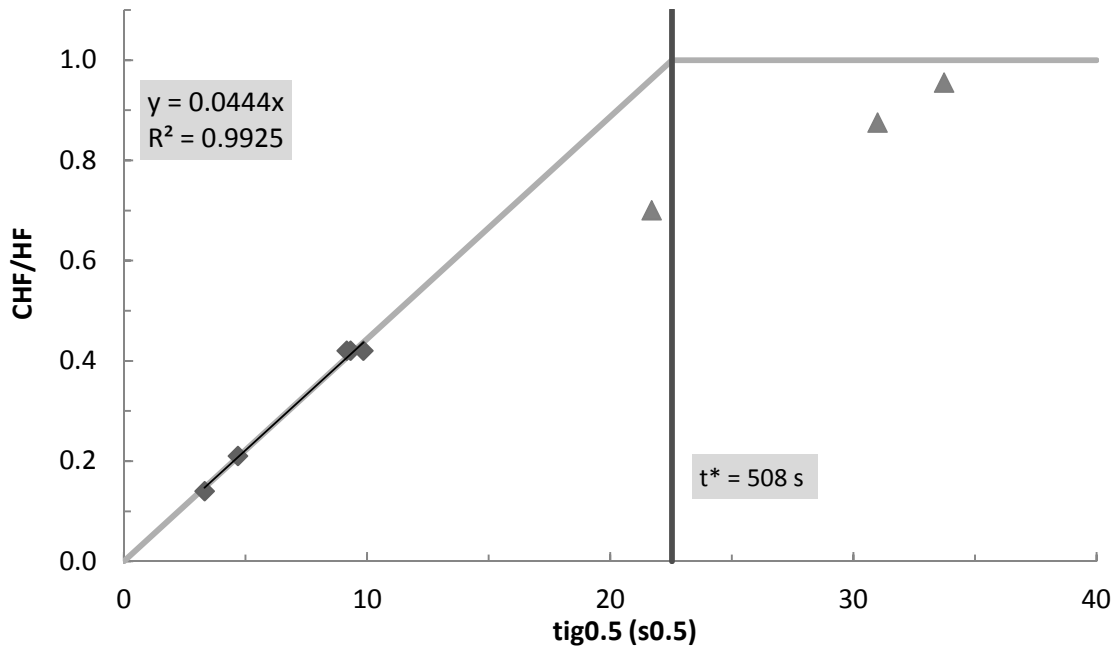


Figure A(C)-2. Plot of $\dot{q}_{cr}'' / \dot{q}_e''$ versus $\sqrt{t_{ig}}$

CONDUCT BURNING-RATE DATA ANALYSIS

1. Estimate $\Delta h_{c,eff}$

There are two approaches in estimating the effective heat of combustion via calorimeter tests: by using the peak in HRR or the average heat released over the entire test. In this example, $\Delta h_{c,eff}$ will be estimated by considering the total heat released divided by the total amount of mass loss during a test. Cone test results at 25, 50 and 75 kW/m² are summarized below (see Table A(C)-4):

Table A(C)-4. Estimation of effective heat-of-combustion using cone calorimeter test results at applied heat flux of 25, 50 and 75 kW/m²

Heat Flux (kW/m ²)	t _{start} (s)	Mass _{start} (g)	t _{end} (s)	Mass _{end} (g)	Total HR (kW/m ²)	Total ML (g/m ²)	Δh _{c, eff} (kJ/g)
25	0	222.7	1330	0.0	539.9	222.7	24.2
50	0	236.9	838	0.0	586.8	236.9	24.8
75	0	221.1	645	0.0	550.9	221.1	24.9
Average							24.6

$$\Delta h_{c, \text{eff}} = 24.6 \text{ kJ/g}$$

2. Estimate Δh_g

Recall $\Delta h_g \equiv \frac{\dot{q}_{net}''}{\dot{m}''} = \frac{\dot{q}_e'' + \dot{q}_f'' - \dot{q}_l''}{\dot{m}''}$; therefore, when plotting mass-loss rates at

different radiant-heat-flux levels during steady-burning condition, the reciprocal of the slope of the best-fit line should be the heat-of-gasification (see Table A(C)-5 and Figure A(C)-3).

$$\Delta h_g = 2.9 \text{ kJ/g}$$

Table A(C)-5. Estimation of effective heat-of-gasification using cone calorimeter test results at applied heat flux of 25, 50 and 75 kW/m²

Heat Flux (kW/m ²)	t _{start} (s)	t _{end} (s)	Total ML (g)	MLR (g/m ² s)
25	0	1330	222.7	16.7
50	0	838	236.9	28.3
75	0	645	221.1	34.3

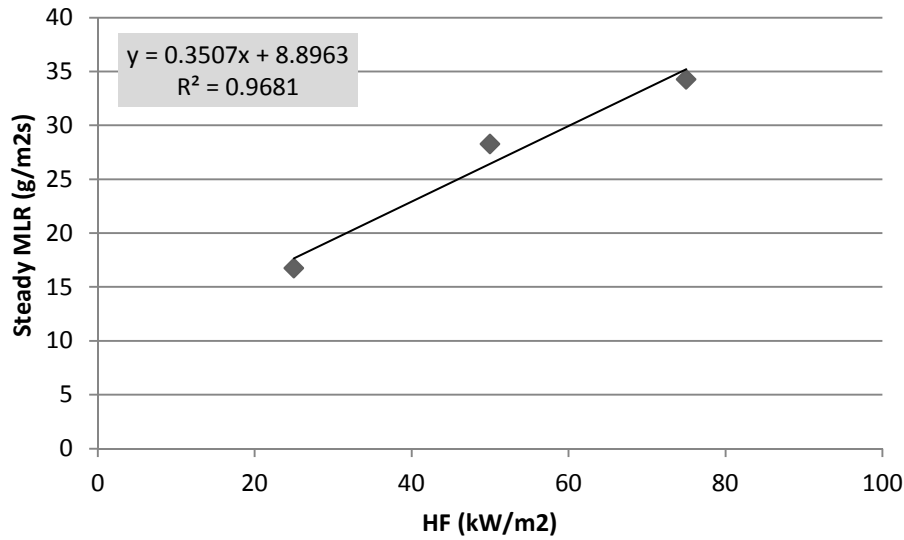


Figure A(C)-3. Plot of steady MLR versus different applied heat-flux levels – 25, 50 and 75 kW/m²

Obtain Uncertainty for Estimated Parameters

UNCERTAINTY FOR MEASURED PARAMETERS

1. δT_{∞}

Fluctuation in ambient temperature during testing is estimated to be less than $\pm 10\%$ of reported measurement data.

2. $\delta \dot{q}_{cr}''$

The resolution of bracketing experiment was 1 kW/m²; hence, uncertainty can be estimated as ± 0.5 kW/m².

3. δh_c

Considering that the reference values sited in the *Guide* for different apparatuses and set-up have two significant figures, uncertainty for this convection coefficient can be estimated as ± 0.5 W/m²K.

4. $\delta \varepsilon$

Based on literature review, black PMMA's emissivity should be within $\pm 10\%$ of what has been approximated in this example.

UNCERTAINTY FOR ESTIMATED PARAMETERS USING IGNITION-DATA ANALYSIS

1. δT_{ig}

See Chapter 4 for detail.

$$\begin{aligned}\frac{\partial \dot{q}_{cr}''}{\partial T_{ig}} &= \frac{h_c + 4\varepsilon\sigma T_{ig}^3}{\varepsilon} \\ &= \frac{\left(0.012 \frac{kW}{m^2 K}\right) + 4(0.9)\left(5.67 \times 10^{-11} \frac{kW}{K^4 m^2}\right)\left((318 + 273)K\right)^3}{(0.9)}\end{aligned}$$

$$\approx 0.06015 \frac{kW}{m^2 K}$$

$$\begin{aligned}\frac{\partial \dot{q}_{cr}''}{\partial \varepsilon} &= \frac{-\dot{q}_{cr}'' + \sigma(T_{ig}^4 - T_\infty^4)}{\varepsilon} \\ &= \frac{-\left(10.5 \frac{kW}{m^2}\right) + \left(5.67 \times 10^{-11} \frac{kW}{K^4 m^2}\right)\left(\left((318 + 273)K\right)^4 - \left((20 + 273)K\right)^4\right)}{(0.9)}\end{aligned}$$

$$\approx -4.445 \frac{kW}{m^2}$$

$$\begin{aligned}\frac{\partial \dot{q}_{cr}''}{\partial h_c} &= \frac{T_{ig} - T_\infty}{\varepsilon} \\ &= \frac{\left((318 + 273)K\right) - \left((20 + 273)K\right)}{(0.9)}\end{aligned}$$

$$\approx 331.1K$$

$$\begin{aligned}\frac{\partial \dot{q}_{cr}''}{\partial T_\infty} &= \frac{-h_c - 4\varepsilon\sigma T_\infty^3}{\varepsilon} \\ &= \frac{-\left(0.012 \frac{kW}{m^2 K}\right) - 4(0.9)\left(5.67 \times 10^{-11} \frac{kW}{K^4 m^2}\right)\left((20 + 273)K\right)^3}{(0.9)}\end{aligned}$$

$$\approx -0.01904 \frac{kW}{m^2 K}$$

Therefore,

$$\begin{aligned} \delta T_{ig} &= \left(\frac{\partial \dot{q}_{cr}''}{\partial T_{ig}} \right)^{-1} \sqrt{ \left(\delta \dot{q}_{cr}'' \right)^2 - \left(\left(\frac{\partial \dot{q}_{cr}''}{\partial \varepsilon} \delta \varepsilon \right)^2 + \left(\frac{\partial \dot{q}_{cr}''}{\partial h_c} \delta h_c \right)^2 + \left(\frac{\partial \dot{q}_{cr}''}{\partial T_{\infty}} \delta T_{\infty} \right)^2 \right)} \\ &= \left(0.06015 \frac{kW}{m^2 K} \right)^{-1} \sqrt{ \left(0.5 \frac{kW}{m^2} \right)^2 - \left(\left(\left(-4.445 \frac{kW}{m^2} \right) (0.09) \right)^2 + \left((331.1K) \left(0.5 \times 10^{-3} \frac{kW}{m^2 K} \right) \right)^2 + \left(\left(-0.01904 \frac{kW}{m^2 K} \right) (2K) \right)^2 \right)} \\ &\approx 4.11K \end{aligned}$$

2. $\delta(k\rho c)$

See Chapter 4 for detail.

The uncertainty of the slope of the best-fit line, $0.0444 \text{ s}^{-0.5}$, can be estimated through calculating 2 times the standard error of the slope, which is $\pm 0.00136 \text{ s}^{-0.5}$.

$$\begin{aligned} \frac{\partial(k\rho c)}{\partial(\text{slope})} &= \frac{-8}{\pi \cdot (\text{slope})^3} \left(\frac{\varepsilon \dot{q}_{cr}''}{T_{ig} - T_{\infty}} \right)^2 \\ &= \frac{-8}{\pi \cdot (0.0444 \text{ s}^{-0.5})^3} \left(\frac{(0.9) \left(10.5 \frac{kJ}{m^2} \right)}{((318 + 273)K) - ((20 + 273)K)} \right)^2 \\ &\approx -29.33 \frac{kJ^2}{m^4 K^2 s^{0.5}} \end{aligned}$$

$$\begin{aligned} \frac{\partial(k\rho c)}{\partial \varepsilon} &= \frac{8}{\pi \cdot (\text{slope})^2} \left(\frac{\dot{q}_{cr}''}{T_{ig} - T_{\infty}} \right)^2 \varepsilon \\ &= \frac{8}{\pi \cdot (0.0444s^{-0.5})^2} \left(\frac{\left(\frac{kJ}{m^2} \right)}{\left((318 + 273)K \right) - \left((20 + 273)K \right)} \right)^2 (0.9) \\ &\approx 1.446 \frac{kJ^2}{m^4 K^2 s} \end{aligned}$$

$$\begin{aligned} \frac{\partial(k\rho c)}{\partial \dot{q}_{cr}''} &= \frac{8}{\pi \cdot (\text{slope})^2} \left(\frac{\varepsilon}{T_{ig} - T_{\infty}} \right)^2 \dot{q}_{cr}'' \\ &= \frac{8}{\pi \cdot (0.0444s^{-0.5})^2} \left(\frac{(0.9)}{\left((318 + 273)K \right) - \left((20 + 273)K \right)} \right)^2 \left(\frac{kJ}{m^2} \right) \\ &\approx 0.1239 \frac{kJ}{m^2 K^2} \end{aligned}$$

$$\begin{aligned} \frac{\partial(k\rho c)}{\partial T_{ig}} &= \frac{-8}{\pi \cdot (\text{slope})^2} \left(\frac{\varepsilon \dot{q}_{cr}''}{T_{ig} - T_{\infty}} \right)^2 \frac{1}{T_{ig} - T_{\infty}} \\ &= \frac{-8}{\pi \cdot (0.0444s^{-0.5})^2} \left(\frac{(0.9) \left(\frac{kJ}{m^2} \right)}{\left((318 + 273)K \right) - \left((20 + 273)K \right)} \right)^2 \frac{1}{\left((318 + 273)K \right) - \left((20 + 273)K \right)} \\ &\approx -0.00437 \frac{kJ^2}{m^4 K^3 s} \end{aligned}$$

$$\begin{aligned}
\frac{\partial(k\rho c)}{\partial T_\infty} &= \frac{8}{\pi \cdot (\text{slope})^2} \left(\frac{\varepsilon \dot{q}_{cr}''}{T_{ig} - T_\infty} \right)^2 \frac{1}{T_{ig} - T_\infty} \\
&= \frac{8}{\pi \cdot (0.0444s^{-0.5})^2} \left(\frac{(0.9) \left(10.5 \frac{kJ}{m^2} \right)}{((318 + 273)K) - ((20 + 273)K)} \right)^2 \frac{1}{((318 + 273)K) - ((20 + 273)K)} \\
&\approx 0.00437 \frac{kJ^2}{m^4 K^3 s}
\end{aligned}$$

Therefore,

$$\begin{aligned} \delta(k\rho c) &= \sqrt{\left(\frac{\partial(k\rho c)}{\partial(\text{slope})} \delta(\text{slope})\right)^2 + \left(\frac{\partial(k\rho c)}{\partial \varepsilon} \delta \varepsilon\right)^2 + \left(\frac{\partial(k\rho c)}{\partial \dot{q}_{cr}''} \delta \dot{q}_{cr}''\right)^2} \\ &\quad + \sqrt{\left(\frac{\partial(k\rho c)}{\partial T_{ig}} \delta T_{ig}\right)^2 + \left(\frac{\partial(k\rho c)}{\partial T_{\infty}} \delta T_{\infty}\right)^2} \\ &= \sqrt{\left(\left(-29.33 \frac{kJ^2}{m^4 K^2 s^{0.5}}\right)(0.00136 s^{-0.5})\right)^2 + \left(\left(1.446 \frac{kJ^2}{m^4 K^2 s}\right)(0.09)\right)^2} \\ &\quad + \sqrt{\left(\left(-0.1239 \frac{kJ}{m^2 K^2}\right)\left(0.5 \frac{kW}{m^2}\right)\right)^2 + \left(\left(-0.00436 \frac{kJ^2}{m^4 K^3 s}\right)(4.1K)\right)^2} \\ &\quad + \sqrt{\left(\left(0.00436 \frac{kJ^2}{m^4 K^3 s}\right)(2K)\right)^2} \\ &\approx 0.151 \frac{kJ^2}{m^4 K^2 s} \end{aligned}$$

UNCERTAINTY FOR ESTIMATED PARAMETERS USING BURNING-RATE DATA ANALYSIS

1. $\delta\Delta h_{c,eff}$

This parameter is estimated by considering the average of the total heat released divided by the total amount of mass loss during three cone tests at 25, 50 and 75 kW/m² heat-flux levels. Assuming the estimated $\Delta h_{c,eff}$ at each test results in normal distribution, confidence interval with $\alpha = 0.05$ (95%) can be predicted using student t distribution with a sample size of three, which is ± 0.9 kJ/g.

2. $\delta\Delta h_g$

See Chapter 4 for detail.

The uncertainty of the slope ($=1/\Delta h_g=0.351$ g/kJ) can be estimated through calculating 2 times the standard error of the slope of the best-fit line, which is ± 0.127 .

Therefore, the uncertainty in Δh_g is

$$\begin{aligned} \frac{d(\Delta h_g)}{d(\text{slope})} &= -\frac{1}{(\text{slope})^2} \\ &= -\frac{1}{\left(0.351 \frac{\text{g}}{\text{kJ}}\right)^2} \\ &\approx -8.13 \frac{\text{kJ}^2}{\text{g}^2} \end{aligned}$$

Therefore,

$$\begin{aligned} \delta(\Delta h_g) &= \sqrt{\left(\frac{d(\Delta h_g)}{d(\text{slope})} \delta(\text{slope})\right)^2} \\ &= \sqrt{\left(\left(-8.13 \frac{\text{kJ}^2}{\text{g}^2}\right) (0.1274 \text{ g / kJ})\right)^2} \\ &\approx 1.036 \frac{\text{kJ}}{\text{g}} \end{aligned}$$

UNCERTAINTY SUMMARY

Table A(C)-6. Summary of model-parameter table with estimated values with uncertainty

Ignition Parameters	T_∞	$20 \pm 2 \text{ }^\circ\text{C}$
	T_{ig}	$318 \pm 4 \text{ }^\circ\text{C}$
	\dot{q}_{cr}''	$10.5 \pm 0.5 \text{ kW/m}^2$
	$k\rho c$	$0.649 \pm 0.151 \text{ kJ}^2/\text{m}^4\text{K}^2\text{s}$
Burning-Rate Parameters	$\Delta h_{c,eff}$	$24.6 \pm 0.9 \text{ kJ/g}$
	Δh_g	$2.9 \pm 1.0 \text{ kJ/g}$
	h_c	$12 \pm 0.5 \text{ W/m}^2\text{K}$
	ε	0.9 ± 0.09

Validation

Analyze Simulation Quality

DETERMINE DATA AND MODEL OUTPUT UNCERTAINTY TO MAKE COMPARISON

1. Conduct uncertainty analysis of data

From the experiment work done by Beaulieu and Dembsey¹ on thermally-thick behaving black PMMA using AFM apparatus, the experiment uncertainty in time-to-ignition and mass-loss rate at steady burning were determined as ± 2 s and ± 3 g/m²s, respectively. The test results were compared with other literature values using different apparatuses such as cone calorimeter in this work, which were considered as consistent. This uncertainty information will be used when comparing modeling output to experiment data.

2. Conduct uncertainty analysis for MLR profile modeling

Because uncertainty information of the data is found in terms of time-to-ignition and mass-loss rate, mass-loss-rate profile is considered as the modeling output of interest for comparison purposes. For Simple Analytical Models, time-to-ignition (t_{ig}) and steady-burning rate (\dot{m}'') are needed when simulating the mass-release-rate profile. The uncertainty in MLR profile in modeling can be determined via considering the uncertainties in the calculation results below:

$$t_{ig} \pm \delta t_{ig}$$
$$\dot{m}'' \pm \delta \dot{m}''$$

To determine the uncertainty in time-to-ignition, recall:

$$\frac{\dot{q}_{cr}''}{\dot{q}_e''} = F(t_{ig}) = \begin{cases} \frac{2 h_{ig} \sqrt{t_{ig}}}{\sqrt{\pi k \rho c}} & t_{ig} \leq t^* \\ 1 & t_{ig} > t^* \end{cases}$$

Knowing that all heat-flux levels of interest, 25, 50 and 75 kW/m², are above the critical heat flux, time-to-ignition should be smaller than t^* . Hence, uncertainty in t_{ig} can be estimated from linear-regression process as:

$$\frac{\dot{q}_{cr}''}{\dot{q}_e''} = \frac{2 h_{ig}}{\sqrt{\pi k \rho c}} \sqrt{t_{ig}}$$

The above equation can be re-written as below after conducting linear regression:

$$y \text{ estimate} = (\text{slope})\sqrt{t_{ig}}$$

Therefore,

$$t_{ig} = \left(\frac{y \text{ estimate}}{\text{slope}} \right)^2$$

Assuming that the y estimate and slope are independent and propagating the uncertainties in these two variables in estimating the time to ignition, the following calculation can be made:

$$\delta t_{ig} = \sqrt{\left(\frac{\partial t_{ig}}{\partial (y \text{ estimate})} \delta (y \text{ estimate}) \right)^2 + \left(\frac{\partial t_{ig}}{\partial (\text{slope})} \delta (\text{slope}) \right)^2}$$

where

$$\frac{\partial t_{ig}}{\partial (y \text{ estimate})} = \frac{2 \cdot (y \text{ estimate})}{(\text{slope})^2}$$

$$\frac{\partial t_{ig}}{\partial (\text{slope})} = - \frac{2 \cdot (y \text{ estimate})^2}{(\text{slope})^3}$$

with $\delta (y \text{ estimate})$ and $\delta (\text{slope})$ estimated through calculating 2 times the standard error of the y estimate and slope of the best-fit line, which are 0.002365 and 0.001363 s^{-0.5}, respectively.

To determine the uncertainty in steady-heat-release rate at post-ignition stage, recall:

$$\Delta h_g \equiv \frac{\dot{q}_{net}''}{\dot{m}''} = \frac{\dot{q}_e'' + \dot{q}_f'' - \dot{q}_l''}{\dot{m}''}$$

Above equation can be rearranged to

$$\dot{m}'' = \frac{1}{\Delta h_g} \dot{q}_e'' + \frac{\dot{q}_f'' - \dot{q}_l''}{\Delta h_g}$$

The steady-burning rate at post-ignition stage is determined by the best-fit line obtained when data are plotted as steady-burning rate versus applied heat flux. The uncertainty in steady-burning rate can be determined by considering 2 times the standard error of the y estimates, i.e., \dot{m}'' , which is obtained through linear-regression process: **± 4.5 g/m²s.**

COMPARE DATA WITH SIMULATION RESULTS WITH CONSIDERATION OF UNCERTAINTIES

Parameters in this simple analytical pyrolysis model have been estimated with cone calorimeter test data from 25, 50 and 75 kW/m². To check the quality of the modeling using the estimated parameters, three cases have been simulated and compared with experiment data, with the consideration of their uncertainty bands as shown in table and figures below (see Table A(C)-7).

Table A(C)-7. Comparison of time-to-ignition at different heat-flux levels from actual experiment and pyrolysis modeling

Heat-Flux Level	Actual t_{ig} (s) $t_{ig} \pm \delta t_i$	Model t_{ig} (s) $t_{ig} \pm \delta t_i$
25 kW/m ²	87 ± 2	90 ± 12
50 kW/m ²	22 ± 2	22 ± 5
75 kW/m ²	11 ± 2	10 ± 3

All three cases show good overlap between the data and simulation of time-to-ignition and the mass-loss rate during steady burning, considering the uncertainties, i.e., the parameter estimation was conducted successfully (see Figure A(C)-4, Figure A(C)-5 and Figure A(C)-6).

MLR at 25 kW/m²

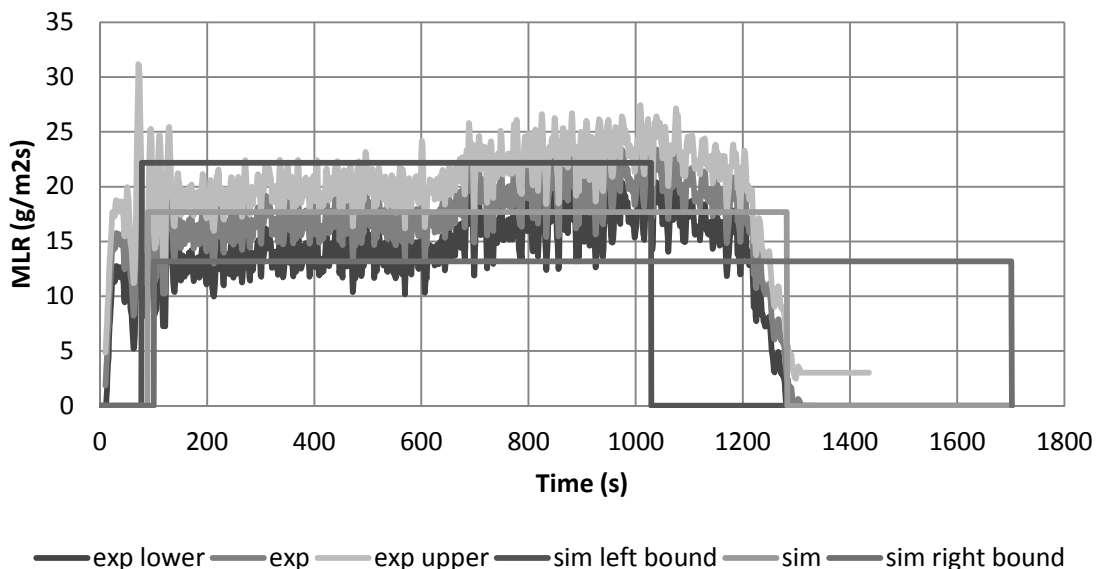


Figure A(C)-4. Mass-loss rate (MLR) comparisons for PMMA between actual MLR from experiment (exp) and modeled MLR (sim) at 25 kW/m². Note that data shown were used to estimate model-parameter values.

MLR at 50 kW/m²

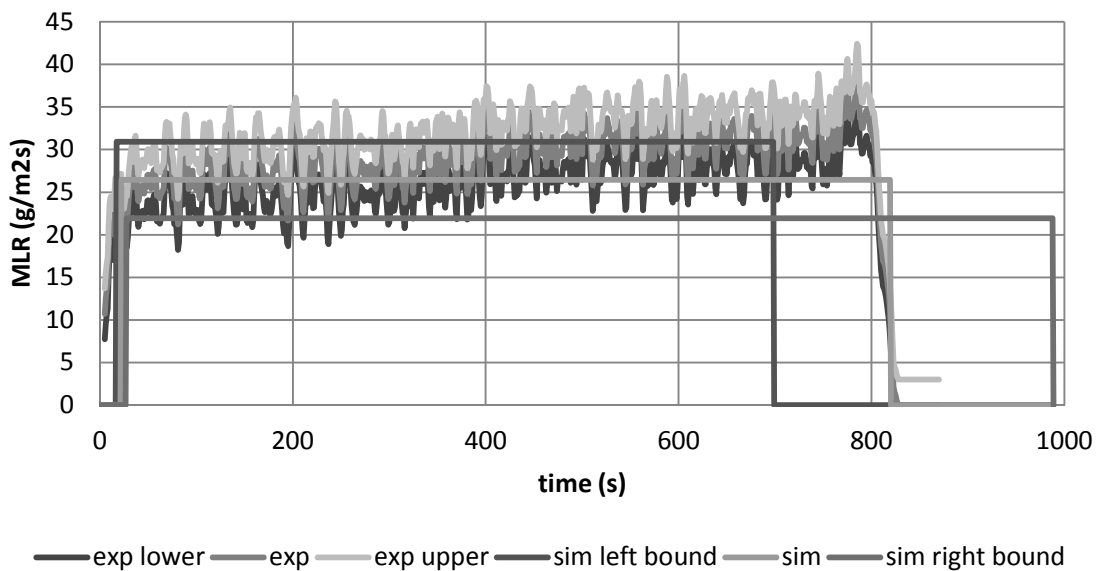


Figure A(C)-5. Mass-loss rate (MLR) comparisons for PMMA between actual MLR from experiment (exp) and modeled MLR (sim) at 50 kW/m². Note that data shown were used to estimate model-parameter values.

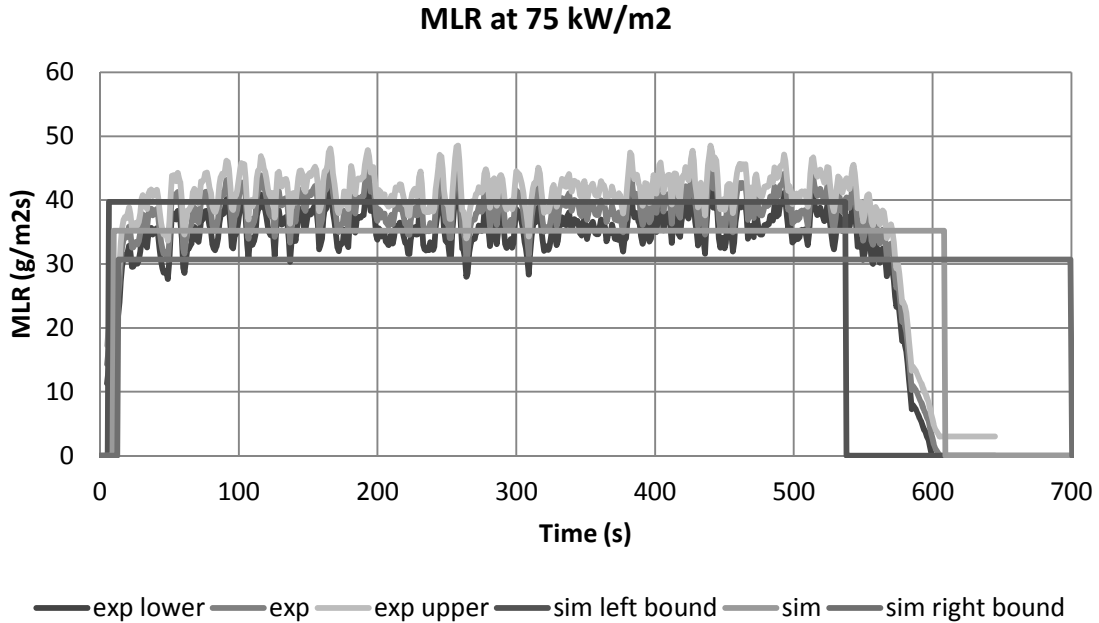


Figure A(C)-6. Mass-loss rate (MLR) comparisons for PMMA between actual MLR from experiment (exp) and modeled MLR (sim) at 75 kW/m². Note that data shown were used to estimate model-parameter values.

Validate Simulation Quality upon Extrapolation

In this example, cone calorimeter data at applied heat flux of 25, 50, and 75 kW/m² were used to estimate the unknown model parameters. In order to check the performance of modeling with the estimated parameters, PMMA AFM tests¹ conducted under 28.4 and 60 kW/m² are used to compare with modeling outputs – time-of-ignition and MLR at steady-burning stage (see Table A(C)-8).

Table A(C)-8. Comparison of time-to-ignition at different heat-flux levels from actual experiment and pyrolysis modeling

Heat-Flux Level	Actual t_{ig} (s) $t_{ig} \pm \delta t_i$	Model t_{ig} (s) $t_{ig} \pm \delta t_i$
28.4 kW/m ²	102 ± 2	70 ± 12
60 kW/m ²	31 ± 2	16 ± 5

In modeling time-to-ignition, the model’s outputs are shorter than those from AFM tests for both heat-flux levels. This discrepancy can be explained by considering the in-depth absorption of radiation during heating of PMMA. The data from AFM tests,

where IR lamps are used to heat the samples, possibly were subject to in-depth radiative absorption delaying ignition, knowing that the PMMA samples are somewhat transparent. However, this phenomenon is not accounted for in modeling assumptions and in parameter estimation process where cone calorimeter test data is used – in the cone, radiation is absorbed mostly on the surface.

In modeling the MLR at steady-burning stage, both cases show good overlap between the data and simulation, considering the uncertainties (see

Figure A(C)-7. Mass-loss rate (MLR) comparisons for PMMA between actual MLR from experiment (exp) and modeled MLR (sim) at 28.4 kW/m². Note that data shown were not included in the model-parameter-estimation process; hence, this case is considered as extrapolation case.

and Figure A(C)-8).

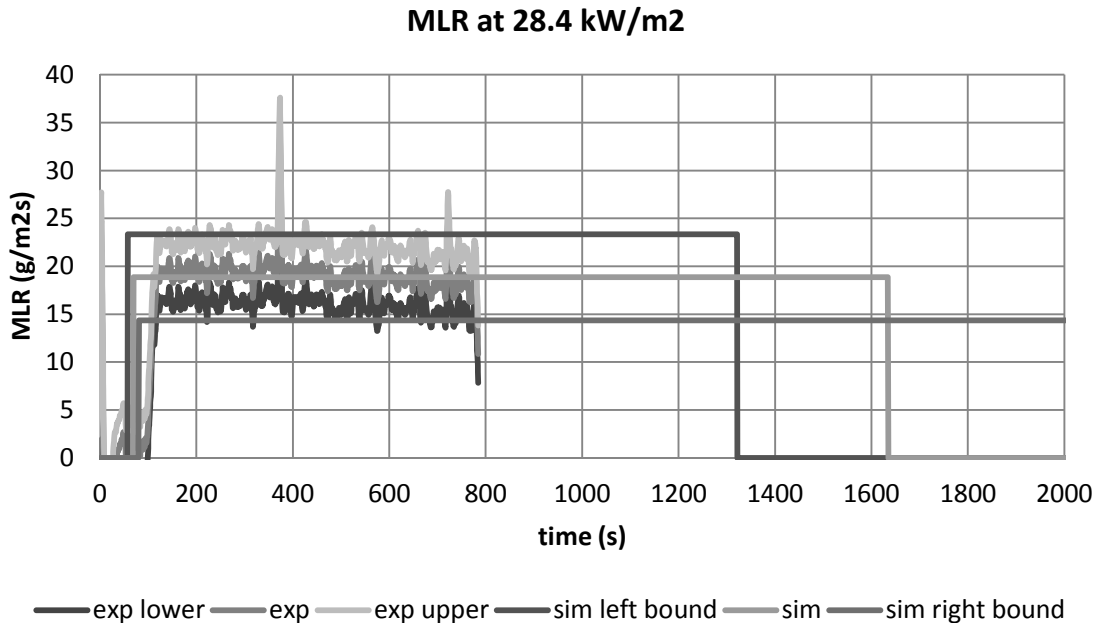


Figure A(C)-7. Mass-loss rate (MLR) comparisons for PMMA between actual MLR from experiment (exp) and modeled MLR (sim) at 28.4 kW/m². Note that data shown were not included in the model-parameter-estimation process; hence, this case is considered as extrapolation case.

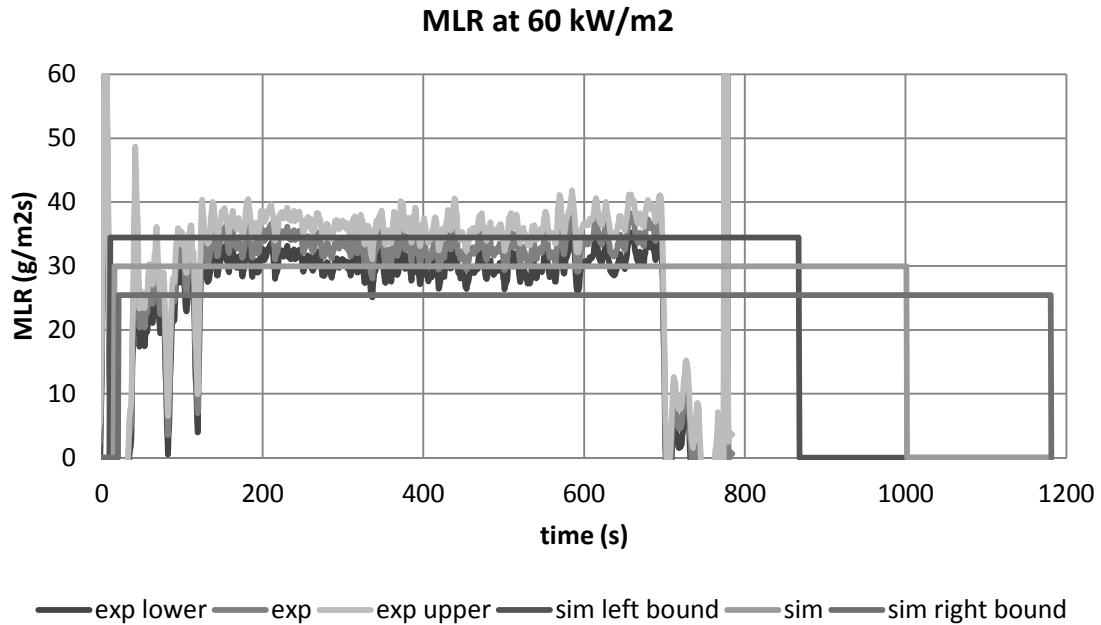


Figure A(C)-8. Mass-loss rate (MLR) comparisons for PMMA between actual MLR from experiment (exp) and modeled MLR (sim) at 60 kW/m². Note that data shown were not included in the model-parameter-estimation process; hence, this case is considered as extrapolation case.

Commentary

When using Simple Analytical Model to simulate pyrolysis of black PMMA (density 1170 kg/m^3 , thickness 18 mm), test data from a bench-scale cone calorimeter experiment at several heat-flux levels have been utilized to estimate the time-to-ignition from exposure to heating and the mass-loss rate at steady-burning stage after ignition. The comparison between the model outputs (time-to-ignition and steady-burning rate) and the data from bench-scale experiment showed good agreement for both checking purposes, where the same heat-flux levels (25, 50, and 75 kW/m^2) used in parameter estimation have been considered, and extrapolation purposes where heat-flux levels (28.4 and 60 kW/m^2) not included in the parameter estimation process have been considered.

Although the modeling predictions of time-to-ignition and steady-burning rate in this example seem to be reasonable, limitations of Simple Analytical Modeling has been acknowledged in literature for modeling black PMMA at relatively high applied heat-flux levels.¹ At high heat-flux levels, the assumption of having an inert condition during pre-ignition stage and neglecting thermal decomposition behavior, such as bubbling, cannot be made where these effects become more profound on the temperature profile and ignition process of PMMA. Therefore, caution should be given when conducting modeling for cases with higher heat-flux levels.

EXAMPLE 4.2 MODELING CORRUGATED CARDBOARD

Measure Parameters

1. *Ambient Temperature*

Direct measurement of ambient temperature is made as 23°C.

2. *Surface Temperature at Ignition*

This parameter will be obtained via Ignition Data Analysis, i.e., no direct measurements will be performed.

3. *Critical Heat Flux for Ignition*

Corrugated cardboard's CHF is measured to between 8 and 10 kW/m² from cone calorimeter testing by bracketing. Hence, CHF is 9 ± 1 kW/m².

4. *Thermal Inertia*

This parameter will be obtained via Ignition Data Analysis, i.e., no direct measurements will be performed.

5. *Effective Heat-of-Combustion*

This parameter will be obtained via Burning-Rate Data Analysis, i.e., no direct measurements will be performed.

6. *Heat-of-Gasification*

This parameter will be obtained via Burning-Rate Data Analysis, i.e., no direct measurements will be performed.

7. *Convection Coefficient*

Because this is a material laid in horizontal position in a cone calorimeter, $h_c = 12$ W/m²K is used based on literature reference.

8. *Surface Emissivity/Absorptivity*

Emissivity is approximated as 0.9.

Summary

Table A(C)-9. Summary of model-parameter table with estimated values via direct measurements, literature search, or approximation

Ignition Parameters	T_{∞}	23 °C
	T_{ig}	Ignition Data Analysis
	\dot{q}_{cr}''	9 kW/m ²
	$k\rho c$	Ignition Data Analysis
Burning-Rate Parameters	$\Delta h_{c,eff}$	Burning-Rate Data Analysis
	Δh_g	Burning-Rate Data Analysis
	h_c	12 W/m ² K
	ε	0.9

Obtain Parameters via Data Analysis

Run Model

SELECT MODEL: THERMALLY THICK MODEL FOR IGNITION ANALYSIS (QUINTIERE AND HARKLEROAD, ASTM E 1321) AND STEADY-BURNING MODEL

UNDERSTAND EXPERIMENT AND FIRE CHARACTERISTICS OF MATERIAL

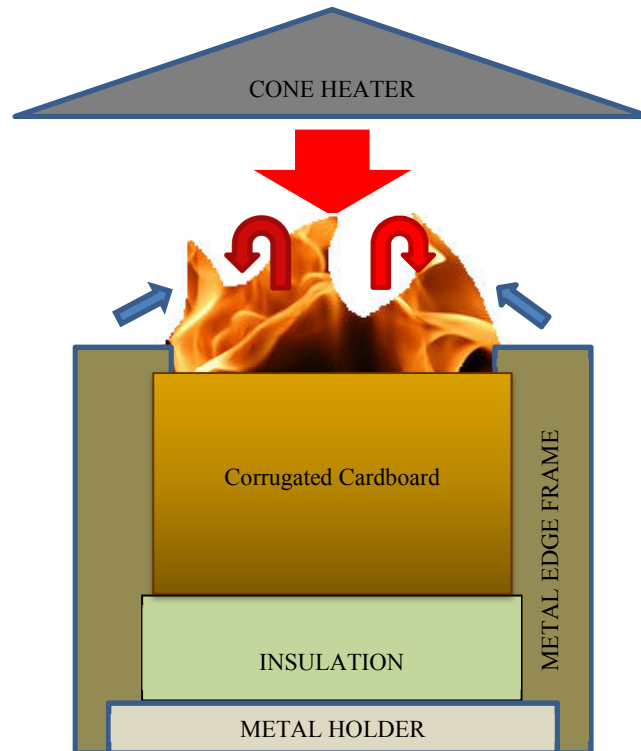


Figure A(C)-9. Simplified representation of a cone calorimeter test of corrugated cardboard

A simplified representation of a cone calorimeter test of triple-layered corrugated cardboard is shown in Figure A(C)-9. The sample is placed on top of an insulation, which sits on a metal holder. Another metal frame is placed on top of the sample, insulation and the holder. A metal edge frame is used as well.

Front Surface: As heating starts by opening the shutter to allow radiation from the cone heater to impinge on sample surface (large red arrow), cooling also begins via natural convection (blue arrows) and re-radiation. The surface decomposes with charring, i.e., surface becoming black and white smoke, which typically indicates moisture loss with heating of the sample. Note that the surface becomes non-uniformly black due to corrugation showing linear shading. As the surface layer is burned away, it exfoliates toward the sides and opens up, allowing the first layer of the corrugation to

appear on the surface. Then the middle flat layer of the cardboard, which separates the two layers of corrugation, starts to burn, allowing the heat release to grow. As this layer is decomposed throughout, the second layer of the corrugation becomes involved in burning process. Followed by the burning of the second corrugation layer, the last flat layer of the cardboard – the back surface of the sample – burns. This results in another growing phase in the heat-release-rate curve. When ignition occurs as the fuel vapor concentration above the surface exceeds its LFL (lower flammable limit), additional heat flux from the flame is introduced on the surface (red arrows).

Back surface: The sample is placed on top of insulation. In the experiment, an air gap of a few millimeters thickness exists between the sample and the insulation due to thermal contact. Nothing leaves through the back face with the insulation when 1D assumption holds for the experiment.

CONFIGURE MODEL CONDITIONS BASED ON UNDERSTANDING OF EXPERIMENT AND MATERIAL CHARACTERISTICS

In the model, the phenomena discussed above are simulated as below. Basic assumptions are as follows:

- Pre-ignition stage is:
 - Inert: non-uniform charring is considered to be evenly distributed
 - Thermally thick: heat transfer does not reach back surface
- Post-ignition stage is:
 - Considered to have instantaneous release of volatiles from solid to gas phase
 - Considered to have a constant thickness: exfoliation of surface layers is neglected
 - Steady burning: heat loss equals heat gain at front surface

ACQUIRE DATA SETS

Cone calorimeter test data of triple layered corrugated cardboard with thickness of 15 mm, density of 116 kg/m^3 and applied heat flux levels ranging from 8 to 75 kW/m^2 are found. For Ignition Data analysis, only time-to-ignition with respect to applied heat-flux data will be used. For burning-rate data analysis, data for the entire testing time duration,

mass loss, and heat release during testing period with respect to applied heat flux will be used.

CONDUCT IGNITION DATA ANALYSIS

1. Estimate T_{ig}

Heat balance at front surface during steady burning is as follow:

$$\varepsilon \dot{q}_{cr}'' = h_c (T_{ig} - T_\infty) + \varepsilon \sigma (T_{ig}^4 - T_\infty^4)$$

Knowing that emissivity is approximated as 0.9, critical heat flux is estimated as 9 kW/m², and heat-transfer in cone calorimeter experiment is estimated as 12.0 W/m²K, ignition temperature, T_{ig} is calculated as:

$$T_{ig} = 293 \text{ }^\circ\text{C}$$

2. Estimate h_{ig}

h_{ig} is the total-heat-transfer coefficient at ignition; therefore, at steady-state burning stage, the following can be defined:

$$\varepsilon \dot{q}_{cr}'' \equiv h_{ig} (T_{ig} - T_\infty)$$

Knowing the ignition temperature, h_{ig} can be calculated:

$$h_{ig} = 30.0 \text{ W/m}^2\text{K}$$

3. Calculate $\dot{q}_{cr}'' / \dot{q}_e''$ versus $\sqrt{t_{ig}}$ from ignition data

Table A(C)-10. $\dot{q}_{cr}'' / \dot{q}_e''$ versus $\sqrt{t_{ig}}$

Heat Flux (kW/m ²)	t_{ig} (s)	CHF/HF	$t_{ig}^{0.5}$ (s ^{0.5})
8	NI		
10	387	0.9000	19.67
15	103	0.6000	10.15
20	52	0.4500	7.21
25	32	0.3600	5.66
25	34	0.3600	5.83
25	33	0.3600	5.74
25	28	0.3600	5.29
40	9	0.2250	3.00
40	11	0.2250	3.32
50	11	0.1800	3.32
60	8	0.1500	2.83
60	8	0.1500	2.83
75	2	0.1200	1.41

4. Plot $\dot{q}_{cr}'' / \dot{q}_e''$ versus $\sqrt{t_{ig}}$ to estimate the time needed to reach “steady-state” burning, t^* and thermal inertia, $k\rho c$

$$\text{Recall } \frac{\dot{q}_{cr}''}{\dot{q}_e''} = F(t_{ig}) = \begin{cases} \frac{2 h_{ig} \sqrt{t_{ig}}}{\sqrt{\pi k \rho c}} & t_{ig} \leq t^* \\ 1 & t_{ig} > t^* \end{cases} \quad \text{for piloted-ignition data, where } t^* \text{ is}$$

the time when $\dot{q}_{cr}'' / \dot{q}_e'' = 1$. Thermal inertia can be estimated from the best-fit line through

$t = 0$. Its slope at $0 < t < t^*$ is $\frac{2 h_{ig}}{\sqrt{\pi k \rho c}}$; therefore, $k\rho c = \frac{4 h_{ig}^2}{\pi \cdot (slope)^2}$. Note that in the

analysis, few data points at lower heat-flux levels with large time-to-ignition data were excluded (see Figure A(C)-10, open circles) to increase fitness of the best-fit line. This approach is reasonable, considering that at this region analysis assumptions of having inert and thermally thick conditions are less likely to be satisfied.

$$k\rho c = 0.297 \text{ kJ}^2/\text{m}^4\text{K}^2\text{s}$$

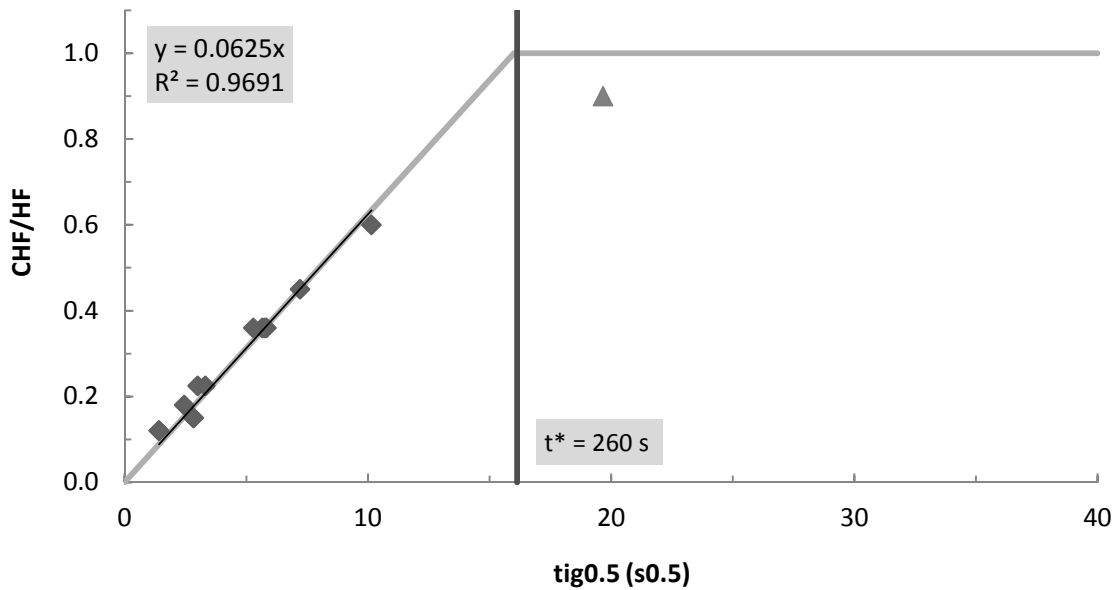


Figure A(C)-10. Plot of $\dot{q}_{cr}'' / \dot{q}_e''$ versus $\sqrt{t_{ig}}$

CONDUCT BURNING-RATE DATA ANALYSIS

1. Estimate $\Delta h_{c,eff}$

There are two approaches in estimating the effective heat-of-combustion via calorimeter tests: by using the peak in HRR or the average heat released over the entire test. In this example, $\Delta h_{c,eff}$ will be estimated by considering the average heat-release rate divided by the average mass-loss rate during a test. Cone test results ranging from 15 to 75 kW/m² are used:

$$\Delta h_{c,eff} = 13.9 \text{ kJ/g}$$

2. Estimate Δh_g

Recall $\Delta h_g \equiv \frac{\dot{q}_{net}''}{\dot{m}''} = \frac{\dot{q}_e'' + \dot{q}_f'' - \dot{q}_l''}{\dot{m}''}$; therefore, when plotting mass-loss rates at

different radiant-heat-flux levels during steady-burning condition, the reciprocal of the slope of the best-fit line should be the heat-of-gasification (see Table A(C)-11 and Figure A(C)-11).

$$\Delta h_g = 21.6 \text{ kJ/g}$$

Table A(C)-11. Estimation of effective heat-of-gasification using cone calorimeter test results at applied heat flux ranging between 25 and 75 kW/m²

Heat Flux (kW/m ²)	avgMLR (g/m ² s)
25	6.70
25	6.59
40	6.93
50	7.95
60	8.64
60	9.09
75	8.30

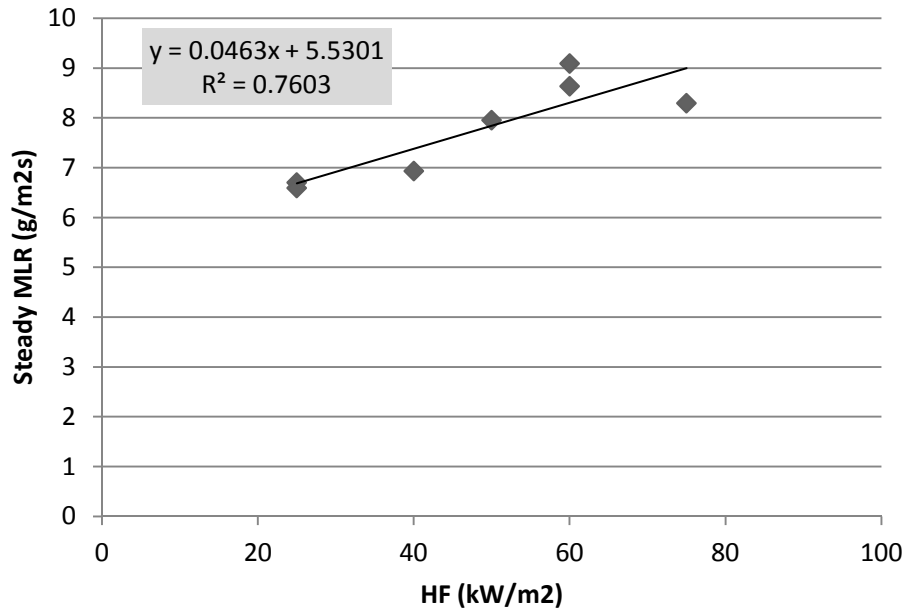


Figure A(C)-11. Plot of steady MLR versus different applied heat-flux levels – 25 to 75 kW/m²

Obtain Uncertainty for Estimated Parameters

UNCERTAINTY FOR MEASURED PARAMETERS

1. δT_{∞}

Fluctuation in ambient temperature during testing is estimated to be less than $\pm 15\%$ of reported measurement data.

2. $\delta \dot{q}_{cr}''$

The resolution of bracketing experiment was 2 kW/m^2 ; hence, uncertainty can be estimated as $\pm 1 \text{ kW/m}^2$.

3. δh_c

Considering that the reference values sited in the *Guide* for different apparatuses and set-up have two significant figures, uncertainty for this convection coefficient can be estimated as $\pm 0.5 \text{ W/m}^2\text{K}$.

4. $\delta \varepsilon$

Based on literature review, cardboard's emissivity should be within $\pm 10\%$ of what has been approximated in this example.

UNCERTAINTY FOR ESTIMATED PARAMETERS USING IGNITION DATA ANALYSIS

1. δT_{ig}

See Chapter 4 for detail.

$$\begin{aligned} \frac{\partial \dot{q}_{cr}''}{\partial T_{ig}} &= \frac{h_c + 4\varepsilon\sigma T_{ig}^3}{\varepsilon} \\ &= \frac{\left(0.012 \frac{kW}{m^2 K}\right) + 4(0.9)\left(5.67 \times 10^{-11} \frac{kW}{K^4 m^2}\right)\left((293 + 273)K\right)^3}{(0.9)} \\ &\approx 0.05446 \frac{kW}{m^2 K} \\ \frac{\partial \dot{q}_{cr}''}{\partial \varepsilon} &= \frac{-\dot{q}_{cr}'' + \sigma(T_{ig}^4 - T_{\infty}^4)}{\varepsilon} \\ &= \frac{-\left(9 \frac{kW}{m^2}\right) + \left(5.67 \times 10^{-11} \frac{kW}{K^4 m^2}\right)\left(\left((293 + 273)K\right)^4 - \left((23 + 273)K\right)^4\right)}{(0.9)} \\ &\approx -4.018 \frac{kW}{m^2} \\ \frac{\partial \dot{q}_{cr}''}{\partial h_c} &= \frac{T_{ig} - T_{\infty}}{\varepsilon} \\ &= \frac{\left((293 + 273)K\right) - \left((23 + 273)K\right)}{(0.9)} \\ &\approx 300.0K \end{aligned}$$

$$\begin{aligned}\frac{\partial \dot{q}_{cr}''}{\partial T_{\infty}} &= \frac{-h_c - 4\varepsilon\sigma T_{\infty}^3}{\varepsilon} \\ &= \frac{-\left(0.012 \frac{kW}{m^2 K}\right) - 4(0.9)\left(5.67 \times 10^{-11} \frac{kW}{K^4 m^2}\right)((23 + 273)K)^3}{(0.9)} \\ &\approx -0.01922 \frac{kW}{m^2 K}\end{aligned}$$

Therefore,

$$\begin{aligned}\delta T_{ig} &= \left(\frac{\partial \dot{q}_{cr}''}{\partial T_{ig}}\right)^{-1} \sqrt{\left(\delta \dot{q}_{cr}''\right)^2 - \left(\left(\frac{\partial \dot{q}_{cr}''}{\partial \varepsilon} \delta \varepsilon\right)^2 + \left(\frac{\partial \dot{q}_{cr}''}{\partial h_c} \delta h_c\right)^2 + \left(\frac{\partial \dot{q}_{cr}''}{\partial T_{\infty}} \delta T_{\infty}\right)^2\right)} \\ &= \left(0.05446 \frac{kW}{m^2 K}\right)^{-1} \sqrt{\left(1 \frac{kW}{m^2}\right)^2 - \left[\left(\left(-4.018 \frac{kW}{m^2}\right)(0.09)\right)^2 + \left(300.0K\right)\left(0.5 \times 10^{-3} \frac{kW}{m^2 K}\right)\right]^2 + \left[\left(-0.01922 \frac{kW}{m^2 K}\right)(3.45K)\right]^2} \\ &\approx 16.9K\end{aligned}$$

2. $\delta(k\rho c)$

See Chapter 4 for detail.

The uncertainty of the slope of the best-fit line, $0.0620 \text{ s}^{-0.5}$, can be estimated through calculating 2 times the standard error of the slope, which is $\pm 0.00282 \text{ s}^{-0.5}$.

$$\begin{aligned}\frac{\partial(k\rho c)}{\partial(\text{slope})} &= \frac{-8}{\pi \cdot (\text{slope})^3} \left(\frac{\varepsilon \dot{q}_{cr}''}{T_{ig} - T_{\infty}}\right)^2 \\ &= \frac{-8}{\pi \cdot (0.0620 \text{ s}^{-0.5})^3} \left(\frac{(0.9) \left(9 \frac{kJ}{m^2}\right)}{\left((293 + 273)K\right) - \left((23 + 273)K\right)}\right)^2 \\ &\approx -9.612 \frac{kJ^2}{m^4 K^2 s^{0.5}}\end{aligned}$$

$$\begin{aligned} \frac{\partial(k\rho c)}{\partial \varepsilon} &= \frac{8}{\pi \cdot (\text{slope})^2} \left(\frac{\dot{q}_{cr}''}{T_{ig} - T_{\infty}} \right)^2 \varepsilon \\ &= \frac{8}{\pi \cdot (0.0620s^{-0.5})^2} \left(\frac{\left(\frac{kJ}{9 \frac{s}{m^2}} \right)}{((293 + 273)K) - ((23 + 273)K)} \right)^2 \quad (0.9) \\ &\approx 0.662 \frac{kJ^2}{m^4 K^2 s} \end{aligned}$$

$$\begin{aligned} \frac{\partial(k\rho c)}{\partial \dot{q}_{cr}''} &= \frac{8}{\pi \cdot (\text{slope})^2} \left(\frac{\varepsilon}{T_{ig} - T_{\infty}} \right)^2 \dot{q}_{cr}'' \\ &= \frac{8}{\pi \cdot (0.060s^{-0.5})^2} \left(\frac{(0.9)}{((293 + 273)K) - ((23 + 273)K)} \right)^2 \left(\frac{kJ}{9 \frac{s}{m^2}} \right) \\ &\approx 0.0662 \frac{kJ}{m^2 K^2} \end{aligned}$$

$$\begin{aligned} \frac{\partial(k\rho c)}{\partial T_{ig}} &= \frac{-8}{\pi \cdot (\text{slope})^2} \left(\frac{\varepsilon \dot{q}_{cr}''}{T_{ig} - T_{\infty}} \right)^2 \frac{1}{T_{ig} - T_{\infty}} \\ &= \frac{-8}{\pi \cdot (0.0620s^{-0.5})^2} \left(\frac{(0.9) \left(\frac{kJ}{9 \frac{s}{m^2}} \right)}{((293 + 273)K) - ((23 + 273)K)} \right)^2 \frac{1}{((293 + 273)K) - ((23 + 273)K)} \\ &\approx -0.00221 \frac{kJ^2}{m^4 K^3 s} \end{aligned}$$

$$\begin{aligned}
\frac{\partial(k\rho c)}{\partial T_\infty} &= \frac{8}{\pi \cdot (\text{slope})^2} \left(\frac{\varepsilon \dot{q}_{cr}''}{T_{ig} - T_\infty} \right)^2 \frac{1}{T_{ig} - T_\infty} \\
&= \frac{8}{\pi \cdot (0.0620s^{-0.5})^2} \left(\frac{(0.9) \left(9 \frac{kJ}{m^2} \right)}{((293 + 273)K) - ((23 + 273)K)} \right)^2 \frac{1}{((293 + 273)K) - ((23 + 273)K)} \\
&\approx 0.00221 \frac{kJ^2}{m^4 K^3 s}
\end{aligned}$$

Therefore,

$$\begin{aligned}
\delta(k\rho c) &= \sqrt{\left(\frac{\partial(k\rho c)}{\partial(\text{slope})} \delta(\text{slope}) \right)^2 + \left(\frac{\partial(k\rho c)}{\partial \varepsilon} \delta \varepsilon \right)^2 + \left(\frac{\partial(k\rho c)}{\partial \dot{q}_{cr}''} \delta \dot{q}_{cr}'' \right)^2} \\
&\quad + \sqrt{\left(\frac{\partial(k\rho c)}{\partial T_{ig}} \delta T_{ig} \right)^2 + \left(\frac{\partial(k\rho c)}{\partial T_\infty} \delta T_\infty \right)^2} \\
&= \sqrt{\left(\left(-9.612 \frac{kJ^2}{m^4 K^2 s^{0.5}} \right) (0.00282s^{-0.5}) \right)^2 + \left(\left(0.662 \frac{kJ^2}{m^4 K^2 s} \right) (0.09) \right)^2} \\
&\quad + \sqrt{\left(\left(-0.0662 \frac{kJ}{m^2 K^2} \right) \left(1 \frac{kW}{m^2} \right) \right)^2 + \left(\left(-0.00221 \frac{kJ^2}{m^4 K^3 s} \right) (16.9K) \right)^2} \\
&\quad + \sqrt{\left(\left(0.00221 \frac{kJ^2}{m^4 K^3 s} \right) (3.45K) \right)^2} \\
&\approx 0.101 \frac{kJ^2}{m^4 K^2 s}
\end{aligned}$$

UNCERTAINTY FOR ESTIMATED PARAMETERS USING BURNING-RATE DATA ANALYSIS

1. $\delta \Delta h_{c,eff}$

This parameter is estimated by considering the average of the heat-release rate divided by the average mass-loss rate during cone tests at 15 to 75 kW/m² heat-flux levels. Assuming the estimated $\Delta h_{c,eff}$ at each test results in normal distribution, confidence interval with $\alpha = 0.05$ (95%) can be predicted using student t distribution with a sample size of nine, which is ± 1.3 kJ/g.

2. $\delta\Delta h_g$

See Chapter 4 for detail.

The uncertainty of the slope ($=1/\Delta h_g=0.04625\text{g/kJ}$) can be estimated through calculating 2 times the standard error of the slope of the best-fit line, which is +/- 0.02323. Therefore, the uncertainty in Δh_g is

$$\begin{aligned} \frac{d(\Delta h_g)}{d(\text{slope})} &= -\frac{1}{(\text{slope})^2} \\ &= -\frac{1}{\left(0.04625 \frac{\text{g}}{\text{kJ}}\right)^2} \\ &\approx -467 \frac{\text{kJ}^2}{\text{g}^2} \end{aligned}$$

Therefore,

$$\begin{aligned} \delta(\Delta h_g) &= \sqrt{\left(\frac{d(\Delta h_g)}{d(\text{slope})} \delta(\text{slope})\right)^2} \\ &= \sqrt{\left(\left(-467 \frac{\text{kJ}^2}{\text{g}^2}\right)(0.02323 \text{ g / kJ})\right)^2} \\ &\approx 10.9 \frac{\text{kJ}}{\text{g}} \end{aligned}$$

UNCERTAINTY SUMMARY

Table A(C)-12. Summary of model-parameter table with estimated values with uncertainty

Ignition Parameters	T_∞	$23 \pm 3.45 \text{ }^\circ\text{C}$
	T_{ig}	$293 \pm 17 \text{ }^\circ\text{C}$
	\dot{q}_{cr}''	$9 \pm 1 \text{ kW/m}^2$
	$k\rho c$	$0.297 \pm 0.101 \text{ kJ}^2/\text{m}^4\text{K}^2\text{s}$
Burning-Rate Parameters	$\Delta h_{c,eff}$	$13.9 \pm 1.3 \text{ kJ/g}$
	Δh_g	$21.6 \pm 10.9 \text{ kJ/g}$
	h_c	$12 \pm 0.5 \text{ W/m}^2\text{K}$
	ε	0.9 ± 0.09

Validation

Analyze Simulation Quality

DETERMINE DATA AND MODEL OUTPUT UNCERTAINTY TO MAKE COMPARISON

1. Conduct uncertainty analysis of data

The uncertainty in the mass-loss-rate data used for comparison between data and model outputs is estimated via statistical approach, taking the standard deviation (0.58 g/sm^2) from the mean of a steady burning of five identical PMMA tests conducted in a cone calorimeter.² The estimated uncertainty is 1.4 g/sm^2 , which is found by calculating the 95% confidence interval applying student t distribution with a sample size of five.

The uncertainty in time-to-ignition data used for comparison is estimated via statistical approach, taking two to four identical cone calorimeter test data at heat fluxes ranging from 25 to 75 kW/m^2 of this cardboard. 95% confidence interval is calculated for each heat-flux level assuming student t distribution.

2. Conduct uncertainty analysis for MLR profile modeling

Because uncertainty information of the data is found in terms of time-to-ignition and mass-loss rate, mass-loss-rate profile is considered as the modeling output of interest for comparison purposes. For Simple Analytical Models, time-to-ignition (t_{ig}) and steady-burning rate (\dot{m}'') are needed when simulating the mass-release-rate profile. The uncertainty in MLR profile in modeling can be determined via considering the uncertainties in these calculation results as below:

$$t_{ig} \pm \delta t_{ig}$$
$$\dot{m}'' \pm \delta \dot{m}''$$

To determine the uncertainty in time-to-ignition, recall:

$$\frac{\dot{q}_{cr}''}{\dot{q}_e''} = F(t_{ig}) = \begin{cases} \frac{2 h_{ig} \sqrt{t_{ig}}}{\sqrt{\pi k \rho c}} & t_{ig} \leq t^* \\ 1 & t_{ig} > t^* \end{cases}$$

Knowing that all of heat-flux levels of interest, 25, 50, and 75 kW/m^2 , are above the critical heat flux, time-to-ignition should be smaller than t^* . Hence, uncertainty in t_{ig} can be estimated from linear-regression process as below:

$$\frac{\dot{q}_{cr}''}{\dot{q}_e''} = \frac{2 h_{ig}}{\sqrt{\pi k \rho c}} \sqrt{t_{ig}}$$

The above equation can be re-written as below after conducting linear regression:

$$y \text{ estimate} = (\text{slope}) \sqrt{t_{ig}}$$

Therefore,

$$t_{ig} = \left(\frac{y \text{ estimate}}{\text{slope}} \right)^2$$

Assuming that the y estimate and slope are independent and propagating the uncertainties in these two variables in estimating the time to ignition, the following calculation can be made:

$$\delta t_{ig} = \sqrt{\left(\frac{\partial t_{ig}}{\partial (y \text{ estimate})} \delta (y \text{ estimate}) \right)^2 + \left(\frac{\partial t_{ig}}{\partial (\text{slope})} \delta (\text{slope}) \right)^2}$$

where

$$\frac{\partial t_{ig}}{\partial (y \text{ estimate})} = \frac{2 \cdot (y \text{ estimate})}{(\text{slope})^2}$$

$$\frac{\partial t_{ig}}{\partial (\text{slope})} = - \frac{2 \cdot (y \text{ estimate})^2}{(\text{slope})^3}$$

with $\delta (y \text{ estimate})$ and $\delta (\text{slope})$ estimated through calculating 2 times the standard error of the y estimate and slope of the best-fit line.

To determine the uncertainty in steady-heat-release rate at post-ignition stage, recall:

$$\Delta h_g \equiv \frac{\dot{q}_{net}''}{\dot{m}''} = \frac{\dot{q}_e'' + \dot{q}_f'' - \dot{q}_l''}{\dot{m}''}$$

Above equation can be rearranged to

$$\dot{m}'' = \frac{1}{\Delta h_g} \dot{q}_e'' + \frac{\dot{q}_f'' - \dot{q}_l''}{\Delta h_g}$$

The steady-burning rate at post-ignition stage is determined by the best-fit line obtained when data is plotted as steady-burning rate versus applied heat flux. The uncertainty in steady-burning rate can be determined by considering 2 times the standard

error of the y estimates, i.e., \dot{m}'' , which is obtained through linear-regression process: \pm 1.1 g/m²s.

COMPARE DATA WITH SIMULATION RESULTS WITH CONSIDERATION OF UNCERTAINTIES

Parameters in this simple analytical pyrolysis model have been estimated with cone calorimeter test data from 25, 50, and 75 kW/m². To check the quality of the modeling using the estimated parameters, three cases have been simulated and compared with experiment data with the consideration of their uncertainty bands as shown in Table

A(C)-13 and figures –

Figure A(C)-12, Figure A(C)-13 and Figure A(C)-14 – below.

Table A(C)-13. Comparison of time-to-ignition at different heat-flux levels from actual experiment and pyrolysis modeling

Heat Flux Level	Actual t_{ig} (s) $t_{ig} \pm \delta t_i$	Model t_{ig} (s) $t_{ig} \pm \delta t_i$
25 kW/m ²	32 ± 4	34 ± 10
50 kW/m ²	18 ± 89	8 ± 5
75 kW/m ²	2 ± 5	4 ± 3

All three cases show good overlap between the data and simulation of time-to-ignition and the mass-loss rate during steady burning, considering the uncertainties, i.e., the parameter estimation was conducted successfully.

MLR at 25 kW/m²

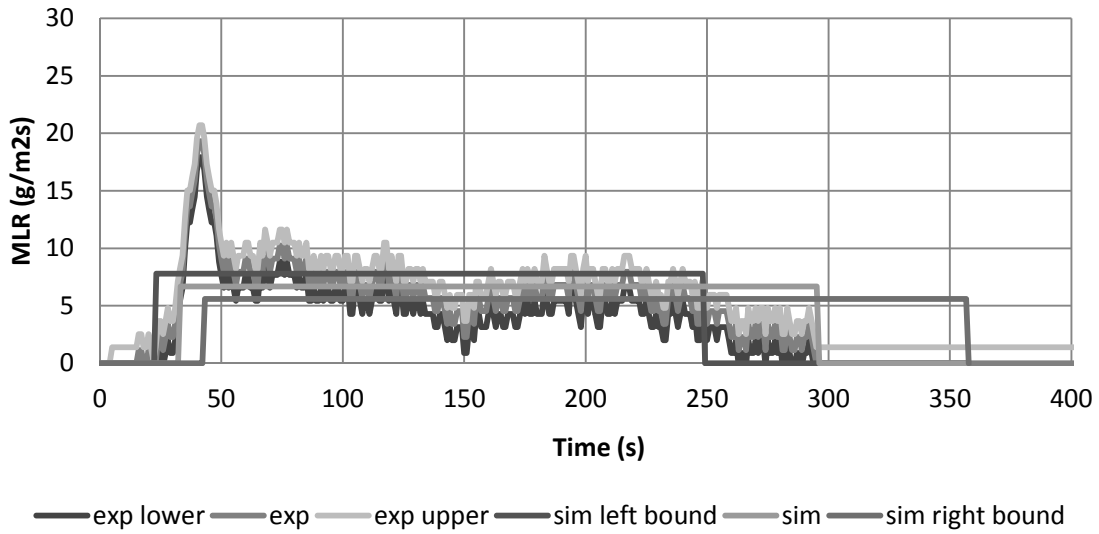


Figure A(C)-12. Mass-loss rate (MLR) comparisons for corrugated cardboard between actual MLR from experiment (exp) and modeled MLR (sim) at 25 kW/m². Note that data shown were used to estimate model-parameter values.

MLR at 50 kW/m²

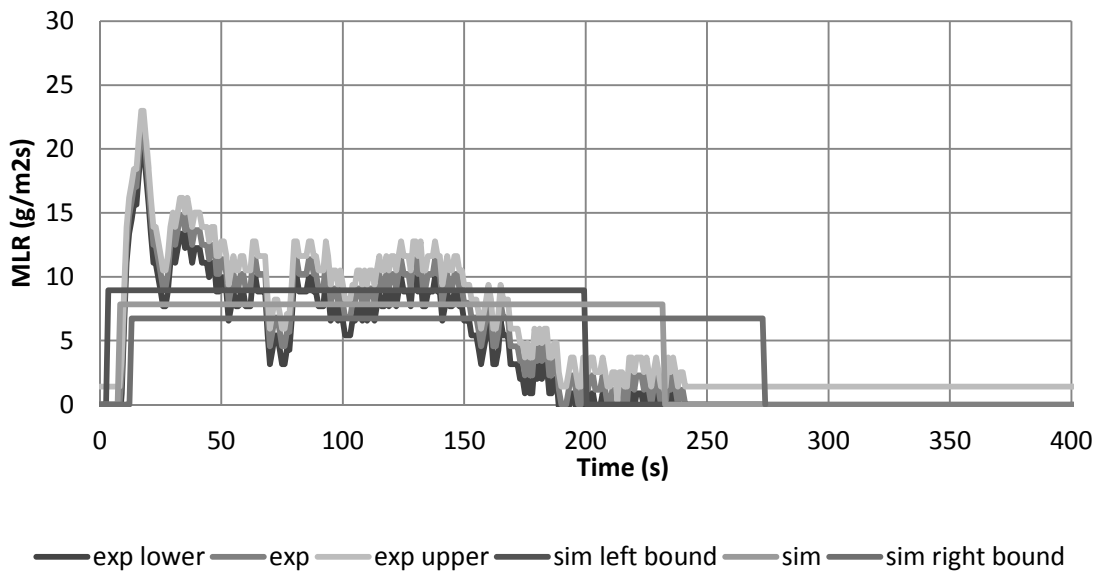


Figure A(C)-13. Mass-loss rate (MLR) comparisons for corrugated cardboard between actual MLR from experiment (exp) and modeled MLR (sim) at 50 kW/m². Note that data shown were used to estimate model-parameter values.

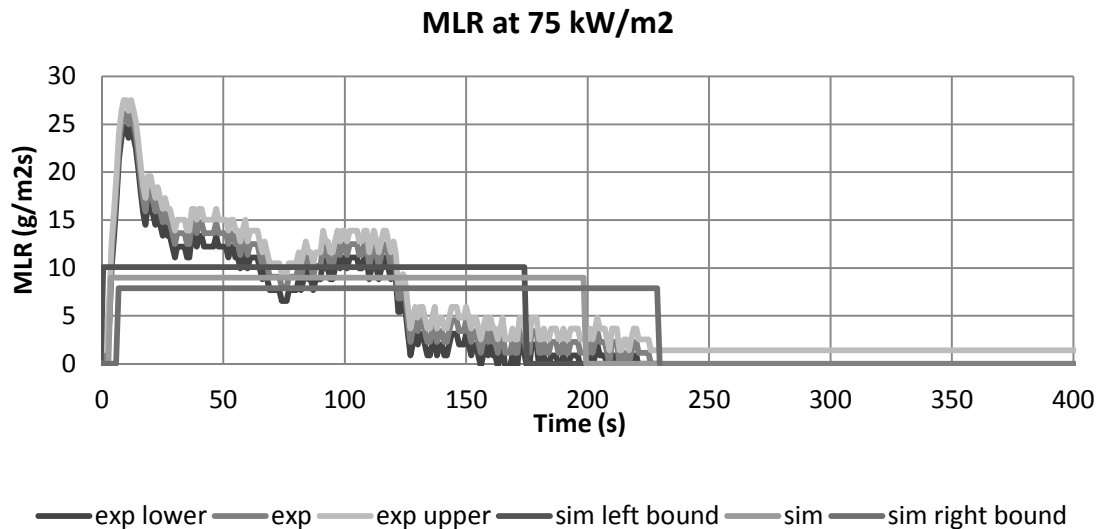


Figure A(C)-14. Mass-loss rate (MLR) comparisons for corrugated cardboard between actual MLR from experiment (exp) and modeled MLR (sim) at 75 kW/m². Note that data shown were used to estimate model-parameter values.

Validate Simulation Quality upon Extrapolation

In this example, cone calorimeter data at applied heat flux ranging from 8 to 75 kW/m² were used to estimate the unknown model parameters. Assuming that the estimated parameters for this corrugated cardboard will be used in pyrolysis modeling at applied heat-flux levels that are within above range, no additional check becomes necessary.

Commentary

When using Simple Analytical Model to simulate pyrolysis of triple-layered corrugated cardboard (density 116 kg/m³, thickness 15 mm), test data from a bench-scale cone calorimeter experiment at several heat-flux levels have been utilized to estimate the time-to-ignition from exposure to heating and the mass-loss rate at steady-burning stage after ignition. The comparison between the model outputs (time-to-ignition and steady-

burning rate) and the data from bench-scale experiment showed good agreement for both checking purposes, where the same heat-flux levels (25, 50, and 75 kW/m²) used in parameter estimation have been considered.

Although the modeling predictions of time-to-ignition and steady-burning rate in this example seems to be reasonable, limitation of this Simple Analytical Modeling should be noted, which is that the model is for thermally-thick-behaving materials and steady burning after ignition.

EXAMPLE 4.3 MODELING FIRE-RETARDED FRP COMPOSITE

Measure Parameters

1. Ambient Temperature

Direct measurement of ambient temperature is made as 23°C.

2. Surface Temperature at Ignition

This parameter will be obtained via Ignition Data Analysis, i.e.- no direct measurements will be performed.

3. Critical Heat Flux for Ignition

Corrugated cardboard's CHF is measured to between 28 and 30 kW/m² from cone calorimeter testing by bracketing. Hence, CHF is 29 ± 1 kW/m².

4. Thermal Inertia

This parameter will be obtained via Ignition Data Analysis, i.e., no direct measurements will be performed.

5. Effective Heat-of-Combustion

This parameter will be obtained via Burning-Rate Data Analysis, i.e., no direct measurements will be performed.

6. Heat-of-Gasification

This parameter will be obtained via Burning-Rate Data Analysis, i.e., no direct measurements will be performed.

7. Convection Coefficient

Because this is a material laid in horizontal position in a cone calorimeter, $h_c = 12$ W/m²K is used based on literature reference.

8. Surface Emissivity/Absorptivity

Emissivity is approximated as 0.9.

Summary

Table A(C)-14. Summary of model-parameter table with estimated values via direct measurements, literature search, or approximation

Ignition Parameters	T_{∞}	23 °C
	T_{ig}	Ignition Data Analysis
	\dot{q}_{cr}''	29 kW/m ²
	$k\rho c$	Ignition Data Analysis
Burning-Rate Parameters	$\Delta h_{c,eff}$	Burning-Rate Data Analysis
	Δh_g	Burning-Rate Data Analysis
	h_c	12 W/m ² K
	ε	0.9

Obtain Parameters via Data Analysis

Run model

SELECT MODEL: THERMALLY THICK MODEL FOR IGNITION ANALYSIS (QUINTIERE AND HARKLEROAD, ASTM E 1321) AND STEADY-BURNING MODEL

UNDERSTAND EXPERIMENT AND FIRE CHARACTERISTICS OF MATERIAL

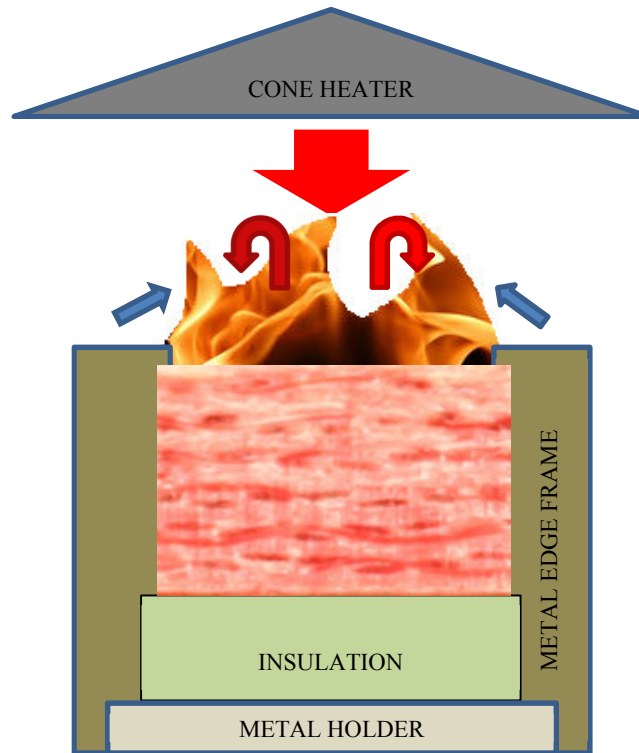


Figure A(C)-15. Simplified representation of a cone calorimeter test of fire-retarded fiberglass-reinforced polymer (FRP) composite

A simplified representation of a cone calorimeter test of fire-retarded fiberglass-reinforced polymer (FRP) composite is shown in Figure A(C)-15. The sample is placed on top of an insulation, which sits on a metal holder. Another metal frame is placed on top of the sample, insulation, and the holder. A metal edge frame is used as well.

Front Surface: As heating starts by opening the shutter to allow radiation from the cone heater to impinge on the sample surface (large red arrow), cooling also begins via natural convection (blue arrows) and re-radiation. The surface decomposes with charring, i.e., surface becoming black and white smoke, which typically indicates moisture loss with heating of the sample. Note that the surface becomes non-uniformly black. As thermal decomposition of the resin with additive progresses, the blackened

surface becomes white, as the resin leaves a white powder-type residue (possible due to decomposition of the fire-retardant additive). Shrinkage or regression during pyrolysis can be considered to be minimal for this material. When ignition occurs as the fuel-vapor concentration above the surface exceeds its LFL (lower flammable limit), additional heat flux from the flame is introduced on the surface (red arrows).

Back surface: The sample is placed on top of insulation. In the experiment, an air gap of a few millimeters thickness exists between the sample and the insulation due to thermal contact. Nothing leaves through the back face with the insulation when 1D assumption holds for the experiment.

CONFIGURE MODEL CONDITIONS BASED ON UNDERSTANDING OF EXPERIMENT AND MATERIAL CHARACTERISTICS

In the model, the phenomena discussed above are simulated as below. Basic assumptions are as follows:

- Pre-ignition stage is:
 - Inert: non-uniform charring is considered to be evenly distributed
 - Thermally thick: heat transfer does not reach back surface
- Post-ignition stage is:
 - Considered to have instantaneous release of volatiles from solid to gas phase
 - Considered to have a constant thickness
 - Steady burning: heat loss equals heat gain at front surface after ignition

ACQUIRE DATA SETS

Cone calorimeter test data of fire-retarded fiberglass-reinforced polymer (FRP) composite with thickness of 9.2 mm, density of 1900 kg/m^3 , and applied heat-flux levels ranging from 20 to 75 kW/m^2 is found. For Ignition Data analysis, only time-to-ignition with respect to applied heat-flux data will be used. For burning-rate data analysis, data for the entire testing-time duration, mass loss and heat release during testing period with respect to applied heat flux will be used.

CONDUCT IGNITION DATA ANALYSIS

1. Estimate T_{ig}

Heat balance at front surface during steady burning is as follow:

$$\varepsilon \dot{q}_{cr}'' = h_c (T_{ig} - T_\infty) + \varepsilon \sigma (T_{ig}^4 - T_\infty^4)$$

Knowing that emissivity is approximated as 0.9, critical heat flux is estimated as 9 kW/m², and heat transfer coefficient in cone calorimeter experiment is estimated as 12.0 W/m²K, ignition temperature, T_{ig} is calculated as:

$$\mathbf{T_{ig} = 523 \text{ }^\circ\text{C}}$$

2. Estimate h_{ig}

h_{ig} is the total heat-transfer coefficient at ignition; therefore, at steady-state burning stage, the following can be defined:

$$\varepsilon \dot{q}_{cr}'' \equiv h_{ig} (T_{ig} - T_\infty)$$

Knowing the ignition temperature, h_{ig} can be calculated:

$$\mathbf{h_{ig} = 52.2 \text{ W/m}^2\text{K}}$$

3. Calculate $\dot{q}_{cr}'' / \dot{q}_e''$ versus $\sqrt{t_{ig}}$ from ignition data

Table A(C)-15. $\dot{q}_{cr}'' / \dot{q}_e''$ versus $\sqrt{t_{ig}}$

Heat Flux (kW/m ²)	t _{ig} (s)	CHF/HF	t _{ig} ^{0.5} (s ^{0.5})
28	NI		
30	484	0.9667	22.00
40	269	0.7250	16.40
40	242	0.7250	15.56
50	143	0.5800	11.96
50	195	0.5800	13.96
50	178	0.5800	13.34
50	183	0.5800	13.53
60	132	0.4833	11.49
75	72	0.3867	8.49
75	83	0.3867	9.11
75	96	0.3867	9.80
75	98	0.3867	9.90

4. Plot $\dot{q}_{cr}'' / \dot{q}_e''$ versus $\sqrt{t_{ig}}$ to estimate the time needed to reach “steady-state” burning, t* and thermal inertia, kρc

$$\text{Recall } \frac{\dot{q}_{cr}''}{\dot{q}_e''} = F(t_{ig}) = \begin{cases} \frac{2 h_{ig} \sqrt{t_{ig}}}{\sqrt{\pi k \rho c}} & t_{ig} \leq t^* \\ 1 & t_{ig} > t^* \end{cases} \quad \text{for piloted-ignition data where } t^* \text{ is}$$

the time when $\dot{q}_{cr}'' / \dot{q}_e'' = 1$. Thermal inertia can be estimated from the best-fit line through

t = 0. Its slope at 0 < t < t* is $\frac{2 h_{ig}}{\sqrt{\pi k \rho c}}$; therefore, $k \rho c = \frac{4 h_{ig}^2}{\pi \cdot (\text{slope})^2}$. Note that in the

analysis, all data points at lower heat-flux levels with large time-to-ignition data were included, for this gave a better fitness of the best-fit line (see Figure A(C)-16).

$$k \rho c = 1.834 \text{ kJ}^2/\text{m}^4\text{K}^2\text{s}$$

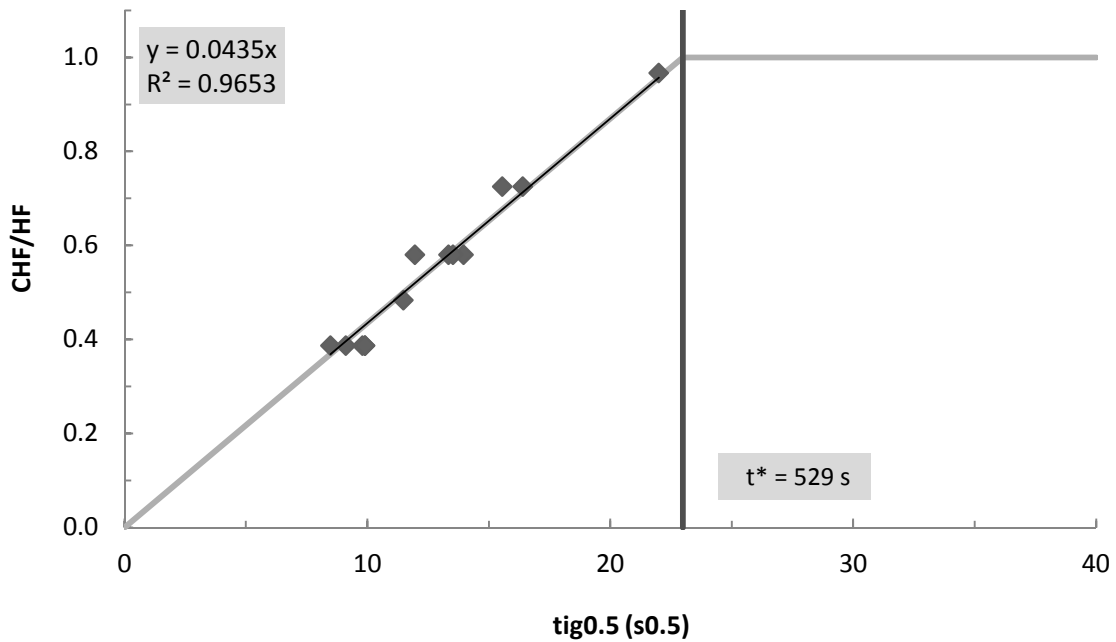


Figure A(C)-16. Plot of $\dot{q}_{cr}'' / \dot{q}_e''$ versus $\sqrt{t_{ig}}$

CONDUCT BURNING-RATE DATA ANALYSIS

1. Estimate $\Delta h_{c,eff}$

There are two approaches in estimating the effective heat-of-combustion via calorimeter tests: by using the peak in HRR or the average heat released over the entire test. In this example, $\Delta h_{c,eff}$ will be estimated by considering the average heat-release rate divided by the average mass-loss rate during a test. Cone test results ranging from 30 to 75 kW/m² are used:

$$\Delta h_{c,eff} = 18.3 \text{ kJ/g}$$

2. Estimate Δh_g

Recall $\Delta h_g \equiv \frac{\dot{q}_{net}''}{\dot{m}''} = \frac{\dot{q}_e'' + \dot{q}_f'' - \dot{q}_l''}{\dot{m}''}$; therefore, when plotting mass-loss rates at different radiant heat-flux levels during steady-burning condition, the reciprocal of the

slope of the best-fit line should be the heat-of-gasification (see Table A(C)-16 and Figure A(C)-17).

$$\Delta h_g = 13.7 \text{ kJ/g}$$

Table A(C)-16. Estimation of effective heat-of-gasification using cone calorimeter test results at applied heat flux ranging between 25 and 75 kW/m²

Heat Flux (kW/m ²)	avgMLR (g/m ² s)
25	6.70
25	6.59
40	6.93
50	7.95
60	8.64
60	9.09
75	8.30

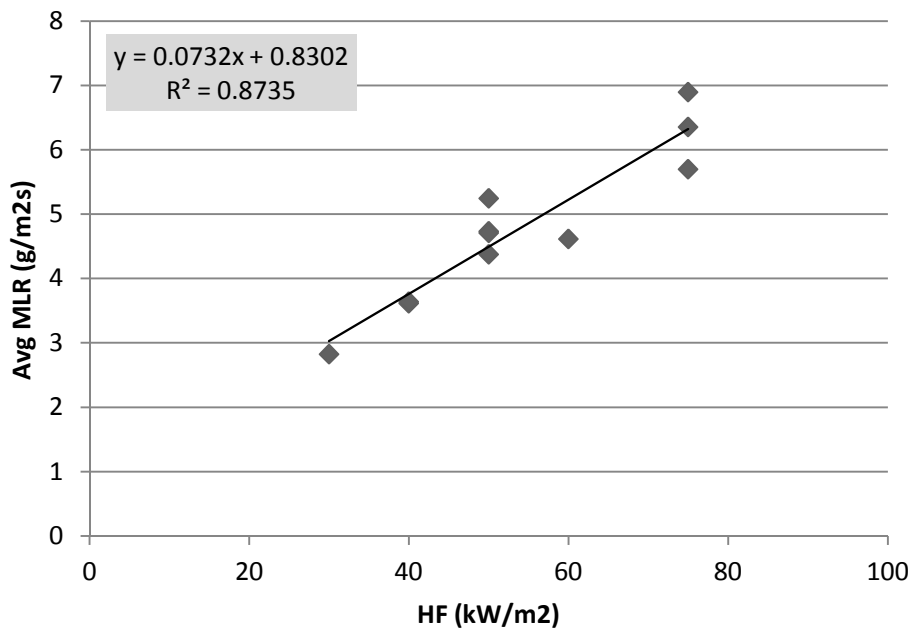


Figure A(C)-17. Plot of steady MLR versus different applied heat-flux levels – 25 to 75 kW/m²

Obtain Uncertainty for Estimated Parameters

UNCERTAINTY FOR MEASURED PARAMETERS

1. δT_{∞}

Fluctuation in ambient temperature during testing is estimated to be less than $\pm 15\%$ of reported measurement data.

2. $\delta \dot{q}_{cr}''$

The resolution of bracketing experiment was 2 kW/m^2 ; hence, uncertainty can be estimated as $\pm 1 \text{ kW/m}^2$.

3. δh_c

Considering that the reference values cited in the *Guide* for different apparatuses and set-up have two significant figures, uncertainty for this convection coefficient can be estimated as $\pm 0.5 \text{ W/m}^2\text{K}$.

4. $\delta \epsilon$

Emissivity measurement of fire-retarded FRP composite sample (preconditioned in an oven to remove moisture) was conducted using a pyrometer at an optical-property-measuring laboratory (ASTM E408). The average value of three measurements were 0.912 with a confidence interval of ± 0.007 (student t distribution, $\alpha = 0.05$, sample size of 3). This is close to what has been assumed in the analysis. Additionally, considering that the surface becomes black as soon as it is exposed to heating from the cone, emissivity of thermally degrading plywood should be within $\pm 10\%$ of what has been approximated in this example.

UNCERTAINTY FOR ESTIMATED PARAMETERS USING IGNITION DATA ANALYSIS

1. δT_{ig}

See Chapter 4 for detail.

$$\begin{aligned}\frac{\partial \dot{q}_{cr}''}{\partial T_{ig}} &= \frac{h_c + 4\varepsilon\sigma T_{ig}^3}{\varepsilon} \\ &= \frac{\left(0.012 \frac{kW}{m^2 K}\right) + 4(0.9)\left(5.67 \times 10^{-11} \frac{kW}{K^4 m^2}\right)\left((523 + 273)K\right)^3}{(0.9)} \\ &\approx 0.1277 \frac{kW}{m^2 K}\end{aligned}$$

$$\begin{aligned}\frac{\partial \dot{q}_{cr}''}{\partial \varepsilon} &= \frac{-\dot{q}_{cr}'' + \sigma(T_{ig}^4 - T_\infty^4)}{\varepsilon} \\ &= \frac{-\left(9 \frac{kW}{m^2}\right) + \left(5.67 \times 10^{-11} \frac{kW}{K^4 m^2}\right)\left(\left((523 + 273)K\right)^4 - \left((23 + 273)K\right)^4\right)}{(0.9)} \\ &\approx -7.413 \frac{kW}{m^2}\end{aligned}$$

$$\begin{aligned}\frac{\partial \dot{q}_{cr}''}{\partial h_c} &= \frac{T_{ig} - T_\infty}{\varepsilon} \\ &= \frac{\left((523 + 273)K\right) - \left((23 + 273)K\right)}{(0.9)} \\ &\approx 555.6 K\end{aligned}$$

$$\begin{aligned}\frac{\partial \dot{q}_{cr}''}{\partial T_\infty} &= \frac{-h_c - 4\varepsilon\sigma T_\infty^3}{\varepsilon} \\ &= \frac{-\left(0.012 \frac{kW}{m^2 K}\right) - 4(0.9)\left(5.67 \times 10^{-11} \frac{kW}{K^4 m^2}\right)\left((23 + 273)K\right)^3}{(0.9)} \\ &\approx -0.01922 \frac{kW}{m^2 K}\end{aligned}$$

Therefore,

$$\begin{aligned}
\delta T_{ig} &= \left(\frac{\partial \dot{q}_{cr}''}{\partial T_{ig}} \right)^{-1} \sqrt{(\delta \dot{q}_{cr}'')^2 - \left(\left(\frac{\partial \dot{q}_{cr}''}{\partial \varepsilon} \delta \varepsilon \right)^2 + \left(\frac{\partial \dot{q}_{cr}''}{\partial h_c} \delta h_c \right)^2 + \left(\frac{\partial \dot{q}_{cr}''}{\partial T_\infty} \delta T_\infty \right)^2 \right)} \\
&= \left(0.1277 \frac{kW}{m^2 K} \right)^{-1} \sqrt{\left(1 \frac{kW}{m^2} \right)^2 - \left(\left(-7.413 \frac{kW}{m^2} \right) (0.09) \right)^2 + \left(555.6 K \left(0.5 \times 10^{-3} \frac{kW}{m^2 K} \right) \right)^2 + \left(-0.01922 \frac{kW}{m^2 K} (3.45 K) \right)^2} \\
&\approx 5.4 K
\end{aligned}$$

2. $\delta(kpc)$

See Chapter 4 for detail.

The uncertainty of the slope of the best-fit line, $0.04349 s^{-0.5}$, can be estimated through calculating 2 times the standard error of the slope, which is $\pm 0.001384 s^{-0.5}$.

$$\begin{aligned}
\frac{\partial(kpc)}{\partial(slope)} &= \frac{-8}{\pi \cdot (slope)^3} \left(\frac{\varepsilon \dot{q}_{cr}''}{T_{ig} - T_\infty} \right)^2 \\
&= \frac{-8}{\pi \cdot (0.04349 s^{-0.5})^3} \left(\frac{(0.9) \left(29 \frac{s}{m^2} \right)}{((523 + 273)K) - ((23 + 273)K)} \right)^2 \\
&\approx -84.35 \frac{kJ^2}{m^4 K^2 s^{0.5}}
\end{aligned}$$

$$\begin{aligned} \frac{\partial(k\rho c)}{\partial \varepsilon} &= \frac{8}{\pi \cdot (\text{slope})^2} \left(\frac{\dot{q}_{cr}''}{T_{ig} - T_{\infty}} \right)^2 \varepsilon \\ &= \frac{8}{\pi \cdot (0.04349s^{-0.5})^2} \left(\frac{\left(\frac{kJ}{m^2} \right)}{\left((523 + 273)K \right) - \left((23 + 273)K \right)} \right)^2 \quad (0.9) \\ &\approx 4.076 \frac{kJ^2}{m^4 K^2 s} \end{aligned}$$

$$\begin{aligned} \frac{\partial(k\rho c)}{\partial \dot{q}_{cr}''} &= \frac{8}{\pi \cdot (\text{slope})^2} \left(\frac{\varepsilon}{T_{ig} - T_{\infty}} \right)^2 \dot{q}_{cr}'' \\ &= \frac{8}{\pi \cdot (0.04349s^{-0.5})^2} \left(\frac{(0.9)}{\left((523 + 273)K \right) - \left((23 + 273)K \right)} \right)^2 \left(\frac{kJ}{m^2} \right) \\ &\approx 0.1265 \frac{kJ}{m^2 K^2} \end{aligned}$$

$$\begin{aligned} \frac{\partial(k\rho c)}{\partial T_{ig}} &= \frac{-8}{\pi \cdot (\text{slope})^2} \left(\frac{\varepsilon \dot{q}_{cr}''}{T_{ig} - T_{\infty}} \right)^2 \frac{1}{T_{ig} - T_{\infty}} \\ &= \frac{-8}{\pi \cdot (0.04349s^{-0.5})^2} \left(\frac{(0.9) \left(\frac{kJ}{m^2} \right)}{\left((523 + 273)K \right) - \left((23 + 273)K \right)} \right)^2 \frac{1}{\left((523 + 273)K \right) - \left((23 + 273)K \right)} \\ &\approx -0.007337 \frac{kJ^2}{m^4 K^3 s} \end{aligned}$$

$$\begin{aligned}
\frac{\partial(k\rho c)}{\partial T_\infty} &= \frac{8}{\pi \cdot (\text{slope})^2} \left(\frac{\varepsilon \dot{q}_{cr}''}{T_{ig} - T_\infty} \right)^2 \frac{1}{T_{ig} - T_\infty} \\
&= \frac{8}{\pi \cdot (0.04349s^{-0.5})^2} \left(\frac{(0.9) \left(29 \frac{kJ}{m^2} \right)}{((523 + 273)K) - ((23 + 273)K)} \right)^2 \frac{1}{((523 + 273)K) - ((23 + 273)K)} \\
&\approx 0.007337 \frac{kJ^2}{m^4 K^3 s}
\end{aligned}$$

Therefore,

$$\begin{aligned}
\delta(k\rho c) &= \sqrt{\left(\frac{\partial(k\rho c)}{\partial(\text{slope})} \delta(\text{slope}) \right)^2 + \left(\frac{\partial(k\rho c)}{\partial \varepsilon} \delta \varepsilon \right)^2 + \left(\frac{\partial(k\rho c)}{\partial \dot{q}_{cr}''} \delta \dot{q}_{cr}'' \right)^2} \\
&\quad + \sqrt{\left(\frac{\partial(k\rho c)}{\partial T_{ig}} \delta T_{ig} \right)^2 + \left(\frac{\partial(k\rho c)}{\partial T_\infty} \delta T_\infty \right)^2} \\
&= \sqrt{\left(\left(-84.35 \frac{kJ^2}{m^4 K^2 s^{0.5}} \right) (0.001384s^{-0.5}) \right)^2 + \left(\left(4.076 \frac{kJ^2}{m^4 K^2 s} \right) (0.09) \right)^2} \\
&\quad + \sqrt{\left(\left(-1265 \frac{kJ}{m^2 K^2} \right) \left(1 \frac{kW}{m^2} \right) \right)^2 + \left(\left(-0.007337 \frac{kJ^2}{m^4 K^3 s} \right) (5.4K) \right)^2} \\
&\quad + \sqrt{\left(\left(0.007337 \frac{kJ^2}{m^4 K^3 s} \right) (3.45K) \right)^2} \\
&\approx 0.408 \frac{kJ^2}{m^4 K^2 s}
\end{aligned}$$

UNCERTAINTY FOR ESTIMATED PARAMETERS USING BURNING-RATE DATA ANALYSIS

1. $\delta \Delta h_{c,eff}$

This parameter is estimated by considering the average of the heat-release rate divided by the average mass-loss rate during cone tests at 30 to 75 kW/m² heat-flux levels. Assuming the estimated $\Delta h_{c,eff}$ at each test results in normal distribution, confidence interval with $\alpha = 0.05$ (95%) can be predicted using student t distribution with a sample size of 10, which is ± 6.7 kJ/g.

2. $\delta\Delta h_g$

See Chapter 4 for detail.

The uncertainty of the slope ($=1/\Delta h_g=0.07324\text{g/kJ}$) can be estimated through calculating 2 times the standard error of the slope of the best-fit line, which is +/- 0.01858. Therefore, the uncertainty in Δh_g is

$$\begin{aligned} \frac{d(\Delta h_g)}{d(\text{slope})} &= -\frac{1}{(\text{slope})^2} \\ &= -\frac{1}{\left(0.07324 \frac{\text{g}}{\text{kJ}}\right)^2} \\ &\approx -186.4 \frac{\text{kJ}^2}{\text{g}^2} \end{aligned}$$

Therefore,

$$\begin{aligned} \delta(\Delta h_g) &= \sqrt{\left(\frac{d(\Delta h_g)}{d(\text{slope})} \delta(\text{slope})\right)^2} \\ &= \sqrt{\left(\left(-186.4 \frac{\text{kJ}^2}{\text{g}^2}\right) (0.01858 \text{g} / \text{kJ})\right)^2} \\ &\approx 3.5 \frac{\text{kJ}}{\text{g}} \end{aligned}$$

UNCERTAINTY SUMMARY

Table A(C)-17. Summary of model-parameter table with estimated values with uncertainty

Ignition Parameters	T_∞	$23 \pm 3.45 \text{ }^\circ\text{C}$
	T_{ig}	$523 \pm 5 \text{ }^\circ\text{C}$
	\dot{q}_{cr}''	$29 \pm 1 \text{ kW/m}^2$
	$k\rho c$	$1.834 \pm 0.408 \text{ kJ}^2/\text{m}^4\text{K}^2\text{s}$
Burning-Rate Parameters	$\Delta h_{c,eff}$	$18.3 \pm 6.7 \text{ kJ/g}$
	Δh_g	$13.7 \pm 3.5 \text{ kJ/g}$
	h_c	$12 \pm 0.5 \text{ W/m}^2\text{K}$
	ε	0.9 ± 0.09

Validation

Analyze Simulation Quality

DETERMINE DATA AND MODEL OUTPUT UNCERTAINTY TO MAKE COMPARISON

1. Conduct uncertainty analysis of data

The uncertainty in the mass-loss rate data used for comparison between data and model outputs is estimated via statistical approach, taking the standard deviation (0.58 g/sm²) from the mean of a steady burning of five identical PMMA tests conducted in a Cone calorimeter.² The estimated uncertainty is 1.4 g/sm², which is found by calculating the 95% confidence interval applying student t distribution with a sample size of five.

The uncertainty in time-to-ignition data used for comparison is estimated via statistical approach, taking four to five identical cone calorimeter test data at heat fluxes at 50 and 75 kW/m² of this FRP composite. 95% confidence interval is calculated for each heat-flux level assuming student t distribution.

2. Conduct uncertainty analysis for MLR profile modeling

Because uncertainty information of the data is found in terms of time-to-ignition and mass-loss rate, mass-loss-rate profile is considered as the modeling output of interest for comparison purposes. For Simple Analytical Models, time-to-ignition (t_{ig}) and steady-burning rate (\dot{m}'') are needed when simulating the mass-release-rate profile. The uncertainty in MLR profile in modeling can be determined via considering the uncertainties in these calculation results as below:

$$t_{ig} \pm \delta t_{ig}$$
$$\dot{m}'' \pm \delta \dot{m}''$$

To determine the uncertainty in time-to-ignition, recall:

$$\frac{\dot{q}_{cr}''}{\dot{q}_e''} = F(t_{ig}) = \begin{cases} \frac{2 h_{ig} \sqrt{t_{ig}}}{\sqrt{\pi k \rho c}} & t_{ig} \leq t^* \\ 1 & t_{ig} > t^* \end{cases}$$

Knowing that all of heat-flux levels of interest, 50 and 75 kW/m², are above the critical heat flux, time-to-ignition should be smaller than t^* . Hence, uncertainty in t_{ig} can be estimated from linear-regression process as below:

$$\frac{\dot{q}_{cr}''}{\dot{q}_e''} = \frac{2 h_{ig}}{\sqrt{\pi k \rho c}} \sqrt{t_{ig}}$$

Above equation can be re-written as below after conducting linear regression:

$$y \text{ estimate} = (\text{slope}) \sqrt{t_{ig}}$$

Therefore,

$$t_{ig} = \left(\frac{y \text{ estimate}}{\text{slope}} \right)^2$$

Assuming that the y estimate and slope are independent and propagating the uncertainties in these two variables in estimating the time to ignition, the following calculation can be made:

$$\delta t_{ig} = \sqrt{\left(\frac{\partial t_{ig}}{\partial (y \text{ estimate})} \delta (y \text{ estimate}) \right)^2 + \left(\frac{\partial t_{ig}}{\partial (\text{slope})} \delta (\text{slope}) \right)^2}$$

where

$$\frac{\partial t_{ig}}{\partial (y \text{ estimate})} = \frac{2 \cdot (y \text{ estimate})}{(\text{slope})^2}$$

$$\frac{\partial t_{ig}}{\partial (\text{slope})} = - \frac{2 \cdot (y \text{ estimate})^2}{(\text{slope})^3}$$

with $\delta (y \text{ estimate})$ and $\delta (\text{slope})$ estimated through calculating 2 times the standard error of the y estimate and slope of the best-fit line.

To determine the uncertainty in the steady-heat-release rate at post-ignition stage, recall:

$$\Delta h_g \equiv \frac{\dot{q}_{net}''}{\dot{m}''} = \frac{\dot{q}_e'' + \dot{q}_f'' - \dot{q}_l''}{\dot{m}''}$$

The above equation can be rearranged to

$$\dot{m}'' = \frac{1}{\Delta h_g} \dot{q}_e'' + \frac{\dot{q}_f'' - \dot{q}_l''}{\Delta h_g}$$

The steady-burning rate at post-ignition stage is determined by the best-fit line obtained when data is plotted as steady-burning rate versus applied heat flux. The uncertainty in steady-burning rate can be determined by considering 2 times the standard

error of the y estimates, i.e. \hat{m} , which is obtained through linear-regression process: \pm 0.9 g/m²s.

COMPARE DATA WITH SIMULATION RESULTS WITH CONSIDERATION OF UNCERTAINTIES

Parameters in this simple analytical pyrolysis model have been estimated with cone calorimeter test data from 50 and 75 kW/m². To check the quality of the modeling using the estimated parameters, three cases have been simulated and compared with experiment data with the consideration of their uncertainty bands as shown in Table A(C)-18 and figures – Figure A(C)-18 and Figure A(C)-19 – below.

Table A(C)-18. Comparison of time-to-ignition at different heat-flux levels from actual experiment and pyrolysis modeling

Heat-Flux Level	Actual t_{ig} (s) $t_{ig} \pm \delta t_i$	Model t_{ig} (s) $t_{ig} \pm \delta t_i$
50 kW/m ²	175 ± 36	178 ± 42
75 kW/m ²	89 ± 14	79 ± 27

Both cases show good overlap between the data and simulation of time-to-ignition and the mass-loss rate during steady burning considering the uncertainties, i.e., the parameter estimation was conducted successfully. Note that when calculating the burnout time in pyrolysis modeling, it was assumed that only 29% of the initial weight is lost and 71% of polymer (resin and additive) residue with inert fiberglass mats remain.

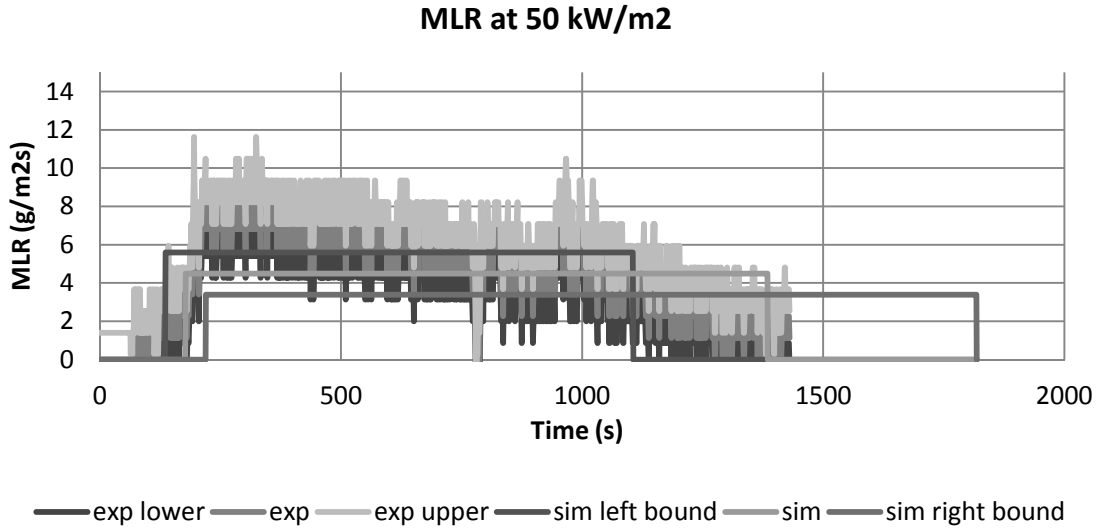


Figure A(C)-18. Mass-loss rate (MLR) comparisons for fire-retarded FRP composite between actual MLR from experiment (exp) and modeled MLR (sim) at 50 kW/m². Note that data shown were used to estimate model-parameter values.

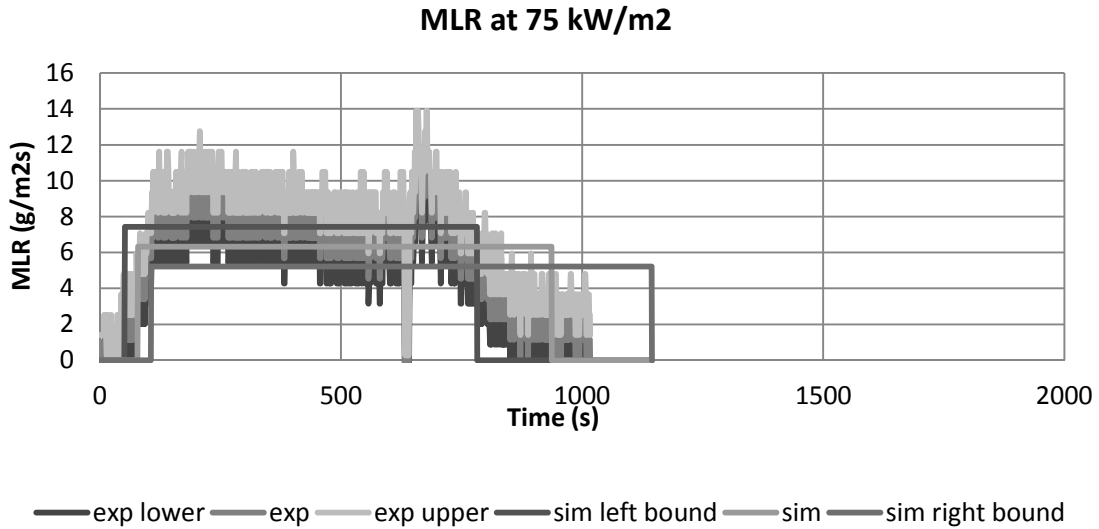


Figure A(C)-19. Mass-loss rate (MLR) comparisons for fire-retarded FRP composite between actual MLR from experiment (exp) and modeled MLR (sim) at 75 kW/m². Note that data shown were used to estimate model-parameter values.

Validate Simulation Quality upon Extrapolation

In this example, cone calorimeter data at applied heat flux ranging from 25 to 75 kW/m² were used to estimate the unknown model parameters. Assuming that the estimated parameters for this corrugated cardboard will be used in pyrolysis modeling at applied heat-flux levels that are within the above range, no additional check becomes necessary.

Commentary

When using Simple Analytical Model to simulate pyrolysis of a fire-retarded fiberglass-reinforced polymer (FRP) composite (density 2100 kg/m³, thickness 8.9 mm, 71 wt% of composite remains as residue), test data from a bench-scale cone calorimeter experiment at several heat-flux levels have been utilized to estimate the time-to-ignition from exposure to heating and the mass-loss rate at steady-burning stage after ignition. The comparison between the model outputs (time-to-ignition and steady-burning rate) and the data from bench-scale experiment showed good agreement for both checking purposes where the same heat-flux levels (50 and 75 kW/m²) used in parameter estimation have been considered.

Although the modeling predictions of time-to-ignition and steady-burning rate in this example seems to be reasonable, limitation of this Simple Analytical Modeling should be noted, which is that the model is for thermally-thick-behaving materials and steady burning after ignition.

EXAMPLE 4.4 MODELING PLYWOOD

Measure Parameters

1. Ambient Temperature

Direct measurement of ambient temperature is made as 20°C.

2. Surface Temperature at Ignition

This parameter will be obtained via Ignition Data Analysis, i.e., no direct measurements will be performed.

3. Critical Heat Flux for Ignition

By bracketing to within +/- 0.5 kW/m² in cone calorimeter tests, \dot{q}_{cr}'' has been determined to be 14.5 kW/m² (see Table A(C)-26). Ignition data is provided below for this plywood with thickness of 11.1 ± 0.1 mm, density of 542 ± 11 kg/m³ (t-distribution, $\alpha = 0.05$, sample size of 10):

Table A(C)-19. Ignition data from cone calorimeter tests of plywood

Heat Flux (kW/m ²)	t _{ig} (s)
14	NI
15	572

4. Thermal Inertia

This parameter will be obtained via Ignition Data Analysis, i.e., no direct measurements will be performed.

5. Effective Heat of Combustion

This parameter will be obtained via Burning-Rate Data Analysis, i.e., no direct measurements will be performed.

6. Heat-of-Gasification

This parameter will be obtained via Burning-Rate Data Analysis, i.e., no direct measurements will be performed.

7. Convection Coefficient

Because this is a material laid in horizontal position in a cone calorimeter, $h_c = 12 \text{ W/m}^2\text{K}$ is used based on literature reference.

8. Surface Emissivity/Absorptivity

Emissivity is approximated as 0.9.

Summary

Table A(C)-20. Summary of model-parameter table with estimated values via direct measurements, literature search, or approximation

Ignition Parameters	T_∞	20 °C
	T_{ig}	Ignition Data Analysis
	\dot{q}_{cr}''	14.5 kW/m ²
	$k\rho c$	Ignition Data Analysis
Burning-Rate Parameters	$\Delta h_{c,eff}$	Burning-Rate Data Analysis
	Δh_g	Burning-Rate Data Analysis
	h_c	12 W/m ² K
	ε	0.9

Obtain Parameters via Data Analysis

Run model

SELECT MODEL: THERMALLY THICK MODEL FOR IGNITION ANALYSIS (QUINTIERE AND HARKLEROAD, ASTM E 1321) AND STEADY-BURNING MODEL

UNDERSTAND EXPERIMENT AND FIRE CHARACTERISTICS OF MATERIAL

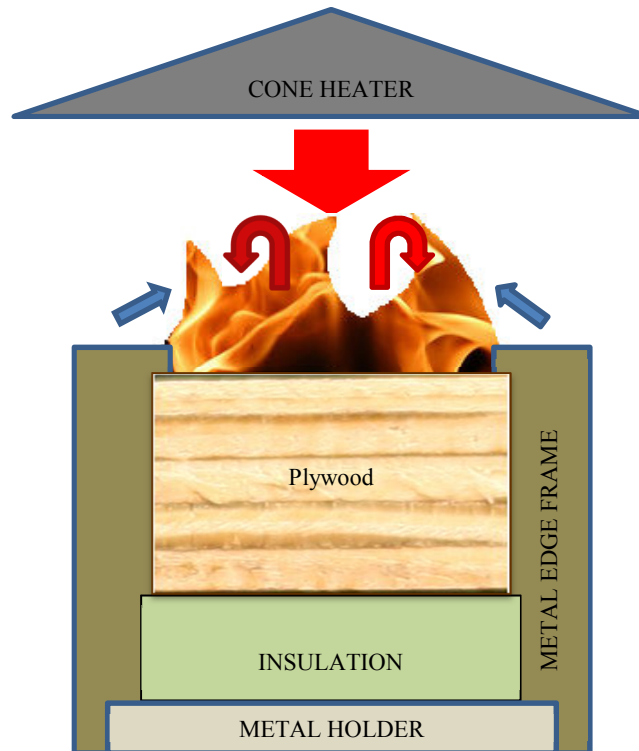


Figure A(C)-20. Simplified representation of a cone calorimeter test of plywood

A simplified representation of a cone calorimeter test of plywood is shown in Figure A(C)-20. The sample is placed on top of an insulation, which sits on a metal holder. Another metal frame is placed on top of the sample, insulation, and the holder. A metal edge frame is used as well.

Front Surface: As heating starts by opening the shutter to allow radiation from the cone heater to impinge on sample surface (large red arrow), cooling also begins via natural convection (blue arrows) and re-radiation. The surface decomposes with moisture loss at first appearing as white smoke followed by thermal decomposition of the wood component. When ignition occurs as the fuel-vapor concentration above the surface exceeds its LFL (lower flammable limit), additional heat flux from the flame is introduced on the surface (red arrows). As decomposition occurs under flaming

condition, relatively uniform cracks appear on the surface with some shrinkage, allowing easy evacuation of the pyrolyzates to the gas phase even as the pyrolysis front propagates toward in-depth. Near the burn-out leaving grey residue, the center of the sample bends upward then quickly falls apart resulting in flameout.

Back surface: The sample is placed on top of insulation. In the experiment, an air gap of a few millimeters thickness exist between the sample and the insulation resulting in some thermal resistance. Due to the insulation, nothing leaves through the back face when 1D assumption holds for the experiment.

CONFIGURE MODEL CONDITIONS BASED ON UNDERSTANDING OF EXPERIMENT AND MATERIAL CHARACTERISTICS

In the model, the phenomena discussed above are simulated as below. Basic assumptions are as follows:

- Pre-ignition stage is:
 - Inert: decomposition before ignition is neglected
 - Thermally thick: heat transfer does not reach back surface
- Post-ignition stage is:
 - Considered to have instantaneous release of volatiles from solid to gas phase: any mass-transportation effect on pyrolysis is neglected, and pyrolysis is considered as surface phenomena only
 - Considered to have a constant thickness: shrinkage, regression and bending at end of plywood is neglected
 - Steady burning: heat loss equals heat gain at front surface

ACQUIRE DATA SETS

Cone calorimeter test data of Douglas Fir plywood with thickness of 11.1 ± 0.1 mm (student t distribution, $\alpha = 0.05$, sample size of 10), density of 542 ± 11 kg/m³ (student t distribution, $\alpha = 0.05$, sample size of 10) and applied heat-flux levels ranging from 14 to 100 kW/m² is found. For ignition data analysis, only time-to-ignition with respect to applied heat-flux data will be used. For burning-rate data analysis, data for the entire testing time duration, mass loss and heat release during testing period with respect to applied heat flux will be used.

CONDUCT IGNITION DATA ANALYSIS

1. Estimate T_{ig}

Heat balance at front surface during steady burning is as follow:

$$\varepsilon \dot{q}_{cr}'' = h_c (T_{ig} - T_\infty) + \varepsilon \sigma (T_{ig}^4 - T_\infty^4)$$

Knowing that emissivity is approximated as 0.9, critical heat flux is estimated as 14.5 kW/m^2 , and heat transfer coefficient in cone calorimeter experiment is estimated as $12.0 \text{ W/m}^2\text{K}$, ignition temperature, T_{ig} is calculated as:

$$T_{ig} = 377 \text{ }^\circ\text{C}$$

2. Estimate h_{ig}

h_{ig} is the total heat-transfer coefficient at ignition; therefore, at steady-state-burning stage, the following can be defined:

$$\varepsilon \dot{q}_{cr}'' \equiv h_{ig} (T_{ig} - T_\infty)$$

Knowing the ignition temperature, h_{ig} can be calculated:

$$h_{ig} = 36.5 \text{ W/m}^2\text{K}$$

3. Calculate $\dot{q}_{cr}'' / \dot{q}_e''$ versus $\sqrt{t_{ig}}$ from ignition data

Table A(C)-21. $\dot{q}_{cr}'' / \dot{q}_e''$ versus $\sqrt{t_{ig}}$

Heat Flux (kW/m ²)	t_{ig} (s)	CHF/HF	$t_{ig}^{0.5}$ (s ^{0.5})
14	NI		
15	572	0.9667	23.92
25	102	0.5800	10.08
50	27	0.2900	5.16
75	9	0.1933	3.06
100	3	0.1450	1.63

4. Plot $\dot{q}_{cr}'' / \dot{q}_e''$ versus $\sqrt{t_{ig}}$ to estimate the time needed to reach “steady-state” burning, t^* and thermal inertia, $k\rho c$

$$\text{Recall } \frac{\dot{q}_{cr}''}{\dot{q}_e''} = F(t_{ig}) = \begin{cases} \frac{2 h_{ig} \sqrt{t_{ig}}}{\sqrt{\pi k \rho c}} & t_{ig} \leq t^* \\ 1 & t_{ig} > t^* \end{cases} \quad \text{for piloted-ignition data, where } t^* \text{ is}$$

the time when $\dot{q}_{cr}'' / \dot{q}_e'' = 1$. Thermal inertia can be estimated from the best-fit line through

$t = 0$. Its slope at $0 < t < t^*$ is $\frac{2 h_{ig}}{\sqrt{\pi k \rho c}}$; therefore, $k \rho c = \frac{4 h_{ig}^2}{\pi \cdot (\text{slope})^2}$. Note that in the

analysis, few data points at lower heat-flux levels with large time-to-ignition data were excluded (see Figure A(C)-21, open circles) to increase fitness of the best-fit line. This approach is reasonable, considering that at this region analysis assumptions of having inert and thermally thick conditions are less likely to be satisfied.

$$k \rho c = 0.501 \text{ kJ}^2/\text{m}^4\text{K}^2\text{s}$$

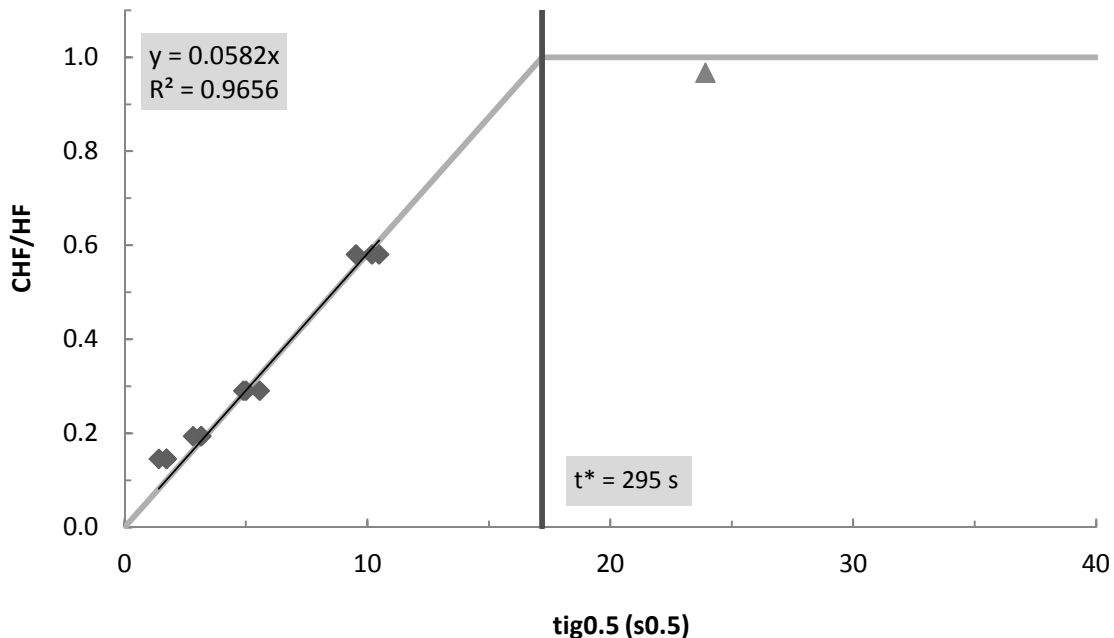


Figure A(C)-21. Plot of $\dot{q}_{cr}'' / \dot{q}_e''$ versus $\sqrt{t_{ig}}$

CONDUCT BURNING-RATE DATA ANALYSIS

1. Estimate $\Delta h_{c,eff}$

There are two approaches in estimating the effective heat of combustion via calorimeter tests: by using the peak in HRR or the average heat released over the entire test. In this example, $\Delta h_{c,eff}$ will be estimated by considering the total heat released divided by the total amount of mass loss during a test. Nine cone test results at 25, 50, and 75 kW/m² are used to calculate the effective heat-of-combustion with its confidence interval using student t distribution and $\alpha = 0.05$:

$$\Delta h_{c,eff} = 14.4 \pm 1.2 \text{ kJ/g}$$

2. Estimate Δh_g

Recall $\Delta h_g \equiv \frac{\dot{q}_{net}''}{\dot{m}''} = \frac{\dot{q}_e'' + \dot{q}_f'' - \dot{q}_l''}{\dot{m}''}$; therefore, when plotting mass-loss rates at different radiant heat-flux levels during steady-burning condition, the reciprocal of the slope of the best-fit line should be the heat-of-gasification. Note that for this material – Douglas Fir plywood – a strict steady-burning phase does not exist where a constant MLR appears. Therefore, an average MLR value will be used to estimate heat-of-gasification (see Table A(C)-22 and Figure A(C)-22).

$$\Delta h_g = 8.0 \text{ kJ/g}$$

Table A(C)-22. Estimation of effective heat-of-gasification using cone calorimeter test results at applied heat flux ranging between 25 and 75 kW/m²

Heat Flux (kW/m ²)	Avg MLR (g/m ² s)
25	7.1
25	6.5
25	8.0
75	13.6
50	11.0
50	10.2
75	13.6
75	13.7
75	12.9

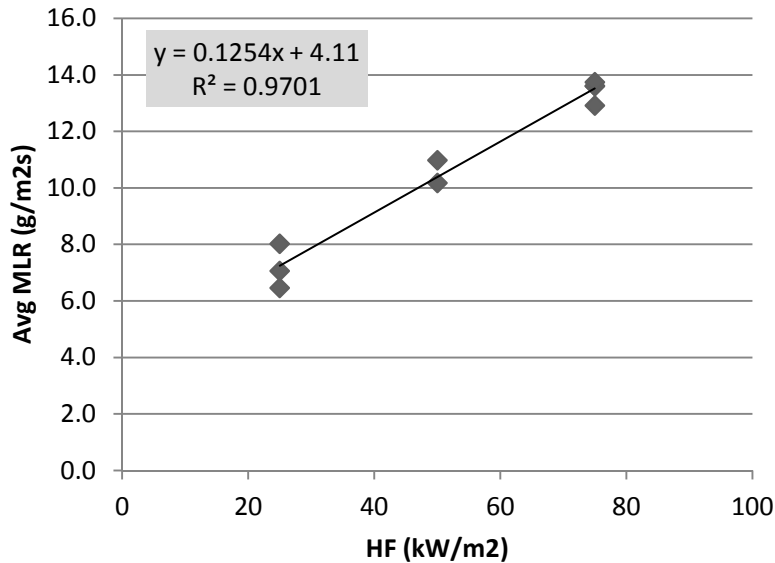


Figure A(C)-22. Plot of steady MLR versus different applied heat-flux levels – 25 to 75 kW/m²

Obtain Uncertainty for Estimated Parameters

UNCERTAINTY FOR MEASURED PARAMETERS

1. δT_{∞}

Fluctuation in ambient temperature during testing is estimated to be less than $\pm 10\%$ of reported measurement data.

2. $\delta \dot{q}_{cr}''$

The resolution of bracketing experiment was 1 kW/m²; hence, uncertainty can be estimated as ± 0.5 kW/m². To be conservative, ± 1 kW/m² will be used in the analysis.

3. δh_c

Considering that the reference values sited in the *Guide* for different apparatuses and set-up have two significant figures, uncertainty for this convection coefficient can be estimated as ± 0.5 W/m²K.

4. $\delta \varepsilon$

Emissivity measurement of dry-plywood sample (preconditioned in an oven to remove moisture) was conducted using a pyrometer at an optical-property-measuring laboratory (ASTM E408). The average value of three measurements were 0.891 with a confidence interval of ± 0.018 (student t distribution, $\alpha = 0.05$, sample size of three).

This is close to what has been assumed in the analysis. Additionally, considering that the

surface becomes black as soon as it is exposed to heating from the cone, emissivity of thermally degrading plywood should be within $\pm 10\%$ of what has been approximated in this example.

UNCERTAINTY FOR ESTIMATED PARAMETERS USING IGNITION DATA ANALYSIS

1. δT_{ig}

See Chapter 4 for detail.

$$\begin{aligned}\frac{\partial \dot{q}_{cr}''}{\partial T_{ig}} &= \frac{h_c + 4\varepsilon\sigma T_{ig}^3}{\varepsilon} \\ &= \frac{\left(0.012 \frac{kW}{m^2 K}\right) + 4(0.9)\left(5.67 \times 10^{-11} \frac{kW}{K^4 m^2}\right)\left((377 + 273)K\right)^3}{(0.9)} \\ &\approx 0.0756 \frac{kW}{m^2 K}\end{aligned}$$

$$\begin{aligned}\frac{\partial \dot{q}_{cr}''}{\partial \varepsilon} &= \frac{-\dot{q}_{cr}'' + \sigma(T_{ig}^4 - T_{\infty}^4)}{\varepsilon} \\ &= \frac{-\left(14.5 \frac{kW}{m^2}\right) + \left(5.67 \times 10^{-11} \frac{kW}{K^4 m^2}\right)\left(\left((377 + 273)K\right)^4 - \left((20 + 273)K\right)^4\right)}{(0.9)} \\ &\approx -5.330 \frac{kW}{m^2}\end{aligned}$$

$$\begin{aligned}\frac{\partial \dot{q}_{cr}''}{\partial h_c} &= \frac{T_{ig} - T_{\infty}}{\varepsilon} \\ &= \frac{\left((377 + 273)K\right) - \left((20 + 273)K\right)}{(0.9)} \\ &\approx 397K\end{aligned}$$

$$\begin{aligned}\frac{\partial \dot{q}_{cr}''}{\partial T_{\infty}} &= \frac{-h_c - 4\varepsilon\sigma T_{\infty}^3}{\varepsilon} \\ &= \frac{-\left(0.012 \frac{kW}{m^2 K}\right) - 4(0.9)\left(5.67 \times 10^{-11} \frac{kW}{K^4 m^2}\right)\left((20 + 273)K\right)^3}{(0.9)} \\ &\approx -0.01904 \frac{kW}{m^2 K}\end{aligned}$$

Therefore,

$$\begin{aligned} \delta T_{ig} &= \left(\frac{\partial \dot{q}_{cr}''}{\partial T_{ig}} \right)^{-1} \sqrt{(\delta \dot{q}_{cr}'')^2 - \left(\left(\frac{\partial \dot{q}_{cr}''}{\partial \varepsilon} \delta \varepsilon \right)^2 + \left(\frac{\partial \dot{q}_{cr}''}{\partial h_c} \delta h_c \right)^2 + \left(\frac{\partial \dot{q}_{cr}''}{\partial T_\infty} \delta T_\infty \right)^2 \right)} \\ &= \left(0.0756 \frac{kW}{m^2 K} \right)^{-1} \sqrt{\left(1 \frac{kW}{m^2} \right)^2 - \left(\left(-5.33 \frac{kW}{m^2} \right) (0.09) \right)^2 + \left(397 K \right) \left(0.5 \times 10^{-3} \frac{kW}{m^2 K} \right)^2 + \left(-0.01904 \frac{kW}{m^2 K} \right) (2K) \right)^2} \\ &\approx 11.3K \end{aligned}$$

2. $\delta(k\rho c)$

See Chapter 4 for detail.

The uncertainty of the slope of the best-fit line, $0.0444 \text{ s}^{-0.5}$, can be estimated through calculating 2 times the standard error of the slope, which is $\pm 0.00136 \text{ s}^{-0.5}$.

$$\begin{aligned} \frac{\partial(k\rho c)}{\partial(\text{slope})} &= \frac{-8}{\pi \cdot (\text{slope})^3} \left(\frac{\varepsilon \dot{q}_{cr}''}{T_{ig} - T_\infty} \right)^2 \\ &= \frac{-8}{\pi \cdot (0.0582 \text{ s}^{-0.5})^3} \left(\frac{(0.9) \left(14.5 \frac{kJ}{m^2} \right)}{((377 + 273)K) - ((20 + 273)K)} \right)^2 \\ &\approx -17.3 \frac{kJ^2}{m^4 K^2 s^{0.5}} \end{aligned}$$

$$\begin{aligned} \frac{\partial(k\rho c)}{\partial \varepsilon} &= \frac{8}{\pi \cdot (\text{slope})^2} \left(\frac{\dot{q}_{cr}''}{T_{ig} - T_{\infty}} \right)^2 \varepsilon \\ &= \frac{8}{\pi \cdot (0.0582s^{-0.5})^2} \left(\frac{\left(\frac{kJ}{14.5 \frac{s}{m^2}} \right)}{((377 + 273)K) - ((20 + 273)K)} \right)^2 \varepsilon \quad (0.9) \\ &\approx 1.12 \frac{kJ^2}{m^4 K^2 s} \end{aligned}$$

$$\begin{aligned} \frac{\partial(k\rho c)}{\partial \dot{q}_{cr}''} &= \frac{8}{\pi \cdot (\text{slope})^2} \left(\frac{\varepsilon}{T_{ig} - T_{\infty}} \right)^2 \dot{q}_{cr}'' \\ &= \frac{8}{\pi \cdot (0.0582s^{-0.5})^2} \left(\frac{(0.9)}{((377 + 273)K) - ((20 + 273)K)} \right)^2 \left(\frac{kJ}{14.5 \frac{s}{m^2}} \right) \\ &\approx 0.0693 \frac{kJ}{m^2 K^2} \end{aligned}$$

$$\begin{aligned} \frac{\partial(k\rho c)}{\partial T_{ig}} &= \frac{-8}{\pi \cdot (\text{slope})^2} \left(\frac{\varepsilon \dot{q}_{cr}''}{T_{ig} - T_{\infty}} \right)^2 \frac{1}{T_{ig} - T_{\infty}} \\ &= \frac{-8}{\pi \cdot (0.0582s^{-0.5})^2} \left(\frac{(0.9) \left(\frac{kJ}{14.5 \frac{s}{m^2}} \right)}{((377 + 273)K) - ((20 + 273)K)} \right)^2 \frac{1}{((377 + 273)K) - ((20 + 273)K)} \\ &\approx -0.00282 \frac{kJ^2}{m^4 K^3 s} \end{aligned}$$

$$\begin{aligned} \frac{\partial(k\rho c)}{\partial T_\infty} &= \frac{8}{\pi \cdot (\text{slope})^2} \left(\frac{\varepsilon \dot{q}_{cr}''}{T_{ig} - T_\infty} \right)^2 \frac{1}{T_{ig} - T_\infty} \\ &= \frac{8}{\pi \cdot (0.0582s^{-0.5})^2} \left(\frac{(0.9) \left(14.5 \frac{kJ}{m^2} \right)}{((377 + 273)K) - ((20 + 273)K)} \right)^2 \frac{1}{((377 + 273)K) - ((20 + 273)K)} \\ &\approx 0.00282 \frac{kJ^2}{m^4 K^3 s} \end{aligned}$$

Therefore,

$$\begin{aligned} \delta(k\rho c) &= \sqrt{\left(\frac{\partial(k\rho c)}{\partial(\text{slope})} \delta(\text{slope}) \right)^2 + \left(\frac{\partial(k\rho c)}{\partial \varepsilon} \delta \varepsilon \right)^2 + \left(\frac{\partial(k\rho c)}{\partial \dot{q}_{cr}''} \delta \dot{q}_{cr}'' \right)^2} \\ &\quad + \sqrt{\left(\frac{\partial(k\rho c)}{\partial T_{ig}} \delta T_{ig} \right)^2 + \left(\frac{\partial(k\rho c)}{\partial T_\infty} \delta T_\infty \right)^2} \\ &= \sqrt{\left(\left(-17.3 \frac{kJ^2}{m^4 K^2 s^{0.5}} \right) (0.00318s^{-0.5}) \right)^2 + \left(\left(1.12 \frac{kJ^2}{m^4 K^2 s} \right) (0.09) \right)^2} \\ &\quad + \sqrt{\left(\left(0.0693 \frac{kJ}{m^2 K^2} \right) \left(1 \frac{kW}{m^2} \right) \right)^2 + \left(\left(-0.00282 \frac{kJ^2}{m^4 K^3 s} \right) (11.3K) \right)^2} \\ &\quad + \sqrt{\left(\left(0.00282 \frac{kJ^2}{m^4 K^3 s} \right) (2K) \right)^2} \\ &\approx 0.138 \frac{kJ^2}{m^4 K^2 s} \end{aligned}$$

UNCERTAINTY FOR ESTIMATED PARAMETERS USING BURNING-RATE DATA ANALYSIS

1. $\delta\Delta h_{c,eff}$

Cone test results at 25, 50, and 75 kW/m² are used to calculate the effective heat-of-combustion. Uncertainty of this value is estimated with its confidence interval using student t distribution and $\alpha = 0.05$: ± 1.2 kJ/g

2. $\delta\Delta h_g$

See Chapter 4 for detail.

The uncertainty of the slope ($=1/\Delta h_g=0.125\text{g/kJ}$) can be estimated through calculating 2 times the standard error of the slope of the best-fit line, which is ± 0.167 .

Therefore, the uncertainty in Δh_g is

$$\begin{aligned} \frac{d(\Delta h_g)}{d(\text{slope})} &= -\frac{1}{(\text{slope})^2} \\ &= -\frac{1}{\left(0.125 \frac{\text{g}}{\text{kJ}}\right)^2} \\ &\approx -63.6 \frac{\text{kJ}^2}{\text{g}^2} \end{aligned}$$

Therefore,

$$\begin{aligned} \delta(\Delta h_g) &= \sqrt{\left(\frac{d(\Delta h_g)}{d(\text{slope})} \delta(\text{slope})\right)^2} \\ &= \sqrt{\left(\left(-63.6 \frac{\text{kJ}^2}{\text{g}^2}\right) (0.0167 \text{g/kJ})\right)^2} \\ &\approx 1.06 \frac{\text{kJ}}{\text{g}} \end{aligned}$$

UNCERTAINTY SUMMARY

Table A(C)-23. Summary of model-parameter table with estimated values with uncertainty

Ignition Parameters	T_∞	$20 \pm 2 \text{ }^\circ\text{C}$
	T_{ig}	$377 \pm 11 \text{ }^\circ\text{C}$
	\dot{q}_{cr}''	$14.5 \pm 1 \text{ kW/m}^2$
	$k\rho c$	$0.501 \pm 0.138 \text{ kJ}^2/\text{m}^4\text{K}^2\text{s}$
Burning-Rate Parameters	$\Delta h_{c,eff}$	$14.4 \pm 1.2 \text{ kJ/g}$
	Δh_g	$8.0 \pm 1.1 \text{ kJ/g}$
	h_c	$12 \pm 0.5 \text{ W/m}^2\text{K}$
	ε	0.9 ± 0.09

Validation

Analyze Simulation Quality

DETERMINE DATA AND MODEL OUTPUT UNCERTAINTY TO MAKE COMPARISON

1. Conduct uncertainty analysis of data

The uncertainty in the mass-loss rate data used for comparison between data and model outputs is estimated via statistical approach, taking the standard deviation (0.58 g/sm^2) from the mean of a steady burning of five identical PMMA tests conducted in a cone calorimeter.² The estimated uncertainty is 1.4 g/sm^2 , which is found by calculating the 95% confidence interval applying student t distribution with a sample size of five.

The uncertainty in time-to-ignition data used for comparison is estimated via statistical approach, taking three to four identical cone calorimeter test data at heat fluxes ranging from 25 to 75 kW/m^2 of this plywood. 95% confidence interval is calculated for each heat-flux level assuming student t distribution.

2. Conduct uncertainty analysis for MLR profile modeling

Because uncertainty information of the data is found in terms of time-to-ignition and mass-loss rate, the mass-loss-rate profile is considered as the modeling output of interest for comparison purposes. For Simple Analytical Models, time-to-ignition (t_{ig}) and steady-burning rate (\dot{m}'') are needed when simulating the mass-release-rate profile. The uncertainty in MLR profile in modeling can be determined via considering the uncertainties in the calculation results below:

$$t_{ig} \pm \delta t_{ig}$$
$$\dot{m}'' \pm \delta \dot{m}''$$

To determine the uncertainty in time to ignition, recall:

$$\frac{\dot{q}_{cr}''}{\dot{q}_e''} = F(t_{ig}) = \begin{cases} \frac{2 h_{ig} \sqrt{t_{ig}}}{\sqrt{\pi k \rho c}} & t_{ig} \leq t^* \\ 1 & t_{ig} > t^* \end{cases}$$

Knowing that all of heat-flux levels of interest, 25, 50, and 75 kW/m^2 , are above the critical heat flux, time-to-ignition should be smaller than t^* . Hence, uncertainty in t_{ig} can be estimated from linear-regression process as below:

$$\frac{\dot{q}_{cr}''}{\dot{q}_e''} = \frac{2 h_{ig}}{\sqrt{\pi k \rho c}} \sqrt{t_{ig}}$$

Above equation can be re-written as below after conducting linear regression:

$$y \text{ estimate} = (\text{slope}) \sqrt{t_{ig}}$$

Therefore,

$$t_{ig} = \left(\frac{y \text{ estimate}}{\text{slope}} \right)^2$$

Assuming that the y estimate and slope are independent and propagating the uncertainties in these two variables in estimating the time to ignition, the following calculation can be made:

$$\delta t_{ig} = \sqrt{\left(\frac{\partial t_{ig}}{\partial (y \text{ estimate})} \delta (y \text{ estimate}) \right)^2 + \left(\frac{\partial t_{ig}}{\partial (\text{slope})} \delta (\text{slope}) \right)^2}$$

where

$$\frac{\partial t_{ig}}{\partial (y \text{ estimate})} = \frac{2 \cdot (y \text{ estimate})}{(\text{slope})^2}$$

$$\frac{\partial t_{ig}}{\partial (\text{slope})} = - \frac{2 \cdot (y \text{ estimate})^2}{(\text{slope})^3}$$

with $\delta (y \text{ estimate})$ and $\delta (\text{slope})$ estimated through calculating 2 times the standard error of the y estimate and slope of the best-fit line, which are 0.0653 and 0.00318 s^{-0.5}, respectively.

To determine the uncertainty in the steady-heat-release rate at post-ignition stage, recall:

$$\Delta h_g \equiv \frac{\dot{q}_{net}''}{\dot{m}''} = \frac{\dot{q}_e'' + \dot{q}_f'' - \dot{q}_l''}{\dot{m}''}$$

The above equation can be rearranged to

$$\dot{m}'' = \frac{1}{\Delta h_g} \dot{q}_e'' + \frac{\dot{q}_f'' - \dot{q}_l''}{\Delta h_g}$$

The steady-burning rate at post-ignition stage is determined by the best-fit line obtained when data is plotted as steady-burning rate versus applied heat flux. The

uncertainty in steady-burning rate can be determined by considering 2 times the standard error of the y estimates, i.e., \dot{m}'' , which is obtained through linear-regression process: \pm **1.1 g/m²s**.

COMPARE DATA WITH SIMULATION RESULTS WITH CONSIDERATION OF UNCERTAINTIES

Parameters in this simple analytical pyrolysis model have been estimated with cone calorimeter test data from 25, 50, and 75 kW/m². To check the quality of the modeling using the estimated parameters, three cases have been simulated and compared with experiment data with the consideration of their uncertainty bands as shown in Table A(C)-24 and figures below.

Table A(C)-24. Comparison of time-to-ignition at different heat-flux levels from actual experiment and pyrolysis modeling

Heat-Flux Level	Actual t_{ig} (s) $t_{ig} \pm \delta t_i$	Model t_{ig} (s) $t_{ig} \pm \delta t_i$
25 kW/m ²	93 ± 43	99 ± 25
50 kW/m ²	15 ± 3	25 ± 12
75 kW/m ²	9 ± 4	11 ± 8

All three cases show good overlap between the data and simulation of time-to-ignition and the mass-loss rate during steady burning considering the uncertainties, i.e., the parameter estimation was conducted successfully (see Figure A(C)-23, Figure A(C)-24 and Figure A(C)-25).

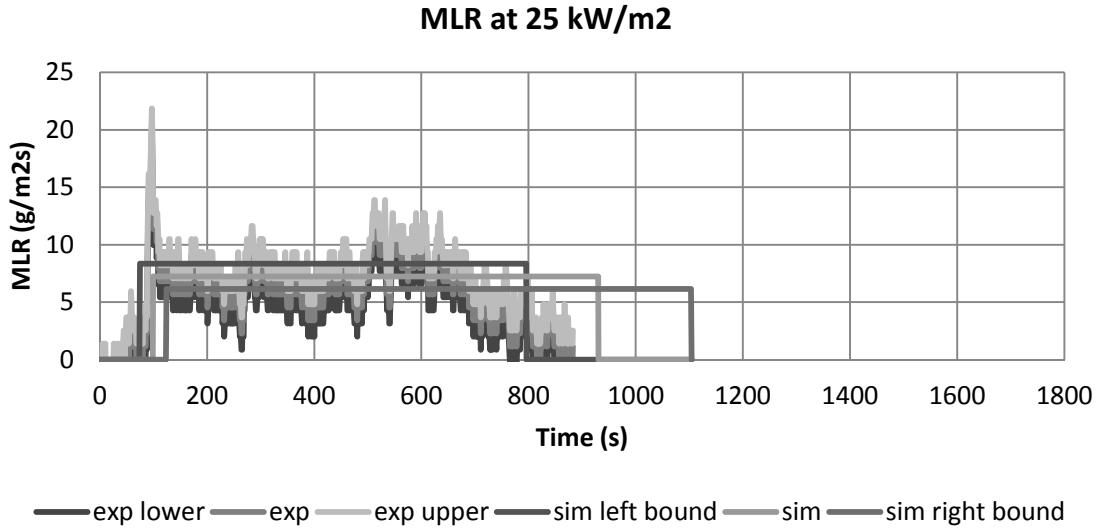


Figure A(C)-23. Mass-loss rate (MLR) comparisons for plywood between actual MLR from experiment (exp) and modeled MLR (sim) at 25 kW/m². Note that data shown were used to estimate model-parameter values.

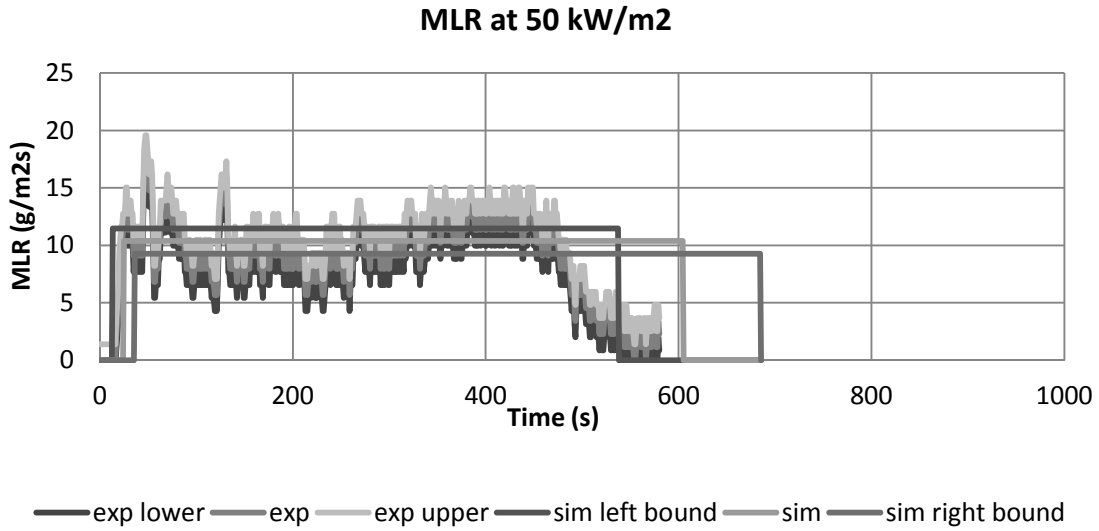


Figure A(C)-24. Mass-loss rate (MLR) comparisons for plywood between actual MLR from experiment (exp) and modeled MLR (sim) at 50 kW/m². Note that data shown were used to estimate model-parameter values.

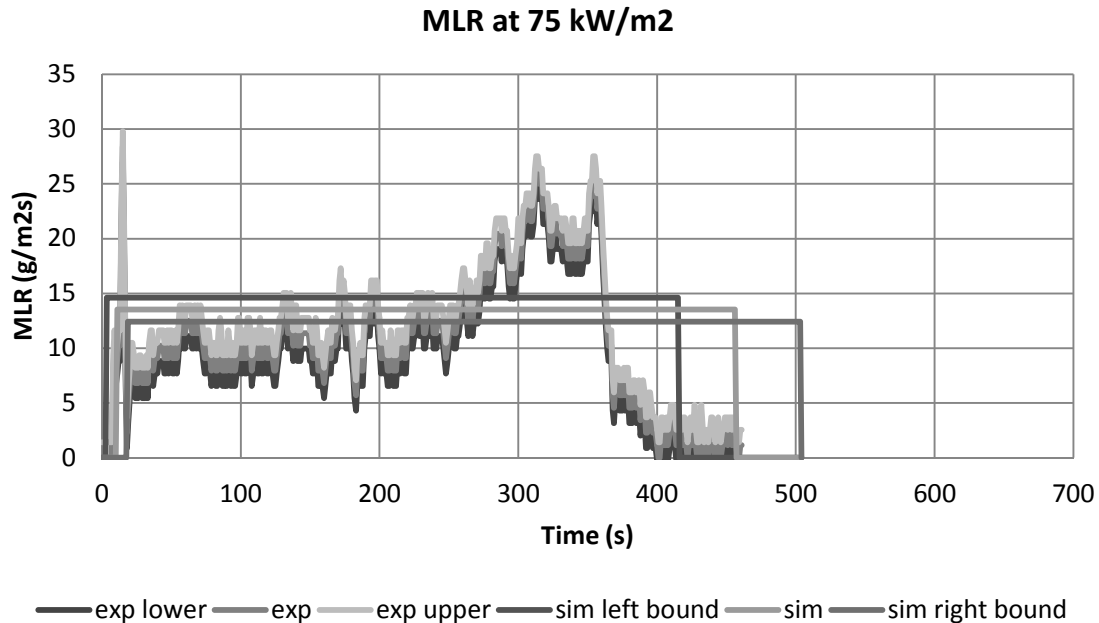


Figure A(C)-25. Mass Loss rate (MLR) comparisons for plywood between actual MLR from experiment (exp) and modeled MLR (sim) at 75 kW/m². Note that data shown were used to estimate model-parameter values.

Commentary

When using Simple Analytical Model to simulate pyrolysis of Douglas Fir plywood, test data from a bench-scale cone calorimeter experiment at several heat-flux levels have been utilized to estimate the time-to-ignition from exposure to heating and the mass-loss rate at steady-burning stage after ignition. The comparison between the model outputs (time-to-ignition and steady-burning rate) and the data from bench-scale experiment showed good agreement for both checking purposes, where the same heat flux levels (25, 50 and 75 kW/m²) used in parameter estimation have been considered.

Although the modeling predictions of time-to-ignition and steady-burning rate in this example seems to be reasonable, limitation of this Simple Analytical Modeling should be noted, which is that the model is for thermally-thick-behaving materials and steady burning after ignition.

EXAMPLE 4.5 MODELING GRP WITH BALSA WOOD CORE SANDWICH COMPOSITE

This material is composed of approximately 1 mm thickness of laminated glass-reinforced polymer (GRP) over approximately 25 mm thickness of resin-soaked balsa wood core as a skin layer (sandwich construction). The resin used in the GRP and with balsa wood is vinyl ester (VEX). The light-weight balsa wood core acts as an insulating layer for the thin GRP skin and allows the ignition data to behave thermally-thin. This thermal behavior is examined by plotting $1/t_{ig}^n$ vs. applied heat flux where its best fitness of a linear regression occurs near $n = 0.9$.

Measure Parameters

1. Ambient Temperature

Direct measurement of ambient temperature is made as 20°C.

2. Surface Temperature at Ignition

This parameter will be obtained via Ignition Data Analysis, i.e., no direct measurements will be performed.

3. Critical Heat Flux for Ignition

By bracketing to within $\pm 2.5 \text{ kW/m}^2$ in cone calorimeter tests, \dot{q}_{cr}'' has been determined to be 12.5 kW/m^2 . Ignition data is provided below for this sandwich composite with thickness of $\sim 1 \text{ mm}$ of GRP skin layer on surfaces out of 28 mm of the entire composite, density of 500 kg/m^3 (see Table A(C)-25):

Table A(C)-25. Ignition data from cone calorimeter tests for GRP with balsa wood core sandwich composite

Heat Flux (kW/m ²)	t_{ig} (s)
10	NI
15	792

4. *Thermal Inertia*

This parameter will be obtained via Ignition Data Analysis, i.e., no direct measurements will be performed.

5. *Effective Heat-of-Combustion*

This parameter will be obtained via BurningRate Data Analysis, i.e., no direct measurements will be performed.

6. *Heat-of-Gasification*

This parameter will be obtained via Burning-Rate Data Analysis, i.e., no direct measurements will be performed.

7. *Convection Coefficient*

Because this is a material laid in horizontal position in a cone calorimeter, $h_c = 12 \text{ W/m}^2\text{K}$ is used based on literature reference.

8. *Surface Emissivity/Absorptivity*

Emissivity is approximated as 0.9.

Summary

Table A(C)-26. Summary of model-parameter table with estimated values via direct measurements, literature search, or approximation

Ignition Parameters	T_∞	20 °C
	T_{ig}	Ignition Data Analysis
	\dot{q}_{cr}''	12.5 kW/m ²
	$k\rho c$	Ignition Data Analysis
Burning-Rate Parameters	$\Delta h_{c,eff}$	Burning-Rate Data Analysis
	Δh_g	Burning-Rate Data Analysis
	h_c	12 W/m ² K
	ε	0.9

Obtain Parameters via Data Analysis

Run model

SELECT MODEL: THERMALLY THIN MODEL FOR IGNITION ANALYSIS AND STEADY-BURNING MODEL

UNDERSTAND EXPERIMENT AND FIRE CHARACTERISTICS OF MATERIAL

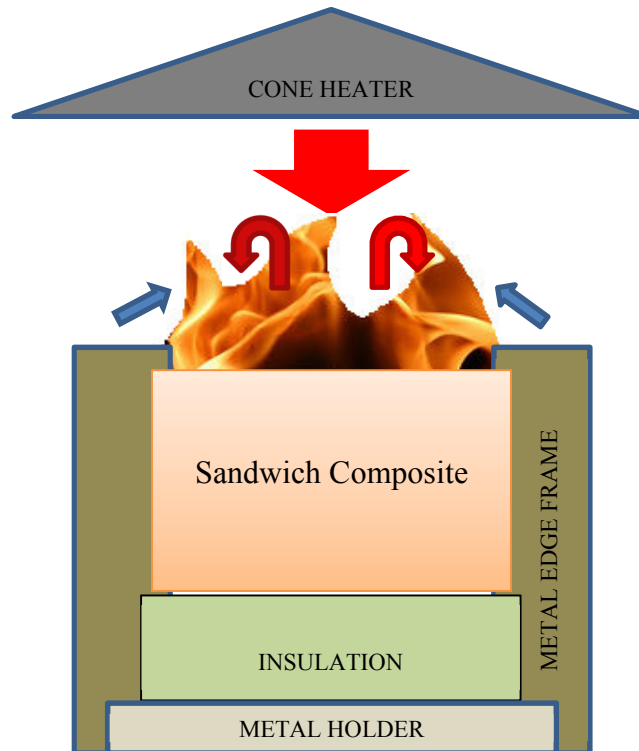


Figure A(C)-26. Simplified representation of a cone calorimeter test of sandwich composite

A simplified representation of a cone calorimeter test of this sandwich composite is shown in Figure A(C)-26. The sample is placed on top of an insulation, which sits on a metal holder. Another metal frame is placed on top of the sample, insulation and the holder. A metal edge frame is used as well.

Front Surface: As heating starts by opening the shutter to allow radiation from the cone heater to impinge on sample surface (large red arrow), cooling also begins via natural convection (blue arrows) and re-radiation. The surface decomposes with small bubbles appearing on the surface and blackening. When ignition occurs as the fuel-vapor concentration above the surface exceeds its LFL (lower flammable limit), additional heat flux from the flame is introduced on the surface (red arrows). The flame height and its intensity are the greatest when the resin in the skin layer (GRP composite) is pyrolyzing.

After the skin layer is consumed, the flame become shorter and scatters on the surface as the fuel vapor produced in the balsa wood core layer is diffusing through the inert glass layers left in the skin layer on the surface. This short and scattering flame continues throughout flameout.

Back surface: The sample is placed on top of insulation. In the experiment, an air gap of a few millimeters thickness exist between the sample and the insulation resulting in some thermal resistance. Due to the insulation, nothing leaves through the back face when 1D assumption holds for the experiment.

CONFIGURE MODEL CONDITIONS BASED ON UNDERSTANDING OF EXPERIMENT AND MATERIAL CHARACTERISTICS

In the model, the phenomena discussed above are simulated as below. Basic assumptions are as follows:

- Pre-ignition stage is:
 - Inert: decomposition with bubbling and changing color on THE surface before ignition is neglected
 - Thermally thin GRP skin: heat transfer reaches back surface quickly, and the surface layer (vinylester resin GRP) is considered to have uniform temperature throughout
 - Control volume for ignition analysis is the thermally-thin GRP skin layer on the front surface facing the heating source
- Post-ignition stage is:
 - Considered to have instantaneous release of volatiles from solid to gas phase: any mass-transportation effect on pyrolysis is neglected, and pyrolysis is considered as surface phenomenon only
 - Considered to have a constant thickness
 - Steady burning: heat loss equals heat gain at front surface
 - 30% of the GRP skin layer (density of 2000 kg/m^3) is consumed via burning, and this information is used to calculate the model's burnout-time prediction

ACQUIRE DATA SETS

Cone calorimeter test data of this sandwich composite panel with thickness of 28 mm, density of 500 and applied heat flux levels ranging from 15 to 90 kW/m² is found. For ignition data analysis, only time to ignition with respect to applied heat flux data will be used. For burning rate data analysis, data for the entire testing time duration, mass loss and heat release during testing period with respect to applied heat flux will be used.

CONDUCT IGNITION DATA ANALYSIS

1. Estimate T_{ig}

Heat balance at front surface during steady burning is as follow:

$$\varepsilon \dot{q}_{cr}'' = h_c (T_{ig} - T_\infty) + \varepsilon \sigma (T_{ig}^4 - T_\infty^4)$$

Knowing that emissivity is approximated as 0.9, critical heat flux is estimated as 12.5 kW/m², and heat transfer coefficient in Cone calorimeter experiment is estimated as 12.0 W/m²K, ignition temperature, T_{ig} is calculated as:

$$T_{ig} = 350 \text{ }^\circ\text{C}$$

2. Estimate h_{ig}

h_{ig} is the total heat transfer coefficient at ignition; therefore, at steady state burning stage, following can be defined:

$$\varepsilon \dot{q}_{cr}'' \equiv h_{ig} (T_{ig} - T_\infty)$$

Knowing the ignition temperature, h_{ig} can be calculated:

$$h_{ig} = 34.1 \text{ W/m}^2\text{K}$$

3. Calculate $\dot{q}_{cr}'' / \dot{q}_e''$ versus t_{ig} from ignition data

Table A(C)-27. $\dot{q}_{cr}'' / \dot{q}_e''$ versus $\sqrt{t_{ig}}$

Heat Flux (kW/m ²)	t_{ig} (s)	CHF/HF	Heat Flux (kW/m ²)	t_{ig} (s)	CHF/HF
10	NI		50	42	0.2500
15	792	0.8333	50	50	0.2500
15	1017	0.8333	50	43	0.2500
15	703	0.8333	50	47	0.2500
20	243	0.6250	50	46	0.2500
20	297	0.6250	50	35	0.2500
20	702	0.6250	50	45	0.2500
20	1044	0.6250	50	44	0.2500
20	256	0.6250	50	60	0.2500
20	266	0.6250	50	55	0.2500
25	139	0.5000	60	34	0.2083
25	191	0.5000	60	38	0.2083
30	89	0.4167	75	24	0.1667
30	123	0.4167	75	22	0.1667
35	93	0.3571	80	26	0.1563
35	82	0.3571	80	21	0.1563
35	93.0	0.3571	85	24.00	0.1471
35	98	0.3571	85	19	0.1471
40	55	0.3125	90	21	0.1389
40	66	0.3125	90	21.00	0.1389

4. Plot $\dot{q}_{cr}'' / \dot{q}_e''$ versus t_{ig} to estimate the time needed to reach “steady-state” burning, t^* and thermal capacity, $\rho c \delta$

$$\text{Recall } \frac{\dot{q}_{cr}''}{\dot{q}_e''} = F(t_{ig}) = \begin{cases} \frac{h_{ig} t_{ig}}{\rho c \delta} & t_{ig} \leq t^* \\ 1 & t_{ig} > t^* \end{cases} \quad \text{for piloted ignition data where } t^* \text{ is the}$$

time when $\dot{q}_{cr}'' / \dot{q}_e'' = 1$. Thermal inertia can be estimated from the best fit line through $t =$

0. Its slope at $0 < t < t^*$ is $\frac{h_{ig}}{\rho c \delta}$; therefore, $\rho c \delta = \frac{h_{ig}}{(\text{slope})}$. Note that in the analysis, few

data points at lower heat flux levels with large time to ignition data were excluded (see Figure A(C)-27, open circles) to increase fitness of the best-fit line. This approach is reasonable considering that at this region analysis assumptions of having inert, thermally-thin and negligible heat loss conditions are less likely to be satisfied.

$$\rho c \delta = 7.625 \text{ kJ/m}^2\text{K}$$

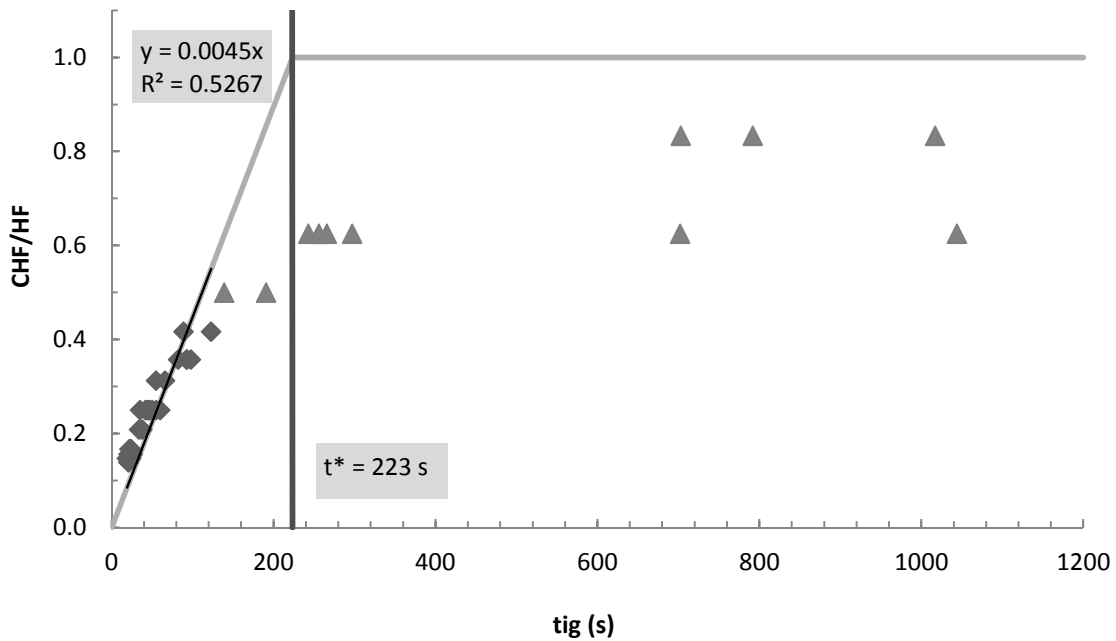


Figure A(C)-27. Plot of $\dot{q}_{cr}'' / \dot{q}_e''$ versus $\sqrt{t_{ig}}$

CONDUCT BURNING RATE DATA ANALYSIS

1. Estimate $\Delta h_{c,eff}$

There are two approaches in estimating the effective heat of combustion via calorimeter tests: by using the peak in HRR or the average heat released over the entire test. In this example, $\Delta h_{c,eff}$ will be estimated by considering the average peak heat released divided by the average peak mass loss during a test. Cone test results ranging from 30 to 90 kW/m² are used to calculate the effective heat of combustion with its confidence interval using student t distribution and $\alpha = 0.05$:

$$\Delta h_{c,eff} = 23.5 \pm 2.1 \text{ kJ/g}$$

2. Estimate Δh_g

Recall $\Delta h_g \equiv \frac{\dot{q}_{net}''}{\dot{m}''} = \frac{\dot{q}_e'' + \dot{q}_f'' - \dot{q}_l''}{\dot{m}''}$; therefore, when plotting mass loss rates at different radiant heat flux levels during steady burning condition, the reciprocal of the

slope of the best-fit line should be the heat-of-gasification. Note that for this material – sandwich composite – a strict steady-burning phase does not exist where a constant MLR appears. The burning of the resin in the front surface-skin layer (vinyl-ester resin GRP composite) occurs with ignition and lasts about 1 min. or so with increasing mass-loss rate and heat-release rate showing up as the initial peak in the MLR and HRR curve. Considering that the model control volume is the first GRP skin layer and HoG is estimated to calculate the energy necessary for gasification of the GRP skin layer, HoG is calculated in the time interval where the initial peaks of the MLR and HRR curve are found; hence, both MLR and HRR are found from the peak averaged values at different heat-flux levels (see Table A(C)-28 and Figure A(C)-28).

$$\Delta h_g = 8.0 \text{ kJ/g}$$

Table A(C)-28. Estimation of effective heat-of-gasification using cone calorimeter test results at applied heat flux ranging between 30 and 90 kW/m²

Heat Flux (kW/m ²)	peakAvgMLR (g/m ² s)
30	10.53
30	12.09
35	12.53
35	12.75
35	12.01
35	12.68
40	12.69
40	13.26
50	12.87
50	12.12
50	12.27
60	14.39
60	16.14
75	17.31
75	17.85
80	16.08
85	17.51
90	20.20
90	20.18

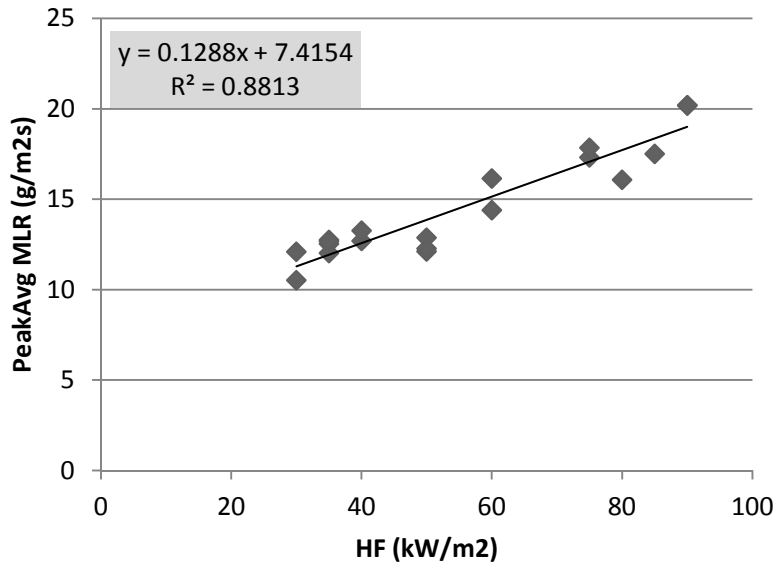


Figure A(C)-28. Plot of steady MLR versus different applied heat-flux levels – 25 to 75 kW/m²

Obtain Uncertainty for Estimated Parameters

UNCERTAINTY FOR MEASURED PARAMETERS

1. δT_{∞}

Fluctuation in ambient temperature during testing is estimated to be less than $\pm 25\%$ of reported measurement data.

2. $\delta \dot{q}_{cr}''$

The resolution of bracketing experiment was 5 kW/m²; hence, uncertainty can be estimated as ± 2.5 kW/m².

3. δh_c

Considering that the reference values sited in the *Guide* for different apparatuses and set-up have two significant figures, uncertainty for this convection coefficient can be estimated as ± 0.5 W/m²K.

4. $\delta \epsilon$

Emissivity measurement of this sample was conducted using an IR camera with its surface blackened – 0.92 ± 0.02 . This is close to what has been assumed in the analysis. The emissivity uncertainty is considered to be $\pm 10\%$ of what has been approximated in this example.

UNCERTAINTY FOR ESTIMATED PARAMETERS USING IGNITION DATA ANALYSIS

1. δT_{ig}

See Chapter 4 for detail.

$$\begin{aligned}\frac{\partial \dot{q}_{cr}''}{\partial T_{ig}} &= \frac{h_c + 4\varepsilon\sigma T_{ig}^3}{\varepsilon} \\ &= \frac{\left(0.012 \frac{kW}{m^2 K}\right) + 4(0.9)\left(5.67 \times 10^{-11} \frac{kW}{K^4 m^2}\right)\left((350 + 273)K\right)^3}{(0.9)}\end{aligned}$$

$$\approx 0.06818 \frac{kW}{m^2 K}$$

$$\begin{aligned}\frac{\partial \dot{q}_{cr}''}{\partial \varepsilon} &= \frac{-\dot{q}_{cr}'' + \sigma(T_{ig}^4 - T_{\infty}^4)}{\varepsilon} \\ &= \frac{-\left(12.5 \frac{kW}{m^2}\right) + \left(5.67 \times 10^{-11} \frac{kW}{K^4 m^2}\right)\left(\left((350 + 273)K\right)^4 - \left((20 + 273)K\right)^4\right)}{(0.9)}\end{aligned}$$

$$\approx -4.863 \frac{kW}{m^2}$$

$$\begin{aligned}\frac{\partial \dot{q}_{cr}''}{\partial h_c} &= \frac{T_{ig} - T_{\infty}}{\varepsilon} \\ &= \frac{\left((350 + 273)K\right) - \left((20 + 273)K\right)}{(0.9)}\end{aligned}$$

$$\approx 367 K$$

$$\begin{aligned}\frac{\partial \dot{q}_{cr}''}{\partial T_{\infty}} &= \frac{-h_c - 4\varepsilon\sigma T_{\infty}^3}{\varepsilon} \\ &= \frac{-\left(0.012 \frac{kW}{m^2 K}\right) - 4(0.9)\left(5.67 \times 10^{-11} \frac{kW}{K^4 m^2}\right)\left((20 + 273)K\right)^3}{(0.9)}\end{aligned}$$

$$\approx -0.01904 \frac{kW}{m^2 K}$$

Therefore,

$$\begin{aligned} \delta T_{ig} &= \left(\frac{\partial \dot{q}_{cr}''}{\partial T_{ig}} \right)^{-1} \sqrt{(\delta \dot{q}_{cr}'')^2 - \left(\left(\frac{\partial \dot{q}_{cr}''}{\partial \varepsilon} \delta \varepsilon \right)^2 + \left(\frac{\partial \dot{q}_{cr}''}{\partial h_c} \delta h_c \right)^2 + \left(\frac{\partial \dot{q}_{cr}''}{\partial T_\infty} \delta T_\infty \right)^2 \right)} \\ &= \left(0.0682 \frac{kW}{m^2 K} \right)^{-1} \sqrt{\left(2.5 \frac{kW}{m^2} \right)^2 - \left[\left(\left(-4.86 \frac{kW}{m^2} \right) (0.09) \right)^2 + \left((367 K) \left(0.5 \times 10^{-3} \frac{kW}{m^2 K} \right) \right)^2 + \left(\left(-0.01904 \frac{kW}{m^2 K} \right) (5 K) \right)^2 \right]} \\ &\approx 36.0 K \end{aligned}$$

2. $\delta(\rho c \delta)$

See Chapter 4 for detail.

The uncertainty of the slope of the best-fit line, 0.004475 /s, can be estimated through calculating 2 times the standard error of the slope, which is +/- 0.000379 /s.

$$\begin{aligned} \frac{\partial(\rho c \delta)}{\partial(\text{slope})} &= \frac{-1}{(\text{slope})^2} \left(\frac{\varepsilon \dot{q}_{cr}''}{T_{ig} - T_\infty} \right) \\ &= \frac{-1}{(0.004475 / s)^2} \left(\frac{(0.9) \left(12.5 \frac{s}{m^2} \right)}{((350 + 273) K) - ((20 + 273) K)} \right) \\ &\approx -1702 \frac{kJ \cdot s}{m^2 K} \end{aligned}$$

$$\begin{aligned} \frac{\partial(\rho c \delta)}{\partial \varepsilon} &= \frac{1}{(\text{slope})} \left(\frac{\dot{q}_{cr}''}{T_{ig} - T_{\infty}} \right) \varepsilon \\ &= \frac{1}{(0.004475 / s)} \left(\frac{\left(\frac{kJ}{m^2} \right)}{\left((350 + 273)K \right) - \left((20 + 273)K \right)} \right) (0.9) \\ &\approx 8.464 \frac{kJ}{m^2 K} \end{aligned}$$

$$\begin{aligned} \frac{\partial(\rho c \delta)}{\partial \dot{q}_{cr}''} &= \frac{1}{(\text{slope})} \left(\frac{\varepsilon}{T_{ig} - T_{\infty}} \right) \\ &= \frac{1}{(0.004475 / s)^2} \left(\frac{(0.9)}{\left((350 + 273)K \right) - \left((20 + 273)K \right)} \right) \\ &\approx 7.617 \frac{s}{K} \end{aligned}$$

$$\begin{aligned} \frac{\partial(\rho c \delta)}{\partial T_{ig}} &= \frac{-1}{(\text{slope})} \left(\frac{\varepsilon \dot{q}_{cr}''}{T_{ig} - T_{\infty}} \right) \frac{1}{T_{ig} - T_{\infty}} \\ &= \frac{-1}{(0.004475 / s)} \left(\frac{(0.9) \left(\frac{kJ}{m^2} \right)}{\left((350 + 273)K \right) - \left((20 + 273)K \right)} \right) \frac{1}{\left((350 + 273)K \right) - \left((20 + 273)K \right)} \\ &\approx -0.0231 \frac{kJ \cdot s}{m^2 K^2} \end{aligned}$$

$$\begin{aligned}
\frac{\partial(\rho c \delta)}{\partial T_{\infty}} &= \frac{1}{(slope)} \left(\frac{\varepsilon \dot{q}_{cr}''}{T_{ig} - T_{\infty}} \right) \frac{1}{T_{ig} - T_{\infty}} \\
&= \frac{1}{(0.004475 / s)} \left(\frac{(0.9) \left(12.5 \frac{kJ}{m^2} \right)}{((350 + 273)K) - ((20 + 273)K)} \right) \frac{1}{((350 + 273)K) - ((20 + 273)K)} \\
&\approx 0.0231 \frac{kJ}{m^2 K^2}
\end{aligned}$$

Therefore,

$$\begin{aligned}
\delta(\rho c \delta) &= \sqrt{\left(\frac{\partial(\rho c \delta)}{\partial (slope)} \delta(slope) \right)^2 + \left(\frac{\partial(\rho c \delta)}{\partial \varepsilon} \delta \varepsilon \right)^2 + \left(\frac{\partial(\rho c \delta)}{\partial \dot{q}_{cr}''} \delta \dot{q}_{cr}'' \right)^2} \\
&\quad + \sqrt{\left(\frac{\partial(\rho c \delta)}{\partial T_{ig}} \delta T_{ig} \right)^2 + \left(\frac{\partial(\rho c \delta)}{\partial T_{\infty}} \delta T_{\infty} \right)^2} \\
&= \sqrt{\left(\left(-1702 \frac{kJ \cdot s}{m^2 K} \right) (0.000379 / s) \right)^2 + \left(\left(8.464 \frac{kJ}{m^2 K} \right) (0.09) \right)^2} \\
&\quad + \sqrt{\left(\left(7.617 \frac{s}{K} \right) \left(2.5 \frac{kW}{m^2} \right) \right)^2 + \left(\left(-0.0231 \frac{kJ}{m^2 K^2} \right) (11.3K) \right)^2} \\
&\quad + \sqrt{\left(\left(0.0231 \frac{kJ}{m^2 K^2} \right) (2.5K) \right)^2} \\
&\approx 19.1 \frac{kJ}{m^2 K}
\end{aligned}$$

UNCERTAINTY FOR ESTIMATED PARAMETERS USING BURNING-RATE DATA ANALYSIS

1. $\delta\Delta h_{c,eff}$

Cone test results ranging from 30 to 90 kW/m² are used to calculate the effective heat-of-combustion. Uncertainty of this value is estimated with its confidence interval using student t distribution and $\alpha = 0.05$: ± 2.1 kJ/g

2. $\delta\Delta h_g$

See Chapter 4 for detail.

The uncertainty of the slope ($=1/\Delta h_g=0.129$ g/kJ) can be estimated through calculating 2 times the standard error of the slope of the best-fit line, which is +/- 0.229. Therefore, the uncertainty in Δh_g is

$$\begin{aligned}\frac{d(\Delta h_g)}{d(\text{slope})} &= -\frac{1}{(\text{slope})^2} \\ &= -\frac{1}{\left(0.129 \frac{\text{g}}{\text{kJ}}\right)^2} \\ &\approx -60.3 \frac{\text{kJ}^2}{\text{g}^2}\end{aligned}$$

Therefore,

$$\begin{aligned}\delta(\Delta h_g) &= \sqrt{\left(\frac{d(\Delta h_g)}{d(\text{slope})}\delta(\text{slope})\right)^2} \\ &= \sqrt{\left(\left(-60.3\frac{\text{kJ}^2}{\text{g}^2}\right)(0.0229\text{g/kJ})\right)^2} \\ &\approx 1.38\frac{\text{kJ}}{\text{g}}\end{aligned}$$

UNCERTAINTY SUMMARY

Table A(C)-29. Summary of model-parameter table with estimated values with uncertainty

Ignition Parameters	T_∞	$20 \pm 5 \text{ }^\circ\text{C}$
	T_{ig}	$350 \pm 36 \text{ }^\circ\text{C}$
	\dot{q}_{cr}''	$12.5 \pm 2.5 \text{ kW/m}^2$
	$\rho c \delta$	$7.625 \pm 19.1 \text{ kJ}^2/\text{m}^4\text{K}^2\text{s}$
Burning-Rate Parameters	$\Delta h_{c,eff}$	$23.5 \pm 2.1 \text{ kJ/g}$
	Δh_g	$8.7 \pm 1.4 \text{ kJ/g}$
	h_c	$12 \pm 0.5 \text{ W/m}^2\text{K}$
	ε	0.9 ± 0.09

Validation

Analyze Simulation Quality

DETERMINE DATA AND MODEL OUTPUT UNCERTAINTY TO MAKE COMPARISON

1. Conduct uncertainty analysis of data

The uncertainty in the mass-loss-rate data used for comparison between data and model outputs is estimated via statistical approach, taking the standard deviation (0.58 g/sm^2) from the mean of a steady burning of five identical PMMA tests conducted in a cone calorimeter.² The estimated uncertainty is 1.4 g/sm^2 , which is found by calculating the 95% confidence interval applying student t distribution with a sample size of five.

The uncertainty in time-to-ignition data used for comparison is estimated via statistical approach, taking three to four identical cone calorimeter test data at heat fluxes ranging from 35 to 75 kW/m^2 of this plywood. 95% confidence interval is calculated for each heat-flux level assuming student t distribution.

2. Conduct uncertainty analysis for MLR profile modeling

Because uncertainty information of the data is found in terms of time-to-ignition and mass-loss rate, the mass-loss-rate profile is considered as the modeling output of interest for comparison purposes. For Simple Analytical Models, time-to-ignition (t_{ig}) and steady-burning rate (\dot{m}'') are needed when simulating the mass-release-rate profile. The uncertainty in the MLR profile in modeling can be determined via considering the uncertainties in these calculation results as below:

$$t_{ig} \pm \delta t_{ig}$$
$$\dot{m}'' \pm \delta \dot{m}''$$

To determine the uncertainty in time to ignition, recall:

$$\frac{\dot{q}_{cr}''}{\dot{q}_e''} = F(t_{ig}) = \begin{cases} \frac{h_{ig} t_{ig}}{\rho c \delta} & t_{ig} \leq t^* \\ 1 & t_{ig} > t^* \end{cases}$$

Knowing that all heat-flux levels of interest, 35, 50, and 75 kW/m^2 , are above the critical heat flux, time-to-ignition should be smaller than t^* . Hence, uncertainty in t_{ig} can be estimated from linear-regression process as below:

$$\frac{\dot{q}_{cr}''}{\dot{q}_e''} = \frac{h_{ig}}{\rho c \delta} t_{ig}$$

The above equation can be re-written as below after conducting linear regression:

$$y \text{ estimate} = (\text{slope}) t_{ig}$$

Therefore,

$$t_{ig} = \frac{y \text{ estimate}}{\text{slope}}$$

Assuming that the y estimate and slope are independent and propagating the uncertainties in these two variables in estimating the time-to-ignition, the following calculation can be made:

$$\delta t_{ig} = \sqrt{\left(\frac{\partial t_{ig}}{\partial (y \text{ estimate})} \delta (y \text{ estimate}) \right)^2 + \left(\frac{\partial t_{ig}}{\partial (\text{slope})} \delta (\text{slope}) \right)^2}$$

where

$$\frac{\partial t_{ig}}{\partial (y \text{ estimate})} = \frac{1}{(\text{slope})}$$

$$\frac{\partial t_{ig}}{\partial (\text{slope})} = -\frac{(y \text{ estimate})}{(\text{slope})^2}$$

with $\delta (y \text{ estimate})$ and $\delta (\text{slope})$ estimated through calculating 2 times the standard error of the y estimate and slope of the best-fit line.

To determine the uncertainty in the steady-heat-release rate at post-ignition stage, recall:

$$\Delta h_g \equiv \frac{\dot{q}_{net}''}{\dot{m}''} = \frac{\dot{q}_e'' + \dot{q}_f'' - \dot{q}_l''}{\dot{m}''}$$

The above equation can be rearranged to

$$\dot{m}'' = \frac{1}{\Delta h_g} \dot{q}_e'' + \frac{\dot{q}_f'' - \dot{q}_l''}{\Delta h_g}$$

The steady-burning rate at post-ignition stage is determined by the best-fit line obtained when data is plotted as steady-burning rate versus applied heat flux. The uncertainty in steady-burning rate can be determined by considering 2 times the standard

error of the y estimates, i.e. \dot{m} , which is obtained through linear regression process: ± 2.1 $\text{g/m}^2\text{s}$.

COMPARE DATA WITH SIMULATION RESULTS WITH CONSIDERATION OF UNCERTAINTIES

Parameters in this simple analytical pyrolysis model have been estimated with cone calorimeter test data from 35, 50 and 75 kW/m². To check the quality of the modeling using the estimated parameters, three cases have been simulated and compared with experiment data with the consideration of their uncertainty bands as shown in Table A(C)-30 and figures below. Note that although the experiment data shows pyrolysis of the entire sandwich composite, from the front surface GRP skin layer to balsa wood core and through the back surface GRP skin layer (blue lines), the modeling results only account for pyrolysis of the front surface GRP skin layer (red lines). The GRP skin layer has a thickness, density, and inert residue fraction, including glass layers, of approximately 1.3 mm, 2000 kg/m³ and 70%, respectively.

Table A(C)-30. Comparison of time-to-ignition at different heat-flux levels from actual experiment and pyrolysis modeling

Heat-Flux Level	Actual t_{ig} (s) $t_{ig} \pm \delta t_i$	Model t_{ig} (s) $t_{ig} \pm \delta t_i$
35 kW/m ²	92 ± 11	80 ± 27
50 kW/m ²	47 ± 5	56 ± 26
75 kW/m ²	23 ± 13	37 ± 26

All three cases show good overlap between the data and simulation of time-to-ignition and the mass-loss rate during steady burning, considering the uncertainties, i.e., the parameter estimation was conducted successfully (see Figure A(C)-29, Figure A(C)-30 and Figure A(C)-31).

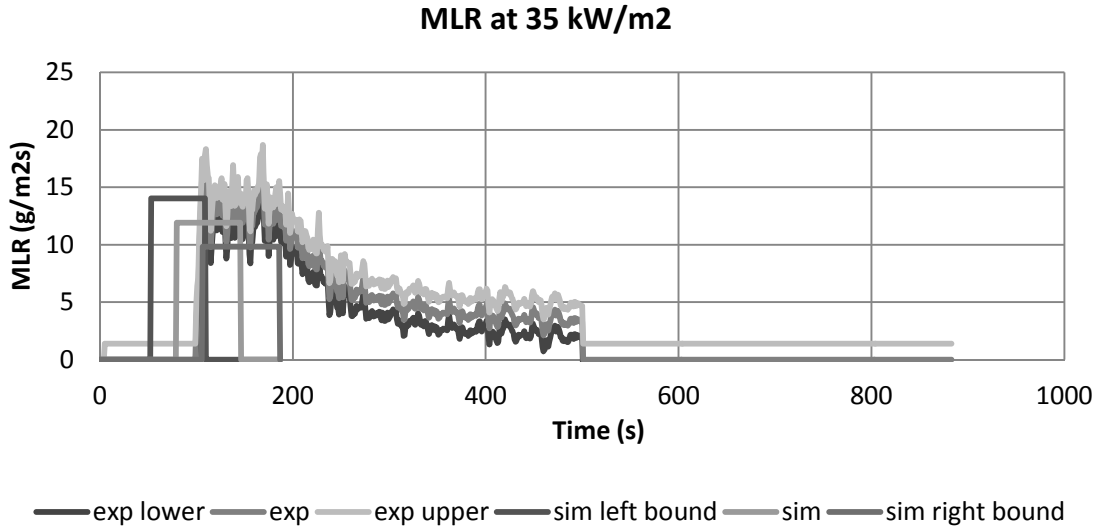


Figure A(C)-29. Mass-loss rate (MLR) comparisons for GRP with balsa wood core sandwich composite between actual MLR from experiment (exp) and modeled MLR (sim) at 25 kW/m². Note that data shown were used to estimate model-parameter values.

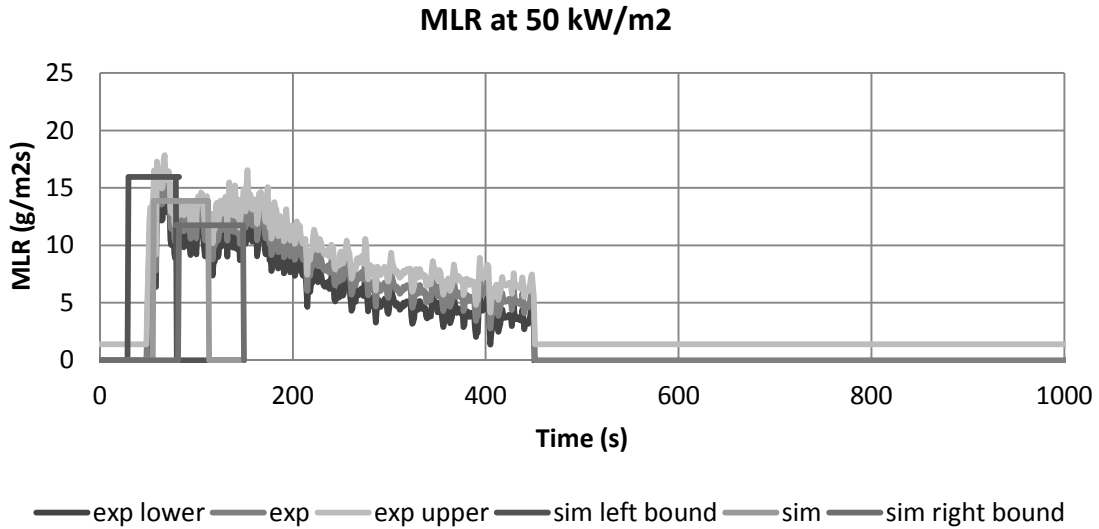


Figure A(C)-30. Mass-loss rate (MLR) comparisons for GRP with balsa wood core sandwich composite between actual MLR from experiment (exp) and modeled MLR (sim) at 50 kW/m². Note that data shown were used to estimate model-parameter values.

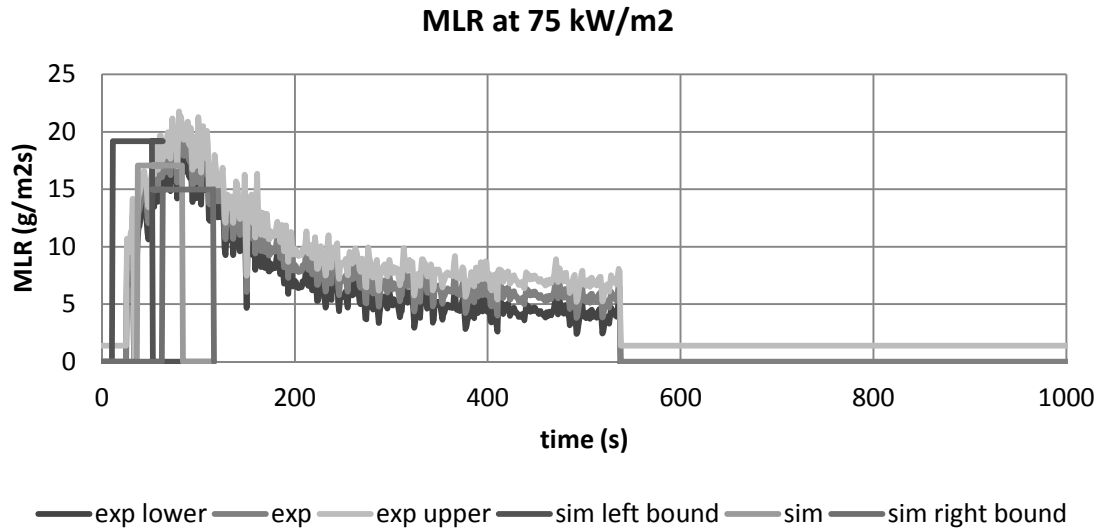


Figure A(C)-31. Mass-loss rate (MLR) comparisons for GRP with balsa wood core sandwich composite between actual MLR from experiment (exp) and modeled MLR (sim) at 75 kW/m². Note that data shown were used to estimate model-parameter values.

Commentary

In this example, Simple Analytical Model is used to simulate pyrolysis of the thermally-thin-behaving GRP skin layer of this sandwich composite (vinyl-ester GRP skin layers with resin-soaked balsa wood core). Test data from a bench-scale cone calorimeter experiment at several heat-flux levels have been utilized to estimate the time-to-ignition from exposure to heating and the mass-loss rate at steady-burning stage after ignition. The comparison between the model outputs (time-to-ignition and steady-burning rate) and the data from bench-scale experiment showed good agreement for both checking purposes where the same heat-flux levels (35, 50 and 75 kW/m²) used in parameter estimation have been considered.

Although the modeling predictions of time-to-ignition and steady-burning rate in this example seems to be reasonable, limitation of this Simple Analytical Modeling should be noted, which is that the model is for thermally-thin-behaving materials and steady burning after ignition.

EXAMPLE 4.6 MODELING THIN FRP COMPOSITE SHEET

The rigid FRP panel chosen for use in full-scale testing is commercially available and advertised for use as ceiling and wall linings in environments designed to be moisture- and mold-free. The panel has a Class C (ASTM E84) flame-spread rating. It is consisted of modified-polyester copolymer and inorganic fillers as the resin base and reinforced with a weave of random-chopped fiberglass. The panel's thickness is 0.09" (2.3 mm) nominal, with a smooth backface and a pebbled, embossed white front surface. When this material is tested for ignition in a cone calorimeter test, thermally thin behavior is observed. This thermal characteristic is examined by plotting $1/t_{ig}^n$ vs. applied heat flux, where its best fitness of a linear regression occurs near $n = 1.0$.

Measure Parameters

1. Ambient Temperature

Direct measurement of ambient temperature is made as 23°C.

2. Surface Temperature at Ignition

This parameter will be obtained via Ignition Data Analysis, i.e., no direct measurements will be performed.

3. Critical Heat Flux for Ignition

By bracketing to within +/- 1 kW/m² in cone calorimeter tests, \dot{q}_{cr}'' has been determined to be 16 kW/m². Ignition data is provided below for this FRP composite with thickness of 2 mm and density of 1500 kg/m³ (see Table A(C)-31):

Table A(C)-31. Ignition data from cone calorimeter tests for thin FRP composite sheet

Heat Flux (kW/m ²)	t_{ig} (s)
15	NI
17	269

4. Thermal Inertia

This parameter will be obtained via Ignition Data Analysis, i.e., no direct measurements will be performed.

5. Effective Heat-of-Combustion

This parameter will be obtained via Burning-Rate Data Analysis, i.e., no direct measurements will be performed.

6. Heat-of-Gasification

This parameter will be obtained via Burning-Rate Data Analysis, i.e., no direct measurements will be performed.

7. Convection Coefficient

Because this is a material laid in horizontal position in a cone calorimeter, $h_c = 12 \text{ W/m}^2\text{K}$ is used based on literature reference.

8. Surface Emissivity/Absorptivity

Emissivity is approximated as 0.9.

Summary

Table A(C)-32. Summary of model-parameter table with estimated values via direct measurements, literature search, or approximation

Ignition Parameters	T_∞	23 °C
	T_{ig}	Ignition Data Analysis
	\dot{q}_{cr}''	16 kW/m ²
	$k\rho c$	Ignition Data Analysis
Burning-Rate Parameters	$\Delta h_{c,eff}$	Burning-Rate Data Analysis
	Δh_g	Burning-Rate Data Analysis
	h_c	12 W/m ² K
	ε	0.9

Obtain Parameters via Data Analysis

Run model

SELECT MODEL: THERMALLY-THIN MODEL FOR IGNITION ANALYSIS AND STEADY-BURNING MODEL

UNDERSTAND EXPERIMENT AND FIRE CHARACTERISTICS OF MATERIAL

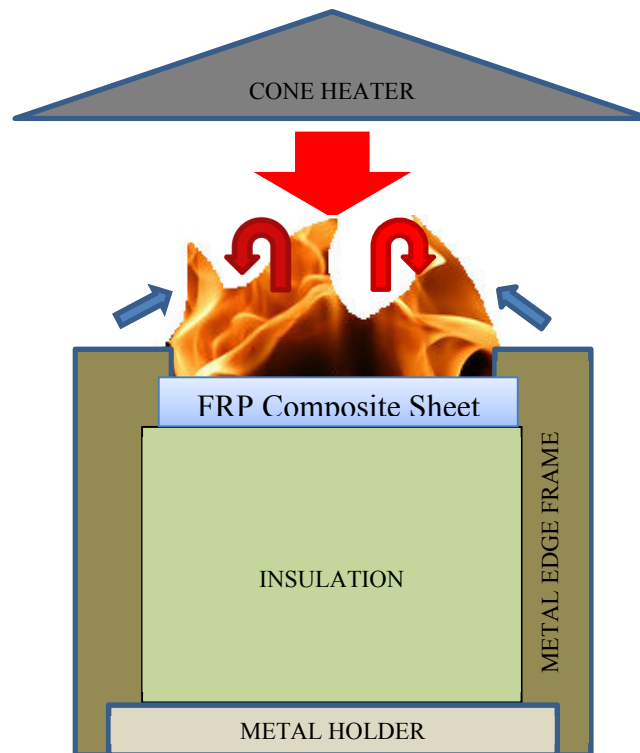


Figure A(C)-32. Simplified representation of a cone calorimeter test of FRP composite sheet

A simplified representation of a cone calorimeter test of this FRP composite sheet is shown in Figure A(C)-32. The sample is placed on top of an insulation, which sits on a metal holder. Another metal frame is placed on top of the sample, insulation and the holder. A metal edge frame is used as well.

Front Surface: As heating starts by opening the shutter to allow radiation from the cone heater to impinge on sample surface (large red arrow), cooling also begins via natural convection (blue arrows) and re-radiation. The surface decomposes with a small crackling sound and the surface becomes black. When ignition occurs as the fuel-vapor concentration above the surface exceeds its LFL (lower flammable limit), additional heat flux from the flame is introduced on the surface (red arrows).

Back surface: The sample is placed on top of insulation. In the experiment, an air gap of a few millimeters thickness exists between the sample and the insulation, resulting in some thermal resistance. Due to the insulation, nothing leaves through the back face when 1D assumption holds for the experiment.

CONFIGURE MODEL CONDITIONS BASED ON UNDERSTANDING OF EXPERIMENT AND MATERIAL CHARACTERISTICS

In the model, the phenomena discussed above are simulated as below. Basic assumptions are as follows:

- Pre-ignition stage is:
 - Inert: decomposition with crackling sound and changing color on the surface before ignition are neglected
 - Thermally thin: heat transfer reaches back surface quickly, and the entire layer is considered to have uniform temperature throughout
- Post-ignition stage is:
 - Considered to have instantaneous release of volatiles from solid to gas phase: any mass-transportation effect on pyrolysis is neglected, and pyrolysis is considered as surface phenomena only
 - Considered to have a constant thickness
 - Steady burning: heat loss equals heat gain at front surface
 - 40% of the FRP composite sheet (density of 1500 kg/m^3) is consumed via burning, and this information is used to calculate the model's burnout time prediction

ACQUIRE DATA SETS

A cone calorimeter test data of this FRP composite sheet with thickness of 2 mm, density of 1500 and applied heat-flux levels ranging from 15 to 75 kW/m^2 is found. For ignition data analysis, only time-to-ignition with respect to applied heat-flux data will be used. For burning-rate data analysis, data for the entire testing time duration, mass loss and heat release during testing period with respect to applied heat flux will be used.

CONDUCT IGNITION DATA ANALYSIS

1. Estimate T_{ig}

Heat balance at front surface during steady burning is as follow:

$$\varepsilon \dot{q}_{cr}'' = h_c (T_{ig} - T_\infty) + \varepsilon \sigma (T_{ig}^4 - T_\infty^4)$$

Knowing that emissivity is approximated as 0.9, critical heat flux is estimated as 16 kW/m^2 , and heat transfer coefficient in cone calorimeter experiment is estimated as $12.0 \text{ W/m}^2\text{K}$, ignition temperature, T_{ig} is calculated as:

$$T_{ig} = 397 \text{ }^\circ\text{C}$$

2. Estimate h_{ig}

h_{ig} is the total heat-transfer coefficient at ignition; therefore, at steady-state-burning stage, the following can be defined:

$$\varepsilon \dot{q}_{cr}'' \equiv h_{ig} (T_{ig} - T_\infty)$$

Knowing the ignition temperature, h_{ig} can be calculated:

$$h_{ig} = 38.5 \text{ W/m}^2\text{K}$$

3. Calculate $\dot{q}_{cr}'' / \dot{q}_e''$ versus t_{ig} from ignition data

Table A(C)-33. $\dot{q}_{cr}'' / \dot{q}_e''$ versus $\sqrt{t_{ig}}$

Heat Flux (kW/m ²)	t_{ig} (s)	CHF/HF
15	NI	
17	269	0.9412
20	207	0.8000
25	106	0.6400
25	117	0.6400
40	42	0.4000
40	52	0.4000
50	37	0.3200
50	39	0.3200
50	37	0.3200
60	26	0.2667
60	26	0.2667
75	24	0.2133
75	25	0.2133

4. Plot $\dot{q}_{cr}'' / \dot{q}_e''$ versus t_{ig} to estimate the time needed to reach “steady-state” burning, t^* and thermal capacity, $\rho c \delta$

$$\text{Recall } \frac{\dot{q}_{cr}''}{\dot{q}_e''} = F(t_{ig}) = \begin{cases} \frac{h_{ig} t_{ig}}{\rho c \delta} & t_{ig} \leq t^* \\ 1 & t_{ig} > t^* \end{cases} \quad \text{for piloted-ignition data, where } t^* \text{ is the}$$

time when $\dot{q}_{cr}'' / \dot{q}_e'' = 1$. Thermal inertia can be estimated from the best-fit line through $t =$

0. Its slope at $0 < t < t^*$ is $\frac{h_{ig}}{\rho c \delta}$; therefore, $\rho c \delta = \frac{h_{ig}}{(\text{slope})}$. Note that in the analysis, few

data points at lower heat-flux levels with large time-to-ignition data were excluded (see Figure A(C)-33, open circles) to increase fitness of the best-fit line. This approach is reasonable, considering that at this region analysis assumptions of having inert, thermally-thin and negligible heat-loss conditions are less likely to be satisfied.

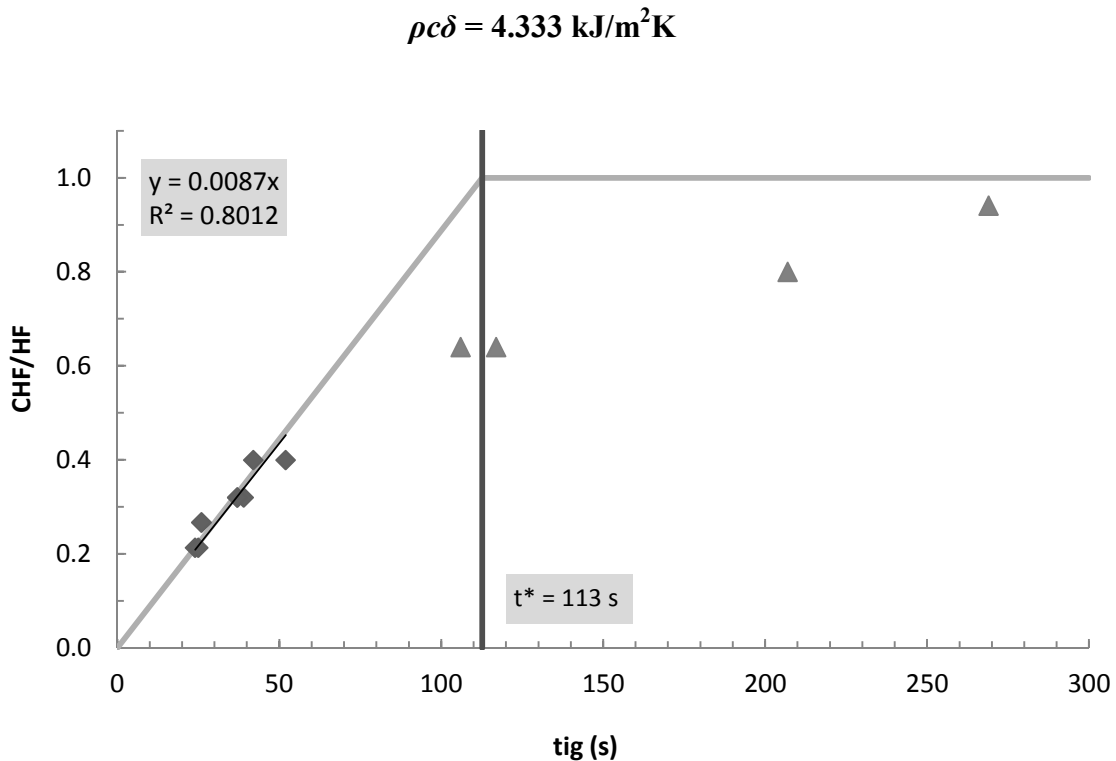


Figure A(C)-33. Plot of $\dot{q}_{cr}'' / \dot{q}_e''$ versus $\sqrt{t_{ig}}$

CONDUCT BURNING-RATE DATA ANALYSIS

1. Estimate $\Delta h_{c,eff}$

There are two approaches in estimating the effective heat-of-combustion via calorimeter tests: by using the peak in HRR or the average heat released over the entire test. In this example, $\Delta h_{c,eff}$ will be estimated by considering the average peak heat released divided by the average peak mass loss during a test. Cone test results ranging from 30 to 90 kW/m² are used to calculate the effective heat-of-combustion with its confidence interval using student t distribution and $\alpha = 0.05$:

$$\Delta h_{c,eff} = 25.5 \pm 1.8 \text{ kJ/g}$$

2. Estimate Δh_g

Recall $\Delta h_g \equiv \frac{\dot{q}_{net}''}{\dot{m}''} = \frac{\dot{q}_e'' + \dot{q}_f'' - \dot{q}_l''}{\dot{m}''}$; therefore, when plotting mass-loss rates at different radiant heat flux-levels during steady-burning condition, the reciprocal of the slope of the best-fit line should be the heat-of-gasification. In this example, average MLR and HRR will be used to estimate heat of gasification (see

Table A(C)-34 and Figure A(C)-34).

$$\Delta h_g = 16.3 \text{ kJ/g}$$

Table A(C)-34. Estimation of effective heat-of-gasification using cone calorimeter test results at applied heat flux ranging between 17 and 75 kW/m²

Heat Flux (kW/m ²)	AvgMLR (g/m ² s)
17	2.23
20	2.64
25	2.61
25	2.85
40	3.80
50	3.84
50	4.72
50	4.58
60	4.69
60	3.34
75	6.44
75	6.16

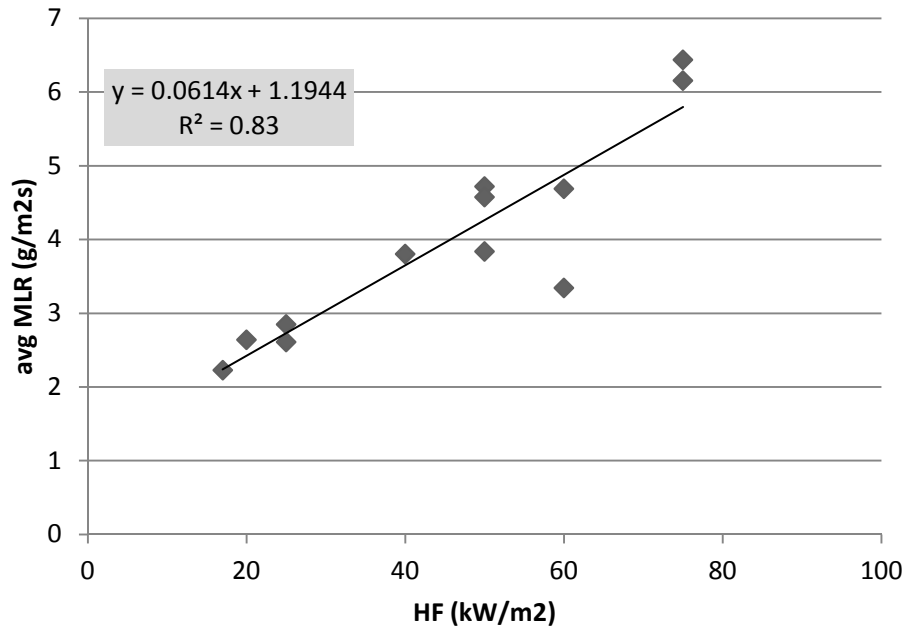


Figure A(C)-34. Plot of steady MLR versus different applied heat-flux levels – 25 to 75 kW/m²

Obtain Uncertainty for Estimated Parameters

UNCERTAINTY FOR MEASURED PARAMETERS

1. δT_{∞}

Fluctuation in ambient temperature during testing is estimated to be less than $\pm 15\%$ of reported measurement data.

2. $\delta \dot{q}_{cr}''$

The resolution of the bracketing experiment was 2 kW/m²; hence, uncertainty can be estimated as ± 1 kW/m².

3. δh_c

Considering that the reference values sited in the *Guide* for different apparatuses and set-up have two significant figures, uncertainty for this convection coefficient can be estimated as ± 0.5 W/m²K.

4. $\delta \epsilon$

The emissivity uncertainty is considered to be $\pm 10\%$ of what has been approximated in this example.

UNCERTAINTY FOR ESTIMATED PARAMETERS USING IGNITION DATA ANALYSIS

1. δT_{ig}

See Chapter 4 for detail.

$$\begin{aligned}\frac{\partial \dot{q}_{cr}''}{\partial T_{ig}} &= \frac{h_c + 4\varepsilon\sigma T_{ig}^3}{\varepsilon} \\ &= \frac{\left(0.012 \frac{kW}{m^2 K}\right) + 4(0.9)\left(5.67 \times 10^{-11} \frac{kW}{K^4 m^2}\right)\left((397 + 273)K\right)^3}{(0.9)}\end{aligned}$$

$$\approx 0.0815 \frac{kW}{m^2 K}$$

$$\begin{aligned}\frac{\partial \dot{q}_{cr}''}{\partial \varepsilon} &= \frac{-\dot{q}_{cr}'' + \sigma(T_{ig}^4 - T_{\infty}^4)}{\varepsilon} \\ &= \frac{-\left(16 \frac{kW}{m^2}\right) + \left(5.67 \times 10^{-11} \frac{kW}{K^4 m^2}\right)\left(\left((397 + 273)K\right)^4 - \left((23 + 273)K\right)^4\right)}{(0.9)}\end{aligned}$$

$$\approx -5.566 \frac{kW}{m^2}$$

$$\begin{aligned}\frac{\partial \dot{q}_{cr}''}{\partial h_c} &= \frac{T_{ig} - T_{\infty}}{\varepsilon} \\ &= \frac{\left((397 + 273)K\right) - \left((23 + 273)K\right)}{(0.9)}\end{aligned}$$

$$\approx 416K$$

$$\begin{aligned}\frac{\partial \dot{q}_{cr}''}{\partial T_{\infty}} &= \frac{-h_c - 4\varepsilon\sigma T_{\infty}^3}{\varepsilon} \\ &= \frac{-\left(0.012 \frac{kW}{m^2 K}\right) - 4(0.9)\left(5.67 \times 10^{-11} \frac{kW}{K^4 m^2}\right)\left((23 + 273)K\right)^3}{(0.9)}\end{aligned}$$

$$\approx -0.01922 \frac{kW}{m^2 K}$$

Therefore,

$$\begin{aligned} \delta T_{ig} &= \left(\frac{\partial \dot{q}_{cr}''}{\partial T_{ig}} \right)^{-1} \sqrt{(\delta \dot{q}_{cr}'')^2 - \left(\left(\frac{\partial \dot{q}_{cr}''}{\partial \varepsilon} \delta \varepsilon \right)^2 + \left(\frac{\partial \dot{q}_{cr}''}{\partial h_c} \delta h_c \right)^2 + \left(\frac{\partial \dot{q}_{cr}''}{\partial T_\infty} \delta T_\infty \right)^2 \right)} \\ &= \left(0.08155 \frac{kW}{m^2 K} \right)^{-1} \sqrt{\left(1 \frac{kW}{m^2} \right)^2 - \left[\left(\left(-5.566 \frac{kW}{m^2} \right) (0.09) \right)^2 + \left((416K) \left(0.5 \times 10^{-3} \frac{kW}{m^2 K} \right) \right)^2 + \left(\left(-0.01922 \frac{kW}{m^2 K} \right) (3.45K) \right)^2 \right]} \\ &\approx 10.3K \end{aligned}$$

2. $\delta(\rho c \delta)$

See Chapter 4 for detail.

The uncertainty of the slope of the best-fit line, 0.008878 /s, can be estimated through calculating 2 times the standard error of the slope, which is +/- 0.000583 /s.

$$\begin{aligned} \frac{\partial(\rho c \delta)}{\partial(\text{slope})} &= \frac{-1}{(\text{slope})^2} \left(\frac{\varepsilon \dot{q}_{cr}''}{T_{ig} - T_\infty} \right) \\ &= \frac{-1}{(0.008878 /s)^2} \left(\frac{(0.9) \left(16 \frac{s}{m^2} \right)}{((397 + 273)K) - ((23 + 273)K)} \right) \\ &\approx -488.4 \frac{kJ \cdot s}{m^2 K} \end{aligned}$$

$$\begin{aligned} \frac{\partial(\rho c \delta)}{\partial \varepsilon} &= \frac{1}{(\text{slope})} \left(\frac{\dot{q}_{cr}''}{T_{ig} - T_{\infty}} \right) \varepsilon \\ &= \frac{1}{(0.008878 / s)} \left(\frac{\left(\frac{kJ}{m^2} \right)}{\left((397 + 273)K \right) - \left((23 + 273)K \right)} \right) (0.9) \\ &\approx 4.818 \frac{kJ}{m^2 K} \end{aligned}$$

$$\begin{aligned} \frac{\partial(\rho c \delta)}{\partial \dot{q}_{cr}''} &= \frac{1}{(\text{slope})} \left(\frac{\varepsilon}{T_{ig} - T_{\infty}} \right) \\ &= \frac{1}{(0.008878 / s)^2} \left(\frac{(0.9)}{\left((397 + 273)K \right) - \left((23 + 273)K \right)} \right) \\ &\approx 4.337 \frac{s}{K} \end{aligned}$$

$$\begin{aligned} \frac{\partial(\rho c \delta)}{\partial T_{ig}} &= \frac{-1}{(\text{slope})} \left(\frac{\varepsilon \dot{q}_{cr}''}{T_{ig} - T_{\infty}} \right) \frac{1}{T_{ig} - T_{\infty}} \\ &= \frac{-1}{(0.008878 / s)} \left(\frac{(0.9) \left(\frac{kJ}{m^2} \right)}{\left((397 + 273)K \right) - \left((23 + 273)K \right)} \right) \frac{1}{\left((397 + 273)K \right) - \left((23 + 273)K \right)} \\ &\approx -0.01160 \frac{kJ \cdot s}{m^2 K^2} \end{aligned}$$

$$\begin{aligned}
\frac{\partial(\rho c \delta)}{\partial T_{\infty}} &= \frac{1}{(\text{slope})} \left(\frac{\varepsilon \dot{q}_{cr}''}{T_{ig} - T_{\infty}} \right) \frac{1}{T_{ig} - T_{\infty}} \\
&= \frac{1}{(0.008878 / s)} \left(\frac{(0.9) \left(16 \frac{kJ}{m^2} \right)}{((397 + 273)K) - ((23 + 273)K)} \right) \frac{1}{((397 + 273)K) - ((23 + 273)K)} \\
&\approx 0.01160 \frac{kJ}{m^2 K^2}
\end{aligned}$$

Therefore,

$$\begin{aligned}
\delta(\rho c \delta) &= \sqrt{\left(\frac{\partial(\rho c \delta)}{\partial(\text{slope})} \delta(\text{slope}) \right)^2 + \left(\frac{\partial(\rho c \delta)}{\partial \varepsilon} \delta \varepsilon \right)^2 + \left(\frac{\partial(\rho c \delta)}{\partial \dot{q}_{cr}''} \delta \dot{q}_{cr}'' \right)^2} \\
&\quad + \sqrt{\left(\frac{\partial(\rho c \delta)}{\partial T_{ig}} \delta T_{ig} \right)^2 + \left(\frac{\partial(\rho c \delta)}{\partial T_{\infty}} \delta T_{\infty} \right)^2} \\
&= \sqrt{\left(\left(-488.4 \frac{kJ \cdot s}{m^2 K} \right) (0.000583 / s) \right)^2 + \left(\left(4.818 \frac{kJ}{m^2 K} \right) (0.09) \right)^2} \\
&\quad + \sqrt{\left(\left(4.337 \frac{s}{K} \right) \left(1 \frac{kW}{m^2} \right) \right)^2 + \left(\left(-0.01160 \frac{kJ}{m^2 K^2} \right) (10.3K) \right)^2} \\
&\quad + \sqrt{\left(\left(0.01160 \frac{kJ}{m^2 K^2} \right) (3.45K) \right)^2} \\
&\approx 4.369 \frac{kJ}{m^2 K}
\end{aligned}$$

UNCERTAINTY FOR ESTIMATED PARAMETERS USING BURNING-RATE DATA ANALYSIS

1. $\delta\Delta h_{c,eff}$

Cone test results ranging from 30 to 75 kW/m² are used to calculate the effective heat-of-combustion. Uncertainty of this value is estimated with its confidence interval using student t distribution and $\alpha = 0.05$: ± 1.8 kJ/g

2. $\delta\Delta h_g$

See Chapter 4 for detail.

The uncertainty of the slope ($=1/\Delta h_g=0.06136$ g/kJ) can be estimated through calculating 2 times the standard error of the slope of the best-fit line, which is +/- 0.01756. Therefore, the uncertainty in Δh_g is

$$\begin{aligned}\frac{d(\Delta h_g)}{d(\text{slope})} &= -\frac{1}{(\text{slope})^2} \\ &= -\frac{1}{\left(0.06136 \frac{\text{g}}{\text{kJ}}\right)^2} \\ &\approx -265.6 \frac{\text{kJ}^2}{\text{g}^2}\end{aligned}$$

Therefore,

$$\begin{aligned}\delta(\Delta h_g) &= \sqrt{\left(\frac{d(\Delta h_g)}{d(\text{slope})} \delta(\text{slope})\right)^2} \\ &= \sqrt{\left(\left(-265.6 \frac{\text{kJ}^2}{\text{g}^2}\right) (0.01756 \text{ g / kJ})\right)^2} \\ &\approx 4.7 \frac{\text{kJ}}{\text{g}}\end{aligned}$$

UNCERTAINTY SUMMARY

Table A(C)-35. Summary of model-parameter table with estimated values with uncertainty

Ignition Parameters	T_{∞}	$23 \pm 3.45 \text{ }^{\circ}\text{C}$
	T_{ig}	$397 \pm 10 \text{ }^{\circ}\text{C}$
	\dot{q}_{cr}''	$16 \pm 1 \text{ kW/m}^2$
	$\rho c \delta$	$4.333 \pm 4.369 \text{ kJ/m}^4\text{K}^2\text{s}$
Burning-Rate Parameters	$\Delta h_{c,eff}$	$25.5 \pm 1.8 \text{ kJ/g}$
	Δh_g	$16.3 \pm 4.7 \text{ kJ/g}$
	h_c	$12 \pm 0.5 \text{ W/m}^2\text{K}$
	ε	0.9 ± 0.09

Validation

Analyze Simulation Quality

DETERMINE DATA AND MODEL OUTPUT UNCERTAINTY TO MAKE COMPARISON

1. Conduct uncertainty analysis of data

The uncertainty in the mass-loss-rate data used for comparison between data and model outputs is estimated via statistical approach, taking the standard deviation (0.58 g/sm^2) from the mean of a steady burning of five identical PMMA tests conducted in a cone calorimeter.² The estimated uncertainty is 1.4 g/sm^2 , which is found by calculating the 95% confidence interval applying student t distribution with a sample size of five

The uncertainty in time-to-ignition data used for comparison is estimated via statistical approach, taking two to three identical cone calorimeter test data at heat fluxes ranging from 25 to 75 kW/m^2 of this FRP composite sheet. 95% confidence interval is calculated for each heat-flux level assuming student t distribution.

2. Conduct uncertainty analysis for MLR profile modeling

Because uncertainty information of the data is found in terms of time-to-ignition and mass-loss rate, the mass-loss-rate profile is considered as the modeling output of interest for comparison purposes. For Simple Analytical Models, time-to-ignition (t_{ig}) and steady-burning rate (\dot{m}'') are needed when simulating the mass-release-rate profile.

The uncertainty in MLR profile in modeling can be determined via considering the uncertainties in these calculation results as below:

$$t_{ig} \pm \delta t_{ig}$$

$$\dot{m}'' \pm \delta \dot{m}''$$

To determine the uncertainty in time to ignition, recall:

$$\frac{\dot{q}_{cr}''}{\dot{q}_e''} = F(t_{ig}) = \begin{cases} \frac{h_{ig} t_{ig}}{\rho c \delta} & t_{ig} \leq t^* \\ 1 & t_{ig} > t^* \end{cases}$$

Knowing that all of heat flux levels of interest, 25, 50, and 75 kW/m², are above the critical heat flux, time-to-ignition should be smaller than t*. Hence, uncertainty in t_{ig} can be estimated from linear-regression process as below:

$$\frac{\dot{q}_{cr}''}{\dot{q}_e''} = \frac{h_{ig}}{\rho c \delta} t_{ig}$$

The above equation can be re-written as below after conducting linear regression:

$$y \text{ estimate} = (\text{slope}) t_{ig}$$

Therefore,

$$t_{ig} = \frac{y \text{ estimate}}{\text{slope}}$$

Assuming that the y estimate and slope are independent and propagating the uncertainties in these two variables in estimating the time-to-ignition, the following calculation can be made:

$$\delta t_{ig} = \sqrt{\left(\frac{\partial t_{ig}}{\partial (y \text{ estimate})} \delta (y \text{ estimate}) \right)^2 + \left(\frac{\partial t_{ig}}{\partial (\text{slope})} \delta (\text{slope}) \right)^2}$$

where

$$\frac{\partial t_{ig}}{\partial (y \text{ estimate})} = \frac{1}{(\text{slope})}$$

$$\frac{\partial t_{ig}}{\partial (\text{slope})} = - \frac{(y \text{ estimate})}{(\text{slope})^2}$$

with $\delta (y \text{ estimate})$ and $\delta (\text{slope})$ estimated through calculating 2 times the standard error of the y estimate and slope of the best-fit line.

To determine the uncertainty in steady heat release rate at post ignition stage, recall:

$$\Delta h_g \equiv \frac{\dot{q}_{net}''}{\dot{m}''} = \frac{\dot{q}_e'' + \dot{q}_f'' - \dot{q}_l''}{\dot{m}''}$$

The above equation can be rearranged to

$$\dot{m}'' = \frac{1}{\Delta h_g} \dot{q}_e'' + \frac{\dot{q}_f'' - \dot{q}_l''}{\Delta h_g}$$

The steady burning rate at post-ignition stage is determined by the best-fit line obtained when data is plotted as steady-burning rate versus applied heat flux. The uncertainty in steady-burning rate can be determined by considering 2 times the standard error of the y estimates, i.e., \dot{m}'' , which is obtained through linear-regression process: $\pm 1.2 \text{ g/m}^2\text{s}$.

COMPARE DATA WITH SIMULATION RESULTS WITH CONSIDERATION OF UNCERTAINTIES

Parameters in this simple analytical pyrolysis model have been estimated with cone calorimeter test data from 25, 50, and 75 kW/m². To check the quality of the modeling using the estimated parameters, three cases have been simulated and compared with experiment data, with the consideration of their uncertainty bands as shown in Table A(C)-36 and figures below. Note the inert residue fraction, including glass layers, of approximately 60% by weight.

Table A(C)-36. Comparison of time-to-ignition at different heat-flux levels from actual experiment and pyrolysis modeling

Heat-Flux Level	Actual t_{ig} (s) $t_{ig} \pm \delta t_i$	Model t_{ig} (s) $t_{ig} \pm \delta t_i$
25 kW/m ²	112 ± 70	72 ± 7
50 kW/m ²	38 ± 3	36 ± 6
75 kW/m ²	25 ± 6	24 ± 6

All three cases show good overlap between the data and simulation of time-to-ignition and the mass-loss rate during steady burning considering the uncertainties, i.e.,

the parameter estimation was conducted successfully (see Figure A(C)-35, Figure A(C)-36 and Figure A(C)-37).

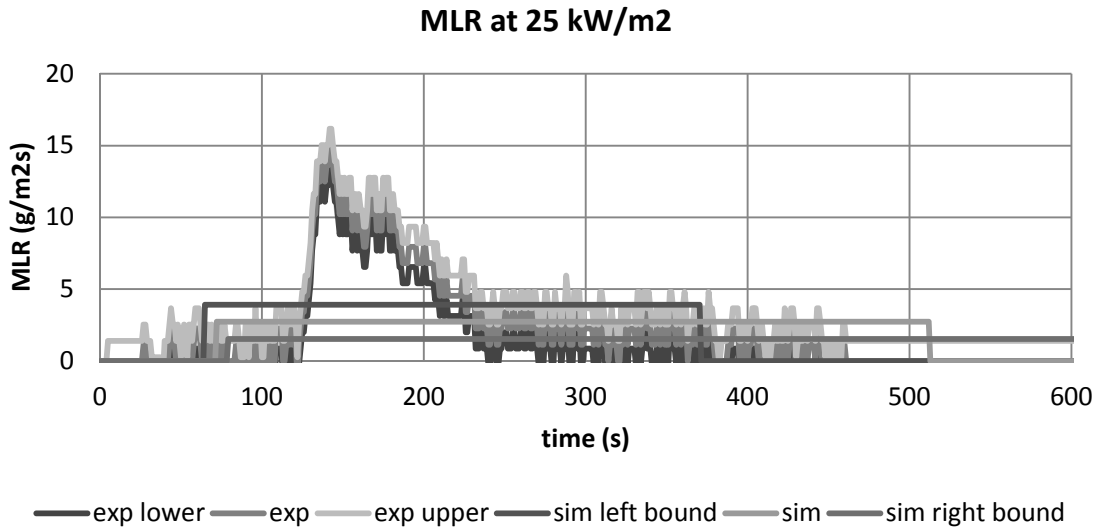


Figure A(C)-35. Mass-loss rate (MLR) comparisons for thin FRP composite sheet between actual MLR from experiment (exp) and modeled MLR (sim) at 25 kW/m². Note that data shown were used to estimate model-parameter values.

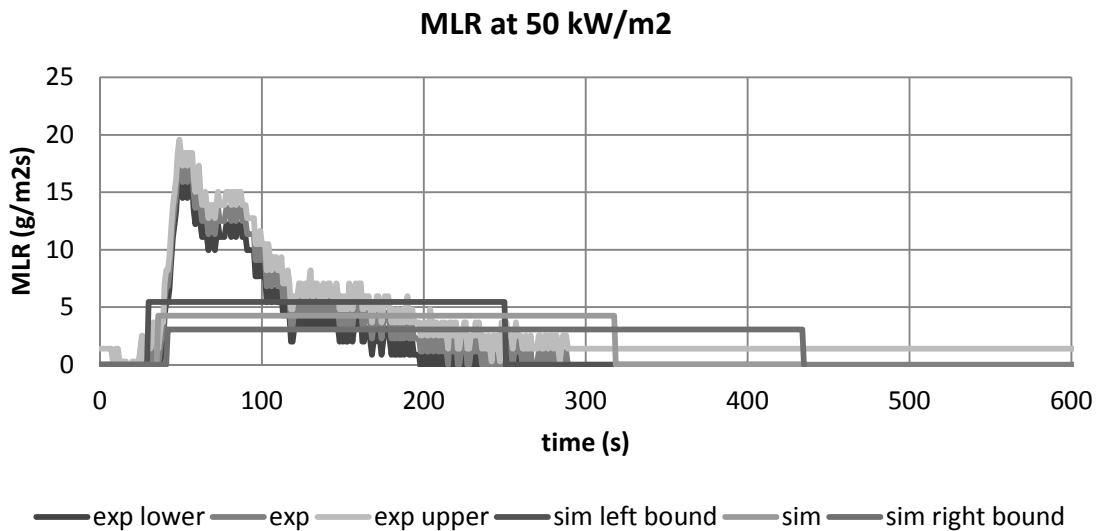


Figure A(C)-36. Mass-loss rate (MLR) comparisons for thin FRP composite sheet between actual MLR from experiment (exp) and modeled MLR (sim) at 50 kW/m². Note that data shown were used to estimate model-parameter values.

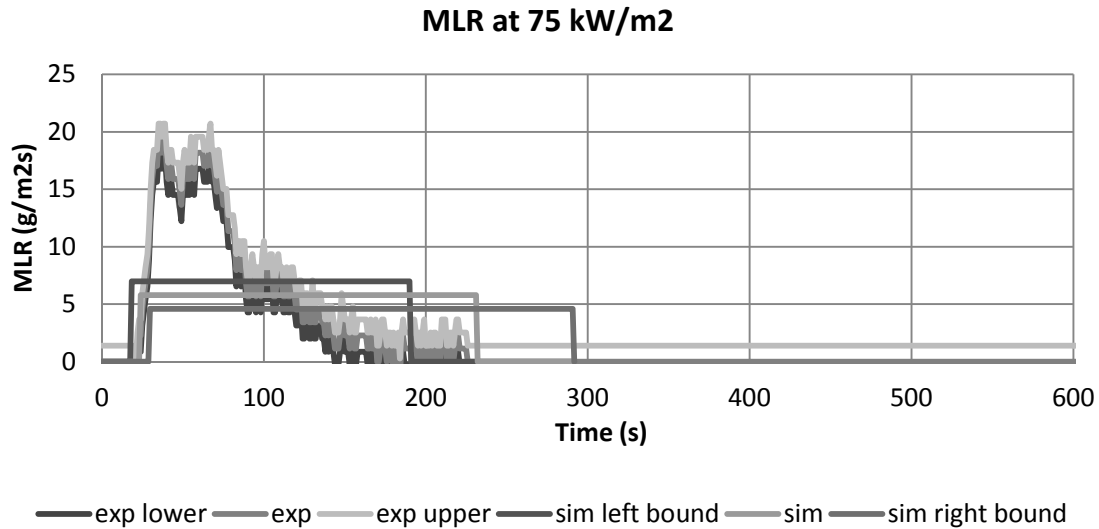


Figure A(C)-37. Mass-loss rate (MLR) comparisons for thin FRP composite sheet between actual MLR from experiment (exp) and modeled MLR (sim) at 75 kW/m². Note that data shown were used to estimate model-parameter values.

Commentary

In this example, Simple Analytical Model is used to simulate pyrolysis of thermally-thin-behaving FRP composite sheet. Test data from a bench-scale cone calorimeter experiment at several heat-flux levels have been utilized to estimate the time-to-ignition from exposure to heating and the mass-loss rate at steady burning stage after ignition. The comparison between the model outputs (time-to-ignition and steady-burning rate) and the data from bench-scale experiment showed good agreement for both checking purposes, where the same heat-flux levels (25, 50, and 75 kW/m²) used in parameter estimation have been considered. To improve modeling results, one may consider taking the peak average of the mass-loss rate and the heat-release rates to estimate heat-of-gasification, for most of the burning occurs near the peak. The tail following the peak (MLR or HRR curve) extends for a longer period of time until flameout, where a smaller percentage of the combustible resin between fiberglass layers is burning off at in-depth.

Although the modeling predictions of time-to-ignition and steady-burning rate in this example seem to be reasonable, limitation of this Simple Analytical Modeling should

be noted, which is that the model is for thermally-thin-behaving materials and steady burning after ignition.

REFERENCES

¹ Beaulieu, P.A.; and Dembsey, N.A., “Flammability Characteristics at Applied Heat Flux Levels up to 200 kW/m²”, *Fire and Materials*, 32:2 (2008) 61-86. [DOI10.1002/fam.948]

² Zhao, Lei, Bench Scale Apparatus Measurement Uncertainty and Uncertainty Effects on Measurement of Fire Characteristics of Material Systems, MS Thesis, Fire Protection Engineering, WPI, 2005-04-27, ETD-050105-182456

Appendix D - Example Solutions for Chapter 5

EXAMPLE 5.1 MODELING PMMA

An example case is shown for a poly(methylmethacrylate), PMMA. Most of the approach and reference values of the input parameters for this simulation were obtained from Stoliarov's work.¹ Note that for this example, three approaches will be used to estimate model parameters: (1) direct measurement, literature search or approximation denoted as Approach A; (2) combination of non-optimization and optimization method denoted as Approach B-GA, B-SCE or B-SHC; and (3) mostly optimization method denoted as Approach C-GA, C-SCE or C-SHC. For optimization routines, Genetic Algorithm (GA), Shuffled Complex Evolution (SCE), or Stochastic Hill-climber (SHC) is applied.

Measure Parameters

When conducting parameter estimation via independent experiments, consider the following:

- Check consistency between model used in experiment analysis and pyrolysis model
- Use statistical approach for determining uncertainty, otherwise, meet equivalency to this requirement

1. Density

Bulk density is measured by the cone calorimeter experiment conducted at room temperature ($\approx 298\text{K}$), weighing sample's mass, and dividing mass with sample volume, which was 1200 kg/m^3 .

$$\rho = 1200 \text{ kg/m}^3$$

2. Thermal Conductivity

This was measured using a Thermoflizer apparatus (SWO Polymertechnik GmbH), which is based on the transient line source method.² The author had mentioned in this work¹ that the values determined from this experiment were significantly lower than the values from the literature, which were ranging from 0.19 to 0.25 W/m-K^3 . The difference in the measurements from different laboratories was explained by the

sensitivity of the thermal conductivity to subtle variations in the polymer structure. See Figure A(D)-1 for comparison.

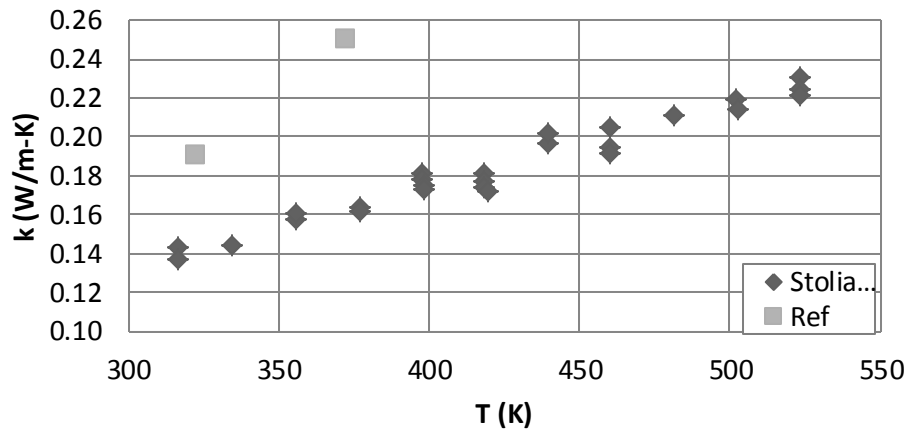


Figure A(D)-1. Thermal conductivity of PMMA

3. Specific-heat Capacity

This was measured using Differential Scanning Calorimetry (DSC). Details of this work are reported in ref⁴. From ref⁴, a figure that compares Stoliarov's measurements to other reference⁵ is reproduced (see Figure A(D)-2). In the simulation in this example, for consistency, Stoliarov's measurements will be used.

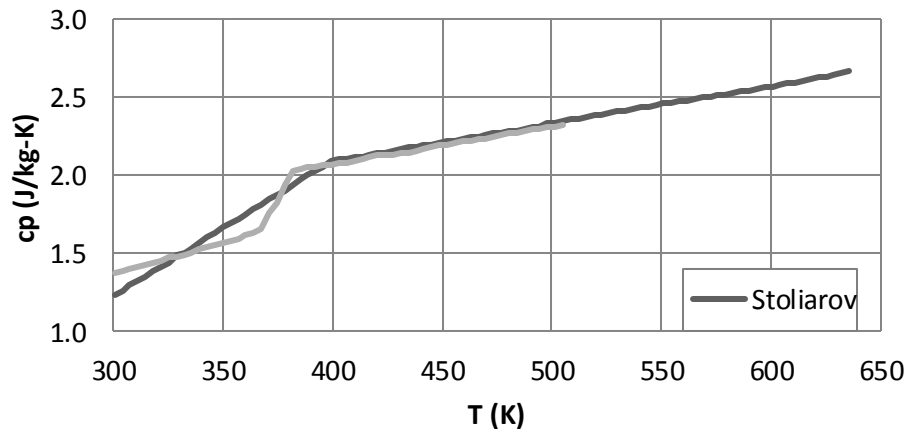


Figure A(D)-2. Heat capacity of PMMA

4. Absorption Coefficient

An expression (based on the assumption of exponential attenuation) that relates the transmissivity (τ) and absorption coefficient (α), where l is the polymer film thickness can be given as below:

$$K_s = \frac{2\ln(1 - r) - \ln\tau}{l}$$

$$\mathbf{K_s = 2700 /m}$$

5. Emissivity

To estimate emissivity of PMMA, average reflectivity was found by averaging the wavelength-dependent reflectivities measured over emissive-power distributions of a blackbody at 1000K, knowing that this temperature is the closest match to radiant-heater temperatures used in the burning-rate measurements. Emissivity of PMMA was estimated to be 1 – reflectivity.

$$\boldsymbol{\varepsilon = 0.85}$$

6. Reaction Order, Pre-exponential Factor and Activation Energy

For this example case, where decomposition kinetics type is 2 (single peak in DTG over entire mass loss temperature range), the following approach is applicable:

Conduct dynamic Thermogravimetric Analysis (TGA) experiments in nitrogen

Thermogravimetric Analysis (TGA) experiments are conducted at various heating rates – 0.05, 0.17 and 0.5 K/s – with samples sizes ranging from 2 to 5 mg. Temperature range used in the tests is from 373 to 1003 K with nitrogen as purging gas. Considering that the decomposition-reaction rate can be written as weight-loss rate measured from TGA tests, reaction rates were calculated by numerical differentiation of mass loss data as:

$$r = \frac{\Delta m / m_0}{\Delta t}$$

Conduct kinetic modeling to obtain kinetic parameters

1. Applying Arrhenius expression and assuming one-step decomposition-reaction mechanism, where virgin material decomposes to fuel vapor leaving no residue with first-order reaction-kinetic model, the reaction rate can be expressed in terms

of weight loss and temperature. Note that n value is pre-determined as 1. This expression is consistent with FDS pyrolysis model.

$$r = A \exp\left(-\frac{E}{RT_s}\right) \left(\frac{1-m}{m_0}\right)^1$$

- Plot $\ln\left(\frac{r}{\left(\frac{1-m}{m_0}\right)^1}\right)$ vs. $\frac{1}{T}$ for all data obtained from different heating-rate experiments.

Applying log to each side of the equation and rearranging it gives the following:

$$\ln\left(\frac{r}{\left(\frac{1-m}{m_0}\right)^1}\right) = \ln(A) - \frac{E}{RT}$$

Therefore, plotting LHS term versus 1/Ts allows determination of activation energy (slope) and the pre-exponential coefficient (intercept) as shown in Figure A(D)-3 (reproduced from reference¹).

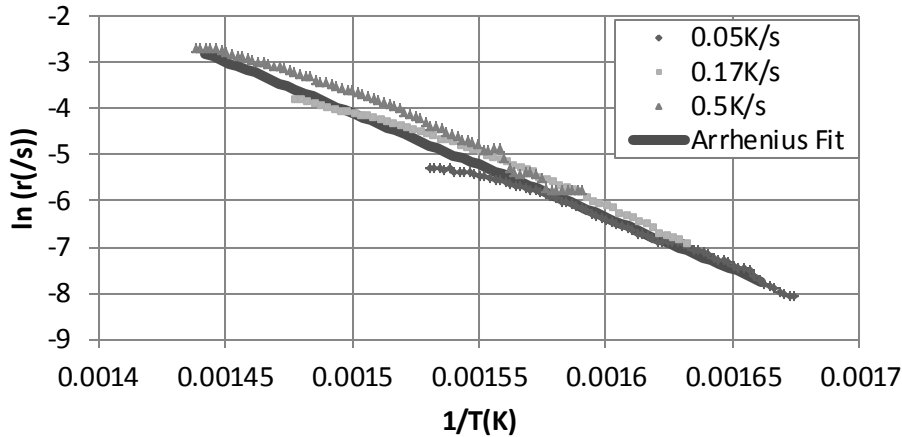


Figure A(D)-3. Kinetic modeling for decomposition of PMMA under nitrogen atmosphere: Arrhenius equation with n = 1 reaction model is used.

- According to the good fitness of the linear trendline to the overall data with different heating rates, first-order approximation utilized in this kinetic modeling seems to be appropriate. The final estimated kinetic parameter values are:

$$A = 8.5 \times 10^{12} \text{ (s)}; E = 1.88 \times 10^5 \text{ (J/mol)}$$

7. Heat of Reaction

Heat-of-decomposition reaction was measured by Stoliarov in his previous work using Differential Scanning Calorimetry (DSC) with nitrogen as purging gas.⁴ Heat is normalized by its initial sample weight.

$$\Delta H_r = 870 \text{ kJ/kg}$$

Summary

The uncertainties in the estimated properties are as follows (see Table A(D)-1) for measured values. Note that these are determined from the data scatter and expressed as ± 2 normalized standard errors. The standard errors are normalized by their mean. Exceptions are the uncertainties in emissivity and absorption coefficient, where crude estimates are given by the author due to lack of information. Note that although modeling PMMA can be done by direct mode, i.e., model parameters are estimated via direct measurements, literature search, and/or approximations, for comparison purposes two other approaches are considered in this example – using some or mostly optimization to estimate unknowns.

Table A(D)-1. Summary of estimated uncertainty for each model parameter

	No	Condense Phase ($i=1$)		Uncertainty (%)
Material Property	1	ρ_i	Density	± 5
	2	k_i	Thermal conductivity	± 15
	3	c_i	Specific-heat capacity	± 15
	4	κ_i	Absorption coefficient	± 50
Parameters for Specifying Conditions	5	ε_i	Emissivity	± 20
		Heterogeneous RxN ($k=1$)		
Kinetic Parameters and Heats assuming n^{th} order model and Arrhenius-type expression	6	n_k	Reaction order	N/A
		Z_k	Pre-exponential factor	± 50
		E_k	Activation energy	± 3
	7	ΔH_k	heat	± 15

Obtain Parameters via Numerical Optimization

Run model or Run Model in Pair with Numerical Optimization

Select model: GPYRO

Understand bench-scale experiment set-up for modeling simple cases

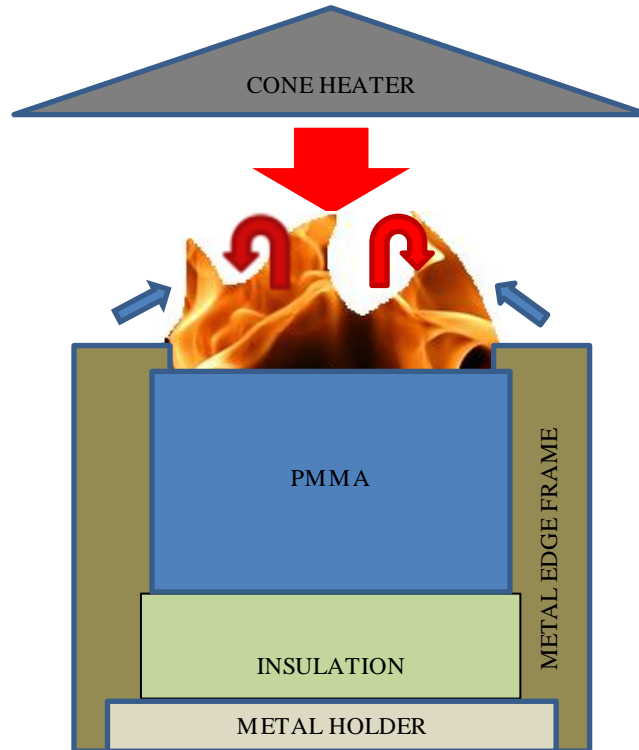


Figure A(D)-4. Simplified representation of a cone calorimeter test of PMMA

A simplified representation of a cone calorimeter test of PMMA is shown in Figure A(D)-4. The sample is placed on top of an insulation, which sits on a metal holder. Another metal frame is placed on top of the sample, insulation and the holder. A metal edge frame is used as well to allow the sample to be stationary with good contact between underlying insulation during decomposition with surface regression.

Front Surface: As heating starts by opening the shutter to allow radiation from the cone heater to heat the sample surface (large red arrow), cooling also begins via natural convection (blue arrows) and re-radiation. The surface decomposes with bubbling with respect to temperature increase occurring through heat conduction and/or in-depth radiative transport. The pyrolyzates leave through the surface until complete burn-off, because this material leaves no residue. When ignition occurs as the fuel-vapor concentration above the surface exceeds its LFL (lower flammable limit), additional heat

flux from the flame is introduced on the surface (red arrows). Regression of the sample surface with respect to consumption of PMMA in pyrolysis occurs.

Back surface: The sample is placed on top of insulation. In the experiment, an air gap of a few millimeters thickness exist between the sample and the insulation due to thermal contact. Due to the insulation, nothing leaves through the back face when 1D assumption holds for the experiment.

Configure model conditions based on understanding of experiment set-up

In the model, the phenomena discussed above are simulated as below. Basic assumptions are as follows:

- Instantaneous release of volatiles from solid to the gas phase
- Local thermal equilibrium between the solid and the volatiles
- No condensation of gaseous products
- No porosity effects

Further details can be found from the *Technical Reference*⁶ and *User's Guide*⁷ of FDS (<http://www.fire.nist.gov/fds/documentation.html>).

When conducting the FDS simulation for the cone calorimeter set-up, the metal edge frame will be ignored and backing is insulated. Gas-phase combustion will be turned off by assuming that the ambient oxygen concentration is less than 10% ($Y_{O_2} = 0$). Heat flux from the cone is set by using EXTERNAL_FLUX at the sample surface. The ignition phenomenon is interpreted as the following in the simulations: when mass-burning rate is above $10 \text{ kW/m}^2 / \Delta H_c$, (criteria based on experiment observations¹), additional heat flux of 20 kW/m^2 is added to EXTERNAL_FLUX to include the heating from the flame, assuming that the flame is transparent. This is the reference value found from the work of Beaulieu⁸, where actual measurement of the flame heat flux of a black PMMA was conducted. The heat-of-combustion was determined using a microscale combustion calorimeter⁹ operating in the following condition: pyrolysis in nitrogen atmosphere by heating samples (2 to 4 mg) at a fixed rate of 1 K/s from 373 to 1173 K. The value is normalized by initial sample weight: $\Delta H_c = 24100 \text{ kJ/kg}$

Acquire data sets that can represent burning behavior of interestⁱ or that can be used in numerical optimization process in pair with pyrolysis modeling for obtaining unknown model parameter valuesⁱⁱ

1. Maximum heat-flux level of interest for this parameter estimation is approximately 100kW/m^2 .
2. Cone calorimeter test data of thick PMMA (thickness, δ ranging from 24 ~ 29 mm) impinged with effective heat fluxes (EHF) of 23, 46, and 69 kW/m^2 is found to show the burning behavior under various heat flux levels that are less than 100 kW/m^2 . Data were reproduced from Stolarov's paper,¹ which are shown in Figure A(D)-5:

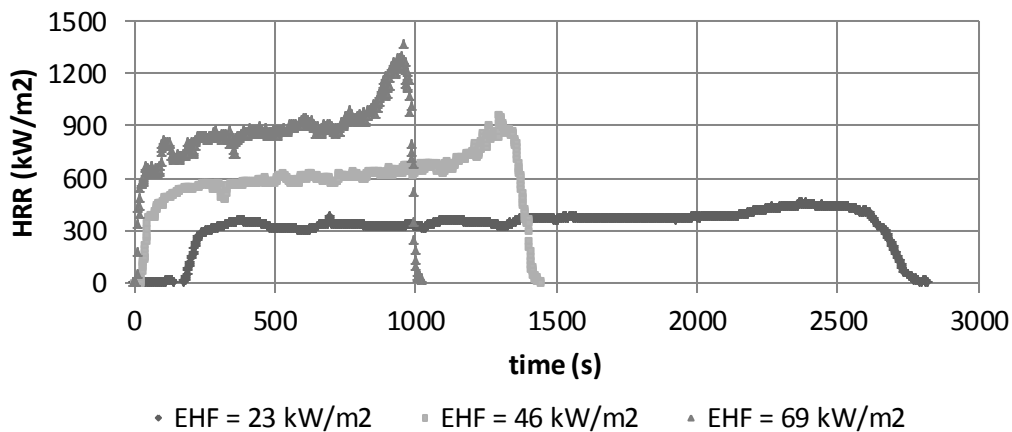


Figure A(D)-5. Cone experiment results of PMMA with effective heat flux and thickness ranging from 23 to 69 kW/m^2 and 24 to 29 mm, respectively

Select numerical optimization routine

- Genetic Algorithm (GA)
- Shuffled Complex Evolution (SCE)
- Stochastic Hill-climber (SHC)
- See Chapter 5 for more description of each optimization routine.

ⁱ The simulations are conducted in a direct mode (i.e., all input values are obtained through other sources, such as references or independent measurements); hence, no data will be used to optimize the final results. However, cone calorimeter test data will be used to make the comparison between the simulation results and experiment data.

ⁱⁱ To conduct simulations, unknown parameters need to be obtained via numerical optimization for independent measurements of those parameters are cumbersome and impossible in most cases.

Conduct simulations for these cases to compare simulation output to experiment data, or conduct numerical optimization in pair with simulations using experiment data as targets

Simulations with GPYRO for the above three cases with $\underline{\text{EHF}} = 23 \text{ kW/m}^2$, $\underline{\text{EHF}} = 46 \text{ kW/m}^2$, and $\underline{\text{EHF}} = 69 \text{ kW/m}^2$ with sample thickness, $\underline{\delta} = 26 \text{ mm}$ are conducted.

*Obtain Confidence Intervals for Optimized Parameters**

- Baseline case: $\text{HF} = 46 \text{ kW/m}^2$, thickness = 29 mm
- Sensitive parameters varied one at a time from baseline to its max and min by considering uncertainty; however, due to compensation effect, pre-exponential factor and activation energy will be considered in pair to have max and min decomposition temperature
- Uncertainty is considered for GA optimization cases (B-GA, C-GA) only using 50 near-optimal parameter sets
- Integration of uncertainty is calculated by the Law of Propagation of Uncertainty

Parameter Estimation Results

ID		A	B-GA	B-SCE	B-SHC	C-GA	C-SCE	C-SHC	
Parameter	Unit	Measurement, Literature, or Approximation	Comparable Non-optimization and Optimization			Mostly Optimization			
Thermo-physical Property	ρ_i	kg/m ³	1200 ± 60	1200 ± 60			1200 ± 60		
			Measurement	Measurement			Measurement		
	k_i	W/m-K	0.18 ± 0.01	0.30 ± 0.01	0.21	0.33	0.29 ± 0.01	0.29	0.19
			Literature ¹⁰	GA	SCE	SHC	GA	SCE	SHC
	c_i	J/kg-K	2.2 ± 0.1	1.8 ± 0.1	0.7	1.7	2.0 ± 0.1	1.1	1.7
Literature ^{4,10}			GA	SCE	SHC	GA	SCE	SHC	
Optical Property	κ_i	/m	2700 ± 1400	150000 ± 86000	1000000	3600000	2200 ± 500	790000	350000
			Literature ¹⁰	GA	SCE	SHC	GA	SCE	SHC
	ε_i	-	0.85 ± 0.16	0.91 ± 0.01	0.66	0.89	0.66 ± 0.01	0.99	0.54
			Literature ¹	GA	SCE	SHC	GA	SCE	SHC
Thermal Decomposition Kinetics and Heats	n_k	-	1	1			0.5 ± 0.1	0.5	1.5
			Approximated	Approximated			GA	SCE	SHC
	Z_k	/s	(8.5 ± 4.3) x 10 ¹²	(8.5 ± 4.3) x 10 ¹²			(1.3 ± 0.6) x 10 ¹⁶	3.3 x 10 ¹⁵	5.3 x 10 ¹⁹
			Model Fitting with multiple heating rate TGA data	Model Fitting with multiple heating-rate TGA data			GA	SCE	SHC
	E_k	J/mol	(1.88 ± 0.06) x 10 ⁵	(1.88 ± 0.06) x 10 ⁵			(1.77 ± 0.01) x 10 ⁵	2.27 x 10 ⁵	2.43 x 10 ⁵
			Model Fitting with multiple heating rate TGA data	Model Fitting with multiple heating-rate TGA data			GA	SCE	SHC
	ΔH_k	kJ/kg	870 ± 130	870 ± 130			1100 ± 21	1300	520
			Literature ⁴	Literature ⁴			GA	SCE	SHC
Model Dependent Parameter	h_{crz}	W/m ² -K	0	12 ± 3	2	14	38 ± 4	3	-32
			Approximated adiabatic condition at back surface	GA	SCE	SHC	GA	SCE	SHC

Validation

Analyze Simulation Quality

Identify sensitive parameters for model inputs

- $\varepsilon_i, n_k, Z_k, E_k, \Delta H_k$
- See Chapter 5 for detail

Determine data and model output uncertainty

1. Check data reproducibility by repeating identical experimentsⁱⁱⁱ

Data is acquired from five repeating PMMA tests under 49 kW/m² heat-flux level with medium-thickness samples (thickness, δ ranging from 7.7 ~ 9.4 mm).

2. Conduct uncertainty analysis of data

Uncertainty in PMMA cone calorimeter experiment is estimated based on five repeating PMMA tests under 49 kW/m² heat-flux level with medium-thickness samples (thickness, δ ranging from 7.7 ~ 9.4 mm). The surface temperatures measured from these tests showed that the values ranged from 260 to 370°C. The uncertainty of peak HRR, average HRR, time-to-ignition, and time-to peak HRR are estimated by the five repeating PMMA tests via, taking two standard deviation of the difference and normalizing them by the mean of this parameter. Table A(D)-2 shows the analysis results from the tests, which were reproduced from Stolarov's paper.¹ Assume that the uncertainty values estimated for five repeating PMMA tests conducted at 49 kW/m² heat flux level with medium-thickness samples are comparable to those of tests conducted under various heating rates, ranging from 23 to 69 kW/m² using thick PMMA samples.

ⁱⁱⁱ In general, data uncertainty is used to analyze the sensitivity of the input parameters; in numerical optimization to estimate unknown parameters; or to evaluate simulation quality later in the process. In this example, data uncertainty will be accounted for here, where simulation results with its uncertainty band are compared with data with its uncertainty band.

Table A(D)-2. Summary of estimated uncertainty in PMMA cone calorimeter experiments based on 5 repeating tests under 49 kW/m² heat-flux level with medium-thickness sample (7.7 ~ 9.4 mm)

	peakHRR (kW/m ²)	avgHRR (kW/m ²)	t _{ig} (s)	t-peakHRR (s)
Average case	990	560	44	430
Uncertainty (%)	17	7	12	17

3. Conduct uncertainty analysis of model outputs of interest

The baseline case was selected at simulation with EHF = 46 kW/m², thickness = 26 mm. Sensitive parameters – ε_i , n_k , Z_k , E_k , ΔH_k – are varied in the simulations one at a time from baseline case.

- The effect of variation is calculated by considering the peak HRR (peakHRR), average HRR (avgHRR), time to peak HRR (t-peakHRR), and surface temperature (T_s). Results are shown in Table A(D)-3.
- Uncertainty for those modeling outputs is calculated using the Law of Propagation of Uncertainty. Note that when inputs are varied to its uncertainty boundary values – minimum or maximum – the maximum effect was selected in the analysis to estimate the maximum uncertainty.

Table A(D)-3. Comparison between experiment data from cone calorimeter test and modeling outputs using estimated parameter values via either direct measurement, literature search, or approximation (a); measurements and numerical optimization (B-GA, B-SCE, B-SHC); or mostly numerical optimization (C-GA, C-SCE, C-SHC)

	Data	A	B-GA	B-SCE	B-SHC	C-GA	C-SCE	C-SHC
Peak MLR (g/m ² s)	36.9 ±6.3	45.1 ±10.6	40.9 ±5.3	32.6	39.3	27.5 ±0.7	34.4	67.0
Avg MLR (g/m ² s)	24.9 ±1.7	24.2 ±5.2	26.7 ±2.7	25.9	26.6	24.0 ±0.5	26.4	28.0
t to pMLR (s)	1310 ±223	1408 ±252	1285 ±123	1317	1284	1391 ±32	1297	1233
T _s (°c)	350 ±50	413 ±21	433 ±20	407	409	244 ±3	419	343

Compare data with simulation results

1. TG / DTG Predictions at 10 °C/min Heating Rate Using Estimated Kinetic Parameters

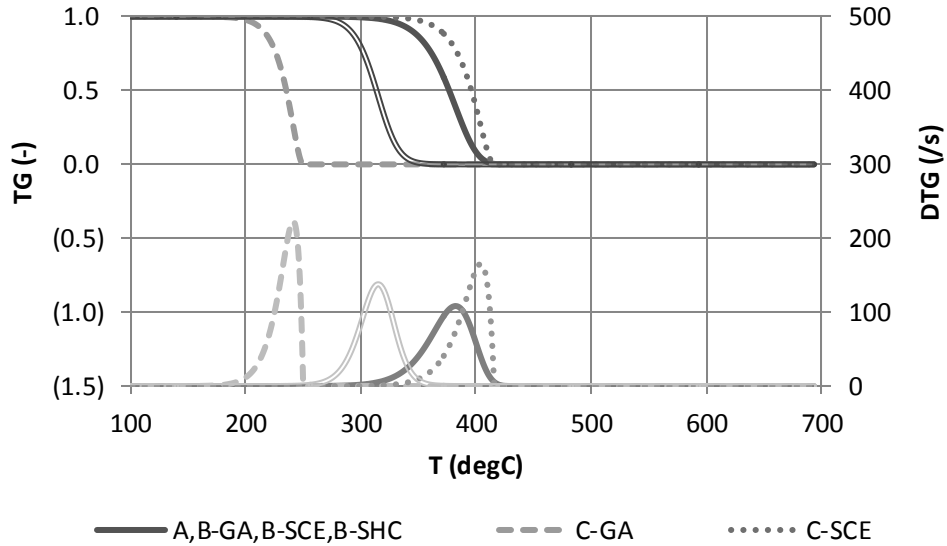


Figure A(D)-6. TG/DTG curves at 10°C/min heating rate with different estimation results for kinetic parameters for thermal decomposition of PMMA

2. Modeling Output: Mass-Loss Rate (MLR)

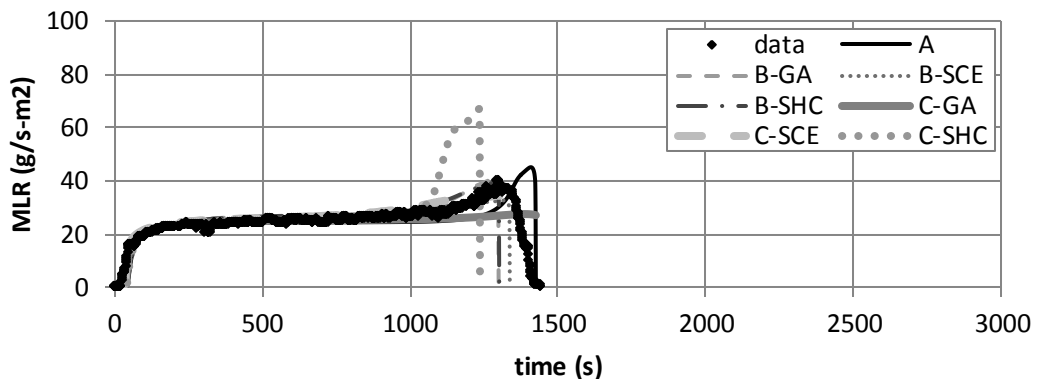


Figure A(D)-7. Mass-loss rate (MLR) comparisons for PMMA between actual MLR from experiment (data) and modeled MLR (A, B-GA, B-SCE, B-SHC, C-GA, C-SCE, C-SHC) at applied heat flux of 46 kW/m². Note that data shown were used to estimate model parameter values via numerical optimization using GA, SCE, or SHC routines.

3. Modeling Output: Surface Temperature (T_{surf})

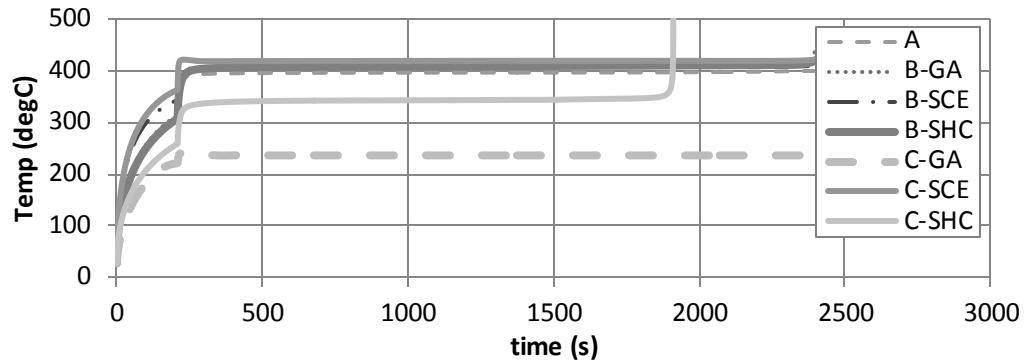


Figure A(D)-8. Surface temperature (T_{surf}) comparisons for PMMA modeling using parameters estimated from different approaches – direct measurement, literature search, or approximation (A); measurement and numerical optimization (B-GA, B-SCE, B-SHC); mostly numerical optimization (C-GA, C-SCE, C-SHC) at applied heat flux of 46 kW/m^2 . Note that data shown were used to estimate model-parameter values via numerical optimization using GA, SCE, or SHC routines.

Validate simulation quality upon extrapolation

1. Modeling Output: Mass Loss Rate (MLR)

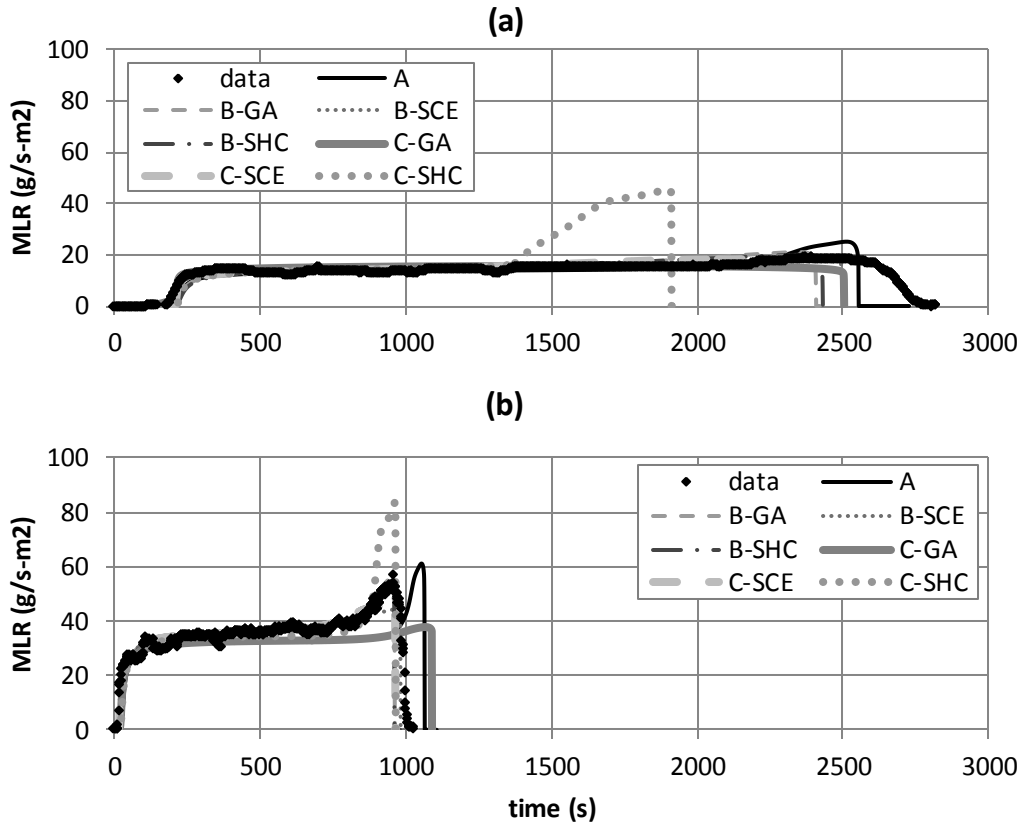


Figure A(D)-9. Mass-loss rate (MLR) comparisons for PMMA between actual MLR from experiment (data) and modeled MLR (A, B-GA, B-SCE, B-SHC, C-GA, C-SCE, C-SHC) at applied heat flux of (a) 23 and (b) 64 kW/m². Note that data shown were not included in the model-parameter-estimation process; hence, these two cases are considered as extrapolation cases.

2. Modeling Output: Surface Temperature (T_{surf})

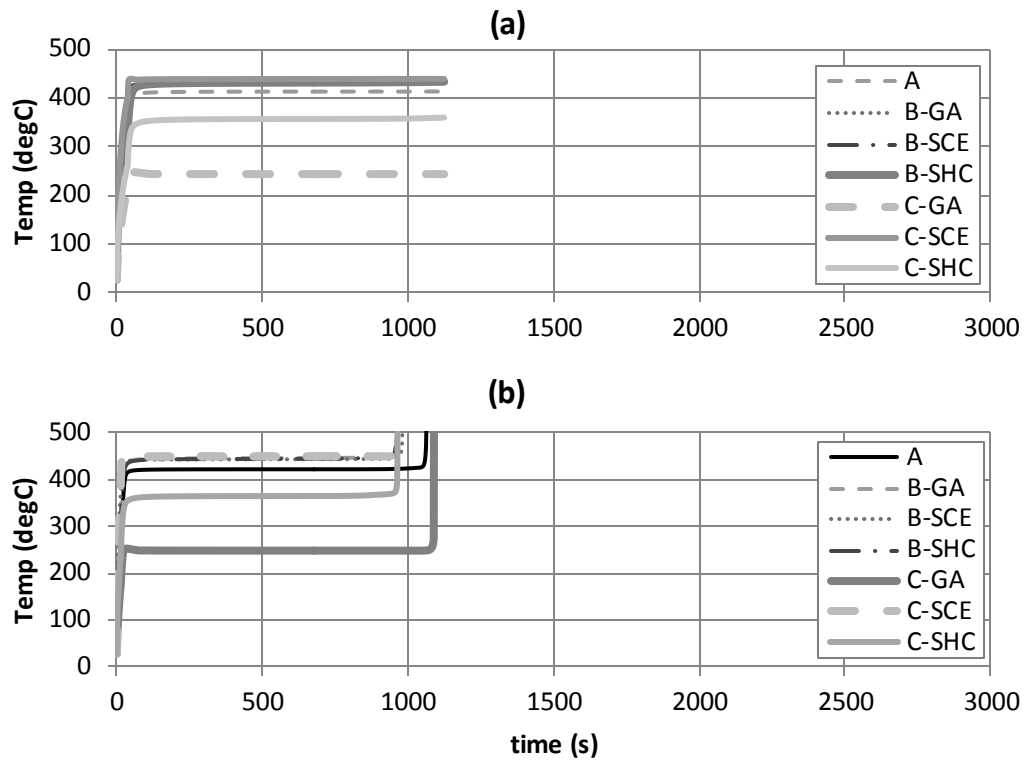


Figure A(D)-10. Surface temperature (T_{surf}) comparisons for PMMA modeling using parameters estimated from different approaches – direct measurement, literature search, or approximation (A); measurement and numerical optimization (B-GA, B-SCE, B-SHC); mostly numerical optimization (C-GA, C-SCE, C-SHC) at applied heat flux of (a) 23 and (b) 64 kW/m^2 . Note that data shown were not included in the model-parameter-estimation process; hence, these two cases are considered as extrapolation cases.

Commentary

General Comments

- TG/DTG
 - Whether kinetic modeling is conducted independently using TGA data (A, B-GA, B-BSE, B-SHC) or as a part of numerical optimization (C-GA, C-SCE, C-SHC), decomposition of PMMA is considered to occur within the temperature range of 200°C to 400°C.
 - Among GA, SCE, and SHC, estimation of SCE was closest, followed by SHC and GA to TGA data.
 - Having surface-temperature data as additional optimization target should have provided constraints to the optimization problem, for kinetic parameters directly determine the surface temperature. However, this approach was not utilized, for uncertainty in surface-temperature measurements was too high – $350 \pm 50^\circ\text{C}$
- Comparison between Data and Computed Modeling Outputs
 - Better agreement between data and modeling outputs for the peak MLR is found when kinetic parameters are estimated through a separate process using TGA data (A, B-GA, B-BSE, B-SHC) than numerical optimization along with estimating other unknowns together (C-GA, C-SCE, C-SHC).
 - Avg MLR and time to peak MLR from all modeling cases show good agreement with data.
 - Simulated surface temperature at steady burning of PMMA is greater (less than 10 s) than that of measurement for cases B-GA, B-SCE, B-SHC, and C-SCE, while simulated surface temperature is lower (greater than 50 s) than that of measurement for case C-GA. Results from cases A and C-SHC are in good agreement.

- MLR
 - Direct Measurement or Optimization at $HF = 46 \text{ kW/m}^2$: Good agreement exists between experiment data and all modeling results, whether modeled with measured parameters or optimized in the time frame of exposure to heating source up to steady burning. However, in the later time, where the peak occurs, result from C-SHC becomes unsatisfying, considering the data with its uncertainty, while others can be considered as satisfying.
 - Direct Measurement or Extrapolation at $HF = 23 \text{ kW/m}^2$: Good agreement exists between experiment data and all modeling results, except for the C-SHC case.
 - Direct Measurement or Extrapolation at $HF = 64 \text{ kW/m}^2$: Good agreement exists between experiment data and all modeling results, except for C-GA and C-SHC cases.

- Surface Temperature
 - See above.

Limitation in Modeling

- When considering limitation of the parameters in simulating PMMA, the modeler should take into account the applicability of the parameters and their associated uncertainties. For example, any assumptions used when determining a parameter value via experiment direct or indirect measurements can be utilized to understand when the parameter value becomes inappropriate. For this example of pyrolysis modeling of PMMA, most consideration can be given to the parameters related to decomposition kinetics.

- In this example, kinetic modeling for this example was conducted with TGA data obtained from a nitrogen environment. However, studies^{8,11,12} have suggested that PMMA decomposes differently with respect to heating rates and availability of oxygen. The decomposition rate of PMMA increases with respect to oxygen concentration, because oxygen aids unzipping of the polymer by being involved in the depolymerization process of the polymer. Also, the oxygen dependency increases at lower heating rates than at higher heating rates. A possible explanation for this can be given by considering the diffusion of oxygen from the nearby gas phase to the condense phase. At lower

heating rates, the decomposition rate is relatively slow; therefore, the time allowed for oxygen to diffuse to the polymer layer and be involved in the decomposition process is relatively longer. However, at higher heating rates, the decomposition rate is relatively higher even without the involvement of oxygen in the decomposition process. This results in shorter time scale for transportation of oxygen via diffusion to the condense phase. In other words, the positive effect of enhancing decomposition by having oxygen involved in the process, compared to decomposition in non-oxidative condition, is compensated by the time necessary for oxygen diffusion to occur from the gas phase to the condense phase. Hence, the increase in decomposition rate of PMMA due to the presence of oxygen in the gas phase is more profound in conditions with lower heating rates than in higher heating rates. Visual observations of the surface phenomena during PMMA decomposition also provide evidence that the above explanation is reasonable. Based on experimental work conducted by Beaulieu,⁸ during decomposition of PMMA, “bubbling” occurs on the surface. The bubbles are relatively large, forming a thick layer of bubbles when irradiated at lower heat-flux levels; and they are smaller, forming a thin bubbling layer, when irradiated at higher heat-flux levels. Considering that bubbling is an effective way for the polymer to enhance oxygen diffusion and larger bubbles entrains more oxygen, reduction in the decomposition rate due to the increasing time necessary for oxygen diffusion at higher heat-flux levels seems plausible with bubbles becoming smaller as increasing from a lower heat flux to a higher heat flux.

- Figure A(D)-11 is TGA a thermogram of PMMA decomposition conducted under constant heating rates – 2, 5, 10, and 20 K/min – and two different environments – nitrogen and air (data obtained from work conducted by Matala¹³). As shown below and discussed earlier, there is significant difference between the curves produced from nitrogen and air tests. This indicates that decomposition kinetics are different in the two cases, and the difference is due to oxygen diffusion from the gas phase surrounding the solid sample surface with respect to the “bubbling” phenomenon.

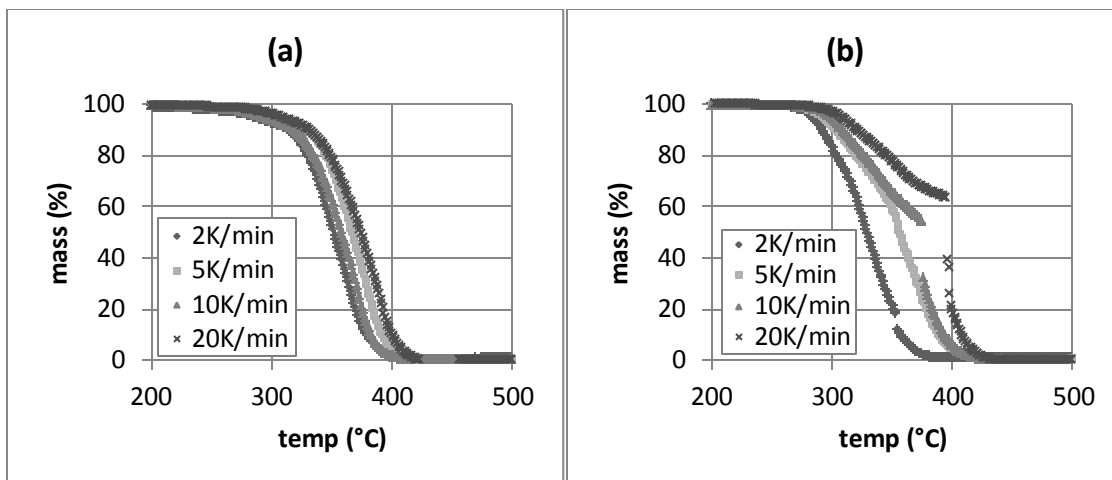


Figure A(D)-11. TGA thermograms of PMMA decomposition conducted under constant heating rates – 2, 5, 10 and 20K/min – and two different environments – (a) nitrogen and (b) air

EXAMPLE 5.2 MODELING CORRUGATED CARDBOARD

An example case is shown for triple-layered corrugated cardboard. Most of the approach and reference values of the input parameters for this simulation were obtained from Chaos' work.^{14,15} Note that for this example, two approaches will be used to estimate model parameters – (1) combination of non-optimization and optimization method denoted as Approach B-GA, B-SCE or B-SHC; and (2) mostly optimization method denoted as Approach C-GA, C-SCE or C-SHC. For optimization routines, Genetic Algorithm (GA), Shuffled Complex Evolution (SCE), or Stochastic Hill-climber (SHC) is applied.

Measure Parameters

When conducting parameter estimation via independent experiments, consider the followings:

- Check consistency between model used in experiment analysis to determine parameter in measurement process and pyrolysis model to mathematically describe the parameter of interest.
- Use statistical approach for determining uncertainty, otherwise meet equivalency to this requirement.

1. *Density*

Although corrugated cardboard is porous and the cross-section is not homogeneous, it is considered a homogeneous single-layer material with relatively low bulk density to account for its porous nature. Bulk density of the virgin fuel material is measured by experiment conducted at room temperature ($\approx 298\text{K}$), weighing sample's mass and dividing mass with sample volume, which is 110 kg/m^3 for this type of corrugated cardboard.

$$\rho = 110 \text{ kg/m}^3$$

2. *Thermal Conductivity*

Not measured; will be obtained via numerical optimization.

3. *Specific-heat Capacity*

Not measured; will be obtained via numerical optimization.

4. Absorption Coefficient

Both virgin fuel and residue solid-phase materials involved in modeling are considered as an opaque material. Therefore, the absorption coefficient is essentially infinity.

$$K_{\text{fuel}} \text{ and } K_{\text{residue}} \rightarrow \infty$$

5. Emissivity

Not measured; will be obtained via numerical optimization.

6. Reaction Order, Pre-exponential Factor and Activation Energy

This example case is determined to have decomposition kinetics type 2 (single peak in DTG over entire mass-loss temperature range) according to TGA experiment conducted in nitrogen atmosphere (see Figure A(D)-12). Based on this information, kinetic parameters will be obtained via a model fitting method using single heating rate TGA data or numerical optimization. Actual TGA data of a generic corrugated cardboard tested in nitrogen environment is shown below. There is less than 10% of moisture loss near 100°C, which has been excluded from the thermogram to only account for the major DTG peak occurring after 200°C. Therefore, kinetic modeling is conducted for a dry-state corrugated cardboard.

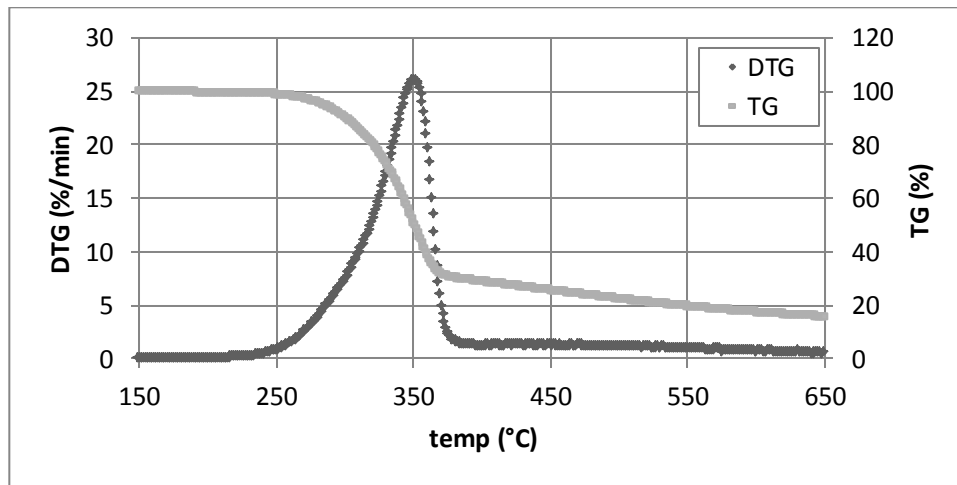


Figure A(D)-12. TGA thermogram (TG and DTG) of corrugated cardboard decomposition conducted under 20K/min heating rate and nitrogen environment

7. Heat of Reaction

Not measured; will be obtained via numerical optimization.

Summary

Among seven categories of parameters, only two have been obtained via direct measurement – fuel virgin bulk density and absorption coefficients of fuel and residue, which are shaded in the table below (see Table A(D)-4). The rest of the unknown parameters, **total of 11 parameters**, should be obtained via numerical optimization in pair with pyrolysis modeling using bench-scale experiment data or equivalent.

Table A(D)-4. Summary of necessary model parameters for simulating pyrolysis of corrugated cardboard

	No	Condense Phase	
		<i>(i=1, fuel)</i>	<i>(i=2, residue)</i>
Material Property	1	ρ_1	ρ_2
	2	k_1	k_2
	3	c_1	c_2
	4	κ_1	κ_2
Parameters for Specifying Conditions	5	ε_1	ε_2
Heterogeneous RxN (<i>k=1</i>)			
Kinetic Parameters and Heats assuming n^{th} order model and Arrhenius-type expression	6	n_1	
		Z_1	
		E_1	
	7	ΔH_1	

Obtain Parameters via Numerical Optimization

Run Model in Pair with Numerical Optimization

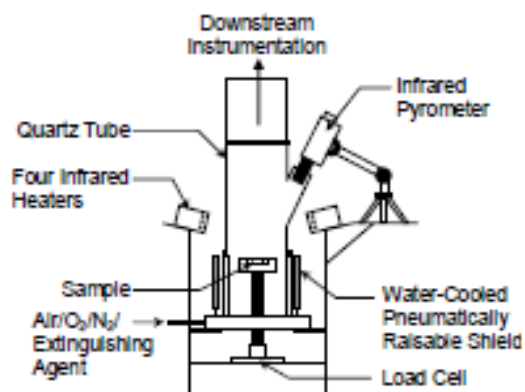


Figure A(D)-13. Schematic of the FPA

Select model: Simplified 1D model based on GPYRO

Understand bench-scale experiment set-up for modeling simple cases: Description reproduced from Chaos' paper¹

A schematic of the FPA used in this study is shown in Figure A(D)-13. The present apparatus differs from that described in the ASTM standard¹⁶ in that high-power high-density infrared heaters (Research Inc., Model 5209) are used, which can yield heat fluxes approaching 120 kW/m^2 . In addition, a humidity control and delivery system¹⁷ can control the relative humidity of the gas supply to the FPA. A flow of 100 SLM of pure nitrogen was used for all experiments (i.e., pyrolytic conditions). In the experiments, insulated circular samples¹⁸ 9.6 cm in diameter were placed on a load cell (0-1000 g range, 0.1 g accuracy, 20 mg peak-to-peak noise), which provided a continuous record of their weight during the pyrolysis process. A water-cooled shield was used to protect the sample from exposure while the heaters stabilized at a specific heat-flux setting. A quartz tube (162 mm inner diameter) shielded the sample and gasification products from room-air entrainment. An infrared pyrometer (Heitronics KT19.81-11) was used to measure surface temperature. The wavelength range of the pyrometer is 8-10 μm , which required modification of the quartz tube used, as quartz is not transparent at these wavelengths. The pyrolysis tests performed in this study cover a heat-flux range of 20-110 kW/m^2 . This ensures that both thermally thin and thick regimes are treated so

that properties determined with the present approach can be applicable to practical fire conditions.

Configure model conditions based on understanding of experiment set-up

Basic assumptions are as follows:

- Instantaneous release of volatiles from solid to the gas phase
- Local thermal equilibrium between the solid and the volatiles
- No condensation of gaseous products
- No porosity effects

Further details can be found from Reference 15.

When conducting the 1D simulation for the FPA set-up, insulation at back surface is not modeled explicitly, but is included as some heat loss to the back surface. In this example case, only FPA experiment with nitrogen as purge gas will be considered; hence, there is no ignition phenomenon to be modeled.

Acquire data sets that can be used in numerical optimization process in pair with pyrolysis modeling for obtaining unknown model parameter values^{iv}

1. The maximum heat-flux level of interest for this parameter estimation is 20 to 110kW/m², considering that estimated parameters will be used in modeling of parallel panel experiment of corrugated cardboard. Fire Propagation Apparatus (FPA) test data of triple-wall corrugated cardboard, i.e., two layers of corrugated cardboard (thickness, δ is 30 mm) impinged with effective heat fluxes (EHF) of 20 to 110 kW/m² is found as shown in Figure A(D)-14. Data were reproduced from Chaos' paper,¹ which are shown below for 20, 60, and 110 kW/m² cases for mass-loss rate (MLR) and surface temperature measurements:

^{iv}To conduct simulations, unknown parameters need to be obtained via numerical optimization, for independent measurements of those parameters are cumbersome and impossible in most cases.

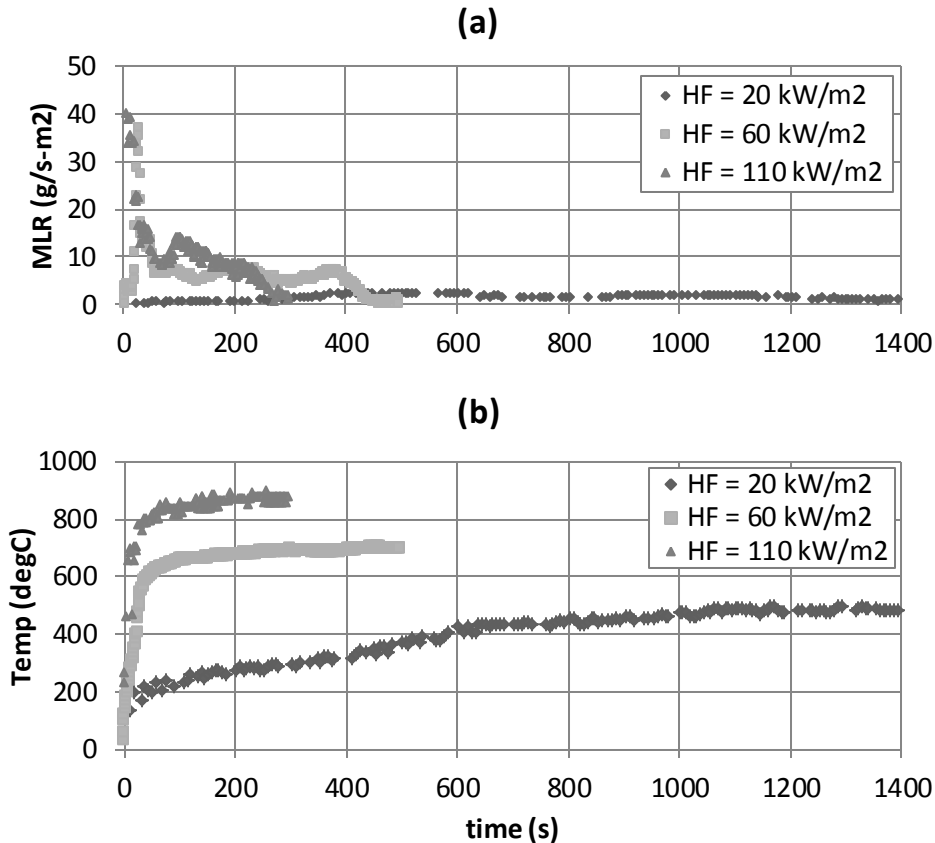


Figure A(D)-14. FPA experiment results of corrugated cardboard with applied heat flux ranging from 20 to 110 kW/m²: (a) Mass-loss rate and (b) surface-temperature measurements using pyrometer

2. Check data reproducibility by repeating identical experiments

Data is acquired from two repeating FPA tests of triple-wall corrugated cardboard under 60 kW/m² heat-flux level with nitrogen atmosphere. Uncertainty analysis will be performed later.

Select numerical optimization routine

- Genetic Algorithm (GA)
- Shuffled Complex Evolution (SCE)
- Stochastic Hill-climber (SHC)
- See Chapter 5 for more description of each optimization routine.

Conduct numerical optimization in pair with simulations using experiment data as targets

Numerous simulations with a simplified version of GPYRO have been used in pair with SCE algorithm to conduct numerical optimization to obtain unknown parameters. Experiment data of mass-loss rate (MLR), cumulative mass loss (CML), and surface-temperature measurements (T_s) generated with various applied heat-flux levels between 20 and 110 kW/m² have been used in the optimization process as targets (i.e., optimization is conducted for unknown parameters to match modeling outputs of interest to certain experiment data).

*Obtain Confidence Intervals for Optimized Parameters**

*Description reproduced from Chaos' paper.¹

As part of the optimization procedure, confidence intervals (CI) were estimated for the material properties obtained. In the literature, optimization results are often reported with no CI estimates due to complexity and problem nonlinearity. This is especially the case for results obtained using evolutionary algorithms, as they lack information available through gradient-optimization methods. In this study, CIs were evaluated using asymptotic methods.¹⁹ These are conceptually appealing and easy to implement, although they may be a poor representation of the actual CIs for highly nonlinear problems. Nevertheless, the computed CIs are useful indications of the reliability of the optimized parameters. Confidence intervals were computed **locally**, that is, at the optimum point found by the optimization scheme. At this optimum point, the standard error of the parameter estimates is approximated by a variance-covariance matrix based on the Jacobian of the model response. This matrix is then used along with the t-distribution at some desired confidence level to derive the CI. The set of equations shown below summarizes this approach:

$$\text{COV} = \frac{\|f(\hat{\mathbf{p}})\|_2^2}{n_d - n_p} (\mathbf{J}^T \mathbf{J})^{-1}; f(\hat{\mathbf{p}}) = y_{\text{exp}_i} - y_{\text{mod}_i}(\hat{\mathbf{p}}); i=1, \dots, n_d$$

$$J = \begin{bmatrix} \left. \frac{\partial y_{\text{mod}1}(\mathbf{p})}{\partial p_1} \right|_{\hat{\mathbf{p}}} & \dots & \left. \frac{\partial y_{\text{mod}1}(\mathbf{p})}{\partial p_{n_p}} \right|_{\hat{\mathbf{p}}} \\ \vdots & \ddots & \vdots \\ \left. \frac{\partial y_{\text{mod}n_d}(\mathbf{p})}{\partial p_1} \right|_{\hat{\mathbf{p}}} & \dots & \left. \frac{\partial y_{\text{mod}n_d}(\mathbf{p})}{\partial p_{n_p}} \right|_{\hat{\mathbf{p}}} \end{bmatrix}$$

$$\hat{\mathbf{p}} = \hat{\mathbf{p}} \pm t^{-1}(CL; n_d - n_p) \sqrt{\text{diag}[\mathbf{COV}]}$$

Where $\hat{\mathbf{p}}$ is the optimum parameter vector (i.e., set of material properties), n_d is the number of data points used for optimization, n_p is the number of parameters (i.e., material properties), \mathbf{COV} and \mathbf{J} are the covariance and Jacobian matrices, respectively, \mathbf{f} is the vector of differences between model results (y_{mod}) and experimental data (y_{exp}), and t^{-1} is the value of the inverse t-distribution at a given confidence level (CL) and degrees of freedom ($n_d - n_p$). The availability of the Jacobian matrix further allows for the computation of the sensitivity of model responses to changes in input parameters (see Table A(D)-5).

Table A(D)-5. Summary of estimated optimum with confidence interval (CI) for each model parameter

	No	Condense Phase			
		<i>i=1 fuel</i>	Optimum ± C.I.	<i>i=2 residue</i>	Optimum ± C.I.
Material Property	1	ρ_1	110 kg/m ³	ρ_2	10.0 ± 6.9 kg/m ³
	2	k_1	0.65 ± 0.15 W/m ² -K	k_2	0.27 ± 0.14 W/m ² -K
	3	c_1	500 ± 40 J/kg-K	c_2	1750 ± 1240 J/kg-K
	4	κ_1	∞	κ_2	∞
Parameters for Specifying Conditions	5	ε_1	0.29 ± 0.02	ε_2	0.98 ± 0.13
		Heterogeneous RxN (<i>k=1</i>)		Optimum ± C.I.	
Kinetic Parameters and Heats Assuming n^{th} order model and Arrhenius-type expression	6		n_1		6.51 ± 2.9
			$\log(Z_1)$		19.1 ± 7.9 Log(/s)
			E_1		242 ± 72 kJ/mol
	7		$\log(\Delta H_1)$		5.95 ± 0.36 Log(J/kg)

Parameter Estimation Results

ID		B-GA	B-SCE	B-SHC	C-GA	C-SCE	C-SHC		
Parameter		Unit	Comparable Non-optimization and Optimization			Mostly Optimization			
Thermo-physical Property	i = 1 (fuel)	ρ_i	kg/m ³	110			110		
				Measurement			Measurement		
		k_i	W/m-K	0.08 ± 0.01			0.13	0.21	0.21
				Measurement			GA	SCE	SHC
		c_i	J/kg-K	2.8	2.3	0.6	2.0	2.4	1.7
				GA	SCE	SHC	GA	SCE	SHC
	i = 2 (residue)	ρ_i	kg/m ³	25	20	11	26	10	43
				GA	SCE	SHC	GA	SCE	SHC
		k_i	W/m-K	0.29	0.32	0.32	0.20	0.35	0.20
				GA	SCE	SHC	GA	SCE	SHC
c_i	J/kg-K	1.5	1.1	0.2	1.0	0.8	2.2		
		GA	SCE	SHC	GA	SCE	SHC		
Optical Property	i = 1 (fuel)	κ_i	/m	10 ⁶			10 ⁶		
				Approximated as opaque			Approximated as opaque		
		ε_i	-	0.88 ± 0.01			0.72	0.50	0.65
	Measurement			GA	SCE	SHC			
	i = 2 (residue)	κ_i	/m	10 ⁶			10 ⁶		
				Approximated as opaque			Approximated as opaque		
ε_i		-	1			0.82	0.93	0.96	
	Approximated			GA	SCE	SHC			
Thermal-Decomposition Kinetics and Heats	n_k	-	1			3.7	3.0	2.2	
			Approximated			GA	SCE	SHC	
	Z_k	/s	1.1 x 10 ²¹			3.9 x 10 ⁶	9.8 x 10 ¹⁹	6.0 x 10 ¹⁴	
			Model Fitting with single-heating-rate TGA data			GA	SCE	SHC	
	E_k	J/mol	2.49 x 10 ⁵			7.0 x 10 ⁴	2.47 x 10 ⁵	3.02 x 10 ⁵	
			Model Fitting with single-heating-rate TGA data			GA	SCE	SHC	
	ΔH_k	kJ/kg	123	512	809	88	54	0.7	
GA			SCE	SHC	GA	SCE	SHC		
Model-Dependent Parameter	h_{crz}	W/m ² -K	19	8	14	10	8	10	
			GA	SCE	SHC	GA	SCE	SHC	
	$n_{kz}(i=1)$	-	5.6	4.6	7.6	0			
GA			SCE	SHC	Approximated				

Validation

Analyze Simulation Quality

Identify sensitive parameters for model inputs

For this case, total of 14 parameters are necessary due to the single-step thermal-decomposition kinetic modeling applied in this problem. Therefore, extensive sensitivity analysis is not necessary to determine sensitive parameters on model output of interest. However, there by Stoliarov²⁰ and Chaos²¹ is conducted for similar cases on considering the effect of variation in material properties on the rate of burning. According to these works, it was recognized that the knowledge of parameters related to emissivity of virgin and char material and the decomposition reaction – Arrhenius pre-exponential factor, activation energy, heats, char yield – are significantly important for predicting the peak, average burning rates and surface temperatures. Based on this result, when determining the uncertainty of the model output, only these parameters will be considered for Case 2 problems, where simulation quality is analyzed by comparing the model output with its uncertainty and the experiment data with its uncertainty. Further details on sensitivity of each parameter can be found in this reference ^{Error! Bookmark not defined.,21}.

Determine data and model output uncertainty to make comparison^v

1. Conduct uncertainty analysis of data: Data is acquired from two repeating FPA tests of triple-wall corrugated cardboard under 60 kW/m² heat-flux level with nitrogen atmosphere.
2. Uncertainty analysis is conducted based on these two data sets. The uncertainty of MLR and surface temperature are estimated by first calculating the standard deviation of the MLR and temperature measurement of the 2 data sets at each time step. Then an average standard deviation is calculated for the time interval of interest (0 < t < 500s). The uncertainty is estimated as ± 2 average standard deviation. Table A(D)-6 shows the analysis results from the tests. Data were provided by FM Global. Note that these estimated uncertainties will be used for

^vData uncertainty is accounted for here because this is required to determine the goodness of near-optimal parameter sets. Optimization targets (experiment data) should be considered with its uncertainty bounds to decide how good the match is between the targets and optimum simulations with its uncertainty.

all other cases with different applied heat-flux levels assuming that these values are comparable to each other.

Table A(D)-6. Summary of estimated uncertainty in triple-wall (2 layers) corrugated cardboard FPA experiments based on 2 repeating tests at 60 kW/m² heat-flux level

	MLR (g/s-m ²)	T _s (K)
± 2 avg standard deviation	± 1.5	± 28

3. Conduct uncertainty analysis of model outputs of interest – MLR and T_s
- Baseline case was selected at simulation with EHF = 60 kW/m², thickness = 30 mm, and the optimum parameter set.
 - Six parameters are varied in the simulations one at a time from baseline case^{vi}. See Table A(D)-7.

Table A(D)-7. Outline of 5 parameter groups – kinetic parameters, heat-of-decomposition reaction and combustion, and emissivity-of-fuel and residue – varied in uncertainty analysis using one-at-a-time method

	E1, A1	ΔH1	ρ2	ε1	ε2
Kinetic parameters	+ , - - , +				
Heat of decomposition reaction		+ -			
Density of residue			+ -		
Emissivity of fuel				+ -	
Emissivity of residue					+ -

- The effect of variation is calculated by considering the change in MLR and surface-temperature profiles from the baseline case. By varying certain parameters at one-at-a-time, average standard deviation of the two

^{vi} Parameter selection is based on known parameter sensitivity. Kinetic parameters are not independent; therefore, activation energy and pre-exponential factor will be considered in pair to give decomposition temperature to be at minimum and maximum in simulation. Although nth order is a kinetic parameter, this is not included in the analysis, because changing this value majorly affects the shape of the DTG peak – increase/decrease in n value results in higher/lower DTG peak and wider/narrower temperature range of decomposition, respectively.

cases (altered and baseline case) are calculated as effects. Results are shown in Table A(D)-8.

- Uncertainty in these modeling outputs (MLR and T_s) is calculated using the Law of Propagation of Uncertainty. Note that when inputs are varied to its uncertainty boundary values – minimum or maximum – the maximum effect was selected in the analysis to estimate the maximum uncertainty.

Table A(D)-8. Comparison between experiment data from fire propagation apparatus test and modeling outputs using estimated parameter values via either measurements and numerical optimization (B-GA, B-SCE, B-SHC) or mostly numerical optimization (C-GA, C-SCE, C-SHC)

	Data	B-GA	B-SCE	B-SHC	C-GA	C-SCE	C-SHC
Peak MLR ($\text{g}/\text{m}^2\text{s}$)	35 ± 4	28	24	53	23	29	N/A
Avg MLR ($\text{g}/\text{m}^2\text{s}$)	5.7 ± 0.6	4.6	5.4	5.9	4.8	6.0	N/A
t to pMLR (s)	27 ± 1	19	13	19	4	12	N/A
T_s at 300 s ($^{\circ}\text{C}$)	696 ± 16	685	682	684	679	679	685

Compare data with simulation results with consideration of uncertainties

1. TG / DTG Predictions at 10 °C/min Heating Rate Using Estimated Kinetic Parameters

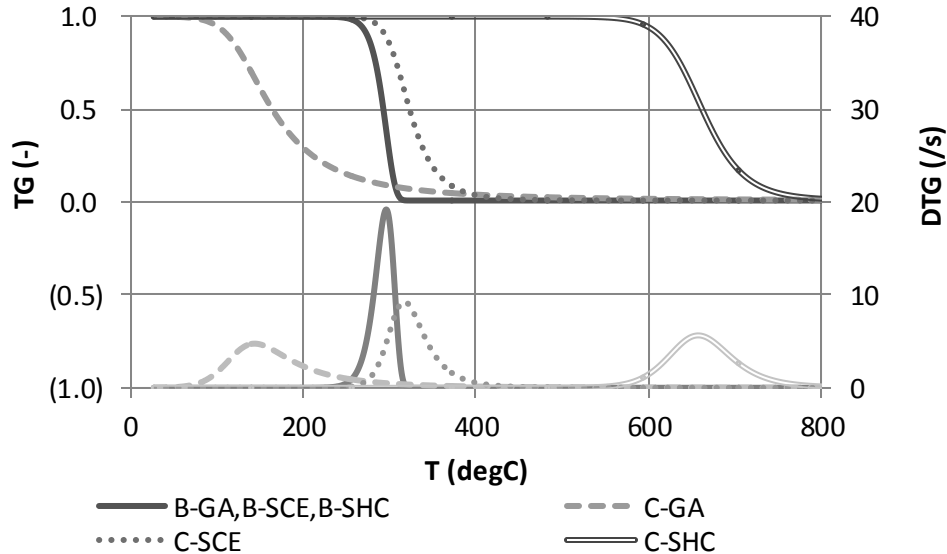


Figure A(D)-15. TG/DTG Curves at 10°C/min heating rate with different estimation results for kinetic parameters for thermal decomposition of corrugated cardboard: For better comparison, TG and DTG thermograms have been scaled to result in 100% conversion.

2. Modeling Output: Mass Loss Rate (MLR)

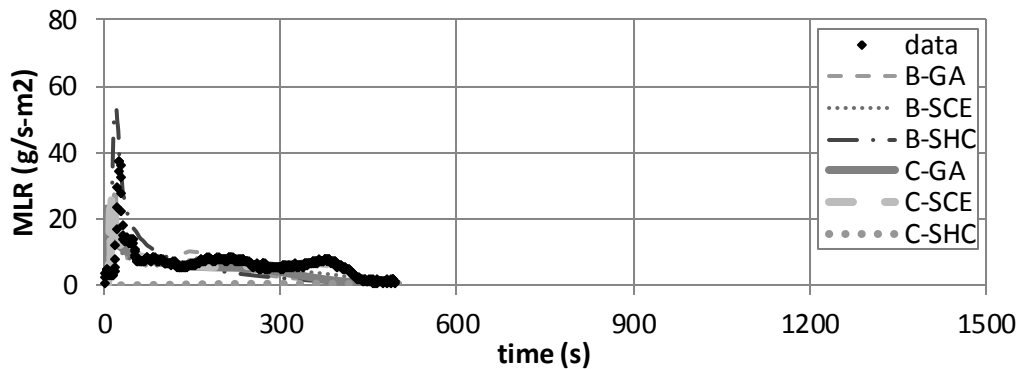


Figure A(D)-16. Mass-loss rate (MLR) comparisons for corrugated cardboard between actual MLR from experiment (data) and modeled MLR (B-GA, B-SCE, B-SHC, C-GA, C-SCE, C-SHC) at applied heat flux of 60 kW/m². Note that data shown were used to estimate model-parameter values via numerical optimization using GA, SCE or SHC routines.

3. Modeling Output: Surface Temperature (T_{surf})

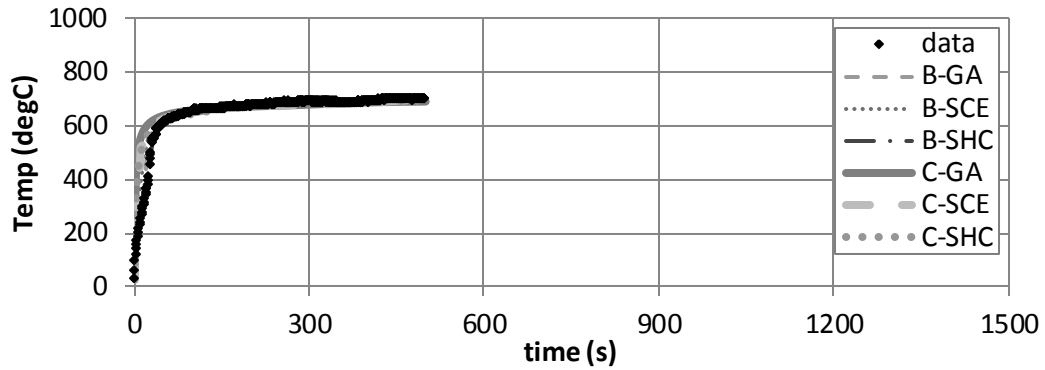


Figure A(D)-17. Surface temperature (T_{surf}) comparisons for corrugated cardboard between actual T_{surf} from experiment (data) and modeled T_{surf} (B-GA, B-SCE, B-SHC, C-GA, C-SCE, C-SHC) at applied heat flux of 60 kW/m^2 . Note that data shown were used to estimate model-parameter values via numerical optimization using GA, SCE or SHC routines.

Validate simulation quality upon extrapolation

1. Modeling Output: Mass Loss Rate (MLR)

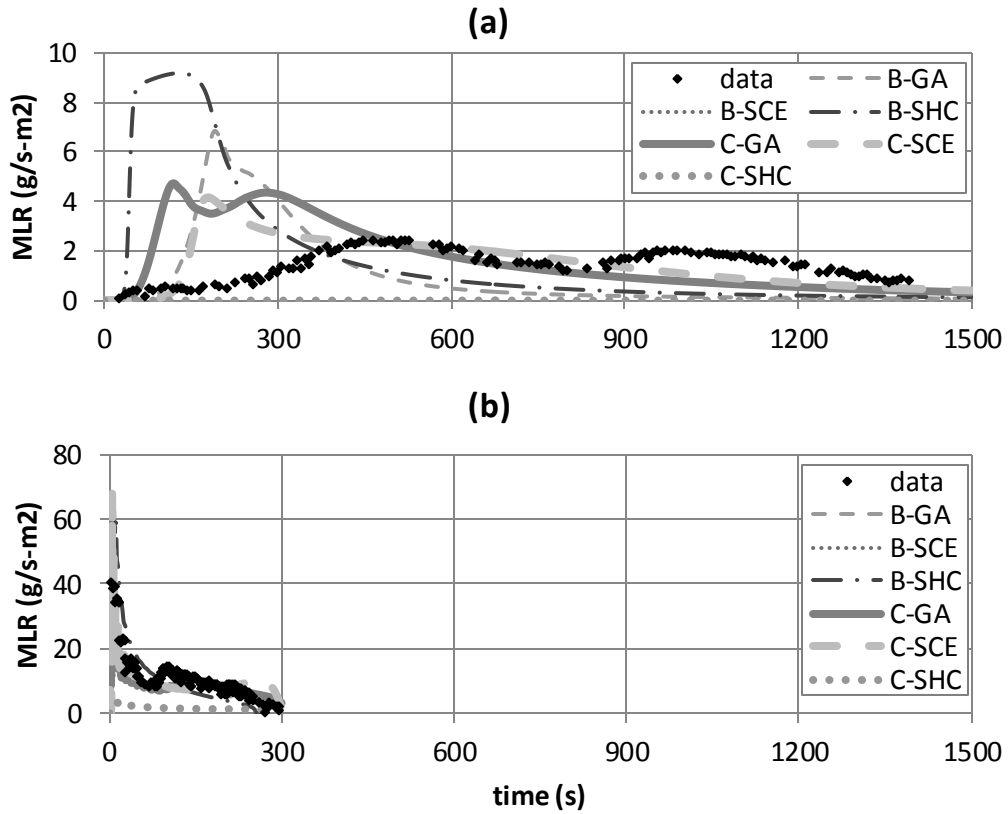


Figure A(D)-18. Mass-loss rate (MLR) comparisons for corrugated cardboard between actual MLR from experiment (data) and modeled MLR (B-GA, B-SCE, B-SHC, C-GA, C-SCE, C-SHC) at applied heat flux of (a) 20 and (b) 110 kW/m². Note that data shown were not included in the model-parameter-estimation process; hence, these two cases are considered as extrapolation cases.

2. Modeling Output: Surface Temperature (T_{surf})

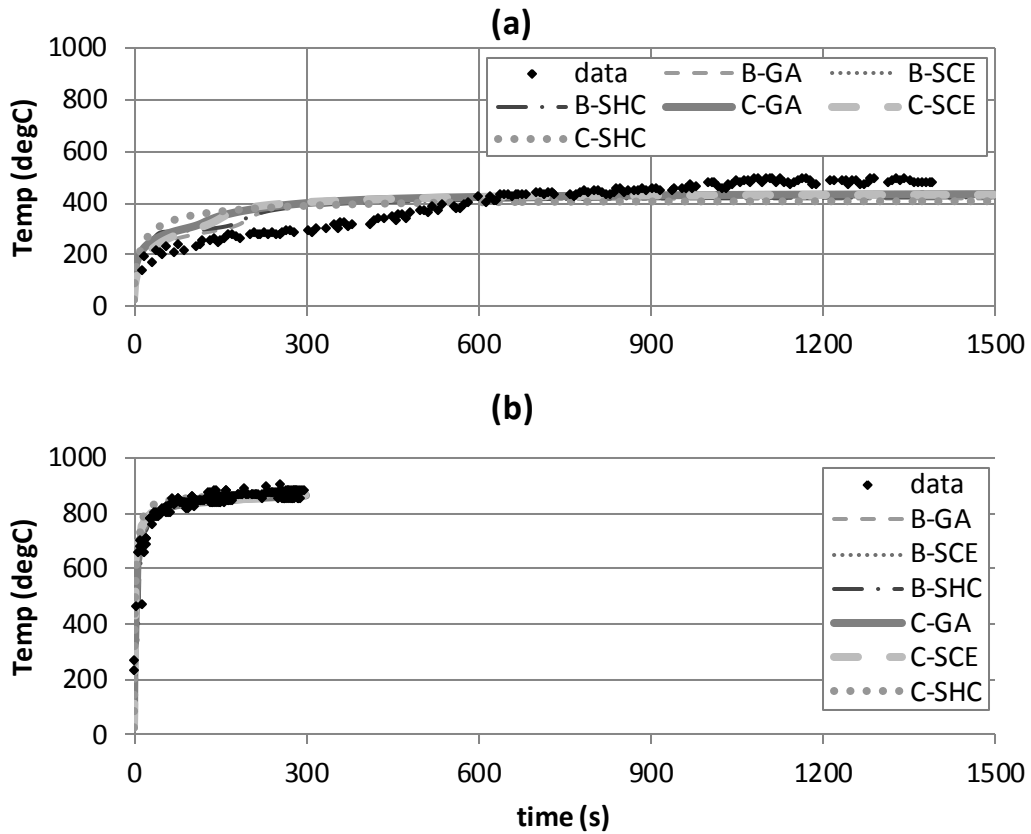


Figure A(D)-19. Surface temperature (T_{surf}) comparisons for corrugated cardboard between actual T_{surf} from experiment (data) and modeled T_{surf} (B-GA, B-SCE, B-SHC, C-GA, C-SCE, C-SHC) at applied heat flux of (a) 20 and (b) 110 kW/m². Note that data shown were not included in the model-parameter-estimation process; hence, these two cases are considered as extrapolation cases.

Commentary

General Comments

- TG/DTG
 - When kinetic modeling is conducted independently using TGA data (B-GA, B-BSE, B-SHC), the DTG peak exist near 300°C.
 - Among GA, SCE and SHC, optimization of SCE of kinetic parameters as part of other unknown parameter estimation is closest to actual TGA data (B-GA, B-SCE, B-SHC), followed by GA and SHC.
 - Optimization of SHC of kinetic parameters along with other unknown parameter estimation is considered as unsuccessful, for decomposition temperature is excessively high (see mass-loss rate optimization and extrapolation results)
- Comparison between Data and Computed Modeling Outputs
 - Generally, better agreement between data and modeling outputs is found when kinetic parameters are estimated through a separate process using TGA data (B-GA, B-BSE, B-SHC) than numerical optimization along with estimating other unknowns together (C-GA, C-SCE, C-SHC).
 - None of the modeled peak MLRs are in quantitative agreement with data.
 - Avg MLR of B-SCE, B-SHC and C-SCE are in good agreement with data.
 - None of the modeled time-to-peak MLRs are in quantitative agreement with data.
 - Surface temperatures at 300 s of B-GA, B-SCE, B-SHC and C-SHC are in good agreement with data.
- MLR
 - Optimization at $HF = 60 \text{ kW/m}^2$: Although the peak may be off for some cases, generally good agreement exists between experiment data and all modeling results, considering the trend, except for that of C-SHC, indicating that optimization of C-SHC – optimizing for all unknowns using SHC – was unsuccessful. Oscillation in the MLR curve is due to the inhomogeneity of sample, corrugated cardboard, which is not captured in

modeling due to the homogeneous assumption made when solving the problem.

- Extrapolation at $HF = 20 \text{ kW/m}^2$: Poor agreement exists between experiment data and all modeling results. None of the modeling cases is able to capture the slow increase in mass-loss rate in the earlier times after exposure to heating source.
- Extrapolation at $HF = 110 \text{ kW/m}^2$: Good agreement exists between experiment data and all modeling results, except for C-SHC case.
- Surface Temperature
 - Optimization at $HF = 60 \text{ kW/m}^2$: Generally good agreement exists between experiment data and all modeling results considering the trend, even for that of C-SHC. Also, when thermal conductivity of the sample at its virgin state was independently measured and that value was used, modeling was able to capture the slow increase in surface temperature up until 400°C followed by a jump up to $\sim 550^\circ\text{C}$.
 - Extrapolation at $HF = 20 \text{ kW/m}^2$: Poor agreement exists between experiment data and all modeling results. None of the modeling cases is able to capture the slow increase in surface temperature in the earlier times after exposure to heating source.
 - Extrapolation at $HF = 110 \text{ kW/m}^2$: Good agreement exists between experiment data and all modeling results, including C-SHC case.

Limitation in Modeling

- When considering limitation of the parameters in modeling corrugated cardboard, the modeler should take into account the applicability of the parameters and their associated uncertainties. For example, any assumptions used when determining a parameter value via experiment direct or indirect measurements can be utilized to understand when the parameter value becomes inappropriate. For this example of pyrolysis modeling of corrugated cardboard, most consideration can be given to the parameters related to decomposition kinetics.

- As shown in the below figure of corrugated cardboard decomposed in TGA at 20 K/min under nitrogen and air atmosphere, the simplified kinetic modeling using one-step decomposition mechanism is only true for a “dry” sample tested in nitrogen. Clearly, for decomposition of a “dry” sample in air results in two distinct DTG peaks. Therefore, the effect of the simplification (one-step) made to kinetic modeling should be addressed when discussing large-scale simulation quality of parallel panel experiment using the optimized parameter set from this exercise.

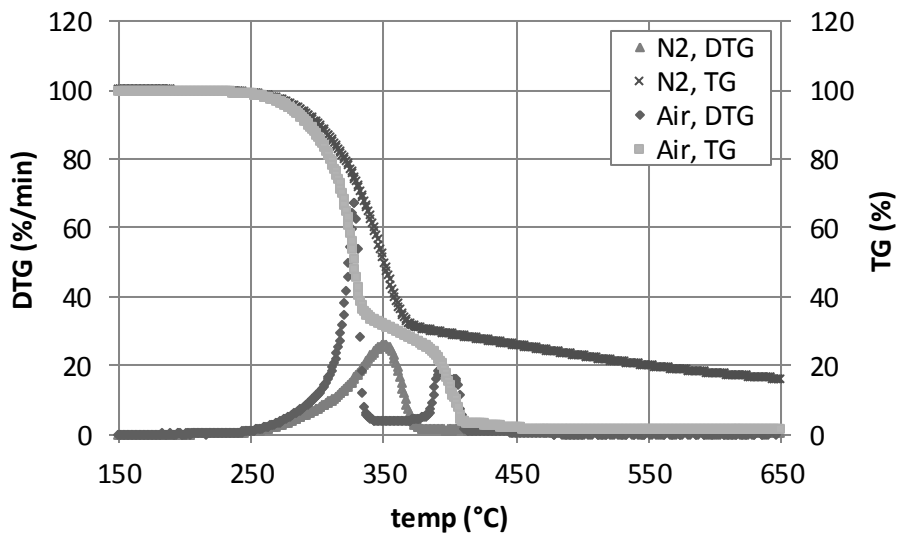


Figure A(D)-20. TGA thermograms of corrugated cardboard decomposition conducted under constant heating rate of 20 °C/min and 2 different environments – nitrogen and air

EXAMPLE 5.3 MODELING MODIFIED ACRYLIC FRP COMPOSITE

An example case is shown for a fiberglass-reinforced polymer (FRP) composite with modified acrylic resin with high-charring inorganic fire-retardant additive. Most of the approach and reference values of the input parameters for this simulation were obtained from Kim and Dembsey's work.²²

Modified acrylic resin (MA) is essentially unsaturated polyester (UPE) with Methacrylic Acid (MMA) replacing most of the styrene monomers. Flame-retarded resin with MA is manufactured by adding a filler-type inorganic additive (A) as an additive, where its loading versus resin is MA:A = 0.38:0.62 by weight. Typical inorganic additives are hydrates such as alumina trihydroxide (ATH) or magnesium hydroxide, antimony trioxide, borax, chalk, silica, etc.²³ Because this additive was known to give a high-charring effect, A was categorized with typical hydroxides used as flame-retardant fillers. These hydroxides work as a flame retardant by resulting in an endothermic dehydration reaction that produces oxides and water.^{24,25} The water produced by this reaction vaporizes, which is an endothermic reaction, and the vapor dilutes the gaseous phase. The oxides remain in the char layer, which adds an insulative effect. This flame retardant is added with a relatively large amount (50 to 65%) comparing to other types of additives. By adding a significant amount of an inorganic flame retardant, the polymer becomes more brittle. Because this is an inorganic additive, inserting this material into the polymer system by 50 to 65 wt% of its original polymer reduces the available fuel within the condensed phase. In addition to this effect, usually the additive has a higher heat capacity compared to the base polymer; hence, the flame retarded polymers with these types of hydroxides require more energy to increase the body temperature to its pyrolysis level. According to the product description, this resin with the flame-retardant additive is formulated to be Class I per ASTM E 84²⁶ (flame spread index < 20 and smoke developed < 225). →Propose two parallel reactions for MA and A thermal decomposition.



Figure A(D)-21. Cross-section of FRP composite with modified-acrylic resin with high-charring inorganic additive

Composite panels were fabricated by vacuum bagging for a relatively high-glass-content composite (31 ± 2 wt% of glass, thickness of 8.8 ± 0.6 mm) using two different types of fiberglass mats that were wetted with resin (see Figure A(D)-21 for cross-section of composite). The two types of fiberglass (E-glass) used in the composite are a chopped-strand mat and a glass-roving woven mat with an area density of 25 g/m^2 and 880 g/m^2 , respectively. The chopped-strand mat is thinner and more porous than the woven mat. The laminate schedule (provided by the manufacturer) is chopped-strand mat and roving alternating three times with another chopped-strand mat layer at the end. Visual inspection of a polished cross-section of the composite slab is consistent with this laminate schedule, but with polymer-resin layers between each fiberglass layer. The chopped-strand mat layer is difficult to identify in the cross section, perhaps because more resin is soaked into this layer than the roving layer. The roving layer is observed as a prominent glass layer possibly because the resin is absorbed only at the fiberglass layer surfaces, leaving the interior with primarily glass. → Apply effective homogeneous single layer of resin, additive. and fiberglass mixture.

Note that for this example, one approach will be used to estimate model parameters – mostly optimization method denoted as Approach GA, SCE, or SHC. For optimization routines, Genetic Algorithm (GA), Shuffled Complex Evolution (SCE) or Stochastic Hill-climber (SHC) is applied.

Measure Parameters

When conducting parameter estimation via independent experiments, consider the following:

- Check consistency between model used in experiment analysis and pyrolysis model.
- Use statistical approach for determining uncertainty; otherwise, meet equivalency to this requirement.

1. Density

Although this FRP composite is porous, due to the nature of the fiberglass and lamination, and therefore the cross-section is not homogeneous, it is considered as an effective homogeneous single-layer material with relatively low bulk density to account for its porous nature. Bulk density of the composite is measured by experiment conducted at room temperature ($\approx 298\text{K}$), weighing the sample's mass and dividing mass with sample volume, which is 1900 kg/m^3 . This density is a mixture of resin (MA), additive (A), and fiberglass (G).

$$\rho_{\text{bulk}} = 1900 \text{ kg/m}^3$$

Also, the resin-with-additive and resin-only sample cured free of fiberglass has been provided by the fabricator. Using this material, the density of resin and additive has been obtained using measurements ($\rho_{\text{MA+A}}$ and ρ_{MA}) and the following correlation (ρ_{MA}):

$$\bar{\rho} = \left(\sum \frac{Y_i}{\rho_i} \right)^{-1}$$

$$\rho_{\text{MA+A}} = 1700 \text{ kg/m}^3$$

$$\rho_{\text{MA}} = 1200 \text{ kg/m}^3$$

$$\rho_{\text{A}} = 2300 \text{ kg/m}^3$$

The density of residue can be found from kinetic modeling, where the weight-loss fraction is estimated for each decomposition reaction.

Density of the fiberglass has been provided by the manufacturer as below:

$$\rho_{\text{G}} = 2600 \text{ kg/m}^3$$

2. *Thermal Conductivity*

Not measured; will be obtained via numerical optimization. However, from literature research, adding inorganic high-charring additives such as hydroxides is known to increase the overall thermal conductivity of the cured resin with additive. Therefore, one can note that the estimated thermal conductivity of the additive, A, should be greater than that of the resin, MA.

3. *Specific-heat Capacity*

Not measured; will be obtained via numerical optimization.

4. *Absorption Coefficient*

Based on visual observation of the composite, every condense-phase material involved in modeling is considered as an opaque material. Therefore, the absorption coefficient is essentially infinity.

$$K \rightarrow \infty$$

5. *Emissivity*

Not measured; will be obtained via numerical optimization.

6. *Reaction Order, Pre-exponential Factor and Activation Energy*

This example case is determined to have decomposition kinetics type 3 (two major peaks – decomposition of resin and additive, respectively – overlapping in DTG over entire mass-loss temperature range) according to TGA and DSC experiments conducted in nitrogen atmosphere. Based on this information, kinetic parameters when using Arrhenius expression and n^{th} order kinetic model – pre-exponential factor, activation energy and n – will be obtained via **Iso-conversional Method (activation energy)** and **model-fitting method (pre-exponential factor and n)**. For modeling fitting method, numerical optimization is conducted with least square method to estimate optimum values for pre-exponential factor and n for each reaction.

Conduct Dynamic Thermogravimetric Analysis (TGA) and Differential Scanning Calorimeter (DSC) Experiments in Nitrogen

Thermogravimetric Analysis (TGA) experiments are conducted at various heating rates – 5, 20, 40, and 60°C/min – with samples sizes near 10 mg for minimal thermal resistance during heating. Temperature range used in the tests is from ambient to 800°C with nitrogen as purging gas.

TGA and DSC data of the decomposable component of the FRP composite, resin and additive cured together (MA+A), and resin only (MA) tested in nitrogen environment with a heating rate of 20°C/min are shown in Figure A(D)-22. Note that DSC data is shown with baseline correction. In the DSC thermogram, a significant endothermic peak is observed for the MA+A sample in 250 to 400°C temperature range, where this is not shown in the MA's thermogram (see green arrow in (b) in Figure A(D)-22). Based on this comparison, the modeler can assume decomposition reaction for the fire-retardant additive, A, in this temperature range followed by that of resin itself, MA, knowing that decomposition of A results in large endothermic reaction.

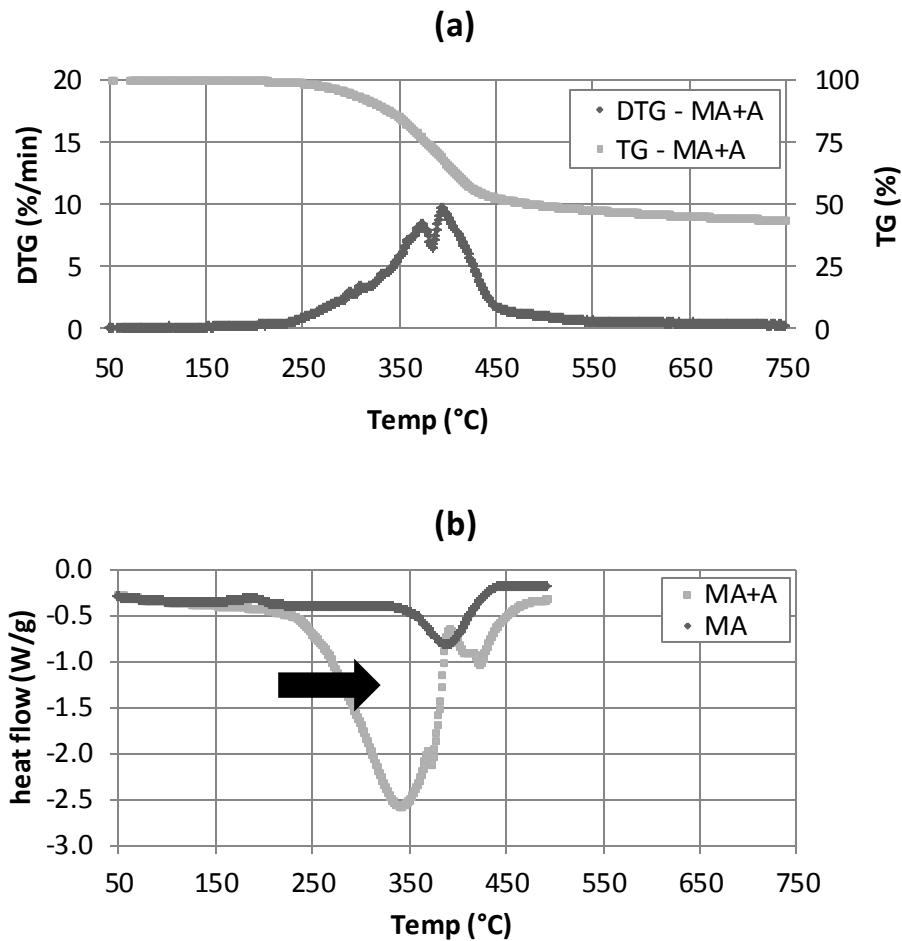


Figure A(D)-22. TGA (a) and DSC (b) thermograms of decomposition of modified-acrylic resin with high-charring additive conducted under 20K/min heating rate and nitrogen environment

Conduct kinetic modeling to obtain kinetic parameters

1. Conduct Iso-conversional Method

Based on this method, activation energy of MA+A and MA are found for $0 < 1-\alpha < 0.2$ (additive decomposition) and $0.1 < 1-\alpha < 0.7$ (resin decomposition) range, respectively (see Figure A(D)-23). According to Iso-conversional Method, two-step reaction mechanism can be proposed as below:



Estimated activation energy for these reactions are 160 ± 3 kJ/mol for decomposition of A and 183 ± 2 kJ/mol for that of MA. Note that slopes, E_a/R , are found via the least-square method. Additionally, considering the uncertainty of $\pm 6\%$ (magnitude of $|\pm 6\%| = 12\%$) in TG data from decomposing MA+A samples, initial weight-loss and char-oxidation reactions that are less than 5% of weight loss are ignored. They can be determined as insignificant changes.

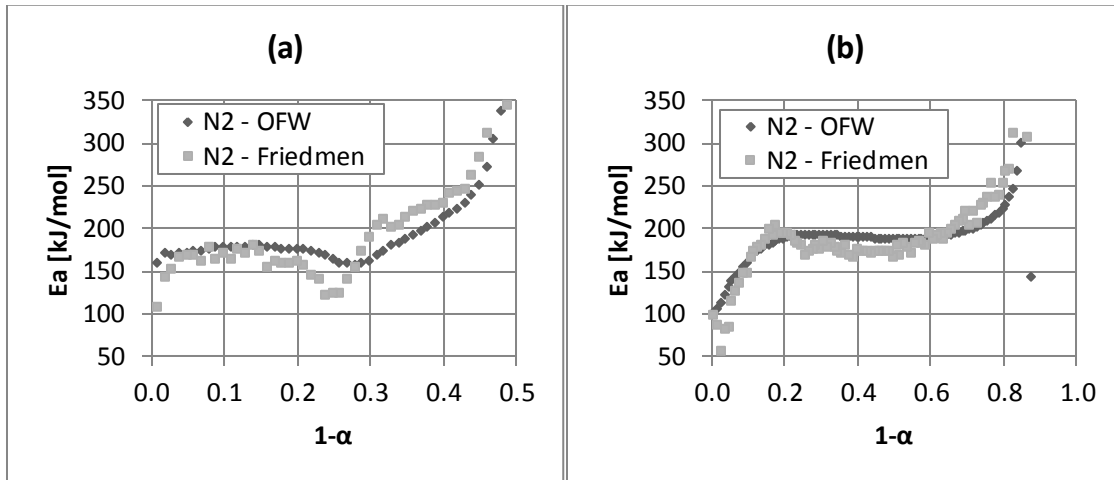


Figure A(D)-23. Estimated activation energy, E_a , with respect to conversion ($1-\alpha$) based on Iso-conversional Method for decomposition of modified-acrylic resin with (a) and without (b) inorganic high-charring additive

2. Conduct model-fitting method using n^{th} order reaction kinetic model ($f(\alpha)$)

Once the minimum number of reactions and their activation energies are estimated by conducting Iso-conversional Method, other kinetic parameters to fully mathematically describe decomposition of MA+A need to be estimated as well. This is done by conducting the model-fitting method with a kinetic model assumed. Typically a

n^{th} order reaction model is used due to its flexibility in providing good fitness between the data and the model. Therefore, n^{th} order will be utilized in this example. Based on the model-fitting method, estimation of total-weight-loss fraction, pre-exponential constant, and n are conducted for each reaction (see Table A(D)-9).

Table A(D)-9. Kinetic parameters for 2-step model – decomposition of additive (+A-R) and resin (R) – for modeling modified-acrylic resin with inorganic high-charring additive

	+A-R	R
Weight Fraction	0.2	0.3
E_a (kJ/mol)	165	183
$\log(A (/s))$	12.2	12.5
$n (/)$	5	1.3

Note that estimation has been done with least-square method by comparing TGA data (TG and DTG from iso-heating rate tests (see Figure A(D)-24) with kinetic modeling's output. The kinetic modeling's output is calculated by applying the Runge-Kutta 4th order method (ODE solving method) to the decomposition ODE equation.

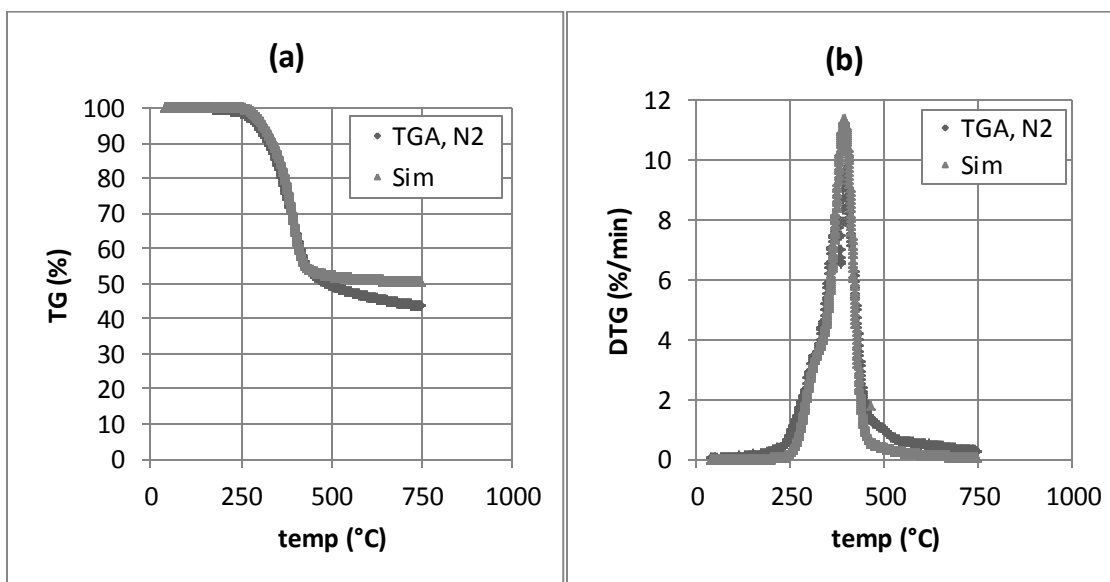


Figure A(D)-24. Comparison of TGA experiment data (TG and DTG) at 20°C/min under nitrogen atmosphere with kinetic modeling results based on model-fitting method for modified-acrylic resin with inorganic high-charring additive

$$\log A_1 = 12.2 \text{ (log(/s))}; E_1 = 1.65 \times 10^5 \text{ (J/mol)}; n_1 = 5$$

$$\log A_2 = 12.5 \text{ (log(/s))}; E_2 = 1.83 \times 10^5 \text{ (J/mol)}; n_2 = 1.3$$

7. Heat of Reaction

For decomposition reaction of the additive, A, three identical DSC experiments are conducted to determine heat-of-reaction: $(3.42 \pm 0.34) \times 10^6$. However, in DSC scans, when the sample is losing mass during the experiment, baseline required to sum energy over temperature range of interest is not stable; therefore, uncertainty should be higher than estimated.

$$\Delta H_1 = 3420 \pm 340 \text{ kJ/kg}$$

For decomposition reaction of the resin, MA, heat of reaction is not measured; will be obtained via numerical optimization.

Summary

Among seven categories of parameters, parameters that have been estimated via direct measurement are shaded in Table A(D)-10. The rest of the unknown parameters, a **total of 16 parameters**, should be obtained via numerical optimization in pair with pyrolysis modeling using bench-scale experiment data or equivalent.

Table A(D)-10. Summary of necessary model parameters for simulating pyrolysis of modified-arylic resin with high-charring additive (MA+A) FRP composite

	No	Condense Phase				
		<i>i=1, A</i>	<i>i=2, A_residue</i>	<i>i=3, MA</i>	<i>i=4, MA_residue</i>	<i>i=5, G</i>
Material Property	1	ρ_1	ρ_2	ρ_3	ρ_4	ρ_5
	2	k_1	k_2	k_3	k_4	k_5
	3	c_1	c_2	c_3	c_4	c_5
	4	κ_1	κ_2	κ_3	κ_4	κ_5
Parameters for Specifying Conditions	5	ε_1	ε_2	ε_3	ε_4	ε_5
		Heterogeneous RxN				
		<i>k = 1, +A-R</i>			<i>k = 2, R</i>	
Kinetic Parameters and Heats assuming n^{th} order model and Arrhenius-type expression	6	n_1			n_2	
		Z_1			Z_2	
		E_1			E_2	
	7	ΔH_1			ΔH_2	

Obtain Parameters via Numerical Optimization

Run Model in Pair with Numerical Optimization

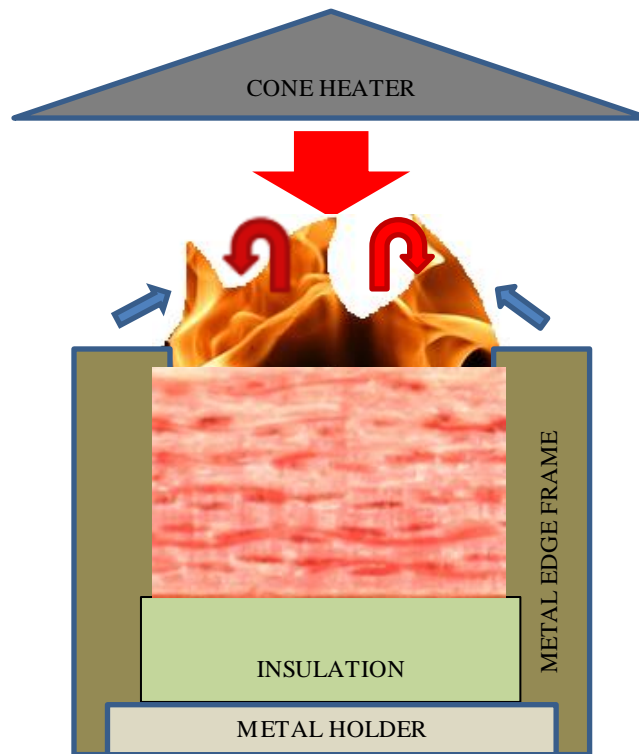


Figure A(D)-25. Simplified representation of a cone calorimeter test of FRP composite

Select model: GPYRO

Understand bench-scale experiment set-up for modeling simple cases

A simplified representation of a cone calorimeter test of FRP composite is shown in Figure A(D)-25. The sample is placed on top of an insulation, which sits on a metal holder. Another metal frame is placed on top of the sample, insulation, and the holder. A metal edge frame is used as well.

Front Surface: As heating starts by opening the shutter to allow radiation from the cone heater to impinge on the sample surface (large red arrow), cooling also begins via natural convection (blue arrows) and re-radiation. The surface decomposes with bubbling with respect to temperature increase occurring through heat conduction and/or in-depth radiative transport. The pyrolyzates leave through the surface until complete burnoff, because this material leaves no residue. When ignition occurs as the fuel-vapor concentration above the surface exceeds its LFL (lower flammable limit), additional heat

flux from the flame is introduced on the surface (red arrows). Regression of the sample surface with respect to consumption of the resin layers in pyrolysis is negligible due to limited expanding of the fiberglass layers upon heating.

Back surface: The sample is placed on top of insulation. In the experiment, an air gap of a few millimeters thickness exists between the sample and the insulation due to thermal contact. Due to the insulation, nothing leaves through the back face when 1D assumption holds for the experiment.

Configure model conditions based on understanding of experiment set-up

In the model, the phenomena discussed above are simulated as below. Basic assumptions are as follows:

- Instantaneous release of volatiles from solid to the gas phase
- Local thermal equilibrium between the solid and the volatiles
- No condensation of gaseous products
- No porosity effects

Further details can be found from the *Technical Reference*⁶ and *User's Guide*⁷ of GPYRO (<http://code.google.com/p/gpyro>).

When conducting the GPYRO simulation for the cone calorimeter set-up, the metal edge frame will be ignored, and backing is insulated. The ignition phenomenon is interpreted as the following in the simulations: at a known time-of-ignition (from experiment data), additional heat flux of 20 kW/m² is applied to the surface to simulate heat flux from the flame. This value is estimated from a measurement from this material pyrolyzing in the cone with a total-heat-flux gauge measuring heat flux impinging on the sample surface (see Figure A(D)-26 – test conducted at 50 kW/m² applied heat flux; from time-of-ignition an increase in measured heat flux is observed due to flame).

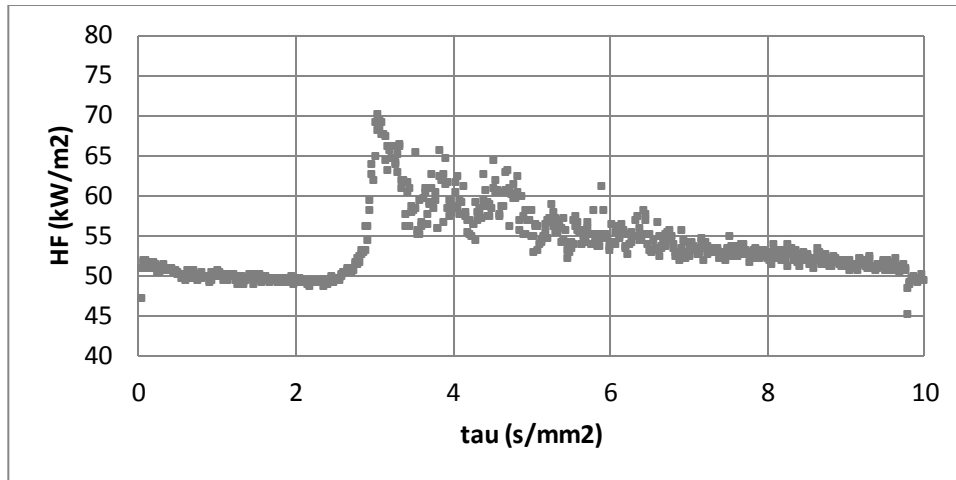


Figure A(D)-26. Heat flux measured during cone calorimeter test of modified-acrylic resin with high-charring additive (MA+A) FRP composite at external-heat-flux level of 50kW/m²: ignition occurs near $\tau = 3$ s/mm², and from this point additional heat flux impinges on the surface due to the flame.

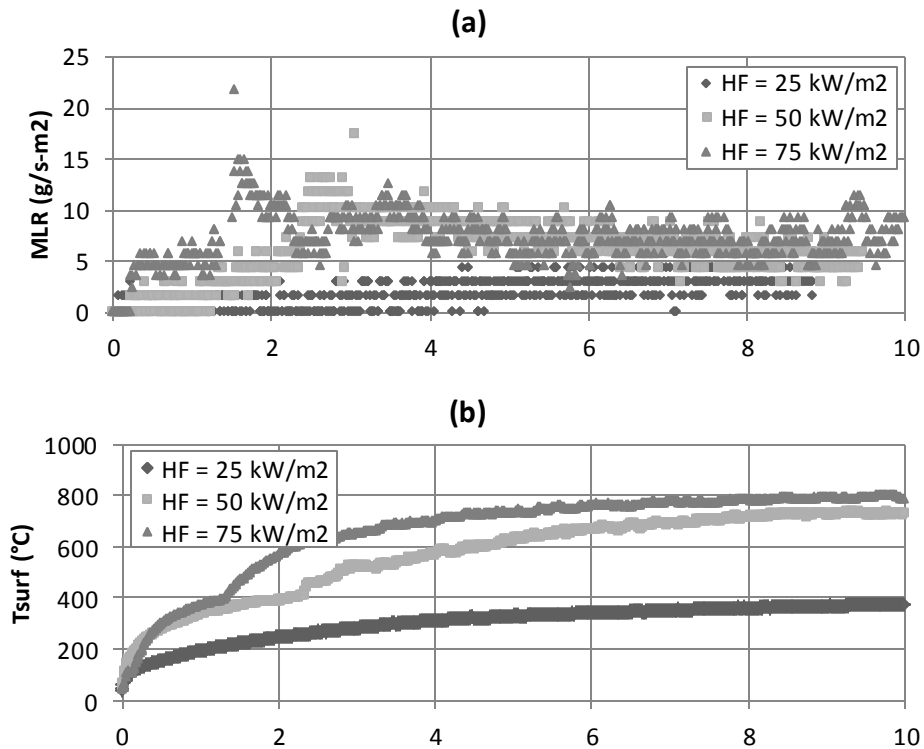
In addition to the parameters introduced in a previous section (see Parameter Estimation Results), the model (GPYRO) has a coefficient (γ , GAMMA) that is used to model radiative heat transfer through the pores. This parameter with T^3 is a model-dependent parameter that is added as another term in the effective thermal conductivity. γ is used for porous fiberglass and decomposed solid species, which results in a more porous state due to the weight loss; therefore, more radiative heat transfer through the gas phase pores, i.e., for condense phase specie $i = 2$ (A_residue), 4 (MA_residue) and 5 (G).

Another set of parameters included as unknowns is the temperature-dependent terms used to describe the variation of thermal conductivity and specific-heat capacity with respect to temperature increase: $k(T) = k_0(T/T_r)^{n_k}$ and $c(T) = c_0(T/T_r)^{n_c}$, respectively, where T_r is a reference temperature. Only properties of fiberglass are allowed to vary with respect to temperature, knowing that for high-glass-content FRP composite, glass may be a controlling factor for its fire behavior. This approach is utilized to give much flexibility during parameter estimation for fiberglass.

Therefore, the **total unknown parameters** of 16 now becomes **21**, including γ , n_k , and n_c .

Acquire data sets that can be used in numerical optimization process in pair with pyrolysis modeling for obtaining unknown model-parameter values^{vii}

1. The maximum heat-flux level of interest for this parameter estimation is 25 to 75 kW/m².
2. Cone calorimeter (cone) test data of modified-acrylic resin with high-charring additive FRP composite (thickness, δ is 8.8 ± 0.6 mm) impinged with effective heat fluxes (EHF) of 25 to 75 kW/m² is obtained and are shown in Figure A(D)-27 for mass-loss rate (MLR), surface, and back face temperature measurements:
3. Check data reproducibility by repeating identical experiments: Data is acquired from three repeating cone tests of MA+A FRP composite under 50 kW/m² heat flux level. Uncertainty analysis will be performed later.



^{vii}To conduct simulations, unknown parameters need to be obtained via numerical optimization, for independent measurements of those parameters are cumbersome and impossible in most cases.

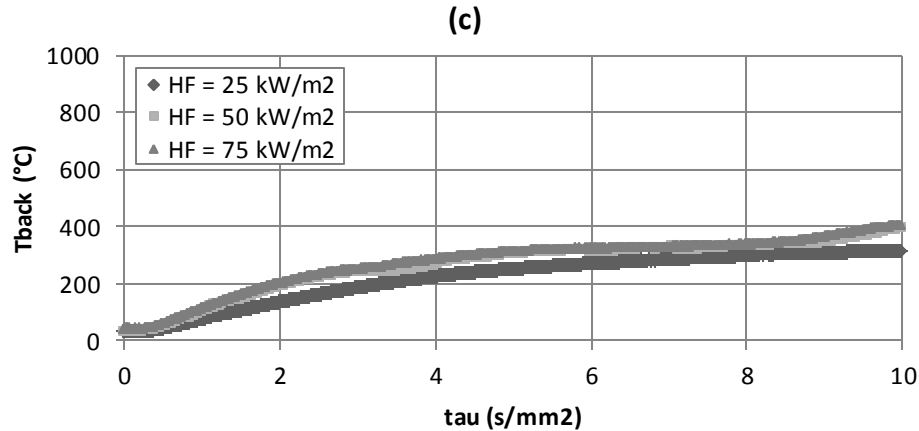


Figure A(D)-27. Cone calorimeter experiment results of modified-acrylic resin with high-charring additive (MA+A) FRP composite with applied heat flux ranging from 25 to 75 kW/m²: (a) mass-loss rate and (b) surface temperature, and (c) back-surface temperature measurements

Select numerical optimization routine

The property estimation for the modified-acrylic composite is conducted by coupling a generalized pyrolysis model for slab experiments developed by Lautenberger and the Genetic Algorithms (GA) for optimization routine.^{27,7} GA was developed based on the mechanics of the Darwinian survival-of-the-fittest theory.

Conduct numerical optimization in pair with simulations using experiment data as targets

Numerous simulations with GPYRO have been used in pair with GA algorithm to conduct numerical optimization to obtain unknown parameters. Experiment data of mass-loss rate (MLR), cumulative mass loss (CML), and surface and back-face temperature measurements (T_s and T_b) generated with a heat-flux level of 50 kW/m² have been used in the optimization process as targets (i.e., optimization is conducted for unknown parameters to match modeling outputs of interest to certain experiment data).

Obtain Confidence Intervals for Optimized Parameters

One possible approach for addressing the uncertainty of a numerically optimized parameter when using GA optimization is to use the near-optimal parameter sets or “best solutions” to generate a relatively large population of parameter sets (see parameter set

fitness after ~ 80 generations in Figure A(D)-28). A multi-objective optimization algorithm, such as the GA applied to pyrolysis modeling, typically produces many near-optimal sets or “best solutions,” which are a set of solutions that represent tradeoffs between many objective functions. Each parameter in each set can be evaluated individually to determine whether the near-optimal value of one parameter changes significantly from one set to another. Also, comparing the model outputs, such as the mass-loss rate and temperature predictions simulated with different near-optimal parameter sets, will allow the user to determine how much the simulation results vary from one set to another within the collection of optimized parameter sets. This numerical experiment may provide insight to the sensitivity of the optimization routine to any changes in the inputs as well as to the uncertainties in the model outputs associated with the optimized parameter values.

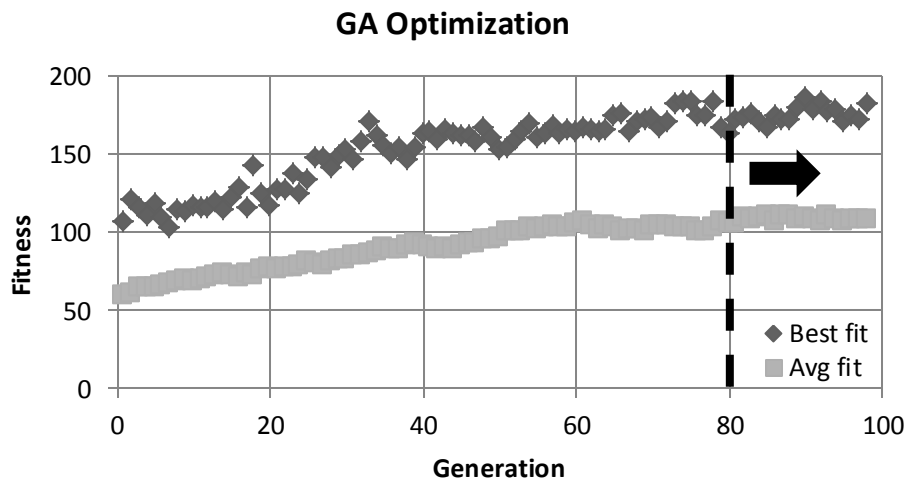


Figure A(D)-28. Increase in model output fitness to targets – mass-loss rate, cumulative mass loss, surface and back-surface temperatures – from genetic algorithm (GA) optimization for estimating unknown parameters from simulating pyrolysis of modified-acrylic resin with high-charring additive (MA+A) FRP composite

Parameter Estimation Results

ID		GA(avg)	GA(best)	SCE	SHC				
Parameter		Comparable Non-optimization and Optimization							
Thermo-physical Property	i = 1 (Resin)	ρ_i	kg/m ³	1200 Measurement					
		k_i	W/m-K	0.23 ± 0.02 GA	0.21 GA	0.54 SCE	0.04 SHC		
		c_i	J/kg-K	1400 ± 100 GA	2200 GA	300 SCE	1300 SHC		
		i = 2 (R_residue)	ρ_i	kg/m ³	253 Measurement, Kinetic Modeling				
			k_i	W/m-K	0.19 ± 0.02 GA	0.12 GA	0.08 SCE	0.31 SHC	
			c_i	J/kg-K	1900 ± 200 GA	1600 GA	1800 SCE	1800 SHC	
	i = 3 (Additive)		ρ_i	kg/m ³	2300 Measurement				
			k_i	W/m-K	1.22 ± 0.10 GA	1.44 GA	0.82 SCE	2.74 SHC	
			c_i	J/kg-K	1200 ± 100 GA	930 GA	2500 SCE	2400 SHC	
		i = 4 (A_residue)	ρ_i	kg/m ³	1558 Measurement, Kinetic Modeling				
			k_i	W/m-K	0.24 ± 0.04 GA	0.22 GA	0.59 SCE	0.36 SHC	
			c_i	J/kg-K	1200 ± 100 GA	2200 GA	300 SCE	780 SHC	
	i = 5 (Glass)		ρ_i	kg/m ³	2600 Reference (MSDS)				
			k_i	W/m-K	0.18 ± 0.02 GA	0.15 GA	0.30 SCE	0.09 SHC	
			c_i	J/kg-K	400 ± 100 GA	170 GA	300 SCE	110 SHC	
		Optical Property	i = 1 (R)	κ_i	/m	10 ⁶ Approximated as Opaque			
				ε_i	-	0.84 ± 0.03 GA	0.81 GA	0.82 SCE	1.24 SHC
				i = 2 (R_res)	κ_i	/m	10 ⁶ Approximated as Opaque		
	ε_i		-		0.90 ± 0.03 GA	0.87 GA	1.00 SCE	0.97 SHC	
	i = 3 (A)		κ_i		/m	10 ⁶ Approximated as Opaque			
ε_i			-	0.81 ± 0.04 GA	0.77 GA	1.00 SCE	0.84 SHC		

	i = 4 (A_res)	κ_i	/m	10^6					
		Approximated as Opaque							
		ε_i	-	0.89 ± 0.03	0.96	1.00	0.42		
				GA	GA	SCE	SHC		
	i = 5 (Glass)	κ_i	/m	10^6					
		Approximated as opaque							
		ε_i	-	0.88 ± 0.02	0.90	1.00	1.41		
				GA	GA	SCE	SHC		
Kinetics and Heats	k = 1 R → R _{residue+vap} ↑	n_k	-	1.3		Model Fitting with Multiple Heating Rate TGA Data			
		Z_k	/s	3.2×10^{12}					
		E_k	J/mol	1.83×10^5					
		ΔH_k	kJ/kg	$(2.5 \pm 0.2) \times 10^3$	2.0×10^3	2.6×10^3	2.6×10^3		
			GA	GA	SCE	SHC			
	k = 2 A → A _{residue + vap} ↑	n_k	-	5.0		Model Fitting with Multiple Heating Rate TGA Data			
		Z_k	/s	1.6×10^{12}					
		E_k	J/mol	1.60×10^5					
ΔH_k		kJ/kg	3760 ± 1130 (30%) Measurement, DSC						
Model Dependent Parameter	n_{kz} (i=5)	-	0.59 ± 0.06	0.58	0.01	0.18			
			GA	GA	SCE	SHC			
	n_c (i=5)	-	0.53 ± 0.06	0.37	0.88	-0.26			
			GA	GA	SCE	SHC			
	Υ (i=2)	m	0.00348 ± 0.00134	0.00051	0.00002	0.02482			
			GA	GA	SCE	SHC			
	Υ (i=4)	m	0.00475 ± 0.00184	0.00625	0.00001	0.05832			
			GA	GA	SCE	SHC			
	Υ (i=5)	m	0.00769 ± 0.00225	0.00001	0.00003	-0.02453			
			GA	GA	SCE	SHC			

Validation

Analyze simulation quality

Identify sensitive parameters for model inputs¹

Global Sensitivity Analysis (Morris Method): For this case, a total of 21 parameters are necessary. In this example case, a structured global sensitivity analysis technique is used to determine the sensitivity of input parameters used in the model. Among various global-analysis techniques, screening design is one of the simplest methods to identify important parameters.^{28,29,30} Typical screening designs are one-at-a-

time (OAT) experiments, where a value is changed and its impact is evaluated in turn. It is known that classical OAT experiments are less meaningful if the model of interest is affected by nonlinearities, which causes a drastically different “sensitivities” when parameter changes around the “control” scenario, depending on the chosen “control” scenarios. To address this limitation, Morris (1991) has proposed a global OAT design method, by covering the entire space in which the parameters may vary independently of the specific initial “control” scenario one may commence the experiment with. A global OAT design assumes that the model is characterized by a large number of parameters and/or is computationally expensive (regarding computational time and computational resources) to run.

Although originally the Morris Method was used for unit-less parameters, for this problem it was used for parameters with units. Because the Method allowed the user to interpret the effect of changes made in the inputs to the model outputs in terms of simulation variation observed in dimensional units (i.e., seconds for time, °C for temperature, and g/m²-s for mass-loss rate), one was able to apply the significance level (see below) directly. This allows the user to rank the sensitivity of each parameter with a quantifiable variation.

Significance level: To identify the sensitive parameters of a model via a sensitivity analysis, there needs to be a measure to determine the sensitivity. This measure, defined as the level of significance, should be able to distinguish which effects shown in the simulation results due to changes made in the inputs are significant and which are not. A typical sensitivity analysis allows the user to rank the input parameters in terms of its sensitivity to model outputs. Defining the level of significance allows the user also to determine how many of the parameters from the top ranking should be set with caution, because those significantly affect the simulation results. The level of significance that defines the sensitivity of an input parameter should be predetermined by the user based on one’s goal of conducting the simulation. When the best simulation accuracy is desired, the level of significance should be determined by the experimental uncertainty obtained by tests identical to the simulation set-up, such as the cone calorimeter tests. For example, if the ignition time has an uncertainty of +/- 20 sec. in the cone calorimeter tests, any changes in the model input that allows more than +/- 20 sec.

in the model output should be considered as a “significant change.” However, there are situations where low simulation accuracy is acceptable for one’s simulation purposes. In these cases, the level of significance can be set by the modeler to be greater than the experimental uncertainty, and this approach results in less parameter being considered as sensitive to model outputs.

→ *In this example case, the significance level is set equal to experiment uncertainty for best simulation accuracy.*

Application: After identifying the necessary parameters for pyrolysis modeling with a model of choice and selecting the significance level, a sensitivity analysis is performed to identify sensitive input parameters to model output. To determine the region of experimentation for Morris’ Method, the minimum and maximum range for each parameter is selected by the user using common sense. Four levels, P1 through P4, are used ($p = \{0, 1/3, 2/3, 1\}$) with an increment of $\Delta = p/[2(p-1)] = 2/3$ following the guide presented by Morris. Four cases are simulated, resulting in four elementary effects for each parameter. See Table A(D)-11.

Table A(D)-11. Summary of unknown model parameters included in sensitivity analysis with searchable space defined with SA min and max: 4 levels (P1 though P4) and an increment of Δ are shown.

	No.		SA Min	SA Max	p1	p2	p3	p4	Δ
MA	1	k_1	0.05	0.50	0.05	0.20	0.35	0.50	0.30
	2	c_1	500	3500	500	1500	2500	3500	2000
	3	ϵ_1	0.01	1.00	0.01	0.34	0.67	1.00	0.66
MA_residue	4	k_2	0.05	0.50	0.05	0.20	0.35	0.50	0.30
	5	c_2	500	3500	500	1500	2500	3500	2000
	6	ϵ_2	0.01	1.00	0.01	0.34	0.67	1.00	0.66
	7	γ_2	0.001	0.100	0.001	0.034	0.067	0.100	0.066
A	8	k_3	0.50	5.00	0.50	2.00	3.50	5.00	3.00
	9	c_3	500	3500	500	1500	2500	3500	2000
	10	ϵ_3	0.01	1.00	0.01	0.34	0.67	1.00	0.66
A_residue	11	k_4	0.10	5.00	0.10	1.73	3.37	5.00	3.27
	12	c_4	500	3500	500	1500	2500	3500	2000
	13	ϵ_4	0.01	1.00	0.01	0.34	0.67	1.00	0.66
	14	γ_4	0.001	0.100	0.001	0.034	0.067	0.100	0.066
Fiberglass	15	k_5	0.05	0.50	0.05	0.20	0.35	0.50	0.30
	16	n_k	0.00	1.00	0.00	0.33	0.67	1.00	0.67
	17	c_5	500	3500	500	1500	2500	3500	2000
	18	n_c	0.00	1.00	0.00	0.33	0.67	1.00	0.67
	19	ϵ_5	0.01	1.00	0.01	0.34	0.67	1.00	0.66
	20	γ_5	0.001	0.100	0.001	0.034	0.067	0.100	0.066
HoR	21	ΔH_2	1.0E+0 5	1.0E+0 7	1.0E+0 5	3.4E+0 6	6.7E+0 6	1.0E+0 7	6.6E+0 6

To calculate an elementary effect, first a baseline case needs to be constructed. The baseline is a group of the entire parameters with their values randomly chosen from **P1 or P2**. This is because there are four levels in this analysis, and when conducting the analysis adding Δ should not exceed the region of experiment. Next, a random order should be created for each case, where this order is used to change the parameter value from its baseline by Δ one at a time. The effect of changing a parameter by Δ is evaluated by running the model and evaluating the changes made in the model output of interest. Using these four effects found from four cases for each parameter, the modeler now can calculate the mean and its standard deviation or variance of changes that occurred due to an increase/decrease made to a single parameter value by Δ . Any parameter resulting in a significant change in model outputs when changed by Δ (i.e., a

large mean and/or standard deviation/variance for changes made in the modeling outputs) are considered to be “sensitive.”

The modeling outputs of interest are as follows for this example case:

- T_s at $\tau = 1 \text{ s/mm}^2$
- T_s at $\tau = 3 \text{ s/mm}^2$
- T_b at $\tau = 1 \text{ s/mm}^2$
- T_b at $\tau = 3 \text{ s/mm}^2$
- $T_{\text{surf-ig}}$ where t_{ig} obtained from experiment data
- $MLR\text{-ig}$ where t_{ig} obtained from experiment data
- MLR_{peak}

Note that kinetic parameters are not included in the sensitivity analysis because when a model-fitting method is used to determine kinetic parameters, any uncertainty in activation energy can be compensated by adjusting the pre-exponential coefficient and vice versa. Therefore, knowing the compensation effect between the estimated activation energy and pre-exponential factor, which is always accounted for in the model-fitting method, the effect of uncertainties in kinetic parameters on modeling outputs of interest is considered to be negligible.

Results: The results are shown with a sensitivity coefficient for each parameter defined as below:

$$SC \equiv \frac{\text{average mean or standard deviation of effects from 4 cases}}{\text{Significance Level}}$$

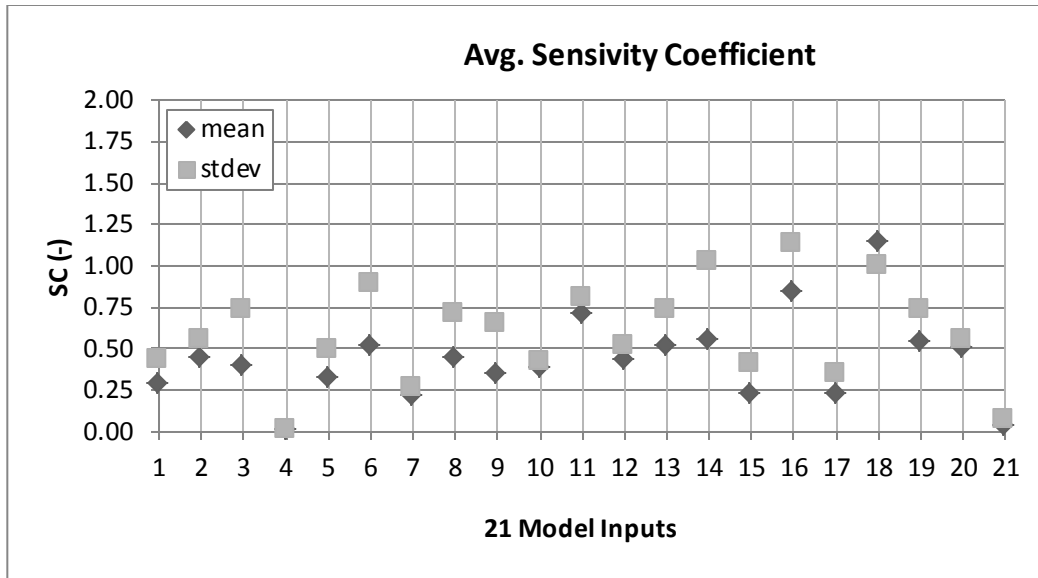


Figure A(D)-29. Sensitivity coefficient (SC) for 21 parameters included in sensitivity analysis

Based on this analysis, Δ changes made in **input parameters, 6, 11, 14, 16 and 18** results in significant changes in the modeling outputs of interest ($SC \geq 1$). See Figure A(D)-29. Therefore, when conducting uncertainty analysis, these parameters will be considered to estimate the uncertainty band of modeling outputs. As noted before, the confidence interval for these parameters will be estimated from near-optimal parameter sets found from numerical optimization using GA. Note that the significance-level set as experiment uncertainty is estimated in the following section; however, it is used to calculate SC in this step.

Determine data and model output uncertainty to make comparison^{viii}

1. Conduct uncertainty analysis of data

Data is acquired from three repeating cone tests of modified-acrylic resin with inorganic high-charring additive FRP composite with relatively high glass content under 50 kW/m^2 heat flux level.

The uncertainties in the MLR and thermocouple measurements at surfaces (front and back) were quantified by comparing data from these three identical FRP composite

^{viii}Data uncertainty is accounted for here because this is required to determine the goodness of near-optimal parameter sets. Optimization targets (experiment data) should be considered with their uncertainty bounds to decide how good the match is between the targets and optimum simulations with their uncertainty.

tests. Note that normalized time, time divided by sample thickness square, i.e., $\tau = \text{time}/\delta^2$, is used to remove the effect of different sample thicknesses when comparing. Because the data is transient, values at different times ($\tau = 1, 3, 5,$ and 7 s/mm^2) from each test have been used to calculate the standard deviation at each time. Then these are averaged and used to estimate uncertainty by applying student t distribution with a sample size of three and calculating the 95% confidence interval. See Table A(D)-12.

Table A(D)-12. Summary of estimated uncertainty in modified-acrylic resin with high-charring additive (MA+A) FRP composite cone calorimeter experiments based on 3 repeating tests at 50 kW/m² heat flux level

	MLR (g/s-m ²)	T _s (°C)	T _b (°C)
± uncertainty	± 2.2	± 67	± 14

2. Conduct uncertainty analysis of model outputs of interest – MLR, T_s and T_b

- Baseline case was selected at simulation with EHF = 50 kW/m², thickness = 8.7 mm, and the best optimum-parameter set.
- Five parameters that were determined to be sensitive to modeling outputs of interest are varied in the simulations one at a time from the baseline case. See Table A(D)-13 for summary.

Table A(D)-13. Outline of 5 parameters – MA_residue emissivity, A_residue thermal conductivity and GAMMA, fiberglass thermal conductivity, and specific heat capacity T dependent terms – varied in uncertainty analysis using one-at-a-time method

No.	Parameter	Optimum±C.I. (α=0.05, t-distribution)	ε ₂	k ₄	γ ₄	n _k	n _c
6	MA_residue Emissivity	0.60 ± 0.04	+ -				
11	A_residue Thermal Conductivity	0.33 ± 0.11		+ -			
14	A_residue GAMMA	0.0095 ± 0.0042			+ -		
16	Fiberglass Thermal Conductivity T Dependent Term	0.30 ± 0.08				+ -	
18	Fiberglass Specific-Heat Capacity T Dependent Term	0.57 ± 0.11					+ -

- The effect of variation is calculated by considering the change in MLR, front and back-surface temperature profiles from baseline case. By varying certain parameters one at a time, standard deviation of the two cases (altered and baseline case) are calculated at each time step and 2 x the maximum standard deviation found from time interval of interest is used as effects. Results are shown in Table A(D)-14.
- Uncertainty in these modeling outputs (MLR and T_s) is calculated using the Law of Propagation of Uncertainty. Note that when inputs are varied to its uncertainty boundary values – minimum or maximum – the maximum effect was selected in the analysis to estimate the maximum uncertainty.

Table A(D)-14. Comparison between experiment data from cone calorimeter test and modeling outputs using estimated parameter values using numerical optimization (GA, SCE, SHC)

	Data	GA(avg)	GA(best)	SCE	SHC
Peak MLR ($\text{g}/\text{m}^2\text{s}$)	27 ± 31	10.7 ± 1.2	11.4	10.6	12.4
Avg MLR ($\text{g}/\text{m}^2\text{s}$)	5.8 ± 1.6	6.3 ± 1.2	6.1	6.2	8.1
t to pMLR (s)	200 ± 70	196	189	189	196
T_s at $\tau = 1 \text{ s}/\text{mm}^2$ ($^{\circ}\text{C}$)	341 ± 54	336 ± 6	327	339	326
T_s at $\tau = 3 \text{ s}/\text{mm}^2$ ($^{\circ}\text{C}$)	541 ± 100	496 ± 6	515	519	450
T_s at $\tau = 5 \text{ s}/\text{mm}^2$ ($^{\circ}\text{C}$)	632 ± 9	583 ± 6	607	611	517
T_b at $\tau = 1 \text{ s}/\text{mm}^2$ ($^{\circ}\text{C}$)	101 ± 14	111 ± 43	117	91	133
T_b at $\tau = 3 \text{ s}/\text{mm}^2$ ($^{\circ}\text{C}$)	240 ± 23	274 ± 43	276	265	289
T_b at $\tau = 5 \text{ s}/\text{mm}^2$ ($^{\circ}\text{C}$)	299 ± 25	302 ± 43	302	302	330

Compare data with simulation results with consideration of uncertainties

1. TG / DTG Predictions at $10^{\circ}\text{C}/\text{min}$ Heating Rate Using Estimated Kinetic Parameters

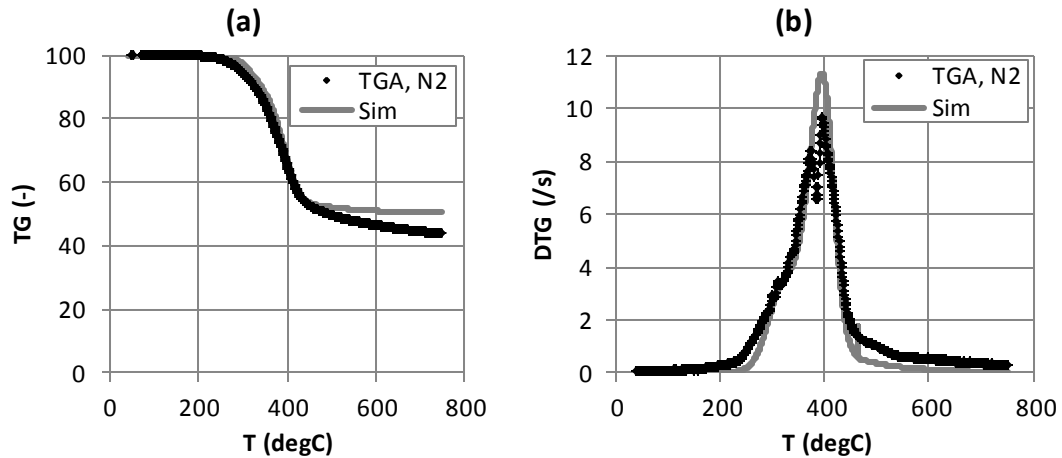


Figure A(D)-30. TG/DTG curves at 10°C/min heating rate with different estimation results for kinetic parameters for thermal decomposition of fire-retarded FRP composite: Testing of resin with additive sample (~10mg) with nitrogen purge

2. Modeling Output: Mass Loss Rate (MLR)

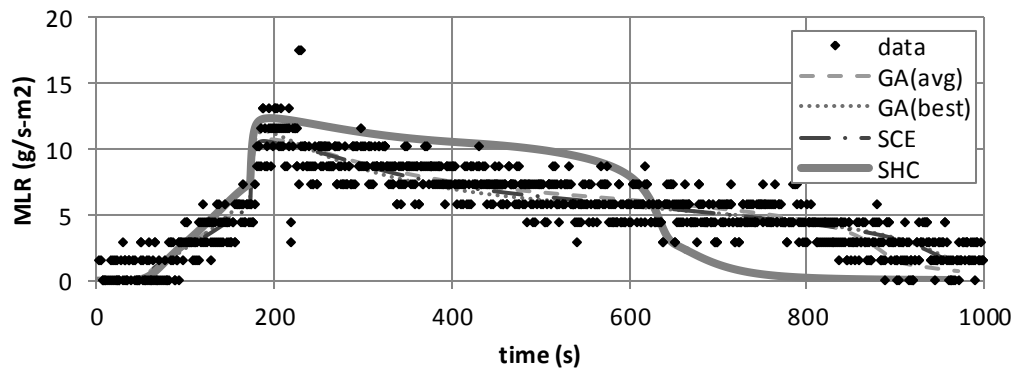


Figure A(D)-31. Mass-loss rate (MLR) comparisons for FRP composite with modified-acrylic resin with high-charring inorganic additive between actual MLR from experiment (data) and modeled MLR (GA, SCE, SHC) at applied heat flux of 50 kW/m². Note that data shown were used to estimate model-parameter values via numerical optimization using GA, SCE, or SHC routines.

3. Modeling Output: Surface Temperature (T_{surf})

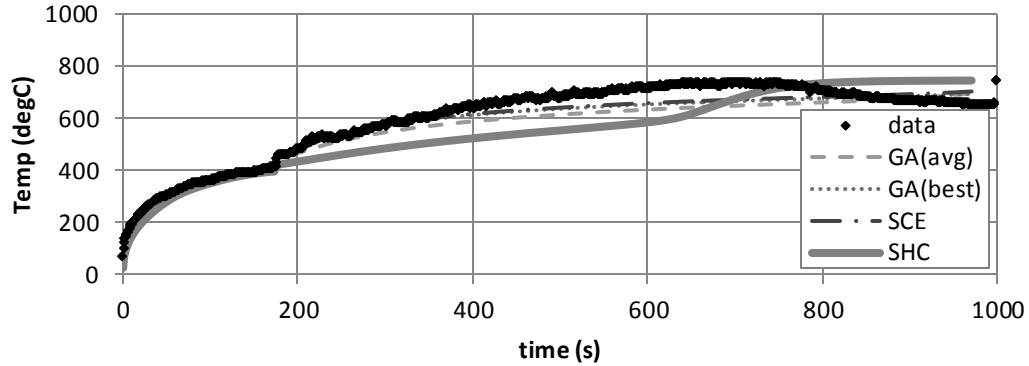


Figure A(D)-32. Surface temperature (T_{surf}) comparisons for FRP Composite with modified-acrylic resin with high-charring inorganic additive between actual T_{surf} from experiment (data) and modeled T_{surf} (GA, SCE, SHC) at applied heat flux of 50 kW/m^2 . Note that data shown were used to estimate model-parameter values via numerical optimization using GA, SCE or SHC routines.

Validate simulation quality upon extrapolation

1. Modeling Output: Mass-Loss Rate (MLR)

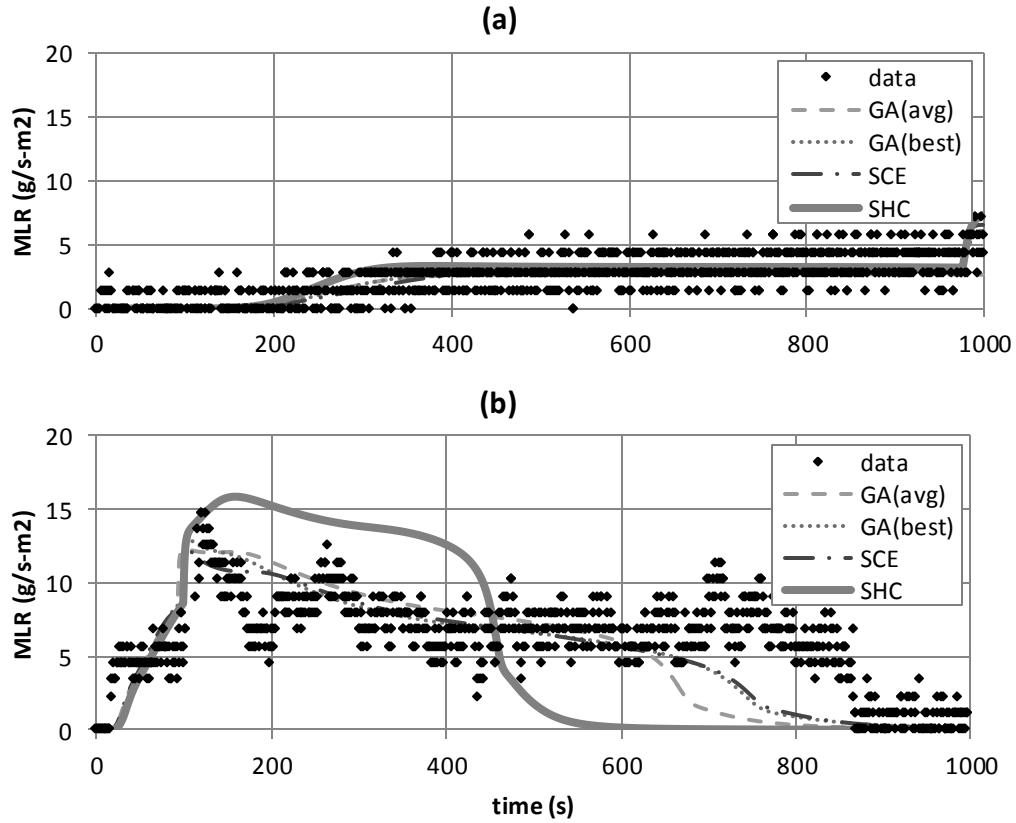


Figure A(D)-33. Mass-loss rate (MLR) comparisons for FRP composite with modified-acrylic resin with high-charring inorganic additive between actual MLR from experiment (data) and modeled MLR (GA, SCE, SHC) at applied heat flux of (a) 25 and (b) 75 kW/m². Note that data shown were not included in the model-parameter-estimation process; hence, these two cases are considered as extrapolation cases.

2. Modeling Output: Surface Temperature (T_{surf})

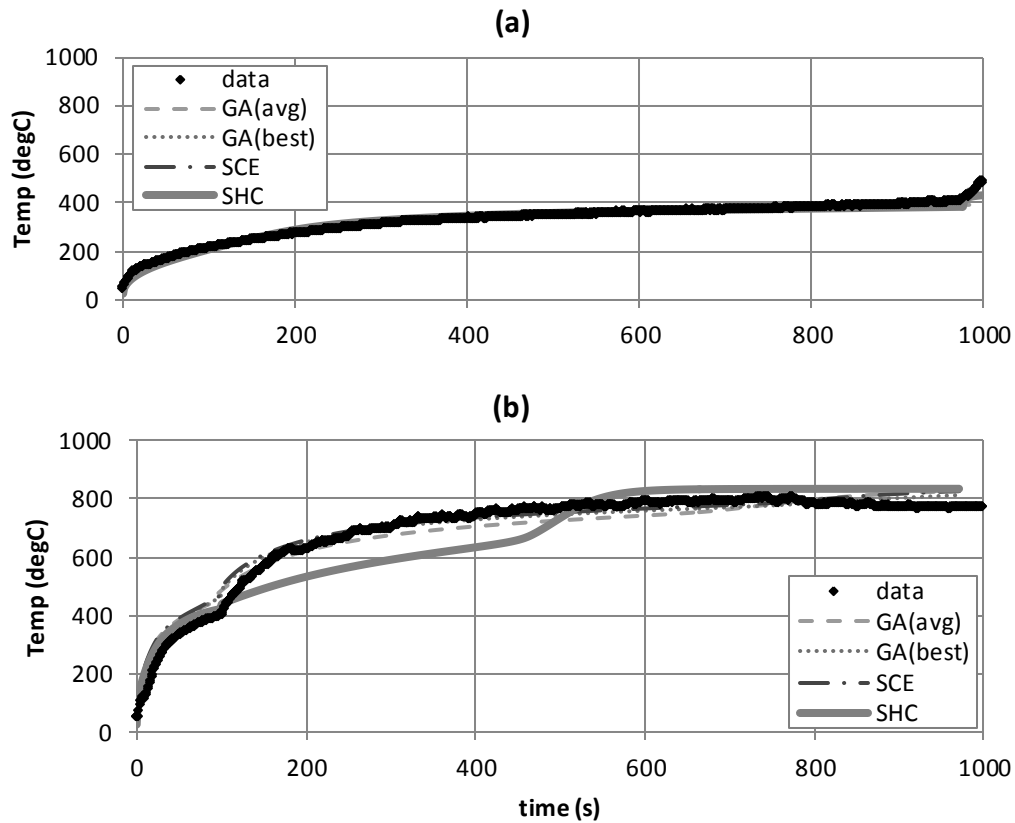


Figure A(D)-34. Surface temperature (T_{surf}) comparisons for FRP composite with modified-acrylic resin with high-charring inorganic additive between actual T_{surf} from experiment (data) and modeled T_{surf} (GA, SCE, SHC) at applied heat flux of (a) 25 and (b) 75 kW/m². Note that data shown were not included in the model-parameter-estimation process; hence, these two cases are considered as extrapolation cases.

Commentary

General Comments

- TG/DTG
 - Good agreement between simulated TG/DTG thermograms and those of actual from TGA experiment is shown when thermal decomposition kinetics is modeled using multiple heating-rate data.
 - The proposed kinetic model does not account for minor mass loss at relatively lower and higher temperature range.
- Comparison Between Data and Computed-Modeling Outputs
 - Modeled peak MLRs are all in quantitative agreement with data, considering its uncertainty.
 - Avg MLRs of modeling are in good agreement with data, except for that of SHC.
 - Modeled time-to-peak MLRs are all in quantitative agreement with data.
 - Modeled surface temperatures at earlier time ($\tau = 1 \text{ s/mm}^2$) show good agreement with data, while at later times ($\tau = 3$ and 5 s/mm^2) modeling results deviate from experiment results; however, considering that there is flame interfering with data collection from surface thermocouple, uncertainty in data should probably be larger.
 - Modeled back-surface temperatures at different times from GA(avg) show good agreement with data, considering the modeling uncertainty. Those from GA(best), SCE, and SHC are off by $\sim 10 \text{ }^\circ\text{C}$ from experiment results.
- MLR
 - Optimization at $\text{HF} = 50 \text{ kW/m}^2$: Generally good agreement exists between experiment data and all modeling results, considering the trend, except for that of SHC, indicating that optimization of SHC was close to being unsuccessful.
 - Extrapolation at $\text{HF} = 25 \text{ kW/m}^2$: Good agreement exists between experiment data and all modeling results. All of the modeling cases are able to capture the slow increase in mass-loss rate in the earlier times after exposure to heating source and a jump near 1000 s due to ignition.

- Extrapolation at $HF = 75 \text{ kW/m}^2$: Good agreement exists between experiment data and all modeling results, except for SHC case. SHC's prediction is slightly higher than data and predictions from other cases; however, considering the uncertainty in the data, this falls within the acceptable bounds.
- Surface Temperature
 - Optimization at $HF = 50 \text{ kW/m}^2$: Generally good agreement exists between experiment data and all modeling results, considering the trend, even for that of SHC. Note that after ignition (post-ignition stage) the flame interferes with data reading of thermocouple on the surface.
 - Extrapolation at $HF = 25 \text{ kW/m}^2$: Good agreement exists between experiment data and all modeling results.
 - Extrapolation at $HF = 75 \text{ kW/m}^2$: Good agreement exists between experiment data and all modeling results, except for the SHC case.

Limitation in Modeling

- When considering limitation of the parameters in modeling this fire-retarded FRP composite, the modeler should take into account the applicability of the parameters and their associated uncertainties. For example, any assumptions used when determining a parameter value via experiment direct or indirect measurements can be utilized to understand when the parameter value becomes inappropriate. For this example, most consideration can be given to the parameters related to decomposition kinetics. One should be cautious that these findings can cause this FRP composite to behave differently under changing conditions, which were not included in the parameter estimation process.
- First, the reaction-order-type kinetic model can be used to fit the DTG data with some degree of satisfaction for all reactions (see +A-R and R). However, the estimated reaction order is high as 5 for +A-R reaction. This indicates that the model is forced to fit the data, knowing that the reaction order of this magnitude is rare to find in the literature. Also, the DSC data confirms that the reaction-order-

type model was inappropriate for +A-R as well. Although the model is giving high correlation coefficients between the data and modeling for +A-R reaction, the DSC data show that +A-R should exist from 200°C and end before 400°C, where a strong endotherm is observed. When the data is fit with a reaction-order-type kinetic model, the additive decomposition temperature range extends beyond 400°C, ending near 600°C.

- Second, the decomposition of the additive reaction is best described by a kinetic model that describes a diffusion controlled reaction (Jander's type model). The model type is reasonable, considering that the model simulates the weight loss to be slow initially with respect to temperature increase and decays relatively fast after the weight-loss rate peak. This modeling becomes suitable for an additive decomposing within a resin-polymer system resulting in a time delay due to the time necessary to degrade the polymer near the additive. Consider the additive being mixed within the resin polymer. For the additive to undergo a decomposition reaction, the degradation of the resin polymer should occur simultaneously, because the additive is aggregated within the resin. Having the additive decomposition temperature lower than that of the resin, the decomposition of the additive is delayed until the temperature is higher to allow the resin to decompose. When this model is actually applied, it provides a good estimate of the slow weight loss at the initial stage near 200°C and the temperature range for the entire reaction. Additionally, when this model is used, the modeling results for weight-loss rate after 300°C matches well with the actual DTG data together with R reaction described with a reaction-order-type kinetic model.
- Third, although kinetic modeling has been conducted to give best fitness between the modeling and the DTG data obtained over various heating rates (5 to 60°C/min), assuming that the kinetics are identical irrespective of heating rates, changes in the kinetic over four heating rates have been noticed. At lower heating rates, the portion of the sample weight consumed via MA_residue oxidation increases, where at higher heating rates it decreases. This can be explained by understanding that the MA_residue oxidation reaction is controlled by oxygen

diffusion from the ambient to the condense phase. At a low heating rate, more time is available for oxygen diffusion with respect to temperature change, allowing an increase in the weight loss due to oxidation. However, when the heating rate is higher, the conditions become the opposite, and pyrolysis reaction (R) dominates. The fitness of the model to DTG data increases when this effect is accounted for in the modeling.

EXAMPLE 5.4 MODELING PLYWOOD

An example case is shown for a non-fire retarded Douglas Fir plywood. Thermal decomposition is modeled with two-step reactions – water loss and decomposition of dry plywood to char. Note that for this example, one approach will be used to estimate model parameters – a combination of non-optimization and manual optimization methods.

Measure Parameters

When conducting parameter estimation via independent experiments, consider the following:

- Check consistency between model used in experiment analysis to determine parameter in measurement process and pyrolysis model to mathematically describe the parameter of interest.
- Use statistical approach for determining uncertainty; otherwise, meet equivalency to this requirement.

1. Density

Although plywood has a laminate structure, this material is considered as a homogeneous single-layer material. Bulk density of the virgin fuel material is measured by experiment conducted at room temperature ($\approx 298\text{K}$), weighing sample's mass, and dividing mass with sample volume, which is $540 \pm 10 \text{ kg/m}^3$.

$$\rho_{\text{wet plywood}} = 540 \text{ kg/m}^3$$

Density of water was found from literature:³¹

$$\rho_{\text{water}} = 1000 \text{ kg/m}^3$$

Based on TGA experiment, moisture content of wet plywood is estimated as 7% by weight. This information is used to estimate density of dry plywood, which is 504 kg/m^3 .

$$\rho_{\text{dry plywood}} = 504 \text{ kg/m}^3$$

Also estimated based on TGA experiment, the weight loss due to thermal decomposition of dry plywood to char is 67%, resulting in:

$$\rho_{\text{char}} = 173 \text{ kg/m}^3$$

2. Thermal Conductivity

Thermal conductivity of water was found from literature:³¹

$$k_{\text{water}} = 0.6 \text{ W/m-K}$$

Thermal conductivity of dry plywood and char were estimated via manual optimization, but with its initial guess based on measurement at 20°C (ASTM C518/E1225):

$$k_{\text{initial guess}} = 0.122 \text{ W/m-K}$$

3. Specific-heat Capacity

Specific-heat capacity of water was found from literature³¹:

$$c_{p \text{ water}} = 4200 \text{ J/kg-K}$$

Specific-heat capacity of dry plywood and char were estimated via manual optimization, but with its initial guess based on measurement at 20°C (ASTM E1269):

$$c_{p \text{ initial guess}} = 1200 \text{ J/kg-K}$$

4. Absorption Coefficient

For simplification, solid-phase species involved in modeling are considered as an opaque material. Therefore, the absorption coefficient is essentially infinity.

$$K \rightarrow \infty$$

5. Emissivity

Emissivity of water and char are approximated as 1. Emissivity of dry plywood is measured using ASTM E903:

$$\epsilon_{\text{dry wood}} = 0.891 \pm 0.018$$

6. Reaction Order, Pre-exponential Factor, and Activation Energy

This example case is determined to have decomposition kinetics type 3 (two major peaks in DTG over entire mass-loss temperature range) according to TGA experiment conducted in nitrogen atmosphere. Based on this information, kinetic parameters will be obtained via the model-fitting method with four iso-heating rate TGA data conducted in air atmosphere.

7. Heat of Reaction

Heat-of-reaction for water loss is measured using DSC:

$$\Delta H_{\text{water loss}} = 2500 \pm 800$$

Heat-of-reaction for decomposition of dry plywood to char is not measured; will be obtained via manual optimization.

Summary

Among seven categories of parameters, most have been obtained via direct measurement, which are shaded in Table A(D)-15. The rest of the unknown parameters, a **total of five parameters**, should be obtained via numerical optimization in pair with pyrolysis modeling using bench-scale experiment data or equivalent.

Table A(D)-15. Summary of necessary model parameters for simulating pyrolysis of plywood

	No	Condense Phase		
		<i>i=1, water</i>	<i>i=2, dry_plywood</i>	<i>i=3, char</i>
Material Property	1	ρ_1	ρ_2	ρ_3
	2	k_1	k_2	k_3
	3	c_1	c_2	c_3
	4	κ_1	κ_2	κ_3
Parameters for Specifying Conditions	5	ε_1	ε_2	ε_3
		Heterogeneous RxN		
		<i>k = 1, water loss</i>		<i>k = 2, wood decomposition</i>
Kinetic Parameters and Heats assuming n^{th} order model and Arrhenius-type expression	6	n_1		n_2
		Z_1		Z_2
		E_1		E_2
	7	ΔH_1		ΔH_2

Obtain Parameters via Numerical Optimization

Run Model in Pair with Numerical Optimization

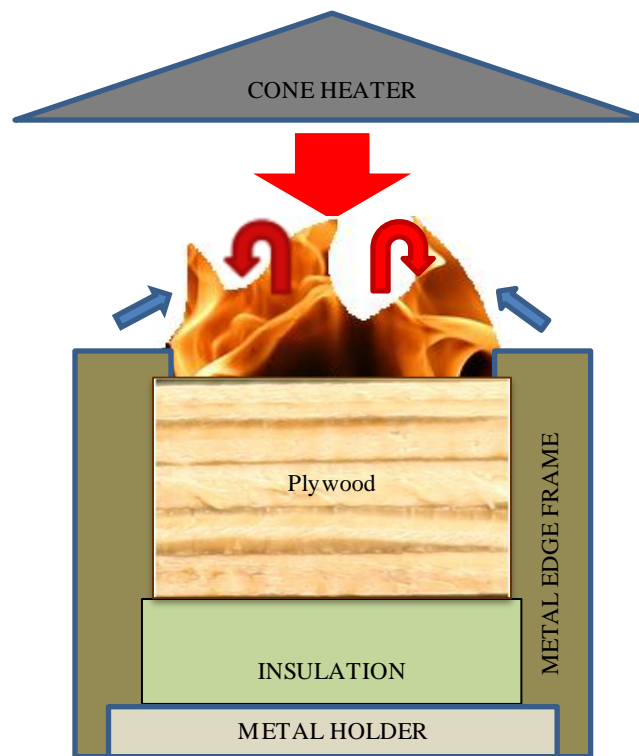


Figure A(D)-35. Simplified representation of a cone calorimeter test of plywood

Select model: GPYRO

Understand bench-scale experiment set-up for modeling simple cases

A simplified representation of a cone calorimeter test of FRP composite is shown in Figure A(D)-35. The sample is placed on top of an insulation, which sits on a metal holder. Another metal frame is placed on top of the sample, insulation, and the holder. A metal edge frame is used as well.

Configure model conditions based on understanding of experiment set-up

In the model, the phenomena discussed above are simulated as below. Basic assumptions are as follows:

- Instantaneous release of volatiles from solid to the gas phase
- Local thermal equilibrium between the solid and the volatiles
- No condensation of gaseous products
- No porosity effects

Further details can be found from the *Technical Reference*⁶ and *User's Guide*⁷ of GPYRO (<http://code.google.com/p/gpyro>).

When conducting the GPYRO simulation for the cone calorimeter set-up, the metal edge frame will be ignored and backing is insulated. The ignition phenomenon is interpreted as the following in the simulations: at a known time-of-ignition (from experiment data), additional heat flux of 20 kW/m² is applied to the surface to simulate heat flux from the flame. This value is estimated from a measurement from this material pyrolyzing in the cone with a total-heat-flux gauge measuring heat flux impinging on the sample surface. Figure A(D)-36 shows the total-heat-flux measurement from sample surface (test conducted at 50 kW/m² applied heat flux). From the time-of-ignition ($\tau \sim 0.1$ s/mm²) an increase above the 50 kW/m² line in measured heat flux is observed due to flame. The oscillation in data in the time interval of ignition to $\tau = 1$ s/mm² is an artifact due to water evaporation, which had condensed near the water-cooled heat-flux gauge.

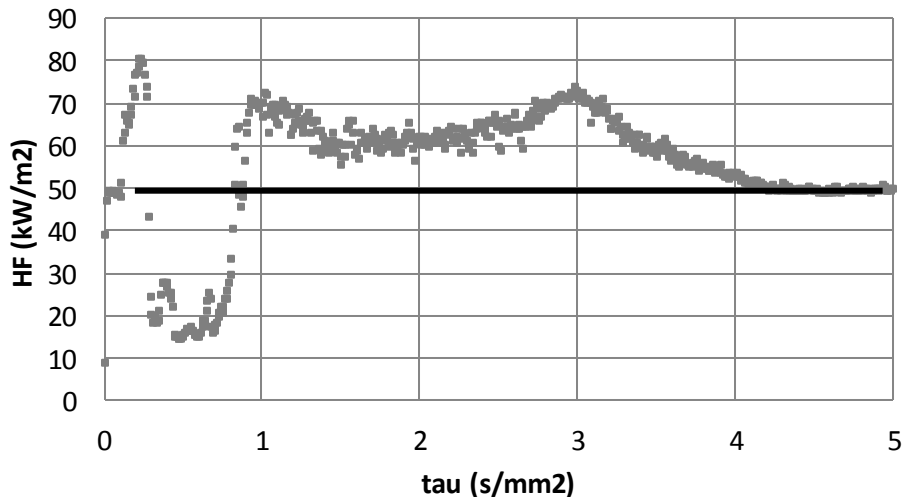


Figure A(D)-36. Total heat flux measured from plywood surface during cone calorimeter test at external-heat-flux level of 50kW/m²: Ignition occurs before $\tau = 1$ s/mm² and from this point additional heat flux impinges on the surface due to the flame

For the back surface, an additional layer of insulation with known properties is modeled to simulate some heat loss through the back. The contact resistance (hcrz) between the FRP composite and the insulation is estimated as roughly 10 W/m²K and that of insulation layer and ambient as 1 W/m²K.

In addition to the parameters introduced in previous section (see Parameter Estimation Results), the model (GPYRO) has a coefficient (γ , GAMMA) that is used to model radiative heat transfer through the pores. This parameter with T3 is a model-dependent parameter that is added as another term in the effective thermal conductivity. γ is used for porous fiberglass and decomposed solid species, which results in a more porous state due to the weight loss; therefore, more radiative heat transfer through the gas-phase pores, i.e., for condense phase specie $i = 2$ (char).

Therefore, the **total unknown parameters** of five now becomes **six** including γ .

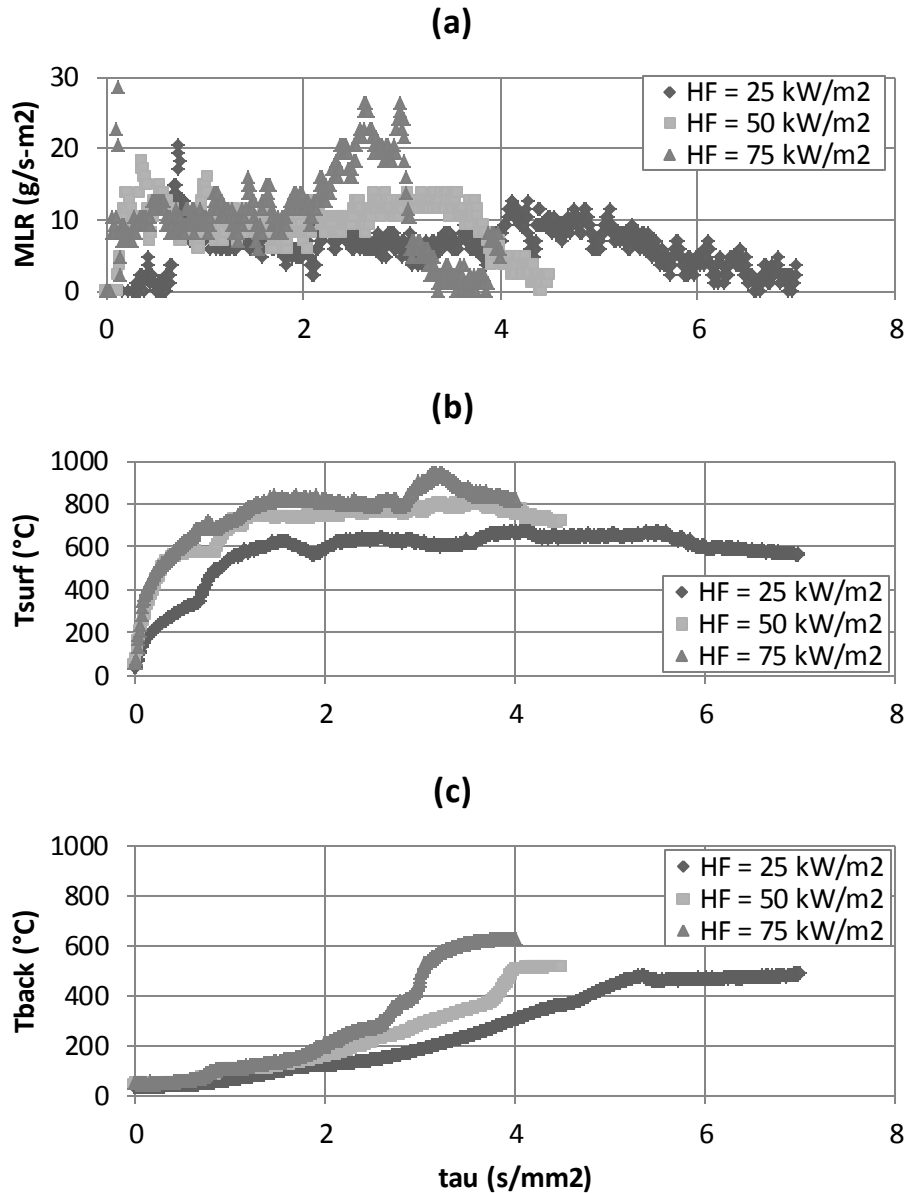


Figure A(D)-37. Cone calorimeter (cone) test data of plywood (thickness, δ is 11.1 ± 0.1 mm, density, ρ is 540 ± 10 kg/m³) impinged with effective heat fluxes (EHF) of 25 to 75 kW/m²

3. Check data reproducibility by repeating identical experiments

Data is acquired from two repeating cone tests of plywood under 50 kW/m² heat-flux level. Uncertainty analysis will be performed later.

Select numerical optimization routine

- Manual optimization
- See Chapter 5 for more description of each optimization routine.

Conduct numerical optimization in pair with simulations using experiment data as targets

Numerous simulations with a simplified version of GPYRO have been used in pair with manual optimization to obtain unknown parameters. Experiment data of mass-loss rate (MLR), surface-temperature measurements (T_s), and back-surface temperature measurements (T_b) generated with various applied heat-flux levels between 25 and 75 kW/m² have been used in the optimization process as targets (i.e., optimization is conducted for unknown parameters to match modeling outputs of interest to certain experiment data).

Obtain Confidence Intervals for Optimized Parameters

For this example case, where manual optimization is used, confidence intervals are approximated as $\pm 10\%$ for each optimized parameter.

Parameter Estimation Results

Parameter		Unit	Comparable Non-optimization and Manual Optimization		
Thermo-physical Property	i = 1 (water)	ρ_i	kg/m ³	1000 Reference ³¹	
		k_i	W/m-K	0.6 Reference ³¹	
		c_i	J/kg-K	4200 Reference ³¹	
	i = 2 (dry_wood)	ρ_i	kg/m ³	504 ± 10 Measurement	
		k_i	W/m-K	0.26 Manual Optimization with Initial Guess of 0.122 measured at 20 °C (dry_wood, ASTM C518/E1225)	
		c_i	J/kg-K	2400 Manual Optimization with Initial Guess of 1200 measured at 20 °C (dry_wood, ASTM E1269)	
	i = 3 (char)	ρ_i	kg/m ³	173 Measurement	
		k_i	W/m-K	0.12 Manual Optimization with Initial Guess of 0.122 measured at 20 °C (dry_wood, ASTM C518/E1225)	
		c_i	J/kg-K	3700 Manual Optimization with Initial Guess of 1200 measured at 20 °C (dry_wood, ASTM E1269)	
	Optical Property	i = 1 (water)	ε_i	-	1.00 Approximated
			i = 2 (dry_wood)	κ_i	/m
		ε_i		-	0.891 ± 0.018 Measurement, ASTM E903
i = 3 (char)		κ_i	/m	10 ⁶ Approximated as opaque	
		ε_i	-	1.00 Approximated	
an		k = 1	n_k	-	5.0

	water → vap↑	Z_k	/s	2.5×10^{12}	Multiple Heating Rate TGA Data
		E_k	J/mol	83×10^4	
		ΔH_k	kJ/kg	2500 ± 800 (30%) Measurement, DSC	
	k = 2 dry_wood → char + vap↑	n_k	-	1.7	Model Fitting with Multiple Heating Rate TGA Data
		Z_k	/s	5.0×10^{16}	
		E_k	J/mol	2.10×10^5	
		ΔH_k	kJ/kg	631 Manual Optimization	
	Model Dependent Parameter	Υ (i=3)	m	0.0036 Manual Optimization	

Validation

Analyze Simulation Quality

Identify sensitive parameters for model inputs

- $\varepsilon_i, \rho_{i=2}, \Delta H_k$
- Kinetic parameters are considered to be certain in this example case

Determine data and model output uncertainty to make comparison^{ix}

1. Conduct uncertainty analysis of data: Data is acquired from two repeating cone tests of plywood under 50 kW/m² heat-flux level.
2. The uncertainties in the MLR and thermocouple measurements on the front surface were quantified by comparing data from these two identical FRP composite tests. Note that the effect of different sample thicknesses was considered to be negligible, for sample thicknesses in two tests were 11.1 and 11.2 mm. Because the data is transient, the standard deviation at each time step was calculated. Then these are averaged and multiplied by 2 to estimate uncertainty: uncertainty in MLR, T_s and T_b are ± 3.4g/sm², ± 54 °C and ± 27 °C, respectively.
3. Assume:

^{ix}Data uncertainty is accounted for here because this is required to determine the goodness of near-optimal parameter sets. Optimization targets (experiment data) should be considered with its uncertainty bounds to decide how good the match is between the targets and optimum simulations with its uncertainty.

- a. Uncertainties are comparable to the same sample tested at various heat flux levels
 - b. Data set found above is close to the averaged curves from multiple identical tests under same conditions
4. Conduct uncertainty analysis of model outputs of interest – MLR and T_s
- Baseline case: $HF = 50 \text{ kW/m}^2$, thickness = 8.7 mm.
 - Sensitive parameters – density of dry_wood and char, emissivity of water, dry_wood and char, heat-of-reaction for drying process and thermal decomposition of dry_wood to char – varied one at a time from baseline to its max and min: $\pm 10\%$ of estimated value or uncertainty limits found from measurement experiment. Results are shown in Table A(D)-16.
 - Kinetic parameters are considered to be certain in this example.
 - Integration of uncertainty is calculated by the Law of Propagation of Uncertainty: uncertainty in model's MLR, T_s and T_b are $\pm 7.2 \text{ g/sm}^2$, $\pm 57 \text{ }^\circ\text{C}$ and $\pm 157 \text{ }^\circ\text{C}$ respectively.

Table A(D)-16. Comparison between experiment data from cone calorimeter test and modeling outputs using estimated parameter values via measurements and manual optimization

	Data (Based on 2 tests, uncertainty as 2 times standard deviation)	Measurements and Manual Optimization
Peak MLR (g/m ² s)	19.9 ± 4.8	18.1 ± 7.2
Avg MLR (g/m ² s)	6.8 ± 0.5	6.6 ± 7.2
t to pMLR (s)	81 ± 113	23
T_s at 100 s (°C)	604 ± 112	628 ± 57
T_s at 200 s (°C)	734 ± 10	670 ± 57
T_s at 300 s (°C)	732 ± 45	689 ± 57
T_b at 100 s (°C)	68 ± 20	56 ± 157
T_b at 200 s (°C)	118 ± 1	185 ± 157
T_b at 300 s (°C)	196 ± 10	291 ± 157

Compare data with simulation results with consideration of uncertainties

1. TG / DTG Predictions at 20 °C/min Heating Rate Using Estimated Kinetic Parameters

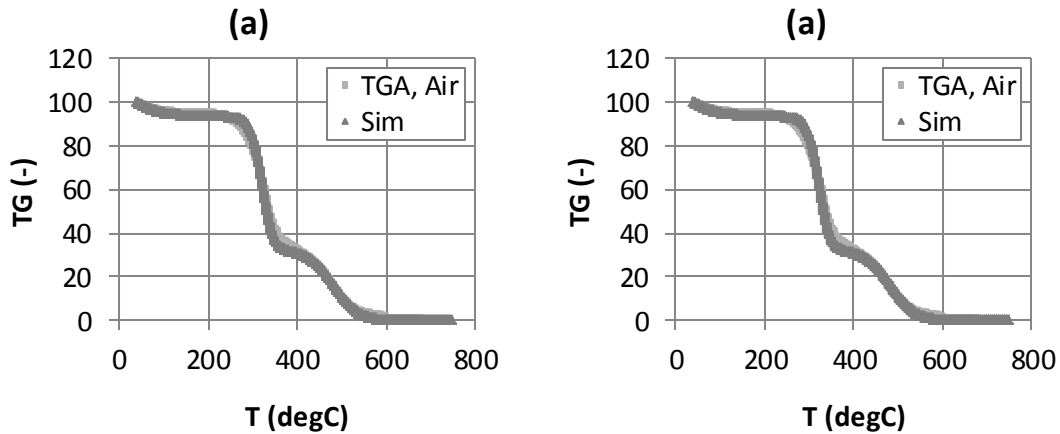


Figure A(D)-38. TG/DTG curves at 20°C/min heating rate with different estimation results for kinetic parameters for thermal decomposition of plywood: testing of plywood sample (~10mg) with air purge

2. Modeling Output: Mass Loss Rate (MLR)

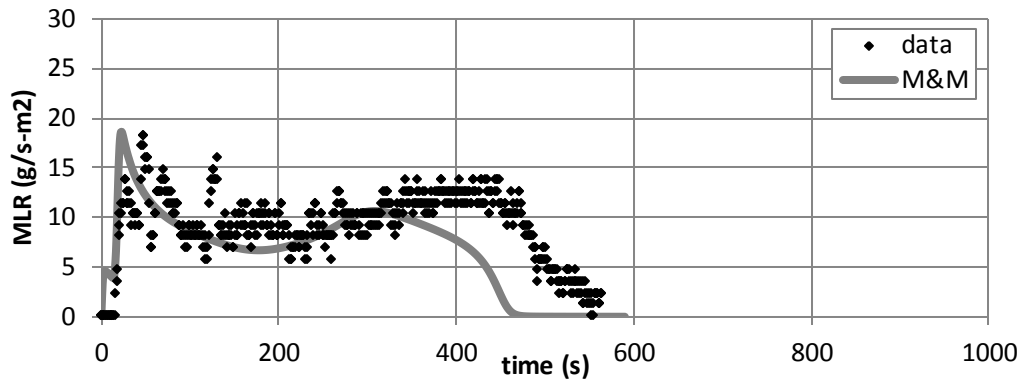


Figure A(D)-39. Mass-loss rate (MLR) comparisons for FRP composite with plywood between actual MLR from experiment (data) and modeled MLR (M&M) at applied heat flux of 50 kW/m². Note that data shown were used to estimate model parameter values via manual optimization.

3. Modeling Output: Surface Temperature (T_{surf})

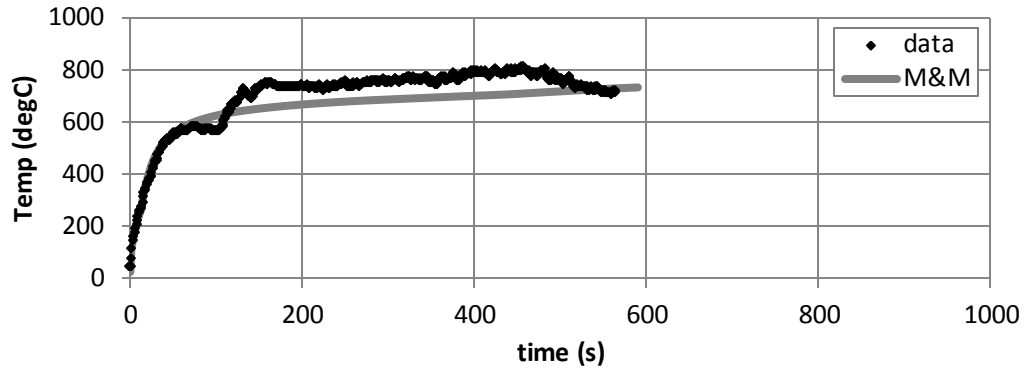


Figure A(D)-40. Surface-temperature (T_{surf}) comparisons for plywood between actual T_{surf} from experiment (data) and modeled T_{surf} (M&M) at applied heat flux of 50 kW/m^2 . Note that data shown were used to estimate model-parameter values via manual optimization.

4. Modeling Output: Back-surface Temperature (T_{back})

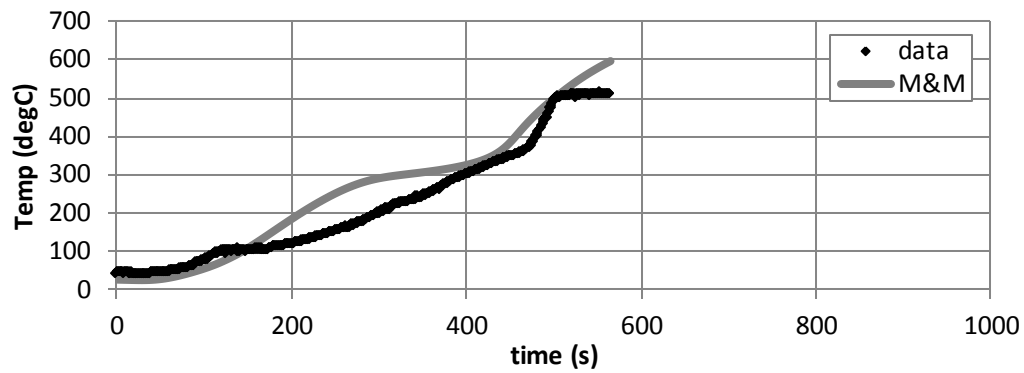


Figure A(D)- 41. Back-surface temperature (T_{back}) comparisons for plywood between actual T_{back} from experiment (data) and modeled T_{back} (M&M) at applied heat flux of 50 kW/m^2 . Note that data shown were used to estimate model-parameter values via manual optimization.

Validate simulation quality upon extrapolation

1. Modeling Output: Mass-Loss Rate (MLR)

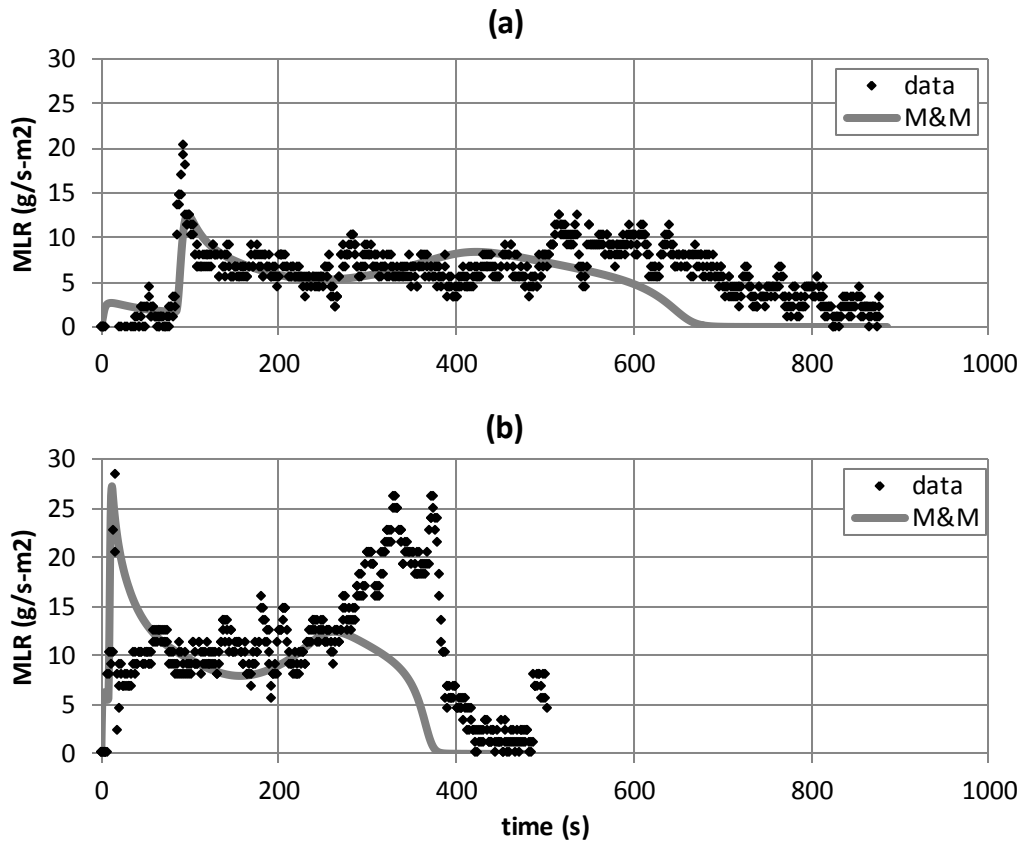


Figure A(D)-42. Mass-loss rate (MLR) comparisons for FRP composite with plywood between actual MLR from experiment (data) and modeled MLR (M&M) at applied heat flux of (a) 25 and (b) 75 kW/m². Note that data shown were not included in the model-parameter-estimation process; hence, these two cases are considered as extrapolation cases.

2. Modeling Output: Surface Temperature (T_{surf})

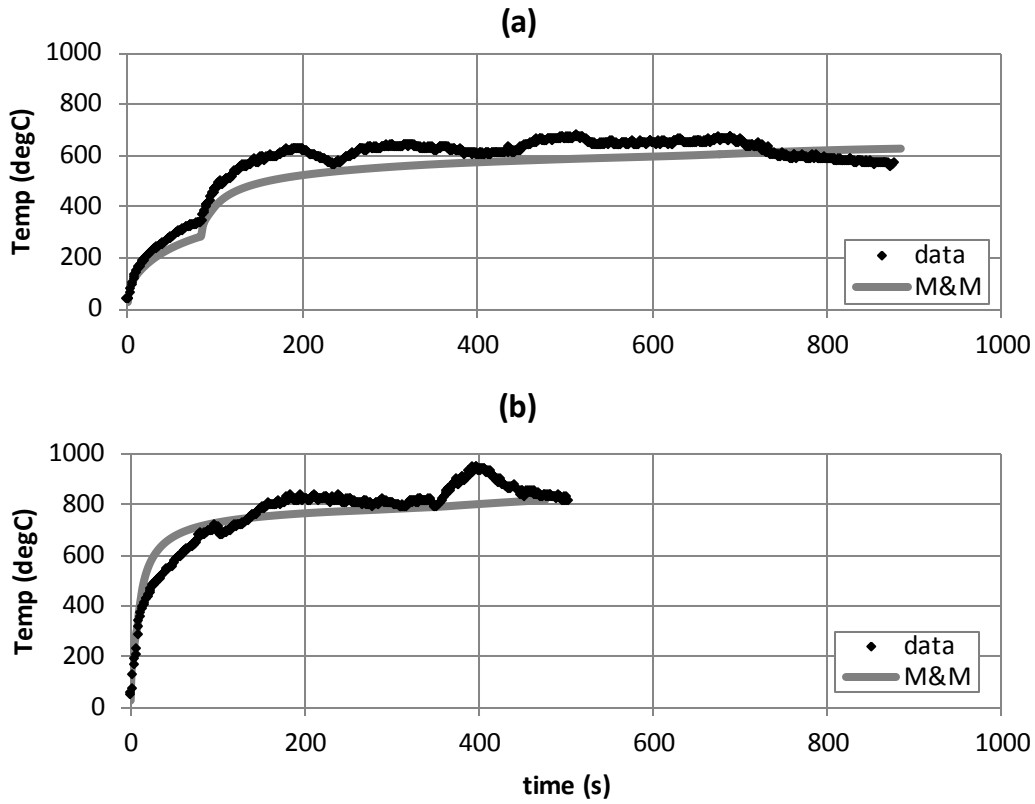
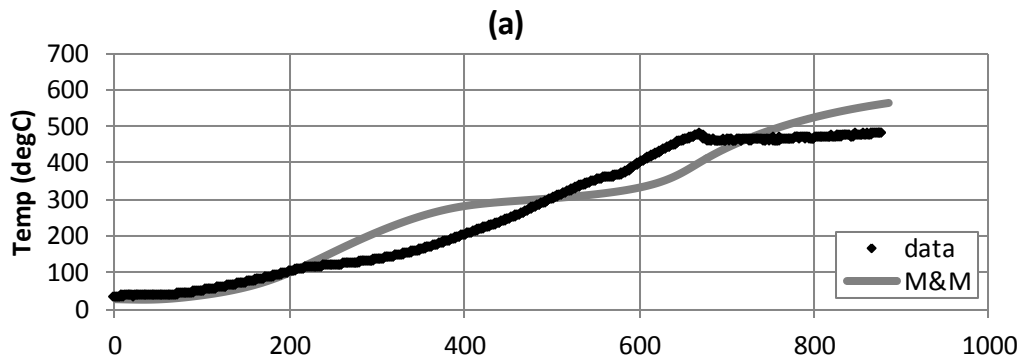


Figure A(D)-43. Surface-temperature (T_{surf}) comparisons for FRP composite with plywood between actual T_{surf} from experiment (data) and modeled T_{surf} (M&M) at applied heat flux of (a) 25 and (b) 75 kW/m². Note that data shown were not included in the model-parameter-estimation process; hence, these two cases are considered as extrapolation cases.

3. Modeling Output: Back-surface Temperature (T_{back})



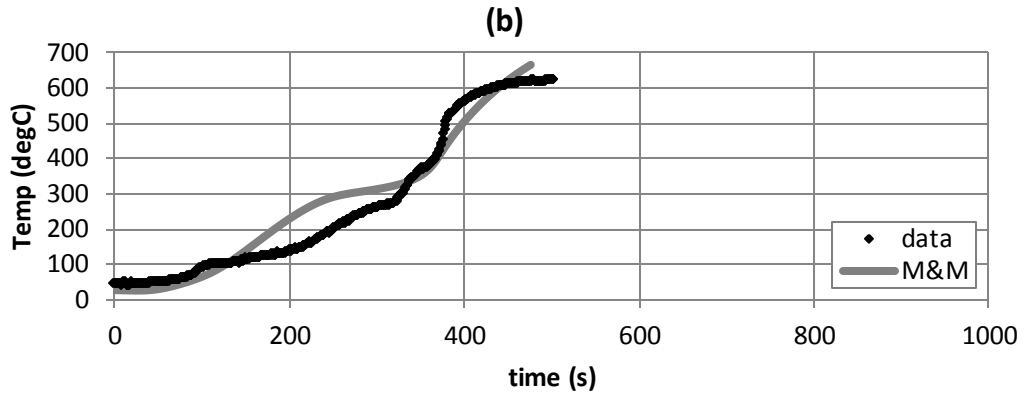


Figure A(D)-44. Back-surface temperature (T_{back}) comparisons for plywood between actual T_{back} from experiment (data) and modeled T_{back} (M&M) at applied heat flux of (a) 25 and (b) 75 kW/m^2 . Note that data shown were not included in the model-parameter-estimation process; hence, these two cases are considered as extrapolation cases.

Commentary

General Comments

- TG/DTG
 - Good agreement between simulated TG/DTG thermograms and those of actual from TGA experiment is shown when thermal decomposition kinetics is modeled using multiple heating rate data.
 - Proposed kinetic model does not account for mass loss due to char oxidation at relatively higher temperature range ($T > 400^{\circ}\text{C}$).
- Comparison Between Data and Computed Modeling Outputs
 - Modeled peak MLR, Avg MLR, time-to-peak MLR, and T_s , and T_b at various times are all in quantitative agreement with data, considering its uncertainty.
- MLR
 - Optimization at $\text{HF} = 50 \text{ kW/m}^2$: Generally good agreement exists between experiment data and all modeling results, considering the trend. Some deviation of modeling results from data is shown at later times, where the second peak is observed in the MLR curve. Near this region, bending of the sample toward the front surface occurs with respect to a rapid temperature increase throughout the back surface. This phenomenon is strictly a 3D behavior, which is not explicitly accounted for in current 1D model. Additionally, mass loss due to minor char oxidation at this region is speculated, for flame height becomes smaller and bending of sample may allow more oxygen to diffuse to the solid phase.
 - Extrapolation at $\text{HF} = 25 \text{ kW/m}^2$: Good agreement exists between experiment data and modeling results. Modeling is able to capture the initial mass-loss-rate peak followed by a decrease qualitatively and quantitatively. A qualitative agreement between data and modeling results exists for the second mass-loss-rate peak; however, actual sample in cone testing extends for a longer period of time ($\sim 100 \text{ s}$), while in modeling burnout time occurs earlier. This is probably due to excluding char oxidation in kinetic modeling.

- Extrapolation at $HF = 75 \text{ kW/m}^2$: Good agreement exists between experiment data and modeling results, except for the second peak in mass-loss-rate curve. See above for discussion.
- Surface Temperature
 - Optimization at $HF = 50 \text{ kW/m}^2$: Generally good agreement exists between experiment data and modeling results, considering the trend. Note that after ignition (post-ignition stage) the flame interferes with data reading of the thermocouple on surface.
 - Extrapolation at $HF = 25 \text{ kW/m}^2$: Good agreement exists between experiment data and modeling results.
 - Extrapolation at $HF = 75 \text{ kW/m}^2$: Good agreement exists between experiment data and modeling results.

Limitation in Modeling

- When considering limitation of the parameters in modeling this plywood, the modeler should take into account the applicability of the parameters and their associated uncertainties. For example, any assumptions used when determining a parameter value via experiment direct or indirect measurements can be utilized to understand when the parameter value becomes inappropriate. For this example, most consideration can be given to the parameters related to decomposition kinetics. One should be cautious that these findings can cause this FRP composite to behave differently under changing conditions, which were not included in the parameter estimation process.
- In this example, drying is simplified as a heterogeneous reaction (i.e., an Arrhenius Law temperature dependence evaporation rate), which occurs near 100°C , based on TGA experiment results. However, water evaporation from a wet wood is governed by transport phenomena of liquid-phase water and vapor diffusion. Additionally, typically the water travels toward the back surface during heating and re-condensation may occur, allowing the back surface to be colder. This phenomenon will not be captured in this modeling.

- Any char oxidation has been considered to be minimal in this example, considering that with a flame sheet on the material surface oxygen diffusion becomes limited. However, when analyzing the cone calorimeter results, some oxidation is speculated, for the sample loses ~4 to 6% more of the initial sample weight comparing to TGA experiment.

REFERENCES

- ¹ Stoliarov, Stanislav I.; Crowley, Sean; Lyon, Richard E.; and Linteris, Gregory T., Prediction of the burning rates of non-charring polymers, *Combustion and Flame*, Volume 156, Issue 5, May 2009, 1068-1083, ISSN 0010-2180, DOI: 10.1016/j.combustflame.2008.11.010.
- ² Lobo, H. and Cohen, C., (1990), Measurement of thermal conductivity of polymer melts by the line-source method. *Polym Eng Sci*, 30: 65–70. doi: 10.1002/pen.760300202.
- ³ Brandrup, J. Immergut, E.H.; Grulke, E.A.; Abe, A.; and Bloch, D.R. (Eds.), *Polymer Handbook*, fourth ed., John Wiley & Sons, New York, 1999.
- ⁴ Stoliarov, S.I.; and Walters, R.N., “Determination of the Heats of Gasification of Polymers Using Differential Scanning Calorimetry,” *Polymer Degradation and Stability*, Vol. 93, 2008, 422-427.
- ⁵ Brandrup, J.; Immergut, E.H.; Grulke, E.A.; Abe, A.; Bloch, D.R., (Eds.), *Polymer Handbook*. 4th ed. New York: John Wiley and Sons, 1999.
- ⁶ Lautenberger, C., Gpyro, A Generalized Pyrolysis Model for Combustible Solids, Technical Reference, Version 0.700, February 19, 2009.
- ⁷ Lautenberger, C., Gpyro, A Generalized Pyrolysis Model for Combustible Solids, Users’ Guide, Version 0.700, February 19, 2009.
- ⁸ Beaulieu, P.A.; and Dembsey, N.A., “Effect of Oxygen on Flame Heat Flux in Horizontal and Vertical Orientations”, *Fire Safety Journal*, 43:6 (2008), 410-428. [DOI10.1016/j.firesaf.2007.11.008].
- ⁹ ASTM Standard D 7309-07, Test Method for Determining Flammability Characteristics of Plastics and Other Solid Materials Using Microscale Combustion Calorimetry, ASTM International, West Conshohocken, PA, 2007.
- ¹⁰ Brandrup, J. Immergut, E.H.; Grulke, E.A.; Abe, A.; and Bloch, D.R., (Eds.), *Polymer Handbook*, fourth ed., John Wiley & Sons, New York, 1999.
- ¹¹ Kashiwagi, T.; and Ohlemiller, T.J., “A study of oxygen effects on nonflaming transient gasification of PMMA and PE during thermal irradiation,” *Proceedings of the Combustion Institute* 19: 815–823 (1982).
- ¹² Kashiwagi T., Polymer combustion and flammability—role of the condensed phase. *Twenty-fifth Symposium (International) on Combustion*, Irvine, CA, 1994; 1423–1437.
- ¹³ Matala, A., “Estimation of Solid Phase Reaction Parameters for Fire Simulation,” MS Thesis, University of Technology, Helsinki, 2008.
- ¹⁴ Chaos, Marcos; Khan, M.; Krishnamoorthy, N.; Chatterjee, P.; Wang, Y.; and Dorofeev, S., Experiments and Modeling of Single- and Triple-Wall Corrugated Cardboard: Effective Material Properties and Fire Behavior, In: *Fire and Materials 2011*, 12th International Conference and Exhibition, 31st January – 2nd February 2011, Fisherman’s Wharf, San Francisco, USA
- ¹⁵ Chaos, M.; Khan, M.M.; Krishnamoorthy, N.; de Ris, J.L.; and Dorofeev, S.B., Bench-Scale Flammability Experiments: Determination of Material Properties Using Pyrolysis Models for Use in CFD Fire Simulations. In: *Interflam 2010*, July 5-7, 2010, Nottingham, UK.
- ¹⁶ ASTM E 2058, 2009, Standard Test Methods for Measurement of Synthetic Polymer Material Flammability Using a Fire Propagation Apparatus (FPA), ASTM International, West Conshohocken, PA, 2009, DOI: 10.1520/E2058-09, www.astm.org
- ¹⁷ Khan, M.M.; de Ris, J.L.; and Ogden, S.D., 2009, Effect of Moisture on Ignition Time of Cellulosic Materials, *Fire Safety Science* 9, 167-178.
- ¹⁸ de Ris, J.L.; and Khan, M.M., 2000, A Sample Holder for Determining Material Properties, *Fire and Materials* 24, 219-226.

-
- ¹⁹ Bates, D.M. & Watts, D.G., 2007. *Nonlinear Regression Analysis and Its Applications*, New York: John Wiley and Sons.
- ²⁰ Stoliarov, S. I.; Safronava, N.; and Lyon, R. E. (2009), The effect of variation in polymer properties on the rate of burning. *Fire and Materials*, 33: 257–271. doi: 10.1002/fam.1003.
- ²¹ Chaos, M.; Khan, M.M.; Krishnamoorthy, N.; de Ris, J.L.; and Dorofeev, S.B., Material Properties for CFD Fire Models, FM Global Open Source CFD Fire Modeling Workshop 2010, <http://docs.google.com/viewer?a=v&pid=sites&srcid=ZGVmYXVsdGRvbWFpbnxmaXJlbW9kZWxpbmd3b3Jrc2hvcHxneDo0NGE0YTlkOWQ3OGUzYWQw>.
- ²² Kim, E.; Dembsey, N.A.; and Dore, C.H., "Property Estimation for Pyrolysis Modeling Applied to Flame Retarded Modified Acrylic FRP Composites", in *Proceedings of Composites & Polycon 2010*, American Composites Manufacturers Association, Mandalay Bay, Las Vegas, NV, USA, February 9-11, 2010, *Best Fire Technical Paper Award at Composites and Polycon 2010*.
- ²³ Kulshreshtha, Anand K.; and Vasile, Cornelia, Handbook of polymer blends and composites, Rapra Technology Limited, c 2002.
- ²⁴ Lewin, M., Synergism and Catalysis in Flame Retardancy of Polymers, *Polym. Adv. Technol.* 12, 215-222 (2001).
- ²⁵ LeVan, S.L., The Chemistry of Solid Wood; Chapter 14, Chemistry of Fire Retardancy, American Chemical Society, 1984.
- ²⁶ Standard Test Method for Surface Burning Characteristics of Building Materials, ASTM E 84-05, ASTM, 100 Barr Harbor Drive, West Conshohocken, PA, U.S.
- ²⁷ Lautenberger, C., "A Generalized Pyrolysis Model for Combustible Solids", Ph.D. Dissertation, Department of Mechanical Engineering, University of California, Berkeley, Fall 2007.
- ²⁸ Cacuci, Dan G.; Ionescu-Bujor, Mihaela; and Navon, Ionel Micheal, *Sensitivity and Uncertainty Analysis; Theory; Volume 1*, Chapman & Hall / CRC Taylor & Francis Group, c 2005.
- ²⁹ Cacuci, Dan G.; Ionescu-Bujor, Michael; and Micheal Navon, Ionel, *Sensitivity and Uncertainty Analysis; Applications to Large-Scale Systems; Volume 2*, Chapman & Hall / CRC Taylor & Francis Group, c 2005.
- ³⁰ Saltelli, A.; Chan, K.; and Scott, E.M., *Sensitivity Analysis*, Wiley, c 2000.
- ³¹ NIST Chemistry WebBook, <http://webbook.nist.gov/>.

Appendix E - Chapter 5 Supplement: Morris' OAT Method

Morris' one-at-a-time (OAT) Method, also known as the Elementary Effect Method,¹ is one of the simplest types of a global sensitivity analysis. This method was developed for a computationally expensive model where a large number of factors are involved in the model calculations. This method is used to rank the factors from factors that have significant influence to model output to those that have negligible effect. The results from applying Morris' method allow the user to categorize the input factors into three groups – factors that have (1) negligible effect, (2) additive effects, or (3) non-linear or interaction effects on the simulation output.

A limitation of this method is that it may identify possible higher-order effects, but it only estimates for the first order effects, i.e., the method does not provide estimations for factor-interactions. Although not discussed further, there is a revised version called the new Morris method that does provide means to estimate the sensitivity of a model due to interactions between two factors known as the second order effect.² The basic principles of the original Morris' OAT method are discussed below.

The range of variation of each component of the vector α of parameters is standardized to the unit interval, and each component is then considered to take on p values in the set $\{0, 1/(p-1), 2/(p-1), 3/(p-1), \dots, 1\}$, so that the region of experimentation becomes an i -dimensional p -level grid. Selecting this region of experiment reasonably for each parameter is an important factor for a successful analysis. An elementary effect of the i^{th} -parameter at a point α is then defined as

$d_i(\alpha) \equiv [R(\alpha_1, \dots, \alpha_{i-1}, \alpha_i + \Delta, \alpha_{i+1}, \dots, \alpha_l) - R(\alpha)] / \Delta$, where Δ is a predetermined multiple of $1/(p-1)$, such that $\alpha_i + \Delta$ is still within the region of experimentation. Note that the base vector α is randomly chosen, and the model is not evaluated at this base vector. A finite distribution F_i of elementary effects for the i^{th} parameter is obtained by sampling α from within the region of experimentation. The number of elements for each F_i is $p^{k-1}[p - \Delta(p-1)]$. For the best economy of design, p is selected as an even number

and Δ is calculated by $p/[2(p-1)]$. Morris showed that applying this selection approach allows the individual input factors to have an equal probability of being selected.

The distribution F_i is then characterized by its mean and standard deviation or variance and is graphically shown in two-dimension, where the mean is the x-axis, and the standard deviation or variance is the y-axis. A high mean indicates a parameter with an important overall influence on the response; a high standard deviation or variance indicates either a parameter interacting with other parameters or a parameter whose effect is nonlinear.

Graphical representation of calculating an elementary effect for each parameter is shown in Figure A(E)-1:

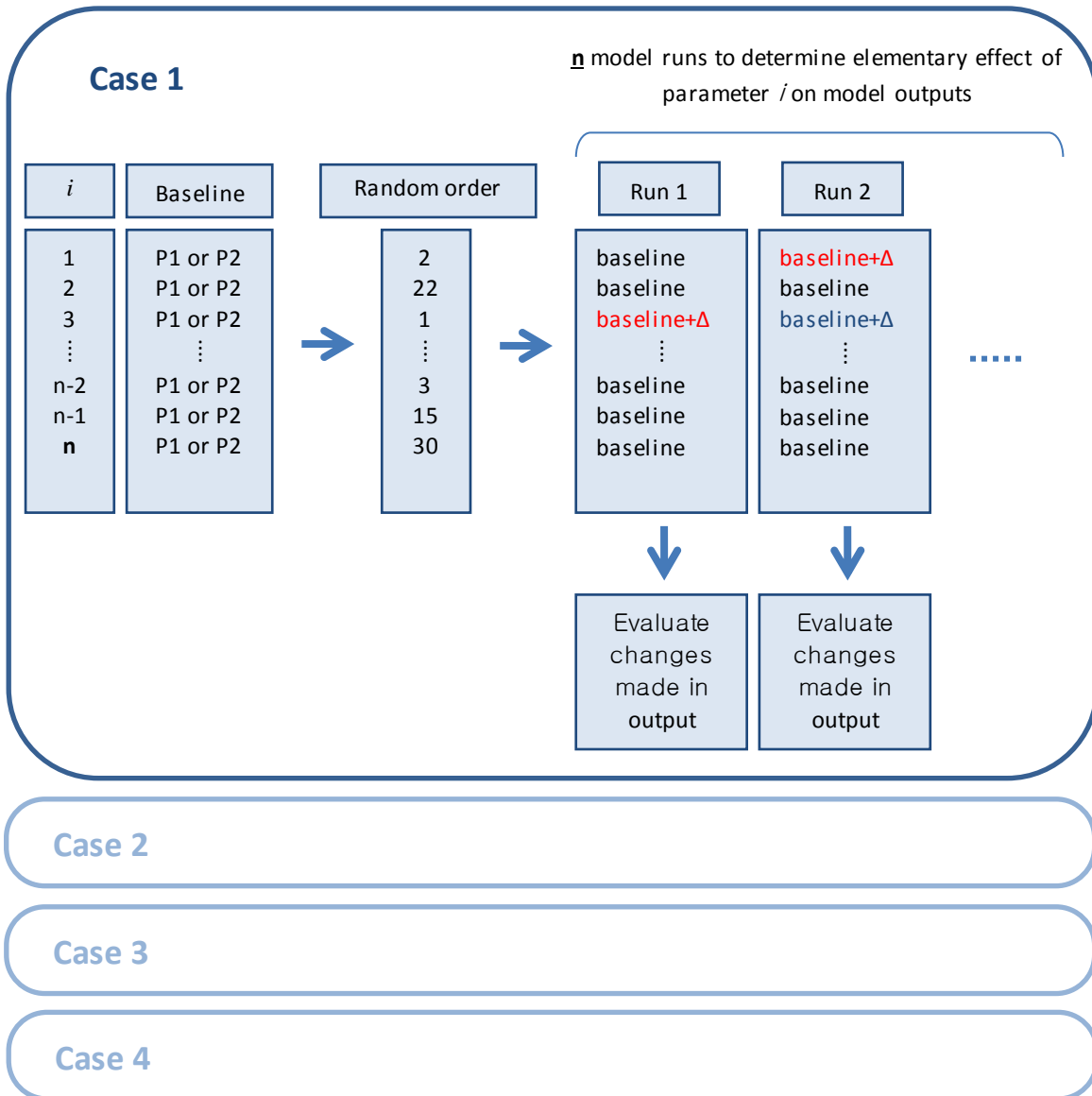


Figure A(E)-1. Schematic of Morris' OAT Method

REFERENCES

- ¹ Morris, M.D., 1991, Factorial sampling plans for preliminary computational experiments. *Technometrics* 33, 161-174.
- ² Campolongo, F.; and Braddock, R., The use of graph theory in the sensitivity analysis of the model output: A second order screening method, *Reliability Engineering and System Safety* 64 (1999) 1–12, doi:10.1016/S0951-8320(02)00109-6

Section 6

CONCLUSIONS AND FUTURE WORKS

CONCLUSIONS

This dissertation consists the following four sections, which covers various aspects of parameter estimation problem for pyrolysis modeling:

Section 2: Evaluating Effects of Applying Different Kinetic Models to Pyrolysis Modeling of Fiberglass Reinforced Polymer Composites

This research evaluates the effects of applying different kinetic models (KMs), developed based on thermal analysis using TGA data, when used in typical 1D pyrolysis models of fiberglass reinforced polymer (FRP) composites. The effect of different KMs is isolated from the FRP heating by conducting pyrolysis modeling based on measured temperature gradients. Mass loss rate (MLR) simulations from this pyrolysis modeling with various KMs show changes in the simulations due to applying different KM approaches are minimal in general. Pyrolysis simulations with the most complex KM are conducted at several heat flux levels. MLR comparison shows there is good overlap between simulations and the experimental data at low incident heat fluxes. Comparison shows there is poor overlap at high incident heat fluxes. These results indicate that increasing complexity of KMs to be used in pyrolysis modeling is unnecessary for these FRP samples; and that the basic assumption of considering thermal decomposition of each computational cell in comprehensive pyrolysis modeling as equivalent to that in a TGA experiment becomes inapplicable at depth and higher heating rates.

Section 3: Evaluation of Pyrolysis Parameters for Fiberglass Reinforced Polymer Composites based on Multi-objective Optimization

This study was conducted to investigate the ability of global, multi-objective and multi-variable optimization methods to estimate material parameters for comprehensive pyrolysis models – thermo-physical and optical properties of two Fiberglass Reinforced Polymer (FRP) composites that share the same fiberglass. With these optimization methods used in pair with a comprehensive pyrolysis model (GPYRO), parameter estimation was carefully conducted with considerations given to applying appropriate thermal decomposition kinetic models and optimization targets.

Suitable kinetic models with different levels of complexity are proposed using independent thermal analysis and their effect on 1D FRP pyrolysis modeling. This procedure shows that changes in the simulations of mass loss rates *integrated* over the cross-section of FRPs at each time step during 1D FRP pyrolysis are minor when different kinetic models are applied. Applicable optimization targets – bench-scale experiment data of mass loss rate and temperature profiles – are found by utilizing the same screening process.

Parameter estimation exercises were conducted with three different kinetic models, from simple to complex. Optimization targets were data from Cone Calorimeter experiments irradiated at a moderate heat flux level of 50kW/m^2 . Estimation results are compared with the following independently measured effective properties – thermal conductivity, specific heat capacity and emissivity of polymer resins and FRPs. Additionally, fiberglass

properties estimated from the parameter estimation exercises conducted for the two FRPs are compared to analyze for consistency in optimized values. The results show that for a well-configured parameter estimation exercise using the optimization method described above, (1) estimated results are within $\pm 100\%$ of the measurements in general; (2) increasing complexity of the kinetic modeling for a single component system has insignificant effect on estimated values; (3) increasing complexity of the kinetic modeling for a multiple component system with each element having different thermal characteristics has positive effect on estimated values; and (4) parameter estimation using an optimization method with appropriate level of complexity in kinetic model and optimization targets can find estimations that can be considered as effective material property values. Overall, a good practice for kinetic modeling for pyrolysis models is to apply a simpler approach for kinetic modeling unless more complex approaches are considered to be necessary.

Section 4: Parameter Estimation for Comprehensive Pyrolysis Modeling: Guidance and Critical Observations

A process for conducting parameter estimation for comprehensive pyrolysis models is proposed in this study. This estimation process was developed based on the following: (1) parameter estimation is about being consistent, applying engineering common-sense and correctly following the steps in this guide; (2) parameter estimation is conducted by breaking down the problem into groups of unknowns of similar character and considering them separately; (3) parameter estimation is conducted in consideration of an appropriate complexity in model set-up using certain approximations for simplifications; and (4) parameter estimation is conducted with direct measurements of parameters from independent experiments, literature search and/or numerical optimization paired with certain pyrolysis models. Additionally, limitations in parameter estimation are discussed by considering example cases. They are shown to demonstrate how simplifying the microstructure, modeling thermal decomposition kinetics and applying numerical optimization method affect the estimation results. The process developed is applied to modeling of real-world materials: thermoplastics (PMMA), corrugated cardboard, fiberglass reinforced polymer composites and plywood. Understanding the limitations in parameter estimation, it was noted that (1) the estimated parameter values are compensated by other parameter values in a parameter set allowing optimization method to optimize for multiple optimal, *linked* parameter sets; however, (2) when modeling is well-configured with optimum complexity, the optimized parameter values may become closer to those of independent measurements, highlighting the possibility of utilizing the optimization method to estimate for effective material properties.

Section 5: Engineering Guide for Estimating Material Pyrolysis Properties for Fire Modeling

With this *Guide*, standardized procedures for obtaining material parameters for input into fire-pyrolysis models are presented, such as empirical, simple analytical and comprehensive pyrolysis models. The different chapters offer guidance to show what pyrolysis models are available for modelers and what may be appropriate for their modeling needs. To provide standardized procedures for obtaining material-pyrolysis parameters for input into fire models, pyrolysis models are grouped into three categories based on their modeling characteristics, understanding that most of the model-input unknowns are related to the solid phase during thermal decomposition. The three categories are

Empirical Models, Simple Analytical Models and Comprehensive Models. For each model category the following information is provided:

- A brief description of its modeling approach and assumptions applied to simplify the problem.
- A typical mathematical formulation with identification of model parameters in the equations.
- Methods of estimating the unknown parameters either by independent measurements or numerical optimization in pair with the model.

Using this information, example cases are introduced for better understanding of the parameter-estimation procedure described for each model category. Additionally, the Appendix provides thorough explanation of example solutions from different chapters.

FUTURE WORKS

In this dissertation, first effort was given to understand thermal decomposition kinetics occurring in a one-dimensional slab using zero-dimensional thermal analysis. The results showed that although comprehensive pyrolysis models have the capability of accommodating highly complex kinetic models, the effect of increasing the complexity in kinetic models have less impact on overall modeling of pyrolysis of a slab. Independent of the level of complexity applied in kinetic models for comprehensive pyrolysis modeling, poor agreement has been reported when modeling pyrolysis at depth and higher heating rates for the FRP composites investigated in this research. Based on this, further research can be proposed for studying the actual changes that occur in the thermal decomposition kinetics with respect to increasing depth and/or heating rates. Author's speculation is that the polymer chain decomposes to monomers and freely leaves the condense-phase to the gas phase at the surface, which can be correlated well with the zero-dimensional thermal analysis (i.e. decomposition conditions are similar for both cases). However, as the pyrolysis front propagates toward the back surface and/or the applied heating rate increases the polymers decompose to higher molecular chains than monomers (production of oligomers, i.e. secondary reactions), which results in reduction in the rate of formation of fuel vapors that travels towards the surface to the gas phase. This would mainly be due to the changes in the thermal decomposition environments (e.g. more high temperature decomposition products are partially encapsulated nearby the new reactants). Initial effort was given to recreate the pyrolysis condition at depth and/or higher heating rates using zero-dimensional thermal analysis – TGA experiment using sample holders with hermetic lids, pin-holed lids, etc. and pressurized TGA experiment. However, the effect of the change in the decomposition environment was minimal in the small-scale experiments. Hence, other methods should be considered such as using pressurized batch reactor, studying as is in the slab set-up, or more.

In the second part of the dissertation, applying multi-variable/objective optimization methods to estimate model parameters for some FRP composites has been investigated. The results showed that although there is a compensation effect between the parameters, when conducted with carefulness in terms of selecting the appropriate

kinetic model and optimization targets, estimated results can be significantly close to their independently measured values. Based on this work, further investigation of “careful” estimation for different materials using multi-variable/objective optimization methods can be proposed to confirm the possibility of accepting the estimated values as effective properties. This can set the basis for developing a future database for model parameters, which can be useful to practitioners. Additionally, knowing that eventually the comprehensive pyrolysis modeling will be used as a sub-model of a computational fluid dynamics simulation in many cases, the parameters estimated from optimization method can be used to conduct multi-dimensional numerical analysis such as flame spread modeling to assess their modeling limitations.

In the last two parts of the dissertation, parameter estimation process for pyrolysis modeling has been proposed and evaluated. Based on this work, the process would need to be further developed by applying the process to different modeling cases. This would require following and understanding the procedure but also documenting well what has been learned throughout the practice.

Appendix A

Kinetic Modeling Effects on Pyrolysis Modeling of Fiberglass Reinforced
Polymer Composites

7th International Seminar of Fire & Explosion Hazards (ISFEH 2013)

Kinetic Modeling Effects on Pyrolysis Modeling of Fiberglass Reinforced Polymer Composites

Kim, E.¹, Dembsey, N.^{1*}, and Shivkumar, S.²

¹WPI, Fire Protection Engineering Dept., Worcester, MA, USA

²WPI, Mechanical Engineering Dept., Worcester, MA, USA

*Corresponding author email: ndembsey@wpi.edu

ABSTRACT

This research evaluates the effects of applying different kinetic models, developed based on thermal analysis using TGA data, when used in typical 1D pyrolysis models of FRP composites. The effect of different kinetic models is isolated from the heating of the FRPs by conducting pyrolysis modeling based on measured temperature gradients. Mass loss rate simulations from this pyrolysis modeling with various kinetic models at moderate applied heat flux (50kW/m²) show that changes in the simulation due to applying different kinetic modeling approaches were minimal. Pyrolysis simulations with the most complex kinetic model that gave the best fitness to TGA data were also conducted at several heat flux levels and the results were compared to those of experiment. Results have shown that although at relatively low incident heat fluxes there is good overlap between simulations and the experimental data, at higher heat flux levels (> 70kW/m²), simulated mass loss rates diverges from the data. These findings are suggestive of the following: (1) increasing complexity of kinetic models to be used in pyrolysis modeling is unnecessary for the FRP samples used in this work; and (2) mass transfer effects are significant for higher incident heat flux levels for FRPs and therefore the typical assumption of negligible mass transfer effects cannot be generally assumed.

KEYWORDS: kinetic modeling, thermal decomposition, thermal analysis, pyrolysis modeling

NOMENCLATURE

<i>a</i>	zero order rxn model slope (/K)	<i>t</i>	time (s)
<i>b</i>	zero order rxn model intercept (-)	Greek	
<i>e</i>	Euler's number (-)	α	conversion (-)
<i>E</i>	activation energy (kJ/mol)	β	heating rate (°C/min)
<i>f</i>	function	Subscripts	
<i>k</i>	rate constant (/s)	p	DTG peak
<i>r</i>	rate (%/min)	0	initial condition
<i>R</i>	gas constant (J/mol-K)		
<i>T</i>	temperature (K)		

INTRODUCTION

For the composites industry designing fiberglass reinforced polymers (FRPs) that have good reaction to fire characteristics is a guess and check operation in many cases. Changes made to the components of the FRP – resin, additives and/or glass – or the microstructure of the FRP affect the overall fire behavior. Traditionally, the effect of the changes made in the FRP are checked via standard fire tests, which can be time consuming and expensive. Therefore, providing an understanding of how typical FRPs decompose under fire conditions and using this information to develop appropriate guidelines for the composite industry to produce fire-safe composites has been a long-term goal for this research.

Towards achieving this goal, virtual materials have been created that can simulate fire behavior of FRPs under different conditions by use of comprehensive pyrolysis models [1,2,3]. To develop accurate virtual materials, the first step is to model the thermal decomposition kinetics of FRPs as this determines the number of solid phase species involved in pyrolysis simulation. Then for every solid phase species, parameters related to their thermo-physical (density, thermal conductivity and specific heat capacity) and optical (emissivity and absorption coefficient) properties need to be determined to create a virtual material that can be used for pyrolysis simulation. Depending on the complexity of the kinetic modeling, virtual material model parameters that need to be estimated may range from less than 10 up to 100 or more.

Kinetic modeling of Thermogravimetric Analysis (TGA) mass loss rate (DTG) data provides the basis of creating virtual materials based on comprehensive pyrolysis modeling of FRPs. Six different kinetic models were investigated as shown in Table 1 where model assumptions applied to estimate kinetic parameters are shown with constant heating rate TGA data used in the modeling.

Table 1. Different kinetic models considered in this study

Model	Model Assumptions / Data	Model	Model Assumptions / Data
A	1 zero order rxn/constant DTG	D	1 or 2 nth order rxn/multi-heating rate
B	1 first order rxn/ peak DTG	E	3 or 4 first order rxn/multi-heating rate
C	1 or 2 first order rxn/multi-heating rate	F	3 or 4 nth order rxn/multi-heating rate

MATERIAL AND EXPERIMENTS

Sample Materials

FRP composite panels were fabricated by vacuum bagging for relatively high glass content composites, using two different types of fiberglass (E-glass) mats – chopped strand mat and a glass roving woven mat – that were wetted with resin. The chopped strand mat is thinner and more porous than the woven mat. The laminate schedule is chopped strand mat and roving alternating 8 and 6 times with another chopped strand mat layer at the end for the brominated unsaturated polyester (BrUPE) and modified acrylic with inorganic additive (MA+A) FRP composites, respectively. Visual inspection (see Figure 1) is made of a polished cross-section of the composite slab to confirm consistency with the provided laminate schedule. BrUPE is an unsaturated polyester resin with bromination for flame retardancy. The bromination is built in to the carbon back bone with 20% by weight, which is typically substituted by replacing the hydrogens. Along with the bromination, antimony trioxide is added as an additive as a synergist that assists the flame retardancy of the polymer resin. MA is a modified acrylic resin. This resin is essentially unsaturated polyester (UPE) with Methacrylic Acid (MMA) replacing most of the styrene monomers. MA+A is a modified acrylic resin (MA) with an inorganic additive (A) as an additive for fire retardancy. Typical inorganic additives are hydrates such as alumina trihydroxide (ATH) or magnesium hydroxide, antimony trioxide, borax, chalk, silica, etc. [4] Because this additive was known to give a high-charring effect with a strong endotherm, A was categorized with typical hydroxides used as flame retardant fillers. These hydroxides works as a flame retardant by resulting in an endothermic dehydration reaction that produces oxides and water [4,5]. The water produced by this reaction vaporizes, which is an endothermic reaction, and the vapor dilutes the gaseous phase. This flame retardant is added with a relatively large amount (50 to 65%) comparing to other types of additives.

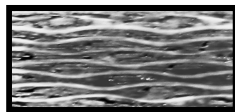


Figure 1. Cross-section of FRP fabricated via vacuum bagging with average glass content of 60 wt%, respectively: two types of fiberglass (E-glass) used in the composite – chopped strand mat (porous) and glass roving woven mat (prominent glass layers in white)

Small-scale TGA/DSC

The instruments used in this study were manufactured from TA Instruments: Thermogravimetric Analysis Q50 (TGA) and the Differential Scanning Calorimetry Q20 (DSC). Throughout this study, TGA and DSC were used for a non-isothermal test purposes and the tests were conducted in nitrogen and air environments to study pyrolysis and oxidation, respectively. Using the TGA, 4 different heating rates of 5, 20, 40 and 60°C/min. were applied to measure the mass loss history of each resin sample up to 800°C. For the DSC, a constant heating rate of 20°C/min. was used to measure the heat flow through the sample during the thermal decomposition of resins up to 500°C using a sample amount of ~ 10 mg in a standard aluminium pan with a punctured lid so that gases may evolve freely away from the pan. The uncertainty in the TG measurements was quantified by plotting 3 or 4 weight loss curves from different tests (TG) with respect to temperature and finding the maximum standard deviation at each temperature ranging from ambient to 750 °C. The maximum standard deviation is then used to calculate 95% confidence intervals for each material by applying the student t distribution with a sample size of 3 or 4. Uncertainties in TG for BrUPE and MA+A resins are estimated to be ± 7 and ± 6 %, respectively.

Bench-scale Cone Calorimeter

Cone Calorimeter (Cone, ASTM E 1354 [6]) is a bench-scale fire test apparatus in which the sample is heated by an electrically powered rod in the shape of a cone. The sample is tested by applying a constant radiative heat flux set via temperature control of the rod. The Cone exposes the sample in an ambient environment which results in a natural flow field as the sample temperature increases allowing convective cooling above the sample surface. The ignition source is an intermittent sparker. Several modifications were made to the standard testing procedure. First, when testing these FRPs, two different types of sample holders were used to produce nominal one-dimensional data: the standard non-insulated square holder with a metal edge frame and a round insulated holder [7]. Second, typically 4 thermocouples were installed to measure temperature change of the sample at various depths: exposed surface, 1/3, 2/3 and back surface. The uncertainties in experimental mass loss rate (MLR) and thermocouple measurements at surfaces (exposed, T_s and back, T_b) were quantified by comparing data from these 3 or 4 identical FRP composite tests tested at 50 and 75kW/m² applied heat flux levels for BrUPE and MA+A composites, respectively. Note that normalized time, time divided by sample thickness square, i.e., $\tau = \text{time}/\delta^2$ is used to remove the effect of different sample thicknesses when comparing. Because the data is transient, values at different times ($\tau = 1, 3, 5 \text{ s/mm}^2$ for BrUPE and 1, 3, 5, 7 s/mm^2 for MA+A composites) from each test have been used to calculate the standard deviation at each time. Then these are averaged and used to estimate uncertainty by applying student t distribution with a sample size of 3 or 4 and calculating the 95% confidence interval. Uncertainties in MLR, T_s and T_b are ± 2.2 or 2.3 g/s-m², ± 67 or 30 °C, ± 14 or 22 °C for BrUPE or MA+A composite. The uncertainty in TC bead location at depth is typically ± 1 mm. These uncertainty values were used to evaluate significant differences between the modeling results and experiment data.

RESULTS AND DISCUSSION

Thermal Decomposition of Resins

To understand thermal decomposition behavior, the iso-conversional method was conducted with iso-heating rate (5, 20, 40 and 60°C/min) TGA data. Typically in kinetic studies, the isothermal rate of degradation or conversion, $d\alpha/dt$, is assumed to be a linear function of the temperature dependent rate constant, $k(T)$, and a temperature independent function of the conversion, $f(\alpha)$, where α indicates the conversion. This equation can be further expanded by using the Arrhenius expression for the rate constant. Within the Arrhenius expression, two more reaction dependent constants are introduced: the pre-exponential constant, A , and the activation energy, E_a (see Eq. 1). The temperature independent function of the conversion, $f(\alpha)$ is dependent upon the mechanism of the chemical reactions.

$$\frac{d\alpha}{dt} = k(T)f(\alpha) = \left[A \exp\left(-\frac{E_a}{RT}\right) \right] f(\alpha) \quad (1)$$

The iso-conversional method, also known as the “model-free method”, is the method applied in this step to identify the minimum number of reactions necessary in the kinetic model. This method requires data from multiple non-isothermal (or dynamic) experiments, i.e. data tested with at least 4 different heating rates. The basis for this method is that at a constant conversion, α , $d\alpha/dt$ and $f(\alpha)$ become constants and therefore, E_a at each conversion is found without the pre-knowledge of the reaction mechanisms. When the E_a is found for the entire degradation process, the results provide insight for the minimum number of steps of elementary reactions needed to address the global reaction [8]. A global reaction composed of a single stage process will show no dependence of E_a on conversion, α . When the global reaction is a complex process, the E_a changes with respect to conversion, α . An increase in E_a with α typically indicates parallel reactions. A decrease in E_a with α suggests that either the process is reversible (concave shape) or there is a change in the rate determining step (convex shape). Therefore, from the iso-conversional method, a minimum number of elementary reactions are indicated. There are two types of iso-conversional methods used in this study to check consistency – Ozawa, Flynn and Wall (OFW) [9,10] and Friedman [11,12]. Using these methods, activation energy with respect to conversion, α is calculated and plotted for both resin systems – BrUPE (see (a) in Figure 2) and MA+A (see (b) in Figure 2).

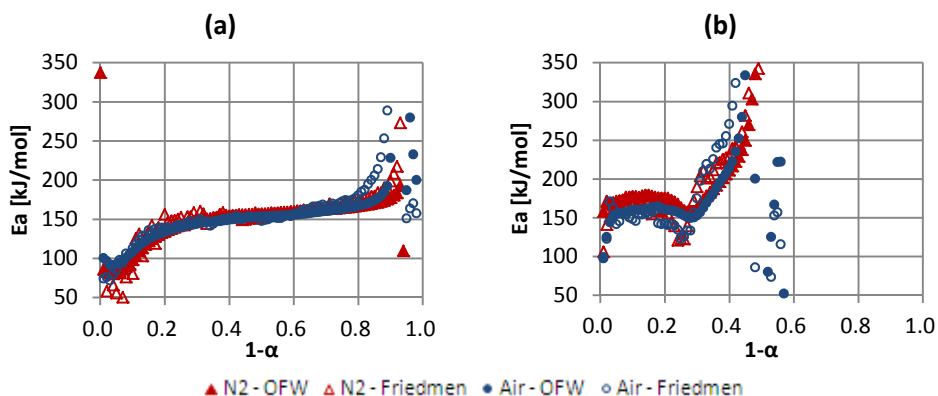


Figure 2. Results from iso-conversional method conducted on BrUPE (a) and MA+A (b) resins: (a) and (b) shows the estimated activation energy of thermal decomposition with respect to conversion (α)

Brominated Unsaturated Polyester Resin: BrUPE

Based on the iso-conversional method, thermal decomposition of BrUPE can be grouped into three stages. The first stage is the initial mass loss where the activation energy increases with respect to α . The changes in the activation energies calculated for each conversion indicate that there is more than one reaction resulting in weight loss. The second stage is the region where most of the mass loss is occurring and is identified with a profound, maximum peak in the DTG thermogram obtained from TGA experiments. As shown in (a) in Figure 2, the activation energies calculated for conversion of BrUPE are relatively constant for both nitrogen and air. This result indicates that a single step reaction can describe the degradation process within this stage. For BrUPE resin decomposing in nitrogen and air, a significant mass loss leaving residue less than 10% of its initial mass is observed at this stage. The third stage is the region where final mass loss is observed at temperatures above 400-500°C leaving almost no mass behind. In this stage, the increase in the activation energy with respect to α occurs for decomposition of BrUPE resin and it occurs earlier for decomposition in air than in nitrogen. This increase in estimated activation energy can be explained by the following: based on the weight loss (TG) and mass loss rate (DTG) thermogram shapes from TGA experiments and the residue yield – 4-5% in nitrogen and less than 2% in air at 800°C, one can speculate that BrUPE decomposition in nitrogen results in a constant increase in activation energy because the weight loss is minimal in this stage, but for BrUPE decomposing in air, it occurs because a parallel, oxidative reaction exists. The oxygen diffusion through the sample seems to delay the decomposition process only slightly, probably because the sample sizes used in this experiment are small.

The results found from conducting the iso-conversional method are consistent with previous research [13,14,15,16] conducted for unsaturated polyester thermoset resins. One thing to note is that BrUPE is identified as thermally less stable than the typical UPE knowing that the initial weight loss occurs up to 10-20% rather than a minor weight loss of less than 10%. This discrepancy is probably due to the antimony trioxide added in BrUPE as a flame retardant additive or other things that may have been added inadvertently acting as an impurity. Even a small amount of impurities are known to affect the integrity or the stability of the polymer performance [17]. Additionally, adding antimony trioxide to a halogenated compound such as UPE is known to have an effect on lowering the charring temperature. After the initial weight loss region follows the major decomposition step. Studies have discovered that the decomposition occurs on the ester chain (-CO-C-) and the unsaturated chain (-C=C-) where the weakest chemical bonding exists [15]. This region exists up to 400°C to 500°C depending on the heating rate and is observed in thermal degradations of BrUPE. In addition to this major decomposition step, weight loss up to 10% of the UPE samples' initial weight is noticed from the tests conducted in air. Considering that this only occurs in oxidative environment, the weight loss is understood as an oxidative degradation reaction that starts around 500°C and above.

Modified Acrylic with Inorganic Additive: MA+A

Based on the iso-conversional method, thermal decomposition of MA+A can be grouped into four stages – three similar to those of BrUPE and one additional stage where decomposition of the additive (A) is observed (see (b) in Figure 2). Although the detailed composition of the additive is unknown, additive (A) decomposition reaction for this conversion region can be assumed due to the following: (1) a strong endothermic peak observed from DSC heat flow measurement at the temperature range (~ 390°C) of this stage; (2) the amount of weight loss at

this stage (~20%) is comparable to that of additive decomposition reaction; and (3) the estimated activation energies, E_a from iso-conversional method in this stage (160 ± 3 kJ/mol with normal distribution, 95% confidence interval) are similar to the reference values found for additive decomposition reaction.

The results found from the iso-conversional method and heat flow measurements show that the decomposition of the inorganic additive used in MA+A that gives high-charring effect is similar to the decomposition of polymers with typical hydroxides used as flame retardant fillers. Among various hydroxides, possibly alumina trihydroxide (ATH, $Al_2(OH)_3$) is used as the unknown additive in the resin and additive mixture considering that (1) the decomposition temperature of the additive is below 250°C; and (2) the weight loss of the additive after its decomposition reaction is approximately 30% of its initial mass. The decomposition temperature of ATH is 240°C and complete weight loss when decomposing to aluminium oxide (Al_2O_3), 35% of weight loss should occur [18,19].

Various Kinetic Modeling Approaches

In this study, 6 different kinetic models are investigated: Model A and B applies single step reaction for BrUPE or MA+A polymer decomposition. Model C and D applies single step for BrUPE and two step for MA+A case where resin and additive decomposition is considered separately. Model E and F are most complex cases proposed from thermal analyses where three step is applied for the additive-free resin case (BrUPE and MA) – decomposition reactions of resin to resin' (R1) and resin' to char (R2) and oxidation reaction of char to residue (R3) – and one step is applied for modeling the additive decomposition (A). See Table 1 for kinetic model summary.

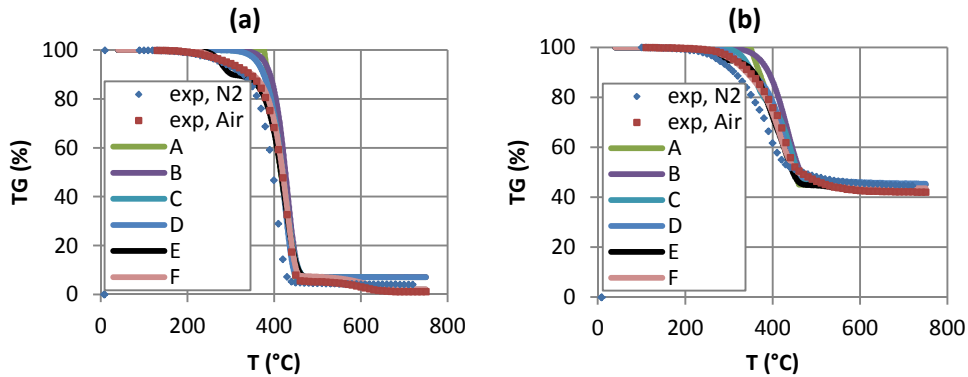


Figure 3. Mass loss rates from TGA experiments (exp) and kinetic modeling (A-F) and are shown for BrUPE (a) and MA+A (b) with 60 °C/min heating rate case. Applying various approaches in kinetic modeling results in minor changes in modeled mass loss rate.

With the number of reactions known, reaction order models ($f(\alpha) = (1 - \alpha)^n$) are investigated in this research with $n = 0, 1$ or n . Zero order reaction is assuming that decomposition is a linear function of temperature (see Eq. (2) and estimation of kinetic parameters are undertaken by data fitting (model fitting method [20,21]) to a single heating rate TGA data (60 °C/min). Note that the slope, a , is estimated as approximately 80% of the DTG peak. When a first or nth order reaction model is applied, kinetic parameters other than activation energy are (1) calculated analytically by assuming at each DTG peak, the second derivative of conversion, α with respect to time is zero and activation energy of each reaction is significantly greater than $2RT_p$ (i.e. $E_a \gg 2RT_p$)

where T_p is the temperature at DTG peak [22] (see (3) and (4)); or (2) estimated using a model fitting method with primarily reaction order kinetic models – $f(\alpha) = 1 - \alpha$ or $(1 - \alpha)^n$ and other models to investigate the reaction controlling factor. Activation energies for each reaction are estimated from the iso-conversional method. Fitness of each kinetic model to TGA data is calculated by least square method. Estimated kinetic parameter values for most complex approach (F in Table 1) are summarized in Table 2 for decomposition of BrUPE and MA+A resins. Note that all cases provide good fitness (minimum r-square value of 0.98 and mostly greater than 0.99) to TGA data (see Figure 3).

$$\alpha = -aT + b \tag{2}$$

$$E_a \approx \frac{RT_p^2}{\beta} \frac{er_p}{(1 - \alpha_0)} \tag{3}$$

$$A \approx \frac{er_p}{(1 - \alpha_0)} \exp\left(\frac{E_a}{RT}\right) \tag{4}$$

Table 2. Estimation of kinetic parameters with most complex kinetic modeling approach (F) for BrUPE and MA+A decomposition. Parameters with * and ** are assumed values and estimated values from iso-conversional method, respectively.

Parameters	Reactions				β (°C/min)	Fitness		
	R1	R2	R3	A		r-square (N2)	r-square (Air)	
BrUPE	weight frac.	0.10	0.83	0.05		5	0.9986	0.9980
	log A (log(/s))	13.9	10.1	7.5		20	0.9992	0.9992
	E_a (kJ/mol)	155**	155**	155**		40	0.9993	0.9998
	n (/)	5	0.7	1*		60	0.9966	0.9997
						avg	0.9984	0.9992
MA+A	weight frac.	0.05	0.30	0.02	0.20	5	0.9981	0.9935
	log A (log(/s))	16.5	12.5	10.5	12.2	20	0.9978	0.9982
	E_a (kJ/mol)	183**	183**	183**	160**	40	0.9991	0.9985
	n (/)	5.0	1.3	1*	5.0	60	0.9992	0.9977
						avg	0.9985	0.9970

Simplified Comprehensive Pyrolysis Modeling

Assuming mass transport effects during pyrolysis are negligible, a typical assumption in comprehensive pyrolysis models; simulating pyrolysis requires an understanding of the heating of a material and the mass loss due to thermal decomposition. These two aspects of pyrolysis can be captured by considering conservation of energy and mass. To evaluate the effect of kinetic modeling on the thermal decomposition of FRPs, the effect of applying different kinetic modeling approaches must be isolated from the heating of the FRPs. By exposing FRPs to various thermal insults and measuring the resultant temperature profiles from the exposed surface to the back surface of the solid, a representation of conservation of energy on the FRPs can be acquired. The changes in temperature measured in the tests account for the heat transport phenomena within the material as well as the heat addition or loss from decomposition reactions. Therefore, to determine mass loss of an FRP, only conservation of mass needs to be considered which is represented by the decomposition kinetics. Decomposition simulations based on the temperature profiles then can be conducted by solving the rate of decomposition ($d\alpha/dt$) computed from a given assumed kinetic model.

To conduct this 1D simplified comprehensive pyrolysis modeling, the solid material is discretized into n+1 number of cells in the z-direction (depth) with equal length of Δz except for

the two cells at the surfaces (front and back) where a half-length ($1/2\Delta z$) is used. In this work, temperature profiles at 4 different locations were obtained via experiments – front and back surfaces, 1/3 and 2/3 depths. With these temperatures known, temperatures at intermediate locations which are unknown are found using 3rd order polynomial at each time step. Note that due to uncertainty in TC bead location at depth (1/3 and 2/3), modeling was repeated with boundary values found from considering the uncertainty in thermocouple bead location. Knowing the temperature of cells at each time step, weight loss of each cell is calculated by solving the rate of decomposition (da/dt) using an ODE solver (Runge-Kutta 4th order). The material's cross-section is considered as an effective homogeneous mixture of resin and fiberglass mats. This approach was utilized because although FRP composites are composed of layers of resin-wetted fiberglass mats stacked one after another, a clear distinction between resin or fiberglass layers was difficult to resolve based on visual inspection of the cross-section for the relatively high glass content FRPs consider.

Simplified pyrolysis modeling of both composites irradiated at 50 kW/m^2 applied heat flux is conducted with different kinetic modeling approaches (A through F) to examine appropriateness of each case. As shown in Figure 4, changes in modeled mass loss rate due to applying different kinetic modeling approaches are minimal except for case A where larger scatter of simulation points occur near the peak and the beginning stage of the final decay. There is some benefit in applying more complex 3 and 4 step decomposition model for modeling BrUPE and MA+A composite (Case E and F), respectively, for they allow the pyrolysis model to capture the small amount of mass loss prior to ignition (shoulder before initial mass loss rate peak) and near mass loss end time. Other than these two advantages, applying more complex kinetic model becomes unnecessary in terms of conducting pyrolysis modeling to calculate mass loss rate.

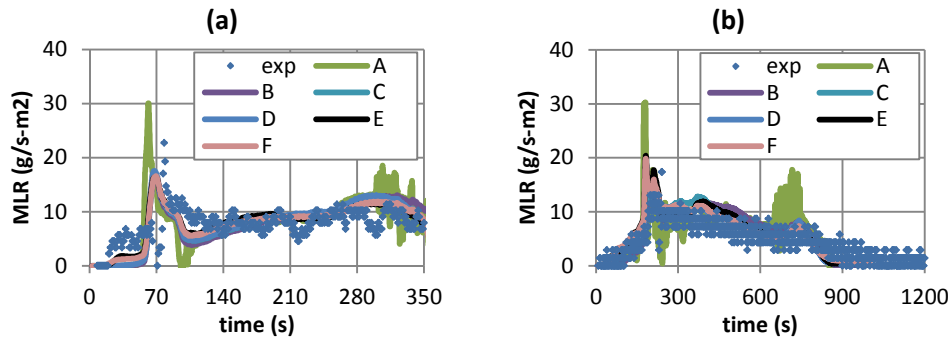


Figure 4. Mass loss rates from Cone Calorimeter experiments (exp) and simplified comprehensive pyrolysis modeling (A-F) and are shown for BrUPE (a) and MA+A (b) FRP composites irradiated at 50 kW/m^2 . Applying various approaches in kinetic modeling results in minor changes in modeled mass loss rate.

Following this work, mass loss rate simulations of BrUPE and MA+A composites with Kinetic Model F were conducted at various incident heat flux levels – applied heat flux levels of 50, 70 and 100 kW/m^2 and 25, 50 and 75 kW/m^2 , respectively. Kinetic Model F was chosen because it had the best fitness to the TGA data as compared to the other models. For modeling of both composites, good agreement with experiment data is shown for cases with relatively low applied heat flux of less than 50 kW/m^2 . At higher heat flux levels, modeling deviates from experiment data for both FRP composites (see Figure 5). For modeling of BrUPE composite at or above 70 kW/m^2 , a secondary peak in mass loss rate, which is comparable to the initial peak immediately after ignition is observed and results in a shorter end time of the simulated mass loss (i.e. time when all decomposable mass is lost due to pyrolysis) than that of experiment. In the experiments, an extended mass loss rate tail exists. Similar to that of BrUPE composite at higher

applied heat flux, modeling results of MA+A FRP composite decomposing at 75 kW/m^2 show a significantly higher mass loss rate peak following ignition than that of experiment resulting in shorter end time of mass loss than that of experiment. This finding indicates that although the temperatures are high enough to result in greater mass loss of the resin system based on TGA data, mass loss is reduced and/or delayed when the FRP is decomposing. This deviation is suggestive that mass transfer effects are significant for higher incident heat flux levels for FRPs likely due to effects of the fiberglass mats and indicate that the typical assumption of negligible mass transfer effects cannot be generally assumed.

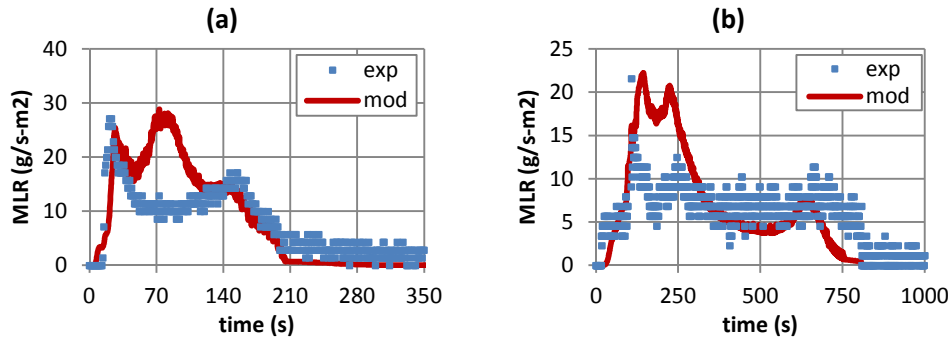


Figure 5. Mass loss rates from Cone Calorimeter experiments (exp) and simplified comprehensive pyrolysis modeling (mod) and are shown for BrUPE (a) and MA+A (b) FRP composites at applied heat flux levels of 100 and 75 kW/m^2 , respectively.

CONCLUSIONS

In this research, effects of applying different kinetic models is evaluated when used in typical 1D pyrolysis modeling where mass transport effects during pyrolysis are assumed to be negligible. The kinetic models are developed based on thermal analysis using TGA data and two FRP composites are used as sample materials – BrUPE and MA+A composites. To examine the effect of kinetic modeling on the thermal decomposition of FRPs, the kinetic modeling approaches are isolated from the heating of the FRPs by conducting pyrolysis modeling which utilizes temperature measurement data from bench-scale experiments of FRP composites as a proxy for conservation of energy. Conservation of mass of the material is represented by decomposition simulation with different kinetic models. Mass loss rate simulations with kinetic models A through F for both materials at moderate applied heat flux (50 kW/m^2) show that changes in the simulation due to applying different kinetic modeling approaches are minimal except for case A. In addition, simulations with the most complex kinetic model (F) that gave best fitness to TGA data are conducted and the mass loss rate results are compared to those of experiment at various heat flux levels. Results show that although at relatively low incident heat fluxes there is good overlap between simulations and the experimental data, at higher heat flux levels ($> 70 \text{ kW/m}^2$), simulated mass loss rates significantly deviate from the experimental data. These findings indicate that (1) increasing complexity of kinetic models to be used in pyrolysis modeling is unnecessary for modeling of the FRP samples used in this research; and (2) mass transfer effects are significant for higher incident heat flux levels for FRPs and therefore the typical assumption of negligible mass transfer effects cannot be generally assumed.

ACKNOWLEDGEMENTS

The authors greatly appreciate the support for this work from DOC NIST Award Number 60NANB8D8106 (Federal Program Officer Dr. Kevin McGrattan). Special thanks go to Charles

Dore for fabricating and donating the FRP composite materials used in this study. Many thanks also to Randall Harris at WPI for conducting the Cone Calorimeter tests.

REFERENCES

1. Kevin McGrattan, Simo Hostikka, Jason Floyd, Howard Baum, Ronald Rehm, William Mell and Randall McDermott, Fire Dynamics Simulator (Version 5) Technical Reference Guide, NIST Special Publication 1018-5, October 29, 2010.
2. S.I. Stolarov, R.E. Lyon, Federal Aviation Administration Technical Note, DOT/FAA/AR-TN08/17, 2008; available for download at <http://www.fire.tc.faa.gov/reports/reports.asp>.
3. Lautenberger, C., Gpyro – A Generalized Pyrolysis Model for Combustible Solids, Technical Reference, Version 0.700, February 19, 2009.
4. Anand K. Kulshreshtha, Cornelia Vasile, *Handbook of Polymer Blends and Composites*, Volume 3, Part 2, Rapra Technology, 2002.
5. LeVan, S.L., *The Chemistry of Solid Wood*; Chapter 14. Chemistry of Fire Retardancy, American Chemical Society, 1984.
6. Standard Test Method for Heat and Visible Smoke Release Rates for Materials and Products Using an Oxygen Consumption Calorimeter, ASTM E 1354-02, ASTM, 100 Barr Harbor Drive, West Conshohocken, PA, U.S.
7. de Ris, J.L. and Khan, M.M., "A sample holder for determining material properties," *Fire and Materials*, 24, 219-226 (2000).
8. S.V. Vyazovkin, A.I. Lesnikovich, An approach to the solution of the inverse kinetic problem in the case of complex processes: Part 1. Methods employing a series of thermoanalytical curves, *Thermochimica Acta*, Volume 165, Issue 2, 15 August 1990, Pages 273-280.
9. T. Ozawa, "A new method of analyzing thermogravimetric data," *Bull.Chem. Soc. Jpn.*, vol. 38, pp. 1881-1886, 1965.
10. J. H. Flynn and L. A. Wall, "A quick, direct method for the determination of activation energy from thermogravimetric data," *J. Polym. Sci. Polym. Lett.*, vol. 4, pp. 323-328, 1966.
11. H. L. Friedman, "Kinetics of thermal degradation of char-forming plastics from Thermogravimetry. Application to a phenolic plastic," *J. Polym. Sci., Pt. C 6*, 183-195 (1964).
12. J. H. Flynn, L. A. Wall, "A quick, direct method for the determination of activation energy from thermogravimetric data," *J. Polym. Sci. Polym. Lett.* 4, 323-328 (1966).
13. Chrissafis, K., Paraskevopoulos, K.M., Bikiaris, D.N., Thermal degradation kinetics of the biodegradable aliphatic polyester, poly(propylene succinate), *Polymer Degradation and Stability* 91 (2006) 60-68
14. Y. S. Yang and L. James Lee, Microstructure formation in the cure of unsaturated polyester resins *Polymer*, Volume 29, Issue 10, October 1988, Pages 1793-1800
15. Chiu, H.T., Chiu, S.H., Jeng, R.E., Chung, J.S., A study of the combustion and fire-retardance behaviour of unsaturated polyester/phenolic resin blends, *Polymer Degradation and Stability* 70 (2000) 505-514
16. Liliana B. Manfredi, Exequiel S. Rodríguez, Maria Wladyka-Przybylak, Analí 'a Va' zquez, Thermal degradation and fire resistance of unsaturated polyester, modified acrylic resins and their composites with natural fibres, *Polymer Degradation and Stability* 91 (2006) 255-261
17. Reich, L., Stivala, S.S., Chapter 6. Factors Affecting Polymer Stability, *Elements of Polymer Degradation*, McGraw-Hill, Inc., c 1971
18. Chen, I., Hwang, S., Chen, S., Chemical Kinetics and Reaction Mechanism of Thermal Decomposition of Aluminum Hydroxide and Magnesium Hydroxide at High Temperatures (973-1123K), *Ind. Eng. Chem. Res.*, **1989**, 28 (6), pp 738-742
19. Hornsby, P. R. (1994), The application of magnesium hydroxide as a fire retardant and smoke-suppressing additive for polymers. *Fire and Materials*, 18: 269-276. doi: 10.1002/fam.810180502
20. Bras, M.L., Rose, N. and Bourbigot, S., The Degradation Front Model – A tool for the Chemical Study of the Degradation of Epoxy Resins in Fire, *Journal of Fire Sciences*, Vol. 14 – May/June (1996)
21. Liu, J., He, D., Xu, L., Yang, H. and Wang, Q., Study of the Kinetics of the Combustion Reaction on Shuangya Mountain Coal Dust by TG, *Journal of Thermal Analysis and Calorimetry*, Vol. 58 (1999) 447-453

22. Lyon RE, Safronava N and Oztekin E. A simple method for determining kinetic parameters for materials in fire models. *Fire Saf Sci* 2011; 10: 765–777.

Appendix B

Thermo-Physical and Optical Parameter Estimation for Pyrolysis Modeling of Fiberglass Reinforced
Polymer Composites

ANTEC 2013

THERMO-PHYSICAL AND OPTICAL PARAMETER ESTIMATION FOR PYROLYSIS MODELING OF FIBERGLASS REINFORCED POLYMER COMPOSITES

*Esther Kim and Nicholas A. Dembsey, WPI, Fire Protection Engineering Dept., Worcester, MA
Satya Shivkumar, WPI, Mechanical Engineering Dept., Worcester, MA*

Abstract

To explore the potential use of modeling for the development of fiberglass reinforced polymers (FRPs) with good fire characteristics, parameter estimation based on comprehensive pyrolysis modeling of an FRP composite is conducted. Kinetic modeling is performed using data from TGA and DSC experiments. Different kinetic models are proposed and their effect on pyrolysis modeling is evaluated using a screening process that involves simulation of 1D FRP pyrolysis. This procedure shows that changes in simulation results (mass loss rate) are minor when different kinetic models are applied. Following this work, a sub-set of these kinetic models are used in a parameter estimation process to examine their effect on the estimated parameters. The results show that different kinetic models affect the successful completion of the estimation process. When completed successfully the estimation process demonstrates the possibility of applying numerical optimization to estimate model parameters that can be reproduced from independent standard measurements.

Introduction

For the composites industry, designing fiberglass reinforced polymers (FRPs) that have good reaction to fire characteristics is a guess and check operation in many cases. Changes made to components of the FRP – resin, additives and/or glass – or the microstructure of the FRP affect the overall fire behavior of the FRP. Traditionally, the effect of the changes made in the FRP are checked via standard fire tests, which can be time consuming and expensive. Therefore, providing an understanding of how typical FRPs decompose under fire conditions and using this information to develop appropriate guidelines for the composite industry to produce fire-safe composites has been a long-term goal for this research.

Towards achieving this goal, virtual materials have been created that can simulate fire behavior of FRPs under different conditions by use of 1D comprehensive pyrolysis models [1, 2, 3]. To develop accurate virtual materials, the first step is to model the thermal decomposition kinetics of FRPs as this determines the number of solid phase species involved in pyrolysis simulation. Then for every solid phase species, parameters related to their thermo-

physical (density, thermal conductivity and specific heat capacity) and optical (emissivity and absorption coefficient) parameters need to be determined to create a virtual material that can be used for pyrolysis simulation. Depending on the complexity of the kinetic modeling, virtual material model parameters that need to be estimated may range from less than 10 up to 100 or more.

Traditionally, estimating unknown model parameters was conducted by making independent measurements for each parameter using standard tests. However, standard tests are typically developed for testing on inert samples (non-decomposing). However many parameters of interest in comprehensive pyrolysis modeling are the result of thermal decomposition. To overcome this current lack of independent measurements of decomposition species, an approach of estimating model parameters by incorporating numerical optimization (e.g. Genetic Algorithm, Shuffled Complex Evolution, etc.) is used [4,5]. This approach has become more appealing recently due to the inexpensive and accessible nature of “high speed” computer resources.

This optimization approach pairs a 1D comprehensive pyrolysis model with a numerical optimization routine to determine the un-measurable parameters for the decomposition species by iteratively comparing model outputs with bench-scale experimental data from the Cone Calorimeter (ASTM E 1354 [6]) such as mass loss rate and temperature profiles. In general, these optimizations incur significant computational expense, i.e. using multiple processors with long duration optimization runs. The level of computational expense is directly related to the complexity of the thermal decomposition kinetics assumed which defines the total number of parameters that need to be optimized. When a numerical optimization method is used to estimate unknown model parameters, generally a unique solution that results in best fitness to the optimization targets is not found. Rather, many near optimum parameter sets can be identified. This indicates that there are compensating effects between optimized model parameter values and there is no unique solution to this optimization problem.

Understanding the above characteristics of utilizing numerical optimization in pyrolysis model parameter estimation processes, a careful parameter estimation

exercise is conducted in this study for a fiberglass reinforced polymer (FRP) composite. The goal of this work is to examine whether parameter estimation via numerical optimization is capable of estimating values that are physically sensible rather than optimizing to non-physical fitting values. When the estimated values from numerical optimization can be considered to present physically meaningful estimation results, which may be reproduced through independent measurements, the compilation of estimated results for different materials may become a starting point of a possible material database for future pyrolysis modeling use.

Sample Material

FRP composite panels were fabricated by vacuum bagging for relatively high glass content composites, using two different types of fiberglass (E-glass) mats – chopped strand mat and a glass roving woven mat – that were wetted with resin. The chopped strand mat is thinner and more porous than the woven mat. The laminate schedule is chopped strand mat and roving alternating 6 times with another chopped strand mat layer at the end. Modified acrylic resin (MA) is used in the composite, which is essentially unsaturated polyester with Methacrylic Acid replacing most of the styrene monomers. An inorganic additive (A) is used for fire retardancy. Typical inorganic additives are hydrates such as alumina trihydroxide (ATH) or magnesium hydroxide, antimony trioxide, borax, chalk, silica, etc. [7] Additive A was known to give a high-charring effect with a strong endotherm and was categorized as a typical hydroxide. These hydroxides work as a flame retardant by an endothermic dehydration reaction that produces oxides and water [8,9]. The water produced by this reaction vaporizes, which is an additional endothermic reaction, and the vapor dilutes the gaseous phase. When these hydroxides decompose it is without re-crystallization or disintegration because they are typically stable crystalline materials. Only some modification of lattice parameter is observed allowing the loss of small stable molecules from the reactant phase, such as H₂O. These molecules travel outward to the interface between the solid and gas phase via diffusion [10,11] in the solid phase. The oxides remain in the char layer, which adds an insulating effect. These flame retardants are added in a relatively large amount (50 to 65% by weight of resin) compared to other types of additives. By adding a significant amount of an inorganic flame retardant, the polymer becomes more brittle. Because this is an inorganic additive, inserting this material into the polymer system by 50 to 65 wt% of the original polymer resin reduces the available fuel within the condensed phase. In addition to this effect, usually the additive has a higher heat capacity compared to the base polymer and hence, the flame retarded polymers with these types of hydroxides require more energy to increase the condensed phase temperature to its pyrolysis level.

Experiments

The "micro-scale" instruments used in this study were manufactured by TA Instruments: Thermogravimetric Analysis Q50 (TGA) and the Differential Scanning Calorimetry Q20 (DSC). Throughout this study, TGA and DSC were used for non-isothermal test purposes and the tests were conducted in nitrogen and air environments to study pyrolysis and oxidation, respectively. In the TGA, 4 different heating rates of 5°C/min., 20°C/min., 40°C/min. and 60°C/min. were applied to measure the mass loss history of the resin and additive sample from 40°C to 800°C. In the DSC, a constant heating rate of 20°C/min. was used to measure the heat flow through the sample during the thermal decomposition of the resin and additive. Tests conducted with the DSC were from 40°C to 500°C where the maximum temperature is lower than that of TGA due to the limitation of the instrument. A sample size of approximately 10 mg was used for each test in a standard aluminium pan with a punctured lid so that gases may evolve freely away from the pan.

Cone Calorimeter (Cone, ASTM E 1354 [6]) is a bench-scale fire test apparatus in which a 1D flat sample is radiatively heated by an electrically powered rod in the shape of a cone. The Cone exposes the sample to a uniform heat flux in an ambient environment which results in a natural convection flow field as the sample temperature increases allowing cooling above the sample surface. The ignition source is an intermittent sparker. The Cone can be used to calculate useful engineering data such as oxygen consumption based heat release rate, mass loss rate, smoke yield and smoke extinction coefficient.

The purpose of the bench-scale testing was to generate 1D pyrolysis data sets appropriate for modeling and parameter estimation. Therefore in addition to the standard Cone measurements thermocouples were added to the 1D sample. Typically 4 thermocouples were installed to measure temperature change of the sample at various depths: exposed front surface, 1/3 and 2/3 in-depths, and unexposed back surface of the sample.

The uncertainties in the mass loss rate (MLR) and thermocouple measurements at surfaces (exposed, T_s and unexposed, T_b) were quantified by comparing data from three identical tests in the Cone Calorimeter with applied heat flux level of 50 kW/m². Note that normalized time, time divided by sample thickness square, i.e., $\tau = \text{time}/\delta^2$ is used to remove the effect of different sample thicknesses when comparing. Because the data is transient, values at different times ($\tau = 1, 3, 5$ and 7 s/mm^2) from each test have been used to calculate the standard deviation at each time. Then these are averaged and used to estimate uncertainty by applying student t distribution with a sample size of 3 and calculating the

95% confidence interval – $\pm 2.2 \text{ g/s-m}^2$, $\pm 67 \text{ }^\circ\text{C}$ and $\pm 14^\circ\text{C}$ for MLR, T_s and T_b .

Thermal Decomposition Kinetic Modeling

The first step to create a given virtual material is to determine the level of complexity needed for the thermal decomposition kinetics of the resin and any additives. Candidate kinetics models are developed based on thermal analysis [12,13,14,15] using TGA and DSC data (see Figure 1). In a reduced form, thermal decomposition of MA+A can be grouped into a maximum of four stages – three for initial (ambient temperature to $\sim 200^\circ\text{C}$), major (200°C to $\sim 500^\circ\text{C}$), and final (500°C to $\sim 700^\circ\text{C}$) resin (MA) decomposition and one additional stage where decomposition of the additive (A) is observed at relatively lower temperatures (200°C to $\sim 400^\circ\text{C}$).

The final kinetic model for the FRP is chosen based on a screening procedure that simulates mass loss during 1D FRP pyrolysis by using bench scale temperature data from the Cone Calorimeter as a proxy for conservation of energy on the FRP. This approach assumes that thermal decomposition is a function of temperature only and products are instantaneously released to the gas phase without interruption, which is typically used in general comprehensive pyrolysis modeling in the fire community [1]. The screening process is capable of decoupling the kinetic simulation from the overall pyrolysis simulation and evaluating the appropriateness of each kinetic model proposed.

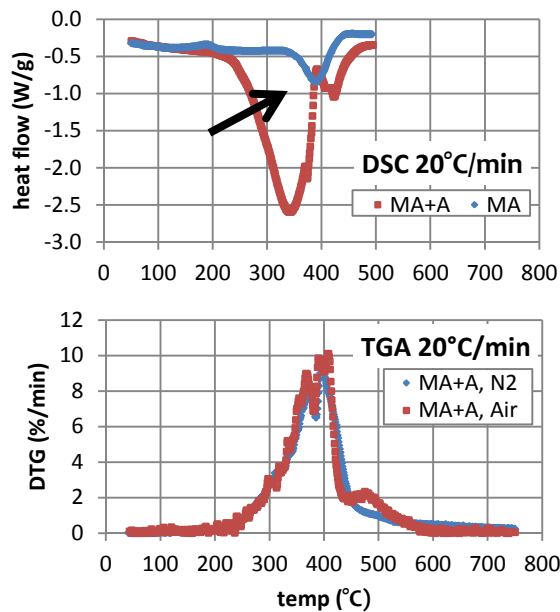


Figure 1. (Top) DSC experiments conducted in N_2 at 20°C/min : strong endothermic peak (\rightarrow) is only found in heat flow measurement of decomposition of resin with

additive (red). (Bottom) DTG from TGA experiments conducted in N_2 and air at 20°C/min .

Six different kinetic models were tested which utilize empirical (Eq.1) or Arrhenius form (Eq.2); $n = 1$ or n th order reaction models, $f(\alpha) = (1-\alpha)^n$ with Arrhenius form; single or multiple reactions, and applying single or multiple iso-heating rate TGA data to estimate kinetic parameter values (see **Error! Reference source not found.**). Note that the fitness of the kinetic models to TGA data increases from approach A to F. The results of the screening procedure for 1D pyrolysis simulation showed the effects of applying these different models on the simulation of mass loss rate should be considered as insignificant (i.e. changes in mass loss rates (MLRs) are less than uncertainty in MLR data).

$$\alpha = aT + b. \quad \text{Eq.1}$$

$$\frac{d\alpha}{dt} = A \exp\left(-\frac{E_a}{RT}\right) f(\alpha) \quad \text{Eq.2}$$

Table 1. Different kinetic models with estimated kinetic parameter values: Parameters with *, ** and *** are assumed values, estimated values from thermal analysis and calculated values from analytical solution, respectively. A and B utilizes single iso-heating rate TGA data and C through F applies multiple rate TGA data.

	Parameters	Reactions			
		R1	R2	R3	A
A	weight frac.		0.55		
	a (/K)		0.009		
	b		6.6		
B	weight frac.		0.55		
	log A (log(/s))		7.8***		
	E (kJ/mol)		126***		
	n (/)		1*		
C	weight frac.		0.35		0.20
	log A (log(/s))		12		11.9
	E (kJ/mol)		183		160
	n (/)		1*		1*
D	weight frac.		0.35		0.20
	log A (log(/s))		12.3		12.6
	E (kJ/mol)		183**		160**
	n (/)		0.9		5
E	weight frac.	0.05	0.30	0.02	0.20
	log A (log(/s))	16.3	12.2	10.2	11.4
	E (kJ/mol)	183**	183**	183**	160**
	n (/)	1*	1*	1*	1*
F	weight frac.	0.05	0.30	0.02	0.20
	log A (log(/s))	16.5	12.5	10.5	12.2
	E (kJ/mol)	183**	183**	183**	160**
	n (/)	5.0	1.3	1*	5.0

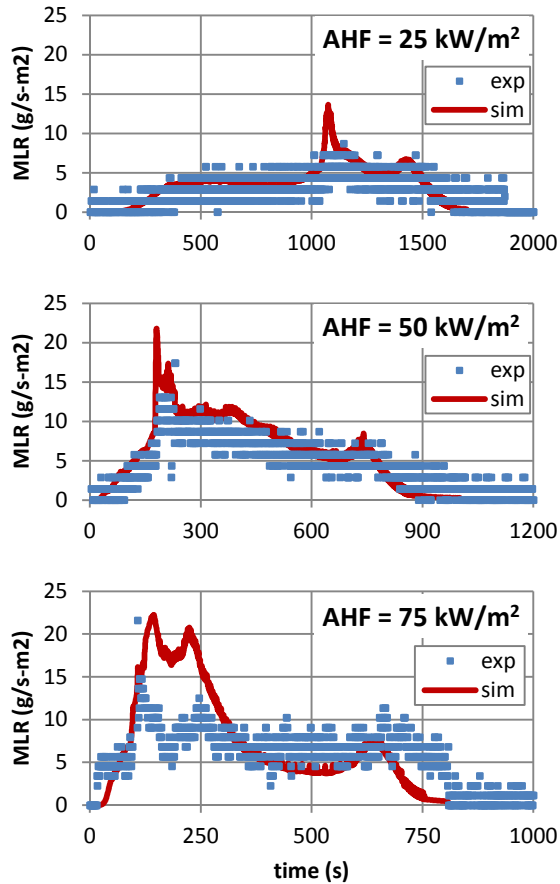


Figure 2. Mass loss rates from Cone Calorimeter experiments (exp) and screening procedure pyrolysis simulations (sim) are shown for MA+A FRP composite. Applied heat flux levels are 25 (top), 50 (middle) and 75 (bottom) kW/m^2 . Simulation results are within the averaged uncertainty bounds of experiment data ($\pm 2.2 \text{ g/s-m}^2$) for top and middle cases.

In Figure 2, screening simulations with kinetic model F (best fitness to TGA data) of mass loss rates are shown for cases with different applied heat flux levels – 25, 50 and 75 kW/m^2 . The results show that at lower heat flux levels good agreement between experiment data and simulations are found where the averaged difference between data and simulations is less than the average uncertainty of mass loss rate data, $\pm 2.2 \text{ g/s-m}^2$. However, at higher heat flux levels, there is a significant deviation in simulation results from measured MLR at earlier times. This is suggestive that at higher heat flux levels, applying assumptions of thermal decomposition being only a function of temperature and having no interruption during release of pyrolysis products becomes inappropriate.

Parameter Estimation via Optimization

The comprehensive pyrolysis modeling and parameter estimation via numerical optimization reported

here are conducted with a generalized pyrolysis model [3,4] that can be applied to a wide variety of condensed phase fuels. The model simultaneously calculates the condensed phase mass conservation, gas phase mass conservation, condensed phase species conservation, and condensed phase energy conservation equations. This model can be applied to 1D systems and is therefore capable of simulating “slab” (Cone Calorimeter) experiments. Extensive details are given in Ref. [3]. In this study, among various optimization routines available in this model, genetic algorithm (GA) is used where multiple near optimal sets that generate similar modeling outputs are found.

Although insignificant changes were observed for simulation of mass loss rate with different kinetic models, three kinetic models (B, C and E) with various complexities are chosen to be used in a parameter estimation process using numerical optimization to examine the effect of kinetic model complexity on the process. With the complexity of the kinetic model determined the number of parameters needed to define the virtual material based on a comprehensive pyrolysis model, GPYRO [Error! Bookmark not defined.] is determined, which are 18, 30 and 38 for B, C and E kinetic model, respectively. Bench-scale experiment data from the Cone is used as optimization targets in parameter estimation – mass loss rate, front and back surface temperature histories. The target data are from a single test with applied heat flux level of 50 kW/m^2 instead of utilizing multiple data sets with different heating rates. This approach was used to ensure that parameter estimation is performed within the bounds of pyrolysis modeling limitation set by the assumptions applied, i.e. assuming thermal decomposition is a function of temperature only and products are instantaneously released to the gas phase without interruption. Otherwise, the effect of modeling results deviating from experimental data at earlier times with higher heat flux levels (see bottom of Figure 2) will be accounted for in the estimated parameter values to compensate for this undesirable deviation. Note that fairly wide searchable range, typically 2-3 orders of magnitude between minimum and maximum value, was applied for each unknown parameter when conducting optimization.

The parameter estimation process was successful for kinetic models B and C (1 and 2 step KM); however, parameter estimation with the most complex kinetic model among the three cases, kinetic model E was unsuccessful. For 1 and 2 step KMs, near optimal parameter sets of 50 and 20 are used, respectively, to estimate the average and uncertainty using 95% confidence intervals applying a student t-distribution of the estimated values. The best-fit cases from parameter estimation with 1 and 2 step KM are shown with experiment data in Figure 3. Both cases are in a good

agreement with the data where modeling outputs are mostly within the uncertainty bands of the experiment data.

Table 2 and Figure 4). The results show that estimated values with 2 step KM are significantly closer to measured values than those with 1 step KM.

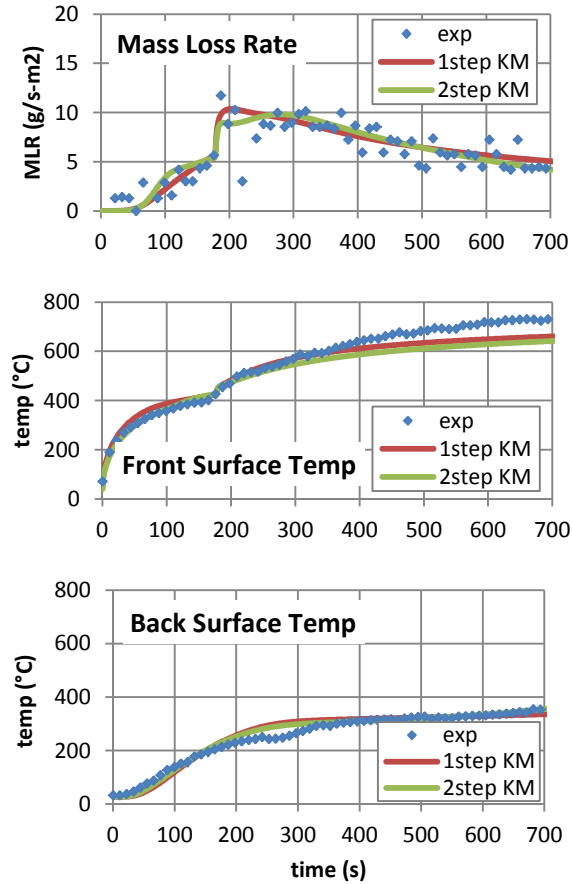


Figure 3. Mass loss rate, front and back surface temperature histories from Cone Calorimeter experiments (exp) and comprehensive pyrolysis modeling results with parameters estimated from numerical optimization using two different kinetic models (1 and 2 step KM) are shown for MA+A FRP composite. Applied heat flux level is 50 kW/m². Modeling outputs are mostly within the uncertainty bands of the experiment data.

The results of the successful optimization strategies – estimation with different kinetic models (1 or 2 step KM) – are evaluated by comparison to independent measurements made with standard tests [16,17,18,19] at temperatures below the FRP’s decomposition temperature – thermal conductivity (k) of resin with additive (MA+A) and the FRP, specific heat capacity (c_p) of MA+A and the FRP, and emissivity (ε) of resin with additive and the FRP composite (see

Table 2. Comparison between measured parameter values for thermal conductivity and emissivity of MA+A and FRP composite and estimated values from numerical optimization: Last column shows the percentage difference between measured and estimated values for two kinetic models where a significant reduction of difference occurs when more complicated kinetic model is used in the estimation process.

	Meas. Value	Estimated Value			% Diff
		KM Type	Avg	\pm 95% C.I. (t-dis)	
k (MA+A) [W/mK]	1.060	1 step	0.349	0.017	67
		2 step	1.018	0.158	4
k (FRP) [W/mK]	0.573	1 step	0.320	0.011	44
		2 step	0.733	0.109	28
ϵ (MA+A) [-]	0.868	1 step	0.790	0.027	9
		2 step	0.849	0.040	2
ϵ (FRP) [-]	0.912	1 step	0.809	0.019	11
		2 step	0.857	0.031	6

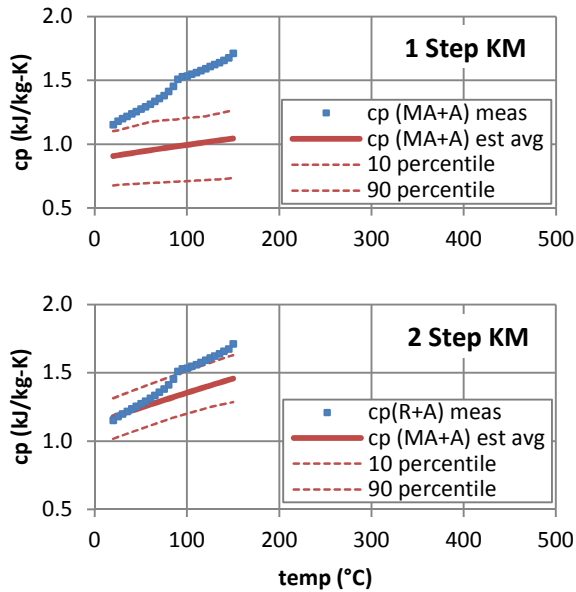


Figure 4. Comparison between measured specific heat values and estimated values from numerical optimization with different kinetic models – 1 Step KM (top) and 2 Step KM (bottom): Results show that when a more complicated kinetic model is used in the estimation process the estimated values become closer to measured values.

Discussion

These findings are suggestive of the following: (1) An optimum level of complexity in kinetic modeling

exists where more complex kinetic models that can reproduce TGA data with higher precision may result in too many unknowns resulting in unsuccessful numerical optimization finding no solution for the given problem (4 step kinetic model case) and where more simple kinetic models may result in estimating parameter values that are inconsistent with values obtained from standard measurements (1 step kinetic model case); (2) With a proper kinetic model with optimum complexity and appropriate experiment data used as optimization targets, parameter estimation via numerical optimization is capable to estimate parameter values that are consistent with values obtained from standard measurements, indicating the possibility of considering certain estimated values as material properties.

Conclusions

In this study, parameter estimation for comprehensive pyrolysis modeling [3,4]] of a FRP composite is conducted to explore the potential to use modeling during the development stage of FRPs with good fire characteristics. To create virtual materials using pyrolysis modeling, first kinetic modeling is conducted with independent thermal analyses using TGA and DSC experimental data. Several kinetic models with different complexity have been proposed and their effect on modeling is evaluated using a screening process that involves mass loss rate simulation of 1D FRP pyrolysis using bench-scale temperature data as a proxy for conservation of energy on the FRP. Through this procedure, it has been shown that insignificant changes occur with respect to changes made in the kinetic model. Knowing this, different kinetic models – 1, 2 or 4 step models – are applied to parameter estimation process to examine their effect on the estimation. The results have shown that estimation based on the 2 step kinetic model is better than that of 1 step kinetic model in terms of having estimated values be more consistent with the independently measured values. The estimation of 4 step model was unsuccessful due to the limitation of the numerical optimization routine. This work presents a possibility of utilizing numerical optimization for parameter estimation to estimate model parameters that can be reproduced from standard measurements when proper kinetic model with optimum complexity is applied and appropriate experiment data are used as optimization targets.

Acknowledgements

The authors greatly appreciate the support for this work from DOC NIST Award Number 60NANB8D8106 (Federal Program Officer Dr. Kevin McGrattan). Special thanks goes to Charles Dore for fabricating and donating the modified acrylic FRP composite materials used in this

study. Many thanks also to Randall Harris at WPI for conducting the Cone Calorimeter tests.

References

1. Kevin McGrattan, Simo Hostikka, Jason Floyd, Howard Baum, Ronald Rehm, William Mell and Randall McDermott, Fire Dynamics Simulator (Version 5) Technical Reference Guide, NIST Special Publication 1018-5, October 29, 2010
2. S.I. Stoliarov, R.E. Lyon, Federal Aviation Administration Technical Note, DOT/FAA/AR-TN08/17, 2008; available for download at <http://www.fire.tc.faa.gov/reports/reports.asp>.
3. Lautenberger, C., Gpyro – A Generalized Pyrolysis Model for Combustible Solids, Technical Reference, Version 0.700, February 19, 2009
- 4 Lautenberger C and Fernandez-Pello C. Optimization algorithms for material pyrolysis property estimation. *Fire Saf Sci* 2011; 10: 751–764.
- 5 Chaos M, Khan MM, Krishnamoorthy N, et al. Evaluation of optimization schemes and determination of solid fuel properties for CFD fire models using bench-scale pyrolysis tests. *P Combust Inst* 2011; 33(2): 2599–2606
- 6 Standard Test Method for Heat and Visible Smoke Release Rates for Materials and Products Using an Oxygen Consumption Calorimeter, ASTM E 1354-02, ASTM, 100 Barr Harbor Drive, West Conshohocken, PA, USA
- 7 Handbook of polymer blends and composites By Anand K. Kulshreshtha, Cornelia Vasile
- 8 Lewin, M., Synergism and Catalysis in Flame Retardancy of Polymers, *Polym. Adv. Technol.* 12, 215-222 (2001)
- 9 LeVan, S.L., The Chemistry of Solid Wood; Chapter 14. Chemistry of Fire Retardancy, American Chemical Society, 1984
- 10 A.K. Galwey, G.M. Lavery, N.A. Baranov and V.B. Okhomikov, *Phil. Trans. R. Soc. London*, A347 (1994) 139, 157
- 11 V.B. Okhotnikov, S.E. Petrov, B.I. Yakobson and N.Z. Lyakhov, *React. Solids*, 2 (1987) 359
- 12 T. Ozawa, "A new method of analyzing thermogravimetric data," *Bull. Chem. Soc. Jpn.*, vol. 38, pp. 1881–1886, 1965.
- 13 J. H. Flynn and L. A. Wall, "A quick, direct method for the determination of activation energy from thermogravimetric data," *J. Polym. Sci. Polym. Lett.*, vol. 4, pp. 323–328, 1966.
- 14 H. L. Friedman, "Kinetics of thermal degradation of char-forming plastics from Thermogravimetry. Application to a phenolic plastic," *J. Polym. Sci., Pt. C* 6, 183-195 (1964)
- 15 J. H. Flynn, L. A. Wall, "A quick, direct method for the determination of activation energy from thermogravimetric data," *J. Polym. Sci. Polym. Lett.* 4, 323-328 (1966).
- 16 Standard Test Method for Steady State Thermal Transmission Properties by Means of the Heat Flow Meter Apparatus, ASTM C518, ASTM, 100 Barr Harbor Drive, West Conshohocken, PA, USA
- 17 Standard Test Method for Thermal Conductivity of Solids by Means of the Guarded Comparative Longitudinal Heat Flow Technique, ASTM E1225, 100 Barr Harbor Drive, West Conshohocken, PA, USA
- 18 Standard Test Method for Determining Specific Heat Capacity by Differential Scanning Calorimetry, ASTM E1269, 100 Barr Harbor Drive, West Conshohocken, PA, USA
- 19 Standard Test Methods for Total Normal Emittance of Surfaces Using Inspection Meter Techniques, ASTM E408, 100 Barr Harbor Drive, West Conshohocken, PA, USA

Appendix C

Evaluation of Different Approaches for Property Estimation for Pyrolysis Modeling Applied
to FRP Composites

Fire and Materials 2011, 12th International Conference

EVALUATION OF DIFFERENT APPROACHES FOR PROPERTY ESTIMATION FOR PYROLYSIS MODELING APPLIED TO FRP COMPOSITES

Esther Kim* & Nicholas Dembsey
Worcester Polytechnic Institute, USA

ABSTRACT

For the composites industry to “design for fire” more thorough understanding of how typical FRPs decompose under fire conditions is needed. The role played by the glass and the resin for FRPs are keys to understanding their fire behavior. The goal of this work is to evaluate the ability of a pyrolysis model and optimization routine pairing to estimate properties of each component of the composite, resin and glass. The composite pyrolysis experimental data used in this work was obtained from tests conducted on a bench scale fire test apparatus, Cone Calorimeter, at various applied heat flux levels with additional instrumentation to measure surface and internal temperatures of the sample and the flame heat flux. Mass loss data, temperature profiles with respect to time at different in-depth locations and heat flux from the flame to sample surface after ignition for boundary condition specification are used in the optimization process. The decomposition kinetics for the resin is modeled using thermal analysis where a series of dynamic experiments of the resin is conducted using thermogravimetric analysis and differential scanning calorimetry. With the approximated decomposition kinetics for the resin determined, simulation of pyrolysis tests of the composite slab in air was performed to estimate the unknown thermophysical properties by Genetic Algorithm (GA) and Shuffled Complex Evolution (SCE) optimization routines. As a part of the property estimation exercise, emphasis was given to evaluating different approaches for estimating properties when applying the optimization technique. This evaluation is achieved by conducting property estimation for the same material with 2 different procedures: running the optimization with Cone data from time of sample exposure to 1) pre-decomposition, or 2) post-decomposition. These numerical experiments are designed to demonstrate the effectiveness of solid phase property estimation when applying partial data from certain times during Cone testing. The estimated properties from these different approaches will be compared and the quality of the estimations will be assessed.

INTRODUCTION

For the composites industry, designing for a FRP that provides good fire characteristics becomes a guess and check operation in many cases. Any changes made to the resin, glass, or the microstructure of the FRP affect the overall fire behavior of the FRP. Traditionally, the effect of the changes made in the FRP is checked by conducting tests via standard fire tests, which can be time consuming and expensive. Therefore, providing an understanding of how typical FRPs decompose under fire conditions and using this information to find an appropriate guideline for the composite industry to produce better fire-safe composites have been a long-term goal for this research.

In this study, an emphasis is given to evaluating the different approaches for estimating the unknown parameters for pyrolysis modeling of the FRP. The parameter estimation process is generally grouped into two parts. The first part is conducted to estimate the parameters related to decomposition kinetics of the resin knowing that the resin is the decomposable component of the system, FRP. The decomposition

kinetics for the resin is modeled using thermal analysis where a series of dynamic experiments of the resin is conducted using thermogravimetric analysis and differential scanning calorimetry. The second part is conducted to estimate the parameters representing the thermophysical properties of the FRP with the estimated kinetic parameters from previous work. When estimating these parameters in this second part, typically a numerical optimization routine is used, along with a pyrolysis model. This study focuses on the second part of the work by evaluating different approaches to estimate thermophysical parameters using a numerical optimization process. Numerical experiments are designed to conduct property estimation for the same FRP material with 2 different procedures and 2 different optimization routines. Estimation is conducted by running the optimization with Cone data from time of sample exposure to the heat source to 1) pre-decomposition, or 2) to post-decomposition.

To conduct property estimation and modeling, complete data sets of decomposition of neat phenolic resin and its FRP composites are presented. Careful experiments were conducted using Thermogravimetric Analysis (TGA) and Differential Scanning Calorimetry (DSC) in order to study the thermal decomposition kinetics. Also, the neat phenolic FRPs were tested under a bench-scale fire test apparatus known as the Cone Calorimeter (ASTM E 1354¹) with additional instrumentation such as thermocouples at various depths and a total heat flux gauge to measure additional heat flux from the flame after ignition. These tests were designed to generate data specifically useful for computer modeling purposes.

The model used in this study is a generalized pyrolysis model developed by Lautenberger^{2,3}, which simulates the heating and decomposition of a chosen material. Like with any other pyrolysis model, this model requires many input parameters found from material properties, which include the pyrolysis kinetics, thermal properties (specific heat capacity, thermal conductivity), and radiative characteristics (surface emissivity, in-depth radiation absorption coefficient). Unfortunately, there are no standardized techniques to determine all of these properties via laboratory tests. Another way of estimating parameters is to use an optimization routine with a pyrolysis model in pair. The current work applies Genetic Algorithm (GA) and Shuffled Complex Evolution (SCE) methodology as an optimizing method coupled with Lautenberger's pyrolysis model^{2,3} to perform parameter estimation.

Using the experimental data of the neat phenolic FRP, an estimation exercise is conducted to find properties of the individual components of the composite, i.e., resin and glass, which are decomposable and inert, respectively.

The property estimation exercise is conducted on a neat phenolic FRP composite tested in a Cone Calorimeter. First, thermal analysis is conducted using thermogravimetric analysis (TGA) and differential scanning (DSC) calorimetry experiment results of the resin to model the decomposition kinetics of the decomposable element of the FRP. With the approximated decomposition kinetics for the resin, simulation of pyrolysis tests of the composite slab in air was performed to estimate the unknown thermophysical properties by optimization. A comparison is done with estimated parameter values using different approaches to evaluate any consistencies in the estimated results.

TESTING MATERIAL

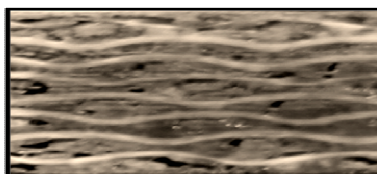
Neat Phenolic Resin

Neat phenolic resin (NP) is a low viscosity, unmodified phenolic resole resin where a flame retardant plasticizer and an acid are used as a catalyst. Phenolic polymers are obtained by polymerizing phenol and formaldehyde⁴. Due to benzene rings built into the chemical chain, this resin has good thermal stability. According to the product description, this resin with the flame retardant additive is formulated to be Class I per ASTM E 84⁵ (flame spread index < 25 and smoke developed index < 450).

FRP Composite Description

Composite panels were fabricated by vacuum bagging for relatively high (60 wt% of glass, average thickness of 9.8 mm) glass content composites, using two different types of fiberglass mats that were wetted with resin (see Figure 1). The two types of fiberglass (E-glass) used in the composite are a chopped strand mat and a glass roving woven mat with an area density of 25 g/m² and 880 g/m², respectively. The chopped strand mat is thinner and more porous than the woven mat. The laminate schedule (provided by the manufacturer) is chopped strand mat and roving alternating eight times for FRP with high glass content (HG) with another chopped strand mat layer at the end. Visual inspection of a polished cross-section of the composite slab is consistent with this laminate schedule, but with polymer resin layers between each fiberglass layer. The chopped strand mat layer is difficult to identify in the cross section, perhaps because more resin is soaked into this layer than the roving layer. The roving layer is observed as a prominent glass layer possibly because the resin is absorbed only at the fiberglass layer surfaces leaving the interior with primarily glass fibers.

Figure 1. Cross-section of Neat Phenolic (NP) FRP fabricated via vacuum bagging with average glass content of 60 wt% and average thickness of 9.8 mm: two types of fiberglass (E-glass) used in the composite – chopped strand mat (25 g/m², highly porous) and glass roving woven mat (880 g/m², prominent glass layers in white)



The layered microstructure is determined to a resolution of 0.3 mm by inspecting a polished cross-section of the composite. Based on visual observation and comparison to global density of the composite sample, approximations of three distinct layers are proposed accounting for the density, ρ of each component of the composite at its non-porous stage – $\rho_{\text{resin}} = 1300 \text{ kg/m}^3$, $\rho_{\text{glass}} = 2600 \text{ kg/m}^3$: porous layer with chopped strand mat with resin (CSM+R), porous layer with some glass roving woven mat (RW+R), and a less-porous layer with glass roving woven mat only (RW). The microstructure of the virtual Neat Phenolic FRP composite is, from the surface, (CSM+R) – (RW+R) – (RW) – (RW+R) repeating 8 times and another (CSM+R) layer at the back face, which resulted in 33 layers.

EXPERIMENT APPARATUSES

Thermogravimetric Analysis (TGA) and Differential Scanning Calorimetry (DSC)

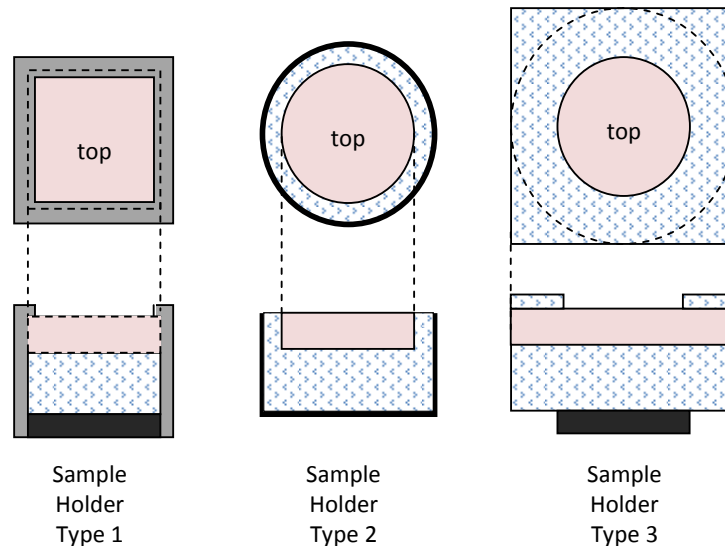
The instruments used in this study were manufactured from TA Instruments: Thermogravimetric Analysis Q50 (TGA) and the Differential Scanning Calorimetry Q20 (DSC). Throughout this study, TGA and DSC were used for non-isothermal test purposes and the tests were conducted in nitrogen to study pyrolysis. Using the TGA, 4 different heating rates of 5°C/min., 20°C/min., 40°C/min. and 60°C/min. were applied to measure the mass loss history of each resin sample from 40°C to 800°C. For the DSC, a constant heating rate of 20°C/min. was used to measure the heat flow through the sample during the thermal decomposition of resins. Tests conducted with the DSC were from 40°C to 500°C where the maximum temperature is lower than that of TGA due to the limitation of the instrument. A sample amount of approximately 10 mg was used for each test in a standard aluminium pan with a punctured lid so that gases may evolve freely away from the pan.

Cone Calorimeter

Cone Calorimeter (Cone, ASTM E 1354¹) is a bench-scale fire test apparatus in which the sample is heated by an electrically heated rod in the shape of a cone. The sample is tested by applying a constant radiative heat flux set via temperature controller of the rod. The Cone exposes the sample in an ambient environment which results in a natural flow field as the sample temperature increases allowing convective cooling above the sample surface. The ignition source is an intermittent sparker. The Cone can be used to calculate useful engineering data such as oxygen consumption based heat release rate (based on the standard), mass loss rate, smoke yield and smoke extinction coefficient.

The purpose of Cone testing was to generate good data sets appropriate for pyrolysis modeling and parameter estimation, and therefore several modifications were made to the standard testing procedure. First, when testing this FRP, three different types of sample holders were used to produce quality one-dimensional data (see Figure 2). Experimental challenges with these FRPs were that significant edge burning, which is a three-dimensional problem, occurs during each test. Because the pyrolysis model of interest in this study has a numerical structure of one-dimension, data that can be considered as one-dimension should be utilized in this parameter estimation exercise using numerical optimization. Hence, caution was given to reduce the edge effect by testing with different sample holders. Sample holder type 1 is a standard specified, non-insulated cone holder that holds a 102 mm x 102 mm (4" x 4") square sample with a metal edge frame. Sample holder type 2 is a round insulated sample dish purposed by de Ris and Khan⁶ that holds a 102 mm (4") diameter circle sample. In this sample dish, the sample is surrounded by Cotronics® paper insulation on the back and sides to limit heat loss, which simplifies the pyrolysis modeling. Sample holder type 3 is composed of ceramic fiberboard (Thermal Ceramics Inc.) that holds a 152 mm (6") diameter circle sample. On top of the sample, a layer of ceramic fiberboard with a hole in the center was placed to limit the sample surface exposure to the cone heater.

Figure 2. Three types of sample holders used in Cone Calorimeter experiment: first and second rows show the top and side view, respectively. Sample is shown in pink, metal edge frame in gray, metal holder in black, and insulation in area with pattern.



Second, 2 thermocouples were installed to measure temperature change of the sample at surface and back face of the sample. The surface thermocouples were affixed via two types of methods: One method was to drill a thermocouple hole from the sample side and allow the hole to reach the surface. A thermocouple

insulated wire was inserted through the side and the bead was able to locate near the surface; hence, from the surface only the bead was visible. Using this method, the center of the bead was located at the surface allowing top half to be exposed to ambient air and the lower half to sit within the sample. A drop of thermal grease or a high temperature adhesive (Resbond 907 Industrial Strength Fireproof Adhesive from Cotronics Corp.) was applied to the bead to ensure good contact between the sample and the bead. Another method was to crimp the thermocouple wire to allow the thermocouple bead to sit on the surface with a minimal amount of thermal grease applied at the bead. The back face thermocouples were affixed with a high temperature adhesive (Resbond 907 Industrial Strength Fireproof Adhesive from Cotronics Corp.).

To evaluate which of the three sample holder types are most appropriate for testing this Neat Phenolic FRP composite with high glass (~60wt%), several Cone tests were conducted at different heat flux levels ranging from 30 to 90 kW/m². Analyzing the results, data from applying type 1 sample holder was utilized in this study for the following reasons: First, considering the temperature increase with respect to one-dimensional heating, although type 3 provides the best condition for one-dimensional approximation, difference between the data from type 3 and type 1 or 2 are about 50°C or less assuming that measurements are made near the centerline of sample. This concurs with Choi's work⁷ on inert materials. Larger size sample has shown to provide the best one-dimensional heat conduction condition comparing to other sample set-ups where regular size (102 mm x 102 mm (4" x 4")) sample is prepared with a metal edge frame, edges exposed, or insulation on the sides and bottom. It was noted that at 80kW/m² of incident heat flux, the centerline temperature difference between that of the larger sample's and centerline temperatures of the regular samples with metal edge frame or insulation on the sides and bottom are approximately 20°C or less within 5 hr period. Second, type 3 results in uncertain burn area due to some decomposition at the sides even with a layer of insulation protecting the sample. This increases the uncertainty in data considered per unit area. However, type 3 allowed visual inspection of the edge burning: when the neat phenolic resin on the back face temperature increased beyond its major decomposition temperature, pyrolyzates traveled around the sample sides and caught fire instead of moving through the composite layers vertically. Even with the resin decomposing in-depth, because the amount of resin residue is sufficient in the composite, the sample was impermeable to pyrolyzates produced from back face resin decomposition. Third, having the edges not exposed as in type 1 and 3 allowed less pyrolyzates to travel horizontally towards the edges, i.e. because the edges are preserved from burning, edges are more impermeable to pyrolyzates. One of the influences from having less pyrolyzates traveling towards the edges is resulting in increased time to ignition.

The uncertainty in the mass loss rate data is estimated via statistical approach, taking the standard deviation (0.58 g/sm²) from the mean of a steady burning of 5 identical PMMA tests conducted in a Cone Calorimeter⁸. The estimated uncertainty is 1.4 g/sm², which is found by calculating the 95% confidence interval applying student t distribution with a sample size of 5. The uncertainty in the thermocouple measurements was quantified by comparing surface and back face temperature data from 3 and 4 identical FRP composite tests with the Neat Phenolic FRP composite with high glass content in the Cone at 70kW/m² and 50kW/m², respectively. Using the normalized time, time divided by sample thickness square, i.e., $\tau = \text{time}/\delta^2$ to remove the effect of different sample thicknesses when comparing, the maximum standard deviation at various normalized times, up to the critical time, τ_c , was 20°C for the surface and 27°C for the back face. Assuming this is approximately equal to one standard deviation, applying student t distribution and calculating the 95% confidence interval becomes $\pm 49^\circ\text{C}$ and $\pm 83^\circ\text{C}$ from the sample mean for surface and back face, respectively. The critical time, τ_c , corresponds to the time of ignition for surface temperature measurements and time when evenly spread flame on sample surface disappearing for back face temperature measurements. For the back face, this time corresponds well with the time when the back face temperature becomes close to the major decomposition temperature of the Neat Phenolic resin. As noted above, after this temperature, edge burning occurs, which is a non-1D phenomenon. These uncertainty values will be used to evaluate significant differences in the modeling results.

KINETIC MODELING OF RESIN DEGRADATION FOR PYROLYSIS MODELING

A series of thermal analyses are conducted on commercial thermoset polymers used in fiberglass reinforced polymer (FRP) composite material. Experiments for thermal analysis are conducted using Thermogravimetric Analysis (TGA) at various heating rates (5, 20, 40 and 60°C/min) and Differential Scanning Calorimetry (DSC) at 20°C/min. These non-isothermal TGA experimental results are used to conduct iso-conversional estimates of activation energy with respect to conversion without pre-determining the kinetic model using an Arrhenius type expression for thermal degradation. Results are also used to determine the minimum number of reactions required in the kinetic model to describe the thermal degradation reactions based on actual weight loss. Then a model fitting method is used where various kinetic models are used to fit the TGA data to the model. The DSC experiments are conducted to use the heat flow information to compare against the analysis results conducted by the TGA. Kinetic modeling is conducted following the steps introduced in this Reference⁹.

PYROLYSIS MODELING FOR LUMPED (TGA) AND SLAB (CONE) EXPERIMENTS

The calculations reported here are conducted with a generalized pyrolysis model^{2,3} that can be applied to a wide variety of condensed phase fuels. The model simultaneously calculates the condensed phase mass conservation, gas phase mass conservation, condensed phase species conservation, and condensed phase energy conservation equations. This model can be applied to both 0D and 1D systems and is therefore capable simulating both “lumped” (thermogravimetric) and “slab” (Cone Calorimeter/FPA) experiments. Extensive details are given in Ref.^{2,3} so only a brief overview is given here. Assumptions inherent in the model, as applied in this paper, include:

- Porosity can either be solved as a property of a species (default) or directly. When porosity is solved directly, it is derived from the condensed-phase mass conservation equation assuming no volume change (shrinkage or swelling).
- When porosity is directly solved, the user-specified thermal conductivity and density are interpreted as those of a nonporous solid. Therefore, the thermal conductivity that appears in the condensed-phase energy conservation equation is $\bar{k} = (1-\psi)\bar{k}_s$ where ψ is porosity and \bar{k}_s is the weighted thermal conductivity of the solid assuming it is nonporous. Similarly, with this formulation, the bulk density is calculated as $\bar{\rho} = (1-\psi)\bar{\rho}_s$ where $\bar{\rho}_s$ is the weighted density of the solid assuming it is nonporous.
- Bulk thermal conductivity \bar{k} has a cut-off value of 0.03W/mK which corresponds to air at 300 to 400K.
- Specific heat is calculated with a weighted or averaged quantity, i.e. $\bar{c}_p = \sum X_i c_{p_i}$ as other solid properties – enthalpy, emissivity, radiation absorption coefficient, permeability, etc.
- Specific heat capacity and effective thermal conductivity vary by as $k(T) = k_0(T/T_r)^{n_k}$ and $c(T) = c_0(T/T_r)^{n_c}$, respectively, where T_r is a reference temperature.
- Radiation heat transfer across pores is accounted for by adding a contribution to the effective thermal conductivity that varies as γT^3 , where γ is a fitting parameter
- Averaged properties in conservation equations are calculated by appropriate mass or volume fraction weighting
- Gas-phase and condensed-phase are in thermal equilibrium

RESULTS AND DISCUSSION

Property estimation exercise for pyrolysis modeling of neat phenolic (NP) FRP composite which contains flame retardant additive is conducted in three parts: First, the kinetic parameters for thermally degrading resin are obtained via kinetic modeling using thermal analysis with non-isothermal experiment data from TGA and DSC tests. Second, parameters other than those related to resin decomposition kinetics are obtained by utilizing optimization routine with a pyrolysis model in pair. Third, a comparison is done with estimated parameter values using different approaches to evaluate any consistencies in the estimated results.

Kinetic modeling for resin degradation

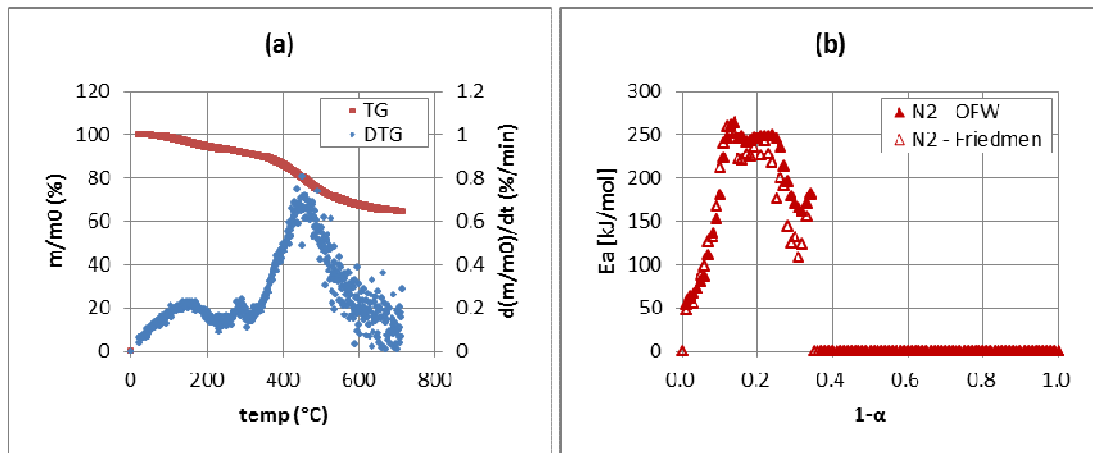
Step 1: Preliminary Experiments with Analysis

Based on preliminary tests on this resin, it was found that when the area to volume (A/V) ratio is changed thermal behavior change as well. Typically, when a polymer sample is cut from a larger sample, the number of mechanically broken polymer bonds increase as the A/V ratio increases. The sample prepared with above method that have high A/V ratio consists polymer chains which are relatively shorter than those found in a larger sample with lower A/V ratio and increased concentration of radicals on the sample surface due to the broken bonds. Polymer samples meeting these conditions can result in changes in their thermogram comparing to those from samples that have lower A/V ratio. In general, the samples appear to be less thermally stable, e.g. increase in initial weight loss at lower temperatures, lower thermal decomposition temperature, higher DTG (weight loss rate) peaks, etc. Considering this effect, relatively larger sample sizes that have low A/V ratio in thermal analysis is recommended.

Step 2: Iso-conversional (Model-free) Method

In Figure 3, the results from two iso-conversional methods introduced by Ozawa, Flynn and Wall^{10,11} (OFW, estimates $-E_a/R$ by plotting $\ln(\beta)$ versus $1/T$) and Friedman^{12,13} (plotting $\ln(da/dT)$ versus $1/T$ to find $-E_a/R$) conducted on the neat phenolic resin are shown. Both methods are used for comparison purposes. The R^2 values for each activation energy value are plotted as well using the least square method. The activation energy becomes more reliable as the R^2 values become closer to 1 where $\alpha = 1 - m/m_0$.

Figure 3. TG and DTG thermograms from TGA experiments conducted in nitrogen with Neat Phenolic Resin (NP) at 5°C/min (a) and results from iso-conversional method conducted on NP resin (b) where the estimated activation energy of thermal decomposition with respect to conversion (1- α) is shown



Step 3: Model Fitting Method

Based on iso-conversional method, 2-step mechanism is proposed as below:



Applying an nth order reaction model, kinetic parameters of the pre-exponential factor (Z), activation energy (E_a), and reaction order (n) are estimated manually as follow:

1. Estimated kinetic parameters using nth order reaction model

	Z (/s)	E _a (kJ/mol)	n (/)	Consumption (%) from Initial Mass
R1	10 ⁸	130	1	14.1
R2	10 ¹⁰	236	1	35.2

Note that these estimated results are simplified and does not represent the actual decomposition kinetics of the given material, i.e. they are empirical values which can only be utilized with this modeling set-up. However, the activation energy for R2 was estimated from iso-conversional method; therefore, the value should be able to represent the actual decomposition kinetics in nitrogen.

Property estimation for Neat Phenolic FRP composite using different approaches

When conducting the Cone simulation for the FRP composite, char oxidation was neglected for modeling simplification. Therefore, decomposition of the neat phenolic resin in nitrogen was used to estimate kinetic parameters and these were used in the cone simulation. Four property estimation cases were built based on the approach of estimation and available optimization routines (GA or SCE). They are summarized as below:

2. Summary of property estimation cases examined in this study constructed using different approaches and optimization routines in pair with pyrolysis model (GPYRO)

Case	Approach	Optimization Routine
1	One step approach: <ul style="list-style-type: none"> Estimate entire property set at pre- decomposition and post decomposition stages using Cone data from 70kW/m² 	GA
2	One step approach: <ul style="list-style-type: none"> Estimate entire property set at pre- decomposition and post decomposition stages using Cone data from 70kW/m² 	SCE
3	Two step approach: <ul style="list-style-type: none"> Estimate properties at pre- decomposition stage using Cone data from 30kW/m² Having above properties fixed, estimate rest using Cone data from 70kW/m² 	GA
4	Two step approach: <ul style="list-style-type: none"> Estimate properties at pre- decomposition stage using Cone data from 30kW/m² Having above properties fixed, estimate rest using Cone data from 70kW/m² 	SCE

The entire property set used in the simulation are shown in the following table:

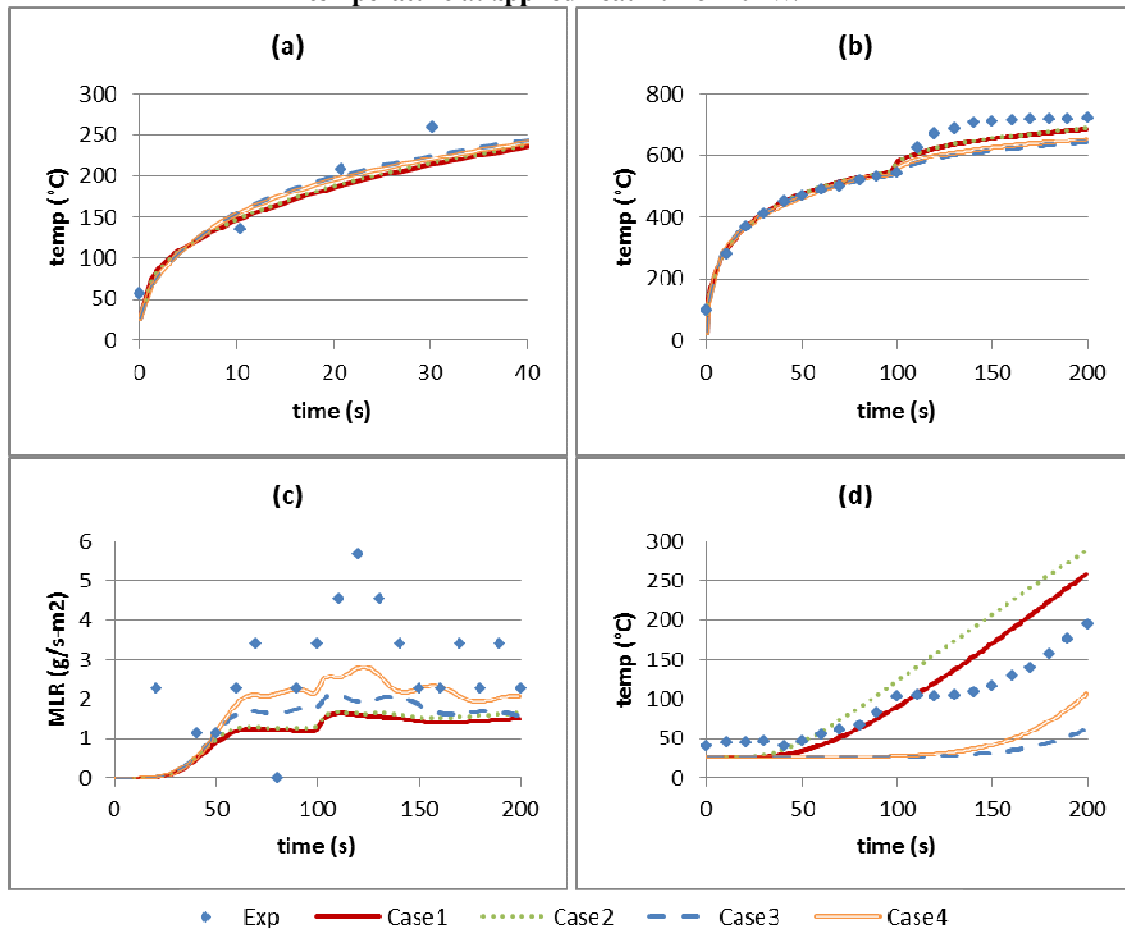
3. Parameter set for Cone simulation

Parameter	Keyword	Resin	Resin'	Char	Fiber Glass
thermal conductivity at T_r	KOZ	Y		Y	Y
thermal conductivity exponent	NKZ	Set as 0.0		Set as 0.0	Y
specific heat capacity at T_r	CO	Y		Y	Y
specific heat capacity exponent	NC	Set as 0.0		Set as 0.0	Y
emissivity	EMIS	Y	Set as 1.0	Y	Y
gamma	GAMMA	Set as 0.0	Y	Y	Y
Heat of Reaction for R1	DHV			Y	
Heat of Reaction for R2	DHV			Y	

To simplify the problem, the exponents of thermal conductivities and specific heat capacities of resin, resin' and char were considered as 0. Only those of fiber glass were expressed as a function of temperature as noted in the previous section on pyrolysis modeling. Considering that the resin quickly becomes black after exposure to the Cone heater, emissivity of the resin' was set as 1.0. Because resin' and char becomes porous as resin decomposes without much shrinkage and fiber glass is porous in nature, a fitting parameter gamma was utilized to account for radiative heat transfer through pores. Additionally, it is assumed that the thermal conductivity and specific heat capacity are the same for resin and resin'. As a boundary condition at the surface, additional constant flame heat flux of 20kW/m² was added to the applied heat flux from the Cone starting at user-specified time of ignition. This value corresponds well with a measured value from actual test. For the back face, actual temperature measurements with respect to time were preferred as a specified boundary condition. However, for cases where this approach proposes heating from the back face, heat loss through the back face was specified instead. In the numerical optimization process, mass loss rate, surface and/or back face temperature measurements were used.

The simulation results with the estimated parameter sets from each case are shown in Figure 4. The first figure (a) is at 30kW/m² and the rest (b, c and d) are at 70kW/m². Note that at 30kW/m² applied heat flux, mass loss rate is negligible (i.e. below uncertainty level) and the back face temperature is at its initial temperature; therefore, they are not shown. Considering the uncertainty of $\pm 49^\circ\text{C}$, surface temperature simulation is in good agreement with the experiment data (a, b) for all cases. For mass loss rate simulation in (c), the results from optimized parameter sets are lower than the actual data even with the consideration of its experiment uncertainty (1.4 g/sm²). This is probably due to the assumption made in the simulation about neglecting char oxidation. Although the magnitude of the mass loss rate may be lower than the actual, note that the trend in changes occurring in the mass loss rate with respect to time is similar. This provides evidence that the microstructure specified in the simulation was well resolved in the simulation. The back face temperature simulations in (d) from all cases are in good agreement with the data considering the uncertainty of $\pm 83^\circ\text{C}$. Simulations from Case 1 and 2 are relatively closer to the data than those from Case 3 and 4, where these are at the outer bounds of the uncertainty band.

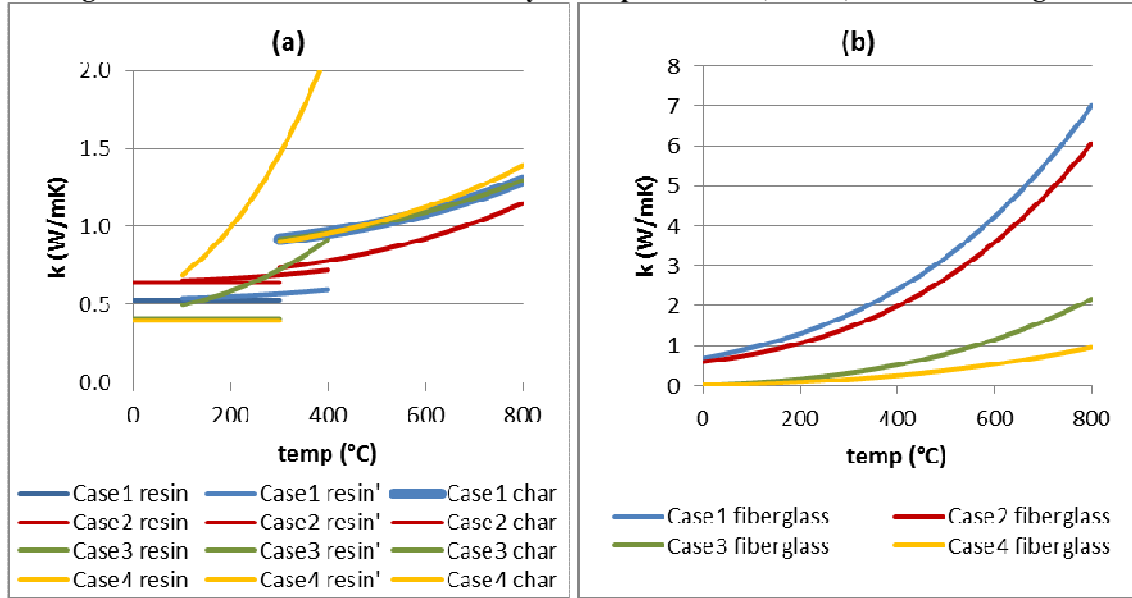
Figure 4. Comparison between simulation results and experiment data: (a) surface temperature at applied heat flux of 30kW/m²; (b) surface temperature, (c) mass loss rate, and (d) back face temperature at applied heat flux of 70kW/m²



Comparison of estimated properties from 4 Cases

The estimated properties of thermal conductivity (Figure 5) and specific heat capacity (Figure 6) from 4 different cases are compared in the figures below. For thermal conductivity of resin and its decomposition products (resin' and char), consistent trend is found for all cases, except for Case 4's resin', which is an outlier. However, it is noteworthy that estimations from Case 3 and 4 are lower at temperatures near ambient (less than 0.5 W/mK) than the others and these values are closer to the reference values of the neat phenolic resin – 0.1 ~ 0.2 W/mK¹⁴. Estimated thermal conductivities of fiber glass from Case 1 and 2 are much higher than those from Case 3 and 4 in general. Considering that the reference value for fiber glass is 0.04 W/mK¹⁵ at temperatures near ambient, estimations from Case 3 and 4 are showing to be closer to the reference values at lower temperatures.

Figure 5. Estimated thermal conductivity for 4 species: resin, resin', char and fiber glass



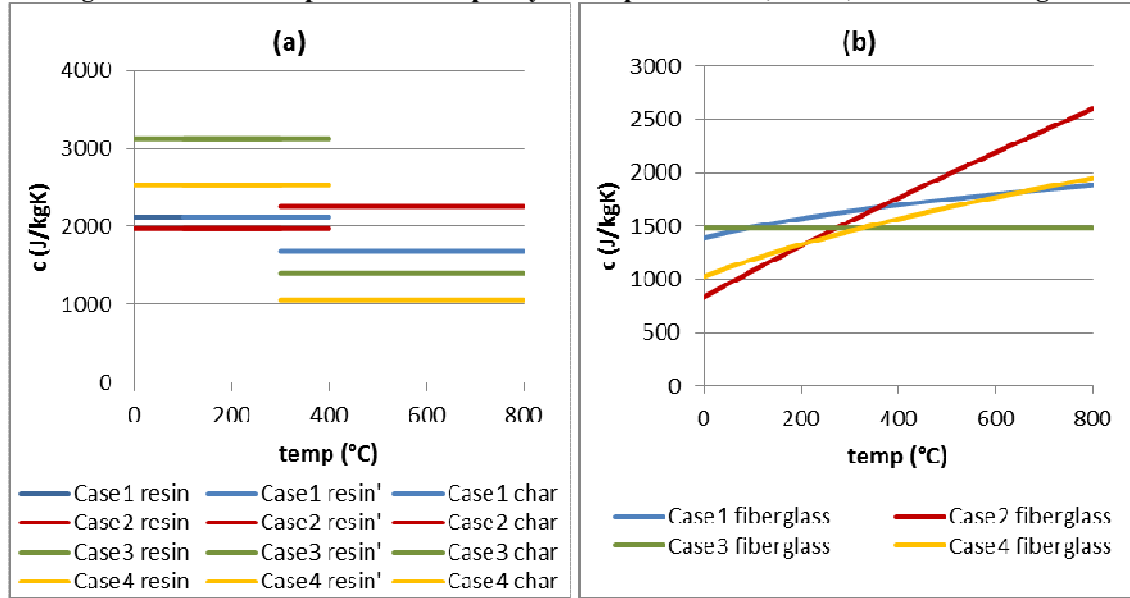
Estimated specific heat capacities of resin and its decomposition products start at higher values at lower temperatures and decreases at higher temperature for Case 1, 3 and 4. For estimation of Case 2, it is the opposite; however, the magnitude of the change is small compared to other cases. Considering that the reference value for neat phenolic resin is near 1700 J/kgK¹⁶, estimations from Case 1 and 2 are showing to be closer to the reference values at lower temperatures. Estimated specific heat capacity of fiber glass from each case show consistency, except for that of Case 2 where steep increase is shown with respect to temperature increase. Reference values for glass and air are 840 J/kgK¹⁷ and near 1000 J/kgK¹⁸, therefore, fiber glass heat capacity should be within this range at ambient temperature. Having this in mind, results from Case 2 and 4 are closer to the reference values.

Parameter estimation of emissivity and heat of reactions were similar for all 4 cases, which are summarized in the following table:

4. Estimated emissivity for 4 species (resin, resin', char and fiber glass) and HoRs for R1 and R2

	Emissivity				Heat of Reaction	
	resin	resin'	char	fiberglass	R1	R2
Case1	1.0	1.0	0.8	0.9	3.0E+04	2.7E+04
Case2	1.0	1.0	0.9	0.7	5.6E+05	1.3E+04
Case3	0.7	1.0	0.9	0.9	3.1E+05	2.5E+05
Case4	0.6	1.0	1.0	0.9	1.0E+06	7.6E+03

Figure 6. Estimated specific heat capacity for 4 species: resin, resin', char and fiber glass



CONCLUSIONS

In this study, parameter estimation for neat phenolic fiberglass reinforced polymer (FRP) composite has been conducted using different approaches and optimization routines in pair with one-dimensional pyrolysis model (GPYRO). With the decomposition kinetics for the resin modeled independently, simulations of Cone tests of the composite at heat flux levels of 30kW/m^2 and 70kW/m^2 were performed to estimate the unknown thermophysical properties via numerical optimization using Genetic Algorithm (GA) or Shuffled Complex Evolution (SCE) optimization routines. Four cases has been explored – Case 1: estimate entire property set using Cone data at 70kW/m^2 up to post-decomposition stage with GA; Case 2: estimate entire property set using Cone data at 70kW/m^2 up to post-decomposition stage with SCE; Case 3: estimate properties at pre-decomposition stage using Cone data at 30kW/m^2 and with those fixed, estimate rest using Cone data at 70kW/m^2 with GA; Case 4: estimate properties at pre-decomposition stage using Cone data at 30kW/m^2 and with those fixed, estimate rest using Cone data at 70kW/m^2 with SCE.

Analyzing the estimation results from 4 cases has presented the following conclusions: First, the two approaches – (1) estimating the entire property set at once or (2) estimating properties in pre-decomposition stage then with those estimated values fixed estimating the rest – generate estimations that are both in good agreement with experiment data. In terms of their estimations compared to reference values, the exercise have shown that approach (2) finds values closer to reference values for thermal conductivity only than approach (1). Considering the computer time and power necessary in the optimization process, approach (1) requires more than approach (2) knowing that the entire parameter set is grouped into two sets for approach (2) and less parameters to optimize in one run means less computation work. For example, when using SCE, the number of processors involved in one optimization run should be similar to the number of unknown parameters to be optimized. Hence, benefit of utilizing approach (2) instead of approach (1) comes from saving computational time and power.

Second, the two optimization routines – GA or SCE – generate estimations that are both in good agreement with experiment data. The major difference between the two routines is GA finds many near optimal solutions (parameter sets) while SCE always converges to one set. However, caution should be given that resulting in one optimized parameter set from SCE does not mean those values are absolute, global

solutions considering GA can develop many near optimal parameter sets using the same experiment data in the optimization process and resulting in similar simulation output quality as in those from SCE.

Third, analyzing 4 cases in this study clearly shows that when numerical optimization is used in the parameter estimation process, the optimized parameter set generated from the exercise should be considered as a linked parameter set along with the pyrolysis model of choice. The different approaches and optimization routines are resulting in different parameter values but the parameter set from each case shows similar simulation output quality. However, determining which values are more physical are significantly limited at this point. This assures the users to be more cautious in extrapolating the information obtained from parameter estimation using numerical optimization.

ACKNOWLEDGMENTS

The authors would like to thank Charles Dore for fabricating the FRP composite materials used in this study. Many thanks also to Randall Harris at WPI for conducting the Cone Calorimeter tests. The authors thank Chris Lautenberger and the computer cluster managers at WPI for helping us run the code.

REFERENCES

- ¹ Standard Test Method for Heat and Visible Smoke Release Rates for Materials and Products Using an Oxygen Consumption Calorimeter, ASTM E 1354-09, ASTM, 100 Barr Harbor Drive, West Conshohocken, PA, U.S.
- ² Lautenberger, C., "A Generalized Pyrolysis Model for Combustible Solids", Ph.D. Dissertation, Department of Mechanical Engineering, University of California, Berkeley, Fall 2007
- ³ Lautenberger, C., Gpyro – A Generalized Pyrolysis Model for Combustible Solids Users' Guide, Version 0.609, July 23, 2008
- ⁴ Odian George, Principles of Polymerization, 3rd ed., John Wiley & Sons, Inc., c1991
- ⁵ Standard Test Method for Surface Burning Characteristics of Building Materials, ASTM E 84-05, ASTM, 100 Barr Harbor Drive, West Conshohocken, PA, U.S.
- ⁶ de Ris, J.L. and Khan, M.M., "A sample holder for determining material properties," *Fire and Materials*, 24, 219-226 (2000).
- ⁷ Keum-Ran Choi, 3D Thermal Mapping of Cone Calorimeter Specimen and Development of a Heat Flux Mapping Procedure Utilizing an Infrared Camera, PhD Dissertation, Fire Protection Engineering, WPI, 2004-08-30, ETD-020205-215634
- ⁸ Lei Zhao, Bench Scale Apparatus Measurement Uncertainty and Uncertainty Effects on Measurement of Fire Characteristics of Material Systems, MS Thesis, Fire Protection Engineering, WPI, 2005-04-27, ETD-050105-182456
- ⁹ Esther Kim, S Shivkumar, N Dembsey, Thermal Degradation Kinetics Modeling for Pyrolysis Modeling Using Fire Retarded Thermoset PolymerResins, INTERFLAM 2010, 5 – 7 July 2010, East Midlands Conference Centre University of Nottingham, UK
- ¹⁰ Ozawa, T., *Bull Chem Soc Jpn* 1965;38;188
- ¹¹ Flynn, J., Wall, L.A., *J Polym Lett* 1966;4:232
- ¹² Friedmen, H.L., *J Polym Sci Part C* 1964;6:183
- ¹³ Friedmen, H.L., *J Polym Lett* 1966;4:232
- ¹⁴ Sidney H. Goodman, Handbook of thermoset plastics, 2nd ed., c 1998, Noyes Publications, ISBN: 0-8155-1421-2
- ¹⁵ http://www.engineeringtoolbox.com/thermal-conductivity-d_429.html
- ¹⁶ Hew-Der Wua, Peter P. Chub and Chen-Chi M. Ma, Thermodynamic properties of the novolac type phenolic resin blended with poly(hydroxyl ether of bisphenol A), *Polymer*, Volume 39, Issue 3, 1998, Pages 703-709, doi:10.1016/S0032-3861(97)00320-0
- ¹⁷ Tipler, Paul A., *Physics for Scientists and Engineers*, 4th Ed., W.H. Freeman, (1999).
- ¹⁸ SFPE Handbook of Fire Protection Engineering, 3rd Ed. c 2002, ISBN/SKU 9780877654513

Appendix D

Evaluation of Different Approaches for Property Estimation for Pyrolysis Modeling Applied to FRP
Composites

Composites 2011

Evaluation of Different Approaches for Property Estimation for Pyrolysis Modeling Applied to FRP Composites

by

Esther Kim¹
Nicholas Dembsey¹

¹ Worcester Polytechnic Institute
Department of Fire Protection Engineering
100 Institute Road
Worcester, MA 01609

Abstract

For the composites industry to “design for fire” more thorough understanding of how typical FRPs decompose under fire conditions is needed. The role played by the glass and the resin for FRPs are keys to understanding their fire behavior. To that end, this study continues work presented at Composites 2010. The goal of this work is to evaluate the ability of a pyrolysis model and optimization routine pairing to estimate properties of each component of the composite, resin and glass. The composite pyrolysis experimental data used in this work was obtained from tests conducted on a bench scale fire test apparatus, Cone Calorimeter, at various applied heat flux levels with additional instrumentation to measure surface and internal temperatures of the sample and the flame heat flux. Mass loss data, temperature profiles with respect to time at different in-depth locations and heat flux from the flame to sample surface after ignition for boundary condition specification are used in the optimization process. The decomposition kinetics for the resin is modeled using thermal analysis where a series of dynamic experiments of the resin is conducted using thermogravimetric analysis and differential scanning calorimetry. With the approximated decomposition kinetics for the resin determined, simulation of pyrolysis tests of the composite slab in air was performed to estimate the unknown thermophysical properties by Genetic Algorithm (GA) and Shuffled Complex Evolution (SCE) optimization routines. As a part of the property estimation exercise, emphasis was given to evaluating different approaches for estimating properties when applying the optimization technique. This evaluation is achieved by conducting property estimation for the same material with 2 different proce-

dures: running the optimization with Cone data from time of sample exposure to 1) pre-decomposition, or 2) post-decomposition. These numerical experiments are designed to demonstrate the effectiveness of solid phase property estimation when applying partial data from certain times during Cone testing. The estimated properties from these different approaches will be compared and the quality of the estimations will be assessed.

1. Introduction

For the composites industry, designing for a FRP that provides good fire characteristics becomes a guess and check operation in many cases. Any changes made to the resin, glass, or the microstructure of the FRP affect the overall fire behavior of the FRP. Traditionally, the effect of the changes made in the FRP is checked by conducting tests via standard fire tests, which can be time consuming and expensive. Therefore, providing an understanding of how typical FRPs decompose under fire conditions and using this information to find an appropriate guideline for the composite industry to produce better fire-safe composites have been a long-term goal for this research. To that end, this work follows the work presented at Composites 2010.

In this study, an emphasis is given to evaluating the different approaches for estimating the unknown parameters for pyrolysis modeling of the FRP. The parameter estimation process is generally grouped into two parts. The first part is conducted to estimate the parameters related to decomposition kinetics of the resin knowing that the resin is the decomposable component of the system, FRP. The decomposition kinetics for the resin is modeled using thermal analysis where a series of dynamic experiments of the resin is conducted using thermogravimetric analysis and differential scanning calorimetry. The second part is conducted to estimate the parameters representing the thermophysical properties of the FRP with the estimated kinetic parameters from previous work. When estimating these parameters in this second part, typically a numerical optimization routine is used, along with a pyrolysis model. This study focuses on the second part of the work by evaluating different approaches to estimate thermophysical parameters using a numerical optimization process. Numerical experiments are designed to conduct property estimation for the same FRP material with 2 different procedures and 2 different optimization routines. Estimation is conducted by running the optimization with Cone data from time of sample exposure to the heat source to 1) pre-decomposition, or 2) to post-decomposition.

To conduct property estimation and modeling, complete data sets of decomposition of neat phenolic resin and its FRP composites are presented. Careful experiments were conducted using Thermogravimetric Analysis (TGA) and Differential Scanning Calorimetry (DSC)

in order to study the thermal decomposition kinetics. Also, the neat phenolic FRPs were tested under a bench-scale fire test apparatus known as the Cone Calorimeter (ASTM E 1354¹) with additional instrumentation such as thermocouples at various depths and a total heat flux gauge to measure additional heat flux from the flame after ignition. These tests were designed to generate data specifically useful for computer modeling purposes.

The model used in this study is a generalized pyrolysis model developed by Lautenberger^{2,3}, which simulates the heating and decomposition of a chosen material. Like with any other pyrolysis model, this model requires many input parameters found from material properties, which include the pyrolysis kinetics, thermal properties (specific heat capacity, thermal conductivity), and radiative characteristics (surface emissivity, in-depth radiation absorption coefficient). Unfortunately, there are no standardized techniques to determine all of these properties via laboratory tests. Another way of estimating parameters is to use an optimization routine with a pyrolysis model in pair. The current work applies Genetic Algorithm (GA) and Shuffled Complex Evolution (SCE) methodology as an optimizing method coupled with Lautenberger's pyrolysis model^{2,3} to perform parameter estimation.

Using the experimental data of the neat phenolic FRP, an estimation exercise is conducted to find properties of the individual components of the composite, i.e., resin and glass, which are decomposable and inert, respectively.

The property estimation exercise is conducted on a neat phenolic FRP composite tested in a Cone Calorimeter. First, thermal analysis is conducted using thermogravimetric analysis (TGA) and differential scanning (DSC) calorimetry experiment results of the resin to model the decomposition kinetics of the decomposable element of the FRP. With the approximated decomposition kinetics for the resin, simulation of pyrolysis tests of the composite slab in air was performed to estimate the unknown thermophysical properties by optimization. A comparison is done with estimated parameter values using different approaches to evaluate any consistencies in the estimated results.

2. Neat Phenolic FRP Composite

2.1. Neat phenolic resin

Neat phenolic resin (NP) is a low viscosity, unmodified phenolic resole resin where a flame retardant plasticizer and an acid are used as a catalyst. Phenolic polymers are obtained by polymerizing phenol and formaldehyde⁴. Due to benzene rings built into the chemical chain, this resin has good thermal stability. According

to the product description, this resin with the flame retardant additive is formulated to be Class I per ASTM E 84⁵ (flame spread index < 25 and smoke developed index < 450).

2.2. FRP composite description

Composite panels were fabricated by vacuum bagging for relatively high (60 wt% of glass, average thickness of 9.8 mm) glass content composites, using two different types of fiberglass mats that were wetted with resin (see Figure 1). The two types of fiberglass (E-glass) used in the composite are a chopped strand mat and a glass roving woven mat with an area density of 25 g/m² and 880 g/m², respectively. The chopped strand mat is thinner and more porous than the woven mat. The laminate schedule (provided by the manufacturer) is chopped strand mat and roving alternating eight times for FRP with high glass content (HG) with another chopped strand mat layer at the end. Visual inspection of a polished cross-section of the composite slab is consistent with this laminate schedule, but with polymer resin layers between each fiberglass layer. The chopped strand mat layer is difficult to identify in the cross section, perhaps because more resin is soaked into this layer than the roving layer. The roving layer is observed as a prominent glass layer possibly because the resin is absorbed only at the fiberglass layer surfaces leaving the interior with primarily glass fibers.

The layered microstructure is determined to a resolution of 0.3 mm by inspecting a polished cross-section of the composite. Based on visual observation and comparison to global density of the composite sample, approximations of three distinct layers are proposed accounting for the density, ρ of each component of the composite at its non-porous stage – $\rho_{\text{resin}} = 1300 \text{ kg/m}^3$, $\rho_{\text{glass}} = 2600 \text{ kg/m}^3$: porous layer with chopped strand mat with resin (CSM+R), porous layer with some glass roving woven mat (RW+R), and a less-porous layer with glass roving woven mat only (RW). The microstructure of the virtual Neat Phenolic FRP composite is, from the surface, (CSM+R) – (RW+R) – (RW) – (RW+R) repeating 8 times and another (CSM+R) layer at the back face, which resulted in 33 layers.

3. Experiment Apparatuses

3.1. Thermogravimetric Analysis (TGA) and Differential Scanning Calorimetry (DSC)

The instruments used in this study were manufactured from TA Instruments: Thermogravimetric Analysis Q50 (TGA) and the Differential Scanning Calorimetry Q20 (DSC). Throughout this study, TGA and DSC were used for non-isothermal test purposes and the tests were conducted in nitrogen to study pyrolysis. Using the TGA, 4 different heating rates of 5°C/min., 20°C/min.,

40°C/min. and 60°C/min. were applied to measure the mass loss history of each resin sample from 40°C to 800°C. For the DSC, a constant heating rate of 20°C/min. was used to measure the heat flow through the sample during the thermal decomposition of resins. Tests conducted with the DSC were from 40°C to 500°C where the maximum temperature is lower than that of TGA due to the limitation of the instrument. A sample amount of approximately 10 mg was used for each test in a standard aluminium pan with a punctured lid so that gases may evolve freely away from the pan.

3.2. Cone Calorimeter

Cone Calorimeter (Cone, ASTM E 1354¹) is a bench-scale fire test apparatus in which the sample is heated by an electrically heated rod in the shape of a cone. The sample is tested by applying a constant radiative heat flux set via temperature controller of the rod. The Cone exposes the sample in an ambient environment which results in a natural flow field as the sample temperature increases allowing convective cooling above the sample surface. The ignition source is an intermittent sparker. The Cone can be used to calculate useful engineering data such as oxygen consumption based heat release rate (based on the standard), mass loss rate, smoke yield and smoke extinction coefficient.

The purpose of Cone testing was to generate good data sets appropriate for pyrolysis modeling and parameter estimation, and therefore several modifications were made to the standard testing procedure. First, when testing this FRP, three different types of sample holders were used to produce quality one-dimensional data (see Figure 2). Experimental challenges with these FRPs were that significant edge burning, which is a three-dimensional problem, occurs during each test. Because the pyrolysis model of interest in this study has a numerical structure of one-dimension, data that can be considered as one-dimension should be utilized in this parameter estimation exercise using numerical optimization. Hence, caution was given to reduce the edge effect by testing with different sample holders. Sample holder type 1 is a standard specified, non-insulated cone holder that holds a 102 mm x 102 mm (4" x 4") square sample with a metal edge frame. Sample holder type 2 is a round insulated sample dish purposed by de Ris and Khan⁶ that holds a 102 mm (4") diameter circle sample. In this sample dish, the sample is surrounded by Cotronics® paper insulation on the back and sides to limit heat loss, which simplifies the pyrolysis modeling. Sample holder type 3 is composed of ceramic fiberboard (Thermal Ceramics Inc.) that holds a 152 mm (6") diameter circle sample. On top of the sample, a layer of ceramic fiberboard with a hole in the center was placed to limit the sample surface exposure to the cone heater.

Second, 2 thermocouples were installed to measure temperature change of the sample at surface and back

face of the sample. The surface thermocouples were affixed via two types of methods: One method was to drill a thermocouple hole from the sample side and allow the hole to reach the surface. A thermocouple insulated wire was inserted through the side and the bead was able to locate near the surface; hence, from the surface only the bead was visible. Using this method, the center of the bead was located at the surface allowing top half to be exposed to ambient air and the lower half to sit within the sample. A drop of thermal grease or a high temperature adhesive (Resbond 907 Industrial Strength Fireproof Adhesive from Cotronics Corp.) was applied to the bead to ensure good contact between the sample and the bead. Another method was to crimp the thermocouple wire to allow the thermocouple bead to sit on the surface with a minimal amount of thermal grease applied at the bead. The back face thermocouples were affixed with a high temperature adhesive (Resbond 907 Industrial Strength Fireproof Adhesive from Cotronics Corp.).

To evaluate which of the three sample holder types are most appropriate for testing this Neat Phenolic FRP composite with high glass (~60wt%), several Cone tests were conducted at different heat flux levels ranging from 30 to 90 kW/m². Analyzing the results, data from applying type 1 sample holder was utilized in this study for the following reasons: First, considering the temperature increase with respect to one-dimensional heating, although type 3 provides the best condition for one-dimensional approximation, difference between the data from type 3 and type 1 or 2 are about 50°C or less assuming that measurements are made near the centerline of sample. This concurs with Choi's work⁷ on inert materials. Larger size sample has shown to provide the best one-dimensional heat conduction condition comparing to other sample set-ups where regular size (102 mm x 102 mm (4" x 4")) sample is prepared with a metal edge frame, edges exposed, or insulation on the sides and bottom. It was noted that at 80kW/m² of incident heat flux, the centerline temperature difference between that of the larger sample's and centerline temperatures of the regular samples with metal edge frame or insulation on the sides and bottom are approximately 20°C or less within 5 hrs. period. Second, type 3 results in uncertain burn area due to some decomposition at the sides even with a layer of insulation protecting the sample. This increases the uncertainty in data considered per unit area. However, type 3 allowed visual inspection of the edge burning: when the neat phenolic resin on the back face temperature increased beyond its major decomposition temperature, pyrolyzates traveled around the sample sides and caught fire instead of moving through the composite layers vertically. Even with the resin decomposing in-depth, because the amount of resin residue is sufficient in the composite, the sample was impermeable to pyrolyzates produced from back face resin decomposition. Third, having the edges not exposed as in type 1 or 3 allowed less pyrolyzates to travel horizontally towards the edges,

i.e. because the edges are preserved from burning, edges are more impermeable to pyrolyzates. One of the influences from having less pyrolyzates traveling towards the edges is resulting in increased time to ignition.

The uncertainty in the mass loss rate data is estimated via statistical approach, taking the standard deviation (0.58 g/sm^2) from the mean of a steady burning of 5 identical PMMA tests conducted in a Cone Calorimeter⁸. The estimated uncertainty is 1.4 g/sm^2 , which is found by calculating the 95% confidence interval applying student t distribution with a sample size of 5. The uncertainty in the thermocouple measurements was quantified by comparing surface and back face temperature data from 3 and 4 identical FRP composite tests with the Neat Phenolic FRP composite with high glass content in the Cone at 70kW/m^2 and 50kW/m^2 , respectively. Using the normalized time, time divided by sample thickness square, i.e., $\tau = \text{time}/\delta^2$ to remove the effect of different sample thicknesses when comparing, the maximum standard deviation at various normalized times, up to the critical time, τ_c , was 20°C for the surface and 27°C for the back face. Assuming this is approximately equal to one standard deviation, applying student t distribution and calculating the 95% confidence interval becomes $\pm 49^\circ\text{C}$ and $\pm 83^\circ\text{C}$ from the sample mean for surface and back face, respectively. The critical time, τ_c , corresponds to the time of ignition for surface temperature measurements and time when evenly spread flame on sample surface disappearing for back face temperature measurements. For the back face, this time corresponds well with the time when the back face temperature becomes close to the major decomposition temperature of the Neat Phenolic resin. As noted above, after this temperature, edge burning occurs, which is a non-1D phenomenon. These uncertainty values will be used to evaluate significant differences in the modeling results.

4. Kinetic Modeling of Resin Degradation for Pyrolysis Modeling

A series of thermal analyses are conducted on commercial thermoset polymers used in fiberglass reinforced polymer (FRP) composite material. Experiments for thermal analysis are conducted using Thermogravimetric Analysis (TGA) at various heating rates (5, 20, 40 and 60°C/min) and Differential Scanning Calorimetry (DSC) at 20°C/min . These non-isothermal TGA experimental results are used to conduct iso-conversional estimates of activation energy with respect to conversion without pre-determining the kinetic model using an Arrhenius type expression for thermal degradation. Results are also used to determine the minimum number of reactions required in the kinetic model to describe the thermal degradation reactions based on actual weight loss. Then a model fitting method is used where vari-

ous kinetic models are used to fit the TGA data to the model. The DSC experiments are conducted to use the heat flow information to compare against the analysis results conducted by the TGA. Kinetic modeling is conducted following the steps introduced in this Reference⁹.

5. Pyrolysis Modeling for Lumped (TGA) and Slab (Cone) Experiments

The calculations reported here are conducted with a generalized pyrolysis model^{2,3} that can be applied to a wide variety of condensed phase fuels. The model simultaneously calculates the condensed phase mass conservation, gas phase mass conservation, condensed phase species conservation, and condensed phase energy conservation equations. This model can be applied to both 0D and 1D systems and is therefore capable simulating both “lumped” (thermogravimetric) and “slab” (Cone Calorimeter/FPA) experiments. Extensive details are given in Ref.^{2,3} so only a brief overview is given here. Assumptions inherent in the model, as applied in this paper, include:

- Porosity can either be solved as a property of a species (default) or directly. When porosity is solved directly, it is derived from the condensed-phase mass conservation equation assuming no volume change (shrinkage or swelling).
- When porosity is directly solved, the user-specified thermal conductivity and density are interpreted as those of a nonporous solid. Therefore, the thermal conductivity that appears in the condensed-phase energy conservation equation is $\bar{k} = (1-\psi)\bar{k}_s$ where ψ is porosity and \bar{k}_s is the weighted thermal conductivity of the solid assuming it is nonporous. Similarly, with this formulation, the bulk density is calculated as $\bar{\rho} = (1-\psi)\bar{\rho}_s$ where $\bar{\rho}_s$ is the weighted density of the solid assuming it is nonporous.
- Bulk thermal conductivity \bar{k} has a cut-off value of 0.03W/mK which corresponds to air at 300 to 400K.
- Specific heat is calculated with a weighted or averaged quantity, i.e. $\bar{c}_p = \sum X_i c_{p_i}$ as other solid properties – enthalpy, emissivity, radiation absorption coefficient, permeability, etc.
- Specific heat capacity and effective thermal conductivity vary by as $k(T) = k_0(T/T_r)^{n_k}$ and $c(T) = c_0(T/T_r)^{n_c}$, respectively, where T_r is a reference temperature.
- Radiation heat transfer across pores is accounted for by adding a contribution to the effective thermal conductivity that varies as γT^3 , where γ is a fitting parameter;

hence,

- Averaged properties in conservation equations are calculated by appropriate mass or volume fraction weighting

Gas-phase and condensed-phase are in thermal equilibrium

6. Results and Discussion

Property estimation exercise for pyrolysis modeling of neat phenolic (NP) FRP composite which contains flame retardant additive is conducted in three parts: First, the kinetic parameters for thermally degrading resin are obtained via kinetic modeling using thermal analysis with non-isothermal experiment data from TGA and DSC tests. Second, parameters other than those related to resin decomposition kinetics are obtained by utilizing optimization routine with a pyrolysis model in pair. Third, a comparison is done with estimated parameter values using different approaches to evaluate any consistencies in the estimated results.

6.1. Kinetic modeling for resin degradation

Step 1: Preliminary Experiments with Analysis

Based on preliminary tests on this resin, it was found that when the area to volume (A/V) ratio is changed thermal behavior change as well. Typically, when a polymer sample is cut from a larger sample, the number of mechanically broken polymer bonds increase as the A/V ratio increases. The sample prepared with above method that have high A/V ratio consists polymer chains which are relatively shorter than those found in a larger sample with lower A/V ratio and increased concentration of radicals on the sample surface due to the broken bonds. Polymer samples meeting these conditions can result in changes in their thermogram comparing to those from samples that have lower A/V ratio. In general, the samples appear to be less thermally stable, e.g. increase in initial weight loss at lower temperatures, lower thermal decomposition temperature, higher DTG (weight loss rate) peaks, etc. Considering this effect, relatively larger sample sizes that have low A/V ratio in thermal analysis is recommended.

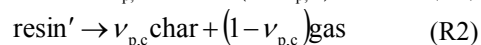
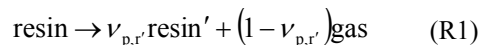
Step 2: Iso-conversional (Model-free) Method

In Figure 3, the results from two iso-conversional methods introduced by Ozawa, Flynn and Wall^{10,11} (OFW, estimates E_a/R by plotting $\ln(\beta)$ versus $1/T$) and Friedman^{12,13} (plotting $\ln(d\alpha/dT)$ versus $1/T$ to find $-E_a/R$) conducted on the neat phenolic resin are shown. Both methods are used for comparison purposes. The R^2 values for each activation energy value are plotted as well using the least square method. The activation en-

ergy becomes more reliable as the R^2 values become closer to 1 where $\alpha = 1 - m/m_0$.

Step 3: Model Fitting Method

Based on iso-conversional method, 2-step mechanism is proposed as below:



Applying an nth order reaction model, kinetic parameters of the pre-exponential factor (Z), activation energy (E_a), and reaction order (n) are estimated manually (see Table 1).

Note that these estimated results are simplified and does not represent the actual decomposition kinetics of the given material, i.e. they are empirical values which can only be utilized with this modeling set-up. However, the activation energy for R2 was estimated from iso-conversional method; therefore, the value should be able to represent the actual decomposition kinetics in nitrogen.

6.2. Property estimation for Neat Phenolic FRP composite using different approaches

When conducting the Cone simulation for the FRP composite, char oxidation was neglected for modeling simplification. Therefore, decomposition of the neat phenolic resin in nitrogen was used to estimate kinetic parameters and these were used in the cone simulation. Four property estimation cases were built based on the approach of estimation and available optimization routines (GA or SCE). They are summarized in Table 2. The entire property set used in the simulation are shown in Table 3.

To simplify the problem, the exponents of thermal conductivities and specific heat capacities of resin, resin' and char were considered as 0. Only those of fiber glass were expressed as a function of temperature as noted in the previous section on pyrolysis modeling. Considering that the resin quickly becomes black after exposure to the Cone heater, emissivity of the resin' was set as 1.0. Because resin' and char becomes porous as resin decomposes without much shrinkage and fiber glass is porous in nature, a fitting parameter gamma was utilized to account for radiative heat transfer through pores. Additionally, it is assumed that the thermal conductivity and specific heat capacity are the same for resin and resin'. As a boundary condition at the surface, additional constant flame heat flux of 20kW/m^2 was added to the applied heat flux from the Cone starting at user-specified time of ignition. This value corresponds well with a measured value from actual test. For the back face, actu-

al temperature measurements with respect to time were preferred as a specified boundary condition. However, for cases where this approach proposes heating from the back face, heat loss through the back face was specified instead. In the numerical optimization process, mass loss rate, surface and/or back face temperature measurements were used.

The simulation results with the estimated parameter sets from each case are shown in Figure 4. The first figure (a) is at 30kW/m^2 and the rest (b, c and d) are at 70kW/m^2 . Note that at 30kW/m^2 applied heat flux, mass loss rate is negligible (i.e. below uncertainty level) and the back face temperature remains at its initial temperature; therefore, they are not shown. Considering the uncertainty of $\pm 49^\circ\text{C}$, surface temperature simulation is in good agreement with the experiment data (a, b) for all cases. For mass loss rate simulation in (c), the results from optimized parameter sets are lower than the actual data even with the consideration of its experiment uncertainty (1.4 g/sm^2). This is probably due to the assumption made in the simulation about neglecting char oxidation. Although the magnitude of the mass loss rate may be lower than the actual, note that the trend in changes occurring in the mass loss rate with respect to time is similar. This provides evidence that the microstructure specified in the simulation was well resolved in the simulation. The back face temperature simulations in (d) from all cases are in good agreement with the data considering the uncertainty of $\pm 83^\circ\text{C}$. These simulations from Case 1 and 2 are relatively closer to the data than those from Case 3 and 4, where these are at the outer bounds of the uncertainty band.

6.3. Comparison of estimated properties from 4 Cases

The estimated properties of thermal conductivity (Figure 5) and specific heat capacity (Figure 6) from 4 different cases are compared in the figures. Consistent trend is found for all cases for estimated thermal conductivity of resin and its decomposition products (resin and char) – thermal conductivity of char is higher than that of resin. The estimations from Case 2, 3 and 4 are lower at temperatures near ambient (less than 0.5 W/mK) than the that of Case 1 and these values are closer to the reference values of the neat phenolic resin – $0.1 \sim 0.2\text{ W/mK}$ ¹⁴. Estimated thermal conductivities of fiber glass from Case 1 and 2 are higher than those from Case 3 and 4 in general. Considering that the reference value for fiber glass is 0.04 W/mK ¹⁵ at temperatures near ambient, estimations from Case 3 and 4 are showing to be closer to the reference values at lower temperatures.

Estimated specific heat capacities of resin and its decomposition products start at higher values at lower temperatures and decreases at higher temperature for all cases. Considering that the reference value for neat COMPOSITES & POLYCON 2010

phenolic resin is near 1700 J/kgK ¹⁶, estimations from Case 1 and 4 are showing to be closer to the reference values at lower temperatures. Estimated specific heat capacity of fiber glass from each case show consistency. Reference values for glass and air are 840 J/kgK ¹⁷ and near 1000 J/kgK ¹⁸, therefore, fiber glass heat capacity should be within this range at ambient temperature. Having this in mind, results from Case 2 and 4 are closer to the reference values.

Parameter estimation of emissivity and heat of reactions were similar for all 4 cases, which are summarized in the table (see Table 4).

7. Conclusions

In this study, parameter estimation for neat phenolic fiberglass reinforced polymer (FRP) composite has been conducted using different approaches and optimization routines in pair with one-dimensional pyrolysis model (GPYRO). With the decomposition kinetics for the resin modeled independently, simulations of Cone tests of the composite at heat flux levels of 30kW/m^2 and 70kW/m^2 were performed to estimate the unknown thermophysical properties via numerical optimization using Genetic Algorithm (GA) or Shuffled Complex Evolution (SCE) optimization routines. Four cases has been explored – Case 1: estimate entire property set using Cone data at 70kW/m^2 up to post-decomposition stage with GA; Case 2: estimate entire property set using Cone data at 70kW/m^2 up to post-decomposition stage with SCE; Case 3: estimate properties at pre-decomposition stage using Cone data at 30kW/m^2 and with those fixed, estimate rest using Cone data at 70kW/m^2 with GA; Case 4: estimate properties at pre-decomposition stage using Cone data at 30kW/m^2 and with those fixed, estimate rest using Cone data at 70kW/m^2 with SCE.

Analyzing the estimation results from 4 cases has presented the following conclusions: First, the two approaches – (1) estimating the entire property set at once, Cases 1 and 2 or (2) estimating properties in pre-decomposition stage then with those estimated values fixed estimating the rest, Cases 3 and 4 – generate estimations that are both in good agreement with experiment data. In terms of their estimations compared to reference values, the exercise have shown that approach (2) finds values closer to reference values for thermal conductivity of the fiberglass only than approach (1). Considering the computer time and power necessary in the optimization process, approach (1) requires more than approach (2) knowing that the entire parameter set is grouped into two sets for approach (2) and less parameters to optimize in one run means less computation work. For example, when using SCE, the number of processors involved in one optimization run should be similar to the number of unknown parameters to be optimized. Hence, benefit of

utilizing approach (2) instead of approach (1) comes from saving computational time and power.

Second, the two optimization routines – GA, Cases 1 and 3 or SCE, Cases 2 and 4 – generate estimations that are both in good agreement with experiment data. The major difference between the two routines is GA finds many near optimal solutions (parameter sets) while SCE always converges to one set. However, caution should be given that resulting in one optimized parameter set from SCE does not mean those values are absolute, global solutions considering GA can develop many near optimal parameter sets using the same experiment data in the optimization process and resulting in similar simulation output quality as in those from SCE.

Third, analyzing 4 cases in this study clearly shows that when numerical optimization is used in the parameter estimation process, the optimized parameter set generated from the exercise should be considered as a linked parameter set along with the pyrolysis model of choice. The different approaches and optimization routines are resulting in different parameter values but the parameter set from each case shows similar simulation output quality. However, methods of determining which values are more physical are significantly limited at this point. This assures the users to be more cautious in extrapolating the information obtained from one parameter estimation case to another using numerical optimization.

Acknowledgments

The authors would like to thank Charles Dore for fabricating the FRP composite materials used in this study. Many thanks also to Randall Harris at WPI for conducting the Cone Calorimeter tests. The authors thank Chris Lautenberger and the computer cluster managers at WPI for helping us run the code.

Reference

¹ Standard Test Method for Heat and Visible Smoke Release Rates for Materials and Products Using an Oxygen Consumption Calorimeter, ASTM E 1354-09, ASTM, 100 Barr Harbor Drive, West Conshohocken, PA, U.S.

² Lautenberger, C., “A Generalized Pyrolysis Model for Combustible Solids”, Ph.D. Dissertation, Department of Mechanical Engineering, University of California, Berkeley, Fall 2007

³ Lautenberger, C., Gpyro – A Generalized Pyrolysis Model for Combustible Solids Users’ Guide, Version 0.609, July 23, 2008

⁴ Odian George, Principles of Polymerization, 3rd ed., John Wiley & Sons, Inc., c1991

⁵ Standard Test Method for Surface Burning Characteristics of Building Materials, ASTM E 84-05, ASTM, 100 Barr Harbor Drive, West Conshohocken, PA, U.S.

⁶ de Ris, J.L. and Khan, M.M., “A sample holder for determining material properties,” *Fire and Materials*, 24, 219-226 (2000).

⁷ Keum-Ran Choi, 3D Thermal Mapping of Cone Calorimeter Specimen and Development of a Heat Flux Mapping Procedure Utilizing an Infrared Camera, PhD Dissertation, Fire Protection Engineering, WPI, 2004-08-30, ETD-020205-215634

⁸ Lei Zhao, Bench Scale Apparatus Measurement Uncertainty and Uncertainty Effects on Measurement of Fire Characteristics of Material Systems, MS Thesis, Fire Protection Engineering, WPI, 2005-04-27, ETD-050105-182456

⁹ Esther Kim, S Shivkumar, N Dembsey, Thermal Degradation Kinetics Modeling for Pyrolysis Modeling Using Fire Retarded Thermoset PolymerResins, INTERFLAM 2010, 5 – 7 July 2010, East Midlands Conference Centre University of Nottingham, UK

¹⁰ Ozawa, T., *Bull Chem Soc Jpn* 1965;38;188

¹¹ Flynn, J., Wall, L.A., *J Polym Lett* 1966;4:232

¹² Friedman, H.L., *J Polym Sci Part C* 1964;6:183

¹³ Friedman, H.L., *J Polym Lett* 1966;4:232

¹⁴ Sidney H. Goodman, Handbook of thermoset plastics, 2nd ed., c 1998, Noyes Publications, ISBN: 0-8155-1421-2

¹⁵ http://www.engineeringtoolbox.com/thermal-conductivity-d_429.html

¹⁶ Hew-Der Wua, Peter P. Chub and Chen-Chi M. Ma, Thermodynamic properties of the novolac type phenolic resin blended with poly(hydroxyl ether of bisphenol A), *Polymer*, Volume 39, Issue 3, 1998, Pages 703-709, doi:10.1016/S0032-3861(97)00320-0

¹⁷ Tipler, Paul A., *Physics for Scientists and Engineers*, 4th Ed., W.H. Freeman, (1999).

¹⁸ SFPE Handbook of Fire Protection Engineering, 3rd Ed. c 2002, ISBN/SKU 9780877654513

Figures:

Figure 1. Cross-section of Neat Phenolic (NP) FRP fabricated via vacuum bagging with average glass content of 60 wt% and average thickness of 9.8 mm: two types of fiberglass (E-glass) used in the composite – chopped strand mat (25 g/m², highly porous) and glass roving woven mat (880 g/m², prominent glass layers in white)

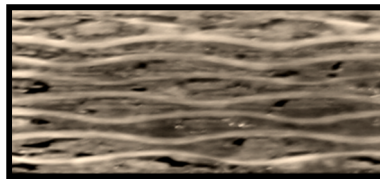


Figure 2. Three types of sample holders used in Cone Calorimeter experiment: first and second rows show the top and side view, respectively. Sample is shown in pink, metal edge frame in gray, metal holder in black, and insulation in area with pattern.

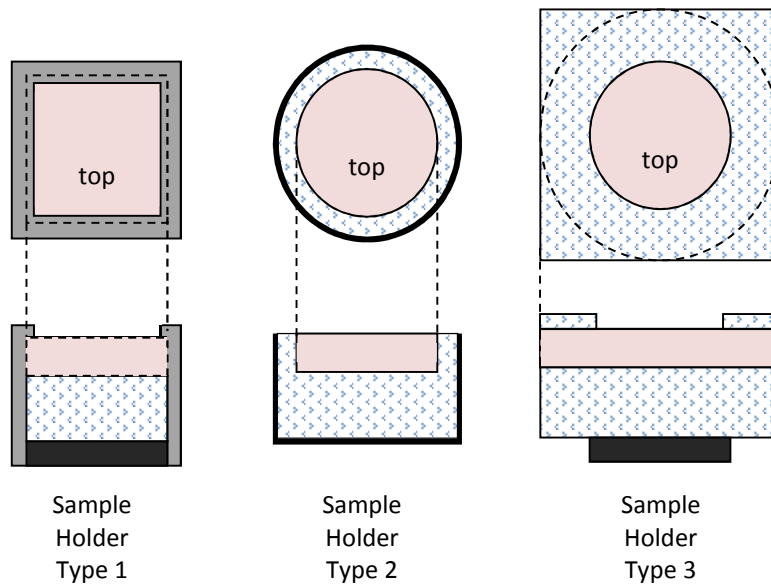


Figure 3. TG and DTG thermograms from TGA experiments conducted in nitrogen with Neat Phenolic Resin (NP) at 5°C/min (a) and results from iso-conversional method conducted on NP resin (b) where the estimated activation energy of thermal decomposition with respect to conversion (1- α) is shown

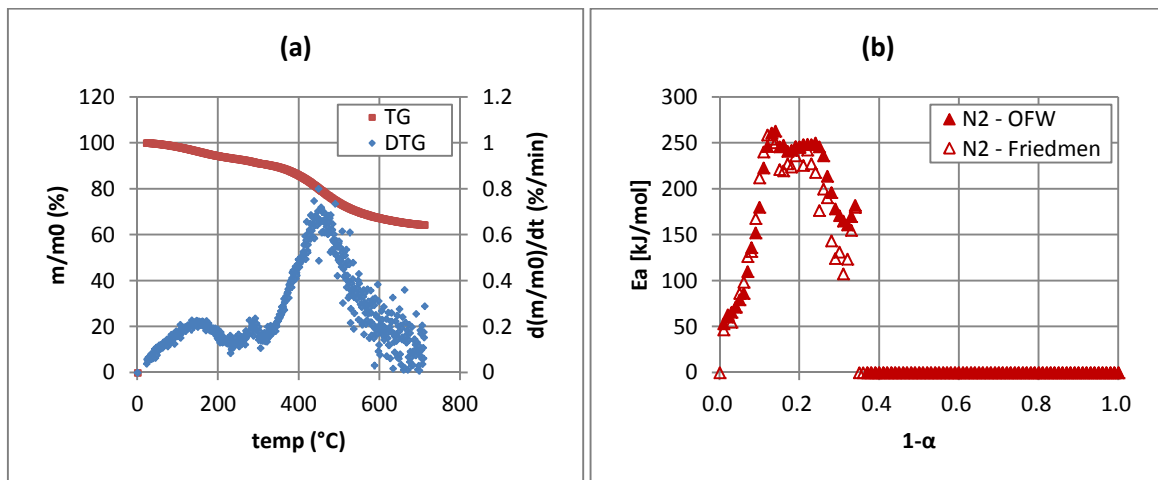


Figure 4. Comparison between simulation results and experiment data: (a) surface temperature at applied heat flux of 30kW/m^2 ; (b) surface temperature, (c) mass loss rate, and (d) back face temperature at applied heat flux of 70kW/m^2

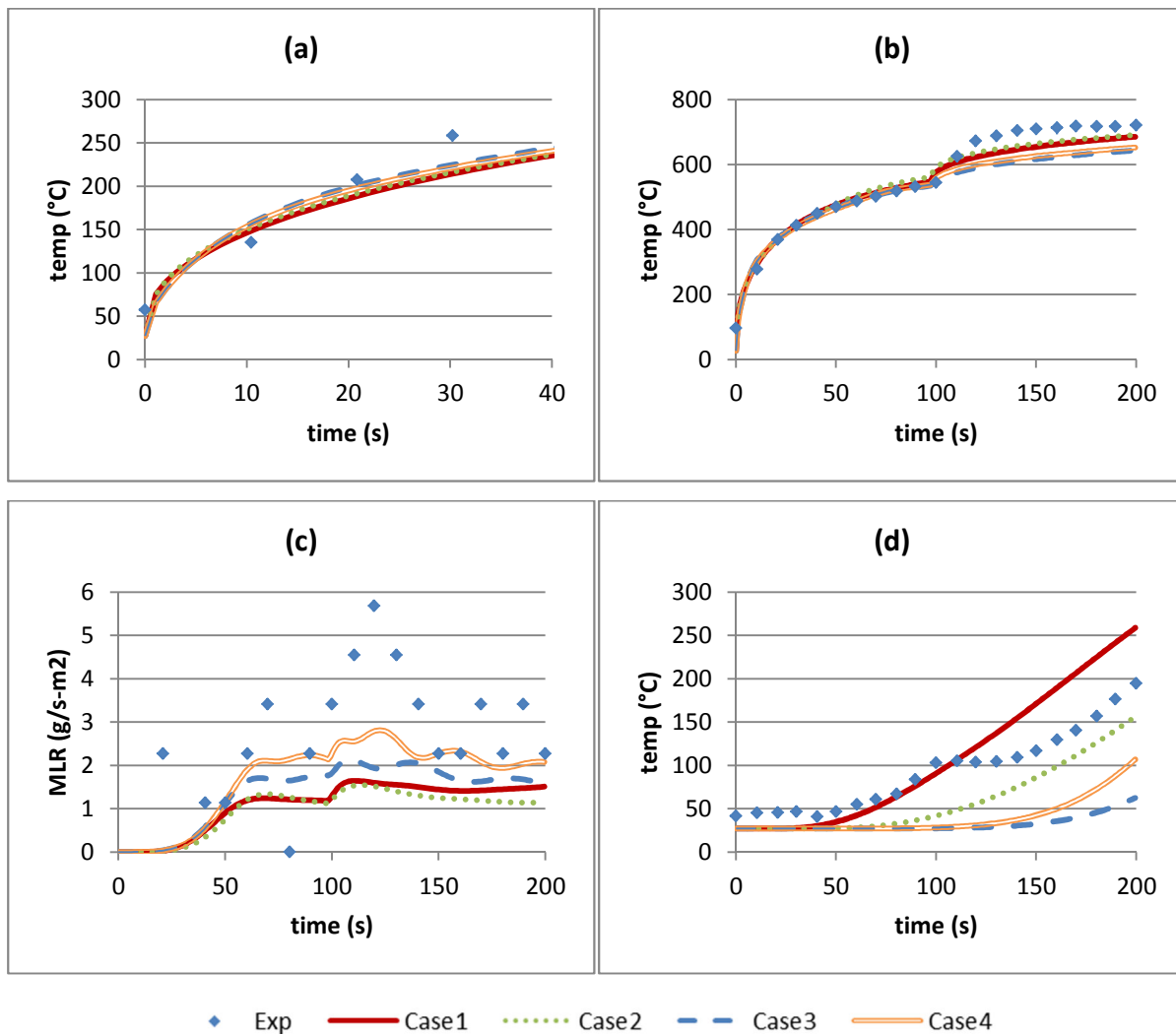


Figure 5. Estimated thermal conductivity for 4 species -- resin, resin', char and fiber glass: values shown below account for the solid component only and exclude the effect of heat transfer through pores modeled via γT^3

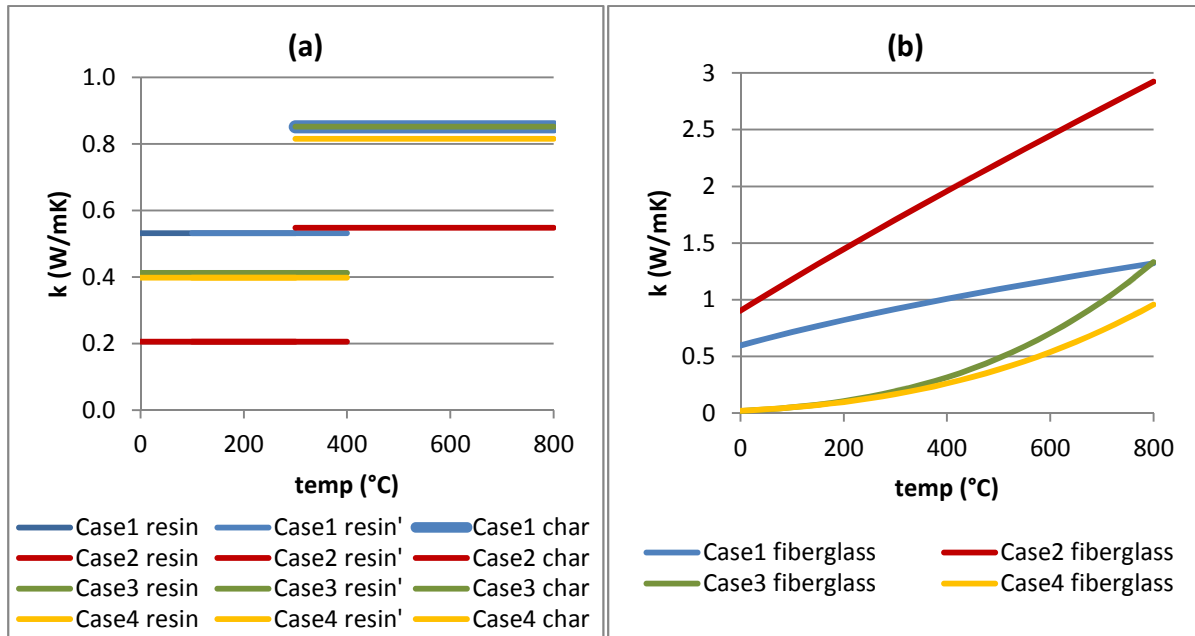
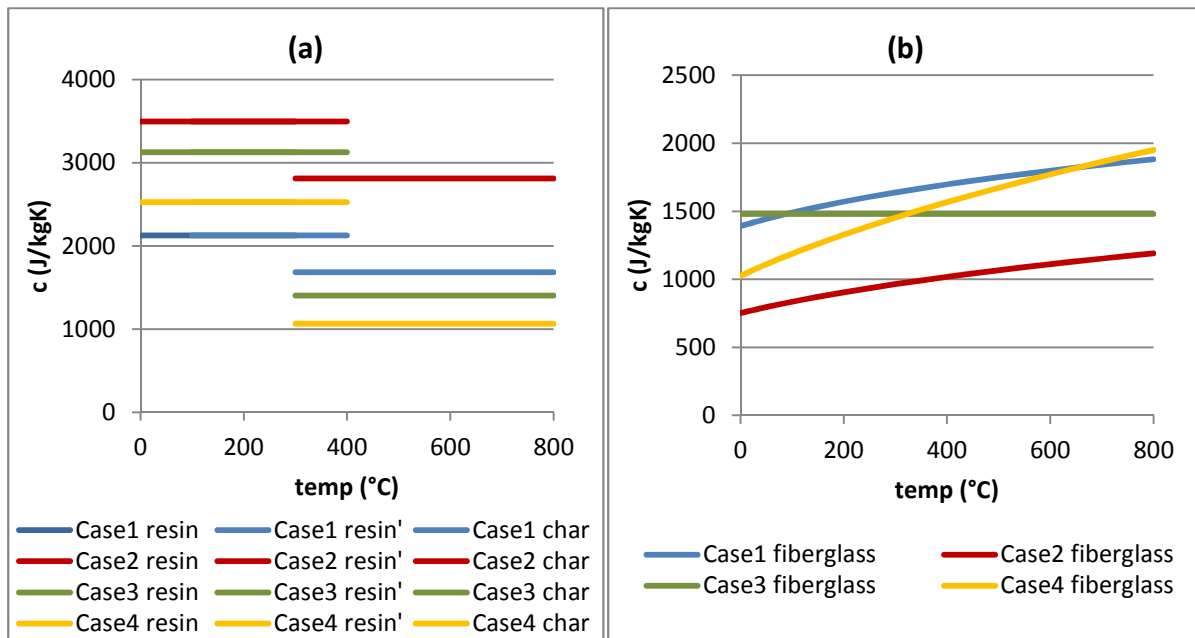


Figure 6. Estimated specific heat capacity for 4 species: resin, resin', char and fiber glass



Tables:

Table 1. Estimated kinetic parameters using nth order reaction model

	Z (/s)	E _a (kJ/mol)	n (/)	Consumption (%) from Initial Mass
R1	10 ⁸	130	1	14.1
R2	10 ¹⁰	236	1	35.2

Table 2. Summary of property estimation cases examined in this study constructed using different approaches and optimization routines in pair with pyrolysis model (GPYRO)

Case	Approach	Optimization Routine
1	One step approach: <ul style="list-style-type: none"> Estimate entire property set at pre- decomposition and post decomposition stages using Cone data from 70kW/m² 	GA
2	One step approach: <ul style="list-style-type: none"> Estimate entire property set at pre- decomposition and post decomposition stages using Cone data from 70kW/m² 	SCE
3	Two step approach: <ul style="list-style-type: none"> Estimate properties at pre- decomposition stage using Cone data from 30kW/m² Having above properties fixed, estimate rest using Cone data from 70kW/m² 	GA
4	Two step approach: <ul style="list-style-type: none"> Estimate properties at pre- decomposition stage using Cone data from 30kW/m² Having above properties fixed, estimate rest using Cone data from 70kW/m² 	SCE

Table 3. Parameter set for Cone simulation

Parameter	Keyword	Resin	Resin'	Char	Fiber Glass
thermal conductivity at T _r	KOZ	Y		Y	Y
thermal conductivity exponent	NKZ	Set as 0.0		Set as 0.0	Y
specific heat capacity at T _r	CO	Y		Y	Y
specific heat capacity exponent	NC	Set as 0.0		Set as 0.0	Y
emissivity	EMIS	Y	Set as 1.0	Y	Y
gamma	GAMMA	Set as 0.0	Y	Y	Y
Heat of Reaction for R1	DHV	Y			
Heat of Reaction for R2	DHV	Y			

Table 4. Estimated emissivity for 4 species (resin, resin', char and fiber glass) and HoRs for R1 and R2

	Emissivity				Heat of Reaction	
	resin	resin'	char	fiberglass	R1	R2
Case1	1.0	1.0	0.8	0.9	3.0E+04	2.7E+04
Case2	1.0	1.0	0.9	0.7	5.6E+05	1.3E+04
Case3	0.7	1.0	0.9	0.9	3.1E+05	2.5E+05
Case4	0.6	1.0	1.0	0.9	1.0E+06	7.6E+03

Appendix E

Thermal Degradation Kinetics Modeling for Pyrolysis Modeling Using Fire Retarded
Thermoset Polymer Resins

Interflam 2010, 12th International Conference on Fire Science and Engineering

THERMAL DEGRADATION KINETICS MODELING FOR PYROLYSIS MODELING USING FIRE RETARDED THERMOSET POLYMER RESINS

E. Kim¹, S. Shivkumar², N. Dembsey¹

¹Fire Protection Engineering, WPI

²Mechanical Engineering, WPI

ABSTRACT

In this study, a series of thermal analyses is conducted to estimate thermal degradation kinetics of two types of thermoset polymer resins, modified acrylic and modified acrylic with inorganic flame retardant additive, which are typically used in fiber reinforced polymer (FRP) composites. As part of parameter estimation for pyrolysis modeling, a simple kinetic modeling method is introduced and applied to construct a set of minimum number of elementary reactions that involves weight loss and to estimate the kinetic parameters. For thermal analysis, Thermogravimetric Analysis (TGA) and Differential Scanning Calorimetry (DSC) experiments are used.

INTRODUCTION

Over the years, an interest towards pyrolysis modeling of real world solid materials in the fire community has been increasing with the development of advanced computer models such as Fire Dynamics Simulator (FDS) from NIST, which is a well-known computational fluid dynamics (CFD) model commonly used by practitioners. When a general comprehensive pyrolysis model – a model that utilizes governing equations for mass, momentum, and energy conservation to capture the thermal behavior of a pyrolyzing material – is used, typically the following parameters are required as input: thermal degradation kinetics related parameters; thermal parameters such as specific heat capacity, thermal conductivity; and radiative characteristics like surface emissivity, in-depth radiation absorption coefficient. Among these various parameters, this study focuses on estimating kinetic parameters because the current practice for kinetic modeling remains at a very simplified stage.

Generally, thermal degradation kinetics is a very complicated problem. Many times there are various reactions occurring simultaneously and the kinetic behaviors change for different conditions such as the particle-size, abrasion or other damage to crystal surfaces, surface impurities and irradiation, local environment, a precursor step, etc. Therefore, modeling the degradation kinetics becomes a highly challenging problem when considerations are given to these test conditions in the modeling process. Kinetic modeling generally is defined as a description of the sequence of chemical steps through which reactants are transformed into products. Although when a material is thermally degrading with numerous reactions, most times there are rate determining steps. Kinetic modeling is conducted to simulate these rate determining steps. To find the rate determining steps for thermally degrading material, one should consider the reaction rate controlling factor(s). There are three factors to consider in reactions of solids where one or a combination of the factors controls the reaction rate. One is the chemical reaction factor that considers a bond redistribution step. This step usually occurs at a reaction interface and is the chemical control of reactivity. Another factor is the reaction

geometry. A systematic variation in the reaction interface area with respect to the changes in the geometry of the reaction interface as the reaction proceeds exerts an important influence on the kinetic behavior. Last is the rate of diffusion of reaction participants. This factor can influence the rate of product formation. Based on the understanding of the reaction rate controlling factors, kinetic models can be developed to describe the thermal degradation of a material.

The purpose of conducting this kinetic modeling is to address the thermal degradation kinetic behavior of a resin sample in milligram scale and extrapolate that information to be used in modeling pyrolysis of real world materials such as the FRPs used in this study in larger scales such as those found in bench-scale or even full-scale tests. One of the major foci of the paper is constructing kinetic models in a consistent manner with minimal information about the resins because for most of the real world materials that are commercially available details regarding the chemical structure of the base polymer, the fire retardant additives, etc. are rarely accessible to the modelers due to the information being proprietary to the manufacturer. The models are intended to be simplified but sophisticated enough to capture the characteristics of the materials such as the fire retardancy via additives within a polymer matrix, environmental effect, etc. To achieve this goal, thermal analyses is conducted on a commercial thermoset polymer used in fiber reinforced polymer (FRP) composites – modified acrylic – with and without fire retardant additive.

KINETIC MODELING METHODOLOGY

There are numerous ways of conducting kinetic modeling for thermal degradation of materials. In this study, the most generalized approach of kinetic modeling is introduced to allow practitioners to follow guidelines to estimate kinetic parameters for pyrolysis modeling. Therefore, the kinetic modeling procedure is developed with minimum number of experiments (TGA/DSC) and thermal analyses (iso-conversional and model fitting methods). The final outcome of kinetic modeling is assembling the minimum number of elementary reactions for thermal degradation of a given material which results in weight loss, identifying the kinetic models for those reactions, and obtaining the kinetic parameters associated with each reaction. A detailed procedure for conducting kinetic modeling (steps 1 through 3) is discussed below:

Step 1: Preliminary Experiments with Analysis

Non-isothermal (dynamic) or isothermal TGA/DSC experiments with various heating rates or temperatures, respectively, should be conducted to study the decomposition of each material in general. The results from TGA experiments – TG (plot of mass loss with respect to temperature) and DTG (plot of mass loss rate with respect to temperature) – and DSC experiments – plot of heat flow with respect to temperature – should be compared in parallel. In this step, factors that can contribute to kinetic behaviors of materials are considered, which are not included in the reaction rate controlling factors discussed earlier – chemical reaction factor, reaction geometry factor, and diffusion rate of reaction participants. Examples of these factors are particle size effects, local environment effects, heating rate effects, effects due to limitations of the experimental set-up, and more¹. These factors are considered to be isolated and controlled when conducting thermal experiments to understand the kinetics which best describe the thermal degradation of the materials' final product stage. After these factors are considered, the most appropriate set of non-isothermal (dynamic) experiments with TGA and DSC should be used in the next step for further analysis.

Step 2: Iso-conversional (Model-free) Method

In this step, more detailed thermal analysis is performed with the data set found from Step 1. Typically in kinetic studies, the isothermal rate of degradation or conversion, $d\alpha/dt$, is assumed to be a linear function of the temperature dependent rate constant, $k(T)$, and a temperature independent function of the conversion, $f(\alpha)$, where α indicates the conversion. This equation can be further expanded by using the Arrhenius expression for the rate constant. Within the Arrhenius expression, two more reaction dependent constants are introduced: the pre-exponential constant, A , and the

activation energy, E_a . (See Eq. 1.) The temperature independent function of the conversion, $f(\alpha)$ is dependent upon the mechanism of chemical reactions.

$$\frac{d\alpha}{dt} = k(T)f(\alpha) = \left[A \exp\left(-\frac{E_a}{RT}\right) \right] f(\alpha) \quad \text{Eq. 1}$$

The iso-conversional method, also known as the “model-free method”, is the method applied in this step to identify the minimum number of reactions necessary in the kinetic model. This method requires data from multiple non-isothermal (or dynamic) experiments, i.e. data tested with at least 4 different heating rates. The basis for this method is that at a constant conversion, α , $d\alpha/dt$ and $f(\alpha)$ become constants. With these terms in Eq. 1 staying as constants, the E_a is found without the pre-knowledge of the reaction mechanisms. When the E_a is found for the entire degradation process, the results provide insight for the minimum number of steps of elementary reactions needed to address the global reaction². A global reaction composed of a single stage process will show no dependence of E_a on conversion, α . When the global reaction is a complex process, the E_a changes with respect to conversion, α . An increase in E_a with α typically indicates parallel reactions. A decrease in E_a with α suggests that either the process is reversible (concave shape) or there is a change in the rate determining step (convex shape). Therefore, by analyzing the shape of the curve plotted with E_a with respect to conversion, α , a minimum number of elementary reactions are suggested.

There are two types of iso-conversional method which will be used in this study to check consistency in the estimation of both analyses. The first method used was introduced by Ozawa, Flynn and Wall^{3,4} (OFW) where the conversion function, $f(\alpha)$ is assumed to be independent of the heating rate. Applying a constant heating rate, $dT/dt = \beta$, Eq. 1 can be re-written as Eq. 2. Hence, $\ln(\beta)$ should have a linear relationship between $1/T$. By plotting $\ln(\beta)$ versus $1/T$ should give a constant slope of $-E_a/R$ for a wide range of conversion.

$$\ln(\beta) = \ln\left(\frac{dT}{dt}\right) = \ln\left(\frac{A \exp\left(-\frac{E_a}{RT}\right) f(\alpha)}{d\alpha/dT}\right) = \ln\left(\frac{Af(\alpha)}{d\alpha/dT}\right) - \frac{E_a}{RT} \quad \text{Eq. 2}$$

Another iso-conversional method is based on Friedman^{5,6}, which is very similar to the OFW method. This method was used to calculate the activation energy, E_a , using a different method for comparison. Instead of plotting $\ln(\beta)$ versus $1/T$, $\ln(d\alpha/dt)$ versus $1/T$ is used to find the slope of $-E_a/R$ (see Eq. 3).

$$\ln\left(\frac{d\alpha}{dt}\right) = \ln\left(A \exp\left(-\frac{E_a}{RT}\right) f(\alpha)\right) = \ln(Af(\alpha)) - \frac{E_a}{RT} \quad \text{Eq. 3}$$

Step 3: Model Fitting Method

After conducting the iso-conversional method to identify the minimum number of reactions required when describing the entire process of a thermally degrading material, the model fitting method should be applied for the following purposes: 1) Identify the rate determining factor to understand more about the thermal degradation kinetics; 2) Estimate kinetic parameters used in the temperature dependent rate constant, $k(T)$, and temperature independent function of conversion, $f(\alpha)$ (see Eq. 1).

The model fitting method is one of various thermal analysis methods that fits the experimental data to a predetermined kinetic model for a single reaction – $f(\alpha)$ or $g(\alpha)$, the integral form of $f(\alpha)$ – expressed in terms of conversion, α . Examples of these models are given in the literature^{7,8} where the models are organized in terms of the most applicable solid state kinetics responsible for a given reaction. The fitness of the data to the model reveals the possible rate determining solid state kinetics for thermal degradation. When using this method, fitting multiple experiment data at once to calculate the kinetic parameters is important to increase the reliability of the results⁹. In the past, a general exercise in pyrolysis modeling was to apply reaction order type models to any kind of solid state degradation kinetics, in most cases a first order reaction model. For many cases, an nth order reaction model ($f(\alpha) = (1 - \alpha)^n$) can be used to fit a range of different kinetics by adjusting the n value .

Therefore, applying this approach is generally accepted. However, one downside for using the n th order reaction model for any kind of kinetics is that the n value may vary significantly and therefore the kinetic modeling becomes merely a data fitting exercise. Another limitation is due to the actual kinetics not being considered when conducting the modeling. There is a high possibility that the kinetic model will misinterpret the material degradation in the conditions which were not considered when obtaining the kinetic parameters for the n th order reaction model. In other words, when kinetic modeling is conducted with TGA non-isothermal experiment data with heating rates of 5 to 60°C/min, the kinetic model may only be good for simulating those heating rates. In this study, the n th order reaction order model was used as a default kinetic model and other various models were also investigated to understand more about degradation kinetics.

MATERIALS AND EXPERIMENTS

There are two different thermoset polymers that are tested in this study. The tested samples are manufactured through the same process as the ones that are used to produce the FRP composites. The samples are fully cured resins which do not contain fiber glass reinforcements. The resins are formulated to be used for FRPs to meet International Building Code Interior Finish requirements¹⁰ for Class I per ASTM E 84¹¹.

Materials tested in this study are the following: The first material is a modified acrylic resin (MA). This resin is essentially unsaturated polyester (UPE) with Methacrylic Acid (MMA) replacing most of the styrene monomers for crosslinking. The second material is a modified acrylic resin with an inorganic additive (A) for fire retardancy. Typical inorganic additives are hydrates such as alumina trihydroxide (ATH) or magnesium hydroxide, antimony trioxide, borax, chalk, silica, etc¹². Because this additive was known to give a high-charring effect with a strong endotherm, it was categorized with typical hydroxides used as flame retardant fillers. These hydroxides work as a flame retardant by resulting in an endothermic dehydration reaction that produces oxides and water^{13,14}. The water produced by this reaction vaporizes, which is an endothermic reaction, and the vapor dilutes the gaseous phase. Note that when these hydroxides decompose without re-crystallization or disintegration they are typically stable crystalline materials. Only some modification of lattice parameter is observed allowing the loss of small stable molecules from the reactant phase, such as H₂O. These molecules travel outward to the interface between the solid and gas phase via diffusion^{15,16}. The oxides remain in the char layer, which adds an insulative effect. This flame retardant is added in a relatively large amount (50 to 65%) compared to other types of additives. By adding a significant amount of an inorganic flame retardant, the polymer becomes more brittle. Because this is an inorganic additive, inserting this material into the polymer system by 50 to 65 wt% of its original polymer reduces the available fuel within the condensed phase. In addition to this effect, usually the additive has a higher heat capacity comparing to the base polymer and hence, the flame retarded polymers with these types of hydroxides require more energy to increase the temperature to its pyrolysis level.

The experimental instruments used in this study were manufactured from TA Instruments: Thermogravimetric Analysis Q50 (TGA) and the Differential Scanning Calorimetry Q20 (DSC). Throughout this study, TGA and DSC were used for a non-isothermal test purposes and the tests were conducted in nitrogen and air environments to study pyrolysis and oxidation, respectively. Using the TGA, 4 different heating rates of 5°C/min., 20°C/min., 40°C/min. and 60°C/min. were applied to measure the mass loss history of each resin sample from 40°C to 800°C. For the DSC, a constant heating rate of 20°C/min. was used to measure the heat flow through the sample during the thermal decomposition of resins. Tests conducted with the DSC were from 40°C to 500°C where the maximum temperature is lower than that of TGA due to the limitation of the instrument. A sample size of approximately 10 mg was used for each test in a standard aluminium pan with a punctured lid so that gases may evolve freely away from the pan.

RESULTS AND DISCUSSION

To apply the kinetic modeling methodology discussed in the previous section, two types of thermoset resins used in fiber glass polymer (FRP) composites are selected, which are the modified acrylic resin (MA) without and with additives (α). When modeling the thermal behavior of these resins, the unknown flame retardant additive (α) is considered to be a filler-type, inorganic, providing high-charring effect to the base polymer. The additive percentage within the resin mixture is 61.9% by weight and it is assumed that the additive is well-mixed within the polymer allowing a uniform concentration of the additive in the samples. The additive effect is modeled by comparing results from these two samples.

Preliminary experiments are conducted as the first step in kinetic modeling and these are done to understand the factors that can contribute to kinetic behaviors of a material. Among various factors, the most consideration was given to the particle size effects because the particle size with respect to the sample mass is proportional to its surface area. Generally in most solid degradations the interface between the solid and the gas phase (i.e. sample surface) becomes important knowing that it provides active sites for degradation reactions to occur. The effect of different sample particle sizes on the TGA test results were determined by changing the surface area to mass ratio in each test. In general, the modified acrylic resin (MA) showed insignificant changes with respect to changes made in the sample size. However, when the resin with additive (MA+ α) size was varied from 1 to 10 mg, the onset temperature for decomposition increased from 280°C to 310°C. Note that separate analysis was performed to ensure that sample mass in this range is small enough to eliminate any temperature gradient within the sample during each TGA test. To account for this effect, the information regarding the sample size for MA+ α was closely monitored and controlled so that the ratio of the interface area between the solid and gas phase to sample volume were similar for all other TGA tests. The effect of sample size to degradation kinetics observed in thermal decomposition of MA+ α resin should be considered when conducting pyrolysis modeling with the kinetic information obtained from this study.

The next step is to conduct the iso-conversional method to construct a set of elementary reactions for thermal decomposition that involves weight loss. As shown in Figure 1, the activation energies calculated for the entire range of conversion ($0.0 \leq \alpha \leq 1.0$) of modified acrylic resin with additive can be categorized into three sets: In the initial weight loss region where conversion ranges from 0.0 to 0.2, the estimated activation energy is relatively steady with respect to conversion. Using a 95% confidence level, the estimated activation energy for this range is 155.5 ± 6.9 or 151.3 ± 3.8 kJ/mol when OFW's or Friedman's methods are used, respectively. By comparing the results from TGA and DSC tests of both samples – without and with additive in modified acrylic resin – this weight loss reaction is considered as additive degradation (see Figure 2 and Figure 3). The test conducted in the TGA with a heating rate of 20 °C/min shows that the onset temperature for the major thermal decomposition of the resin only sample is 341°C, which is 26°C higher than that of the resin with additive sample (315°C). Before this onset temperature, there is less than 10% weight loss most likely due to the escape of impurities, unreacted monomers and non-fully cross-linked oligomers within the polymer resin. The test conducted in the DSC with a heating rate of 20°C/min shows that the weight loss of resin with additive sample within this conversion region incorporates a significant endothermic heat flow, which is speculated to result from the degradation of a flame retardant additive knowing that typically this type of strong endotherm is a desired effect of a fire retardant additive. Therefore, in $0.0 \leq \alpha < 0.2$ region, decomposition reaction for mostly additive is assumed, considering that the resin decomposition is minimal at this stage.

Figure 1: Estimated activation energy (left) and R^2 values for the estimation (right) of modified acrylic resin with an inorganic high charring additive calculated via “iso-conversional” (model free) method

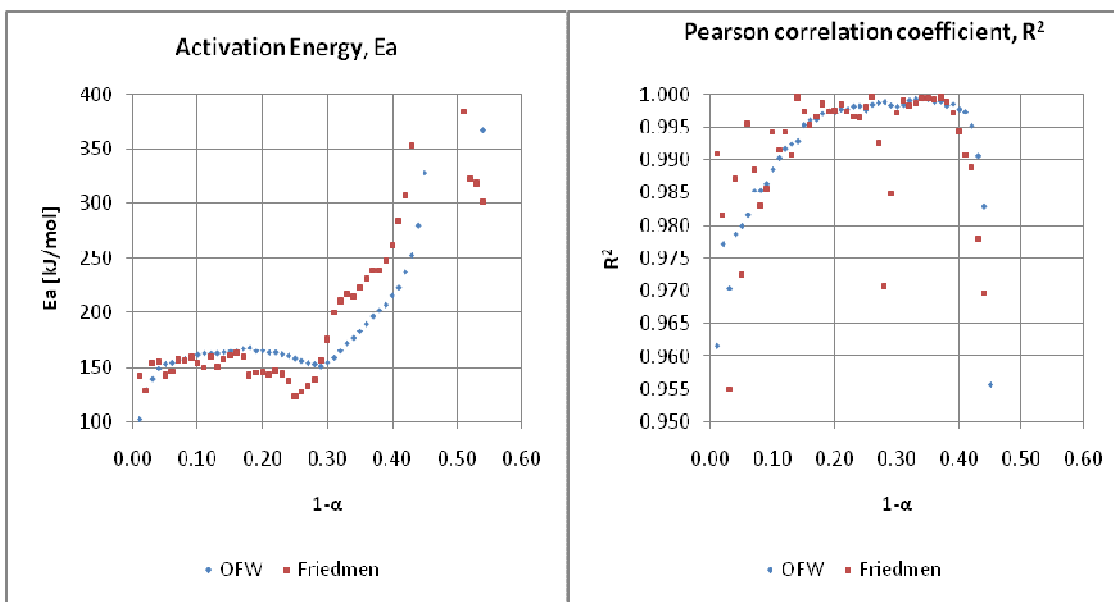


Figure 2. TGA Non-isothermal experiment results with a constant heating rate of 20°C/min for temperatures ranging from ambient to 800°C: TGA and DTG of resin without and with additive tested in air (oxidative) and nitrogen (inert) environments. Note that the results from testing resin only sample is scaled down to a maximum of 38.1% from 100% which is the weight percentage mixed within the resin with additive sample.

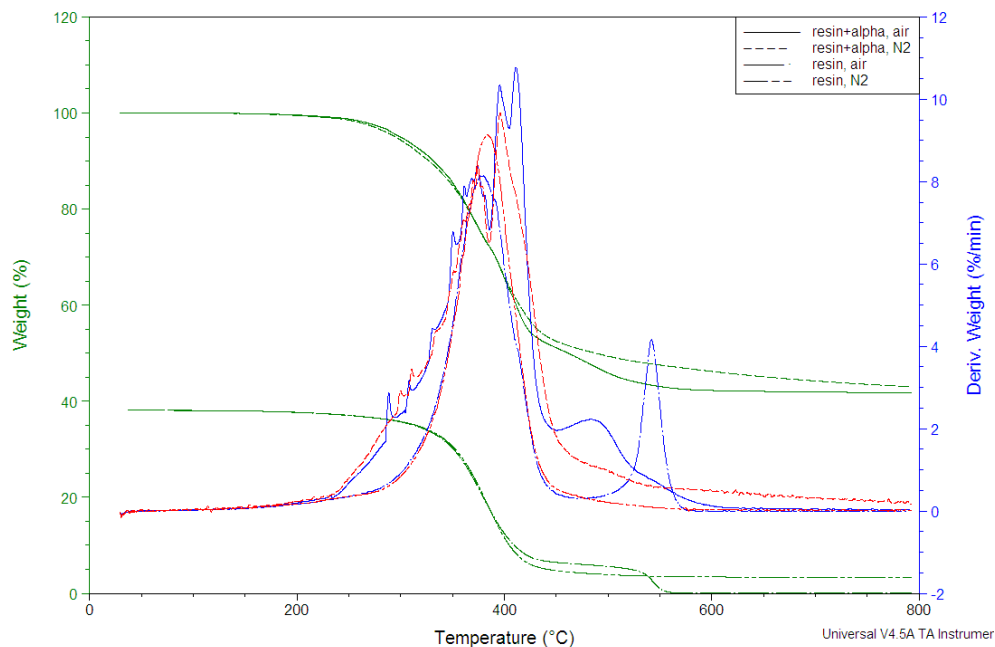
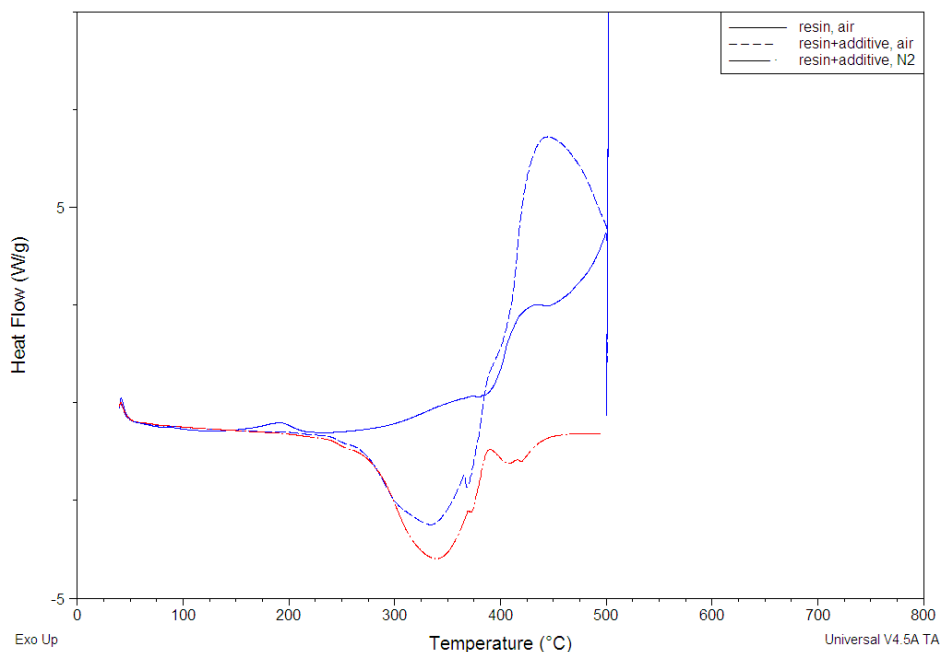


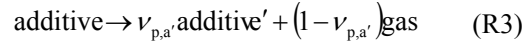
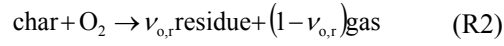
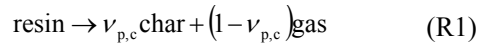
Figure 3. DSC Non-isothermal experiment results with a constant heating rate of 20°C/min for temperatures ranging from ambient to 500°C: Heat flow results of resin without and with additive tested in air (oxidative) and nitrogen (inert) environments. Note that baseline correction has not been applied to the results shown below.



For $0.2 \leq \alpha < 0.4$, the estimation for the activation energy increases as α increases meaning that the kinetics of decomposition are changing. This can be an indication that there is an additional parallel reaction occurring¹⁷. The results from TGA and DSC experiments conducted for samples without and with additive in modified acrylic resin allow one to consider the resin decomposition being responsible for the weight loss. The temperature range of decomposition and the DTG maximum height (i.e. peak mass loss rate) observed in TGA tests on resin with additive sample are similar to those found from tests on the resin only sample. Based on this comparison and assuming that the additive does not interfere with the polymerization process, the degradation reaction that allows the weight loss in this conversion region is modeled as the weight loss due to the modified acrylic resin degradation reaction only.

As conversion increases above 0.4, the activation energy increases with a higher slope than the slope found in the previous region. The change in the slope also suggests that the kinetics is changing in this region. Then the modified acrylic resin with additive sample stops losing its mass resulting in a residue of approximately 40 to 45% of its initial weight. The TGA and DSC tests for the resin samples without and with additive in nitrogen and air environments suggest that the weight loss observed within this region is due to the resin char oxidation. The resin only sample loses about 15% or 25% of its initial weight in the temperature range found in this conversion region when tested in nitrogen (pyrolysis) or air (pyrolysis and oxidation), respectively. Hence, it can be assumed that for this temperature range, resin only sample is involved in a minimum of two reactions – a pyrolysis reaction resulting in a 15% weight loss, which is the later part of the major decomposition step for the resin only sample discussed in the previous stage and oxidation reaction resulting in 10% more. Applying the weight percentage of the resin within the resin with additive sample, 38.1%, the resin with additive sample should lose roughly 6% and 4% of its mass from pyrolysis and oxidation of the resin, respectively. Therefore, a total of 10% of resin with additive sample is due to the resin decomposition assuming that the thermal degradation behavior of the resin is similar whether the additive is mixed with the resin or not. The resin with additive sample loses about 15% or 20% of

its initial weight in the same temperature range when tested in nitrogen (pyrolysis) and air (pyrolysis and oxidation), respectively. Considering that the difference of 5% weight loss between the nitrogen and air test results is comparable to the 4% weight loss due to resin oxidation discussed earlier, no additional oxidation reaction is presumed for this conversion region. The 15% weight loss observed in resin with additive sample tested in nitrogen (pyrolysis) indicate that in addition to the resin's pyrolysis reaction resulting in 6% weight loss, there is approximately 9% decrease in sample mass. This 9% of mass loss can be described by analyzing the TGA and DTG graphs shown in Figure 2. As shown here, the peak temperature for the major decomposition DTG peak of the resin with additive sample is slightly greater than that of the resin only sample which suggests that the 9% of mass loss is due to the major decomposition of the resin from the previous stage extending to this conversion range. Based on this analysis, a total of two reactions are modeled: pyrolysis (15% weight loss) and oxidation (4~5% weight loss) of the modified acrylic resin. Therefore, the full degradation of the resin with additive is:

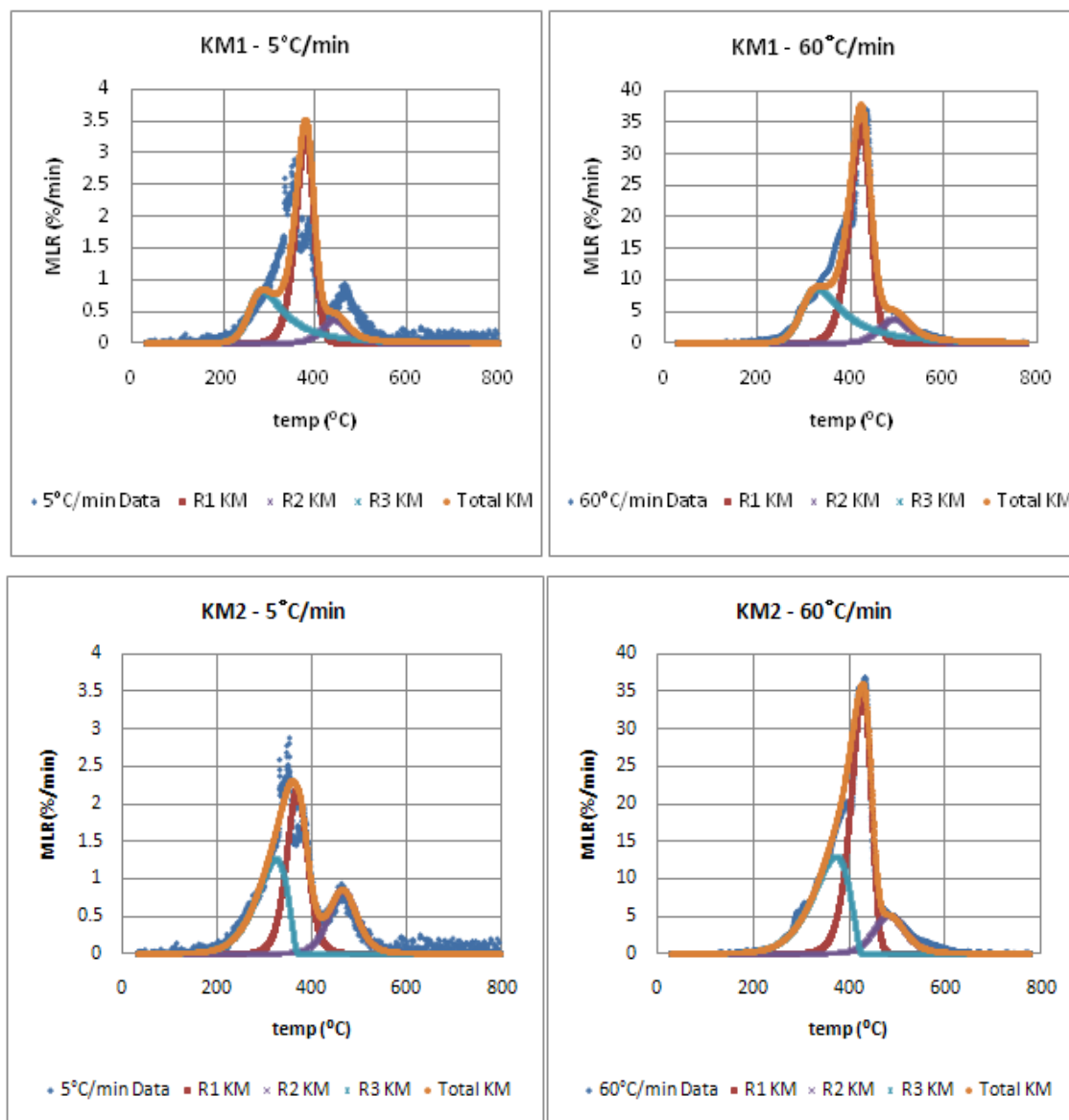


Applying this degradation mechanism, the final step of conducting the model fitting method⁹ is shown where a kinetic model, $f(\alpha)$ (or $g(\alpha)$ in integrated form) is preselected to fit the TGA experiment data to find the kinetic parameters with the best fitness. In this study, a model for a reaction order type kinetics, $f(\alpha) = (1 - \alpha)^n$ is used primarily, considering that this model is typically used for many solid thermal degradations, as well as other types of models available for various solid state reactions^{7,8}. The weight loss with respect to each reaction is optimized based on the findings from conducting the iso-conversional method discussed above. The fitness of the model is compared by considering two factors: (1) the weight loss rate vs. temperature (DTG) shape and (2) the square of the Pearson product moment correlation coefficient, R^2 . Applying a reaction order type kinetic model to conduct model fitting method, the estimation results of the kinetic parameters are summarized in Table 1 and the fitness between the actual DTG and the kinetic modeling is shown in Figure 4.

Table 1: Kinetic parameters estimated from model fitting exercise using Genetic Algorithm (GA): Three steps nth order kinetic model

Reaction	Z (s-1)	E _a (kJ/mol)	n (-)	n _O (-)
R1	1.80E+14	207	1.3	
R2	7.20E+12	207	1.8	1.0
R3	2.80E+11	152	4.9	

Figure 4. Kinetic modeling conducted for modified acrylic resin with inorganic additive: Kinetic Model 1 (KM1) – 3 step mechanism with nth order kinetic model; Kinetic Model 2 (KM2) – 3 step mechanism with 2 nth order kinetic model for R1 and R2, and diffusion controlled model for R3. For KM2 cases, the kinetic parameters and mass fractions for R1 and R2 have been adjusted differently for each heating rate case to give best-fit between the TGA experiment data and kinetic modeling results.



Several findings are summarized as follows based on this model fitting exercise. First, the reaction order type kinetic model can be used to fit the DTG data with some degree of satisfaction for all reactions (see R1, R2 and R3). However, the estimated reaction order is high as 4.9 for R3 reaction. This indicates that the model is forced to fit the data knowing that the reaction order in this magnitude is rare to find in the literature. Also, the DSC data confirms that the reaction order type model was inappropriate for R3 as well (see KM2 cases in Figure 3). Although the model is giving high correlation coefficients between the data and modeling for R3 reaction, the DSC data show that R3

should exist from 200°C and end before 400°C where a strong endotherm is observed. When the data is fit with a reaction order type kinetic model, the additive decomposition temperature range extends beyond 400°C, ending near 600°C.

Second, the decomposition of the additive reaction is best described by a kinetic model that describes a diffusion controlled reaction (see Figure 4) among various other types of models investigated in this paper. The model type is reasonable considering that the model simulates the weight loss to be slow initially with respect to temperature increase and decays relatively fast after the weight loss rate peak. This modeling becomes suitable for an additive decomposing within a resin polymer system resulting in a time delay due to the time necessary to degrade the polymer near the additive. Consider the additive being mixed within the resin polymer. For the additive to undergo a decomposition reaction, the degradation of the resin polymer should occur simultaneously because the additive is aggregated within the resin. Having the additive decomposition temperature lower than that of the resin, the decomposition of the additive is delayed until the temperature is higher to allow the resin to decompose. When this model is actually applied, it provides good estimate of the slow weight loss at the initial stage near 200°C and the temperature range for the entire reaction. Additionally, when this model is used, the modeling results for weight loss rate after 300°C matches well with the actual DTG data together with R1 reaction described with a reaction order type kinetic model.

Third, although kinetic modeling has been conducted to give best fitness between the modeling and the DTG data obtained over various heating rates (5 to 60°C/min) assuming that the kinetics are identical irrespective of heating rates, changes in the kinetics over 4 heating rates have been noticed. At lower heating rates, the portion of the sample weight consumed via R2 (char oxidation) increases where at higher heating rates it decreases. The ratio of weight loss due to R1 (resin pyrolysis) to R2 (char oxidation) is 25:13 for 5°C/min DTG data and 30:8 for that of 60°C/min. This can be explained by understanding that the resin pyrolysis and char oxidation reactions compete and the char oxidation reaction is controlled by oxygen diffusion from the ambient to the condense phase. At a low heating rate, more time is available for oxygen diffusion with respect to temperature change allowing an increase in the weight loss due to oxidation (R2). However, when the heating rate is higher, the conditions become the opposite and the pyrolysis reaction (R1) dominates. The fitness of the model to DTG data significantly increases when this effect is accounted for in the modeling (see Figure 4).

CONCLUSION AND FUTURE WORK

As a part of a property estimation exercise for pyrolysis modeling, a three step kinetic modeling methodology was introduced. The first step is to conduct preliminary experiments to understand factors that contribute to a material's kinetic behavior. The second step is to apply the iso-conversional method to construct sets of elementary reactions which result in weight loss. The last step is conducting a model fitting method to estimate the appropriate kinetic model as well as its kinetic parameters. Two types of thermoset resins, modified acrylic resin (MA) degradation without and with additive (α), were considered as example materials for kinetic modeling.

To conduct kinetic modeling, TGA and DSC experiments were performed on the resins at various heating rates ranging from 5 to 60°C/min. Preliminary experiments on these resins showed that changes made in the sample sizes have an insignificant effect on the overall degradation of MA; however, the onset temperature of thermal decomposition of MA+ α was influenced. Using an iso-conversional method, a three step mechanism was developed as a set of minimum number of elementary reactions required to describe the full degradation of MA+ α – two reactions for polymer resin decomposition (R1 and R2) and one for decomposition of the additive (R3). With a pre-determined three step reaction mechanism, a model fitting method was used to find the kinetic parameters for each reactions.

By conducting the kinetic modeling exercise, the following observations were made: First, although the reaction order type kinetic model can be used to fit the three reactions of DTG with some degree of satisfaction, evidence (high reaction order value and the temperature range where a strong endotherm is observed in the DSC data) exists that the additive degradation reaction was forced to fit this kinetic model. Second, the decomposition of the additive reaction is best described by a kinetic model that describes a diffusion controlled reaction. Third, changes in the kinetics over 4 heating rates have been noticed where at lower heating rates, the portion of the sample weight consumed via R2 (char oxidation) increases and at higher heating rates it decreases.

In this study, a simple method of conducting kinetic modeling for pyrolysis modeling is introduced and is applied to two types of thermoset polymer resins – modified acrylic resin without and with fire retardant additive. In the future, this information will be used in pyrolysis modeling of FRPs and many challenging non-trivial questions regarding the extrapolation of non-dimensional kinetic analysis results to dimensional pyrolysis modeling will need to be answered. Some of these questions are:

- ◆ How should the effect of having different thermal decomposition temperatures with respect to TGA sample sizes be handled when conducting pyrolysis modeling?
- ◆ What are the physics that are necessary in pyrolysis modeling to properly apply this kinetic information?
- ◆ Should there be any modification to the kinetics when pyrolysis modeling is conducted considering that there is a significant change in the testing conditions from kinetic modeling where a sample is decomposing in a milligram scale to pyrolysis modeling where a sample is decomposing in a kilogram scale?

ACKNOWLEDGEMENT

The authors greatly appreciate the support for this work from DOC NIST Award Number 60NANB8D8106 (Federal Program Officer Dr. Kevin McGrattan). Special thanks to Charles Dore for fabricating and donating the resins used in this study.

¹ Handbook of Thermal analysis and Calorimetry. Vol.1: Principles and Practice. M.E. Brown, editor c 1998 Elsevier Science B.V.

² S.V. Vyazovkin and A.I. Lesnikovich, *Thermochim. Acta*, 165 (1990) 273

³ Ozawa, T., *Bull Chem Soc Jpn* 1965;38;188

⁴ Flynn, J., Wall, L.A., *J Polym Lett* 1966;4:232

⁵ Friedmen, H.L., *J Polym Sci Part C* 1964;6:183

⁶ Friedmen, H.L., *J Polym Lett* 1966;4:232

⁷ Bras, M.L., Rose, N. and Bourbigot, S., The Degradation Front Model – A tool for the Chemical Study of the Degradation of Epoxy Resins in Fire, *Journal of Fire Sciences*, Vol. 14 – May/June (1996)

⁸ Liu, J., He, D., Xu, L., Yang, H. and Wang, Q., Study of the Kinetics of the Combustion Reaction on Shuangya Mountain Coal Dust by TG, *Journal of Thermal Analysis and Calorimetry*, Vol. 58 (1999) 447-453

⁹ Burnham, A.K., Weese, R.K., Kinetics of thermal degradation of explosive binders Viton A, Estane, and Kel-F, *Thermochimica Acta* 426 (2005) 85-92

¹⁰ Chapter 8 Interior Finishes, 2006 (IBC) International Building Code, ICC - International Code Council, ISBN 13: 9781580012515, ISBN 10: 1580012515, 2006

¹¹ Standard Test Method for Surface Burning Characteristics of Building Materials, ASTM E 84-05, ASTM, 100 Barr Harbor Drive, West Conshohocken, PA, U.S.

¹² Handbook of polymer blends and composites By Anand K. Kulshreshtha, Cornelia Vasile

¹³ Lewin, M., Synergism and Catalysis in Flame Retardancy of Polymers, *Polym. Adv. Technol.* 12, 215-222 (2001)

¹⁴ LeVan, S.L., The Chemistry of Solid Wood; Chapter 14. Chemistry of Fire Retardancy, American Chemical Society, 1984

¹⁵ A.K. Galwey, G.M. Laverty, N.A. Baranov and V.B. Okhomikov, *Phil. Trans. R. Soc. London*, A347 (1994) 139, 157

-
- ¹⁶ V.B. Okhotnikov, S.E. Petrov, B.I. Yakobson and N.Z. Lyakhov, *React. Solids*, 2 (1987) 359
- ¹⁷ S.V. Vyazovkin and A.I. Lesnikovich, *Thermochim. Acta*, 165 (1990) 273

Appendix F

Property Estimation for Pyrolysis Modeling Applied to Flame Retarded Modified Acrylic FRP Composites

Composites & Polymers 2010

Property Estimation for Pyrolysis Modeling Applied to Flame Retarded Modified Acrylic FRP Composites

by

Esther Kim¹
Nicholas Dembsey¹
Charles Dore²

¹ Worcester Polytechnic Institute
Department of Fire Protection Engineering
100 Institute Road
Worcester, MA 01609

² Abate Fire Technologies, LLC
8238 Sandpoint Blvd
Orlando, FL, 32819, USA

Abstract

For the composites industry to “design for fire” more thorough understanding of how typical FRPs decompose under fire conditions is needed. The role played by the glass and the resin (and additives) for FRPs are keys to understanding their fire behavior. To that end, this study continues work presented at Composites 2009. The goal of this work is to evaluate the ability of a pyrolysis model and genetic algorithm (optimization routine) pairing to estimate properties of each component of the composite, resin and glass. As a part of the property estimation exercise, emphasis was given to estimating the thermal decomposition kinetic parameters of the modified acrylic resin in a simplified manner when an “unknown” flame retardant is included as an additive. When conducting the kinetic modeling, focus was on creating a procedure that only requires general information about the resin and its additive. The reason for this is that typically due to intellectual property concerns exact information on the resin and additive are unavailable. The composite pyrolysis experimental data used in this work was obtained from tests conducted on a bench scale fire test apparatus, Cone Calorimeter, with additional instrumentation to measure surface and internal temperatures of the sample and the flame heat flux. Mass loss data, temperature profiles with respect to time at different in-depth locations and heat flux from the flame to sample surface after ignition for boundary condition specification are

used in the optimization process. The property estimation exercise is conducted on a flame retarded modified acrylic FRP composite. Thermal analysis data from thermogravimetric analysis (TGA) and differential scanning (DSC) calorimetry of the resin with a high-charring flame retardant additive was used to model the decomposition kinetics. With the approximated decomposition kinetics for the resin, simulation of pyrolysis tests of the composite slab in air was performed to estimate the unknown thermophysical properties by genetic algorithm optimization. A validation exercise using the estimated properties is then conducted on composites tested under different external heat fluxes impinging on the sample surface. The quality of the estimated properties is assessed by comparing simulated results to experimental results from tests with different heat fluxes.

1. Introduction

For the composites industry, designing for a FRP that provides good fire characteristics becomes a guess and check operation in many cases. Any changes made to the resin, glass, or the microstructure of the FRP affect the overall fire behavior of the FRP. Traditionally, the effect of the changes made in the FRP is checked by conducting tests via standard fire tests, which can be time consuming and expensive. Therefore, providing an understanding of how typical FRPs decompose under fire conditions and using this information to find an appropriate guideline for the composite industry to produce better fire-safe composites have been a long-term goal for this research. To that end, this work follows the work presented at Composites 2009.

In this study, an emphasis was given to estimating the thermal decomposition kinetic parameters of the modified acrylic resin in a simplified manner when an “unknown” flame retardant is included as an additive. When conducting the kinetic modeling, focus was on creating a procedure that only requires basic information about the resin and its additive such as the weight percentage of the additive within the polymer base, general description of the flame retardant effect of the additive on the overall fire performance of the polymer, existing content of a potential fuel within the additive, etc. The reason for this is that typically due to intellectual property concerns exact information on the resin and additive are unavailable for real world materials.

To conduct property estimation and modeling, complete data sets of decomposition of flame retarded modified acrylic resin and its FRP composites are presented. Careful experiments were conducted using Thermogravimetric Analysis (TGA) and Differential Scanning Calorimetry (DSC) in order to study the thermal decomposition kinetics of the modified acrylic resin with an inorganic high-charring additive. Also, the FRP composites with a glass content of 41.6 wt% were tested

under a bench-scale fire test apparatus known as the Cone Calorimeter (ASTM E 1354 [1]) with additional instrumentations – thermocouples at various depths and total heat flux gauge to measure additional heat flux from the flame after ignition. These were designed to generate data useful for computer modeling purposes.

The model used in this study is a generalized pyrolysis model developed by Lautenberger [2,3], which simulates the heating and decomposition of a chosen material. Like with any other pyrolysis models, this model requires many input parameters found from material properties, which include the pyrolysis kinetics (pre-exponential factor, activation energy, reaction order), thermal properties (specific heat capacity, thermal conductivity), and radiative characteristics (surface emissivity, in-depth radiation absorption coefficient). Unfortunately, there are no standardized techniques to determine all of these properties via laboratory tests. Another way of estimating parameters is to use an optimization routine with a pyrolysis model in pair. The current work applies Genetic Algorithm (GA) as an optimizing method coupled with Lautenberger's pyrolysis model [2,3] to perform parameter estimation.

In this paper, the following work is presented: Thermal analysis is conducted for kinetic modeling of the resin without and with the flame retardant additive, the decomposable element of the FRP. With the approximated decomposition kinetics for the flame retarded resin, simulation of pyrolysis tests of the composite slab in air is performed to estimate the unknown thermo-physical properties by GA optimization. A validation exercise using the estimated properties is then conducted on composites tested under different external heat fluxes. The quality of the estimated properties is assessed by comparing the simulated results to experimental results.

2. Modified Acrylic FRP Composite

2.1. Modified acrylic thermoset resin and high-charring additive

Modified acrylic resin (MA) is essentially unsaturated polyester (UPE) with Methacrylic Acid (MMA) replacing most of the styrene monomers. Flame retarded resin with MA is manufactured by adding a filler type inorganic additive (α) as an additive. Typical inorganic additives are hydrates such as alumina trihydroxide (ATH) or magnesium hydroxide, antimony trioxide, borax, chalk, silica, etc [4]. Because this additive was known to give a high-charring effect, α was categorized with typical hydroxides used as flame retardant fillers. These hydroxides works as a flame retardant by resulting in an endothermic dehydration reaction that produces oxides and water [5,6]. The water produced by this reaction vaporizes, which is an endothermic reaction,

and the vapor dilutes the gaseous phase. The oxides remain in the char layer, which adds an insulative effect. This flame retardant is added with a relatively large amount (50 to 65%) comparing to other types of additives. By adding a significant amount of an inorganic flame retardant, the polymer becomes more brittle. Because this is an inorganic additive, inserting this material into the polymer system by 50 to 65 wt% of its original polymer reduces the available fuel within the condensed phase. In addition to this effect, usually the additive has a higher heat capacity comparing to the base polymer and hence, the flame retarded polymers with these types of hydroxides require more energy to increase the body temperature to its pyrolysis level. According to the product description, this resin with the flame retardant additive is formulated to be Class I per ASTM E 84 [7] (flame spread index < 20 and smoke developed < 225).

2.2. FRP composite description

Composite panels were fabricated by hand lay-up for a relatively low glass content composite (41.6 wt% of glass, average thickness of 7~9 mm) using two different types of fiberglass mats that were wetted with resin. The two types of fiberglass (E-glass) used in the composite are a chopped strand mat and a glass roving woven mat with an area density of 25 g/m² and 880 g/m², respectively. The chopped strand mat is thinner and more porous than the woven mat. The laminate schedule (provided by the manufacturer) is chopped strand mat and roving alternating three times with another chopped strand mat layer at the end. Visual inspection of a polished cross-section of the composite slab is consistent with this laminate schedule, but with polymer resin layers between each fiberglass layer. The chopped strand mat layer is difficult to identify in the cross section, perhaps because more resin is soaked into this layer than the roving layer. The roving layer is observed as a prominent glass layer possibly because the resin is absorbed only at the fiberglass layer surfaces leaving the interior with primarily glass. The layered microstructure is determined to a resolution of 0.10 mm by inspecting a polished cross-section of the composite under a microscope. Based on visual observation and comparison to global density of the composite sample, approximations of three distinct layers are proposed: 100% resin, 100% glass, and 50% resin/50% glass (see Figure 1).

3. Experiment Apparatuses

3.1. Thermogravimetric Analysis (TGA) and Differential Scanning Calorimetry (DSC)

The instruments used in this study were manufactured from TA Instruments: Thermogravimetric Analysis Q50 (TGA) and the Differential Scanning Calorimetry Q20 (DSC). In this study, TGA and DSC were used for a non-isothermal test purposes and the tests were conducted in nitrogen and air environments to study pyroly-

sis and oxidation, respectively. Using the TGA, 4 different heating rates of 5, 20, 40 and 60°C/min were applied to measure the mass loss history of each resin sample from 40 to 800°C. For the DSC, a constant heating rate of 20°C/min was used to measure the heat flow through the sample during the thermal decomposition of resins. Tests conducted with the DSC were from 40 to 500°C where the maximum temperature is lower than that of TGA due to the limitation of the instrument. A sample amount of approximately 10 mg was used for each test in a standard aluminium pan with a punctured lid so that gases may evolve freely away from the pan.

3.2. Cone Calorimeter

Cone Calorimeter (Cone, ASTM E 1354 [1]) is a bench-scale fire test apparatus in which the sample is heated by an electrically heated rod in the shape of a cone. The sample is tested by applying a constant radiative heat flux set via temperature controller of the rod. The Cone exposes the sample in an ambient environment which results in a natural flow field as the sample temperature increases allowing convective cooling above the sample surface. The ignition source is an intermittent sparker. The Cone can be used to calculate useful engineering data such as oxygen consumption based heat release rate (based on the standard), mass loss rate, smoke yield and smoke extinction coefficient.

The purpose of Cone testing was to generate good data sets appropriate for pyrolysis modeling and parameter estimation, and therefore several modifications were made to the standard testing procedure. First, when testing the FRPs, a round insulated sample dish purposed by de Ris and Khan [8] was used instead of the standard specified, non-insulated square sample holder (see Figure 2). In this sample dish, the sample is surrounded by Cotronics® paper insulation on the back and sides to limit heat loss, which simplifies the pyrolysis modeling. Second, 4 thermocouples were installed to measure temperature change of the sample at various depths: surface, 1/3, 2/3 and back face of the sample. The installation of thermocouples on the sample was consistent with the method introduced in Composites 2009 paper [9]. Thermocouple holes were drilled at 1/3 and 2/3 of the sample thickness with a 1.25 mm diameter drill bits. Thermal grease (OmegaTherm Thermally Conductive Silicone Paste, Model OT-201, Omega Engineering) was inserted along with the thermocouples (Omega Precision Fine Wire Thermocouples, Model 5TC-GG-K-30-36, Omega Engineering) to reduce the air gaps within the thermocouple holes. The surface thermocouples were affixed via two types of methods: One method was to drill a thermocouple hole from the sample side and allow the hole to reach the surface. A thermocouple insulated wire was inserted through the side and the bead was able to locate near the surface; hence, from the surface only the bead was visible. Using this method, the center of the bead was located at

COMPOSITES & POLYCON 2010

the surface allowing top half to be exposed to ambient air and the lower half to sit within the sample. A drop of thermal grease was applied to the bead to ensure good contact between the sample and the bead. Another method was to crimp the thermocouple wire to allow the thermocouple bead to sit on the surface with a minimal amount of thermal grease applied at the bead. These two methods were used due to the sample pyrolyzing from a relatively lower temperature around 200°C generating a significant amount of white smoke possibly due to additive degradation. A conventional method of applying a high temperature adhesive (Resbond 907 Industrial Strength Fireproof Adhesive from Cotronics Corp.) was not utilized due to detach of thermocouple bead from the sample surface at an earlier times in the experiment. The back face thermocouples were affixed with Krazy glue.

The uncertainty in the mass loss rate data is estimated via statistical approach, taking the standard deviation (0.58 g/sm²) from the mean of a steady burning of 5 identical PMMA tests conducted in a Cone Calorimeter¹⁰. The estimated uncertainty is 1.4 g/sm², which is found by calculating the 95% confidence interval applying student t distribution with a sample size of 5. The uncertainty in the thermocouple measurements was quantified by comparing back face temperature data from four identical FRP composite tests with unsaturated polyester resin conducted in the Fire Propagation Apparatus (FPA, ASTM E 2058 [11]), a bench-scale test apparatus similar to the Cone Calorimeter assuming that the polyester composites and the modified acrylic composites have similar characteristics. Temperature measurement at the back face of the sample surface was chosen because the exact measurement location is known, i.e. the sample thickness. Other temperature measurements made in various depths have a positional uncertainty of ± 0.625 mm associated with the data. This uncertainty is from the drill bit used to make holes for thermocouple installations, which had a thickness of 1.25 mm diameter. Using the normalized time, time divided by sample thickness square, i.e., $\tau = \text{time}/\delta^2$ to remove the effect of different sample thicknesses when comparing, the maximum deviation at various normalized times, up to the critical time, τ_c , was 16°C. Assuming this is approximately equal to one standard deviation, applying student t distribution with a sample size of 4 and calculating the 95% confidence interval becomes ±25.5°C, hence the magnitude becomes 51°C. The critical time, τ_c , corresponds to the time when evenly spread flame on sample surface disappearing when tested under air. Test data presented in this parameter estimation exercise study is truncated at this critical time of 4 s/mm² because the pyrolysis model is set up with a one-dimensional assumption, which may not be used when flames on the sample surface is not evenly distributed, typically where edge burning is dominant. These uncertainty values will be used to evaluate significant differences in the modeling results

4. Kinetic Modeling of Resin Degradation for Pyrolysis Modeling

The purpose of conducting kinetic modeling in this study is to consider the thermal degradation kinetic behavior of a resin sample in milligram scale and extrapolate that information to be used in modeling pyrolysis of real world materials such as the FRPs in larger scales, i.e. those found in bench-scale or even full-scale tests. One of the major focuses of the paper is at constructing kinetic models in a consistent manner with minimal information about the resins because for most of the real world materials that are commercially available details regarding the chemical structure of the base polymer, the fire retardant additives, etc. are rarely accessible to the modelers due to the information being proprietary to the manufacturer. The models are intended to be simplified but sophisticated enough to capture the characteristics of the materials such as the fire retardancy via additives within a polymer matrix, environmental effect, etc.

To achieve this goal, a series of thermal analyses are conducted on commercial modified acrylic thermoset polymers with flame retardant additives used in fiber reinforced polymer (FRP) composites. Experiments for thermal analysis are conducted using Thermogravimetric Analysis (TGA) at various heating rates (5, 20, 40 and 60°C/min) and Differential Scanning Calorimetry (DSC) at 20°C/min. These non-isothermal TGA experimental results are used to conduct iso-conversional estimates of activation energy with respect to conversion without pre-determining the kinetic model using an Arrhenius type expression for thermal degradation. Results are also used to determine the minimum number of reactions required in the kinetic model to describe the thermal degradation reactions based on actual weight loss. Then a model fitting method is used where various kinetic models are used to fit the TGA data to the model. Kinetic model with the best fitness provides insight to the mechanism of degradation and kinetic parameters other than the activation energy are estimated based on the model of choice. The DSC experiments are conducted to use the heat flow information to compare against the analysis results conducted by the TGA and to determine the heat of reaction for each reaction involved in the thermal degradation process.

5. Pyrolysis Modeling for Lumped (TGA) and Slab (Cone) Experiments

The calculations reported here are conducted with a generalized pyrolysis model [2,3] that can be applied to a wide variety of condensed phase fuels. The model simultaneously calculates the condensed phase mass conservation, gas phase mass conservation, condensed phase species conservation, and condensed phase energy conservation equations. This model can be applied

to both 0D and 1D systems and is therefore capable simulating both “lumped” (TGA) and “slab” (Cone Calorimeter/FPA) experiments. Extensive details are given in Ref. [2,3] so only a brief overview is given here. Assumptions inherent in the model, as applied in this paper, include:

- Porosity can either be solved as a property of a species (default) or directly. When porosity is solved directly, it is derived from the condensed-phase mass conservation equation assuming no volume change (shrinkage or swelling)
- When porosity is directly solved, the user-specified thermal conductivity and density are interpreted as those of a nonporous solid. Therefore, the thermal conductivity and bulk density that appear in the condensed-phase energy conservation equation are $\bar{k} = (1-\psi)\bar{k}_s$ and $\bar{\rho} = (1-\psi)\bar{\rho}_s$ respectively, where ψ is porosity and \bar{k}_s and $\bar{\rho}_s$ are the weighted thermal conductivity and density of the solid assuming it is nonporous
- Bulk thermal conductivity \bar{k} has a cut-off value of 0.03W/mK which corresponds to air at 300 to 400K
- Specific heat is calculated with a weighted or averaged quantity, i.e. $\bar{c}_p = \sum X_i c_{p_i}$ as other solid properties – enthalpy, emissivity, radiation absorption coefficient, permeability, etc.
- Specific heat capacity and effective thermal conductivity vary by as $k(T) = k_0(T/T_r)^{n_k}$ and $c(T) = c_0(T/T_r)^{n_c}$, respectively, where T_r is a reference temperature
- Radiation heat transfer across pores is accounted for by adding a contribution to the effective thermal conductivity that varies as γT^3 , where γ is a fitting parameter
- Averaged properties in conservation equations are calculated by appropriate mass or volume fraction weighting

6. Results and Discussion

6.1. Kinetic modeling for resin degradation

To model the thermal behavior of the resin with an unknown flame retardant additive, two types of samples are prepared for thermal analysis – thermoset modified acrylic polymer resin without and with additives where the additive is known to be a filler-type, inorganic, and

providing high-charring effect to the base polymer. The additive percentage within the resin mixture is 61.9% by weight and it is assumed that the additive is well-mixed within the polymer allowing a uniform concentration of the additive in the samples. The additive effect is modeled by comparing results from these two samples.

Typically in kinetic studies, the isothermal rate of degradation or conversion, da/dt , is assumed to be a linear function of the temperature dependent rate constant, $k(T)$, and a temperature independent function of the conversion, $f(\alpha)$, where α indicates the conversion. This equation can be further expanded by using the Arrhenius expression for the rate constant. Within the Arrhenius expression, two more reaction dependent constants are introduced: the pre-exponential constant, Z , and the activation energy, E_a . The temperature independent function of the conversion, $f(\alpha)$ is dependent upon the mechanism of chemical reactions.

$$\frac{d\alpha}{dt} = f(\alpha)Z \exp\left(-\frac{E_a}{RT}\right) \quad (1)$$

Substituting the linear heating rate $\beta = dT/dt$ into Eq. (1) and taking the natural logarithm of both sides gives the following:

$$\ln \frac{d\alpha}{dT} = \ln\left(\frac{f(\alpha)Z}{\beta}\right) - \frac{E_a}{RT} \quad (2)$$

The iso-conversional method, also known as the model-free method is used to find the minimum number of elementary reactions necessary to describe the global degradation kinetics of the resin. This method uses data tested from different heating rates. Knowing that at a constant conversion, α , da/dt and $f(\alpha)$ become constants (see Eq.(2)), the E_a is found without the pre-knowledge of the reaction mechanisms. The iso-conversional method will give constant activation energies, E_a , over the range of conversion of interest if the reaction is a single-step chemical reaction. If the activation energies, E_a , changes significantly with respect to different conversions, this is an indication for a more complex reaction mechanism.

In

Figure 3, the results from two iso-conversional methods introduced by Ozawa, Flynn and Wall [12,13] (OFW, estimates $-E_a/R$ by plotting $\ln(\beta)$ versus $1/T$) and Friedman [14,15] (plotting $\ln(da/dT)$ versus $1/T$ to find $-E_a/R$) conducted on the modified acrylic resin with additive are shown. Both methods are used for comparison purposes. The R^2 values for each activation energy value are plotted as well using the least square method. The activation energy becomes more reliable as the R^2 values become closer to 1 where $\alpha = 1 - m/m_0$.

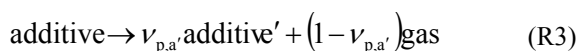
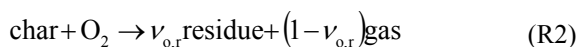
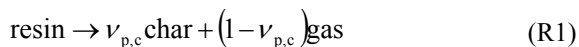
As shown in

Figure 3, the activation energies calculated for the entire range of conversion ($0.0 \leq \alpha \leq 1.0$) of modified acrylic resin with additive can be categorized into three sets: In the initial weight loss region where conversion ranges from 0.0 to 0.2, the estimated activation energy is relatively steady with respect to conversion. Using a 95% confidence level, the estimated activation energy for this range is 155.5 ± 6.9 or 151.3 ± 3.8 kJ/mol when OFW's or Friedman's method is used, respectively. By comparing the results from TGA and DSC tests of both samples – without and with additive in modified acrylic resin – this weight loss reaction is considered as the additive degradation (see Figure 4 and Figure 5). The test conducted in the TGA with a heating rate of 20 °C/min shows that the onset temperature for the major thermal decomposition of the resin only sample is 341°C, which is 26°C higher than that of the resin with additive sample (315°C). Before this onset temperature, there is less than 10% weight loss most likely due to the escape of impurities, unreacted monomers and non-fully cross-linked oligomers within the polymer resin. The test conducted in the DSC with a heating rate of 20°C/min shows that the weight loss of resin with additive sample within this conversion region incorporates a significant endothermic heat flow, which is speculated as a result of a degradation of a flame retardant additive knowing that typically this type of strong endotherm is a desired effect of a fire retardant additive. Therefore, in $0.0 \leq \alpha < 0.2$ region, decomposition reaction for mostly additive is assumed, considering that the resin decomposition is minimal at this stage.

For $0.2 \leq \alpha < 0.4$, the estimation for the activation energy increases as α increases meaning that the kinetics of decomposition are changing. This can be an indication that there is an additional parallel reaction occurring [16]. The results from TGA and DSC experiments conducted for samples without and with additive in modified acrylic resin allow one to consider the resin decomposition being responsible for the weight loss. The temperature range of decomposition and the DTG maximum height (i.e. peak mass loss rate) observed in TGA tests on resin with additive sample are similar to those found from tests on the resin only sample. Based on this comparison and assuming that the additive does not interfere with the polymerization process, the degradation reaction that allows the weight loss in this conversion region is modeled as the weight loss due to the modified acrylic resin degradation reaction only.

As conversion increases above 0.4, the activation energy increases with a higher slope than the slope found in the previous region. The change in the slope also suggests that the kinetics is changing in this region. Then the modified acrylic resin with additive sample stops losing its mass resulting in a residue of approximately 40 to 45%

of its initial weight. The TGA and DSC tests for the resin samples without and with additive in nitrogen and air environments suggest that the weight loss observed within this region is due to the resin char oxidation. The resin only sample loses about 15% or 25% of its initial weight in the temperature range found in this conversion region when tested in nitrogen (pyrolysis) or air (pyrolysis and oxidation), respectively. Hence, it can be assumed that for this temperature range, resin only sample is involved in a minimum of two reactions – a pyrolysis reaction resulting in a 15% weight loss, which is the later part of the major decomposition step for the resin only sample discussed in the previous stage and oxidation reaction resulting in 10% more. Applying the weight percentage of the resin within the resin with additive sample, 38.1%, the resin with additive sample should lose roughly 6% and 4% of its mass from pyrolysis and oxidation of the resin, respectively. Therefore, a total of 10% of resin with additive sample is due to the resin decomposition assuming that the thermal degradation behavior of the resin is similar whether the additive is mixed with the resin or not. The resin with additive sample loses about 15% or 20% of its initial weight in the same temperature range when tested in nitrogen (pyrolysis) and air (pyrolysis and oxidation), respectively. Considering that the difference of 5% weight loss between the nitrogen and air test results is comparable to the 4% weight loss due to resin oxidation discussed earlier, no additional oxidation reaction is presumed for this conversion region. The 15% weight loss observed in resin with additive sample tested in nitrogen (pyrolysis) indicate that in addition to the resin's pyrolysis reaction resulting in 6% weight loss, there is approximately 9% decrease in sample mass. This 9% of mass loss can be described by analyzing the TGA and DTG graphs shown in Figure 4. As shown here, the peak temperature for the major decomposition DTG peak of the resin with additive sample is slightly greater than that of the resin only sample which suggests that the 9% of mass loss is due to the major decomposition of the resin from the previous stage extending to this conversion range. Based on this analysis, a total of two reactions are modeled: pyrolysis (15% weight loss) and oxidation (4~5% weight loss) of the modified acrylic resin. Therefore, the full degradation of the resin with additive is:



Applying this degradation mechanism, a model fitting method [17] is used where a kinetic model, $f(\alpha)$ (or $g(\alpha)$ in integrated form) is preselected to fit the TGA experiment data to find the kinetic parameters with the best fitness. In this study, a model for a reaction order

COMPOSITES & POLYCON 2010

type kinetics, $f(\alpha) = (1 - \alpha)^n$ is used primarily, considering that this model is typically used for many solid thermal degradations, as well as other types of models available for various solid state reactions [18,19] (see Table 1). The weight loss with respect to each reaction is optimized based on the findings from conducting the iso-conversional method discussed above. The fitness of the model is compared by considering two factors: (1) the weight loss rate vs. temperature (DTG) shape and (2) the square of the Pearson product moment correlation coefficient, R^2 . Applying a reaction order type kinetic model to conduct model fitting method, the estimation results of the kinetic parameters are summarized in Table 2 and the fitness between the actual DTG and the kinetic modeling is shown in Figure 6.

Several findings are summarized as follows based on this model fitting exercise. First, the reaction order type kinetic model can be used to fit the DTG data with some degree of satisfaction for all reactions (see R1, R2 and R3). However, the estimated reaction order is high as 4.9 for R3 reaction. This indicates that the model is forced to fit the data knowing that the reaction order in this magnitude is rare to find in the literatures. Also, the DSC data confirms that the reaction order type model was inappropriate for R3 as well (see Figure 5). Although the model is giving high correlation coefficients between the data and modeling for R3 reaction, the DSC data show that R3 should exist from 200°C and end before 400°C where a strong endotherm is observed. When the data is fit with a reaction order type kinetic model, the additive decomposition temperature range extends beyond 400°C, ending near 600°C.

Second, the decomposition of the additive reaction is best described by a kinetic model that describes a diffusion controlled reaction (see Table 1, Jander's type model and Figure 6) among various other types of model investigated in this paper. The model type is reasonable considering that the model simulates the weight loss to be slow initially with respect to temperature increase and decays relatively fast after the weight loss rate peak. This modeling becomes suitable for an additive decomposing within a resin polymer system resulting in a time delay due to the time necessary to degrade the polymer near the additive. Consider the additive being mixed within the resin polymer. For the additive to undergo a decomposition reaction, the degradation of the resin polymer should occur simultaneously because the additive is aggregated within the resin. Having the additive decomposition temperature lower than that of the resin, the decomposition of the additive is delayed until the temperature is higher to allow the resin to decompose. When this model is actually applied, it provides good estimate of the slow weight loss at the initial stage near 200°C and the temperature range for the entire reaction. Additionally, when this model is used, the modeling results for weight loss rate after 300°C matches well with the actual

DTG data together with R1 reaction described with a reaction order type kinetic model.

Third, although kinetic modeling has been conducted to give best fitness between the modeling and the DTG data obtained over various heating rates (5 to 60°C/min) assuming that the kinetics are identical irrespective of heating rates, changes in the kinetic over 4 heating rates have been noticed. At lower heating rates, the portion of the sample weight consumed via R2 (char oxidation) increases where at higher heating rates it decreases. The ratio of weight loss due to R1 (resin pyrolysis) to R2 (char oxidation) is 25:13 for 5°C/min DTG data and 30:8 for that of 60°C/min. This can be explained by understanding that the char oxidation reaction is controlled by oxygen diffusion from the ambient to the condense phase. At a low heating rate, more time is available for oxygen diffusion with respect to temperature change allowing an increase in the weight loss due to oxidation (R2). However, when the heating rate is higher, the conditions become the opposite and pyrolysis reaction (R1) dominates. The fitness of the model to DTG data significantly increases when this effect is accounted for in the modeling (see Figure 6).

6.2. Property estimation for modified acrylic FRP composite

The property estimation for the modified acrylic composite is conducted by coupling a generalized pyrolysis model for slab experiments developed by Lautenberger and the Genetic Algorithms (GA) for optimization routine [2,3]. GA was developed based on the mechanics of the Darwinian survival-of-the-fittest theory. To ensure consistency between the conditions applied in the modeling and the Cone Calorimeter experiments when conducting the parameter estimation, the data from the modified acrylic composite test (external heat flux level of 50kW/m²) was truncated when normalized time, time divided by sample thickness square, i.e., $\tau = \text{time}/\delta^2$ became approximately 4 s/mm² to account for the one-dimensional assumption used in the model (see section 3.2).

Before conducting the optimization to estimate parameters required in the modeling, a global sensitivity analysis called Morris' method, also known as the Elementary Effect method [20], has been applied to the given problem to identify the input parameters which are sensitive to model outputs – mass loss rate and temperature measurement data. Morris' method is a simple OAT (one-at-a-time) sensitivity analysis that allows the model user to rank the factors from factors which have significant influence to model output to those that have negligible effect. When conducting the analysis, the user must first decide the analysis domain for each input parameter by determining the minimum and maximum values for each input based on the user's common sense.

Then following a randomly selected sequence, each input is changed with some equal percentage of the entire range, i.e. the difference between the maximum and minimum, until the entire set of input parameters has been changed once. Whenever an input is changed, the effect on the model output is determined by calculating the magnitude changes made in the output of interest such as the mass loss rate or the in-depth temperature at a certain time. Evaluating the elementary effects for an input is conducted multiple times using multiple random sequences of input parameters for a given set. At the end, the average and standard deviation of the effects are calculated to categorize the input factors into three groups – factors that have 1) negligible effect (low average and standard deviation); 2) additive effects (high average) or; 3) non-linear or interaction effects (high standard deviation) on the simulation output.

After identifying the necessary parameters for pyrolysis modeling with a model of choice and selecting the significance level, Morris' one-at-a-time (OAT) global sensitivity analysis is performed to identify the sensitive input parameters to model output of interest – surface temperatures at various times ($\tau = 1, 2, 3, 4$ s/mm² and ignition) and mass loss rate at ignition, mass loss rate peak, time to mass loss rate peak, and the peak mass loss rate. When conducting the analysis, the kinetic parameters were not included in this analysis, only the heats of reactions were. 4 difference randomized sequences were used ($p = \{0, 1/3, 2/3, 1\}$) with an increment of 2/3 ($\Delta = p/[2(p-1)]$) following the guide presented by Morris. Therefore, 4 cases are simulated for each parameter (total of 32 parameters) which results in 4 elementary effects. In Table 3, the domain of each variable is shown where KOZ is thermal conductivity, NKZ is temperature dependent term in the thermal conductivity, C0 is specific heat capacity, NC is temperature dependent term in the specific heat capacity, EMIS is emissivity, GAMMA is the fitting parameter to address the effective thermal conductivity that varies with T³ to account for radiation heat transfer through pores, and DHV is heat of reaction.

Examples of the results found from Morris' method are shown in Figure 7. The points in the figure stand for each input parameter tested in this sensitivity analysis. The points that are farther away from the origin in Figure 7, whether due to higher average or standard deviation, are the inputs that are sensitive to input changes where the sensitivity is determined based on changes observed in the model outputs of interest listed above. When conducting the optimization to estimate input parameter values using GA routine, an effort was given to determine the minimum number of inputs required in the optimization process to ensure a good match between the experiment data (mass loss rate and temperature measurements) and the model simulation. To determine the minimum number of input parameter set for good optimization, the

number of inputs involved in the optimization was increased, starting from the most sensitive to the insensitive, based on the sensitivity ranking found by Morris' method. According to this exercise, GA requires having at least 19 parameters out of 32 to optimize, which were the following: KOZ (thermal conductivity) of resin, char and glass; NKZ (temperature dependent term in the thermal conductivity) of resin, additive and glass; C0 (specific heat capacity) of resin, additive and glass; NC (temperature dependent term in the specific heat capacity) of additive and glass; EMIS (emissivity) of char, additive and glass; GAMMA (fitting parameter for modeling radiation heat transfer through pores) of char, additive and additive; and DHV (heat of reaction) of reactions R1 and R2. The estimated values are reported in Table 3. This exercise demonstrated that a powerful optimization tool such as GA still do require some degree of freedom during optimization by allowing at least 19 parameters to vary out of 32. Additionally, the optimization results improved significantly when most of the parameters related to fiberglass (thermal conductivity, temperature dependent term in the thermal conductivity, specific heat capacity, temperature dependent term in the specific heat capacity, and emissivity) were included in the optimization process, but based on the sensitivity ranking, allowing GA to optimize for these values. This can be an indication that glass properties used in the model are important in terms of providing good simulation for pyrolysis modeling this FRP composite. Another finding was in general, matching all three stages of the mass loss rate and temperature measurements at surfaces and in-depth – pre-ignition, ignition and post-ignition stage – was challenging without allowing the temperature dependent terms in the thermal conductivity, NKZ and specific heat capacity, NC to be involved in the optimization process, allowing GA to vary those values to find the optimum

Based on the GA parameter estimation, the optimal simulations of mass loss rate and temperatures at various locations are shown in Figure 8. This is for a Cone test of modified acrylic FRP composite conducted under 50kW/m^2 heat flux. As shown in the figure, the optimized parameter set allows the mass loss rate simulation to predict the actual behavior with satisfaction in general, knowing that the uncertainty of the mass loss rate data is 1.4 g/s-m^2 . The difference between the simulation and the experiment data becomes significant near the mass loss rate peak where the maximum difference is approximately 2 times the uncertainty. This is possibly due to the uncertainty associated with the microstructure used in the model. Comparing the model microstructure to that of the actual sample tested in the Cone, the simplified microstructure may have placed more resin near the surface where less is present in the actual sample. By doing so, more resin is decomposed

in the model near ignition time creating a greater mass loss rate peak than that found from the experiment.

The surface temperature profile simulation with the same optimal parameters has a good agreement with the experiment data considering the uncertainty of the data, which is 51°C . At later times ($\tau \rightarrow 4\text{ s/mm}^2$), the back face temperature simulation diverges from the actual test data used in the optimization process and the difference becomes about 60°C increase which is 18% more than the experimental uncertainty of 51°C . A possible explanation for this difference is that in the actual experiment, there are more heat losses to the sides as time progresses although insulation was applied to minimize this effect. When modeling, these heat losses are not captured allowing more heat energy to be conducted through the sample towards the back face and therefore resulting in higher back face temperatures at later times.

6.3. Evaluation for estimated properties

To evaluate the appropriateness of the property estimation, modeling of the same modified acrylic FRP composite tested at different heat flux levels – 25 and 75 kW/m^2 – are conducted. The parameter estimation using the FRP composite Cone test data at an external heat flux of 50 kW/m^2 is performed for the resin (i.e. a mixture of modified acrylic resin and flame retardant additive) and fiberglass in the previous section. In theory, if the parameter estimation was conducted properly, one should be able to model a composite that is tested under different heat flux levels using the estimation as an input to the pyrolysis model with degrees of satisfaction.

In Figure 9, simulation results of mass loss rate and temperature profiles at surface and back face for pyrolysis modeling of modified acrylic composite with inorganic additive irradiated at 25kW/m^2 is compared with the experiment data. The optimized parameter set provides good simulation results for modeling the mass loss rate. Note that the significant oscillations observed in the earlier times of the mass loss rate data is an artifact caused by the Cone igniter, an electrical sparker, touching the sample holder which had affected the load cell reading when inserting the sparker in place before starting the experiment. Additionally, there were numerous flash fires occurring in the test with the igniter in place before a “sustained” ignition of the sample was observed. These flash fires resulted in steady oscillations in the mass loss rate data with similar magnitude and frequency. When conducting the modeling, an additional heat flux from the flame of 20kW/m^2 was added after the sustained ignition time to model flaming condition, neglecting the flash fires observed in pre-ignition time. Considering these two factors, the simulated mass loss rate not being able to model the pre-ignition oscillations is adequate and therefore the mass loss rate simulation is in a good agreement with the actual experiment data.

The surface temperature profile simulation is modeled with satisfaction in the pre-ignition times. For the post-ignition times, the simulated surface temperature becomes significantly lower than the measurement considering the uncertainty of 51°C. The maximum difference is about 70°C, which is 37% greater than the uncertainty. A reasonable explanation for this difference can be given when considering the following: First, based on direct measurement of the flame heat flux to the sample surface and observation of the flame developing after ignition, it is known that nominally the flame requires several minutes to be fully developed for the FRP composite tested in this paper. Second, the surface temperature is sensitive to the flame heat flux and follows the trend of the flame heat flux because the flame and the sample surface are in direct contact. The surface temperature measurement showing an increase after ignition is due to the increasing flame heat flux. This is not resolved in the model where a constant heat flux of 20kW/m² is applied additionally after ignition; hence, while the simulated temperature remains relatively constant after ignition, the actual data shows an increase resulting in a difference greater than the uncertainty at later times ($\tau \rightarrow 10$ s/mm²). The back face temperature simulation is in a good agreement with the experiment data.

The simulation results of mass loss rate and temperature profiles at surface and back face for pyrolysis modeling of modified acrylic composite with inorganic additive irradiated at 75kW/m² is compared with the experiment data in Figure 10. The mass loss rate simulation using the optimized parameter set based on 50kW/m² test provided poor agreement (see baseline case in Figure 10). However, it was found that improvements can be made to the mass loss rate simulations based on numerical experiments which were conducted with different microstructures where a slight variation was given for the layers near the surface by removing the resin with additive layers for a better representation of the actual microstructure of the sample tested (see Modeling 1 and 2 cases in Figure 10). This approach was reasonable because the composites tested under 75 kW/m² heat flux level had a sample thickness of 7.7 mm while the sample used for optimization had a thickness of 8.5 mm. Note that because the samples were fabricated via hand layup method, variations in the order of a millimeter may be typical.

The surface temperature simulation is significantly different from the experimental data. Improvements were made to simulated surface temperature profiles when more fiberglass and less resin with additive layers were present. This is because GA optimized conductivity of the fiberglass layer is much smaller than other solid phase species' conductivities resulting in a steep temperature gradient near the surface as the glass concentration increases. Considering this steep temperature

gradient with the positional uncertainty of the surface thermocouple bead location, a maximum difference between modeling and experiment less than 150°C can be reasonable. The back face temperature simulation resulted in a similar trend observed for modeling 50 kW/m² test case as discussed in the previous section. As τ reaches 4 s/mm², the back face temperature simulation diverges from the experiment data used for comparison. The difference becomes about 70°C increase which is 37% more than the temperature measurement uncertainty of 51°C. A possible reasoning for this difference can be found by considering the model not being able to capture heat losses to the sides because the model uses one-dimensional setup and therefore resulting in more energy being transferred via conduction to the back face of the sample.

7. Conclusions

A property estimation exercise for pyrolysis modeling is conducted on modified acrylic with inorganic high-charring additive FRP composites. To properly model the pyrolysis of the composite, kinetic modeling of the resin degradation, without and with additive, was performed using TGA and DSC experiment data on the resin. Using an iso-conversional method (also known as model-free method), the minimum number of elementary reactions required to describe the full degradation mechanism was proposed – three step mechanism. With a pre-known reaction mechanism, a model fitting method was used to find the kinetic parameters for each reactions.

By conducting the kinetic modeling exercise, the following observations were made: First, although the reaction order type kinetic model can be used to fit the three reactions of DTG with some degree of satisfaction, evidence (high reaction order value and the temperature range where a strong endotherm is observed in the DSC data) exists that the additive degradation reaction was forced to fit this kinetic model. Second, the decomposition of the additive reaction is best described by a kinetic model that describes a diffusion controlled reaction (see Table 1, Jander's type model and Figure 6). Third, changes in the kinetic over 4 heating rates have been noticed where at lower heating rates, the portion of the sample weight consumed via R2 (char oxidation) increases and at higher heating rates it decreases.

The property estimation for the modified acrylic composite is conducted by coupling a generalized pyrolysis model for slab experiments and the Genetic Algorithms (GA) for optimization routine [2,3]. The data used for parameter optimization was from a Cone experiment irradiated at 50kW/m². Before conducting the optimization to estimate parameters required in the modeling, a global sensitivity analysis called Morris' method [20], was applied to identify input parameters which are sensitive to the model outputs of interest – mass loss rate

and temperature measurement data. To determine the minimum number of input parameter set for good optimization, inputs that were identified as sensitive based on the Morris' method were allowed to vary to find an optimum value while the rest set as a constant. From this exercise it was understood that a powerful optimization tool such as GA still do require a degree of freedom during its optimization by allowing at least 19 parameters to vary out of 32. Additionally, the optimization results improved significantly when most of the parameters related to fiberglass are included in the optimization process possibly indicating that the glass properties used in the model are important in terms of providing good simulation for pyrolysis modeling the FRP composite with modified acrylic resin with additive. Another finding was that matching all three stages of the mass loss rate and temperature measurements at surfaces and in-depth – pre-ignition, ignition and post-ignition stage – was challenging without allowing the temperature dependent terms (NKZ and NC) in the thermal conductivity and specific heat capacity vary during optimization process allowing GA to find the optimal values for those parameters. When using the optimized parameter set found via GA optimization, the modeling of mass loss rate and temperature profiles at surface and back face locations were generally in a good agreement with the experiment data considering the uncertainties associated with the data.

The estimated optimized parameter set was used to model Cone tests of the FRP composite with modified acrylic resin with additive conducted under 25 and 75 kW/m² heat fluxes. In general, the simulated mass loss rate and temperature profiles at surface and back face in a good agreement for 25 kW/m² test case but not for 75 kW/m² test case. By conducting additional numerical experiments, it was concluded that the microstructure used in the simulation had a significant impact over determining the quality of the modeling and therefore estimating a good representation of the microstructure of the sample should be accepted as an important task when conducting the parameter estimation for pyrolysis modeling.

In this study, the work demonstrates the possibility of constructing a virtual experiment for composites using a bench-scale pyrolysis test and thermal analysis experiment data. Kinetic modeling of modified acrylic with a fire retardant additive was conducted separately to estimate kinetic parameters. Using a composite tested at one heat flux level (50 kW/m²) and applying the kinetic modeling results for the decomposing resin with additive, an optimization of parameters was conducted and those estimations were used to model the same composite irradiated at different heat flux levels (25 and 75 kW/m²). The parameter estimation and modeling were in a good agreement with the experiment data relatively. However, it was understood that without a good

representation of the microstructure, the simulation quality can become significantly poor. Therefore, the importance of the sample microstructure used in the modeling was recognized.

8. Acknowledgments

The authors greatly appreciate the support for this work from DOC NIST Award Number 60NANB8D8106 (Federal Program Officer Dr. Kevin McGrattan). Special thanks goes to co-author Charles Dore for fabricating and donating the modified acrylic FRP composite materials used in this study. Many thanks also to Randall Harris at WPI for conducting the Cone Calorimeter tests.

9. Reference

-
- ¹ Standard Test Method for Heat and Visible Smoke Release Rates for Materials and Products Using an Oxygen Consumption Calorimeter, ASTM E 1354-09, ASTM, 100 Barr Harbor Drive, West Conshohocken, PA, U.S.
 - ² Lautenberger, C., "A Generalized Pyrolysis Model for Combustible Solids", Ph.D. Dissertation, Department of Mechanical Engineering, University of California, Berkeley, Fall 2007
 - ³ Lautenberger, C., Gpyro – A Generalized Pyrolysis Model for Combustible Solids Users' Guide, Version 0.609, July 23, 2008
 - ⁴ Handbook of polymer blends and composites By Anand K. Kulshreshtha, Cornelia Vasile
 - ⁵ Lewin, M., Synergism and Catalysis in Flame Retardancy of Polymers, *Polym. Adv. Technol.* 12, 215-222 (2001)
 - ⁶ LeVan, S.L., The Chemistry of Solid Wood; Chapter 14. Chemistry of Fire Retardancy, American Chemical Society, 1984
 - ⁷ Standard Test Method for Surface Burning Characteristics of Building Materials, ASTM E 84-05, ASTM, 100 Barr Harbor Drive, West Conshohocken, PA, U.S.
 - ⁸ de Ris, J.L. and Khan, M.M., "A sample holder for determining material properties," *Fire and Materials*, 24, 219-226 (2000).
 - ⁹ Kim, E., Lautenberger, C., and Dembsey, N., Property Estimation for Pyrolysis Modeling Applied to Polyester FRP Composites with Different Glass Contents, COMPOSITES & POLYCON 2009, American Composites Manufacturers Association (ACMA), January 15-17, 2009, Tampa, FL USA
 - ¹⁰ Lei Zhao, Bench Scale Apparatus Measurement Uncertainty and Uncertainty Effects on Measurement of Fire Characteristics of Material Systems, MS Thesis, Fire Protection Engineering, WPI, 2005-04-27, ETD-050105-182456
 - ¹¹ Standard Methods of Test for Measurement of Synthetic Polymer Material Flammability Using a Fire Propagation Apparatus (FPA), ASTM E 2058-03, ASTM, 100 Barr Harbor Drive, West Conshohocken, PA, U.S.
 - ¹² Ozawa, T., *Bull Chem Soc Jpn* 1965;38;188
 - ¹³ Flynn, J., Wall, L.A., *J Polym Lett* 1966;4:232
 - ¹⁴ Friedmen, H.L., *J Polym Sci Part C* 1964;6:183
 - ¹⁵ Friedmen, H.L., *J Polym Lett* 1966;4:232
 - ¹⁶ S.V. Vyazovkin and A.I. Lesnikovich, *Thermochim. Acta*, 165 (1990) 273
 - ¹⁷ Burnham, A.K., Weese, R.K., Kinetics of thermal degradation of explosive binders Viton A, Estane, and Kel-F, *Thermochimica Acta* 426 (2005) 85-92

¹⁸ Bras, M.L., Rose, N. and Bourbigot, S., The Degradation Front Model – A tool for the Chemical Study of the Degradation of Epoxy Resins in Fire, *Journal of Fire Sciences*, Vol. 14 – May/June (1996)

¹⁹ Liu, J., He, D., Xu, L., Yang, H. and Wang, Q., Study of the Kinetics of the Combustion Reaction on Shuangya Mountain

Figures:

Coal Dust by TG, *Journal of Thermal Analysis and Calorimetry*, Vol. 58 (1999) 447-453

²⁰ Morris, M.D., 1991. Factorial sampling plans for preliminary computational experiments. *Technometrics* 33, p.161-174.



Figure 1: Approximation of three distinct layers – 100 wt% resin (yellow), 50-50 wt% resin and glass (red), and 100 wt% glass – in composite microstructure: Modified acrylic FRP with inorganic high-charring flame retardant additive

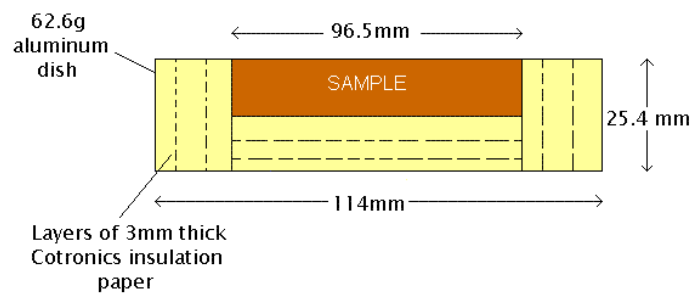


Figure 2: Insulated Sample Holder Designed by de Ris and Khan [8]

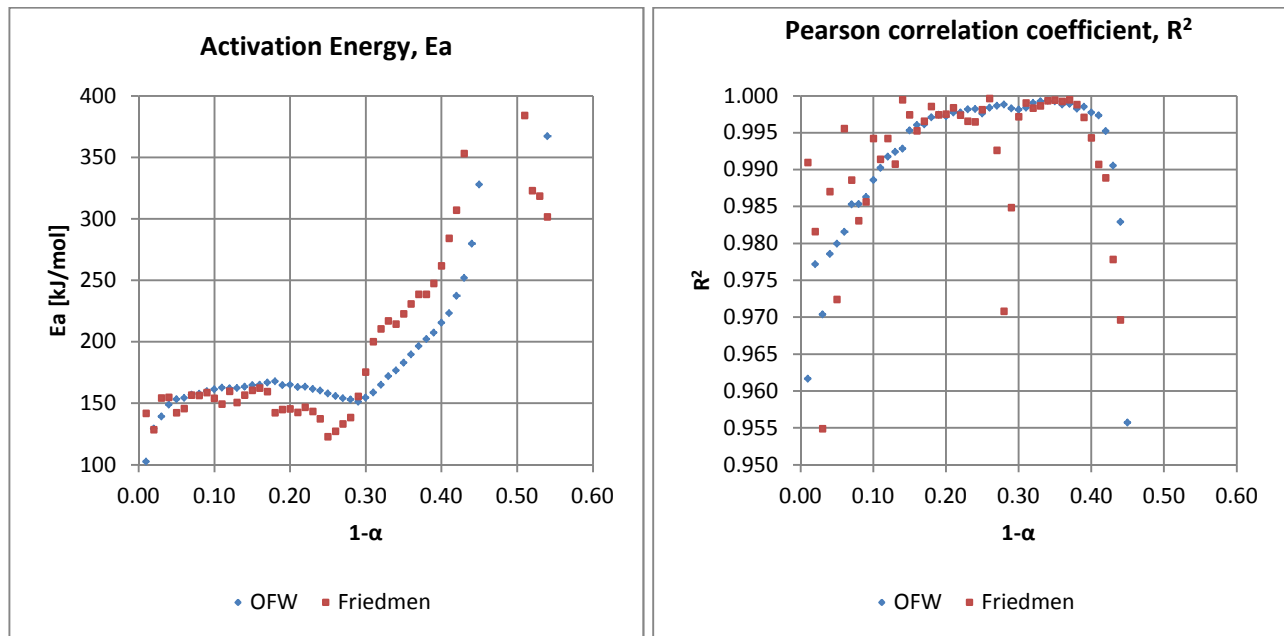


Figure 3: Estimated activation energy (left) and R^2 values for the estimation (right) of modified acrylic resin with an inorganic high charring additive calculated via “iso-conversional” (model free) method

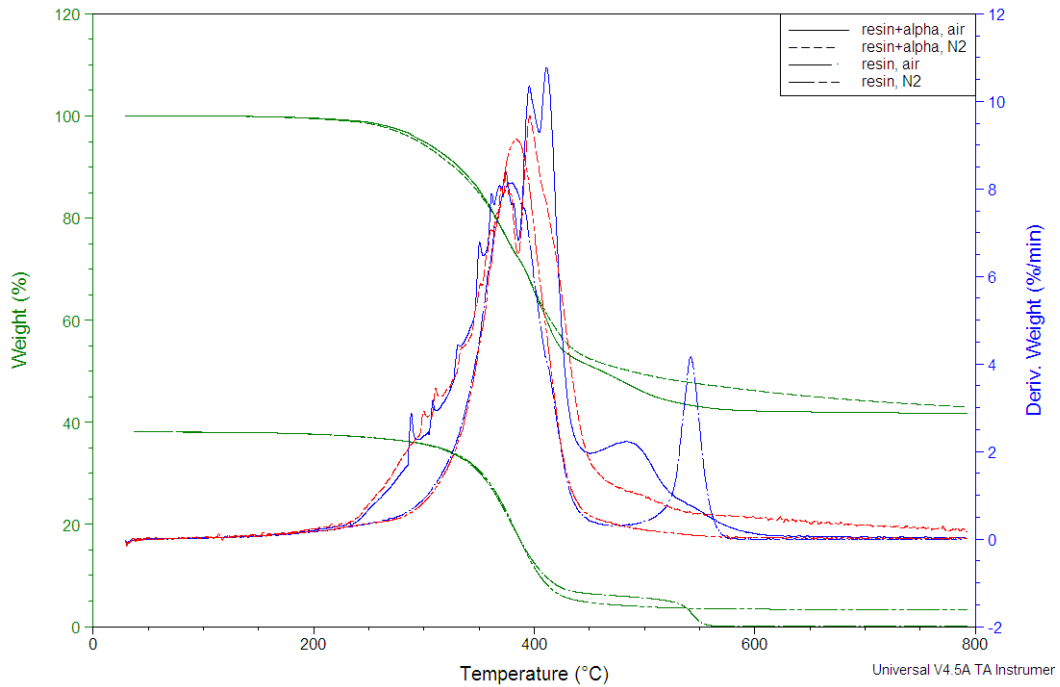


Figure 4. TGA Non-isothermal experiment results with a constant heating rate of 20°C/min for temperatures ranging from ambient to 800°C: TGA and DTG of resin without and with additive tested in air (oxidative) and nitrogen (inert) environments. Note that the results from testing resin only sample is scaled down to a maximum of 38.1% from 100% which is the weight percentage mixed within the resin with additive sample.

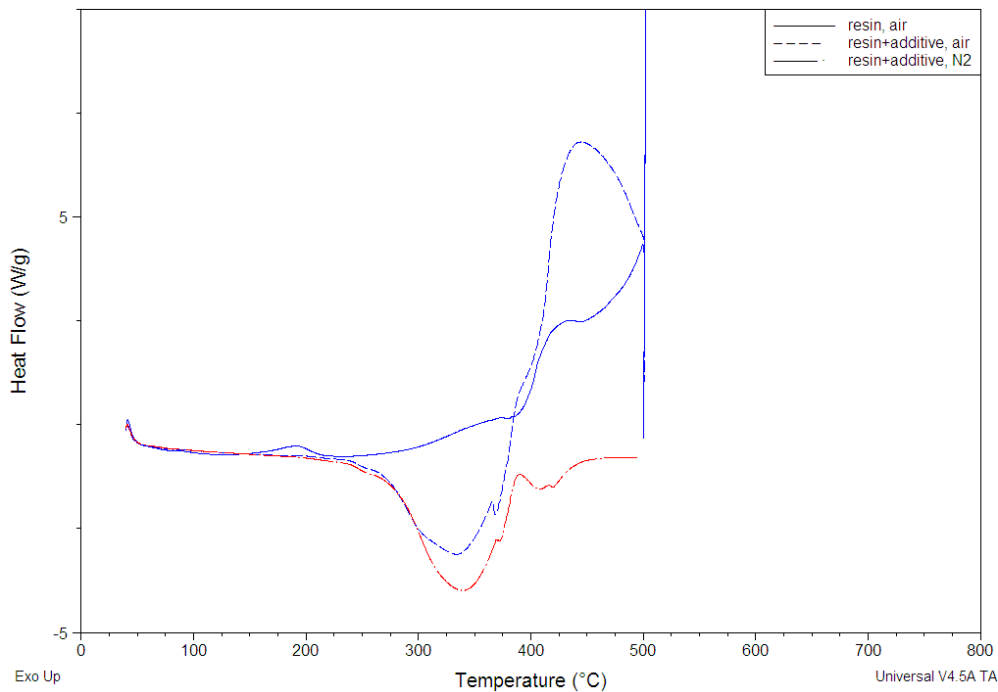


Figure 5. DSC Non-isothermal experiment results with a constant heating rate of 20°C/min for temperatures ranging from ambient to 500°C: Heat flow results of resin without and with additive tested in air (oxidative) and nitrogen (inert) environments. Note that baseline correction has not been applied to the results shown above.

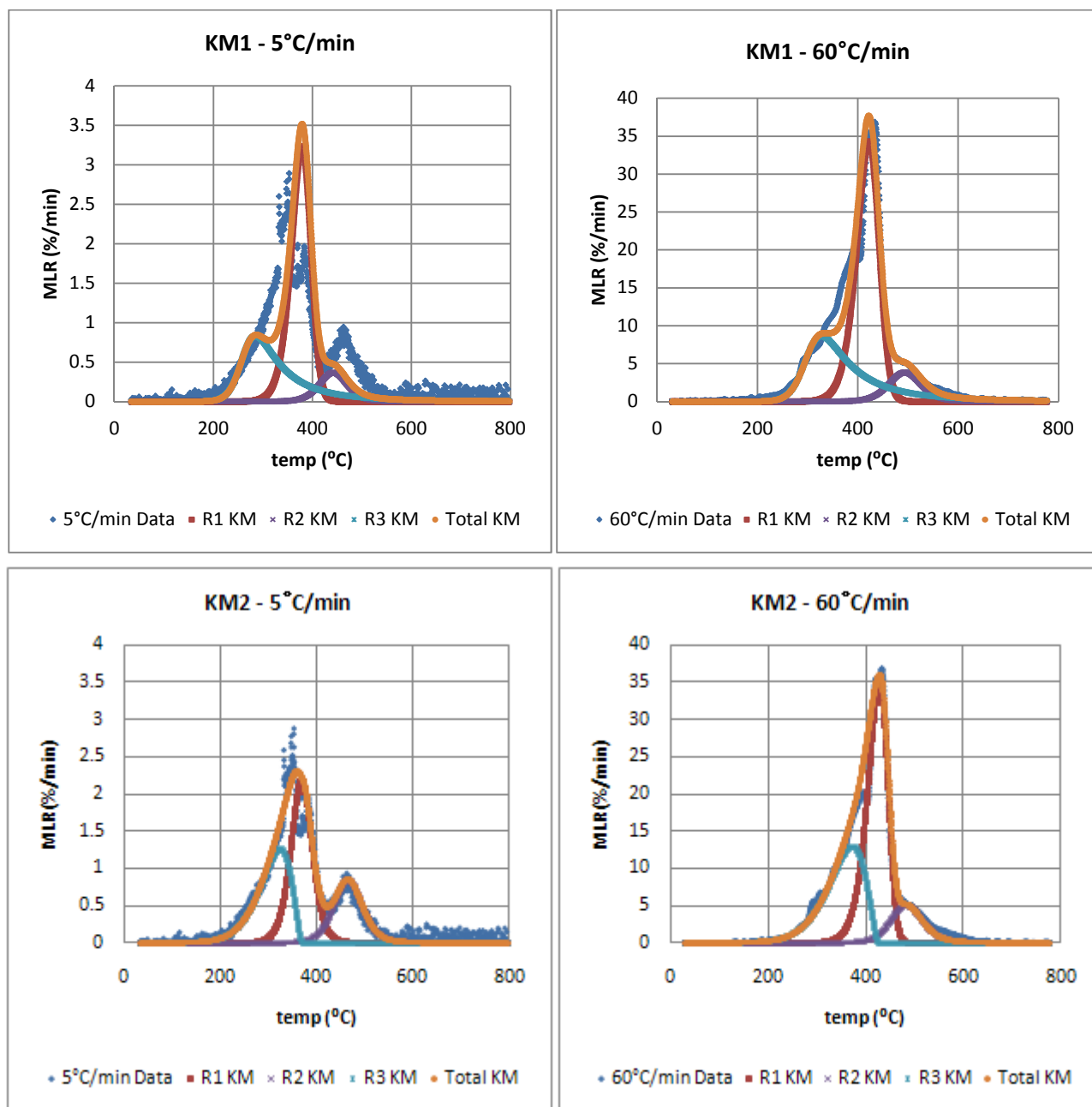


Figure 6. Kinetic modeling conducted for modified acrylic resin with inorganic additive: Kinetic Model 1 (KM1) – 3 step mechanism with nth order kinetic model; Kinetic Model 2 (KM2) – 3 step mechanism with 2 nth order kinetic model for R1 and R2, and diffusion controlled model for R3. For KM2 cases, the kinetic parameters and mass fractions for R1 and R2 have been adjusted differently for each heating rate case to give best-fit between the TGA experiment data and kinetic modeling results.

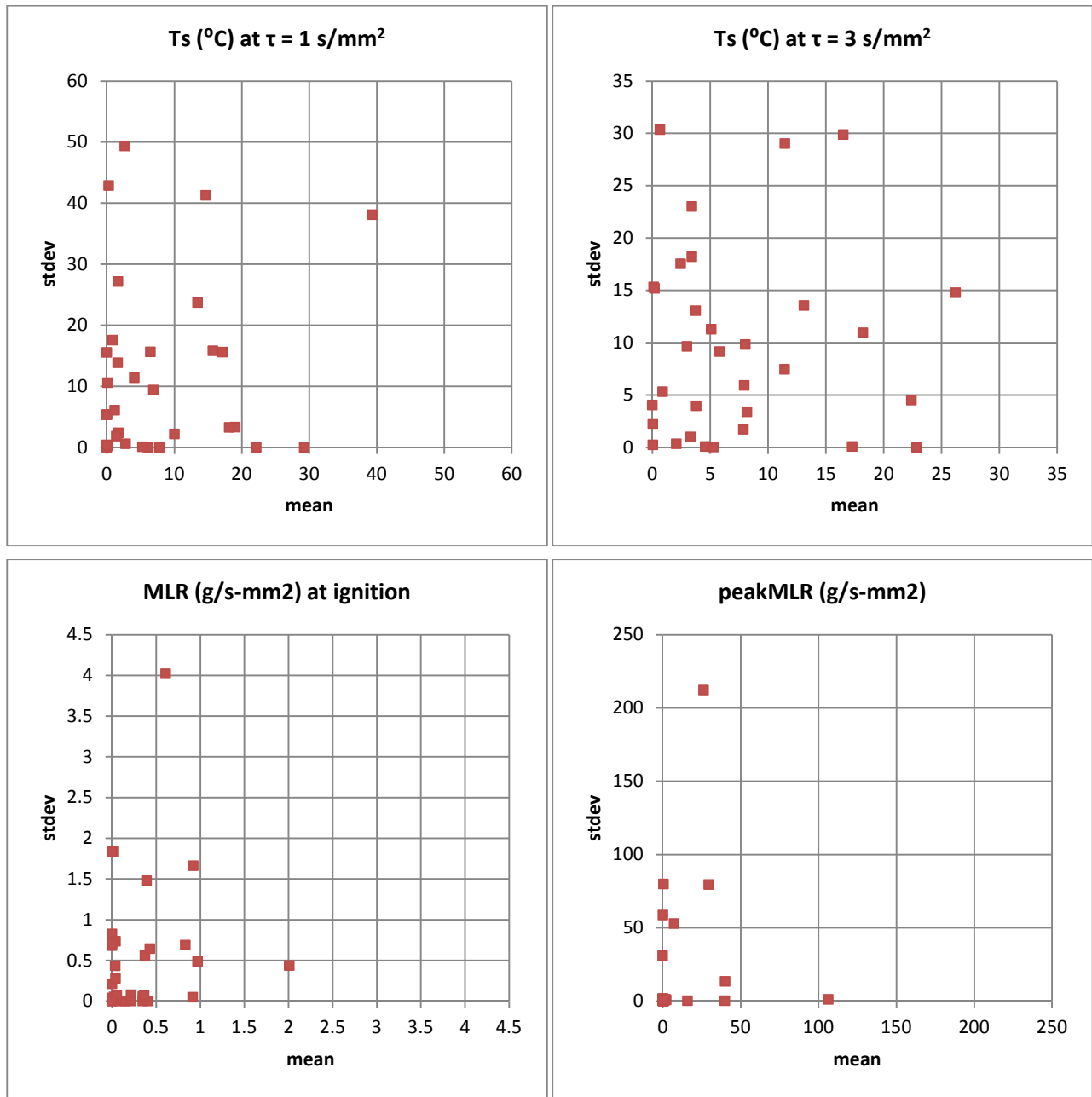


Figure 7. Morris sensitivity analysis applied to modeling of fiber reinforced polymer (FRP) composite: results are analyzed in terms of surface temperature at $\tau = 1$ and 3 s/mm² (top left and right) and mass loss rate at ignition and the peak mass loss rate (lower left and right).

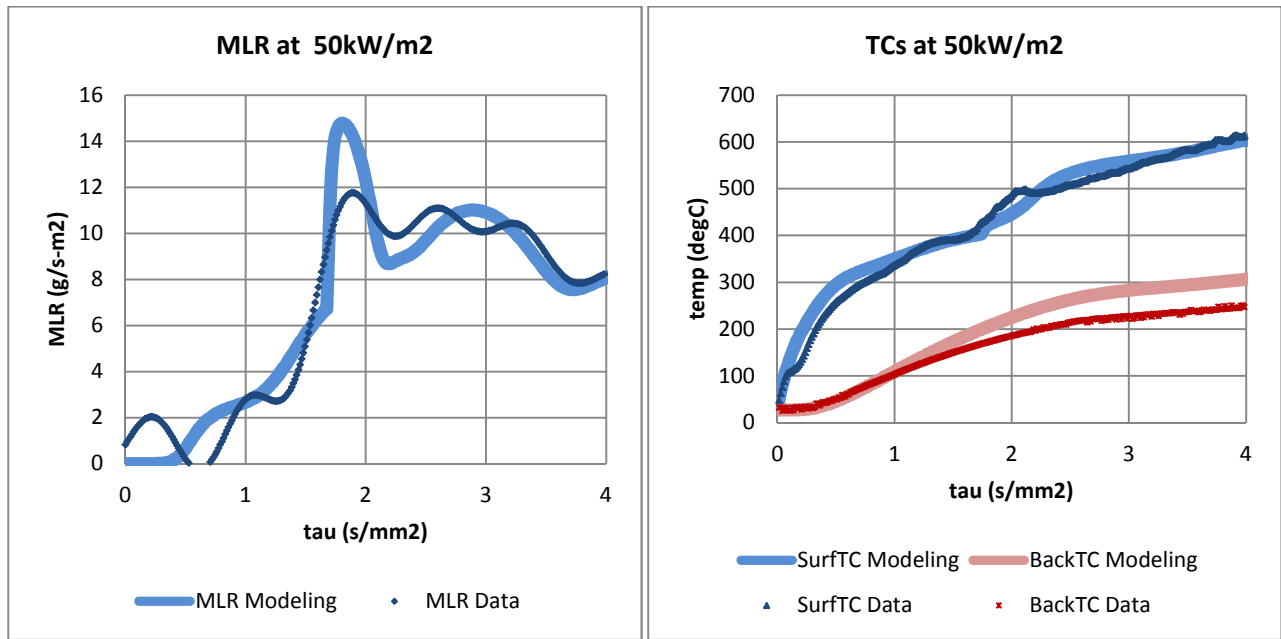


Figure 8. Parameter estimation results via GA optimization for modified acrylic composite with inorganic additive irradiated at a heat flux level of 50kW/m^2 – Comparison of experimental data and simulation are given for mass loss rate (left) and temperature profiles at sample surface and back face (right). The thick lines are used to show modeling results and the points for experiment data.

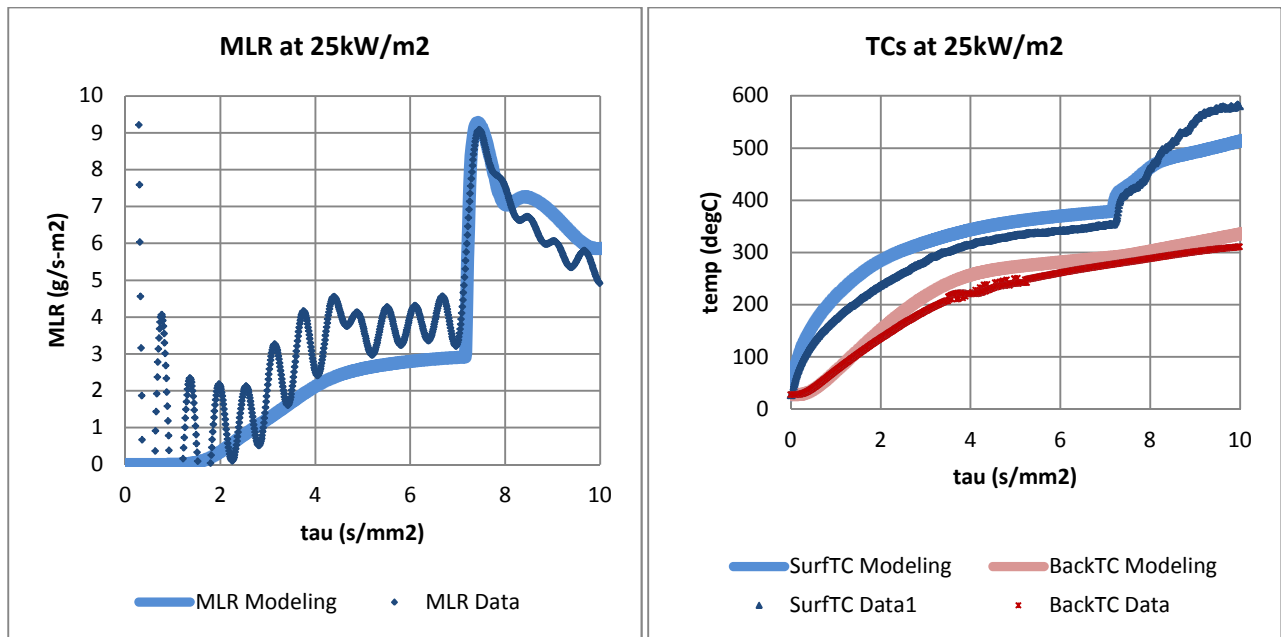


Figure 9. Pyrolysis modeling results of modified acrylic composite with inorganic additive irradiated at a heat flux level of 25kW/m^2 using parameters estimated via GA optimization using experiment data conducted at 50kW/m^2 – Comparison of experimental data and simulation are given for mass loss rate (left) and temperature profiles at sample surface and back face (right). The thick lines are used to show modeling results and the points for experiment data. For simplification in the modeling, additional heat flux due to the flame was applied after ignition. However, numerous flash fires had existed before a “sustained” ignition, which explains significant oscillations observed in the earlier time in the mass loss rate data.

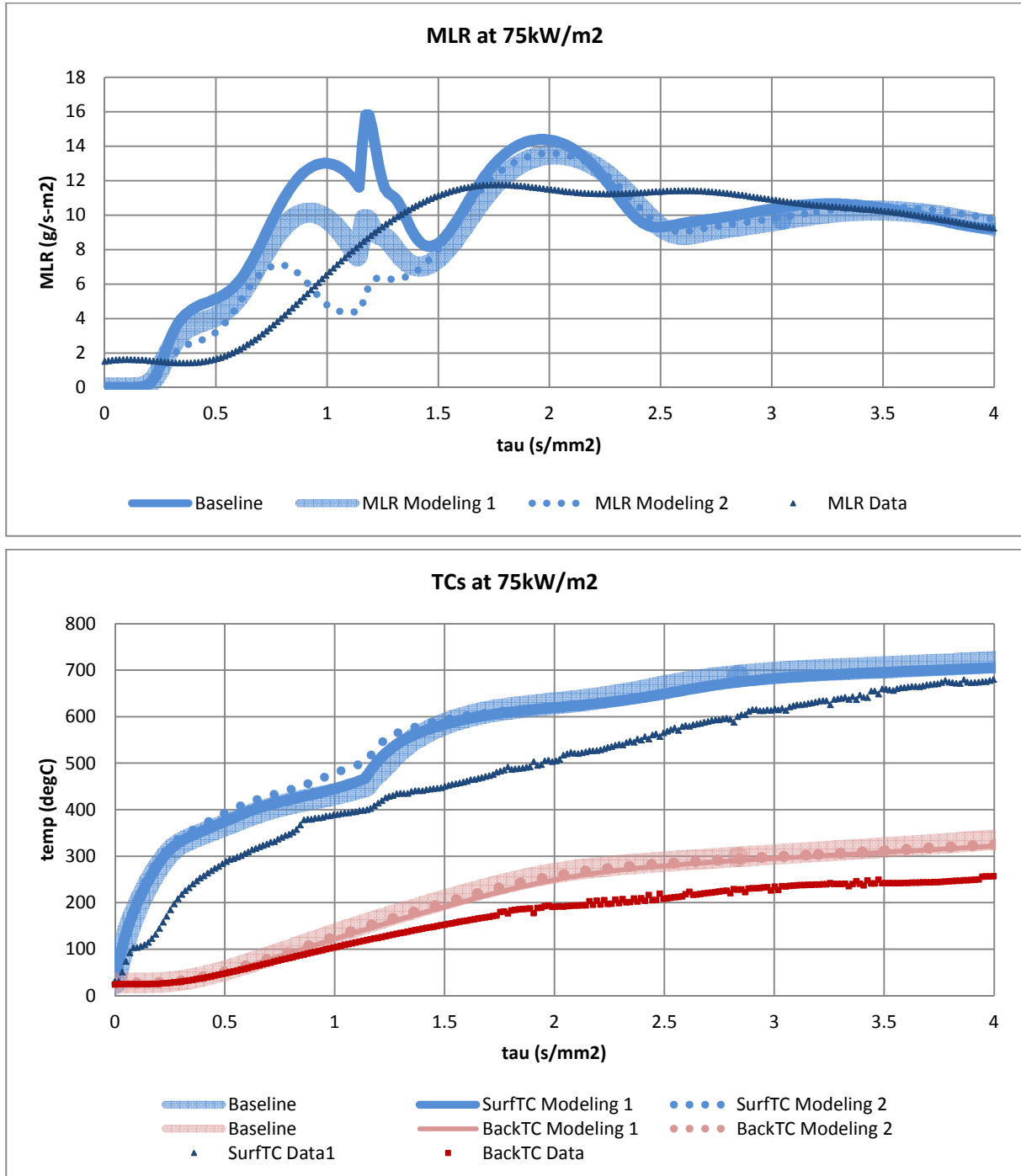


Figure 10. Pyrolysis modeling results of modified acrylic composite with inorganic additive irradiated at a heat flux level of 75kW/m² using parameters estimated via GA optimization using experiment data conducted at 50kW/m² – Comparison of experimental data and simulation are given for mass loss rate (top) and temperature profiles at sample surface and back face (bottom). The thick lines are used to show modeling results and the points for experiment data. There are three cases for modeling – baseline, modeling 1 and 2 – because a numerical experiment was conducted to show that removal of some resin layers near the surface in the microstructure can significantly improve mass loss rate simulations. However, the changes made in the microstructure have insignificant effect on the temperature simulations.

Tables:

Table 1. Kinetic Degradation Functions

Solid State Kinetics	$f(\alpha)$	$g(\alpha)$	
Nucleation and nucleus growing	$\frac{1}{n}(1-\alpha)(-\ln(1-\alpha))^{1-n}$	$(-\ln(1-\alpha))^n$	$n = \frac{1}{4}, \frac{1}{3}, \frac{1}{2}, \frac{2}{3}$ or 1
Phase Boundary Reaction	$(1-\alpha)^n$	$\frac{1-(1-\alpha)}{2\left[1-(1-\alpha)^{1/2}\right]}$ $\frac{1-(1-\alpha)}{3\left[1-(1-\alpha)^{1/3}\right]}$	plane symmetry cylindrical symmetry spherical symmetry
Diffusion	$\frac{1}{2}\alpha^{-1}(-\ln(1-\alpha))^{-1}$ $\frac{3}{2}\left[(1-\alpha)^{-1/3}-1\right]^{-1}$ $\frac{3}{2}(1-\alpha)^{2/3}\left[(1-\alpha)^{1/3}-1\right]^{-1}$	$\frac{\alpha^2}{(1-\alpha)\ln(1-\alpha)+\alpha}$ $1-\frac{2}{3}\alpha-(1-\alpha)^{2/3}$ $\left[(1-\alpha)^{1/3}-1\right]^2$	plane symmetry cylindrical symmetry spherical symmetry Jander's type
Potential Law	$\frac{1}{n}\alpha^{1-n}$	$\alpha^n(0 < n < 2)$	$n = \frac{1}{4}, \frac{1}{3}, \frac{1}{2}$ or $\frac{3}{2}$
Reaction Order	$\frac{1}{n}(1-\alpha)^{1-n}$	$1-(1-\alpha)^{1/2}$ $1-(1-\alpha)^{1/3}$	$n = \frac{1}{2}$ or $\frac{1}{3}$

Table 2: Kinetic parameters estimated from model fitting exercise using Genetic Algorithm (GA): Three steps nth order kinetic model

Reaction	Z (s-1)	E _a (kJ/mol)	n (-)	n ₀ (-)
R1	1.80E+14	207	1.30	
R2	7.20E+12	207	1.80	1.0
R3	2.80E+11	152	4.90	

Table 3: List of parameters necessary for simulating the FRP composite with their region of experimentation for Morris' OAT sensitivity analysis bounded by the minimum and maximum of each parameter explored and their Genetic Algorithm (GA) optimized values. There are 5 solid phase species and each have 4 levels selected by the user and Δ set as $p/[2(p-1)] = 2/3$. The parameter values found via GA optimization are noted in blue and the ones kept as constants are in black.

No	Var	Species & HoRs	SA Min	SA Max	Δ	GA Optimized
1	KOZ	resin	0.05	0.35	0.20	0.27
2	NKZ		0.00	1.00	0.67	0.65
3	CO		500.00	2500.00	1333.33	695
4	NC		0.00	1.00	0.67	0.00
5	EMIS		0.60	1.00	0.27	0.80
6	KOZ	char	0.05	0.35	0.20	0.30
7	NKZ		0.00	1.00	0.67	0.00
8	CO		500.00	2500.00	1333.33	1500
9	NC		0.00	1.00	0.67	0.0
10	EMIS		0.60	1.00	0.27	0.87
11	GAMMA		0.0001	0.0100	0.01	0.060
12	KOZ	additive	10.00	70.00	40.00	40.00
13	NKZ		0.00	1.00	0.67	-0.48
14	CO		500.00	2500.00	1333.33	846
15	NC		0.00	1.00	0.67	0.00
16	EMIS		0.60	1.00	0.27	0.80
17	GAMMA		0.0001	0.0100	0.01	0.057
18	KOZ	additive'	1.00	61.00	40.00	31.00
19	NKZ		0.00	1.00	0.67	0.00
20	CO		500.00	2500.00	1333.33	1500
21	NC		0.00	1.00	0.67	-0.047
22	EMIS		0.60	1.00	0.27	0.799
23	GAMMA		0.0001	0.0100	0.01	0.047
24	KOZ	glass	0.10	1.00	0.60	0.09
25	NKZ		0.00	1.00	0.67	-0.41
26	CO		500.00	2500.00	1333.33	920
27	NC		0.00	1.00	0.67	-0.27
28	EMIS		0.60	1.00	0.27	0.75
29	GAMMA		0.0001	0.0100	0.01	0.001
30	DHV	HoR1	100000	10000000	6600000	1.38×10^6
31	DHV	HoR2	-10000000	-100000	6600000	3.67×10^5
32	DHV	HoR1	3078900	3763100	456133	3.42×10^6

Appendix G

Parameter Estimation for Pyrolysis Modeling Applied to Polyester FRP Composites with Different Glass Contents

Fire and Materials 2009, 11th International Conference

PROPERTY ESTIMATION FOR PYROLYSIS MODELING APPLIED TO POLYESTER FRP COMPOSITES WITH DIFFERENT GLASS CONTENTS

Esther Kim¹
Chris Lautenberger²
Nicholas Dembsey¹

¹ Worcester Polytechnic Institute
Department of Fire Protection Engineering
100 Institute Road
Worcester, MA 01609

²University of California, Berkeley
Department of Mechanical Engineering
Berkeley, CA 94720

ABSTRACT

For the composites industry to “design for fire” more thorough understanding of how typical FRPs decompose under fire conditions is needed. The role played by the glass and the resin (and additives) for FRPs are keys to understanding the fire behavior. The goal of this work is to evaluate the ability of a pyrolysis model and genetic algorithm (optimization routine) pairing to estimate properties of each component of the composite, resin and glass. The composite pyrolysis experimental data used in this work was obtained from tests conducted on a bench scale fire test apparatus, Fire Propagation Apparatus, with additional instrumentation to measure surface and internal temperatures of the sample. Mass loss data and temperature profiles with respect to time at different in-depth locations are used in the optimization process. The property estimation exercise is conducted on a brominated, unsaturated polyester FRP composite with low glass content. Thermal analysis data from thermogravimetric analysis and differential scanning calorimetry of the polyester resin in the composite was used to model the decomposition kinetics. With the approximated decomposition kinetics for the resin, simulation of pyrolysis tests (nitrogen environment) of the composite slab was performed to estimate the unknown thermophysical properties by genetic algorithm optimization. A validation exercise using the estimated properties is then conducted on a composite with high glass content. The quality of the estimated properties is assessed by comparing simulated results to experimental results for the high glass content sample.

1. INTRODUCTION

For the composites industry, designing for a FRP that provides good fire characteristics becomes a guess and check operation in many cases. Any changes made to the resin, glass, or the microstructure of the FRP affect the overall fire behavior of the FRP. Traditionally, the effect of the changes made in the FRP is checked by conducting tests via standard fire tests, which can be time consuming and expensive. Therefore, providing an understanding of how typical FRPs decompose under fire conditions and using

this information to find an appropriate guideline for the composite industry to produce better fire-safe composites have been a long-term goal for this research.

In this study, complete data sets of decomposition of brominated, unsaturated polyester resin and its FRP composites with different glass contents are presented. Careful experiments were conducted using Thermogravimetric Analysis (TGA) and Differential Scanning Calorimetry (DSC) in order to study the thermal decomposition kinetics of the polyester resin. Also, the polyester FRPs with different glass contents – 33 wt% (1A) and 60 wt% (1C) – were tested under a modern bench-scale fire test apparatus known as Fire Propagation Apparatus (FPA, ASTM E 2058[1]) with additional instrumentation such as thermocouples at various depths. These tests were designed to generate data specifically useful for computer modeling purposes.

The model used in this study is a generalized pyrolysis model developed by Lautenberger [2,3], which simulates the heating and decomposition of a chosen material. Like with any other pyrolysis models, this model requires many input parameters found from material properties, which include the pyrolysis kinetics (pre-exponential factor, activation energy, reaction order), thermal properties (specific heat capacity, thermal conductivity), and radiative characteristics (surface emissivity, in-depth radiation absorption coefficient). Unfortunately, there are no standardized techniques to determine all of these properties via laboratory tests. Another way of estimating parameters is to use an optimization routine with a pyrolysis model in pair.

The current work applies Genetic Algorithm as an optimizing method coupled with Lautenberger's pyrolysis model [2,3] to perform parameter estimation. Using the experimental data of the polyester FRP with lower glass content (1A), an estimation exercise is conducted to find properties of the individual components of the composite, i.e., resin and glass, where one is decomposable while the other is inert, respectively. The estimated parameters for these components are used to model the pyrolysis of the same polyester FRP but with higher glass content (1C). The simulated 1C mass loss rate (MLR) and temperatures (TC) will be compared to those of actual experiments to evaluate the appropriateness of the estimation. Additionally, the estimated properties will be compared to those found from the literature [4,5] to check how consistent the estimations are.

2. PYROLYSIS OF FRP COMPOSITE

2.1. FRP composite description

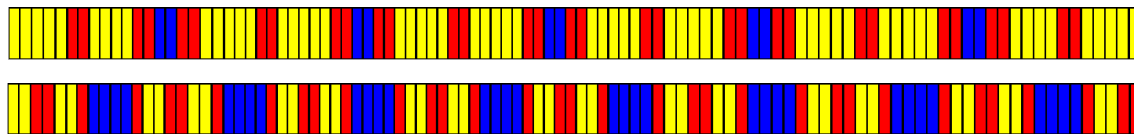
The resin in this study is a commercially prepared unsaturated polyester resin with 20 wt% bromination for its fire retardancy built in to the carbon backbone. Antimony trioxide is added, which acts as a synergist that assists the flame retardancy of the polymer resin. Among the various effects of adding antimony trioxide, the major role of this additive is reacting with the halogen such as bromine and removing the radicals that are essential for combustion chemical reactions to proceed. This additive is also known to delay the escape of halogen from the flame, which increases its concentration and diluting effect [6]. The resin was catalyzed with methyl ethyl ketone peroxide (MEKP). According to the product description, this resin is a low viscosity, thixotropic polyester resin formulated to be Class I per ASTM E 84 [7] (flame spread index < 25 and smoke developed < 450).

Composite panels were fabricated by hand lay-up and vacuum bagging for low (33 wt% of glass, average thickness of 10 mm) and high (60 wt% of glass, average thickness of 6 ~7 mm) glass content composites, respectively, using two different types of fiberglass mats that were wetted with resin. The two types of fiberglass (E-glass) used in the composite are a chopped strand mat and a glass roving woven mat with an area density of 25 g/m² and 880 g/m², respectively. The chopped strand mat is thinner and more porous than the woven mat. The laminate schedule (provided by the manufacturer) is chopped strand mat and roving alternating five times for 1A and eight times for 1C with another chopped strand mat layer at the

end. Visual inspection of a polished cross-section of the composite slab is consistent with this laminate schedule, but with polymer resin layers between each fiberglass layer. The chopped strand mat layer is difficult to identify in the cross section, perhaps because more resin is soaked into this layer than the roving layer. The roving layer is observed as a prominent glass layer possibly because the resin is absorbed only at the fiberglass layer surfaces leaving the interior with primarily glass.

The layered microstructure is determined to a resolution of 0.10 mm and 0.06 ~ 0.07 mm for 1A and 1C, respectively by inspecting a polished cross-section of the composite under a microscope. Based on visual observation and comparison to global density of the composite sample, approximations of three distinct layers are proposed: 100% resin, 100% glass, and 50% resin/50% glass. The microstructure is shown schematically in Figure 1. The lightest “box” represents 100% resin, the medium darkness box represents 50% resin/50% glass, and the darkest box represents 100% glass. Each box has a thickness of 1% of each sample’s average thickness.

Figure 1: Approximation of three distinct layers – 100 wt% resin (yellow), 50-50 wt% resin and glass (red), and 100 wt% glass – in composite microstructure: Unsaturated polyester FRP with low glass content (1A, 33 wt% of glass, top) and with high glass content (1C, 60 wt% of glass, bottom)



2.2. Thermogravimetric Analysis (TGA) and Differential Scanning Calorimetry (DSC)

The instruments used in this study were manufactured from PerkinElmer: Thermogravimetric Analysis 7 (TGA7) and the Differential Scanning Calorimetry 7 (DSC7). Throughout this study, TGA and DSC were used for a non-isothermal test purposes and the tests were conducted in a nitrogen environment. Using TGA7, 4 different heating rates of 5°C/min., 10°C/min., 30°C/min. and 50°C/min. were applied to measure the mass loss history of each resin sample. For each test, a sample amount of 7.5 mg ~ 10.5 mg was used. TGA7 was calibrated using 4 different standard reference materials over the temperature range of ambient to 850°C: Alumel, Nickel, Perkalloy and Iron. Each reference was checked for its magnetic transition temperatures, which should be within +/- 5°C of its reported values. For DSC7, constant heating rates of 10°C/min., 30°C/min., 50°C/min. and 70°C/min. were used to measure the heat flow through the sample during its thermal decomposition. A sample amount of 7.5 ~ 9.5 mg was used for each test. This instrument was calibrated using the standard indium and zinc references for a temperature range of ambient to the maximum temperature available from the instrument, 500°C. The melting points of these references were checked to be within +/- 10% of its reported values. The enthalpy check was performed using indium. The heat of fusion for indium was calibrated to be within 10% of its reference value. A simple baseline subtraction was conducted to eliminate the unnecessary curvatures within the heat flow curve.

2.3. Fire Propagation Apparatus (FPA)

The Fire Propagation Apparatus (FPA, ASTM E 2058[1]) is a bench-scale fire test apparatus where four radiant lamps are used to heat the samples. In the FPA the samples can be tested in a controlled atmosphere (from nitrogen to 40% enhanced oxygen condition) using a long quartz tube. Performing tests on the FPA can deliver useful engineering data such as carbon dioxide generation based heat release rate (based on the standard), mass loss rate, smoke yield and smoke extinction coefficient. The purpose of FPA testing was to generate good data sets appropriate for pyrolysis modelling and parameter estimation, and therefore several modifications were made to the standard testing procedure. First, when testing the polyester FRPs, an insulated sample dish proposed by de Ris and Khan [8] was used instead of the stand-

ard specified, non-insulated aluminium dish. Second, 4 thermocouples were installed to measure temperature change of the sample at various depths: surface, 1/3, 2/3 and back face of the sample. The installation of thermocouples on the sample was consistent with the method introduced in Avila's work [4]. Third, carbon black was applied on the sample surface to allow radiation to be absorbed on the surface of the sample. This approach was taken because the samples (1A and 1C) were somewhat transparent and when tested in the FPA, in-depth absorption of radiation occurred. To incorporate in-depth absorption of radiation into the model requires more parameters than assuming only surface absorption. Therefore, to minimize the number of parameters that need to be optimized, carbon black was used which, should allow surface radiation absorption only. All of the tests were conducted under nitrogen to eliminate the effect of oxidation in the resin degradation kinetics and flame. Limiting the environment to only nitrogen allowed for more simplified kinetics modeling for the resin degradation as well as the pyrolysis modeling of the composite.

The uncertainty for the mass loss rate (MLR) and thermocouple measurements were determined via statistical analysis performed on data from tests with identical conditions. All uncertainties listed in this study are full scale (as opposed to \pm half scale). The uncertainty of MLR for the FPA was determined as 17mg/s (2.4g/sm²) by comparing three PMMA tests performed at 50kW/m² based on the standard which calls for three identical tests to be performed to correctly determine other properties [9]. The uncertainty in the thermocouple measurements was quantified by comparing back face temperature data from four identical 1C tests in the FPA. Temperature measurement at the back face of the sample surface was chosen because the exact measurement location is known, i.e. the sample thickness. Other temperature measurements made in various depths have a positional uncertainty of \pm 0.625 mm associated with the data. This uncertainty is from the drill bit used to make holes for thermocouple installations, which had a thickness of 1.25mm diameter. Using the normalized time, time divided by sample thickness square, i.e., $\tau = \text{time}/\delta^2$ to remove the effect of different sample thicknesses when comparing, the maximum deviation at various normalized times, up to the critical time, τ_c , was 16°C. The critical time, τ_c , corresponds to the time when evenly spread flames on the sample surface disappear when tested under air. Test data presented in this parameter estimation exercise study is truncated at this critical time of 4 s/mm² because the pyrolysis model is set up with a one-dimensional assumption, which may not be used when flames on the sample surface are not evenly distributed, typically where edge burning is dominant. These uncertainty values will be used to evaluate significant differences in the modeling results.

3. PYROLYSIS MODELING FOR LUMPED (TGA) AND SLAB (CONE/ FPA) EXPERIMENTS

The calculations reported here are conducted with a generalized pyrolysis model [2,3] that can be applied to a wide variety of condensed phase fuels. The model simultaneously calculates the condensed phase mass conservation, gas phase mass conservation, condensed phase species conservation, and condensed phase energy conservation equations. This model can be applied to both 0D and 1D systems and is therefore capable simulating both "lumped" (thermogravimetric) and "slab" (Cone Calorimeter/FPA) experiments. Extensive details are given in the following references – 2,3 – so only a brief overview is given here. Assumptions inherent in the model, as applied in this paper, include:

- Porosity can either be solved as a property of a species (default) or directly. When porosity is solved directly, it is derived from the condensed-phase mass conservation equation assuming no volume change (shrinkage or swelling).
- When porosity is directly solved, the user-specified thermal conductivity and density are interpreted as those of a nonporous solid. Therefore, the thermal conductivity that appears in the condensed-phase energy conservation equation is $\bar{k} = (1 - \psi)\bar{k}_s$ where ψ is porosity and \bar{k}_s is the weighted thermal conductivity of the solid assuming it is nonporous. Similarly, with this formula-

tion, the bulk density is calculated as $\bar{\rho} = (1-\psi)\bar{\rho}_s$ where $\bar{\rho}_s$ is the weighted density of the solid assuming it is nonporous.

- Bulk thermal conductivity \bar{k} has a cut-off value of 0.03W/mK which corresponds to air at 300 to 400K.
- Specific heat is calculated with a weighted or averaged quantity, i.e. $\bar{c}_p = \sum X_i c_{p_i}$ as other solid properties – enthalpy, emissivity, radiation absorption coefficient, permeability, etc.
- Specific heat capacity and effective thermal conductivity vary by as $k(T) = k_0(T/T_r)^{n_k}$ and $c(T) = c_0(T/T_r)^{n_c}$, respectively, where T_r is a reference temperature.
- Radiation heat transfer across pores is accounted for by adding a contribution to the effective thermal conductivity that varies as γT^3 , where γ is a fitting parameter
- Averaged properties in conservation equations are calculated by appropriate mass or volume fraction weighting
- All gases escape to the exterior ambient with no resistance to heat or mass transfer
- Negligible heat transfer between the gas phase and the condensed phase inside the decomposing solid
- There is no net shrinkage (volume change) due to reactions or bulk density changes

4. RESULTS AND DISCUSSION

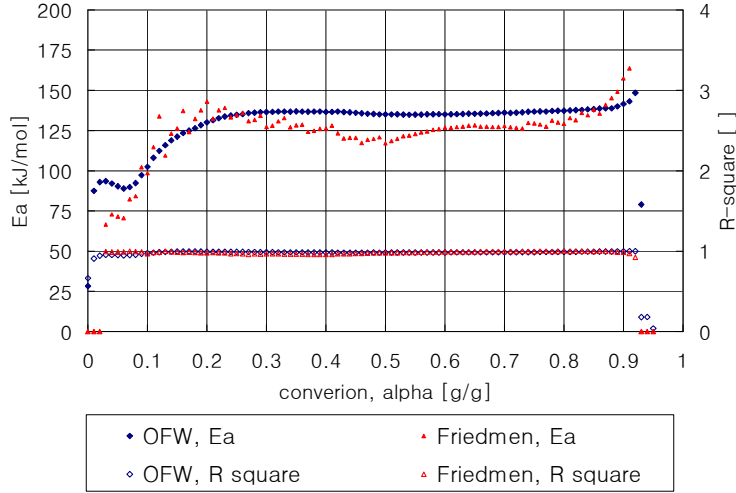
4.1. Kinetics of resin degradation

Typically in kinetic studies, the isothermal rate of degradation or conversion, $d\alpha/dt$, is assumed to be a linear function of the temperature dependent rate constant, $k(T)$, and a temperature independent function of the conversion, $f(\alpha)$, where α indicates the conversion. This equation can be further expanded by using the Arrhenius expression for the rate constant. Within the Arrhenius expression, two more reaction dependent constants are introduced: the pre-exponential constant, Z , and the activation energy, E_a . The temperature independent function of the conversion, $f(\alpha)$ is dependent upon the mechanism of chemical reactions.

$$\frac{d\alpha}{dt} = f(\alpha)Z \exp\left(-\frac{E_a}{RT}\right) \quad (1)$$

The iso-conversional method, also known as the model-free method is used to find the minimum number of elementary reactions necessary to describe the global degradation kinetics of the resin. This method uses data tested from different heating rates. Knowing that at a constant conversion, α , $d\alpha/dt$ and $f(\alpha)$ become constants. With these terms remaining as constants, the E_a is found without the pre-knowledge of the reaction mechanisms. The iso-conversional method will give constant activation energies, E_a , over the range of conversion of interest if the reaction is a single-step chemical reaction. If the activation energies, E_a , changes significantly with respect to different conversions, this is an indication for a more complex reaction mechanism.

Figure 2: Estimated activation energy of unsaturated brominated polyester resin calculated via “isoconversional” (model free) method



In Figure 2, the results from two iso-conversional methods introduced by Ozawa, Flynn and Wall [10,11] (OFW, finding a constant slope of $-Ea/R$ by plotting $\ln(\beta)$ versus $1/T$) and Friedmen [12,13] (plotting $\ln(d\alpha/dT)$ versus $1/T$ to find the slope of $-Ea/R$) conducted on the polyester resin are shown. Both methods are used for comparison purposes. The r-square values for each activation energy value are plotted as well using least square method. The activation energy becomes more reliable as the r-square values become closer to 1. The conversion is calculated as $\alpha = 1 - m/m_0$. As shown in Figure 2, the estimated activation energy ranges from 70 ~ 145 kJ/mol in $0 < \alpha < 0.20$, relatively steady around 120 ~ 145 kJ/mol in $0.20 < \alpha < 0.93$ and 145 kJ/mol and above in $0.93 < \alpha < 1.0$. Based on this result, one can approximate a minimum of three elementary reactions to model the full degradation over $0 < \alpha < 0.97$ range.



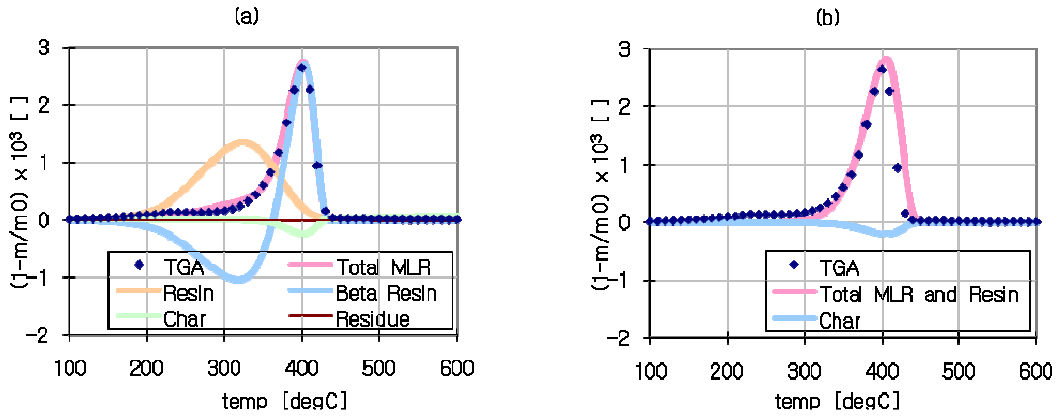
The proposed mechanism is consistent with previous research [14,15,16] conducted for unsaturated polyester thermoset resins. In addition to this three step mechanism, a single step degradation mechanism of resin becoming char and releasing fuel gas (93% weight loss) is modeled and compared to evaluate the necessity of multiple reaction steps. Applying these degradation mechanisms, a model fitting method [17] is used where $f(\alpha)$ is preselected to fit the TGA experiment data to find the kinetic parameters with the best fitness. In this study, a conversion function $f(\alpha) = (1 - \alpha)^n$ is used, which is typically applied for phase boundary reactions. The data fitting software used in this study is Genetic Algorithm (GA) coupled with the pyrolysis model for lumped experiments explained in the previous section. The GA was developed based on the mechanics of the Darwinian survival-of-the-fittest theory [2,3,18].

Table 1: Kinetic parameters estimated from model fitting exercise using Genetic Algorithm (GA): Three step nth order kinetic model and single step nth order kinetic model

Kinetics	Z_1 (/s)	E_{a1} (kJ/mol)	n_1 (-)	Z_2 (/s)	E_{a2} (kJ/mol)	n_2 (-)	Z_3 (/s)	E_{a3} (kJ/mol)	n_3 (-)
3 step n^{th} order	3.42×10^2	56.1	1.03	3.55×10^{11}	174.1	0.80	1.75×10^6	127.6	2.64
Single step n^{th} order				4.92×10^9	151.4	0.90			

The results found from the model fitting exercise are summarized in Table 1 and plotted in Figure 3. As shown in Figure 3, using three steps when modeling the resin degradation gives better fitness of the estimated mass loss rate to the actual TGA experiment data. When three steps are used instead of one, the initial mass loss that starts from 200°C is captured while the temperature needs to increase up to 300°C to initiate any mass loss when using one step reaction (see Figure 3). In addition to the earlier stage of degradation, better fitness is shown after 400 °C for the three step reaction case than that of one step where mass loss rate is expected to rapidly decrease. The total mass loss rate peak observed in ~400°C range spreads over a wider temperature range when a single step reaction is used for resin degradation. This is due to the unresolved initial mass loss when using the single step reaction. An additional mass loss is given at the end of the major mass loss peak after 400°C to compensate for the initial mass loss which should have existed before 200°C. However, these differences in mass loss rate found from applying two resin decomposition mechanisms – three steps vs. single – are subtle.

Figure 3: Kinetic parameters estimated for brominated, unsaturated polyester resin: 3 step mechanism with n^{th} order kinetic model (a) and one step mechanism with n^{th} order kinetic model (b)



4.2. Property estimation for FRP composite: Polyester composite with low glass content (1A)

The property estimation for the polyester composite is conducted by coupling a generalized pyrolysis model for slab experiments developed by Lautenberger and the Genetic Algorithms (GA) for optimization routine [2,3,18]. To reduce the number of parameters to estimate, the FPA experiments for the polyester composite with low glass content, 1A were conducted with certain approaches. For example, carbon black powder was applied on top of the sample surface to eliminate in-depth absorption of radiation. FPA tests were conducted under nitrogen environment to exclude the effect of oxidative decomposition of the resin and flame. Experimental data used in the estimation exercise was truncated when normalized time, time divided by sample thickness square, i.e., $\tau = \text{time}/\delta^2$ became approximately 4 s/mm². This time is noted as the critical time, τ_c , for a typical 1A sample when the pyrolysis can no longer be simplified as a one-dimensional problem. The critical time, τ_c , is identified as time of evenly spread flame on the sample

surface disappearing when tested under air, where edge burning is dominant. Additionally, for further simplification of the problem when modeling, the backface temperature measurement was used as a boundary condition for the condensed phase.

The parameter estimation exercise was conducted for the following two cases: (1) GA1 where the heterogeneous microstructure was incorporated and the three step mechanism for resin decomposition was used; (2) GA2 where a single layer was constructed as a homogeneous structure based on resin and glass weight proportion within the composite and the three step mechanism for resin decomposition was used. For both cases, the same set of parameters is optimized, which are listed in Table 2 along with the estimation results. These parameters were introduced in Section 3 where a brief description of the pyrolysis model used in this study [2,3] is given. The kinetic parameters for resin degradation were pre-determined as described in the previous section. However, the heats of reaction for the three elementary reactions were estimated through parameter estimation exercise as other thermophysical properties, but with its searchable range for optimization set based on Differential Scanning Calorimeter (DSC) experiment results on the polyester resin. Note that the heat of reactions were proportioned to reflect the kinetic modeling, i.e. the first, second and third reactions consumes 20%, 73% and 8% of the total enthalpy, respectively, which is identical to the resin weight loss percentages in each reaction step. The total number of parameters found via optimization was 29 including the heat of reactions.

Table 2: Optimized thermophysical properties from 1A with heterogeneous assumption. For each material (resin, beta-resin, char, residue and glass) conductivity (k_0), conductivity temperature dependency (n_k), heat capacity (c_0), heat capacity temperature dependency (n_c), emissivity (ϵ) and the fitting parameter for radiation heat transfer across pores (γ) are estimated. Additionally, heat of reaction (ΔH) for three resin decomposition kinetic is estimated.

Species		ρ_0 (kg/m ³)	k_0 (W/m-K)	n_k (-)	c_0 (J/kg-K)	n_c (-)	ϵ (-)	γ (m)
Resin	GA1	1350	0.304	0.082	1185	0.093	0.964	0.0000
	GA2		0.261	0.099	1237	0.206	0.969	0.0000
	GA1-GA2 /GA1		14.1%	19.9%	4.4%	120.6%	0.6%	0.0%
Beta resin	GA1	1080	0.317	0.080	1260	0.094	0.973	0.0000
	GA2		0.274	0.087	1318	0.207	0.965	0.0000
	GA1-GA2 /GA1		13.5%	9.1%	4.6%	119.5%	0.8%	0.0%
Char	GA1	95	0.163	0.326	1111	0.464	0.990	0.0046
	GA2		0.169	0.237	1029	0.246	0.991	0.0034
	GA1-GA2 /GA1		3.4%	27.4%	7.4%	46.9%	0.1%	0.0%
Residue	GA1	41	0.168	0.333	1061	0.481	0.985	0.0046
	GA2		0.176	0.236	956	0.247	0.980	0.0036
	GA1-GA2 /GA1		4.6%	29.1%	9.9%	48.7%	0.4%	0.0%
Glass	GA1	2600	0.064	0.328	1069	0.249	0.981	0.0034
	GA2		0.113	0.218	1072	0.194	0.982	0.0050
	GA1-GA2 /GA1		74.9%	33.4%	0.2%	22.3%	0.1%	0.0%
Heat of reaction ΔH (J/kg)		Degradation Reactions				GA1	GA2	GA1-GA2 /GA1
		resin $\rightarrow \nu_{br}$ beta_resin + (1 - ν_{br})gas				3.1E+04	2.2E+04	29.9%
		beta_resin $\rightarrow \nu_c$ char + (1 - ν_c)gas				1.1E+05	8.0E+04	29.9%
		char $\rightarrow \nu_r$ residue + (1 - ν_r)gas				1.1E+04	8.0E+03	29.9%

In Table 2, the estimation of GA1 and GA2 are compared to show how consistent the estimations are. It shows that most of the estimated values of GA2 have a difference of less than 30% when compared to those of GA1, which allows constructing some level of confidence in the optimizing capability of the Genetic Algorithms. Although the comparison has been made for individual parameter estimations and shows results from GA1 and GA2 are somewhat consistent, one should take into account that the Genetic Algorithm optimizes for a group of these individual estimations that gives the best fit to the mass loss rate and temperature data measured at four locations. When compared in groups, typically it shows that a change occurring in one parameter is compensated by a change found from the other. Hence, comparing the pyrolysis modeling results using the estimations from two different set-ups (GA1 and GA2) in groups should present a better sense of optimization consistency. Accounting for the uncertainties associated with the experiments (17mg/s and 16°C for mass loss rate and temperature measurements, respectively), the property estimations with GA1 and GA2 baselines were nominally equivalent. This demonstrates that there is consistency in the estimation for both baselines. Because the two baselines produce similar results, only GA1 is used as a baseline for the pyrolysis modeling study discussed in the next section.

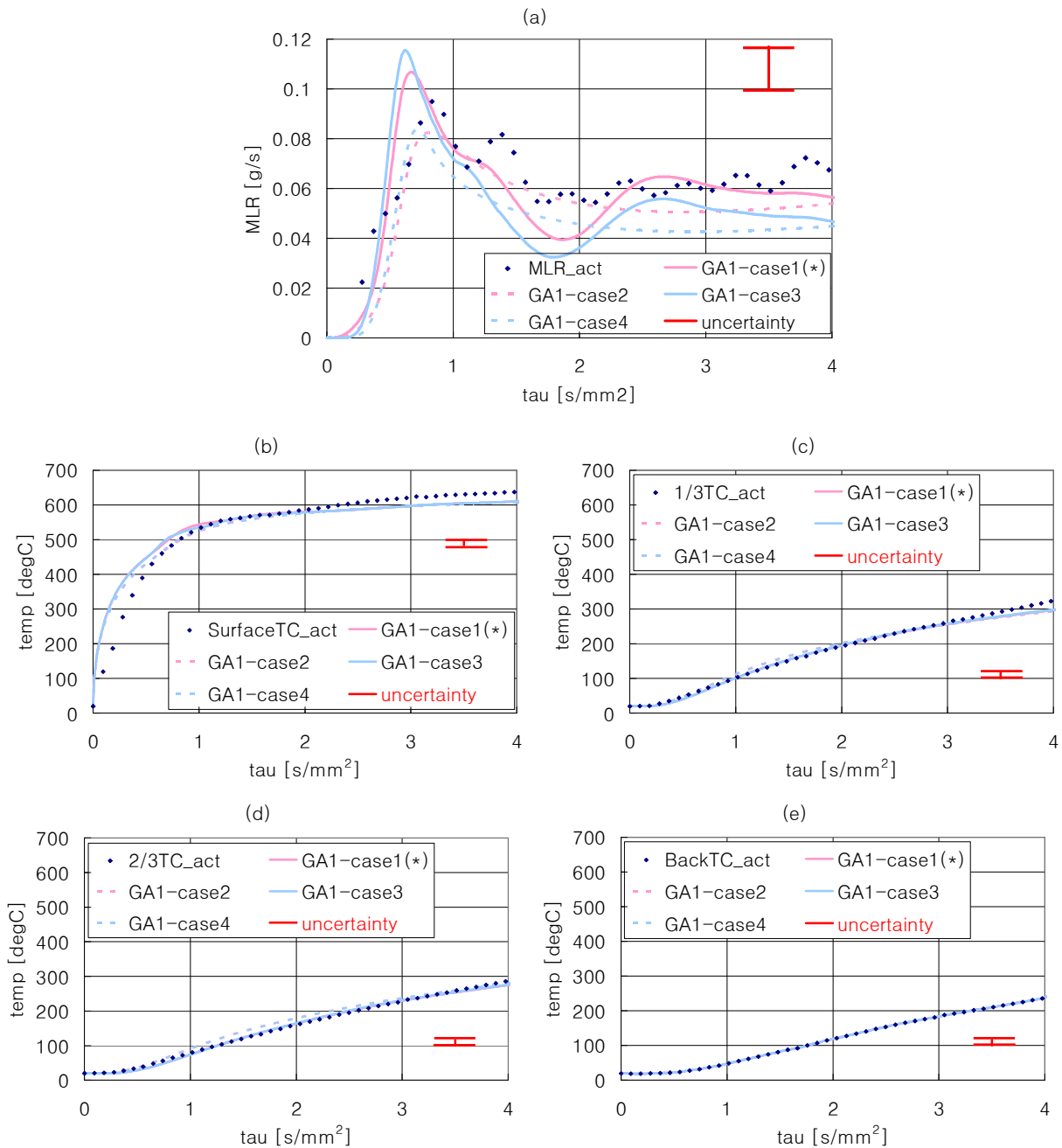
Using the estimated properties found from this study, four cases (as summarized in Table 3) for 1A (sample with low glass content) are modeled to check the fitness of the optimization and compare cases with various modeling conditions. Note that only the results from GA1 are plotted (see Figure 4) in this paper considering that those from GA1 and GA2 are significantly similar. These cases are constructed based on applying different assumptions for the microstructure of the composite (heterogeneous or homogeneous) and degradation mechanism (3 step or single). For every case, the pyrolysis modeling results of mass loss rate and temperatures from surface, 1/3, 2/3 of sample thickness from surface, and backface are plotted with the actual experimental data. The parameter estimations from GA1 set-up should give the best fit for case 1 because the optimization was performed based on the corresponding condition.

Table 3: Testing matrix for parameter estimation of 1A and pyrolysis modeling of 1C – GA1 (case 1: heterogeneous structure and three step degradation kinetic model) is used to optimize the parameter estimation. Using the estimated values, cases 1 through 4 are simulated using a pyrolysis model [2,3].

Parameter Estimation	Pyrolysis Modeling	Microstructure	Resin Degradation Kinetics $f(\alpha) = (1 - \alpha)^n$
GA1	Case 1	Heterogeneous	3 steps
	Case 2	Homogeneous	3 steps
	Case 3	Heterogeneous	Single step
	Case 4	Homogeneous	Single step

In general, one can conclude that the parameter estimations for 1A with GA1 set-up(see Figure 4) was conducted properly and that the modeling results are in a good agreement with the actual experiment data within the uncertainty stated for the experiment (17mg/s and 16°C for mass loss rate and temperature measurements, respectively). In the figure, (a) shows that modeling the mass loss rate had improved qualitatively when microstructure of composite was incorporated as an input (case1 and case3) as oppose to simply assuming as a homogeneous material (case 2 and case 4). However, note that quantitatively the changes should be considered as insignificant taking into account for the uncertainty of 17mg/s. The mass loss rate data shown in the figures were applied with Fast Fourier Transform (FFT) smoothing, which resulted in artificial oscillations with magnitude in the order of 0.01g/s. Therefore, the actual mass loss rate has an initial peak before $\tau = 1$, another smaller peak following around $\tau = 1.4$ with a decreasing trend up until $\tau = 1.8$, and a slowly increasing trend from that point to $\tau = 4$. The minimal point in the mass loss rate data near $\tau = 1.8$ is possibly due to pyrolysis proceeding through the prominent glass layer after decomposing through the resin rich layers. The model was able to capture the large oscillations in the beginning and the decreasing trend followed by an increasing trend near $\tau = 1.8$ in the mass loss rate

Figure 4. Parameter estimation GA1 results for brominated, unsaturated polyester composite with low glass content (1A) – heterogeneous microstructure and 3 step degradation mechanism (case1, * indicates this condition is identical to that of GA1); homogeneous structure and 3 step degradation mechanism (case2); heterogeneous microstructure and a single step degradation mechanism (case3); homogeneous structure and a single step degradation mechanism (case4) – (a) Mass loss rate; (b) Surface temperature; (c) 1/3 of sample thickness in-depth temperature from the surface; (d) 2/3 of sample thickness in-depth temperature from the surface; (e) Backface temperature



generated by pyrolyzing through different layers composed of an alternating decomposable resin and inert glass layers. The simulated temperature results follow well with the actual tests data for all four cases. Note that even with this comparison made without incorporating the positional uncertainty of ± 0.625 mm

for the in-depth thermocouple installation to the temperature measurement uncertainty band, the simulation and actual test data show a good agreement (see (c) and (d) in Figure 4). The simulation and actual data for backface temperature is shown in (e) in Figure 4 as a check to confirm they match perfectly knowing that this was used as a boundary condition in the simulation. Changing the resin decomposition mechanism from 3 step to a single step had an insignificant effect on the simulation results, which is consistent with the results found from kinetic modeling analyses performed in the previous section.

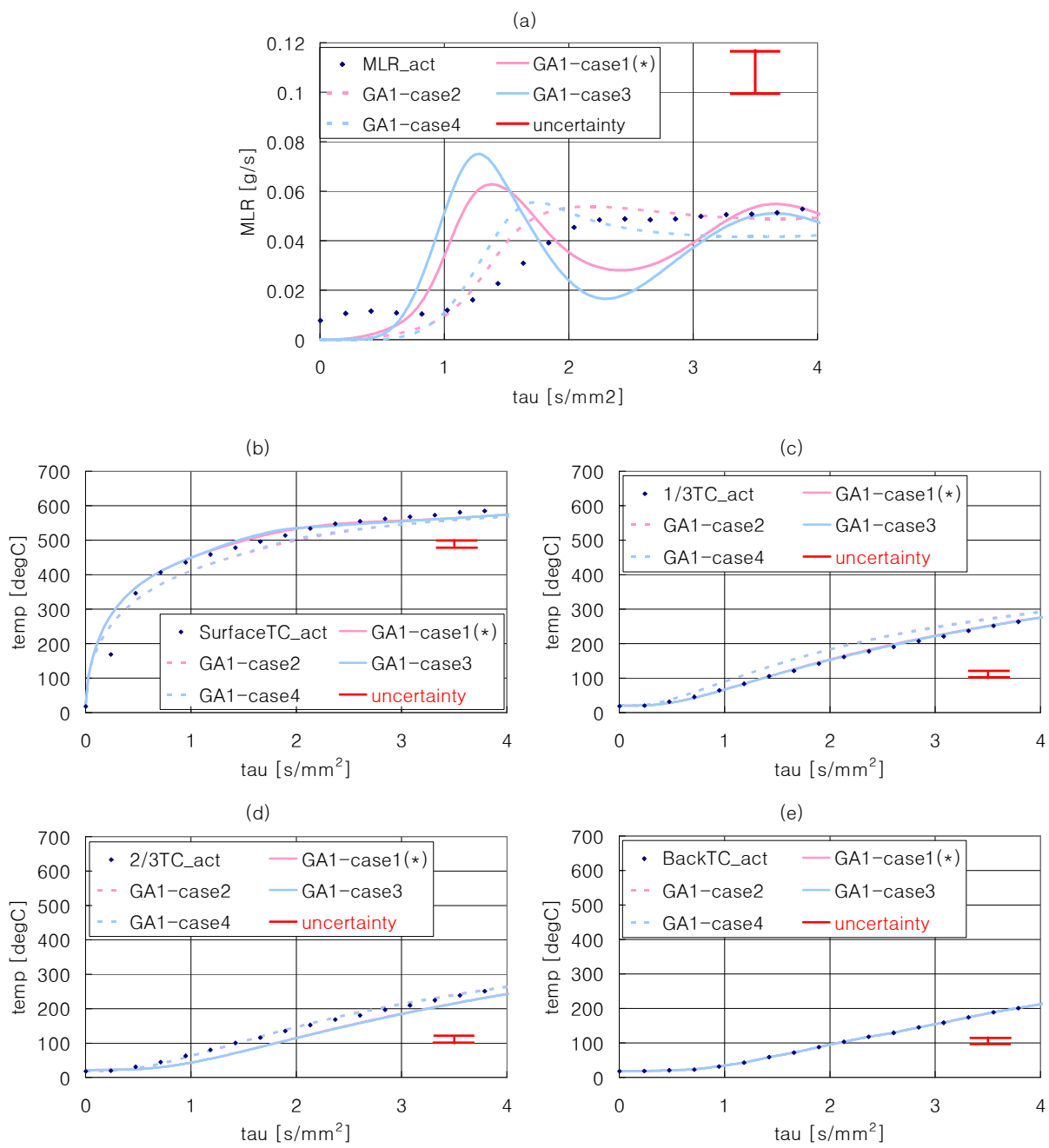
Based on the findings from above analyses, one can conclude the following: (1) Quantitatively, the two baselines – GA1 or GA2 – are nominally equivalent considering the uncertainty associated with the experimental data. There is consistency in the estimation with both baselines. (2) Optimization for parameter estimation using pyrolysis model with GA was conducted with satisfaction in terms of mass loss rate and temperatures at various depths (surface, 1/3 and 2/3 in-depth from surface, and backface) (3) Incorporating the microstructure of the composite improves the mass loss rate simulations in terms of resolving the detailed oscillations and following the trend qualitatively but has less impact on sample temperature predictions. (4) Applying 3 step resin decomposition mechanism instead of a single step has subtle influence in the modeling results.

4.3. Evaluation for estimated properties

To evaluate the correctness of the property estimation, modeling of the same composite as 1A but with higher glass content designated as 1C is conducted. The parameter estimation using 1A pyrolysis FPA test data was for the resin and glass. In theory if the parameter estimation was conducted properly, one should be able to model a composite that is produced with the same type of resin and glass using the estimation as an input to the pyrolysis model with the degrees of satisfaction which was found from comparing the modeling results for 1A as shown in Figure 4.

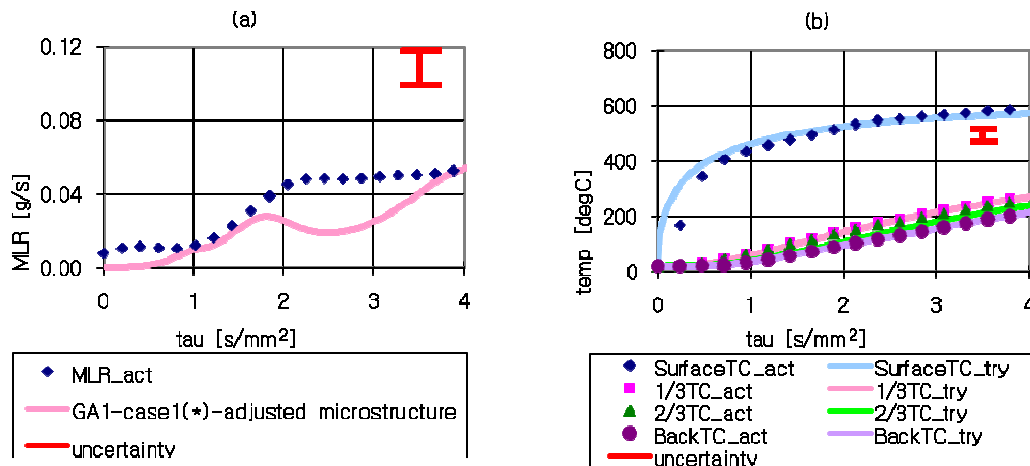
Four cases as in Table 3 for 1C with GA1 baseline (see Figure 5) are simulated using the estimated properties found from 1A. The results are shown in Figure 5 for GA1 where mass loss rate and temperature measurements from surface, 1/3 and 2/3 of sample thickness from surface, and backface are plotted with experimental data. In Figure 5, (a) shows that the simulation results of case 2 and 4 (homogeneous structure with 3 step or single step resin decomposition mechanism assumptions) have the better fit to the actual test data considering the uncertainty of 17mg/s than those of case 1 and 3 (heterogeneous structure with 3 step or single step resin decomposition mechanism assumptions). Although incorporating the microstructure of the composite (assuming heterogeneous) does allow the model to resolve the oscillations in the mass loss rate curve due to pyrolysis through resin and glass alternating layers (case 1 and case 3), this phenomenon is not observed from the experiment. The difference of modeled temperatures at various depths and those from the actual experiment are within the measurement uncertainty and the positional uncertainty of ± 0.625 mm for the 1/3 and 2/3 in-depth thermocouple bead where temperature is actually measured (see (b) through (d) in Figure 5). The positional uncertainty associated with the 1/3 and 2/3 in-depth thermocouple location is interpreted in the context of the simulation results. This is conducted by comparing the simulated temperatures from the exact 1/3 and 2/3 locations as well as temperatures at ± 0.625 mm from the exact locations. The simulation and actual data for backface temperature is shown in (e) in Figure 5 as a check to confirm they are identical knowing that this was used as a boundary condition in the simulation. Similar to 1A simulation results, using either 3 step or a single step for the polyester resin decomposition mechanism was irrelevant in terms of simulating mass loss or temperature changes of 1C.

Figure 5. Pyrolysis modeling results for brominated, unsaturated polyester composite with higher glass content (1C) using estimations based on 1A (GA1) – heterogeneous microstructure and 3 step degradation mechanism (case1, * indicates this condition is identical to that of GA1); homogeneous structure and 3 step degradation mechanism (case2); heterogeneous microstructure and a single step degradation mechanism (case3); homogeneous structure and a single step degradation mechanism (case4) – (a) Mass loss rate; (b) Surface temperature; (c) 1/3 of sample thickness in-depth temperature from the surface; (d) 2/3 of sample thickness in-depth temperature from the surface; (e) Backface temperature



Comparing the results from pyrolysis modeling of 1C (see Figure 5) to those of 1A (see Figure 4), one can find that the major difference is observed from the mass loss rate simulations. In 1C simulations, incorporating the microstructure of the composite has a negative effect on the mass loss rate simulation while it has a positive effect qualitatively when simulating 1A. To find a plausible explanation for this difference, additional pyrolysis modeling numerical experiments were conducted for 1C. For these numerical experiments, minor adjustments to the 1C microstructure were made for the following reason. More uncertainty is introduced when 1C microstructure is estimated visually than for 1A because in 1C (average thickness of 6 ~ 7 mm) more layers are added to a thinner sample comparing to 1A (average thickness of 10 mm). As shown in (a) of Figure 5, the simulation with heterogeneous structure allows an over-prediction of the mass loss rate between $\tau = 1$ and 2 and under-prediction between $\tau = 2$ and 3. This indicated that the proposed microstructure (see Figure 1) for 1C used in the model had more resin on surface than actual followed by layers with more glass than actual. Therefore, when running the model, slight modification was made to the 1C microstructure near the surface within 0.5 mm to resolve the identified problem but the global density was maintained to 40 wt% resin and 60 wt% glass. The simulation results are shown in Figure 6. As shown in this figure, using the same estimated parameters the mass loss rate simulation can be improved without negatively affecting the temperature agreement by simply adjusting the microstructure only to a minimal degree. Therefore, it shows that the simulation agreement with the actual data is sensitive to the microstructure as oppose to poorly conducted parameter estimation.

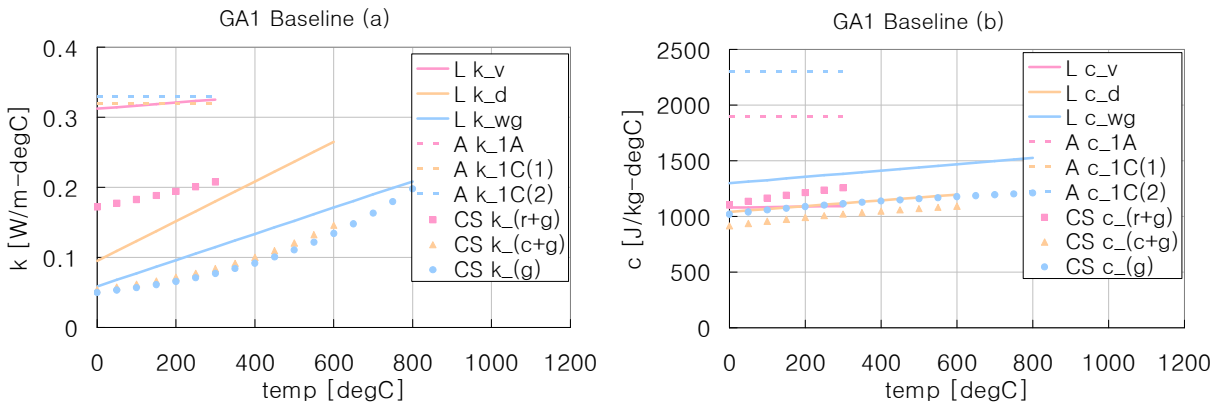
Figure 6. Pyrolysis modeling results for brominated, unsaturated polyester composite with higher glass content (1C) using estimations based on 1A (GA1) but with 1C microstructure near surface slightly adjusted to account for less resin – heterogeneous microstructure and 3 step degradation mechanism (case1, * indicates this condition is identical to that of GA1) – (a) Mass loss rate; (b) Temperature comparisons at various depths (surface, 1/3 and 2/3 of sample thickness in-depth from the surface, and backface temperatures)



To check whether the estimated parameter values from this study are consistent with other references [4,5], a comparison is made for the conductivities and the specific heat capacities of the virgin composite (resin and glass), decomposed composite (char and glass) and fully decomposed composite (glass only). An artificial composite is made with 30 wt% of resin and 70 wt% of glass with the estimated parameters from 1A FPA pyrolysis tests to directly compare the values found from Lattimer's paper [5] where conductivities and heat capacities are experimentally evaluated for a glass reinforced vinyl ester composite found from different stages of pyrolysis. The method used to determine the thermal properties found from Lattimer's work incorporates the effects of voids and cracks generated during pyrolysis. Therefore, effective thermal conductivity and heat capacity are used to compare with Lattimer's data, which are calculated based on volume fraction including the properties of the voids as gas. In addition to Lattimer's

data, thermal properties estimated for 1A and 1C by Avila [4] are plotted for more comparison. As shown in **Error! Not a valid bookmark self-reference.**, the effective thermal properties calculated from estimated parameters using 1A test data for GA1 condition is consistent with other reference values. The average deviation of the estimations found from this study is within 50% of those of Lattimer and Avila for conductivity and heat capacity.

Figure 7: Estimated parameters with GA1 (heterogeneous structure with three steps of degradation kinetic model) estimations – from current study (CS), conductivity, k and specific heat capacity, c for resin and glass (r+g), char and glass (c+g) and glass only (g) assuming constant volume compared with those from the work of Lattimer (L, estimation for virgin composite (v), decomposed composite (d) and woven glass only composite after fully degrading resin (wg)) and Avila (A, estimation for 1A and 1C composites, same samples used in this study).



5. CONCLUSIONS AND FUTURE WORK

A property estimation exercise for pyrolysis modeling is conducted on unsaturated polyester FRP composites with low glass content (1A). To properly model the pyrolysis of the composite, kinetic modeling of the resin degradation was performed using TGA and DSC experiment data on the resin. Using an iso-conversional method (also known as model-free method), the minimum number of elementary reactions required to describe the full degradation mechanism was proposed. Based on this analysis, three step mechanism was constructed. In addition to this three step mechanism, a single step case was also investigated to compare the effect of using a more complicated approach than a simple one step on the overall pyrolysis modeling and property estimation. With a pre-known reaction mechanism, a model fitting method was used to find the kinetic parameters for each reactions.

Property estimation for unsaturated polyester FRP composite was conducted using the 1A FPA pyrolysis test data with a generalized pyrolysis model, Gpyro paired with an optimization routine known as Genetic Algorithm (GA). Two conditions were used to construct a baseline – (1) GA1 where the heterogeneous microstructure was incorporated and the three step mechanism for resin decomposition was used; (2) GA2 where a single layer was constructed as a homogeneous structure based on resin and glass weight proportion within the composite and the three step mechanism for resin decomposition was used. Independent of applying one of these conditions, the estimation was conducted for the same set of parameters for resin and glass as summarized in Table 2. The results demonstrated that whether applying GA1 or GA2 conditions as a baseline, the estimations are nominally identical quantitatively considering the uncertainty of the experiment data; however, this provides evidence that independent of the baselines, the estimation results are consistent. The estimated values were used to model 1A to verify the fitness of the

optimization and compare cases with different microstructures (heterogeneous or homogeneous) and kinetic mechanisms (3 step or single step), which are designated as case 1 through 4. The parameter optimization results showed that the pyrolysis modeling was conducted with satisfaction in terms of mass loss rate and temperatures at various depths (surface, 1/3 and 2/3 in-depth from surface, and backface). The pyrolysis modeling results qualitatively showed that incorporating microstructure of the composite when modeling allows the model to resolve oscillations in the mass loss rate. Changing the kinetics mechanism had a subtle influence for modeling this composite.

To evaluate whether the estimation can represent the components of the composite, resin and glass, a pyrolysis modeling is conducted for a polyester FRP composite with higher glass content (1C) than 1A. The results show a relatively good agreement to the actual test data except for the mass loss rate. Although for 1A applying the heterogeneous microstructure to the modeling did improve the simulation results, it did not for 1C modeling. A reasonable explanation for this poor estimation is due to the uncertainty in the microstructure of 1C near the surface rather than poorly conducted parameter estimation. In addition to 1C modeling, estimated conductivity and heat capacity values are compared with those of other references and confirmed that it was consistent within 50%.

In this study, the work demonstrates the possibility of constructing a virtual experiment for composites using a bench-scale pyrolysis test and thermal analysis experiment data. Using one type of composite (1A), an optimization of parameters was conducted and those estimations were used to model a different type of composite (1C). In the future, the work will be expanded to cases where fire retardant additives have an effect to the degradation kinetics of the composite and composites are decomposing in an oxidative condition such as air. The goal of the work will be to develop an approach that is consistent and simple when performing parameter estimation and modeling for different types of composites in various conditions.

ACKNOWLEDGMENTS

The authors would like to thank Charles Dore for fabricating and donating the polyester FRP composite materials used in this study. Many thanks also to Randall Harris, William Wong and Haejun Park at WPI for assisting the FPA tests.

REFERENCE

-
- ¹ Standard Methods of Test for Measurement of Synthetic Polymer Material Flammability Using a Fire Propagation Apparatus (FPA), ASTM E 2058-03, ASTM, 100 Barr Harbor Drive, West Conshohocken, PA, U.S.
 - ² Lautenberger, C., "A Generalized Pyrolysis Model for Combustible Solids", Ph.D. Dissertation, Department of Mechanical Engineering, University of California, Berkeley, Fall 2007
 - ³ Lautenberger, C., Gpyro – A Generalized Pyrolysis Model for Combustible Solids Users' Guide, Version 0.609, July 23, 2008
 - ⁴ Avila, Melissa B., Dembsey, Nicholas A., Kim, Mi Hyun E., Lautenberger, Chris, Dore, Charles, Fire Characteristics of Polyester FRP Composites with Different Glass Contents, *Composites & Polycon 2007*, American Composites Manufacturers Association, October 17-19, 2007
 - ⁵ Lattimer, Brian Y., Ouellette, Jason, Properties of composite materials for thermal analysis involving fires, *Composites: Part A* 37 (2006) 1068–1081
 - ⁶ Lewin, M., "Synergism and Catalysis in Flame Retardancy of Polymers", *Polym. Adv. Technol.* 12, 215-222 (2001)
 - ⁷ Standard Test Method for Surface Burning Characteristics of Building Materials, ASTM E 84-05, ASTM, 100 Barr Harbor Drive, West Conshohocken, PA, U.S.

-
- ⁸ de Ris, J.L. and Khan, M.M., "A sample holder for determining material properties," *Fire and Materials*, 24, 219-226 (2000).
- ⁹ User's Guide for the Fire Propagation Apparatus (FPA) ASTM E-2058, Fire Testing Technology Limited, PO Box 116, East Grinstead, West Sussex, England.
- ¹⁰ Ozawa, T., *Bull Chem Soc Jpn* 1965;38;188
- ¹¹ Flynn, J., Wall, L.A., *J Polym Lett* 1966;4:232
- ¹² Friedmen, H.L., *J Polym Sci Part C* 1964;6:183
- ¹³ Friedmen, H.L., *J Polym Lett* 1966;4:232
- ¹⁴ Chrissafis, K., Paraskevopoulos, K.M., Bikiaris, D.N., Thermal degradation kinetics of the biodegradable aliphatic polyester, poly(propylene succinate), *Polymer Degradation and Stability* 91 (2006) 60-68
- ¹⁵ Y. S. Yang and L. James Lee, Microstructure formation in the cure of unsaturated polyester resins *Polymer, Volume 29, Issue 10, October 1988, Pages 1793-1800*
- ¹⁶ Chiu, H.T., Chiu, S.H., Jeng, R.E., Chung, J.S., A study of the combustion and fire-retardance behaviour of unsaturated polyester/phenolic resin blends, *Polymer Degradation and Stability* 70 (2000) 505-514
- ¹⁷ Burnham, A.K., Weese, R.K., Kinetics of thermal degradation of explosive binders Viton A, Estane, and Kel-F, *Thermochimica Acta* 426 (2005) 85-92
- ¹⁸ Rein, G., Lautenberger, C., Fernandez-Pello, C., Torero, J.L., Urban, D.L., Application of genetic algorithms and thermogravimetry to determine the kinetics of polyurethane foam in smoldering combustion, *Combustion and Flame* 146 (2006) 95-108

Appendix H

Property Estimation for Pyrolysis Modeling Applied to Polyester FRP Composites with Different
Glass Contents

Composites & Polycon 2009

Property Estimation for Pyrolysis Modeling Applied to Polyester FRP Composites with Different Glass Contents

by

Esther Kim¹
Chris Lautenberger²
Nicholas Dembsey¹

¹ Worcester Polytechnic Institute
Department of Fire Protection Engineering
100 Institute Road
Worcester, MA 01609

² University of California, Berkeley
Department of Mechanical Engineering
Berkeley, CA 94720

Abstract

For the composites industry to “design for fire” more thorough understanding of how typical FRPs decompose under fire conditions is needed. The role played by the glass and the resin (and additives) for FRPs are keys to understanding the fire behavior. To that end, this study continues work presented at Composites 2007 [1]. The goal of this work is to evaluate the ability of a pyrolysis model and genetic algorithm (optimization routine) pairing to estimate properties of each component of the composite, resin and glass. The composite pyrolysis experimental data used in this work was obtained from tests conducted on a bench scale fire test apparatus, Fire Propagation Apparatus, with additional instrumentation to measure surface and internal temperatures of the sample. Mass loss data and temperature profiles with respect to time at different in-depth locations are used in the optimization process. The property estimation exercise is conducted on a brominated, unsaturated polyester FRP composite with low glass content. Thermal analysis data from thermogravimetric analysis and differential scanning calorimetry of the polyester resin in the composite was used to model the decomposition kinetics. With the approximated decomposition kinetics for the resin, simulation of pyrolysis tests (nitrogen environment) of the composite slab was performed to estimate the unknown thermophysical properties by genetic algorithm optimization. A validation exercise using the

estimated properties is then conducted on a composite with high glass content. The quality of the estimated properties is assessed by comparing simulated results to experimental results for the high glass content sample.

1. Introduction

For the composites industry, designing for a FRP that provides good fire characteristics becomes a guess and check operation in many cases. Any changes made to the resin, glass, or the microstructure of the FRP affect the overall fire behavior of the FRP. Traditionally, the effect of the changes made in the FRP is checked by conducting tests via standard fire tests, which can be time consuming and expensive. Therefore, providing an understanding of how typical FRPs decompose under fire conditions and using this information to find an appropriate guideline for the composite industry to produce better fire-safe composites have been a long-term goal for this research. To that end, this work follows the work presented at Composites 2007.

In this study, complete data sets of decomposition of brominated, unsaturated polyester resin and its FRP composites with different glass contents are presented. Careful experiments were conducted using Thermogravimetric Analysis (TGA) and Differential Scanning Calorimetry (DSC) in order to study the thermal decomposition kinetics of the polyester resin. Also, the polyester FRPs with different glass contents – 33 wt% (1A) and 60 wt% (1C) – were tested under a modern bench-scale fire test apparatus known as Fire Propagation Apparatus (FPA, ASTM E 2058[2]) with additional instrumentations such as thermocouples at various depths. These tests were designed to generate data specifically useful for computer modeling purposes.

The model used in this study is a generalized pyrolysis model developed by Lautenberger [3,4], which simulates the heating and decomposition of a chosen material. Like with any other pyrolysis models, this model requires many input parameters found from material properties, which include the pyrolysis kinetics (pre-exponential factor, activation energy, reaction order), thermal properties (specific heat capacity, thermal conductivity), and radiative characteristics (surface emissivity, in-depth radiation absorption coefficient). Unfortunately, there are no standardized techniques to determine all of these properties via laboratory tests. Another way of estimating parameters is to use an optimization routine with a pyrolysis model in pair.

The current work applies Genetic Algorithm as an optimizing method coupled with Lautenberger’s pyrolysis model [3,4] to perform parameter estimation. Using the experimental data of the polyester FRP with lower glass content (1A), an estimation exercise is conducted to

find properties of the individual components of the composite, i.e., resin and glass, where one is decomposable while the other is inert, respectively. The estimated parameters for these components are used to model the pyrolysis of the same polyester FRP but with higher glass content (1C). The simulated 1C mass loss rate (MLR) and temperatures (TC) will be compared to those of actual experiments to evaluate the appropriateness of the estimation. Additionally, the estimated properties will be compared to those found from the literature [1,5] to check how consistent the estimations are.

2. Pyrolysis of FRP Composite

2.1. FRP composite description

The resin in this study is a commercially prepared unsaturated polyester resin with 20 wt% bromination for its fire retardancy built in to the carbon backbone. Antimony trioxide is added, which acts as a synergist that assists the flame retardancy of the polymer resin. Among the various effects of adding antimony trioxide, the major role of this additive is reacting with the halogen such as bromine and removing the radicals that are essential for combustion chemical reactions to proceed. This additive is also known to delay the escape of halogen from the flame, which increases its concentration and diluting effect [6]. The resin was catalyzed with methyl ethyl ketone peroxide (MEKP). According to the product description, this resin is a low viscosity, thixotropic polyester resin formulated to be Class I per ASTM E 84 [7] (flame spread index < 25 and smoke developed < 450).

Composite panels were fabricated by hand lay-up and vacuum bagging for low (33 wt% of glass, average thickness of 10 mm) and high (60 wt% of glass, average thickness of 6 ~7 mm) glass content composites, respectively, using two different types of fiberglass mats that were wetted with resin. The two types of fiberglass (E-glass) used in the composite are a chopped strand mat and a glass roving woven mat with an area density of 25 g/m² and 880 g/m², respectively. The chopped strand mat is thinner and more porous than the woven mat. The laminate schedule (provided by the manufacturer) is chopped strand mat and roving alternating five times for 1A and eight times for 1C with another chopped strand mat layer at the end. Visual inspection of a polished cross-section of the composite slab is consistent with this laminate schedule, but with polymer resin layers between each fiberglass layer. The chopped strand mat layer is difficult to identify in the cross section, perhaps because more resin is soaked into this layer than the roving layer. The roving layer is observed as a prominent glass layer possibly because the resin is absorbed only at the fiberglass layer surfaces leaving the interior with primarily glass.

The layered microstructure is determined to a resolution of 0.10 mm and 0.06 ~ 0.07 mm for 1A and 1C, respectively by inspecting a polished cross-section of the composite under a microscope. Based on visual observation and comparison to global density of the composite sample, approximations of three distinct layers are proposed: 100% resin, 100% glass, and 50% resin/50% glass. The microstructure is shown schematically in Figure 1. The lightest “box” represents 100% resin, the medium darkness box represents 50% resin/50% glass, and the darkest box represents 100% glass. Each box has a thickness of 1% of each sample’s average thickness.

2.2. Thermogravimetric Analysis (TGA) and Differential Scanning Calorimetry (DSC)

The instruments used in this study were manufactured from PerkinElmer: Thermogravimetric Analysis 7 (TGA7) and the Differential Scanning Calorimetry 7 (DSC7). Throughout this study, TGA and DSC were used for a non-isothermal test purposes and the tests were conducted in a nitrogen environment. Using TGA7, 4 different heating rates of 5°C/min., 10°C/min., 30°C/min. and 50°C/min. were applied to measure the mass loss history of each resin sample. For each test, a sample amount of 7.5 mg ~ 10.5 mg was used. TGA7 was calibrated using 4 different standard reference materials over the temperature range of ambient to 850°C: Alumel, Nickel, Perkalloy and Iron. Each reference was checked for its magnetic transition temperatures, which should be within +/- 5°C of its reported values. For DSC7, constant heating rates of 10°C/min., 30°C/min., 50°C/min. and 70°C/min. were used to measure the heat flow through the sample during its thermal decomposition. A sample amount of 7.5 ~ 9.5 mg was used for each test. This instrument was calibrated using the standard indium and zinc references for a temperature range of ambient to the maximum temperature available from the instrument, 500°C. The melting points of these references were checked to be within +/- 10% of its reported values. The enthalpy check was performed using indium. The heat of fusion for indium was calibrated to be within 10% of its reference value. A simple baseline subtraction was conducted to eliminate the unnecessary curvatures within the heat flow curve.

2.3. Fire Propagation Apparatus (FPA)

Similar to the Cone Calorimeter (Cone, ASTM E 1354[8]), the Fire Propagation Apparatus (FPA, ASTM E 2058[9]) is a bench-scale fire test apparatus in which the sample is heated by four radiant lamps as opposed to using an electrically heated coil as a radiant source as in the Cone. There are 6 bulbs within one IR lamp that consist a tungsten wire in argon gas. These bulbs emit with a narrow energy spectrum where the peaks are 1.15 and 0.89 microns [10]. Based on experimental analysis, the lamps are known to provide a uniform heat flux that

is steady within 5kW/m^2 over the specimen surface of up to 60kW/m^2 . A long quartz tube is used to create a desired atmosphere. The atmosphere may be controlled from nitrogen to 40% enhanced oxygen condition. A flow rate of 100 or 200 lpm is run through the bottom of the air chamber depending on the purging gas and therefore the sample is in a flow field during the test. The FPA can be used to calculate useful engineering data such as carbon dioxide generation based heat release rate (based on the standard), mass loss rate, smoke yield and smoke extinction coefficient.

The purpose of FPA testing was to generate good data sets appropriate for pyrolysis modelling and parameter estimation, and therefore several modifications were made to the standard testing procedure. First, when testing the polyester FRPs, an insulated sample dish purposed by de Ris and Khan [11] was used instead of the standard specified, non-insulated aluminium dish (see Figure 2). In this sample dish, the sample is surrounded by Cotronics® paper insulation on the back and sides to limit heat loss, which simplifies the pyrolysis modeling. Second, 4 thermocouples were installed to measure temperature change of the sample at various depths: surface, 1/3, 2/3 and back face of the sample. The installation of thermocouples on the sample was consistent with the method introduced in Composites 2007 paper [1]. Based on experimental analysis, a zone of uniformity with regards to temperature and heat flux was found to be within 32 mm (1.25 in.) radius from the center of the specimen and therefore, all four thermocouple beads were located within this zone. Thermocouple holes were drilled at 1/3 and 2/3 of the sample thickness with a 1.25 mm diameter drill bits. Thermal grease (OmegaTherm Thermally Conductive Silicone Paste, Model OT-201 from Omega Engineering) was inserted along with the thermocouples (Omega Precision Fine Wire Thermocouples, Model 5TC-GG-K-30-36 from Omega Engineering) to reduce the air gaps within the thermocouple holes. The surface and back face thermocouples were affixed with a high temperature adhesive (Resbond 907 Industrial Strength Fireproof Adhesive from Cotronics Corp.) and Crazy glue, respectively. Third, carbon black was applied on the sample surface to allow radiation to be absorbed on the surface of the sample. This approach was taken because the samples (1A and 1C) were somewhat transparent and when tested in the FPA, in-depth absorption of radiation occurred. To incorporate in-depth absorption of radiation into the model requires more parameters than assuming only surface absorption. Therefore, to minimize the number of parameters that need to be optimized, carbon black was used which, should allow surface radiation absorption only. All of the tests were conducted under nitrogen to eliminate the effect of oxidation in the resin degradation kinetics and flame. Limiting the environment to only nitrogen allowed for more simplified kinetics modeling for the resin degradation as well as the pyrolysis modeling of the composite.

The uncertainty for the mass loss rate (MLR) and thermocouple measurements were determined via statistical analysis performed on data from tests with identical conditions. All uncertainties listed in this study are full scale (as opposed to \pm half scale). The uncertainty of MLR for the FPA was determined as 17mg/s (2.4g/sm^2) by comparing three PMMA tests performed at 50kW/m^2 based on the standard which calls for three identical tests to be performed to correctly determine other properties [10]. The uncertainty in the thermocouple measurements was quantified by comparing back face temperature data from four identical 1C tests in the FPA. Temperature measurement at the back face of the sample surface was chosen because the exact measurement location is known, i.e. the sample thickness. Other temperature measurements made in various depths have a positional uncertainty of ± 0.625 mm associated with the data. This uncertainty is from the drill bit used to make holes for thermocouple installations, which had a thickness of 1.25mm diameter. Using the normalized time, time divided by sample thickness square, i.e., $\tau = \text{time}/\delta^2$ to remove the effect of different sample thicknesses when comparing, the maximum deviation at various normalized times, up to the critical time, τ_c , was 16°C . The critical time, τ_c , corresponds to the time when evenly spread flame on sample surface disappearing when tested under air. Test data presented in this parameter estimation exercise study is truncated at this critical time of 4 s/mm^2 because the pyrolysis model is set up with a one-dimensional assumption, which may not be used when flames on the sample surface is not evenly distributed, typically where edge burning is dominant. These uncertainty values will be used to evaluate significant differences in the modeling results

3. Pyrolysis Modeling for Lumped (TGA) and Slab (Cone or FPA) Experiments

The calculations reported here are conducted with a generalized pyrolysis model [3,4] that can be applied to a wide variety of condensed phase fuels. The model simultaneously calculates the condensed phase mass conservation, gas phase mass conservation, condensed phase species conservation, and condensed phase energy conservation equations. This model can be applied to both 0D and 1D systems and is therefore capable simulating both “lumped” (thermogravimetric) and “slab” (Cone Calorimeter/FPA) experiments. Extensive details are given in Ref. [3,4] so only a brief overview is given here. Assumptions inherent in the model, as applied in this paper, include:

- Porosity can either be solved as a property of a species (default) or directly. When porosity is solved directly, it is derived from the condensed-phase mass conservation equation assuming no volume change (shrinkage or swelling).

- When porosity is directly solved, the user-specified thermal conductivity and density are interpreted as those of a nonporous solid. Therefore, the thermal conductivity that appears in the condensed-phase energy conservation equation is $\bar{k} = (1-\psi)\bar{k}_s$ where ψ is porosity and \bar{k}_s is the weighted thermal conductivity of the solid assuming it is nonporous. Similarly, with this formulation, the bulk density is calculated as $\bar{\rho} = (1-\psi)\bar{\rho}_s$ where $\bar{\rho}_s$ is the weighted density of the solid assuming it is nonporous.

- Bulk thermal conductivity \bar{k} has a cut-off value of 0.03W/mK which corresponds to air at 300 to 400K.

- Specific heat is calculated with a weighted or averaged quantity, i.e. $\bar{c}_p = \sum X_i c_{p_i}$ as other solid properties – enthalpy, emissivity, radiation absorption coefficient, permeability, etc.

- Specific heat capacity and effective thermal conductivity vary by as $k(T) = k_0(T/T_r)^{n_k}$ and $c(T) = c_0(T/T_r)^{n_c}$, respectively, where T_r is a reference temperature.

- Radiation heat transfer across pores is accounted for by adding a contribution to the effective thermal conductivity that varies as γT^3 , where γ is a fitting parameter

- Averaged properties in conservation equations are calculated by appropriate mass or volume fraction weighting

- All gases escape to the exterior ambient with no resistance to heat or mass transfer

- Negligible heat transfer between the gas phase and the condensed phase inside the decomposing solid

- There is no net shrinkage (volume change) due to reactions or bulk density changes

-

4. Results and Discussion

4.1. Kinetics of resin degradation

Typically in kinetic studies, the isothermal rate of degradation or conversion, da/dt , is assumed to be a linear function of the temperature dependent rate constant, $k(T)$, and a temperature independent function of the conversion, $f(\alpha)$, where α indicates the conversion. This equation can be further expanded by using the Arrhenius

expression for the rate constant. Within the Arrhenius expression, two more reaction dependent constants are introduced: the pre-exponential constant, Z , and the activation energy, E_a . The temperature independent function of the conversion, $f(\alpha)$ is dependent upon the mechanism of chemical reactions.

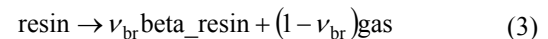
$$\frac{d\alpha}{dt} = f(\alpha)Z \exp\left(-\frac{E_a}{RT}\right) \quad (1)$$

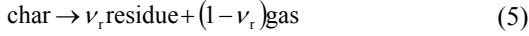
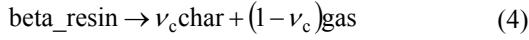
Substituting the linear heating rate $\beta = dT/dt$ into Eq. (1) and taking the natural logarithm of both sides gives the following:

$$\begin{aligned} \ln \frac{d\alpha}{dT} &= \ln \left(\frac{f(\alpha)}{\beta} Z \exp\left(-\frac{E_a}{RT}\right) \right) \\ &= \ln \left(\frac{f(\alpha)Z}{\beta} \right) - \frac{E_a}{RT} \end{aligned} \quad (2)$$

The iso-conversional method, also known as the model-free method is used to find the minimum number of elementary reactions necessary to describe the global degradation kinetics of the resin. This method uses data tested from different heating rates. Knowing that at a constant conversion, α , da/dt and $f(\alpha)$ become constants. With these terms in Eq.(2) remaining as constants, the E_a is found without the pre-knowledge of the reaction mechanisms. The iso-conversional method will give constant activation energies, E_a , over the range of conversion of interest if the reaction is a single-step chemical reaction. If the activation energies, E_a , changes significantly with respect to different conversions, this is an indication for a more complex reaction mechanism.

In Figure 3, the results from two iso-conversional methods introduced by Ozawa, Flynn and Wall [12,13] (OFW, finding a constant slope of $-E_a/R$ by plotting $\ln(\beta)$ versus $1/T$) and Friedman [14 , 15] (plotting $\ln(da/dT)$ versus $1/T$ to find the slope of $-E_a/R$) conducted on the polyester resin are shown. Both methods are used for comparison purposes. The r-square values for each activation energy value are plotted as well using least square method. The activation energy becomes more reliable as the r-square values become closer to 1. The conversion is calculated as $\alpha = 1 - m/m_0$. As shown in Figure 3, the estimated activation energy ranges from 70 ~ 145 kJ/mol in $0 < \alpha < 0.20$, relatively steady around 120 ~ 145 kJ/mol in $0.20 < \alpha < 0.93$ and 145 kJ/mol and above in $0.93 < \alpha < 1.0$. Based on this result, one can approximate a minimum of three elementary reactions to model the full degradation over $0 < \alpha < 0.97$ range.





The proposed mechanism is consistent with previous research [16,17,18] conducted for unsaturated polyester thermoset resins. In addition to this three steps mechanism, a single step degradation mechanism of resin becoming char and releasing fuel gas (93% weight loss) is modeled and compared to evaluate the necessity of multiple reaction steps. Applying these degradation mechanisms, a model fitting method [19] is used where $f(\alpha)$ is preselected to fit the TGA experiment data to find the kinetic parameters with the best fitness. In this study, a conversion function $f(\alpha) = (1 - \alpha)^n$ is used, which is typically applied for phase boundary reactions. The data fitting software used in this study is Genetic Algorithm (GA) coupled with the pyrolysis model for lumped experiments explained in the previous section. The GA was developed based on the mechanics of the Darwinian survival-of-the-fittest theory [3,4,20].

The results found from model fitting exercise are summarized in Table 1 and plotted in Figure 4. As shown in Figure 4, using three steps when modeling the resin degradation gives better fitness of the estimated mass loss rate to the actual TGA experiment data. When three steps are used instead of one, the initial mass loss that starts from 200°C is captured while the temperature needs to increase up to 300°C to initiate any mass loss when using one step reaction (see total mass loss rate in (a) and (c) of Figure 4). In addition to the earlier stage of degradation, better fitness is shown after 400 °C for the three steps reactions case than that of one step where mass loss rate is expected to rapidly decrease. The total mass loss rate peak observed in ~400°C range spreads over a wider temperature range when a single step reaction is used for resin degradation. This is due to the unresolved initial mass loss when using single step reaction. An additional mass loss is given at the end of the major mass loss peak after 400°C to compensate for the initial mass loss which should have existed before 200°C. However, these differences in mass loss rate found from applying two resin decomposition mechanisms – three steps vs. single – are subtle. Comparing the difference at various heating rates emphasizes more that the effect of changing resin degradation mechanism from 3 steps to single is insignificant (see (b) and (d) of Figure 4).

4.2. Property estimation for FRP composite using polyester composite with low glass content (1A)

The property estimation for the polyester composite is conducted by coupling a generalized pyrolysis model for slab experiments developed by Lautenberger and the

Genetic Algorithms (GA) for optimization routine [3,4,20]. To reduce the number of parameters to estimate, the FPA experiments for the polyester composite with low glass content, 1A were conducted with certain approaches. For example, carbon black powder was applied on top of the sample surface to eliminate in-depth absorption of radiation. FPA tests were conducted under nitrogen environment to exclude the effect of oxidative decomposition of the resin and flame. Experimental data used in the estimation exercise was truncated when normalized time, time divided by sample thickness square, i.e., $\tau = \text{time}/\delta^2$ became approximately 4 s/mm². This time is noted as the critical time, τ_c , for a typical 1A sample when the pyrolysis can no longer be simplified as a one-dimensional problem. The critical time, τ_c , is identified as time of evenly spread flame on sample surface disappearing when tested under air, where edge burning is dominant. Additionally, for further simplification of the problem when modeling, the backface temperature measurement was used as a boundary condition for the condensed phase.

The parameter estimation exercise was conducted for the following two cases: (1) GA1 where the heterogeneous microstructure was incorporated and three steps mechanism for resin decomposition was used; (2) GA2 where a single layer was constructed as a homogeneous structure based on resin and glass weight proportion within the composite and three steps mechanism for resin decomposition was used. For both cases, the same set of parameters is optimized, which are listed in Table 2 along with the estimation results. These parameters were introduced in Section 3 where a brief description of the pyrolysis model used in this study [3,4] is given. The kinetic parameters for resin degradation were predetermined as described in the previous section. However, the heats of reaction for the three elementary reactions were estimated through parameter estimation exercise as other thermophysical properties, but with its searchable range for optimization set based on Differential Scanning Calorimeter (DSC) experiment results on the polyester resin. Note that the heat of reactions were proportioned to reflect the kinetic modeling, i.e. the first, second and third reactions consumes 20%, 73% and 8% of the total enthalpy, respectively, which is identical to the resin weight loss percentages in each reaction step. The total number of parameters that was found via optimization was 29 including the heat of reactions. These estimations are used as two different baselines – GA1 and GA2 – for pyrolysis modeling study discussed in the next section. In Table 2, the estimation of GA1 and GA2 are compared to show how consistent the estimations are. It shows that most of the estimated values of GA2 have a difference of less than 30% when compared to those of GA1, which allows constructing some level of confidence in the optimizing capability of the Genetic Algorithms. Although the comparison has been made for individual parameter estimations and shown that results

from GA1 and GA2 are somewhat consistent, one should take into account that the Genetic Algorithm optimizes for a group of these individual estimations that gives the best fit to the mass loss rate and temperature data measured at four locations. When compared in groups, typically it shows that a change occurred in one parameter is compensated by a change found from the other. Hence, comparing the pyrolysis modeling results using the estimations from two different set-ups (GA1 and GA2) in groups should present a better sense of optimization consistency.

Using the estimated properties found from GA1 and GA2 conditions, four cases (as summarized in Table 3) for 1A (sample with low glass content) are modeled to check the fitness of the optimization and compare cases with various modeling conditions (see Figure 5 and Figure 6). These cases are constructed based on applying different assumptions for the microstructure of the composite (heterogeneous or homogeneous) and degradation mechanism (3 steps or single). For every case, the pyrolysis modeling results of mass loss rate and temperatures from surface, 1/3, 2/3 of sample thickness from surface, and backface are plotted with the actual experimental data. The parameter estimations from GA1 and GA2 set-ups should give the best fit for case 1 and case 2, respectively because the optimization was performed based on the corresponding conditions.

In general, from Figure 5 and Figure 6 one can conclude that the parameter estimations for 1A with two set-ups – GA1 and GA2 – were conducted properly and that the two baselines are nominally equivalent knowing that both modeling results are in a good agreement with the actual experiment data within the uncertainty stated for the experiment (17mg/s and 16°C for mass loss rate and temperature measurements, respectively). This also demonstrates that the parameter estimations for GA1 and GA2 conditions are consistent. In both figures, (a) shows that modeling the mass loss rate had improved qualitatively when microstructure of composite was incorporated as an input (case1 and case3) as oppose to simply assuming as a homogeneous material (case 2 and case 4). However, note that quantitatively the changes should be considered as insignificant taking into account for the uncertainty of 17mg/s. The mass loss rate data shown in the figures were applied with Fast Fourier Transform (FFT) smoothing, which resulted in artificial oscillations with magnitude in the order of 0.01g/s. Therefore, the actual mass loss rate has an initial peak before $\tau = 1$, another smaller peak following around $\tau = 1.4$ with a decreasing trend up until $\tau = 1.8$, and a slowly increasing trend from that point to $\tau = 4$. The minimal point in the mass loss rate data near $\tau = 1.8$ is possibly due to pyrolysis proceeding through the prominent glass layer after decomposing through the resin rich layers. The model was able to capture the large oscillations in the beginning and the decreasing trend followed by an

increasing trend near $\tau = 1.8$ in the mass loss rate generated by pyrolyzing through different layers composed of an alternating decomposable resin and inert glass layers. The simulated temperature results follow well with the actual tests data for all four cases. Note that even with this comparison made without incorporating the positional uncertainty of ± 0.625 mm for the in-depth thermocouple installation to the temperature measurement uncertainty band, the simulation and actual test data show a good agreement (see (c) and (d) in Figure 5 and Figure 6). The simulation and actual data for backface temperature is shown in (e) in Figure 5 and Figure 6 as a check to confirm they match perfectly knowing that this was used as a boundary condition in the simulation. Changing the resin decomposition mechanism from 3 steps to a single step had an insignificant effect on the simulation results, which is consistent with the results found from kinetic modeling analyses performed in the previous section.

Based on the findings from above analyses, one can conclude the following: (1) Optimization for parameter estimation using pyrolysis model with GA was conducted with satisfaction in terms of mass loss rate and temperatures at various depths (surface, 1/3 and 2/3 in-depth from surface, and backface) for both conditions with consistency – GA1 and GA2. Quantitatively, the two baselines are nominally equivalent considering the uncertainty associated with the experimental data. (2) Incorporating the microstructure of the composite improves the mass loss rate simulations in terms of resolving the detailed oscillations and following the trend qualitatively but has less impact on sample temperature predictions. (3) Applying 3 steps resin decomposition mechanism than a single step has subtle influence in the modeling results.

4.3. Evaluation for estimated properties

To evaluate the correctness of the property estimation, modeling of the same composite as 1A but with higher glass content designated as 1C is conducted. The parameter estimation using 1A pyrolysis FPA test data was for the resin and glass. In theory if the parameter estimation was conducted properly, one should be able to model a composite that is produced with the same type of resin and glass using the estimation as an input to the pyrolysis model with the degrees of satisfaction which was found from comparing the modeling results for 1A as shown in Figure 5 and Figure 6.

Four cases as in Table 3 for 1C with two baselines – GA1 and GA2 – are simulated using the estimated properties found from 1A. The results are shown in Figure 7 and Figure 8 where mass loss rate and temperature measurements from surface, 1/3 and 2/3 of sample thickness from surface, and backface are plotted with experimental data. As it was with 1A simulations, applying

GA1 or GA2 as a baseline have an insignificant effect on the 1C modeling results. In both Figure 7 and Figure 8, (a) shows that the simulation results of case 2 and 4 (homogeneous structure with 3 steps or single step resin decomposition mechanism assumptions) have the better fit to the actual test data considering the uncertainty of 17mg/s than those of case 1 and 3 (heterogeneous structure with 3 steps or single step resin decomposition mechanism assumptions). Although incorporating the microstructure of the composite (assuming heterogeneous) does allow the model to resolve the oscillations in the mass loss rate curve due to pyrolysis through resin and glass alternating layers (case 1 and case 3), this phenomenon is not observed from the experiment. The difference of modeled temperatures at various depths and those from the actual experiment are within the measurement uncertainty and the positional uncertainty of ± 0.625 mm for the 1/3 and 2/3 in-depth thermocouple bead where temperature is actually measured (see (b) through (d) in Figure 7 and Figure 8). The positional uncertainty associated with the 1/3 and 2/3 in-depth thermocouple location is interpreted in the context of the simulation results. This is conducted by comparing the simulated temperatures from the exact 1/3 and 2/3 locations as well as temperatures at ± 0.625 mm from the exact locations. The simulation and actual data for back-face temperature is shown in (e) in Figure 7 and Figure 8 as a check to confirm they are identical knowing that this was used as a boundary condition in the simulation. Similar to 1A simulation results, using either 3 steps or a single step for the polyester resin decomposition mechanism was irrelevant in terms of simulating mass loss or temperature changes of 1C.

Comparing the results from pyrolysis modeling of 1C (see Figure 7 and Figure 8) to those of 1A (see Figure 5 and Figure 6), one can find that the major difference is observed from the mass loss rate simulations. In 1C simulations, for both GA1 and GA2 conditions, incorporating the microstructure of the composite have a negative effect on the mass loss rate simulation while it has a positive effect qualitatively when simulating 1A. To find a plausible explanation for this difference, additional pyrolysis modeling numerical experiments were conducted for 1C. For these numerical experiments, minor adjustments to the 1C microstructure were made for the following reason. More uncertainty is introduced when 1C microstructure is estimated visually than for 1A because in 1C (average thickness of 6 ~ 7 mm) more layers are added to a thinner sample comparing to 1A (average thickness of 10 mm). As shown in (a) of Figure 7 and Figure 8, the simulation with heterogeneous structure allows an over-prediction of the mass loss rate between $\tau = 1$ and 2 and under-prediction between $\tau = 2$ and 3. This indicated that the proposed microstructure (see Figure 1) for 1C used in the model had more resin on surface than actual followed by layers with more glass than actual. Therefore, when running the model, slight modi-

fication was made to the 1C microstructure near the surface within 0.5 mm to resolve the identified problem but the global density was maintained to 40 wt% resin and 60 wt% glass. The simulation results are shown in Figure 9. As shown in this figure, using the same estimated parameters the mass loss rate simulation can be improved without negatively affecting the temperature agreement by simply adjusting the microstructure only to a minimal degree. Therefore, it shows that the simulation agreement with the actual data is sensitive to the microstructure as oppose to the parameter estimation was poorly conducted.

To check whether the estimated parameter values from this study are consistent with other references [1,5], a comparison is made for the conductivities and the specific heat capacities of the virgin composite (resin and glass), decomposed composite (char and glass) and fully decomposed composite (glass only). An artificial composite is made with 30 wt% of resin and 70 wt% of glass with the estimated parameters from 1A FPA pyrolysis tests to directly compare the values found from Lattimer's paper [5] where conductivities and heat capacities are experimentally evaluated for a glass reinforced vinyl ester composite found from different stages of pyrolysis. The method used to determine the thermal properties found from Lattimer's work incorporates the effects of voids and cracks generated during pyrolysis. Therefore, effective thermal conductivity and heat capacity are used to compare with Lattimer's data, which are calculated based on volume fraction including the properties of the voids as gas. In addition to Lattimer's data, thermal properties estimated for 1A and 1Cs by Avila [1] are plotted for more comparison. As shown in Figure 10, the effective thermal properties calculated from estimated parameters using 1A test data for both GA1 and GA2 conditions are consistent with other reference values. The average deviation of the estimations found from this study is within 50% of those of Lattimer and Avila for conductivity and heat capacity.

5. Conclusions and Future Work

A property estimation exercise for pyrolysis modeling is conducted on unsaturated polyester FRP composites with low glass content (1A). To properly model the pyrolysis of the composite, kinetic modeling of the resin degradation was performed using TGA and DSC experiment data on the resin. Using an iso-conversional method (also known as model-free method), the minimum number of elementary reactions required to describe the full degradation mechanism was proposed. Based on this analysis, three steps mechanism was constructed. In addition to this three steps mechanism, a single step case was also investigated to compare the effect of using a more complicated approach than a simple one step on the overall pyrolysis modeling and property

estimation. With a pre-known reaction mechanism, a model fitting method was used to find the kinetic parameters for each reaction.

Property estimation for unsaturated polyester FRP composite was conducted using the 1A FPA pyrolysis test data with a generalized pyrolysis model, Gpyro paired with an optimization routine known as Genetic Algorithm (GA). Two conditions were used to construct a baseline – (1) GA1 where the heterogeneous microstructure was incorporated and three steps mechanism for resin decomposition was used; (2) GA2 where a single layer was constructed as a homogeneous structure based on resin and glass weight proportion within the composite and three steps mechanism for resin decomposition was used. Independent of applying one of these conditions, the estimation was conducted for the same set of parameters for resin and glass as summarized in Table 2.

The estimated values were used to model 1A to verify the fitness of the optimization and compare cases with different microstructures (heterogeneous or homogeneous) and kinetic mechanisms (3 steps or single step), which are designated as case 1 through 4. For both GA1 and GA2 conditions, the parameter optimization results showed that the pyrolysis modeling was conducted with satisfaction in terms of mass loss rate and temperatures at various depths (surface, 1/3 and 2/3 in-depth from surface, and backface). It also demonstrated that whether applying GA1 or GA2 conditions as a baseline, the simulation results are nominally identical quantitatively considering the uncertainty of the experiment data, however, estimation based on GA1 and GA2 conditions are consistent. The pyrolysis modeling results qualitatively showed that incorporating microstructure of the composite when modeling allows the model to resolve oscillations in the mass loss rate. Changing the kinetics mechanism had a subtle influence for modeling this composite.

To evaluate whether the estimation can represent the components of the composite, resin and glass, a pyrolysis modeling is conducted for a polyester FRP composite with higher glass content (1C) than 1A. The results show a relatively good agreement to the actual test data except for the mass loss rate. Although for 1A applying the heterogeneous microstructure to the modeling did improve the simulation results, it did not for 1C modeling. A reasonable explanation for this poor estimation is due to the uncertainty in the microstructure of 1C near the surface rather than poorly conducted parameter estimation. In addition to 1C modeling, estimated conductivity and heat capacity values are compared with those of other references and confirmed that it was consistent within 50%.

In this study, the work demonstrates the possibility of constructing a virtual experiment for composites using a bench-scale pyrolysis test and thermal analysis experi-

ment data. Using one type of composite (1A), an optimization of parameters was conducted and those estimations were used to model a different type of composite (1C). In the future, the work will be expanded to cases where fire retardant additives have an effect to the degradation kinetics of the composite and composites are decomposing in an oxidative condition such as air. The goal of the work will be to develop an approach that is consistent and simple when performing parameter estimation and modeling for different types of composites in various conditions.

Acknowledgments

The authors would like to thank Charles Dore for fabricating and donating the polyester FRP composite materials used in this study. Many thanks also to Randall Harris, William Wong and Haejun Park at WPI for assisting the FPA tests.

Reference

- ¹ Avila, Melissa B., Dembsey, Nicholas A., Kim, Mihyun E., Lautenberger, Chris, Dore, Charles, Fire Characteristics of Polyester FRP Composites with Different Glass Contents, *Composites & Polycon 2007*, American Composites Manufacturers Association, October 17-19, 2007
- ² Standard Methods of Test for Measurement of Synthetic Polymer Material Flammability Using a Fire Propagation Apparatus (FPA), ASTM E 2058-03, ASTM, 100 Barr Harbor Drive, West Conshohocken, PA, U.S.
- ³ Lautenberger, C., "A Generalized Pyrolysis Model for Combustible Solids", Ph.D. Dissertation, Department of Mechanical Engineering, University of California, Berkeley, Fall 2007
- ⁴ Lautenberger, C., Gpyro – A Generalized Pyrolysis Model for Combustible Solids Users' Guide, Version 0.609, July 23, 2008
- ⁵ Lattimer, Brian Y., Ouellette, Jason, Properties of composite materials for thermal analysis involving fires, *Composites: Part A 37* (2006) 1068–1081
- ⁶ Lewin, M., "Synergism and Catalysis in Flame Retardancy of Polymers", *Polym. Adv. Technol.* 12, 215-222 (2001)
- ⁷ Standard Test Method for Surface Burning Characteristics of Building Materials, ASTM E 84-05, ASTM, 100 Barr Harbor Drive, West Conshohocken, PA, U.S.
- ⁸ Standard Test Method for Heat and Visible Smoke Release Rates for Materials and Products Using an Oxygen Consumption Calorimeter, ASTM E 1354-02, ASTM, 100 Barr Harbor Drive, West Conshohocken, PA, U.S.
- ⁹ Standard Methods of Test for Measurement of Synthetic Polymer Material Flammability Using a Fire Propaga-

tion Apparatus (FPA), ASTM E 2058-03, ASTM, 100 Barr Harbor Drive, West Conshohocken, PA, U.S.

¹⁰ User's Guide for the Fire Propagation Apparatus (FPA) ASTM E-2058, Fire Testing Technology Limited, PO Box 116, East Grinstead, West Sussex, England.

¹¹ de Ris, J.L. and Khan, M.M., "A sample holder for determining material properties," *Fire and Materials*, 24, 219-226 (2000).

¹² Ozawa, T., *Bull Chem Soc Jpn* 1965;38;188

¹³ Flynn, J., Wall, L.A., *J Polym Lett* 1966;4:232

¹⁴ Friedmen, H.L., *J Polym Sci Part C* 1964;6:183

¹⁵ Friedmen, H.L., *J Polym Lett* 1966;4:232

¹⁶ Chrissafis, K., Paraskevopoulos, K.M., Bikiaris, D.N., Thermal degradation kinetics of the biodegradable aliphatic polyester, poly(propylene succinate), *Polymer Degradation and Stability* 91 (2006) 60-68

¹⁷ Y. S. Yang and L. James Lee, Microstructure formation in the cure of unsaturated polyester resins *Polymer, Volume 29, Issue 10, October 1988, Pages 1793-1800*

¹⁸ Chiu, H.T., Chiu, S.H., Jeng, R.E., Chung, J.S., A study of the combustion and fire-retardance behaviour of unsaturated polyester/phenolic resin blends, *Polymer Degradation and Stability* 70 (2000) 505-514

¹⁹ Burnham, A.K., Weese, R.K., Kinetics of thermal degradation of explosive binders Viton A, Estane, and Kelf, *Thermochimica Acta* 426 (2005) 85-92

²⁰ Rein, G., Lautenberger, C., Fernandez-Pello, C., Toro, J.L., Urban, D.L., Application of genetic algorithms and thermogravimetry to determine the kinetics of polyurethane foam in smoldering combustion, *Combustion and Flame* 146 (2006) 95-108

Figures:

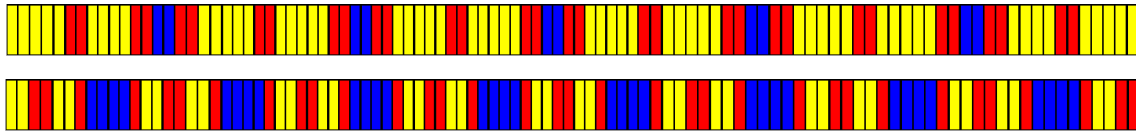


Figure 1: Approximation of three distinct layers – 100 wt% resin (yellow), 50-50 wt% resin and glass (red), and 100 wt% glass – in composite microstructure: Unsaturated polyester FRP with low glass content (1A, 33 wt% of glass, top) and with high glass content (1C, 60 wt% of glass, bottom)

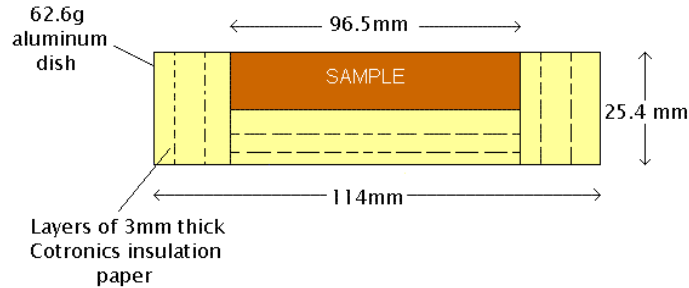


Figure 2: Insulated Sample Holder Designed by de Ris and Khan [11]

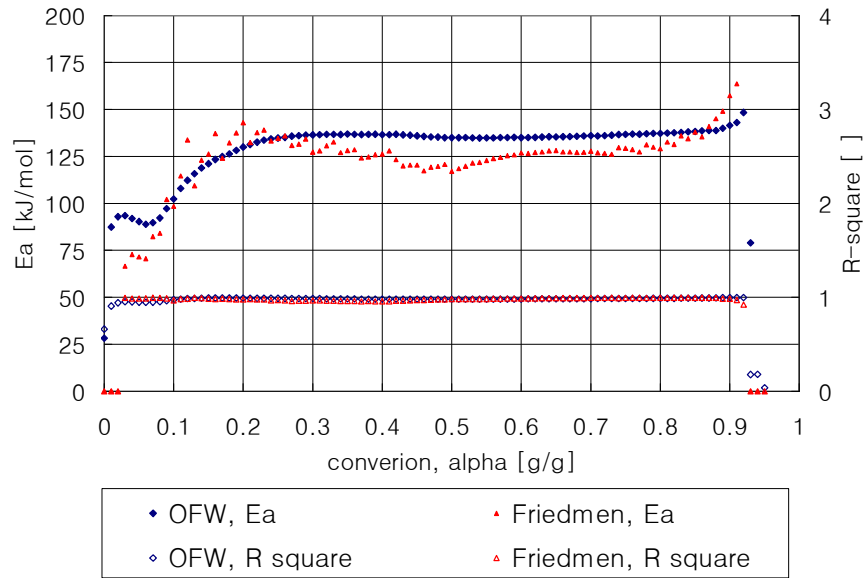


Figure 3: Estimated activation energy of unsaturated brominated polyester resin calculated via “isoconversional” (model free) method

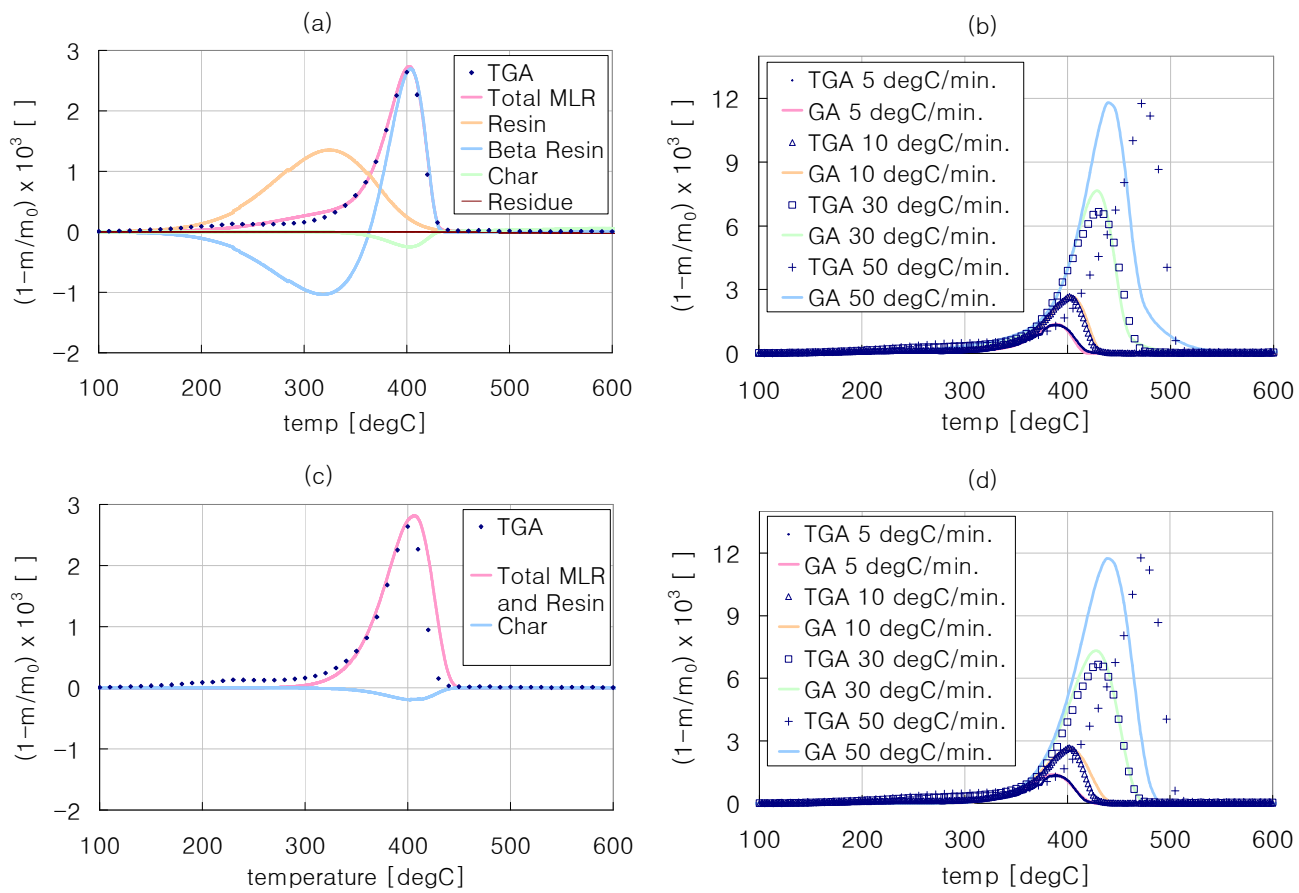


Figure 4: Kinetic parameters estimated for brominated, unsaturated polyester resin: 3 steps mechanism with nth order kinetic model (a,b) and one step mechanism with nth order kinetic model (c,d)

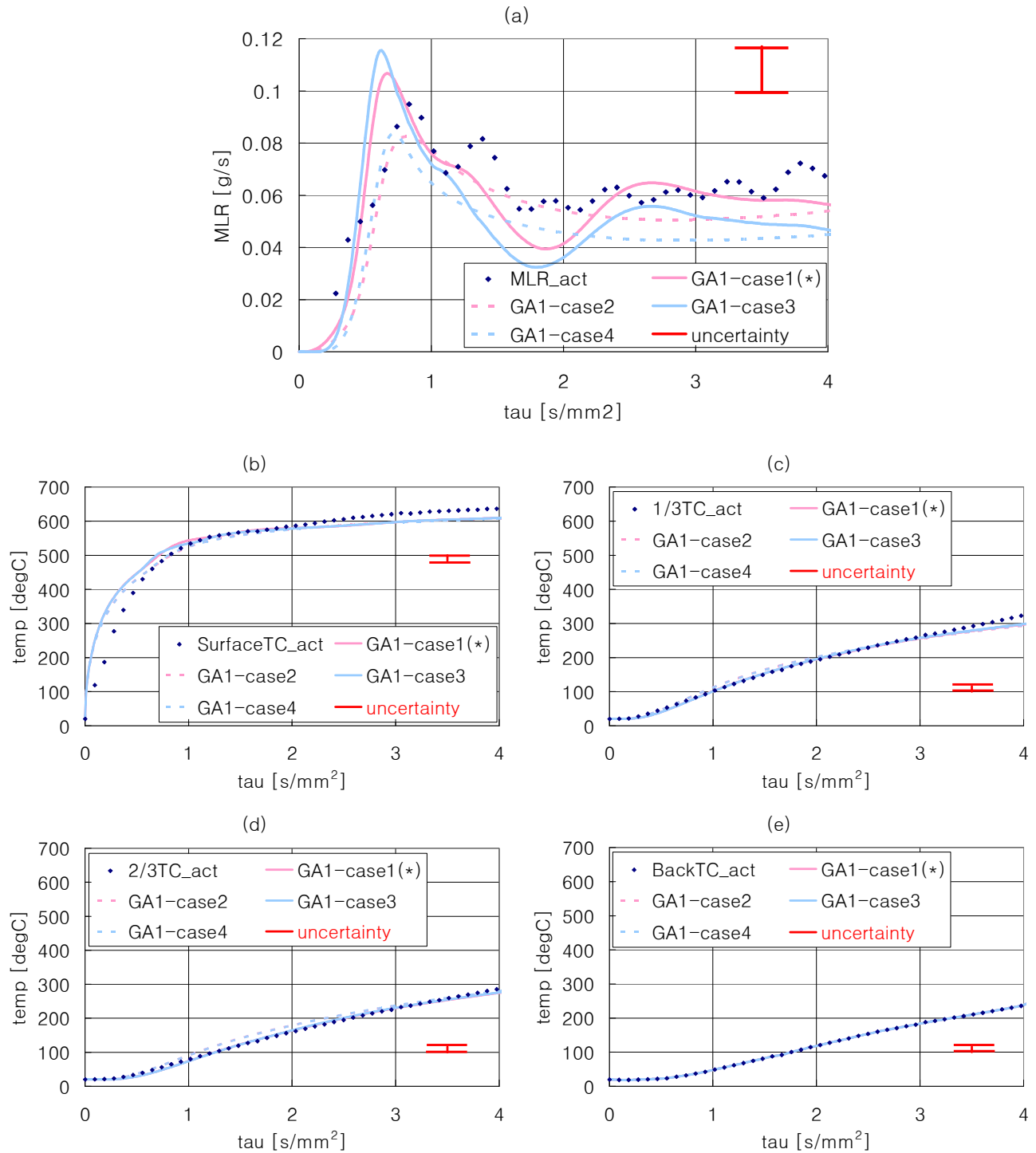


Figure 5. Parameter estimation GA1 results for brominated, unsaturated polyester composite with low glass content (1A) – heterogeneous microstructure and 3 steps degradation mechanism (case1, * indicates this condition is identical to that of GA1); homogeneous structure and 3 steps degradation mechanism (case2); heterogeneous microstructure and a single step degradation mechanism (case3); homogeneous structure and a single step degradation mechanism (case4) – (a) Mass loss rate; (b) Surface temperature; (c) 1/3 of sample thickness in-depth temperature from the surface; (d) 2/3 of sample thickness in-depth temperature from the surface; (e) Backface temperature

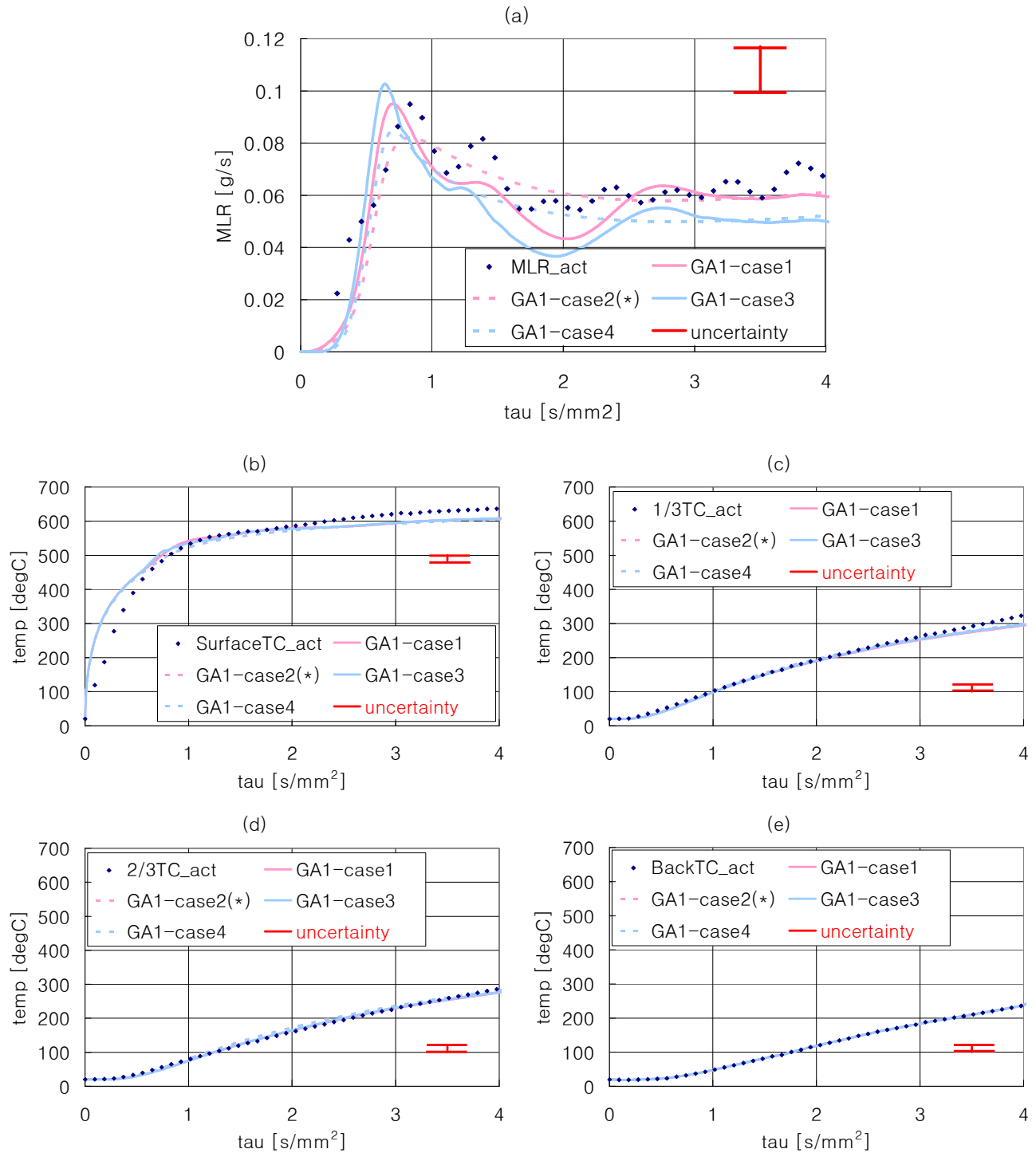


Figure 6. Parameter estimation GA2 results for brominated, unsaturated polyester composite with low glass content (1A) – heterogeneous microstructure and 3 steps degradation mechanism (case1); homogeneous structure and 3 steps degradation mechanism (case2, * indicates this condition is identical to that of GA2); heterogeneous microstructure and a single step degradation mechanism (case3); homogeneous structure and a single step degradation mechanism (case4) – (a) Mass loss rate; (b) Surface temperature; (c) 1/3 of sample thickness in-depth temperature from the surface; (d) 2/3 of sample thickness in-depth temperature from the surface; (e) Backface temperature

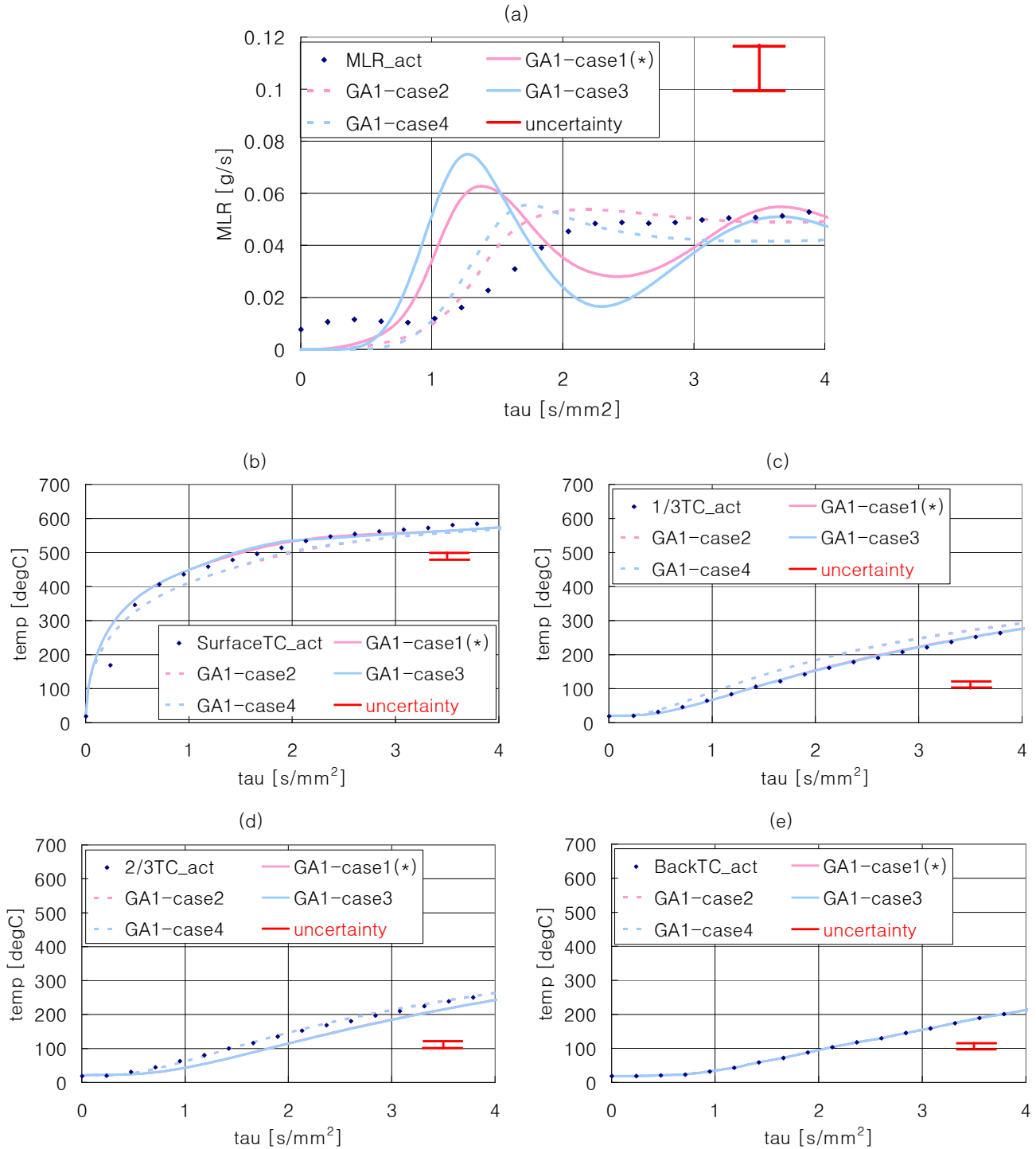


Figure 7. Pyrolysis modeling results for brominated, unsaturated polyester composite with higher glass content (1C) using estimations based on 1A (GA1) – heterogeneous microstructure and 3 steps degradation mechanism (case1, * indicates this condition is identical to that of GA1); homogeneous structure and 3 steps degradation mechanism (case2); heterogeneous microstructure and a single step degradation mechanism (case3); homogeneous structure and a single step degradation mechanism (case4) – (a) Mass loss rate; (b) Surface temperature; (c) 1/3 of sample thickness in-depth temperature from the surface; (d) 2/3 of sample thickness in-depth temperature from the surface; (e) Backface temperature

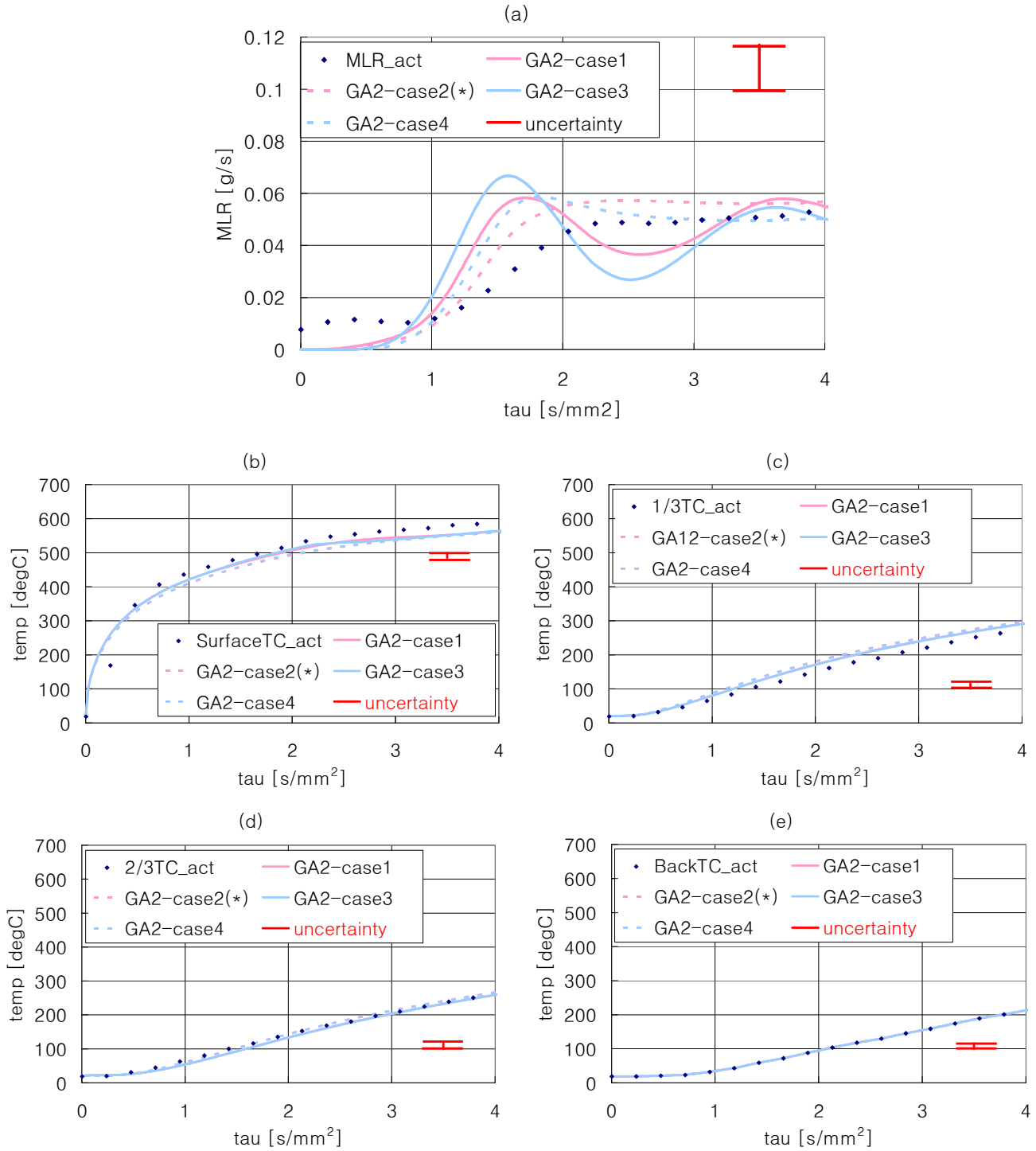


Figure 8: Pyrolysis modeling results for brominated, unsaturated polyester composite with higher glass content (1C) using estimations based on 1A (GA2) – heterogeneous microstructure and 3 steps degradation mechanism (case1); homogeneous structure and 3 steps degradation mechanism (case2, * indicates this condition is identical to that of GA2); heterogeneous microstructure and a single step degradation mechanism (case3); homogeneous structure and a single step degradation mechanism (case4) – (a) Mass loss rate; (b) Surface temperature; (c) 1/3 of sample thickness in-depth temperature from the surface; (d) 2/3 of sample thickness in-depth temperature from the surface; (e) Backface temperature

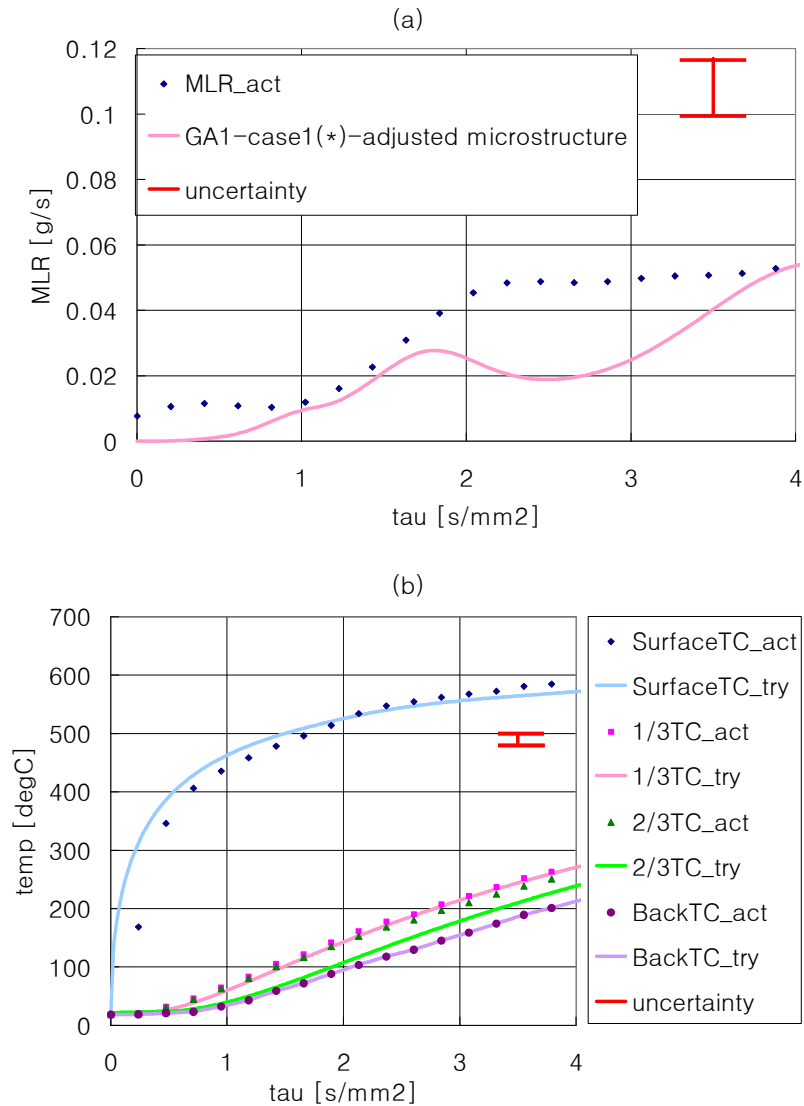


Figure 9. Pyrolysis modeling results for brominated, unsaturated polyester composite with higher glass content (1C) using estimations based on 1A (GA1) but with 1C microstructure near surface slightly adjusted to account for less resin – heterogeneous microstructure and 3 steps degradation mechanism (case1, * indicates this condition is identical to that of GA1) – (a) Mass loss rate; (b) Temperature comparisons at various depths (surface, 1/3 and 2/3 of sample thickness in-depth from the surface, and back-face temperatures)

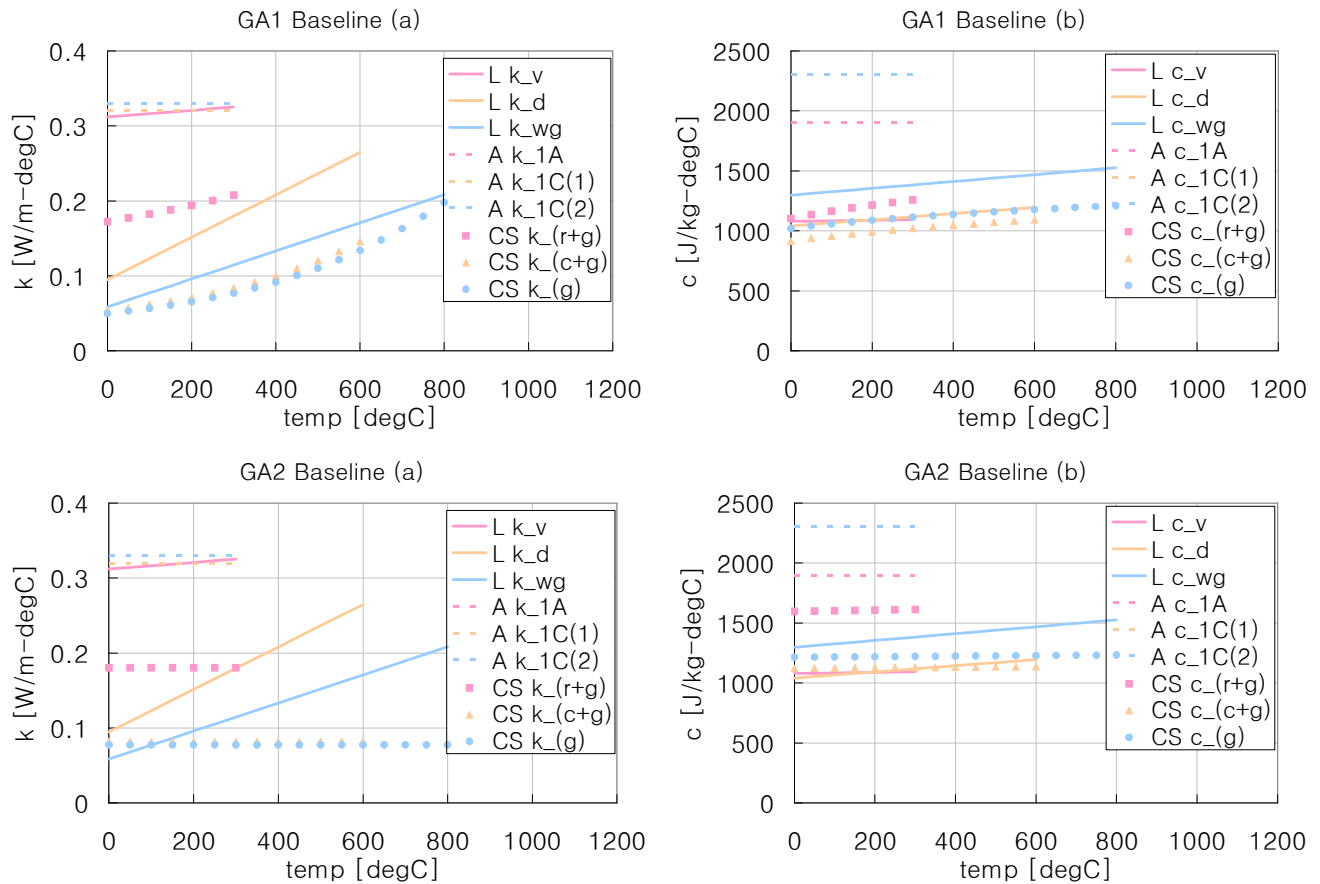


Figure 10: Estimated parameters with two different baselines – GA1 (heterogeneous structure with three steps of degradation kinetic model) and GA2 (homogeneous structure with three steps of degradation kinetic model) estimations – from current study (CS), conductivity, k and specific heat capacity, c for resin and glass (r+g), char and glass (c+g) and glass only (g) assuming constant volume compared with those from the work of Lattimer (L, estimation for virgin composite (v), decomposed composite (d) and woven glass only composite after fully degrading resin (wg)) and Avila (A, estimation for 1A and 1C composites, same samples used in this study).

Tables:

Table 1: Kinetic parameters estimated from model fitting exercise using Genetic Algorithm (GA): Three steps nth order kinetic model and single step nth order kinetic model

Kinetics	Z_1 (s-1)	E_{a1} (kJ/mol)	n_1 (-)	Z_2 (s-1)	E_{a2} (kJ/mol)	n_2 (-)	Z_3 (s-1)	E_{a3} (kJ/mol)	n_3 (-)
3 steps nth order	3.42×10^2	56.1	1.03	3.55×10^{11}	174.1	0.80	1.75×10^6	127.6	2.64
Single step nth order				4.92×10^9	151.4	0.90			

Table 2: Optimized thermophysical properties from 1A with heterogeneous assumption. For each material (resin, beta-resin, char, residue and glass) conductivity (k_0), conductivity temperature dependency (n_k), heat capacity (c_0), heat capacity temperature dependency (n_c), emissivity (ϵ) and the fitting parameter for radiation heat transfer across pores (γ) are estimated. Additionally, heat of reaction (ΔH) for three resin decomposition kinetic is estimated.

Species		ρ_0	k_0	n_k	c_0	n_c	ϵ	γ
		(kg/m ³)	(W/m-K)	(-)	(J/kg-K)	(-)	(-)	(m)
Resin	GA1	1350	0.304	0.082	1185	0.093	0.964	0.0000
	GA2		0.261	0.099	1237	0.206	0.969	0.0000
	GA1-GA2 /GA1 (%)		14.1	19.9	4.4	120.6	0.6	0.0
Beta resin	GA1	1080	0.317	0.080	1260	0.094	0.973	0.0000
	GA2		0.274	0.087	1318	0.207	0.965	0.0000
	GA1-GA2 /GA1 (%)		13.5	9.1	4.6	119.5	0.8	0.0
Char	GA1	95	0.163	0.326	1111	0.464	0.990	0.0046
	GA2		0.169	0.237	1029	0.246	0.991	0.0034
	GA1-GA2 /GA1 (%)		3.4	27.4	7.4	46.9	0.1	0.0
Residue	GA1	41	0.168	0.333	1061	0.481	0.985	0.0046
	GA2		0.176	0.236	956	0.247	0.980	0.0036
	GA1-GA2 /GA1 (%)		4.6	29.1	9.9	48.7	0.4	0.0
Glass	GA1	2600	0.064	0.328	1069	0.249	0.981	0.0034
	GA2		0.113	0.218	1072	0.194	0.982	0.0050
	GA1-GA2 /GA1 (%)		74.9	33.4	0.2	22.3	0.1	0.0
Heat of reaction ΔH (J/kg)		Degradation Reactions				GA1	GA2	GA1-GA2 /GA1 (%)
		resin $\rightarrow v_{br}$ beta_resin + (1 - v_{br})gas				3.1E+04	2.2E+04	29.9
		beta_resin $\rightarrow v_c$ char + (1 - v_c)gas				1.1E+05	8.0E+04	29.9
		char $\rightarrow v_r$ residue + (1 - v_r)gas				1.1E+04	8.0E+03	29.9

Table 3: Testing matrix for parameter estimation of 1A and pyrolysis modeling of 1C – GA1 (case 1: heterogeneous structure and three steps degradation kinetic model) and GA2 (case 2: homogeneous structure and three steps degradation kinetic model) are used to optimize the parameter estimation. Using the estimated values, cases 1 through 4 are simulated using a pyrolysis model [3,4].

Parameter Estimation	Pyrolysis Modeling	Microstructure	Resin Degradation Kinetics $f(\alpha) = (1 - \alpha)^n$
GA1	Case 1	Heterogeneous	3 steps
	Case 2	Homogeneous	3 steps
	Case 3	Heterogeneous	Single step
	Case 4	Homogeneous	Single step
GA2	Case 1	Heterogeneous	3 steps
	Case 2	Homogeneous	3 steps
	Case 3	Heterogeneous	Single step
	Case 4	Homogeneous	Single step

Appendix I

The Role of Decomposition Kinetics in Pyrolysis Modeling: Application to a Fire Retardant Polyester Composite

Fire Safety Science - Proceedings of the 9th International Symposium

The Role of Decomposition Kinetics in Pyrolysis Modeling – Application to a Fire Retardant Polyester Composite

CHRIS LAUTENBERGER¹, ESTHER KIM², NICHOLAS DEMBSEY², and CARLOS FERNANDEZ-PELLO¹

¹University of California, Berkeley
Department of Mechanical Engineering
Berkeley, CA 94720

²Worcester Polytechnic Institute
Department of Fire Protection Engineering
100 Institute Road
Worcester, MA 01609

ABSTRACT

This work assesses the effect of decomposition kinetics on overall pyrolysis behavior using experimental data from thermogravimetric analysis (TGA) and Fire Propagation Apparatus (FPA) experiments. TGA data are presented for an unsaturated brominated polyester resin (reinforcement free), and the FPA is used to investigate the pyrolysis behavior of a fiber reinforced polymer (FRP) composite slab with matrix comprised of the same resin tested via TGA. Three different kinetic models are fit to the TGA data: single-step n^{th} order, 3-step n^{th} order, and 3-step n^{th} order with one autocatalytic step. These kinetics models are then used to simulate the pyrolysis of a composite slab in the FPA, with thermophysical properties estimated by genetic algorithm optimization. It is shown that the two 3-step mechanisms provide nearly identical calculations of total mass loss rate (MLR) in the FPA, while the single-step mechanism provides similar, but quantitatively different, MLR predictions. Although no broad conclusions regarding the importance of multi-step thermal decomposition kinetics can be drawn on the basis of a single study, detailed reaction mechanisms may be superfluous unless TGA curves show multiple distinct reaction peaks and/or all thermophysical properties/model input parameters are precisely known.

KEYWORDS: modeling, heat transfer, pyrolysis, composites

NOMENCLATURE LISTING

c	specific heat capacity (J/kg-K)	β	heating rate (K/min)
E	activation energy (J/mole)	γ	radiant conductivity length (m)
h	specific enthalpy (J/kg)	δ	thickness (m)
h_c	convective heat transfer coefficient (W/m ² -K)	ε	emissivity (-)
ΔH	change in enthalpy (J/kg)	κ	radiant absorption coefficient (m ⁻¹)
k	thermal conductivity (W/m-K)	ρ	density (kg/m ³)
K	# of condensed phase reactions	σ	Stefan-Boltzmann constant (W/m ² -K ⁴)
m	mass (kg), autocatalytic exponent (-)	ϕ	generic variable
m''	mass per unit area (kg/m ²)	ψ	porosity
\dot{m}''	mass flux (kg/m ² s)	$\dot{\omega}'''$	volumetric reaction rate (kg/m ³ -s)
M	# of condensed phase species	Subscripts	
n	reaction order (-), property exponent (-)	d	destruction
N	# of gas phase species	f	formation
\dot{q}''	heat flux (W/m ²)	g	gaseous
\dot{Q}'''	volumetric heat release rate (W/m ³)	i	condensed phase species i
t	time (s)	j	gas phase species j
T	temperature (K)	k	reaction k
X	volume fraction (-)	r	reference or radiative
Y	mass fraction (-)	s	solid
z	distance (m)	vol	volatilization
Z	pre-exponential factor (s ⁻¹)	0	at $t = 0$ or $z = 0$
Greek		∞	ambient, or at the end of an experiment
α	conversion	δ	At $z = \delta$

INTRODUCTION

Bench-scale flammability tests such as the Cone Calorimeter and Fire Propagation Apparatus (FPA) provide a mechanism to assess a material's reaction to fire. From these laboratory tests, a material's overall flammability can be evaluated on the basis of measured quantities such as heat release rate or mass loss rate (MLR) history, species yields, smoke production rate, heat of combustion, etc. Furthermore, by conducting experiments at multiple heat flux levels, apparent material fire properties such as thermal inertia, ignition temperature, and heat of gasification can be determined. These quantities are useful for establishing relative rankings of material flammability or as input to semi-empirical fire growth models.

In recent years, detailed physics-based pyrolysis models have seen increased usage in the fire community. For example, Fire Dynamics Simulator Version 5 (FDS5) contains a comprehensive pyrolysis model capable of simulating the thermal decomposition of both charring and noncharring solids. This pyrolysis model can accommodate multi-step decomposition kinetics, layered composition, and in-depth absorption of radiation. However, inclusion of these physical phenomena comes at a price: a large number of adjustable parameters ("material properties") must be specified to characterize a particular material. These properties include pyrolysis kinetics (pre-exponential factor, activation energy, reaction order), thermal properties (specific heat capacity, thermal conductivity), and radiative characteristics (surface emissivity, in-depth radiation absorption coefficient). For many of these material properties, there are no standardized and widely accepted techniques to determine these properties from laboratory tests. The number of adjustable parameters becomes onerous when multi-step reactions with multiple condensed phase species having temperature-dependent thermal properties are considered.

An optimal pyrolysis modeling strategy balances complexity with minimizing the number of adjustable input parameters. This can be accomplished by including only essential physics or reactions in a simulation, and omitting all extraneous physics and reactions. However, it is not always obvious what constitutes "essential" or "extraneous" physics and reactions. This multifaceted and complex issue cannot be completely resolved in a single paper, so here we focus on one particular aspect: decomposition kinetics. Using a fire retardant polyester composite as an example, we investigate whether a multi-step kinetic mechanism extracted from thermogravimetric analysis (TGA) provides a more "accurate" description of solid fuel slab pyrolysis (e.g. in an FPA experiment) than a single-step global n^{th} order Arrhenius reaction (the conventional pyrolysis modeling paradigm in the fire community). This fiber reinforced polymer (FRP) composite is considered a representative "practical" heterogeneous material.

Below, a methodology is presented that can be used to assess the minimum number of reaction steps that must be included in a decomposition mechanism to capture the major features of differential thermogravimetric (DTG) curves. First, two different three-step decomposition mechanisms and a single-step global mechanism are fit to DTG curves obtained at four heating rates between 5 K/min and 50 K/min under nitrogen. Next, holding these kinetic parameters fixed, an FPA experiment of a 1 cm thick FRP composite (with matrix comprised of the same resin tested via TGA) irradiated at 50 kW/m² under nitrogen is simulated with the three different decomposition mechanisms.

CONDENSED PHASE PYROLYSIS MODEL

The calculations reported here are conducted with a generalized pyrolysis model [1], similar to that used in FDS5, that can be applied to a wide variety of condensed phase fuels. This model can be applied to both 0D and 1D systems and is therefore capable simulating both "lumped" (thermogravimetric) and "slab" (Cone Calorimeter/FPA) experiments. Extensive details are given in Ref. [1] so only a brief overview is given here. Assumptions inherent in the model, as applied in this paper, include:

- Each condensed phase species has well-defined "properties": bulk density, specific heat capacity, effective thermal conductivity, and porosity. An overbar denotes a weighted or averaged quantity, i.e.
$$\bar{k} = \sum X_i k_i .$$
- Specific heat capacity and effective thermal conductivity vary by as $\phi(T) = \phi_0 (T/T_r)^{n_\phi}$ where T_r is a reference temperature, ϕ_0 is the value of k or c at T_r , and n_ϕ specifies the temperature dependency of ϕ

- Radiation heat transfer across pores is accounted for by adding a contribution to the effective thermal conductivity that varies as γT^3 , where γ is a fitting parameter
- Averaged properties in conservation equations are calculated by appropriate mass or volume fraction weighting
- All gases escape to the exterior ambient with no resistance to heat or mass transfer
- Negligible heat transfer between the gas phase and the condensed phase inside the decomposing solid
- There is no net shrinkage (volume change) due to reactions or bulk density changes

The one-dimensional (slab) transient conservation equations are given as Eqs. 1-4:

Condensed phase mass conservation:

$$\frac{\partial \bar{\rho}}{\partial t} = -\dot{\omega}_{fg}'' \quad (1)$$

Gas phase mass conservation:

$$\frac{\partial(\rho_g \bar{\psi})}{\partial t} + \frac{\partial \dot{m}''}{\partial z} = \dot{\omega}_{fg}'' \quad (2)$$

Condensed phase species conservation:

$$\frac{\partial(\bar{\rho} Y_i)}{\partial t} = \dot{\omega}_{fi}'' - \dot{\omega}_{di}'' \quad (3)$$

Condensed phase energy conservation:

$$\frac{\partial(\bar{\rho} h)}{\partial t} = \frac{\partial}{\partial z} \left(\bar{k} \frac{\partial T}{\partial z} \right) + \sum_{k=1}^K \dot{Q}_{s,k}'' + \sum_{i=1}^M (\dot{\omega}_{fi}'' - \dot{\omega}_{di}'') h_i \quad (4)$$

The gaseous mass flux at any point in the decomposing solid is calculated by integrating Eq. 2 from the back face to the front face:

$$\dot{m}''(z) = \dot{m}''_{\delta} + \int_{\delta}^z \left(\dot{\omega}_{fg}'' - \frac{\partial(\rho_g \bar{\psi})}{\partial t} \right) \quad (5)$$

where, since the back face is assumed impermeable, $\dot{m}''_{\delta} = 0$. When discretized, the above equations yield a system of coupled algebraic equations that are solved numerically. The recommendations of Patankar [2] are followed closely. Due to the nonlinearity introduced by the source terms and temperature-dependent thermophysical properties, a fully-implicit formulation is adopted for solution of all equations. The condensed phase energy conservation equation is solved using a computationally efficient tridiagonal matrix algorithm (TDMA). The condensed phase mass and condensed phase species conservation equations are solved with a customized fully implicit solver that uses overrelaxation to prevent divergence. Source terms are split into positive and negative components to ensure physically realistic results and prevent negative mass fractions or densities from occurring [2]. Newton iteration is used to extract the temperature from the weighted enthalpy and the condensed phase species mass fractions [1].

The initial conditions describe the state of the solid (density, species mass fractions) at $t=0$. The “front-face” boundary condition (where radiation from the FPA heaters is incident) is a convective-radiative balance. Following de Ris and Khan [3], the back-face of the FRP composite loses heat to the underlying sample holder (3 mm Cotronics ceramic paper thermal insulation) proportional to an inverse contact resistance. The sample holder is treated in the model as a separate layer, with its temperature-dependent thermal properties estimated from de Ris and Khan [3].

The above governing equations can also be used to simulate thermogravimetric experiments. Since this involves only a single 0D lumped particle ($Bi \ll 1$), the preceding coupled partial differential equations

become coupled (transient) ordinary differential equations, i.e. only a single control volume (representing a thermogravimetric sample) is considered. Since the particle temperature is assumed equal to the atmosphere temperature (which increases linearly with time) the condensed phase energy conservation (Eq. 4) is replaced with the following relation:

$$T = T_0 + \beta t \quad (6)$$

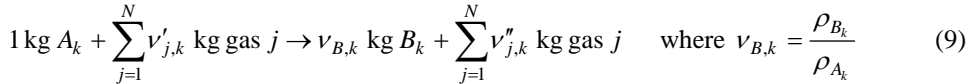
The condensed phase mass and species conservation equations (Eqs. 1 and 3) remain unchanged, with the exception that the partial time derivative becomes a total time derivative since there is no spatial variation in mass or species (homogeneous particle). Differential thermogravimetric curves are calculated from the formation rate of gases normalized by the initial particle bulk density:

$$\frac{d}{dt} \left(\frac{m''}{m_0''} \right) = - \frac{\dot{\omega}_{fg}''}{\bar{\rho}|_{t=0}} \quad (7)$$

Thermogravimetric curves are then calculated by integrating Eq. 7:

$$1 - \alpha(t) = \frac{m''}{m_0''}(t) = 1 - \frac{1}{\bar{\rho}|_{t=0}} \int_0^t \dot{\omega}_{fg}''(\tau) d\tau \quad (8)$$

The governing equations presented earlier contain several source terms attributed to chemical reactions ($\dot{\omega}_{fg}''$, $\dot{\omega}_{fi}''$, $\dot{\omega}_{di}''$, and $\dot{Q}_{s,k}''$) that must be quantified. Heterogeneous reaction stoichiometry can be written in general form as:



Each reaction k converts a condensed phase species having index A_k to a condensed phase species having index B_k . Gases may be consumed or produced in the process, but it is assumed here for simplicity that $\nu'_{j,k} = 0$ and $N = 1$. The destruction rate of condensed phase species A_k by reaction k is calculated as:

$$\dot{\omega}_{dA_k}'' = f \left(\frac{\bar{\rho} Y_{A_k}}{\bar{\rho}|_{t=0}} \right) \bar{\rho}|_{t=0} Z_k \exp \left(- \frac{E_k}{RT} \right) \quad (10)$$

The term $f(\bar{\rho} Y_{A_k} / \bar{\rho}|_{t=0})$ on the RHS of Eq. 10 is the kinetic model, described in greater detail below. The formation rate of condensed phase species B_k by reaction k is related to bulk density ratios:

$$\dot{\omega}_{fB_k}'' = \nu_{B,k} \dot{\omega}_{dA_k}'' = \frac{\rho_{B_k}}{\rho_{A_k}} \dot{\omega}_{dA_k}'' \quad (11)$$

The formation rate of all gases (conversion rate of condensed phase mass to gas phase mass) by reaction k is:

$$\dot{\omega}_{fg_k}'' = (1 - \nu_{B,k}) \dot{\omega}_{dA_k}'' = \left(1 - \frac{\rho_{B_k}}{\rho_{A_k}} \right) \dot{\omega}_{dA_k}'' \quad (12)$$

Associated with each reaction k is a heat of reaction $\Delta H_{vol,k}$ and the source term appearing in Eq. 4 is calculated as the volumetric formation rate of gases multiplied by $\Delta H_{vol,k}$:

$$\dot{Q}_{s,k}'' = - \dot{\omega}_{fg_k}'' \Delta H_{vol,k} \quad (13)$$

The total source terms appearing in the conservation equations are obtained by summing over all reactions:

$$\dot{\omega}_{di}''' = \sum_{k=1}^K \delta_{i,A_k} \dot{\omega}_{dA_k}''' \quad \delta_{i,A_k} = \begin{cases} 1 & \text{if } i = A_k \\ 0 & \text{if } i \neq A_k \end{cases} \quad (14)$$

$$\dot{\omega}_{fi}''' = \sum_{k=1}^K \delta_{i,B_k} \dot{\omega}_{fB_k}''' \quad \delta_{i,B_k} = \begin{cases} 1 & \text{if } i = B_k \\ 0 & \text{if } i \neq B_k \end{cases} \quad (15)$$

$$\dot{\omega}_{fg}''' = \sum_{k=1}^K \dot{\omega}_{fg_k}''' \quad (16)$$

DESCRIPTION OF RESIN AND COMPOSITE SLAB

The resin in this study is a commercially prepared brominated unsaturated polyester resin with 20% bromination by mass built in to the carbon back bone. Antimony trioxide is added to enhance flame retardancy. The resin was catalyzed with methyl ethyl ketone peroxide (MEKP). According to the product description, this resin is a low viscosity, thixod polyester resin formulated to be Class I per ASTM E84 (flame spread index < 25 and smoke developed < 450).

Composite panels (33% glass by mass and approximately 10 mm in thickness) were fabricated by hand lay-up using two different types of fiberglass mats that were fully wetted with resin. The two types of fiberglass (E-glass) used in the composite are a chopped strand mat and a glass roving with an area density of 25 g/m² and 880 g/m², respectively. The chopped strand mat is thinner and more porous than the roving. The laminate schedule (provided by the manufacturer) is chopped strand mat and roving alternating five times with another chopped strand mat layer at the end. Visual inspection of a polished cross-section of the composite slab is consistent with this laminate schedule, but with polymer resin layers between each fiberglass layer. The chopped strand mat layer is difficult to identify in the cross section, perhaps because more resin is soaked into this layer than the roving layer. The roving layer is observed as a prominent glass layer possibly because the resin is absorbed only at the fiberglass layer surfaces leaving the interior with primarily glass.

The layered microstructure is determined to a resolution of ~0.07 mm by inspecting a polished cross-section of the composite under a microscope. Based on visual observation and comparison to global density of the composite sample, approximations of three distinct layers are proposed: 100% resin, 100% glass, and 50% resin/50% glass. The microstructure is shown schematically in Fig. 1. The lightest “box” represents 100% resin, the medium darkness box represents 50% resin/50% glass, and the darkest box represents 100% glass. Each box has a thickness of ~0.07 mm.



Fig. 1. Approximation of three distinct layers in composite microstructure.

THERMAL DECOMPOSITION OF RESIN POLYMER

The resin's thermal stability is investigated via TGA using a PerkinElmer Thermogravimetric Analysis 7 (TGA7) instrument. Experiments are conducted under nitrogen at heating rates of 5 K/min, 10 K/min, 30 K/min, and 50 K/min. The initial mass of each sample ranges from ~7.5 mg to ~10.5 mg.

Apparent number of reaction steps – isoconversional method

Thermogravimetric experiments are often analyzed using a kinetic model of the form:

$$\frac{d\alpha}{dt} = f(\alpha)Z \exp\left(-\frac{E}{RT}\right) \quad (17)$$

Eq. 17 can also be obtained after dividing Eq. 10 by $\bar{\rho}|_{t=0}$, considering only a single condensed phase species, and defining the conversion $\alpha = 1 - \bar{\rho}/\bar{\rho}|_{t=0}$. Substituting the linear heating rate $\beta = dT/dt$ into Eq. 17 and taking the natural logarithm of both sides gives:

$$\ln \frac{d\alpha}{dT} = \ln \left(\frac{f(\alpha)}{\beta} Z \exp \left(-\frac{E}{RT} \right) \right) = \ln \left(\frac{f(\alpha)Z}{\beta} \right) + \ln \left(\exp \left(-\frac{E}{RT} \right) \right) = \ln \left(\frac{f(\alpha)Z}{\beta} \right) - \frac{E}{RT} \quad (18)$$

Eq. 18 can be used to determine the activation energy E as a function of α by plotting $\ln(d\alpha/dT)$ against $1/T$. The slope of the line is $-E/R$ [4]. If the activation energy determined via this so-called “isoconversional” (or “model free”) method is not a function of α , this is indicative of a single step reaction. If however the activation energy varies significantly with conversion, then multiple reactions having different activation energies likely occur.

As an example, Fig. 2 shows the apparent activation energy as a function of conversion determined with the above method for the brominated polyester resin described earlier. It can be seen from Fig. 2 that the apparent activation energy increases from ~ 70 kJ/mol to ~ 145 kJ/mol in the range $0 < \alpha < 0.2$. Over the range $0.2 < \alpha < 0.9$, the activation energy is relatively constant, varying between ~ 125 kJ/mol and ~ 140 kJ/mol. For $\alpha > 0.9$, the apparent activation energy increases, approaching 200 kJ/mol. The activation energy calculated in this way should be viewed as an estimate, rather than an exact value. What is more important than the specific value of activation energy at a particular conversion is the number of fundamental steps that this type of plot elucidates.

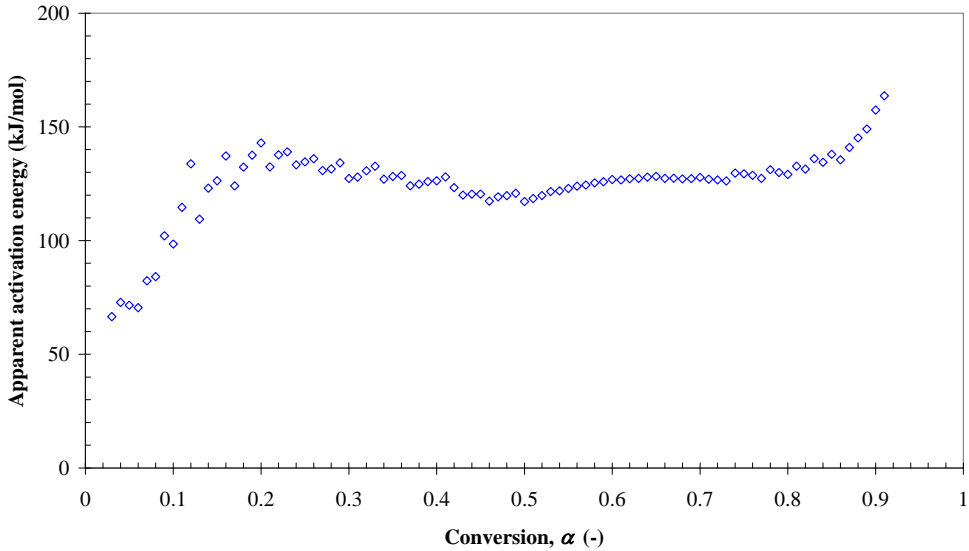


Fig. 2. Apparent activation energy of unsaturated brominated polyester resin calculated via “isoconversional” (model free) method [4].

Based on Fig. 2 and the above discussion, it can be concluded that at least three primary reactions occur. Reaction 1 is dominant over $0 < \alpha < 0.2$, reaction 2 is dominant over $0.2 < \alpha < 0.9$, and reaction 3 is dominant for $\alpha > 0.9$. On this basis, a 3-step mechanism is postulated:



In Eq. 19, the species beta_resin is an intermediate species that is formed in the early stages of pyrolysis; referring to Fig. 2 above, beta_resin is fully formed when the conversion value has reached approximately 0.2. This beta_resin species is analogous to the β -foam species used in previous work [5]. Similarly, char is an intermediate species that is formed when the conversion value has reached approximately 0.93. Although approximately 97% conversion was observed at the end of each TGA experiments, complete mass loss (100% conversion) was assumed in the modeling for simplicity.

For the reaction mechanism in Eq. 19, it follows from Eqs. 9, 11, and 12 that $v_{br} = \rho_{\text{beta_resin}} / \rho_{\text{resin}} = 0.80$ and $v_c = \rho_{\text{char}} / \rho_{\text{beta_resin}} = 0.07 \rho_{\text{resin}} / 0.80 \rho_{\text{resin}} = 0.088$. The single-step approximation to the above reaction mechanism used here is: $\text{resin} \rightarrow v_{c,ss} \text{char} + (1 - v_{c,ss}) \text{gas}$, where $v_{c,ss} = \rho_{\text{char}} / \rho_{\text{resin}} = 0.07$.

Kinetic models

In the three-step reaction mechanism, two different forms of $f(\alpha)$ are contemplated for the second step (Eq. 19.2):

$$f(\alpha) = (1 - \alpha)^n \quad \text{standard } n^{\text{th}} \text{ order reaction} \quad (20a)$$

$$f(\alpha) = \alpha^m (1 - \alpha)^n \quad \text{autocatalytic reaction} \quad (20b)$$

Eq. 20a represents current “standard” practice for condensed phase kinetic modeling in the fire community, and Eq. 20b is an autocatalytic reaction, which arises from chemical considerations because polyester thermostat resin thermal decomposition is probably caused by free radical depolymerization. Depolymerization is the same process as polymerization except the chain length becomes shorter rather than longer. An autocatalytic reaction means that the reaction product (here, free radicals) is the catalyst for the reaction itself. A thermal insult on the polymer generates free-radicals that start to attack other parts of the polymer. Essentially, free radicals attack on the polymer breaks chemical bonds, promoting further degradation of the unreacted polymer. The α^m part of the kinetic model in Eq. 20b is attributed to attack by free radicals and the $(1 - \alpha)^n$ part of the kinetic model in Eq. 20b is because the absolute reaction rate drops as the sample mass decreases since there is less polymer to pyrolyze. Thus, Eq. 20b is considered a more “fundamental” kinetic decomposition model than Eq. 20a because it attempts to simulate the postulated chemical decomposition mechanism (free radical depolymerization).

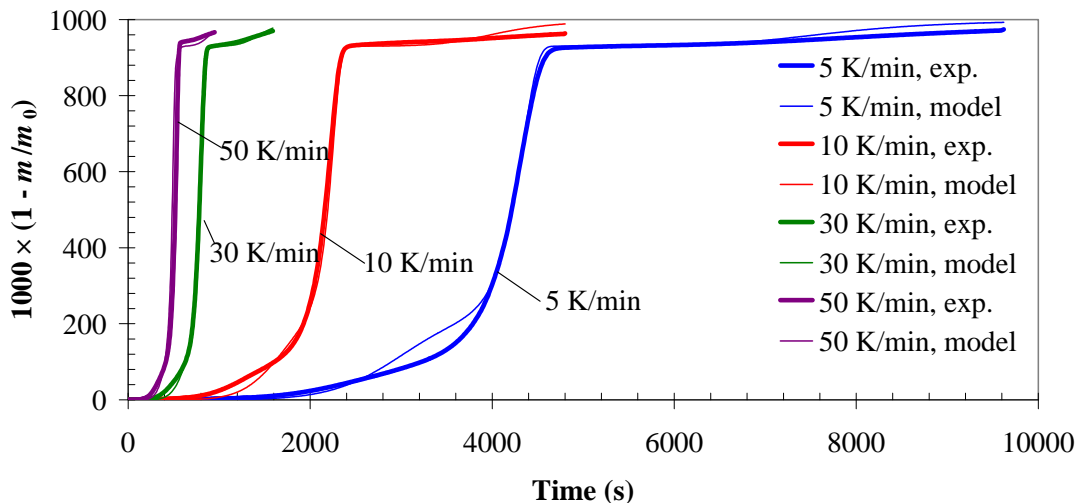
Numerical simulation of TGA experiments

First, the model described earlier is used to simulate the thermogravimetric experiments. Kinetic parameters are estimated via genetic algorithm optimization [1] for three separate reaction mechanisms/kinetic models which are labeled as: a) Three-step autocatalytic, b) Three-step n^{th} order, c) Single-step n^{th} order. The three-step autocatalytic assumes that steps 1 and 3 are n^{th} order, and that step 2 is autocatalytic. The three-step n^{th} order and the single-step n^{th} order assume that all steps are n^{th} order. The best-fit results are shown in Fig. 3, with best-fit kinetic parameters listed in Table 1.

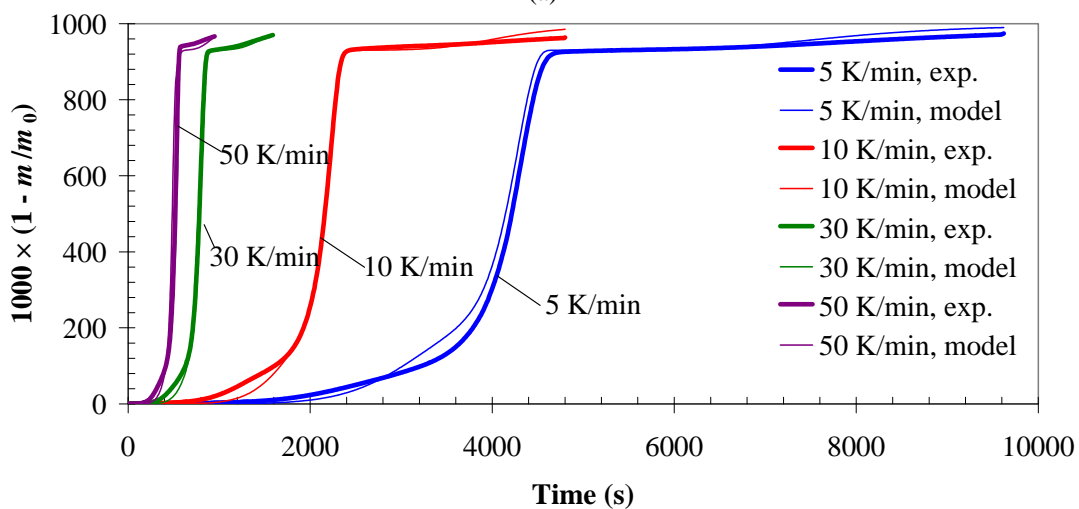
It can be seen from Fig. 3 that the two 3-step mechanisms (n^{th} order and autocatalytic) capture better the early and late stages of mass loss than the single-step reaction. The 3-step mechanisms approach zero remaining mass at long times, whereas 7% of the sample’s mass remains at the end of the simulation with the single-step mechanism. Experimentally, less than 3% of the sample mass remained at the end of a TGA run as residue. There is little difference between the three-step autocatalytic mechanism (case a) and the three-step n^{th} order mechanism (case b), suggesting that the additional parameter (m) introduced for the autocatalytic reaction may be extraneous. On balance, the autocatalytic reaction mechanism does provide a slightly better fit to the 5 K/min TG data between 4000 and 4800 s. It appears from Fig. 3 that the models provide a better fit to the experimental data at higher heating rates; however, this is a nuance of plotting the results as a function of time rather than temperature because the data from the lower heating rates appear stretched on the plots, and the data from the higher heating rates appear compressed.

Table 1. Optimized kinetics parameters for three different kinetic models. (a) Three-step autocatalytic; (b) Three-step n^{th} order; (c) Single-step n^{th} order.

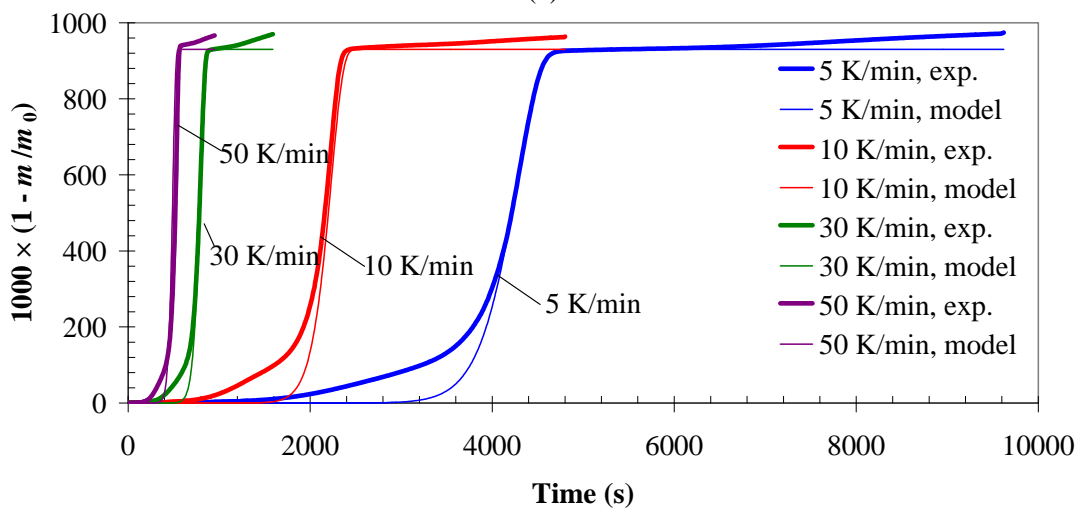
	Z_1 (s ⁻¹)	E_1 (kJ/mol)	n_1 (-)	Z_2 (s ⁻¹)	E_2 (kJ/mol)	n_2 (-)	m_2	Z_3 (s ⁻¹)	E_3 (kJ/mol)	n_3 (-)
a	4.39×10^2	55.8	1.09	2.19×10^{11}	170.1	0.87	0.61	5.66×10^6	139.0	2.47
b	3.42×10^2	56.1	1.03	3.55×10^{11}	174.1	0.80	0	1.75×10^6	127.6	2.64
c	-	-	-	4.92×10^9	151.4	0.90	0	-	-	-



(a)



(b)



(c)

Fig. 3. Comparison of experimental and modeled thermogravimetric curves for three different kinetic models. (a) three-step autocatalytic; (b) three-step n^{th} order; (c) Single-step n^{th} order.

SIMULATION OF FPA EXPERIMENTS

The preceding TGA experiments were conducted with polyester resin that contained no glass reinforcements. This same resin forms the matrix of the FRP composite slab (having woven glass reinforcements) that is tested in the FPA. It was shown in Fig. 1 that the composite slab is far from homogeneous, with distinct layers of 100% glass, 100% resin, and a 50%/50% mixture of resin and glass. However, as a first approximation and to focus on decomposition kinetics, the heterogeneous FRP composite slab is modeled here as an equivalent homogeneous slab having the same global glass content as the FRP composite (33% by mass). It is assumed here that the glass is inert and that only the resin reacts. We plan to address the effect of layered structure on slab pyrolysis behavior in future work.

The FPA experiments involve irradiating (under nitrogen) circular FRP composite samples with a radius of 9.7 cm (area of 74 cm²) at 50 kW/m² and measuring the resultant mass loss. To facilitate temperature measurements, thermocouples are positioned at the sample surface, 1/3 and 2/3 of its thickness, and at its back face. The sample holder consists of 3 mm Cotronics ceramic paper thermal insulation [3]. To ensure that most of the incident radiation is absorbed at the irradiated surface, samples are coated with a thin layer of carbon black in accordance with ASTM E2058. The composite tested here (referred to as material “1a”) has a thickness of 10.2 mm and a glass content of 33% by mass.

In the numerical simulations of the FPA experiments, the kinetics coefficients extracted earlier from TGA are held fixed. Three separate cases (corresponding to each kinetic model) are considered: 3-step autocatalytic, 3-step n^{th} order, and single step. First, the unknown model input parameters (thermophysical properties, reaction enthalpies, and surface emissivities) are estimated by genetic algorithm optimization [1] from the FPA data for the n^{th} order case since it is the standard model in the fire community and was shown to provide a very good fit to the TGA data in Fig 3. Next, the 3-step autocatalytic mechanism is assessed by holding fixed all input parameters and swapping the 3-step n^{th} order mechanism for the 3-step autocatalytic mechanism. The final simulation involves replacing the three-step reaction mechanism with the single-step reaction mechanism. The calculated MLR for each case is compared to the available experimental data to assess how the complexity of the reaction mechanism affects global decomposition behavior of a composite slab.

In the simulations, four condensed phase “pseudo” species are tracked: resin_glass (33% glass by mass bonded to 67% resin by mass), betaresin_glass (a mixture of beta resin and glass), char_glass (a mixture of char and glass), and porous_glass (the glass reinforcements that remain after all resin has pyrolyzed, leaving behind a porous glass structure consisting primarily of woven glass reinforcements).

As explained in Ref. [1], the bulk density of condensed phase species mixtures can be calculated as $\bar{\rho} = \sum (Y_i / \rho_i)^{-1} = \sum X_i \rho_i$. Here, the bulk density of species resin_glass is calculated from the density of the resin (1350 kg/m³) and the glass (2600 kg/m³) as $\rho_{\text{resin_glass}} = \sum (Y_i / \rho_i)^{-1} = 1605 \text{ kg/m}^3$. Using the relation $\rho_{\text{resin_glass}} = \sum X_i \rho_i = X_{\text{resin}} \rho_{\text{resin}} + X_{\text{glass}} \rho_{\text{glass}}$, the volume fraction of glass in species resin_glass is calculated to be 0.20. The bulk density of species betaresin_glass is calculated as:

$$\rho_{\text{betaresin_glass}} = \sum X_i \rho_i = X_{\text{beta_resin}} \rho_{\text{beta_resin}} + X_{\text{glass}} \rho_{\text{glass}} = 0.8 \times 0.8 \times 1350 + 0.2 \times 2600 = 1384 \text{ kg/m}^3$$

where use has been made of the relation $v_{\text{br}} = \rho_{\text{beta_resin}} / \rho_{\text{resin}} = 0.80$. Finally, the bulk densities of species char_glass and porous_glass are $\rho_{\text{char_glass}} = \sum X_i \rho_i = 0.8 \times 0.07 \times 1350 + 0.2 \times 2600 = 596 \text{ kg/m}^3$ and $\rho_{\text{porous_glass}} = 0.2 \times 2600 = 520 \text{ kg/m}^3$.

The above bulk density calculations (and the governing equations presented earlier) assume that there is no net volume change in the unpyrolyzed vs. pyrolyzed sample. The kinetic mechanism from the TGA experiments (involving resin with no reinforcements) must be adapted to fit into the above framework. Specifically, Eq. 19 becomes:

$$\text{resin_glass} \rightarrow \nu_{\text{brg}} \text{betaresin_glass} + (1 - \nu_{\text{brg}}) \text{gas} \quad (21.1)$$

$$\text{betaresin_glass} \rightarrow \nu_{\text{cg}} \text{char_glass} + (1 - \nu_{\text{cg}}) \text{gas} \quad (21.2)$$

$$\text{char_glass} \rightarrow \nu_{\text{pg}} \text{porous_glass} + (1 - \nu_{\text{pg}}) \text{gas} \quad (21.3)$$

For the reaction mechanism in Eq. 21, it follows from Eqs. 9, 11, and 12:

$$\nu_{\text{brg}} = \rho_{\text{betaresin_glass}} / \rho_{\text{resin_glass}} = 0.86, \quad \nu_{\text{cg}} = \rho_{\text{char_glass}} / \rho_{\text{betaresin_glass}} = 0.43, \quad \text{and}$$

$$\nu_{\text{pg}} = \rho_{\text{porous_glass}} / \rho_{\text{char_glass}} = 0.87.$$

The kinetics coefficients in Eq. 21 (resin/glass reaction mechanism) are the same as in Eq. 19 (reaction mechanism for 100% resin) except that the pre-exponential factors determined by thermogravimetric analysis are multiplied by the pyrolyzable volume fraction (0.8, as calculated above). An alternative is to multiply the pre-exponential factors by the pyrolyzable mass fraction, but this is not investigated here.

A comparison of the optimized model calculations and the experimental data is shown in Fig. 4 for the 3-step n^{th} order mechanism. The thermophysical properties used in these calculations are listed in Table 2 (ΔH_{vol} is 1.3×10^5 J/kg, 2.3×10^5 J/kg, and 1.4×10^6 J/kg respectively for reactions 1, 2, and 3). Fig. 4a-4c compare the measured and modeled temperatures. The maximum deviation from the experimental data is ~60 K, approximately consistent with the global measurement uncertainty of 50 K [6] indicating that the calculated temperature traces match the experimental data. The measured and calculated MLR is shown in Fig. 4d. The model correctly captures the general “dual peak” shape of the MLR curve. However, the second peak is over-calculated compared to the experimental data.

The reason for the over-calculation of the second MLR peak may be due to different pyrolyzable mass fractions of resin (i.e., different resin conversions) in the TGA and FPA experiments. From the TGA kinetic modeling above, 93% of the resin’s mass pyrolyzes in the first two steps of the reaction mechanism to form “char”. Assuming that in the FPA experiments the resin reacts to form char, but that this char does not further react, the total mass loss per unit area is: $0.67 \times 0.93 \times 1605 \text{ kg/m}^3 \times 10.2 \text{ mm} = 10.2 \text{ kg/m}^2$ (where 0.67 is the pyrolyzable mass fraction and the 0.93 factor assumes that the char does not further react, i.e. the final resin conversion is 0.93). The cumulative mass loss calculated by the model after 900 s is 10.5 kg/m^2 (resin conversion of 0.96) because in the model some of the char has reacted, i.e. char_glass has started reacting to form porous_glass. In comparison, the experimental data show a cumulative mass loss of only 7.6 kg/m^2 (resin conversion of 0.69) after 900 s. It appears that the resin conversion is different in the TGA and FPA experiments. Although this finding has practical ramifications, the main focus of this paper is *relative* changes in slab pyrolysis behavior caused by decomposition kinetics. The differences encountered here may be caused (indirectly) by experimental error in the temperature measurements. If the measured temperature is hotter than the actual temperature of the condensed phase, the optimized model would over-predict the MLR since its thermophysical properties are optimized to make the calculated temperatures match the experimental data. Another contributing effect may be the heterogeneous nature of the composite, which is approximated here as a homogeneous equivalent. The woven glass layers could act as a thermal barrier (thereby limiting resin pyrolysis) or a physical barrier (thereby preventing pyrolyzed resin from escaping). A model that explicitly considers the laminated microstructure would be required to capture this effect.

Table 2. Optimized thermophysical properties used in slab pyrolysis simulations.

Species	ρ_0 (kg/m ³)	k_0 (W/m-K)	n_k (-)	c_0 (J/kg-K)	n_c (-)	ε (-)	γ (m)
resin_glass	1600	0.240	0.116	1465	0.180	0.98	0
betaresin_glass	1384	0.278	0.239	1331	0.184	0.98	0
char_glass	596	0.130	0.165	938	0.026	1.00	2.5×10^{-3}
porous_glass	520	0.130	0.173	924	0.025	1.00	3.7×10^{-3}
Cotronics	168	0.028	1.270	800	0.190	1.00	0

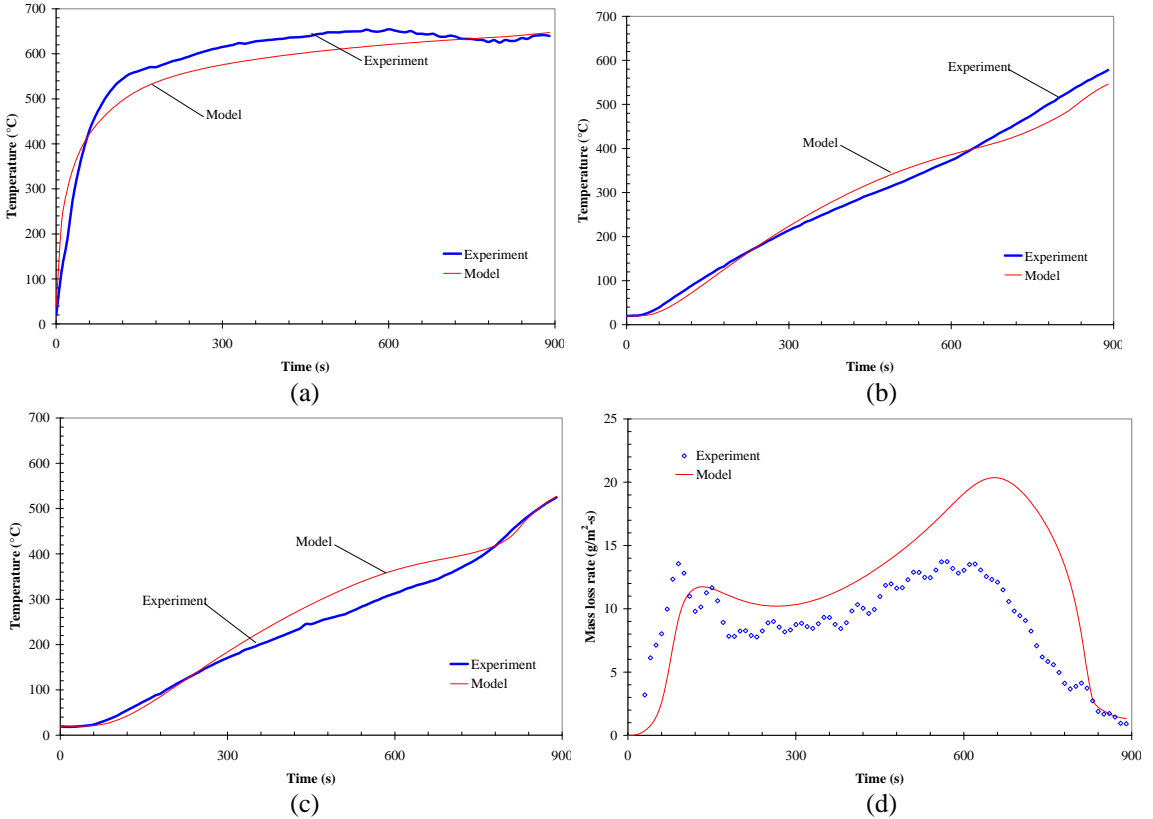


Fig. 4. Comparison of calculations (3-step n^{th} order) and experimental data for pyrolysis of FRP polyester composite in FPA at 50 kW/m^2 under N_2 . (a) Surface T ; (b) 2/3 thickness T ; (c) Back face T ; (d) MLR.

Next, the thermophysical properties determined above (Table 2) are held constant, and the two additional kinetic models are investigated. Their effect on the calculated MLR is shown in Fig. 5. There are minor differences between the calculated MLR curve for the two 3-step mechanisms (n^{th} order and autocatalytic). This is expected since these mechanisms provide similar fits to the TGA data (Fig. 3). However, the MLR calculated with the single-step mechanism is quantitatively different from the 3-step mechanisms. The early MLR is suppressed, with greater MLR at later times. This is consistent with Fig. 3, which shows that for the single step reaction mechanism the initial mass loss is not captured, but the later stages are.

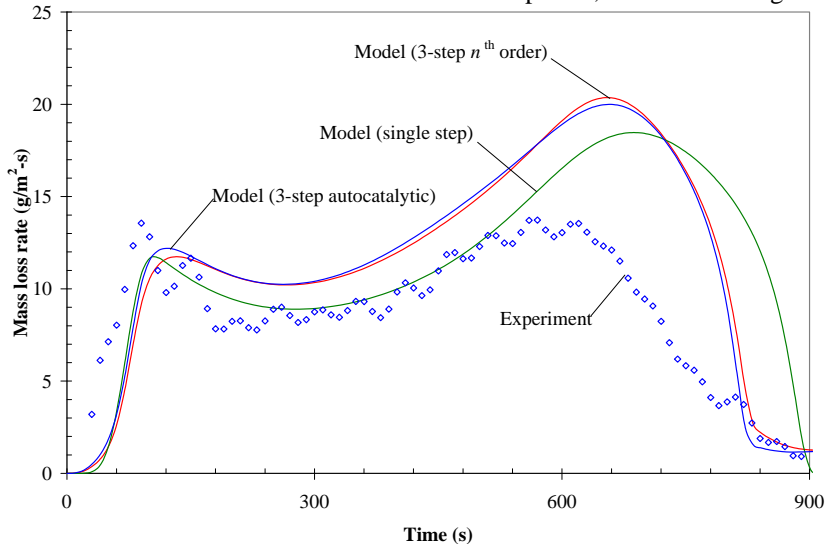


Fig. 5. Comparison of measured and modeled MLR in FPA for three different kinetic models.

CONCLUDING REMARKS

In the example presented in this paper, a 3-step n^{th} order reaction mechanism and a 3-step reaction mechanism with a main autocatalytic step provided nearly identical calculations of thermogravimetric curves and slab pyrolysis in the Fire Propagation Apparatus (FPA) under nitrogen. Compared to the 3-step mechanisms, a single-step decomposition mechanism provides quantitatively different, but similar, MLR predictions of the FPA data. The 3-step n^{th} order mechanism requires specification of 19 additional model input parameters (two values each of Z , E , n , and ΔH_{vol} , two values each of k_0 , n_k , c_0 , n_c , ε , and one value of γ) over the single step reaction case. In view of the marginal difference between the single-step and the 3-step calculations shown in Fig. 5, it is apparent that for this particular case introducing additional complexity (and degrees of freedom) is superfluous. Essentially, uncertainties in microstructure/anisotropy, material properties, heats of reaction, boundary conditions, experimental measurements, and inter-batch/inter-manufacturer variations dwarf any uncertainty in the decomposition kinetics as determined from TGA.

Although it is difficult to justify use of a multi-step for the material modeled here, no broad conclusions regarding the importance of multi-step thermal decomposition kinetics can be drawn on the basis of a single study. Multi-step reaction mechanisms may be justified for materials with DTG curves that show multiple reaction peaks. If a material's DTG curve can't be fit using an n^{th} order reaction, one of the more fundamental kinetic models (e.g., autocatalytic) may be appropriate. If a material shows endothermic behavior in inert environments but exothermic behavior in oxidative environments, a reaction mechanism that includes an endothermic pyrolysis step and an exothermic oxidative step may be warranted. Finally, the additional complexity introduced by multi-step reaction mechanisms may be justified if all other model input parameters (thermophysical properties, radiation characteristics) are accurately known.

ACKNOWLEDGEMENTS

The authors would like to thank Mr. Charles Dore for fabricating the FRP Composites used in this study. The UC Berkeley authors would like to thank the National Science Foundation for support under Award 0730556, "Tackling CFD Modeling of Flame Spread on Practical Solid Combustibles".

REFERENCES

- [1] Lautenberger, C., "A Generalized Pyrolysis Model for Combustible Solids", Ph.D. Dissertation, Department of Mechanical Engineering, University of California, Berkeley, Fall 2007. See also <http://code.google.com/p/gpyro>.
- [2] Patankar, S.V., *Numerical Heat Transfer and Fluid Flow*, Hemisphere Publishing Corporation, New York, 1980.
- [3] de Ris, J.L. and Khan, M.M., (2000) A Sample Holder for Determining Material Properties, *Fire and Materials* 24: 219-226, [http://dx.doi.org/10.1002/1099-1018\(200009/10\)24:5<219::AID-FAM741>3.0.CO;2-7](http://dx.doi.org/10.1002/1099-1018(200009/10)24:5<219::AID-FAM741>3.0.CO;2-7)
- [4] Friedman, H.L., (1964) Kinetics of Thermal Degradation of Char Forming Plastics from Thermogravimetry: Application to a Phenolic Plastic, *Journal of Polymer Sci Part C* 6: 183-195, <http://www3.interscience.wiley.com/journal/114174190/abstract>
- [5] Rein, G., Lautenberger, C., Fernandez-Pello, A.C., Torero, J.L., and Urban, D.L., (2006) Application of Genetic Algorithms and Thermogravimetry to Determine the Kinetics of Polyurethane Foam in Smoldering Combustion, *Combustion and Flame* 146: 95-108, <http://dx.doi.org/10.1016/j.combustflame.2006.04.013>
- [6] Avila, M.B., Dembsey, N.A., and Dore, C., (2008) Effect of Resin Type and Glass Content on the Reaction to Fire Characteristics of Typical FRP Composites, *Composites Part A Applied Science and Manufacturing*, accepted for publication.